Non-Covalent Interactions in Aqueous Media: Molecular Recognition Studies Through Circular Dichroism and Self-Assembly of Discrete Aggregates

Thesis by

Jonathan Eric Forman

In Partial Fulfillment of the Requirements

for the Degree of

Doctor of Philosophy

California Institute of Technology

Pasadena, California

1996

(Defended February 20, 1996)

Acknowledgments

There are numerous individuals and organizations that have contributed in some way to making this thesis possible and in keeping my time in graduate school interesting. I will attempt to acknowledge those that are most memorable, for the positive things that they helped to bring about and for the defining moments they created. As has been typical of all I've written during my time at Caltech, this list of acknowledgments won't be short.

It has been an honor and a pleasure to work as a graduate student for Dennis Dougherty. I am continually amazed at Dennis' brilliance as a scientist, and even more

amazed that he can be such a brilliant scientist without losing track of important aspects of his life outside science. I have immense respect for this man, and have benefited greatly from his guidance. I have greatly appreciated his encouragement of bringing my own ideas and directions into my projects. If nothing else, Dennis has taught me the importance of critically thinking about what I'm doing and where the work is going. I have been fortunate to have had the opportunity to work with Dennis' graduate advisor Kurt Mislow, and I value the insights he has provided. I also want to thank the other members of my Ph.D. committee for their comments about my work (and my choice of tie's); I have greatly benefited from my interactions with Andy Myers, Jackie Barton, and Doug Rees.

I cannot thank Rich Barrans enough for all the help he provided in the early stages of my graduate education. My success with the circular dichroism project can be directly attributed to him, and I have learned a lot from working with such a thoughtful and careful scientist. Pat Kearney and Sandro Mecozzi deserve credit for all the insight (criticism) they have provided towards my work. The other members of the "Molecular Recognition" group that I've had the opportunity to interact with include Leslie Jimenez, Laura Mizoue, Wenge Zhong, Alison McCurdy, and Sarah Ngola. Jennifer Ma and Eric Co deserve credit for their contributions to the "Self-Assembly" project. Bill Schaefer and Richard Marsh solved the host **P** crystal structure. I thank Josef Michl for providing a program for doing INDO/S calculations as well as helpful comments on the results. Finally Bob Kumpf and Anthony West deserve credit for their patience in helping me with calculations.

Justin Gallivan, Jeff Clites, Sandro Mecozzi, Pat Kearney, and Heike Thompson all deserve credit for "happily" proofreading parts of this somewhat lengthy thesis. I could not have done it without their critical comments and insights. The five comma's in this paragraph are all for Jeff.

There are quite a few people that have made my life at Caltech somewhat easier, and I cannot leave them out of these acknowledgments. Most notable is Susanne Lin. Others include Tom Dunn and Guy Duremburg (both of whom have gone above and beyond the

call of duty to help me with various problems I've encountered–like printing e-mail messages on "unknown" laser writers), Mick Murray, Kraig Anderson (Kraig will not be mentioned anywhere else in these acknowledgments in order to avoid potential problems with his security clearance and/or lawsuits against him), Dave Shultz, Piotr Kaszynski, Voyle Coleman, Margaret Lindstrom, and members of various research groups that I've had the opportunity to work with. I suppose it would also be appropriate to thank the American tax payers for all the money that appeared in the form of a National Institutes of Health Bioorganic/Bioinorganic Training Grant, a National Research Service Award Training Grant, and financial support of the molecular recognition work from the Office of Naval Research.

There are few places that have as much to offer a motorcycle rider than Southern California (despite emission canisters, Harley's, and GSXR squids), my sanity would not have survived graduate school without the Angeles Crest Highway and the likes of the "Caltech Motorcycle Club" (Chris Claypool, Neil Farrow, Mike Slessor, Karl Terry, and anyone else that came riding with us), Bob and Shelly Stuart, Richard Yee, Joe, Neil with the Harley, Bob and Gary McDaniels, John Kincaid, Steve Pershing, Mike Karbacher, Fulton, Dennis and Tony and the breakfast crowd at Newcombs, the guys at Pro-Italia, Glen, Raul, Roy Ruben, Bobby and Mondo from Pasadena Suzuki, Terry and Marlene McGarry, Jim Green, Gerry, The CLASS School, The Fastrack School, Tab, the "clubhouse" guys, Cagiva Motor Corporation, Suzuki North America, Z-Custom Leathers, AGV Helmets, Alpine Star Boots, Bates Gloves, *Performance Bike*, the California Highway Patrol and the Los Angeles County Sheriff's Department, and of course Chris' buddy with the skin graft and pierced nipple and all the other Angeles Crest squids that made for some good stories.

Other extra curricular activities have included my (recent and so-far brief) career as a novice road racer at Willow Springs International Raceway. I cannot describe in words the fun and excitement of road racing (although no one believes me when I tell them it is

safer than motorcycle riding on the street). Chris Claypool (and to a lesser extent, the California Highway Patrol) deserves credit for giving me the incentive to obtain the racing license, Susanne Lin donated the "race bike", and the following members of the Willow Springs Motorcycle Club have significantly contributed to my enjoyment of the sport: Bill Fennessy, John Kagel, Andrea and John Hilton, Bob Light, Paul, Eric and Ray on the GS500's, Danny Farnsworth ("I'm the nicest guy you'll ever meet, unless you piss me off, so don't piss me off"; this guy even has a Caltech connection), Skip O'Brien, Dave Neal, and all the 500 novice regulars. The best advice I've had in the last five and a half years (well, the only suggestion that worked on the first try): Turn 8-sixth gear, wide open!

Going on the offensive with the "Lads" was never dull, the "core" (Mick Murray, Chris Kenyon, and Neil Farrow), 556, Pueblo Taco's and the Ranchero Truck, Anne at Denny's, Big Wednesday at Toes, Guy, Steve-O, The 35er, the Old Town Pub, Lucky B's, and all the "Rager" regulars will not be forgotten. "I am not responsible for the actions of Neil Farrow!"

My close friends Juneko Robinson, Cheryl Vincent, and Mickey Millman have provided great encouragement through my extended stay in school, as have various members of my family (most notably Ron Forman and Miriam Wechsler). I must also thank my mother and travel agent, Jane Levy, for making arrangements for a "detour" through the Czech Republic; another highlight of the five and a half years at Caltech. Finally, I am indebted to Heike Thompson for sharing her insights on life. Our conversations have helped to keep me sane during the writing of this manuscript and I hope our friendship will continue for many years to come.

Abstract

The application of circular dichroism (CD) spectroscopy to the study of molecular recognition phenomena in chiral water-soluble cyclophane hosts is described. The CD method produces results that complement and expand upon previous NMR studies. This includes allowing the measurement of larger binding constants by allowing studies to be carried out at lower concentrations.

Using the excitonic chirality method, these studies have provided a means of assigning the absolute stereochemistry of the ethenoanthracene building blocks used in preparation of the hosts. This information, along with an x-ray structure of one of the cyclophane molecules, has provided important information concerning host structure. The x-ray structure and CD spectral changes observed on guest binding have also served to provide direct experimental evidence for binding conformations of the hosts.

The chiral hosts have been shown to induce CD in achiral chromophoric guests. Analysis of this induced CD using INDO/S and coupled-oscillator calculations has provided valuable information concerning the conformations of the bound guest. These data complement information obtained in NMR studies (*D* values) and provide additional insights into the important factors that govern the binding event.

Finally, preliminary studies of self-assembling systems in aqueous media are reported. These studies employ etheno- and ethanoanthracene based structures designed to form aggregates with well defined order and discrete stoichiometries. These molecules are designed to aggregate through hydrophobic forces. The aggregate is kept from becoming a micelle using polar groups strategically placed to complement one another within the assembling structure.

Table of Contents

List of Figures

Chapter 3: Stereochemical Assignments and Molecular Conformations of Cyclophane Host Molecules.

Chapter 8: Miscellaneous Laboratory Projects.

List of Tables

Chapter 5: Larger Hosts and Higher Order Stoichiometries.

Chapter 6: Chiral Recognition of Inorganic Metal Complexes by Cyclophane Host Molecules.

Chapter 7: Progress Toward Self-Assembling Systems in Aqueous Media.

Chapter 1:
Non-Covalent Interactions in Aqueous Media.

Chapter 1

Non-Covalent Interactions in Aqueous Media.

1.1 Introduction

Non-covalent bonding interactions play an important role both as primary and as secondary stabilizing forces for a wide variety of inter- and intra-molecular processes across a range of fields of study. These forces include hydrogen bonding, Coulombic attractions,[1] van der Waals interactions,[1] π-π interactions,[1] cation-π interactions,[3] and the collection of phenomena termed hydrophobic interactions.[1,4] Table 1.1 lists the important non-covalent forces and provides representative examples of each.

Interaction	Distance Dependence	Example
Hydrogen bonding[1,2]	Only occurs at very short distances (typically ≤ sum of van der Waals radii of the heavy atoms involved)	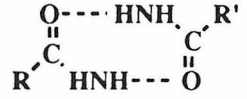
Electrostatic (Coulombic)[1]	1/r	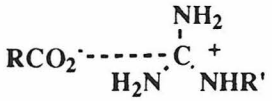
van der Waals forces[1]	$1/r^2$	*n*-Alkane crystals
π-π Interactions[1]	$1/r^6$	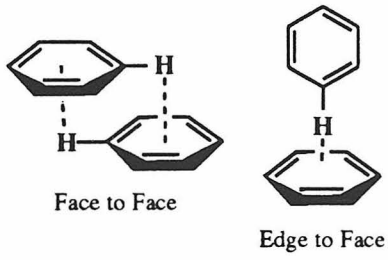 Face to Face Edge to Face
Cation-π interactions[3]	$1/r^n$ (n < 2)	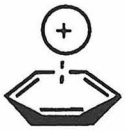
Hydrophobic forces[1,4]	$1/r^n$ (n < 2)	Surfactant aggregation in water

Table 1.1. Representative non-covalent interactions.

In biological systems, non-covalent forces provide secondary intramolecular stabilizing interactions that induce proteins to fold into stable tertiary structures as well as providing the primary stabilizing interactions that hold non-covalently bound subunits together in a well-defined manner (Figure 1.1).[5] The weak nature of these forces also make them ideally suited for holding small molecules in specific binding sites where they

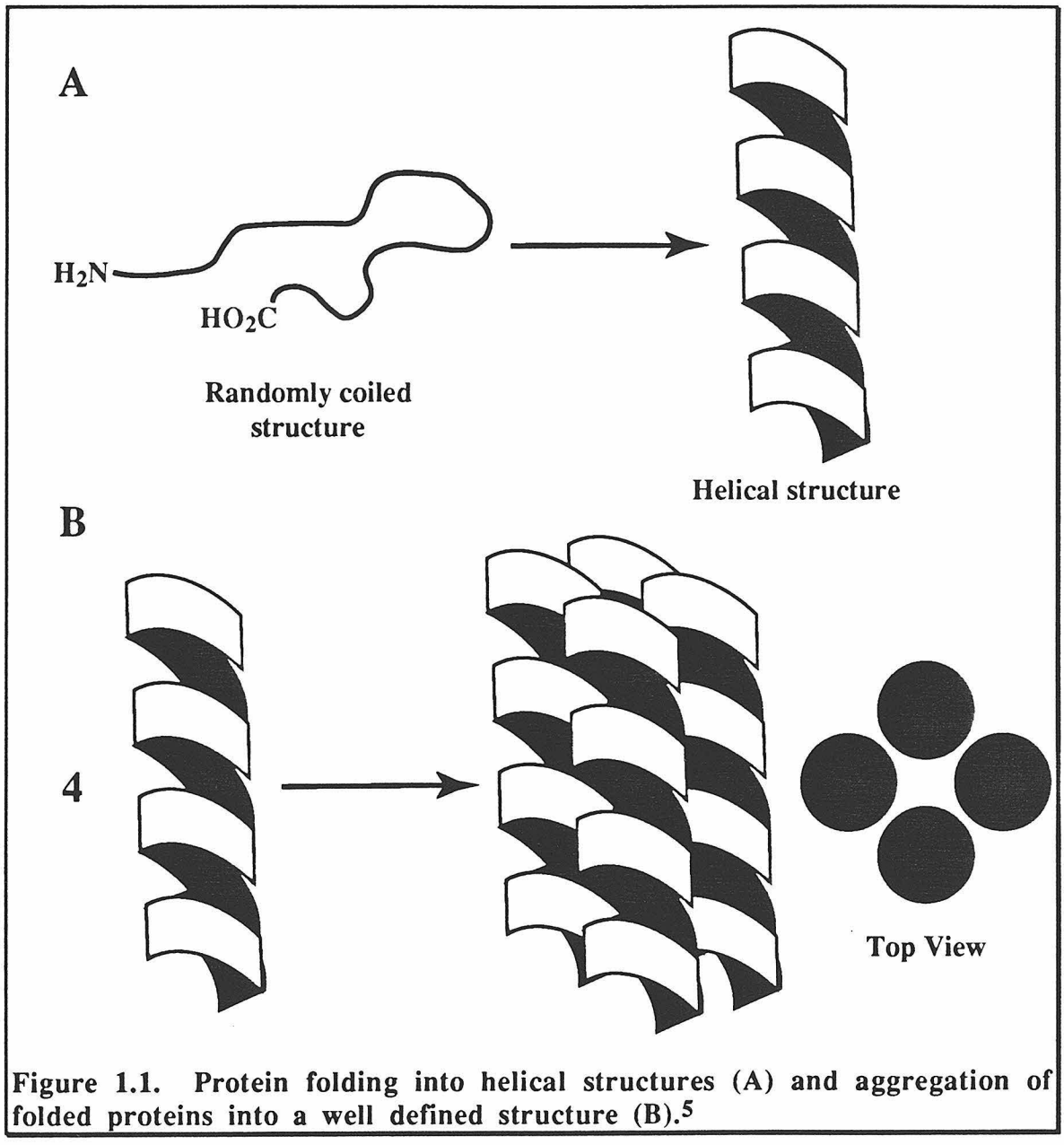

Figure 1.1. Protein folding into helical structures (A) and aggregation of folded proteins into a well defined structure (B).[5]

can regulate biological process.[6] Figure 1.2 shows a model for the binding site of the D_2-dopaminergic neuroreceptor.[7] It can be seen that the ligand (dopamine) is held in the binding site through a combination of hydrogen bonding, π-stacking, and electrostatic interactions.[7]

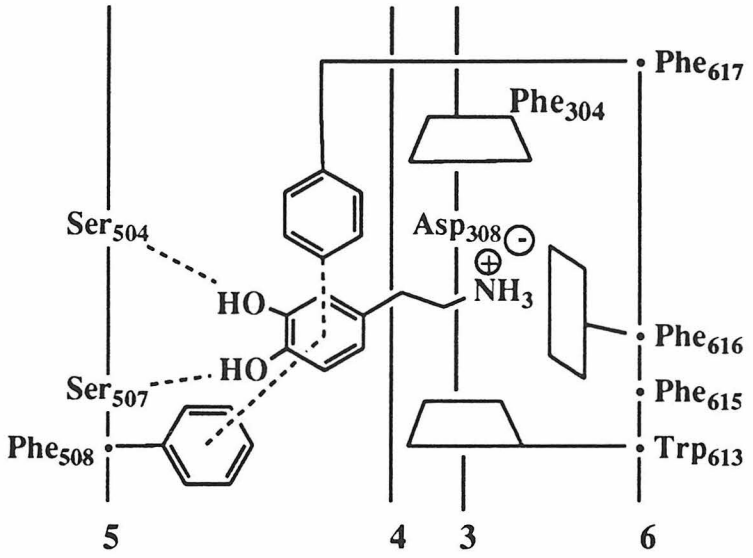

Figure 1.2. Proposed structure of the dopamine binding site in the D_2-dopaminergic neuroreceptor (the numbers refer to the receptor subunits).[7]

Biological systems provide some of the most elegant examples of the use of non-covalent interactions for carrying out specific functions, but the use of non-covalent interactions is not limited to the realm of biology. Langmuir-Blodgett films, for example, can be used to modify the surface properties of a material.[8] These films arise through non-covalent association of surfactant molecules with solid surfaces. Figure 1.3 illustrates the formation of a Langmuir-Blodgett film of the salt of arachidic acid.[6] A graphite slab is pulled through a monolayer of the salt on water (Figure 1.3A), the alkyl tails adhere to the graphite surface through weak van der Waals forces (Figure 1.3B).[9] Repeated dipping of the graphite results in multilayer formation (Figure 1.3C);[9] the layers add in such a way as to segregate their hydrophobic and hydrophilic regions (Figure 1.3D).

The important role played by non-covalent forces has lead to a great effort toward the design and study of synthetic systems that exploit non-covalent interactions to form supramolecular complexes. It is the purpose of this manuscript to report the results of a number of studies on such supramolecular systems carried out in the Dougherty group at the California Institute of Technology. The studies of molecular recognition and self-assembly described herein were inspired heavily by biological systems and as such were performed primarily in aqueous media.

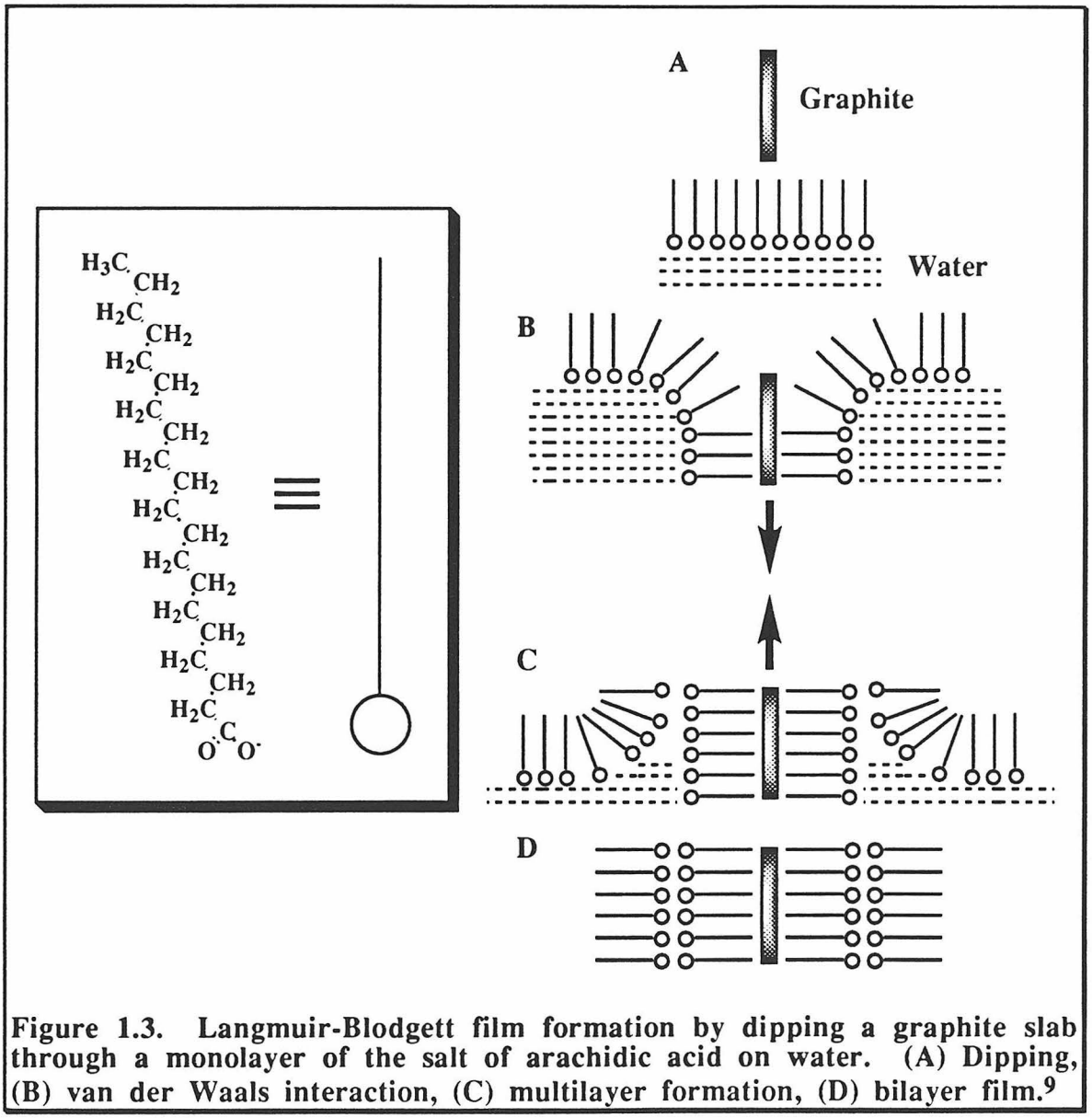

Figure 1.3. Langmuir-Blodgett film formation by dipping a graphite slab through a monolayer of the salt of arachidic acid on water. (A) Dipping, (B) van der Waals interaction, (C) multilayer formation, (D) bilayer film.[9]

1.2 Molecular Recognition

1.2.1 General

"Molecular recognition" encompasses a broad array of intermolecular interactions in a large variety of processes, and as such is not limited to the context of the work in this manuscript. For this reason we limit our definition of "molecular recognition" specifically to the encapsulation of smaller "guest" molecules by larger "host" molecules (Figure 1.4).[10]

The strength of the binding interactions observed with the various host-guest systems are highly dependent on the solvent medium.[16a,17] In non-polar organic solvents, for example, the hosts can take advantage of the strong interactions between hydrogen bond donors and acceptors or between oppositely charged functional groups.[17] Figure 1.4B illustrates a cyclophane (**1**) receptor that binds barbiturate guests (such as **2**) in chloroform. The guest is drawn out of the solvent environment and into the binding site, where it is stabilized by the formation of six hydrogen bonds.[11] Molecular recognition in aqueous media is more relevant to biological phenomena, and has spawned a wide variety of cyclophane-based host systems.[10chjq,12,16,18-32] In aqueous media, functional groups capable of forming hydrogen bonds or participating in electrostatic interactions are strongly solvated; this results in the attenuation (but not the complete absence[32]) of the interactions that these groups undergo.[17] On the other hand, hydrophobic forces become very strong in an aqueous environment, as illustrated in Figure 1.4C where a guest with large hydrophobic surface area (azulene, **3**) is drawn out of the aqueous environment into the cavity of a cyclophane receptor (**4**) that is less polar than the aqueous solvent.[12ad]

There exist a wide variety of synthetic host-guest systems that make use of non-covalent forces for the stabilization of the guest molecule in the host binding site (generally a molecular cavity). Figure 1.5 gives some representative examples of the various classes

of host molecules. Such hosts include crown ethers and cryptands,[13] calix[n]arenes,[14] cyclodextrins,[15] and a variety of cyclophane structures.[16] All of these structures contain a central cavity that serves as the binding site for the guest.

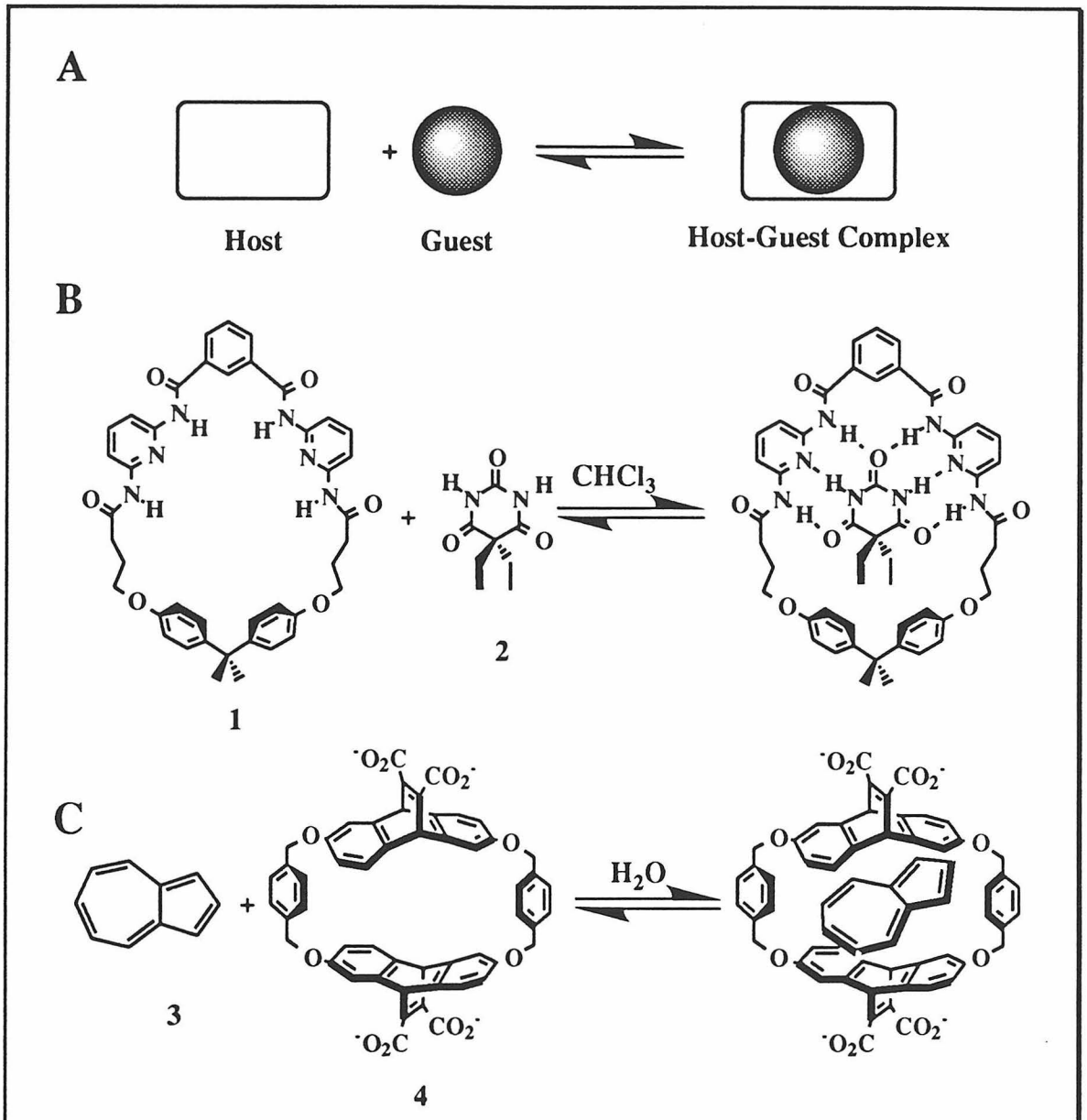

Figure 1.4. Host-Guest interactions (molecular recognition) as a general phenomenon (A), in organic media (B),[11] and in aqueous media (C).[12ad]

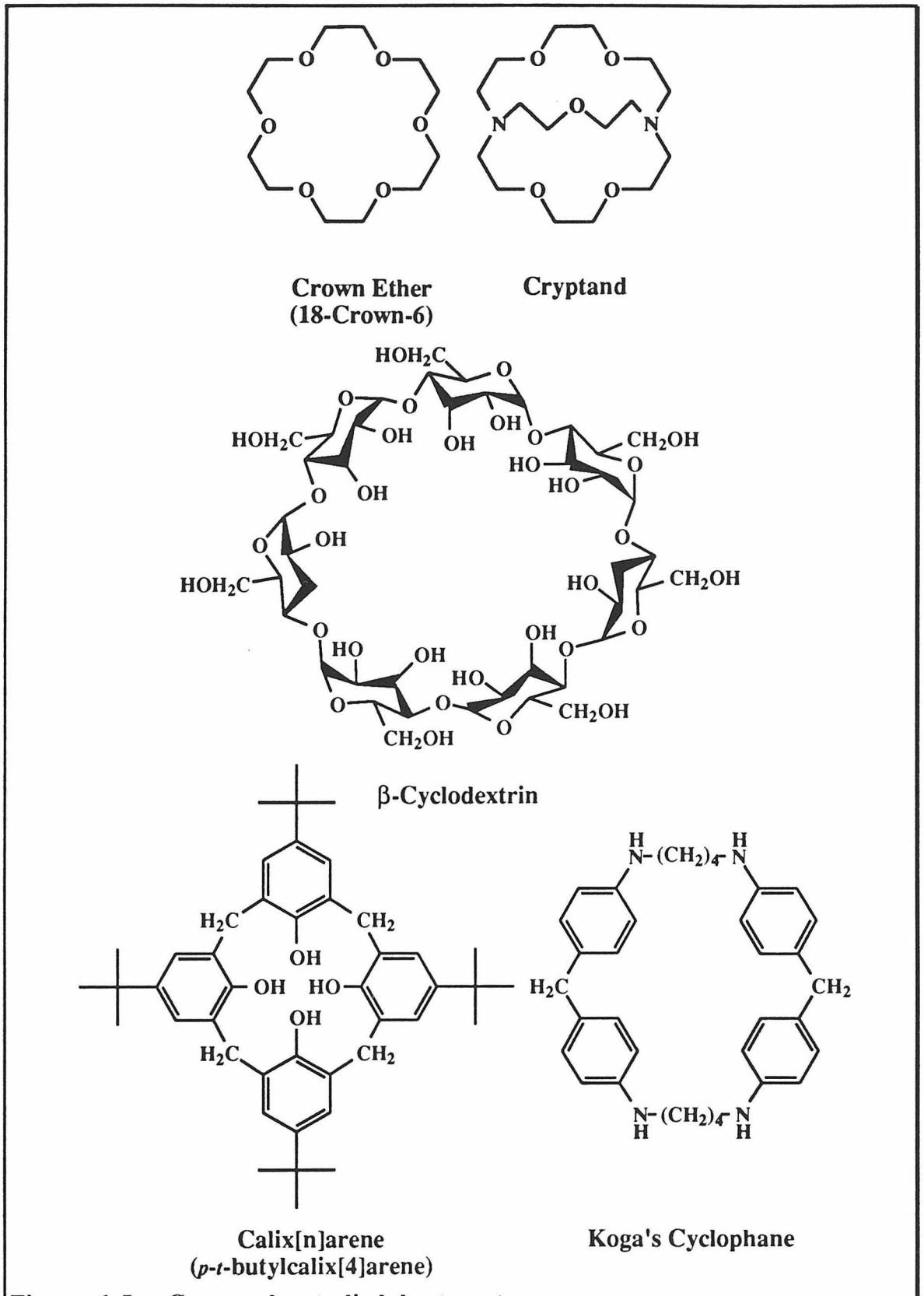

Figure 1.5. Commonly studied host systems.

1.2.2 Dougherty Group Studies

Molecular recognition studies in the Dougherty group have focused on the study of cyclophane receptors of the general structure shown in Figure 1.6 (this includes the receptor of Figure 1.4C).[12] These hosts are based around two ethenoanthracene units that serve to provide rigid, concave hydrophobic surfaces for formation of a cavity-like binding site.[12im] Two of these ethenoanthracene units are linked together through variable regions, hereafter referred to as linkers.[12im] Figure 1.6 illustrates a number of linkers that have been employed.[12,33] The ethenoanthracene units also serve to hold the solubilizing groups (R in Figure 1.6) external to the binding site, so that their influence on binding is minimized.[12im] The ethenoanthracene units are chiral, with C_2-symmetry, and give rise to a host structure with a maximum symmetry of D_2.[12im]

The synthesis of the ethenoanthracene unit is shown in Figure 1.7.[12im] Anthraflavic acid (**5**) is reduced with aluminum amalgam to provide 2,6-dihyroxyanthracene (**6**). After protection of the hydroxyl groups, the anthracene derivative (**7**) undergoes an asymmetric Diels-Alder reaction with (-)-dimenthyl fumarate (**8**) in the presence of an excess of diethylaluminum chloride. The Diels-Alder reaction provides the ethanoanthracene diastereomers **9a** and **9b** (*syn* and *anti* respectively); these diastereomers are separated so that they can be converted into enantiomerically pure product. The etheno bridge is incorporated by reaction of **9** with diphenyldiselenide in the presence of potassium *t*-butoxide; this reaction is immediately followed by deprotection of the phenols to give ethenoanthracenes **10a** and **10b**. Transesterification with methanol provides the enantiomerically pure ethenoanthracenes **11a** and **11b**. The ethenoanthracene units are macrocyclized with the appropriate linker precursor (a dibromide or ditosylate) under high-dilution conditions in DMF with cesium carbonate as base to provide the tetramethyl ester **12** (Figure 1.8).[12im] Hydrolysis of the esters provides the water-soluble receptor **13**.

The major isolable byproducts of the macrocyclization are the trimer (**14**) and tetramer (**15**) oligomers of the host structures (Figure 1.9).[12i]

Chapters 2-6 and 8 of this manuscript report studies of primarily two hosts from Figure 1.6, hosts **P** and **C** (Figure 1.10). The names of these hosts are derived from the linkers, **P** for *para*-xylyl and **C** for *trans*-1,4-cyclohexyl. Like all of the hosts shown in Figure 1.6, these two hosts are general receptors for a variety of neutral and cationic organic guests in an aqueous environment.[12]

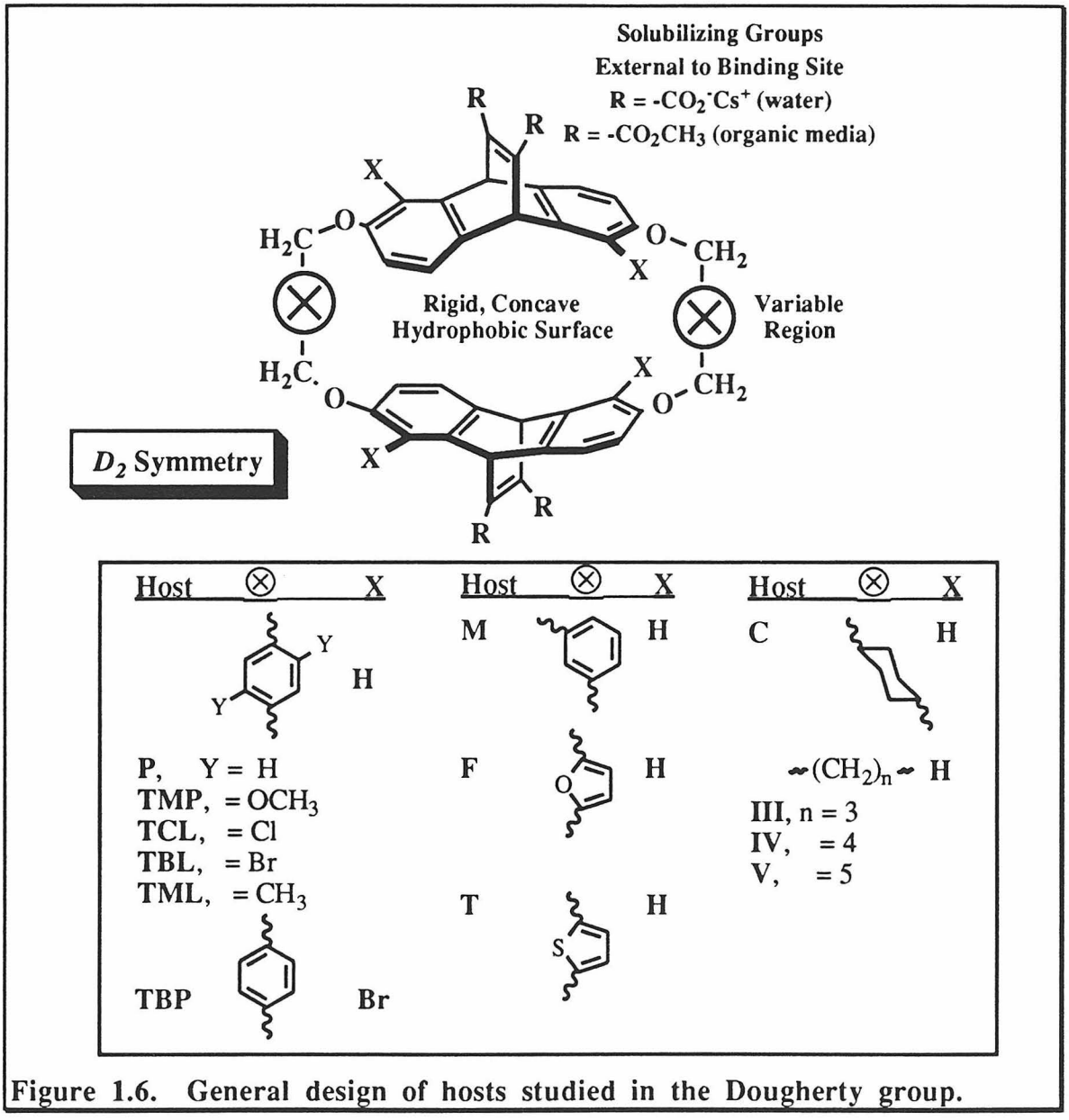

Figure 1.6. General design of hosts studied in the Dougherty group.

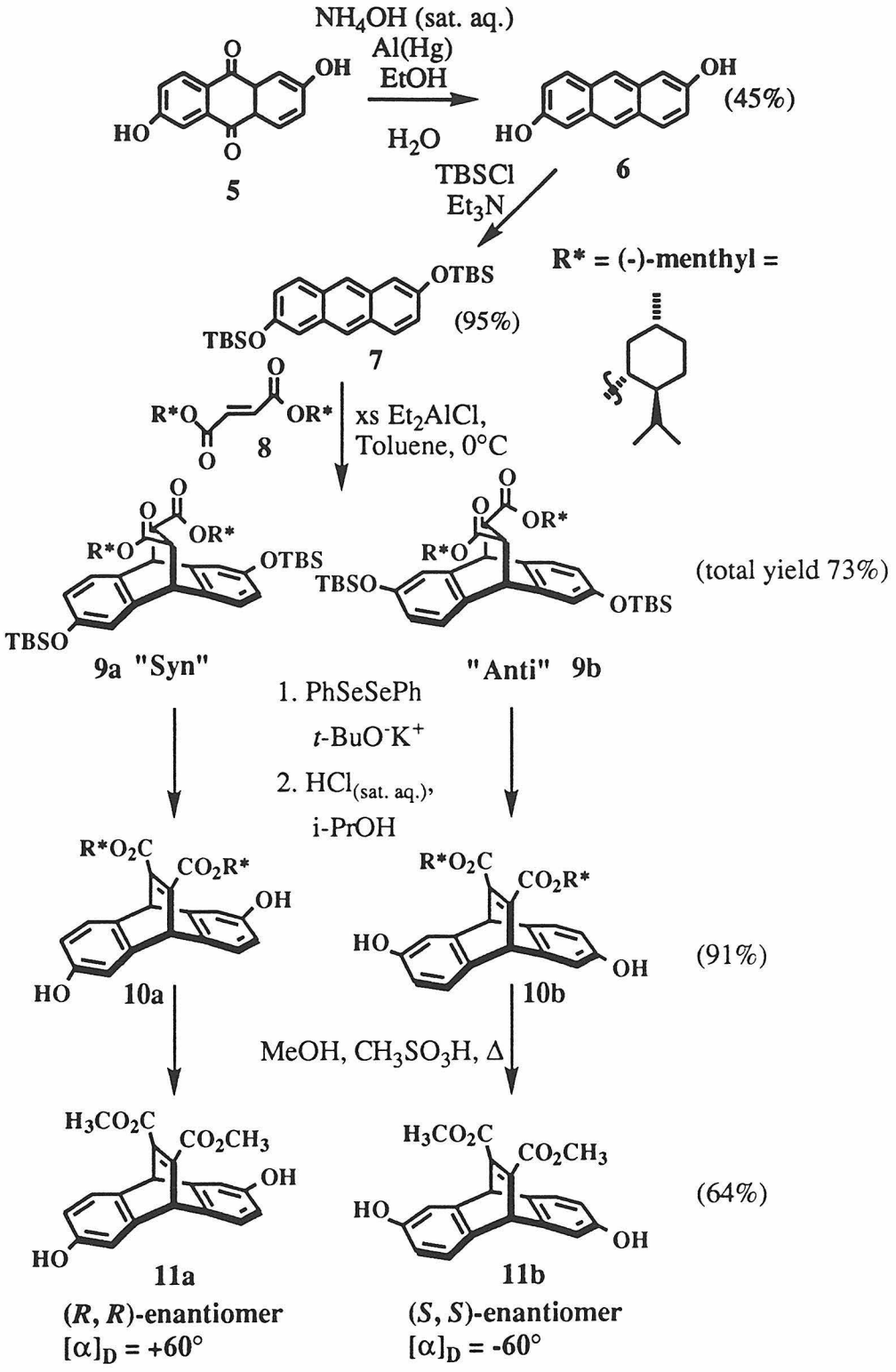

Figure 1.7. Synthesis of enantiomerically pure ethenoanthracene units.[12im]

Table 1.2 lists binding constants for representative guest molecules. These guests include electron-deficient neutral molecules (**16**, **17**), iminium ions (**18**, **19**), quaternary ammonium ions (**20**), sulfonium ions (**21**), guanidinium ions (**22**), and the neuroreceptor acetylcholine (**23**).[12h] Some general trends can be observed from the data in Table 1.2: for neutral guests (such as isoquinoline, **16**) the binding constants observed for both hosts are the same, while charged guests (**18**-**21**) generally show greater affinity for host **P** than for host **C**.[12i] Another interesting observation is that with guests of the same size and shape (**17** and **19**), a charged guest (**19**) always shows higher binding affinity than an uncharged one (**17**).[12i]

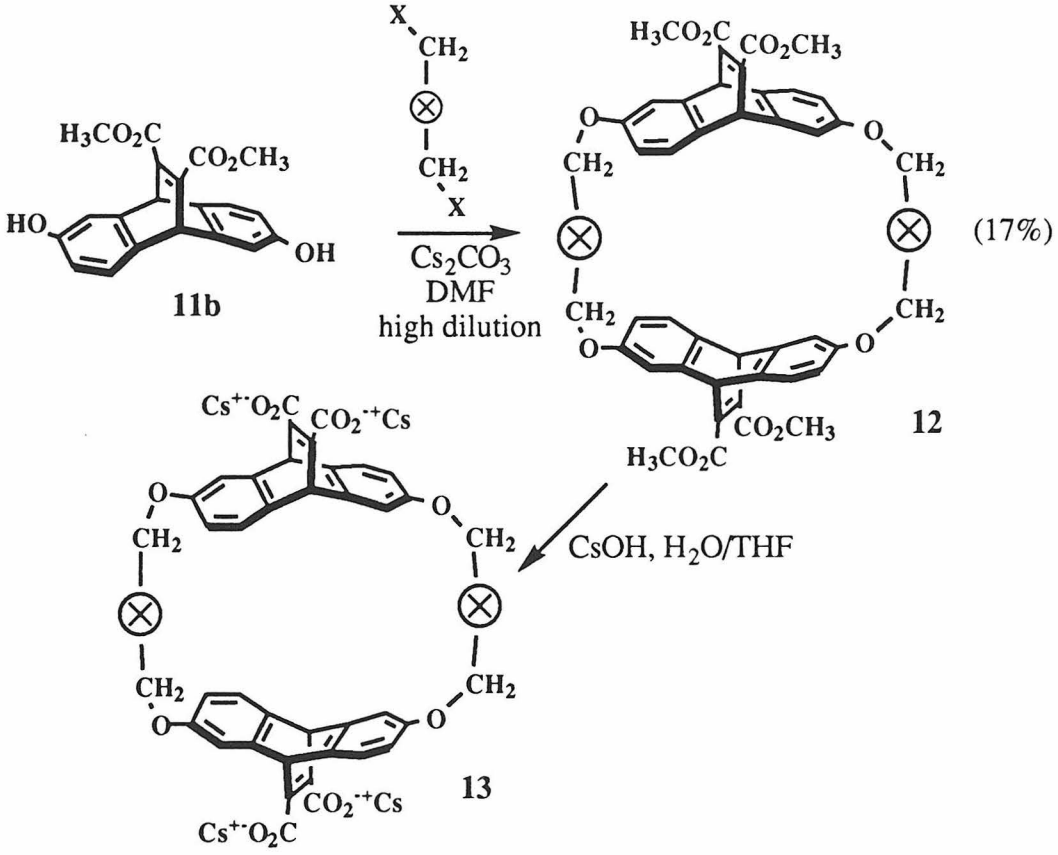

Figure 1.8. Macrocyclization to prepare host molecules.[12im]

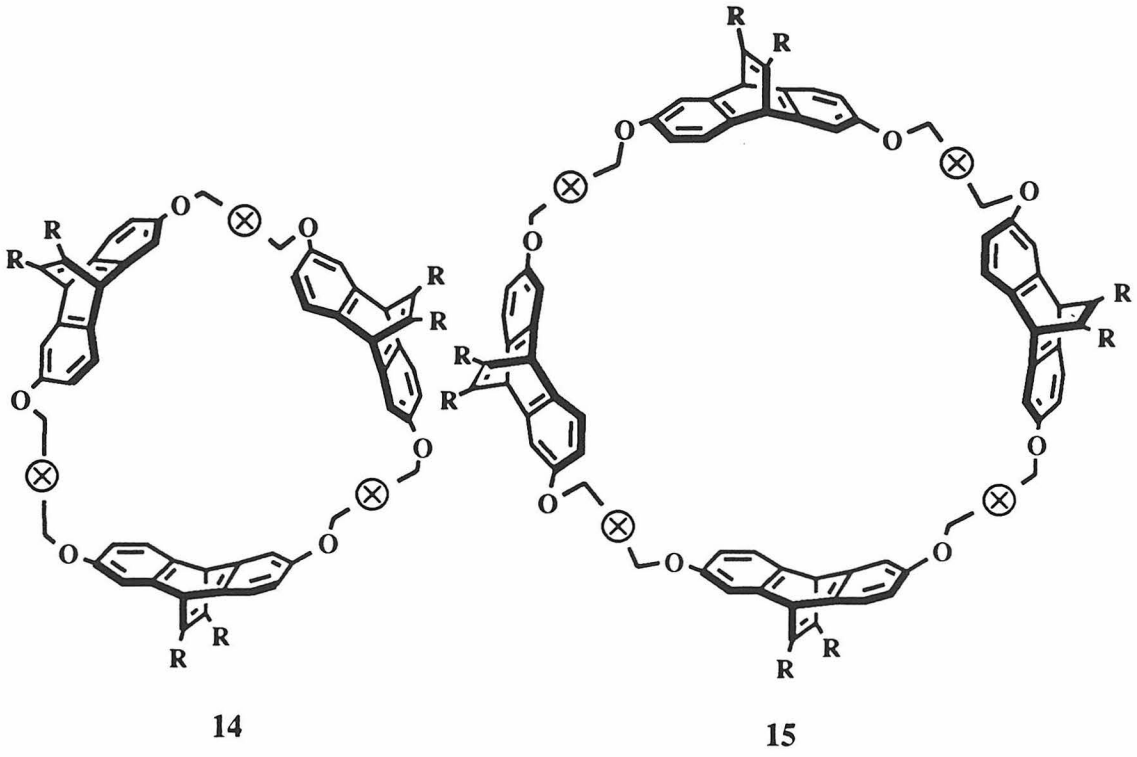

14 15

Figure 1.9. Higher oligomers of host molecules.[12i]

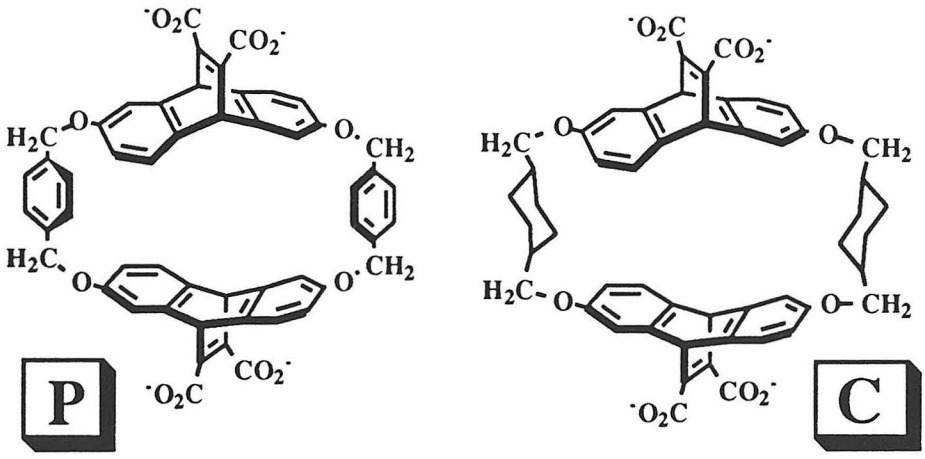

Figure 1.10. Hosts P and C.[12i]

Guest	$-\Delta G°_a$ (kcal/mol) [P]	$-\Delta G°_a$ (kcal/mol) [C]
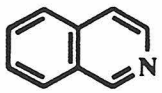 16	6.3	6.3
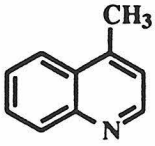 17	5.9	6.0
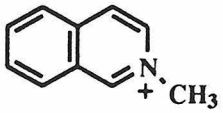 18	7.3	6.0
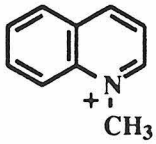 19	8.4	6.3
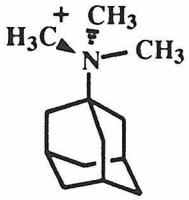 20	6.7	5.6
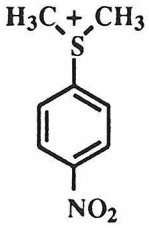 21	5.7	4.5
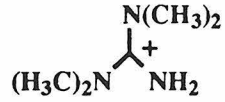 22	4.7	N/A
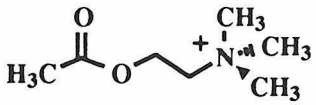 23	6.2	N/A

Table 1.2. Representative guests and their binding constants with hosts P and C in aqueous borate buffer (pH 9). Values are accurate to ± 0.2 kcal.[12adi]

The host and guest interact through a number of non-covalent interactions. These include hydrophobic attractions between the organic guest and host cavity, weak electrostatic forces from the remote carboxylate solubilizing groups and cationic guests, and a strong cation-π effect[3b,12dhi] which is evident in the binding preference for charged guests by host **P** (a cavity with a greater number of aromatic rings than host **C**). The observation of a cation-π effect in the binding behavior of the hosts is of primary interest in the study of such systems.

1.2.3 The Cation-π Effect in Molecular Recognition

The cation-π effect (Figure 1.11) can qualitatively be thought of as the interaction between a positive charge and the negatively charged face of a benzene ring, or more specifically with the benzene quadrupole moment.[3b] The quadrupole moment of benzene is depicted in Figure 1.11. As shown in the Figure, the faces of the ring represent regions of negative charge, while the periphery of the ring represents a region of positive charge.[3b] Qualitatively, the magnitude of a cation-π effect is dominated by the cation-quadrupole interaction. Quantitatively, however, contributions from induced dipoles, polarizability, dispersion forces, and charge transfer cannot be ignored.[3b] This binding force is thought to be important in a number of biological binding sites,[3b,34] including those for the neurotransmitter acetylcholine (**23**)[3b,12h] and has been invoked to explain cation selectivity in a number of biological cation channels.[3b,34] Cation-π interactions are also known to be important in the gas-phase[3b,35] and have been observed with a number of other synthetic host systems in aqueous media.[12,23d,25o,27b,29a,36]

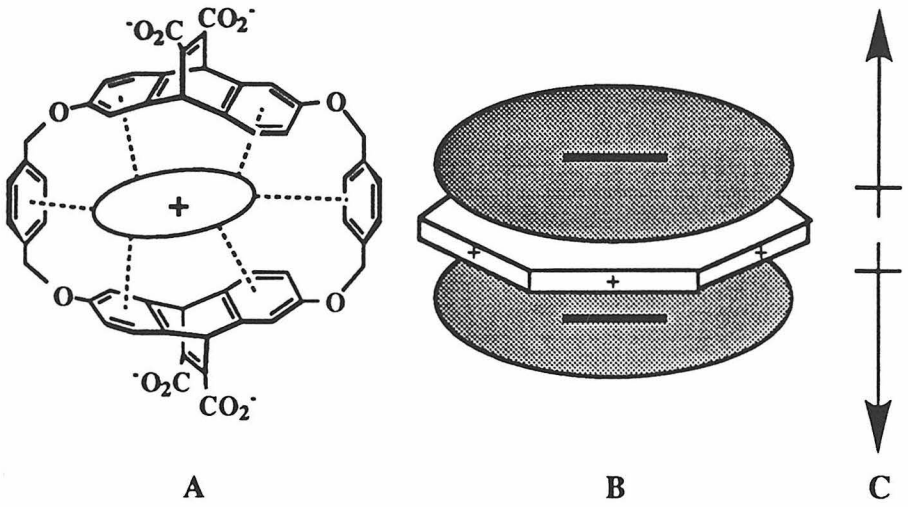

Figure 1.11. The cation-π effect idealized for host P (A), quadrupole moment of benzene (B); quadrupole moments can be thought of as being derived from two dipole moments arranged in such a way as to create no net dipole (C).[3]

1.3 Self-Assembly

1.3.1 General

Self-assembly is a type of molecular recognition, in which a number of smaller molecules combine in a specific manner to produce a supramolecular array of well defined structure.[17,37] Like molecular recognition, the term "self-assembly" has broad usage throughout the literature and self-assembly processes can be divided into a number of classes; Table 1.3 provides descriptions and representative examples of these classes.[17,37c] The studies described in this manuscript (Chapter 7) fall into the class of *Strict* (or *Equilibrium*) *Self-Assembly* (Table 1.3, Class 1).[17,37c] In these processes the formation of the assembly is a reversible equilibrium process, and requires that the assembly itself represent a thermodynamic minimum.[17,37] The same combination of non-covalent forces

that allows for the formation of host-guest complexes are used in self-assembly processes; however, the self-assembled structures tend to be far more ordered than loosely associated host-guest complexes (the structure is more precise than simply encapsulating a guest in a cavity). The formation of ordered assemblies is highly entropically unfavorable; consequently, most of the reported structures self-assemble through enthalpically favorable processes.[17,37]

Class	Self-Assembly	Definition	Example(s)
1	Strict (or Equilibrium) Self-Assembly	The product forms spontaneously (and reversibly) upon combining the component parts under proper conditions.	Tobacco Mosaic Virus,[38] metal chelates.[37c]
2	Irreversible (or Kinetic) Self-Assembly	A self-assembly process that involves irreversible bond forming reactions.	Cascade reactions,[37c,39] formation of self-assembled monolayers.[40]
3	Precursor Modification Followed by Self-Assembly	One or more of the component parts must be modified before self-assembly can occur.	GTP binding to tubulin before polymerization into microtubules occurs.[41]
4	Self-Assembly with Post-Modification	The initial assembly requires modification (usually by an external agent) before it can attain functional competence.	Self-splicing and self-cleaving RNA's,[42] template assisted formation of catenanes.[43]
5	Assisted Self-Assembly	An external agent that is not part of the final assembly is required to accompany the assembly process.	"Molecular chaperone" proteins mediate many protein assembly processes.[44]
6	Directed Self-Assembly	A temporary "template" participates as a structural element in the assembly process, but does not appear in the final assembled product.	Template assisted self-replication.[45-47]
7	Self-Assembly with Intermittent Processing	Combinations of classes **1-6**, this allows for sequential alterations of self-assembly and irreversible modifications to provide a highly-controlled process.	Ribosome biogenesis,[48] bacteriophage assembly.[49]

Table 1.3. Definitions of self-assembly.[35c]

The most elegant examples of self-assembly come from biological systems.[17,37] The Tobacco Mosaic Virus (TMV), for example, forms from the self-assembly of 2130 protein subunits and a single strand of viral RNA into a spiral cylinder of protein which surrounds the RNA (Figure 1.12).[38] This assembly occurs spontaneously at physiological pH both *in vivo* and *in vitro*; at low pH the protein subunits will assemble into the spiral

cylinder without the presence of the RNA (Figure 1.12).[38] The formation of TMV represents a process which is both spontaneous and cooperative.[17,37,38] Biological molecules are very large and can create microenvironments that are less polar than the aqueous solvent medium. This allows strong non-covalent interactions (hydrogen bonding) to occur without attenuation from solvent, thus providing a strong enthalpic contribution to the formation of the structure.[17,37]

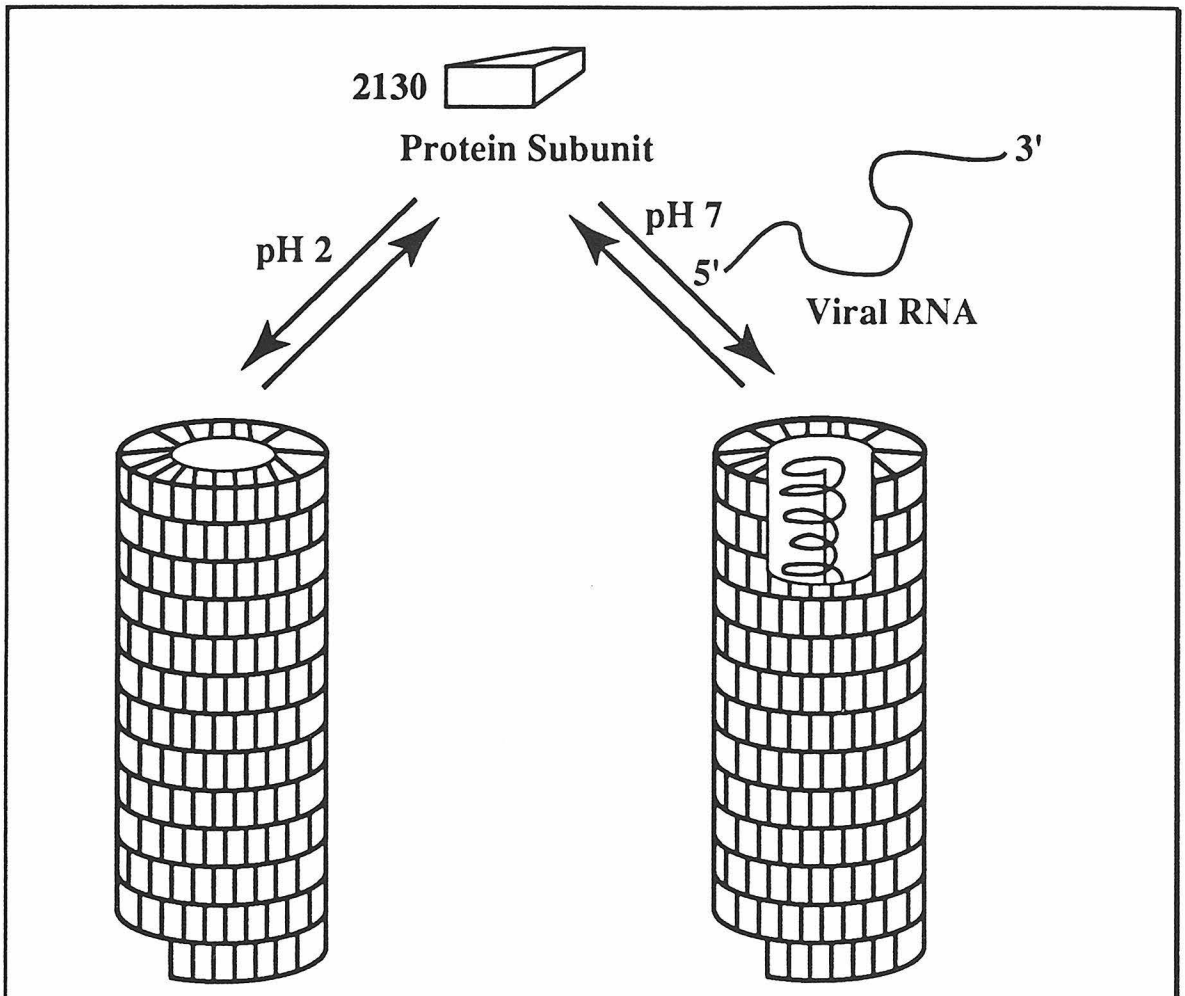

Figure 1.12. Self-assembly of the Tobacco Mosaic Virus at low and physiological pH.[38]

Given the requirements for enthalpic control of the assembly process, the majority of reported strictly non-covalent synthetic systems have relied on hydrogen bonding in

non-polar solvents (Figure 1.13).[17,37,50,51] A number of systems have been reported which assemble into highly ordered structures in solution,[17,36,50,51-56] in the solid state (from non-polar solutions),[51,57-60] and in liquid-crystalline phases.[61] Hydrogen bonding has also been used to self-assemble solution-phase structures with cavities capable of encapsulating guest molecules.[53ab,55,57c] The choice of structure is critical for the assembly of component units into highly organized structures with discrete stoichiometry (Figure 1.13) instead of into infinite arrays (Figure 1.14).[17,37] Figures 1.13 and 1.14 illustrate how the size of a substituent (*t*-butyl vs methyl vs ethyl ester) determines if a small aggregate (**26**) or a specific type of solid array is formed (**27** or **28**).[17a,51,52aef,57b]

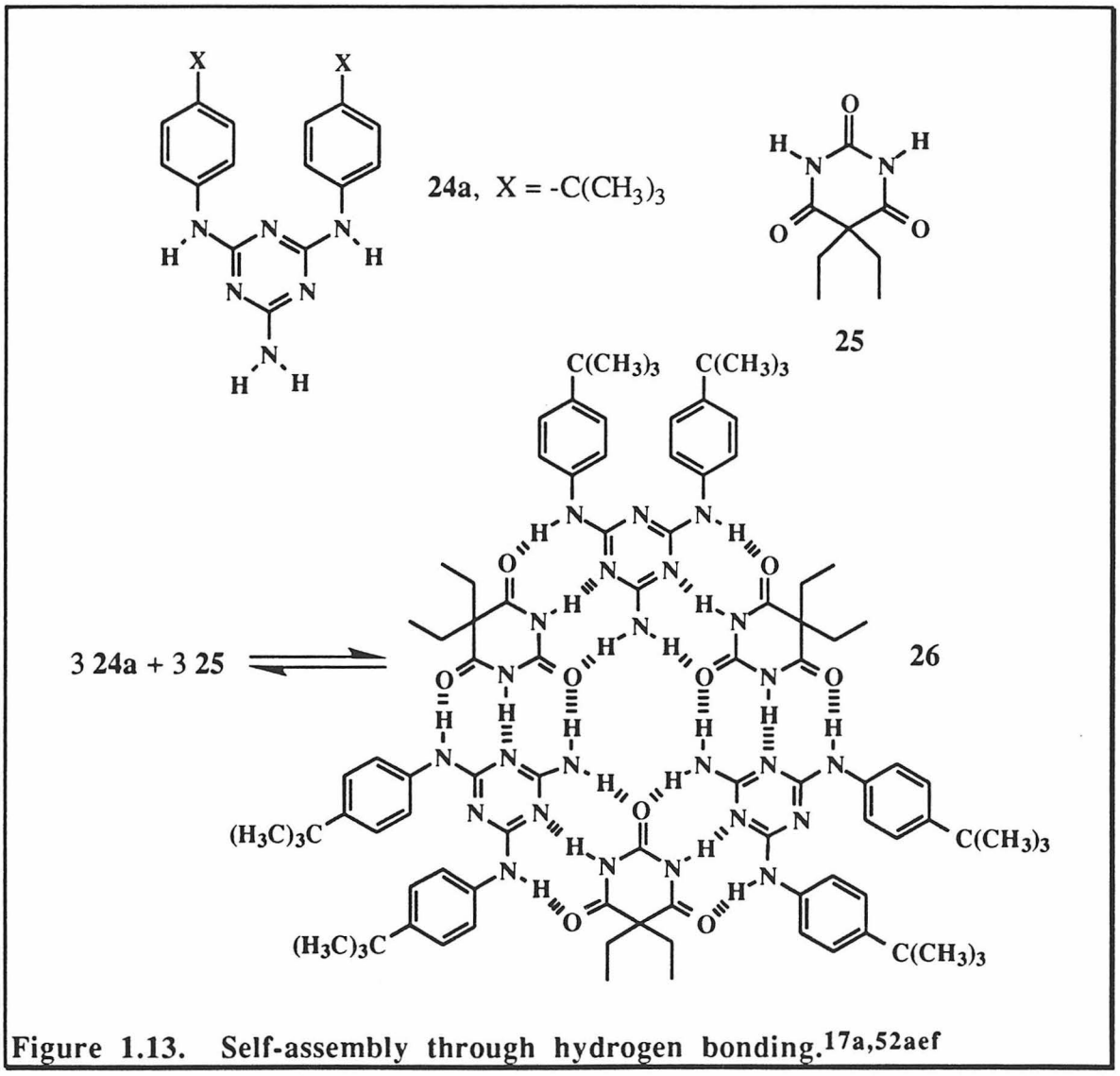

Figure 1.13. Self-assembly through hydrogen bonding.[17a,52aef]

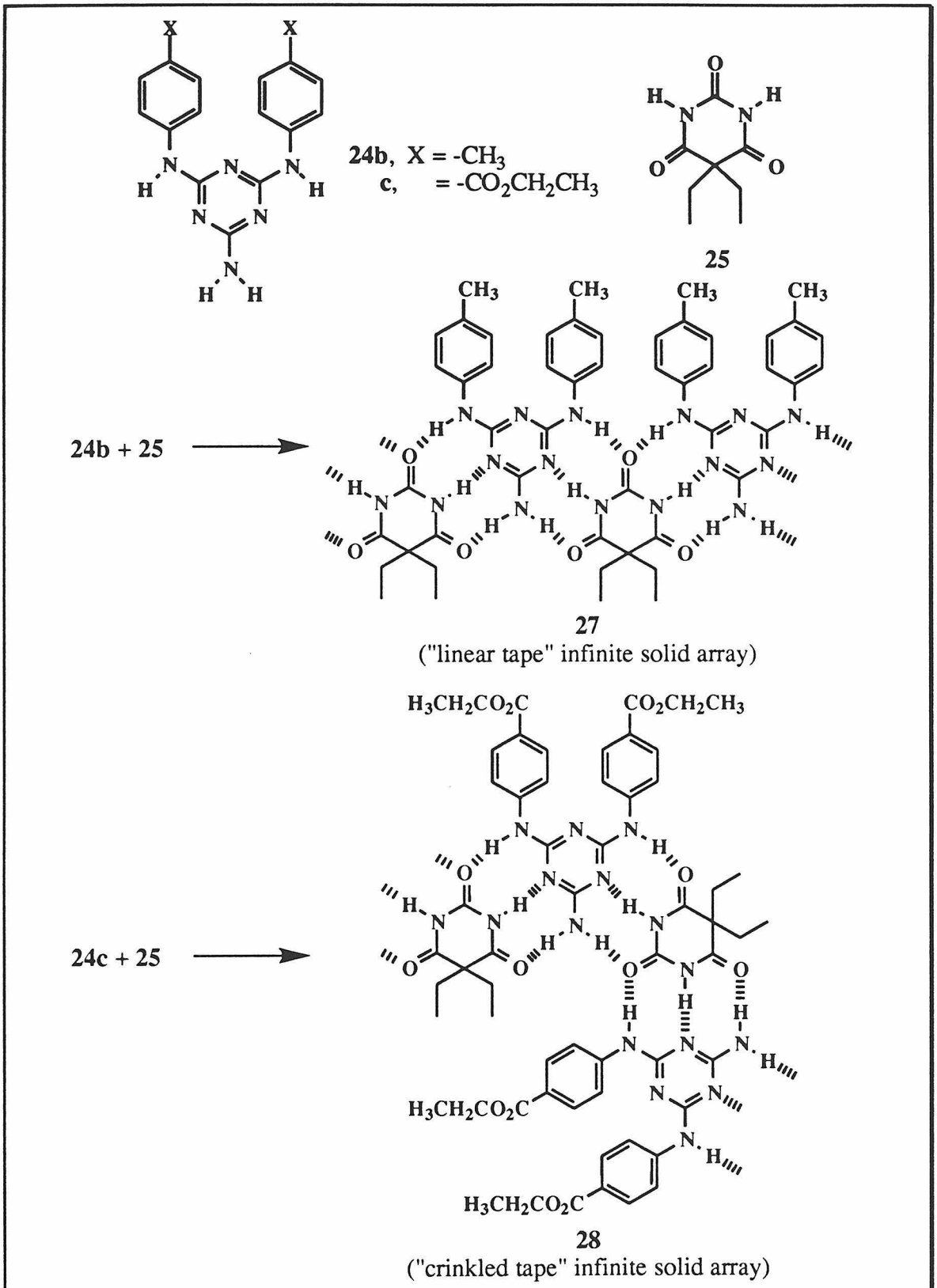

Figure 1.14. Self-assembly through hydrogen bonding to give infinite solid arrays.[17a,57b]

Other non-covalent forces have seen less application in solution-phase synthetic self-assembling systems (but have been successfully used to create specific solid state structures;[62] the use of π-π interactions has even been employed[63]). While representing one type of covalent interaction, coordinate covalent bonding (dative bonding) is weak enough to be reversible and has attracted a large amount of attention for formation of self-assembling structures (Figures 1.15-1.17).[17,37] Such structures include double and triple helix "helicates" derived from tetrahedral and octahedral metal centers respectively (Figure 1.15),[63-68] square arrays (Figure 1.16),[69] and capped structures (Figure 1.17).[70] Metal coordination has also been used to create infinite arrays,[71] to form structures containing internal cavities for guest binding,[72] and to organize arrays of peptides.[73] These metal complexes form through spontaneous and cooperative processes and as such represent ex-

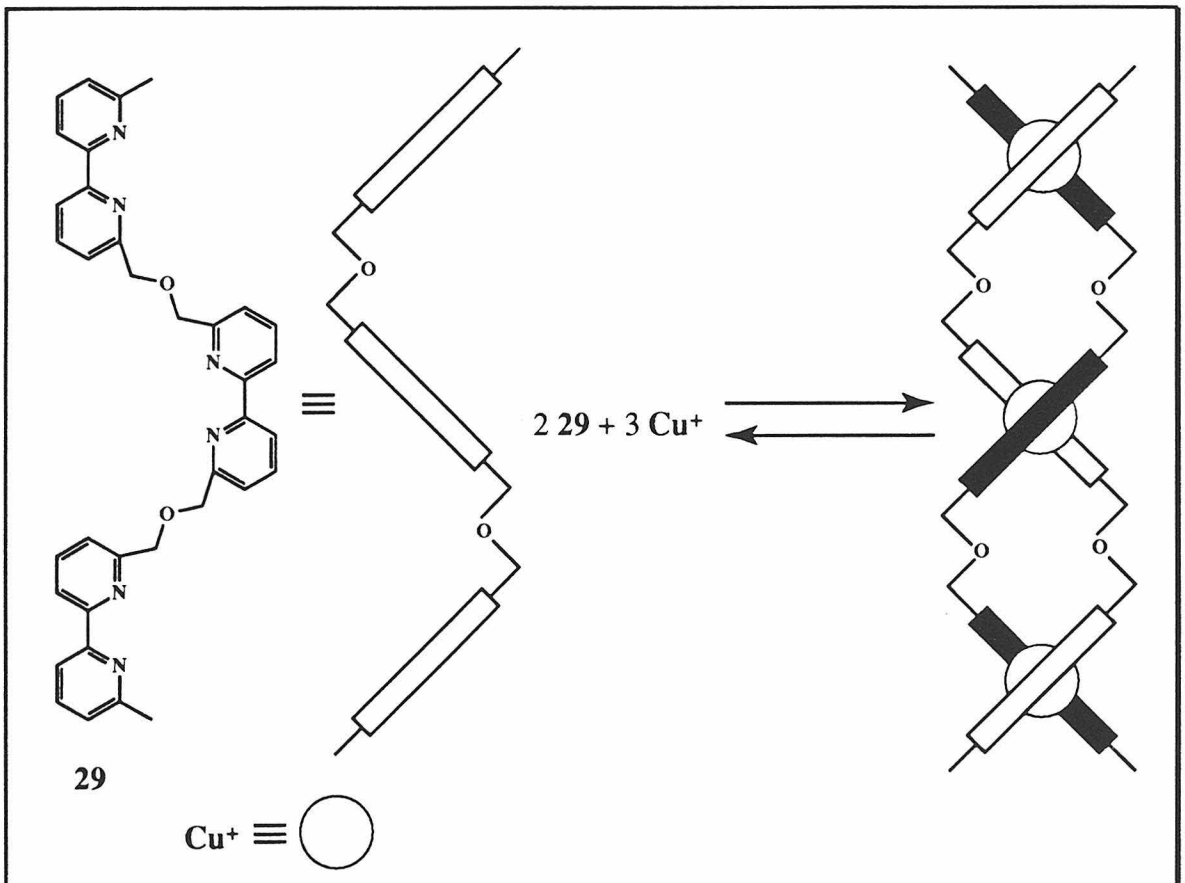

Figure 1.15. Self-assembly through coordinate covalent bonding: formation of a double helicate structure.[64]

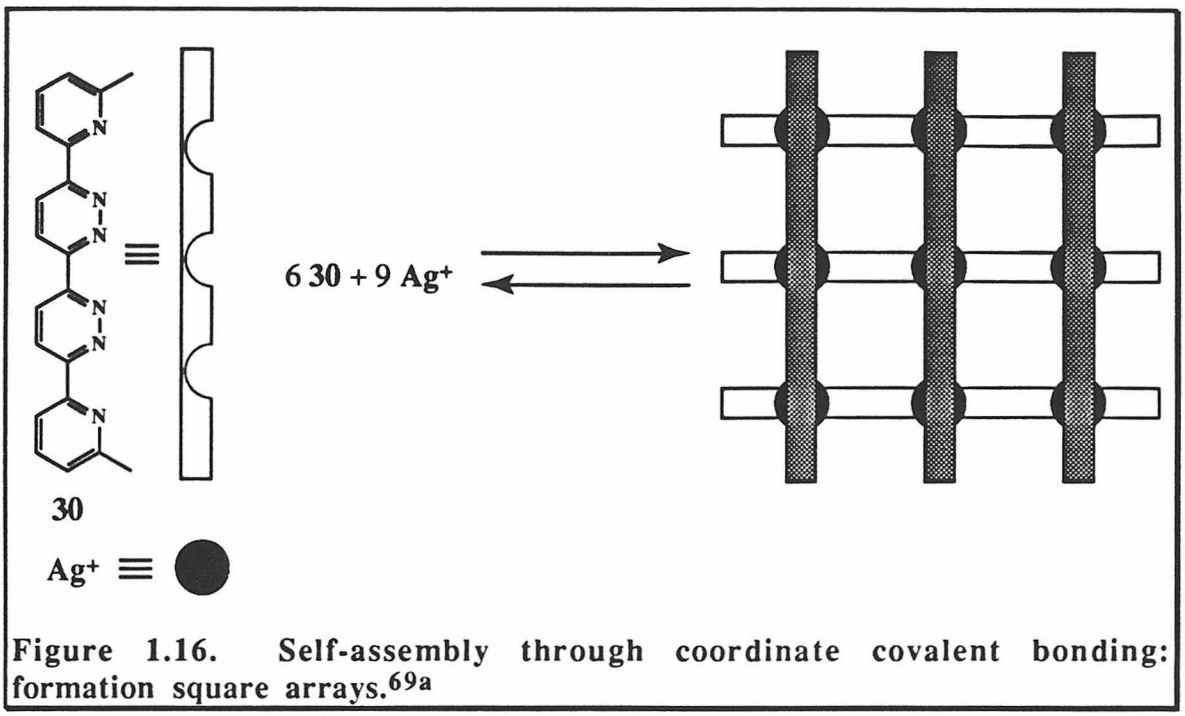

Figure 1.16. Self-assembly through coordinate covalent bonding: formation square arrays.[69a]

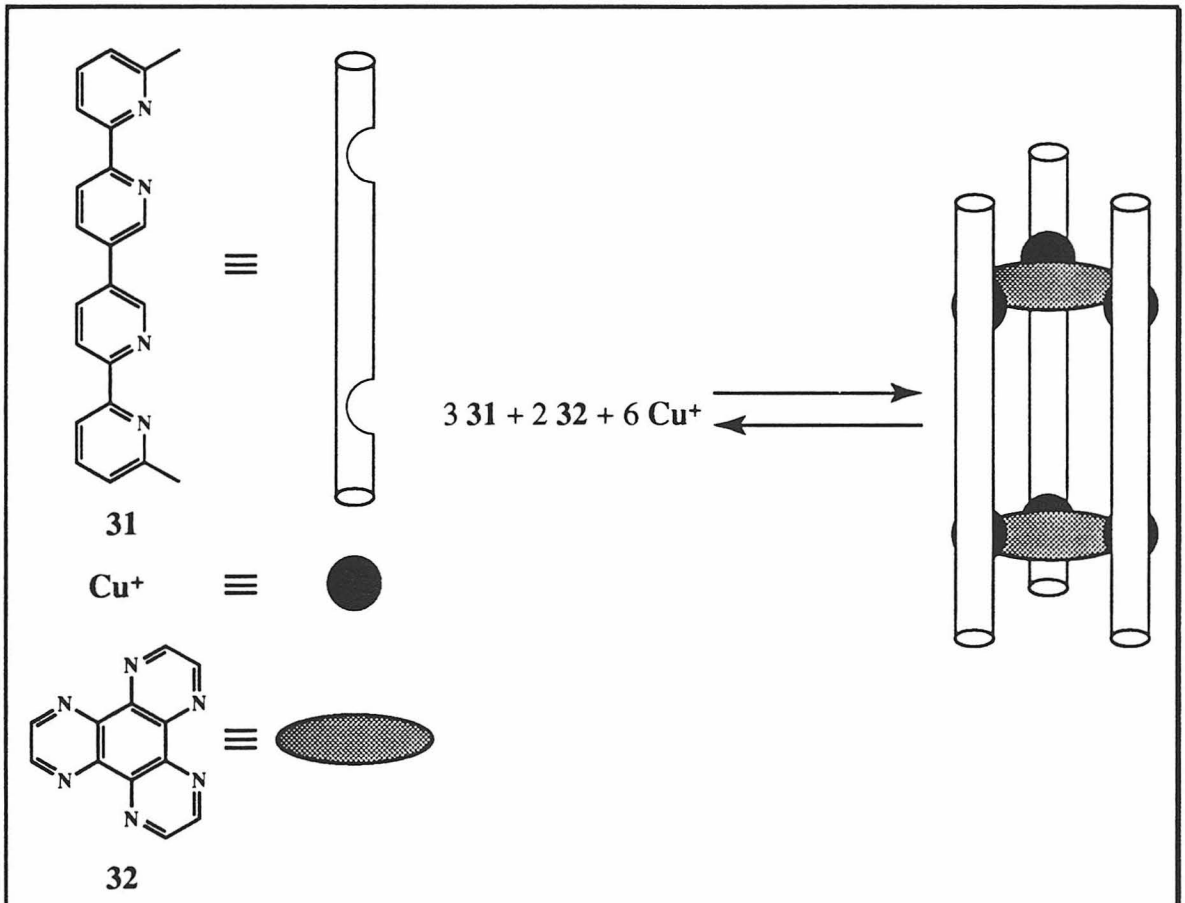

Figure 1.17. Self-assembly through coordinate covalent bonding: formation of capped structures.[70a]

amples of *strict self-assembly* (Table 1.3).[17,37] Metal coordination represents an attractive alternative to hydrogen bonding because it can occur in aqueous solvents, although its relevance to biological self-assembly is not clear.

Synthetic systems that self-assemble through strictly non-covalent interactions in aqueous media are more difficult to design, but are more interesting to study given their biological relevance. Assembly of small molecules from aqueous media into highly organized structures is possible, but the majority of reported systems fall out of solution as extended structures in gel or solid phases.[17a,74-77] Figure 1.18 illustrates such a self-assembly process. In the presence of potassium or ammonium ions, guanosine monophosphate (**33**, as well as molecules of similar structures) will form tetrameric arrays templated about the cation; the "G-quartets" then stack upon one another to give liquid-crystalline like "gel" phases.[17,75] These G-quartets also have biological significance, as they can form from guanosine-containing polynucleotides.[78]

Small molecules can be induced to aggregate from aqueous solution into organized structures,[74] although formation of such aggregates tends to be entropically driven (classical hydrophobic effect)[4b] and these structures are much more loosely organized than the previously described self-assembled structures. One of the most common of such aggregates is the micelle.[4b,79] These roughly spherical aggregates assemble through the aggregation of surfactant molecules above a certain critical aggregation concentration (CAC) in water (Figure 1.19). The micelle structure is such that the aggregate compartmentalizes its hydrophobic region (the alkyl tails of the surfactant molecules) to the interior of a sphere whose surface is made up of the hydrophilic head groups of the surfactant components (Figure 1.19).[4b,79] This compartmentalization of hydrophobic and hydrophilic regions is a common motif in biological systems.[5]

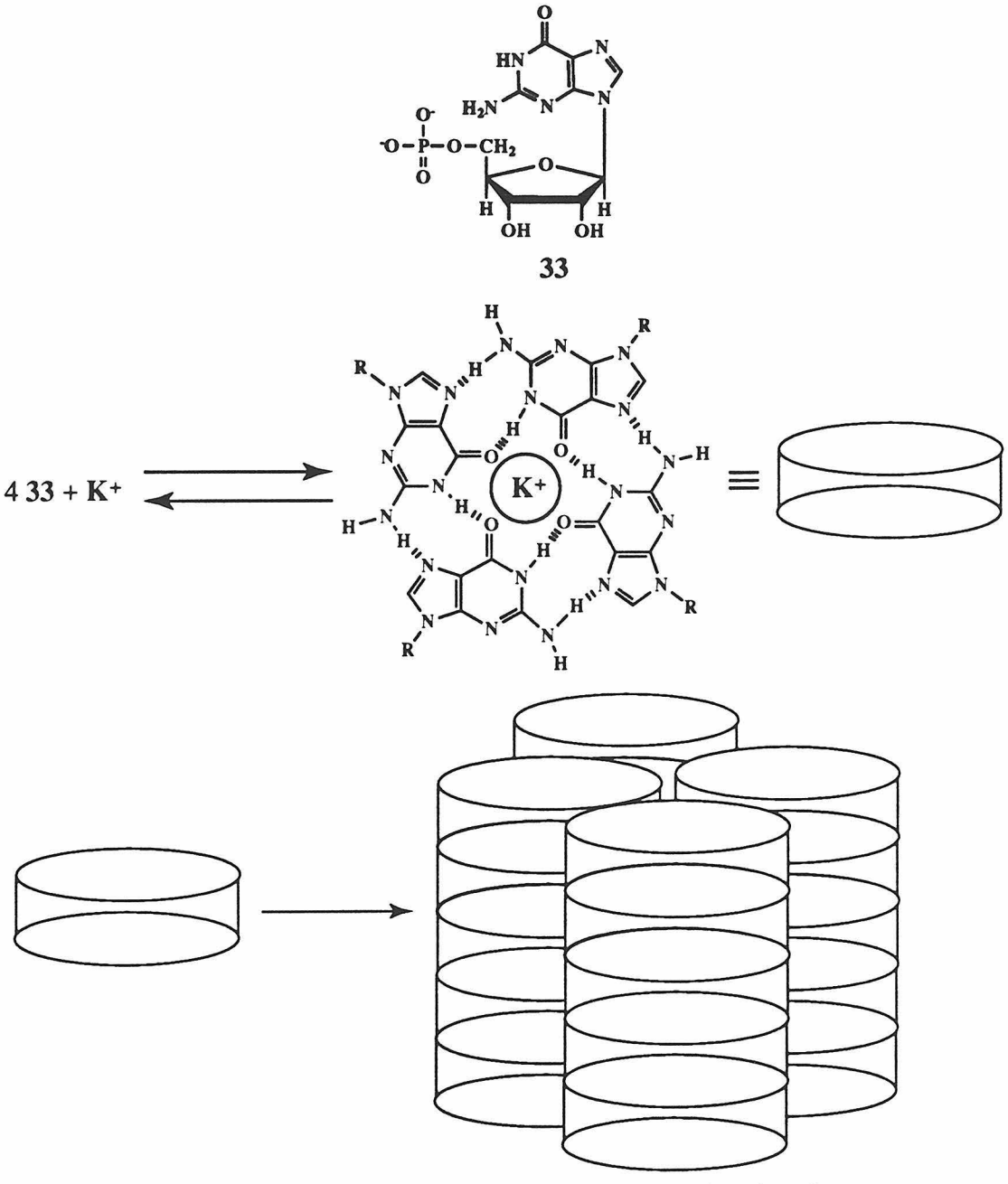

Figure 1.18. The formation of ordered phases out of an aqueous environment.[17a,75cd]

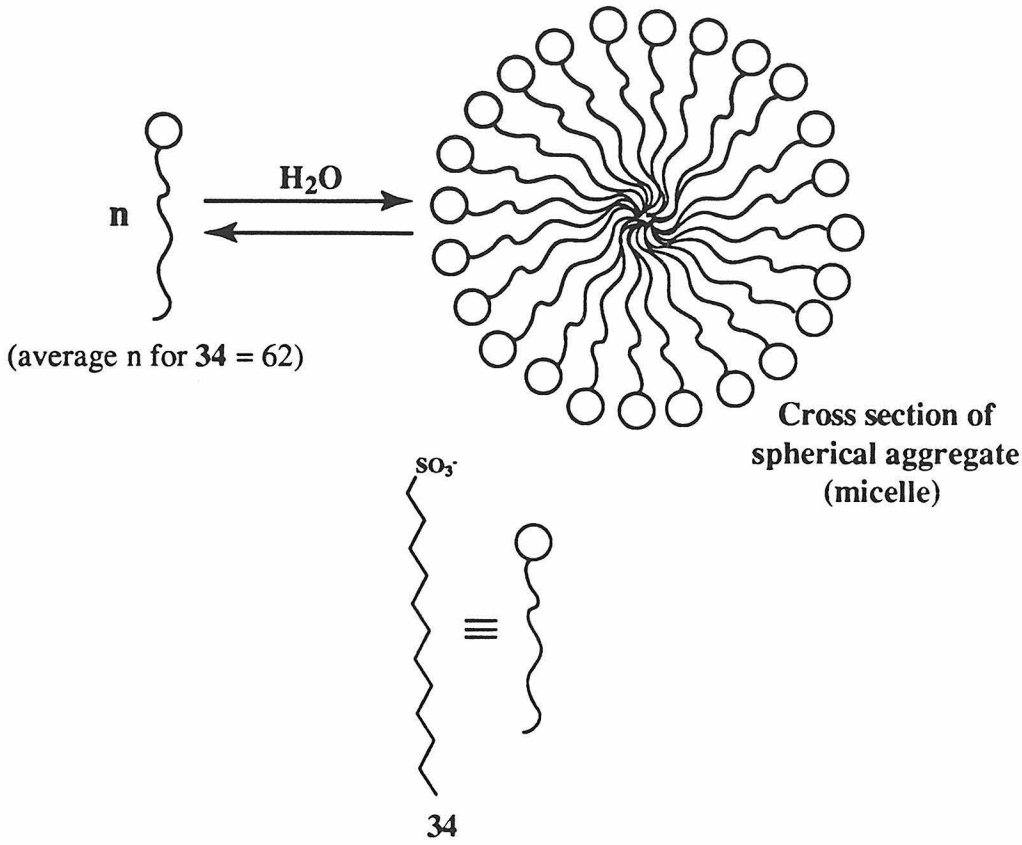

Figure 1.19. Sodium dodecyl sulfate (34) micelle formation.[4b,78]

1.3.2 Dougherty Group Studies

Chapter 7 describes some of the initial attempts in the Dougherty group at creating strictly non-covalent aqueous systems for self-assembly. These studies have focused on molecules derived from the same ethenoanthracene units (**11**) as our host systems. The structures (**35** and **36**) are proposed to take on "U-shaped" conformations (Figure 1.20) that enable two such molecules to combine to form a dimer (Figure 1.21). The assembly into a dimeric structure is proposed to be driven by a combination of hydrophobic and other more directional (hydrogen bonding and electrostatic) non-covalent forces. The ethenoanthracene unit (with its aryl side chains) provides a hydrophobic surface that should

give the molecules a high propensity toward micelle-like aggregation; appending the molecules with polar groups that can form hydrogen bonds or salt bridges should allow these interactions to occur and hold the aggregate to a dimeric stoichiometry (Figure 1.21).

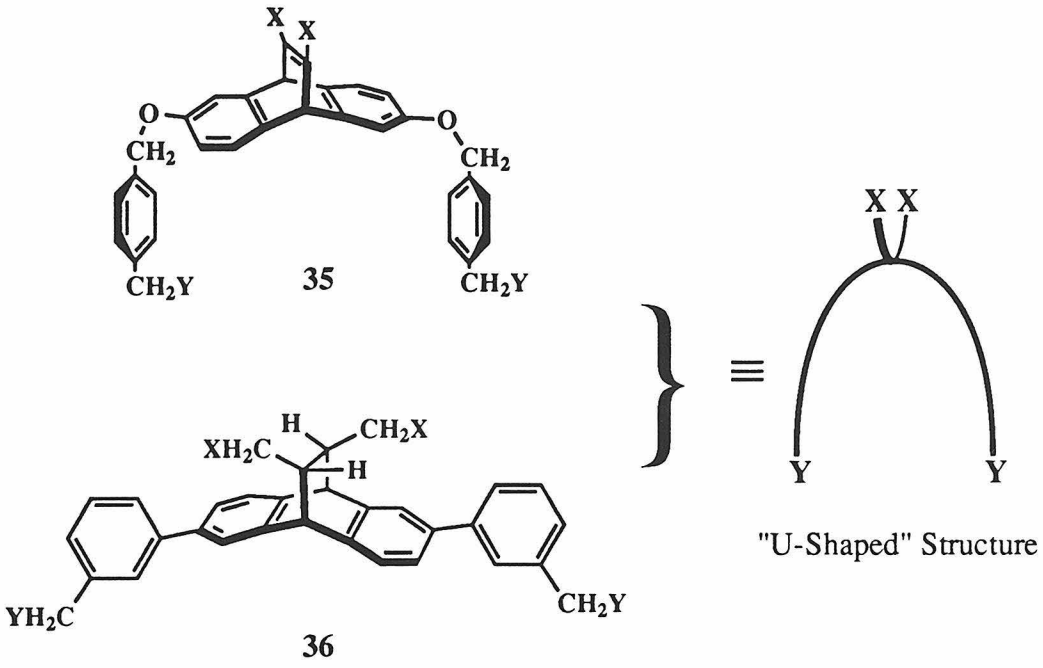

X, Y = Charged or polar functional groups that are complementary to each other.

Figure 1.20. Proposed structures for self-assembling molecules.

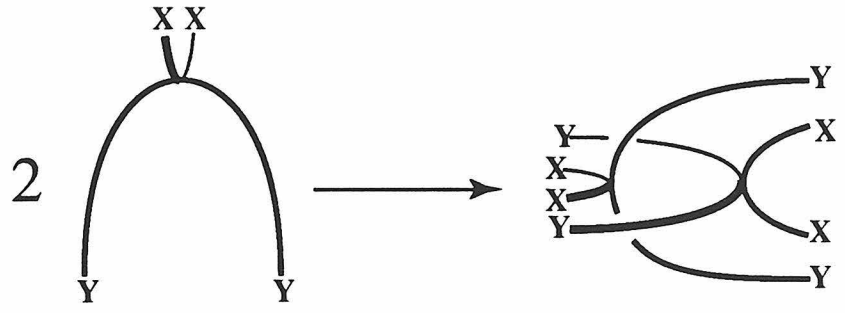

X, Y = Charged or polar functional groups that are complementary to each other.

Figure 1.21. Proposed scheme for self-assembly of molecules with structures like 35 and 36 in an aqueous environment.

While a large portion of the driving force for the formation of these structures may come from an entropic effect (hydrophobic aggregation), the study of these structures in an aqueous environment using strictly non-covalent forces to bring about assembly is quite relevant to biological processes. The potential for learning how to bring about the controlled and specific aggregation of small molecules in an aqueous environment has provided the impetus for the studies that will be described in Chapter 7.

1.4 References and Footnotes

1. Delaage, M. in *Molecular Recognition Mechanisms*, M. Delaage (ed), VCH, 1991, 1-13.

2. (a) Jeffrey, G. A.; Saenger, W.; *Hydrogen Bonding in Biological Structures*, Springer-Verlag, 1991. (b) Vinogradov, S. N.; Linnell, R. H.; *Hydrogen Bonding*, van Nostrand Reinhold Company, 1971. (c) Pimentel, G. C.; McClellan, A. L.; *The Hydrogen Bond*, Freeman and Company, 1960.

3. (a) Mecozzi, S.; West, A. P., Jr.; Dougherty, D. A.; *Submitted.* (b) Dougherty, D. A.; *Science* **1996**, *271*, 163-168.

4. (a) Blokzijl, W.; Engberts, J. B. F. N.; *Angew. Chem., Int. Ed. Engl.* **1993**, *32*, 1545-1579. (b) Tanford, C.; *The Hydrophobic Effect: Formation of Micelles and Biological Membranes*, Wiley Interscience, 1973.

5. (a) Merz, K. M., Jr.; Le grande, S. M. (eds); *The Protein Folding Problem and Tertiary Structure*, Birkhäuser, Boston, 1994. (b) Lehninger, A. L.; *Biochemistry*, Worth Publishers, Inc.; New York, 1976.

6. Hulme, H. C.; *Receptor Biochemistry*, Oxford University Press, New York, 1990.

7. Hiber, M. F.; Trumpp-Kallmeyer, S.; Bruinvels, A.; Hoflack, J.; *Mol. Pharm.* **1991**, *40*, 8-15.

8. (a) Petty, M. C.; *Langmuir-Blodgett Films: An Introduction*, Cambridge University Press, 1996. (b) Roberts, G. G. (ed); *Langmuir-Blodgett Films*, Plenum, 1990.

9. Frommer, J.; *Angew. Chem., Int. Ed. Engl.* **1992**, *31*, 1298-1328.

10. For general references on host-guest chemistry: (a) Izatt, R. M.; Pawlak, K.; Bradshaw, J. S.; Bruening, R. L.; *Chem. Rev.* **1995**, *95*, 2529-2586. (b) Brodessor, G.; Güther, R.; Hoss, R.; Meier, S.; Ottens-Hildebrandt, S.; Schmitz, J.; Vögtle, F.; *Pure Appl. Chem.* **1993**, *65*, 2325-2328. (c) Seel, C.; Vögtle, F.; *Angew. Chem., Int. Ed. Engl.* **1992**, *31*, 528-549. (d) Izatt, R. M.; Bradshaw, J. S.; Pawlak, K.; Bruening, R. L.; Tarbet, B. J.; *Chem. Rev.* **1992**, *92*, 1261-1354. (e) Schneider, H.-J.; *Angew. Chem., Int. Ed. Engl.* **1991**, *30*, 1417-1436. (f) Izatt, R. M.; Pawlak, K.; Bradshaw, J. S.; Bruening, R. L.; *Chem. Rev.* **1991**, *91*, 1721-2085. (g) Schneider, H.-J.; Dürr, H. (eds); *Frontiers in Supramolecular Organic Chemistry and Photochemistry*, VCH, 1991. (h) Atwood, J. L. (ed); *Inclusion Phenomena and Molecular Recognition*, Plenum, 1990. (i) Murakami, Y. (ed); *New Frontiers in Supramolecular Chemistry*, Mita Press: Tokyo, 1990. (j) Roberts, S. M.; *Molecular Recognition: Chemical and Biochemical Problems*, The Royal Society of Chemistry: Cambridge, UK, 1989. (k) Vögtle, F.; *Supramolecular Chemistry*, Wiley, 1989. (l) Vögtle, F.; Weber, E. (eds); *Top. Curr. Chem.* **1986**, *136*. (m) Vögtle, F.; Weber, E. (eds); *Top. Curr. Chem.* **1986**, *132*. (n) Lehn, J.-M.; *Science* **1985**, *227*, 849-856. (o) Boschke, F. L. (ed); *Top. Curr. Chem.* **1985**, *128*. (p) Vögtle,

F. (ed); *Top. Curr. Chem.* **1984**, *121*. (q) Yoshida, Z.-I.; Ise, N.; ***Biomimetic Chemistry***, Elsevier, 1983. (r) Vögtle, F.; Weber, E. (eds); ***Host-Guest Complex Chemistry-Macrocycles, Synthesis, Structures, Applications***; Springer, 1985. (s) Vögtle, F. (ed); *Top. Curr. Chem.* **1982**, *101*. (t) Vögtle, F. (ed); *Top. Curr. Chem.* **1981**, *98*.

11. Chang, S.-K.; Hamilton, A. D.; *J. Am. Chem. Soc.* **1988**, *110*, 1318-1319.

12. (a) Forman, J. E.; Barrans, R. E., Jr.; Dougherty, D. A.; *J. Am. Chem. Soc.* **1995**, *117*, 9213-9228. (b) Dougherty, D. A.; Kearney, P.C.; Mizoue, L.S.; Kumpf, R. A.; Forman, J. E.; McCurdy, A.; in *Computational Approaches in Supramolecular Chemistry*, G. Wipff (ed), NATO ASI Series, 1994. (c) Forman, J. E.; Marsh, R. E.; Schaefer, W. P.; Dougherty, D. A.; *Acta. Cryst. Section B*, **1993** *B49*, 892-896. (d) Kearney, P. C.; Mizoue, L. S.; Kumpf, R. A.; Forman, J. E.; McCurdy, A.; Dougherty, D. A. *J. Am. Chem. Soc.* **1993**, *115*, 9907-9919. (e) McCurdy, A.; Jimenez, L.; Stauffer, D. A.; Dougherty, D. A. *J. Am. Chem. Soc.* **1992**, *114*, 10314-10321. (f) Stauffer, D. A.; Barrans, R. E., Jr.; Dougherty, D. A. *Angew. Chem., Int. Ed. Engl.* **1990**, *29*, 915-918. (g) Stauffer, D. A.; Barrans, R. E., Jr.; Dougherty, D. A. *J. Org. Chem.* **1990**, *55*, 2762-2767. (h) Stauffer, D. A.; Dougherty, D. A. *Science* **1990**, *250*, 1558-1560. (i) Petti, M. A.; Shepodd, T. J.; Barrans, R. E., Jr.; Dougherty, D. A. *J. Am. Chem. Soc.* **1988**, *110*, 6825-6840. (j) Shepodd, T. J.; Petti, M. A.; Dougherty, D. A. *J. Am. Chem. Soc.* **1988**, *110*, 1983-1985. (k) Stauffer, D. A.; Dougherty, D. A. *Tetrahedron Lett.* **1988**, *29*, 6039-6042. (l) Shepodd, T. J.; Petti, M. A.; Dougherty, D. A. *J. Am. Chem. Soc.* **1986**, *108*, 6085-6087. (m) Petti, M. A.; Shepodd, T. J.; Dougherty, D. A.; *Tetrahedron Lett.* **1986**, *27*, 807-810.

13. (a) An, H. Y.; Bradshaw, J. S.; Izatt, R. M.; *Chem. Rev.* **1994**, *94*, 939-991. (b) An, H. Y.; Bradshaw, J. S.; Izatt, R. M.; *Chem. Rev.* **1992**, *92*, 543-572. (c) Cooper, S. R. (ed); *Crown Compounds: Towards Future Applications*, VCH, 1992. (d) Hiraoka, M. (ed); *Crown Ethers and Analogous Compounds*, Elsevier, 1992. (e) Inoue, Y.; Gokel, G. W. (eds); *Cation Binding by Macrocycles: Complexation of Cationic Species by Crown Ethers*, Marcell Dekker, 1990. (f) Patai, S.; Rappoport, Z. (eds); *Crown Ethers and Analogs*, John Wiley and Sons, 1989. (g) Lindoy, L. F.; *The Chemistry of Macrocyclic Ligand Complexes*, Cambridge University Press, 1989. (h) Izatt, I.; Christensen, J. J. (eds); *Progress Macrocyclic Chemistry, Vol. 3*, Wiley, 1986. (i) Izatt, I.; Christensen, J. J. (eds); *Progress Macrocyclic Chemistry, Vol. 2*, Wiley, 1982. (j) Izatt, I.; Christensen, J. J. (eds); *Progress Macrocyclic Chemistry, Vol. 1*, Wiley, 1979.

14. (a) Vicens, J.; Böhmer, V. (eds); *Calixarenes-a Versatile Class of Macrocyclic Compounds*, Kluwer Academic Publishers, 1991. (b) Gutsche, C. D.; *Calixarenes*, The Royal Society of Chemistry: Cambridge, UK, 1989.

15. (a) Wenz, G.; *Angew. Chem., Int. Ed. Engl.* **1994**, *33*, 803-822. (b) Szejtli, J.; *Cyclodextrin Technology*, Kluwer, 1988. (c) Duchene, D. (ed); *Cyclodextrins and Their Industrial Uses*, Ed. Sante: Paris, 1987. (d) Szejtli, J.; *Cyclodextrins and their Inclusion Complexes*, Akademiai Kiado: Budapest, 1982. (e) Bender, M. L.; Komiyama, M.; *Cyclodextrin Chemistry*, Springer-Verlag, 1978.

16. (a) Diederich, F.; *Cyclophanes*; The Royal Society of Chemistry: Cambridge, UK, 1991. (b) Vögtle, F. (ed); *Top. Curr. Chem.* **1983**, *115*. (c) Vögtle, F. (ed); *Top. Curr. Chem.* **1983**, *113*.

17. (a) Lawrence, D. S.; Jiang, T.; Levett, M.; *Chem. Rev.* **1995**, *95*, 2229-2260. (b) König, B.; *J. Prakt. Chem.* **1995**, 337, 339-346.

18. (a) Miyake, M.; Kirisawa, K.; Koga, K. *Chem. Pharm. Bull.* **1993**, *41*, 1211-1213. (b) Miyake, M.; Kirisawa, K.; Koga, K. *Heterocycles,* **1993**, *36*, 1845-1849. (c) Miyake, M.; Kirisawa, K.; Koga, K. *Chem. Pharm. Bull.* **1992**, *40*, 3124-3126. (d) Miyake, M.; Kirisawa, K.; Koga, K. *Tetrahedron Lett.* **1991**, *32*, 7295-7298. (e) Lai, C. F.; Odashima, K.; Koga, K. *Chem. Pharm. Bull.* **1989**, *37*, 2351-2384. (f) Odashima, K.; Kawakami, H.; Miwa, A.; Sasaki, I.; Koga, K. *Chem. Pharm. Bull.* **1989**, *37*, 257-259. (g) Kawakami, H.; Yoshino, O.; Odashima, K.; Koga, K. *Chem. Pharm. Bull.* **1985**, *33*, 5610-5613. (h) Odashima, K.; Iitaka, Y.; Itai, A.; Koga, K. *Chem. Pharm. Bull.* **1985**, *33*, 4478-4484. (i) Odahima, K.; Spoga, T.; Koga, K. *Tetrahedron Lett.* **1981** *22*, 5311-5314. (j) Odashima, K.; Itai, A.; Iitaka, Y.; Koga, K. *J. Am. Chem. Soc.* **1980**, *102*, 2504-2505. (k) Soga, T.; Odashima, K.; Koga, K.; *Tetrahedron Lett.* **1980** *21*, 4351-4354.

19. (a) Tabushi, L.; Yamamura, K.; Nonoguchi, H.; Hirotsu, K.; Higuchi, T. *J. Am. Chem. Soc.* **1984**, *106*, 2621-2625. (b) Tabushi, E.; Kimura, Y.; Yamamura, K. *J. Am. Chem. Soc.* **1981**, *103*, 6486-6492. (c) Tabushi, E.; Sasaki, H.; Kuroda, Y. *J. Am. Chem. Soc.* **1976**, *98*, 5727-5728.

20. (a) Peterson, B. R.; Mordasiniidenti, T.; Diederich, F.; *Chem. Biol.* **1995**, *2*, 139-146. (b) Peterson, B. R.; Wallimann, P.; Carcanague, D. R.; Diederich, F. *Tetrahedron*, **1995**, *51*, 401-421. (c) Peterson, B. R.; Diederich, F. *Angew. Chem., Int. Ed. Engl.* **1994**, *33*, 1625-1628. (d) Diederich, F.; Carcabague, D. R.; *Helv. Chim. Acta* **1994**, *77*, 800-818. (e) Tamchang, S. W.; Jimenez, L.; Diederich, F.; *Helv. Chim. Acta* **1993**, *76*, 2616-2639. (f) Chao, I.; Diederich, F.; *Rec. Trav.*

Chim. **1993**, *112*, 335-338. (g) Jorgensen, W. L.; Nguyen, T. B.; Sanford, E. M.; Chao, I.; Houk, K. N.; Diederich, F.; *J. Am. Chem. Soc.* **1992**, *114*, 4003-4004. (h) Smithrud, D. B.; Wyman, T. B.; Diederich, F. J. *J. Am. Chem. Soc.* **1991**, *113*, 5420-5426. (i) Georgiadis, T. M.; Georgiadis, M. M.; Diederich, F.; *J. Org. Chem.* **1991**, *56*, 3362-3369. (j) Castro, P. P.; Diederich, F.; *Tetrahedron Lett.* **1991**, *32*, 6277-6280. (k) Carcanague, D. R.; Diederich, F.; *Angew. Chem., Int. Ed. Engl.* **1990**, *29*, 769-771. (l) Seward, E. M.; Hopkins, R. B.; Sauerer, W.; Tam, S. W.; Diederich, F.; *J. Am. Chem. Soc.* **1990**, *112*, 1783-1790. (m) Smithrud, D. B.; Sanford, E. M.; Chao, I.; Ferguson, S. B.; Carcanague, D. R.; Evanseck, J. D.; Houk, K. N.; Diederich, F. *Pure Appl. Chem.* **1990**, *62*, 2227-2236. (n) Hester, M. R.; Uyeki, M. A.; Diederich, F.; *Israel J. Chem.* **1989**, *29*, 201-212. (o) Ferguson, S. B.; Seward, E. M.; Sanford, E. M.; Hester, M.; Uyeki, M.; Diederich, F.; *Pure Appl. Chem.* **1989**, *61*, 1523-1528. (p) Jimenez, L.; Diederich, F.; *Tetrahedron Lett.* **1989**, *30*, 2759-2762. (q) Dharanipragada, R.; Ferguson, S. B.; Diederich, F.; *J. Am. Chem. Soc.* **1988**, *110*, 1679-1690. (r) Ferguson, S. B.; Seward, E. M.; Diederich, F.; Sanford, E. M.; Chou, A.; Inocenio-Szweda, P.; Knobler, C. B. *J. Org. Chem.* **1988**, *53*, 5593-5595. (s) Diederich, F.; Schumann, G.; Chao, I.; *J. Org. Chem.* **1988**, *53*, 2744-2757. (t) Seward, E.; Diederich, F.; *Tetrahedron Lett.* **1987**, *28*, 5111-5114. (u) Dharanipragada, R.; Diederich, F.; *Tetrahedron Lett.* **1987**, *28*, 2443-2446. (v) Diederich, F.; Dick, K.; Griebel, D.; *J. Am. Chem. Soc.* **1986**, *108*, 2273-2286. (w) Rubin, Y.; Dick, K.; Diederich F.; Georgiadis, T. M.; J. Org. Chem. 1986, 51, 3270-3278. (x) Schumann, G.; Diederich, F.; *Tetrahedron Lett.* **1986**, *27*, 4249-4252. (y) Diederich, F.; Dick, K.; *Chem. Ber.* **1985**, *118*, 3817-3829. (z) Krieger, C.; Diederich, F.; *Chem. Ber.* **1985**, *118*, 3620-3631. (aa) (y) Diederich, F.; Dick, K.; Griebel, D.; *Chem. Ber.* **1985**, *118*, 3588-3619. (bb) Diederich, F.; Dick, K.; *Angew, Chem., Int. Ed. Engl.* **1984**, *23*, 810-812. (cc)

Diederich, F.; Dick, K.; *Angew, Chem., Int. Ed. Engl.* **1983**, *22*, 715-716. (dd) Diederich, F.; Dick, K.; *Tetrahedron Lett.* **1982**, *23*, 3167-3170.

21. (a) Seel, C.; Vögtle, F. *Angew. Chem., Int. Ed. Engl.* **1991**, *30*, 442-444. (b) Ebmeyer, F.; Vögtle, F. In *Bioorganic Chemistry Frontiers*; Springer-Verlag: Berlin, 1990, Vol. 1, 145-158.

22. (a) Bernardo, A. R.; Stoddart, J. F.; Kaifer, A. E. *J. Am. Chem. Soc.* **1992**, *114*, 10624-10631. (b) Goodnow, T. T.; Reddington, M. V.; Stoddart, J. F.; Kaifer, A. E. *J. Am. Chem. Soc.* **1991**, *113*, 4335-4337.

23. (a) Cudic, P.; Zinic, M.; Tomisic, V.; Simeon, V.; Vigneron, J.-P.; Lehn, J.-M.; *J. Chem. Soc., Chem. Commun.* **1995**, 1073-1075. (b) Meric, R.; Lehn, J.-M.; Vigneron, J.-P. *J. Chem. Soc., Chem. Commun.* **1993**, 129-131. (c) Dhaenens, M.; Lehn, J.-M.; Visneron, J.-P. *J. Chem. Soc., Perkin Trans. 2*, **1993**, 1379-1382. (d) Dhaenens, M.; Lehn, J.-M.; Fernandez, M.-J. *New J. Chem.* **1991**, *15*, 873-877. (e) Slamaschwok, A.; Lehn, J.-M.; *Biochemistry* **1990**, *29*, 7895-7903. (f) Lehn, J.-M. *Angew. Chem., Int. Ed. Engl.* **1988**, *27*, 89-112. (f) Hosseini, M. W.; Blacker, A. J.; Lehn, J.-M.; *J. Chem. Soc., Chem. Commun.* **1988**, 596-598. (g) Dhaenens, M.; Lacombe, L.; Lehn, J.-M.; Vigneron, J.-P. *J. Chem. Soc., Chem. Commun.* **1984**, 1097-1099.

24. (a) Whitlock, B. J.; Whitlock, H. W. *J. Am. Chem. Soc.* **1994**, *116*, 2301-2311. (b) Cochran, J. E.; Parrott, T. J.; Whitlock, B. J.; Whitlock, H. W. *J. Am. Chem. Soc.* **1992**, *114*, 2269-2270. (c) Whitlock, B. J.; Whitlock, H. W. *J. Am. Chem. Soc.* **1990**, *112*, 3910-3915.

25. (a) Baldes, R.; Schneider, H.-J.; *Angew Chem., Int. Ed. Engl.* **1995**, *34*, 321-323. (b) Ikeda, T.; Yoshida, K.; Schneider, H.-J.; *J. Am. Chem. Soc.* **1995**, *117*, 1453-1454. (c) Schneider, U.; Schneider, H.-J.; *Chem. Ber.* **1994**, *127*, 2455-2469. (d) Schneider, H.-J.; *Chem. Soc. Rev.* **1994**, *23*, 227-234. (e) Eliseev, A. V.; Schneider, H.-J.; *J. Am. Chem. Soc.* **1994**, *116*, 6081-6088. (f) Schneider, H.-J.; Schneider, U.; *J. Inclusion Phenom. Mol. Rec.* **1994**, *19*, 67-83. (g) Eliseev, A. V.; Schneider, H.-J.; *Angew. Chem., Int. Ed. Engl.* **1993**, *32*, 1331-1333. (h) Schneider, H.-J.; Kramer, R.; Rammo, J.; *J. Am. Chem. Soc.* **1993**, *115*, 8980-8984. (i) Schneider, H.-J.; Werner, F.; Blatter, T.; *J. Phys. Org. Chem.* **1993**, *6*, 590-594. (j) Schneider, H.-J.; Blatter, T.; Eliseev, A.; Rudiger, V.; Raevsky, O. A.; *Pure Appl. Chem.* **1993**, *65*, 2329-2334. (k) Schneider, H.-J.; Blatter, T.; Palm, B.; Pfingstag, U.; Rudiger, V.; Theis, I.; *J. Am. Chem. Soc.* **1992**, *114*, 7704-7708. (l) Schneider, H.-J.; Schiestel, T.; Zimmermann, P.; *J. Am. Chem. Soc.* **1992**, *114*, 7698-7703. (m) Schneider, H.-J.; Fei, X.; *J. Chem. Soc. Perkin 2* **1992**, 387-391. (n) Schneider, H-J.; Theis, I.; *J. Org. Chem.* **1992**, *57*, 3066-3070. (o) Schneider, H.-J.; *Angew. Chem., Int. Ed. Engl.* **1991**, *30*, 1417-1436. (p) Schneider, H.-J.; Blatter, T.; Simova, S.; *J. Am. Chem. Soc.* **1991**, *113*, 1996-2000. (q) Schneider, H.-J.; Blatter, T.; Zimmermann, P.; *Angew. Chem., Int. Ed. Engl.* **1990**, *29*, 1161-1162. (r) Schneider, H.-J.; Ruf, D.; *Angew. Chem., Int. Ed. Engl.* **1990**, *29*, 1159-1160. (s) Schneider, H.-J.; Kramer, R.; Theis, I.; Zhou, M. Q.; *J. Chem. Soc., Chem. commun.* **1990**, 276-278. (t) Schneider, H.-J.; Theis, I.; *Angew. Chem., Int. Ed. Engl.* **1989**, *28*, 753-754. (u) Schneider, H.-J.; Juneja, R. K.; Simova, S.; *Chem. Ber.* **1989**, *122*, 1211-1213. (v) Schneider, H.-J.; Blatter, T.; Simova, S.; Theis, I.; *J. Chem. Soc., Chem. Commun.* **1989**, 580-581. (w) Kumar, S.; Schneider, H.-J.; *J. Chem. Soc. Perkin 2* **1989**, 245. (x) Schneider, H.-J.; Guttes, D.; Schneider, U.; *J. Am. Chem. Soc.* **1988**, *110*, 6449-6454. (y) Schneider, H.-J.; Kramer, R.; Simova, S.; Schneider, U.; *J. Am. Chem. Soc.* **1988**, *110*, 6442-6448.

(z) Schneider, H.-J.; Sangwan, N. K.; *Angew. Chem., Int. Ed. Engl.* **1987**, *26*, 896-897. (aa) Schneider, H.-J.; Pohlman, J.; *Bioorg. Chem.* **1987**, *15*, 183-193. (bb) Schneider, H.-J.; Schneider, U.; *J. Org. Chem.* **1987**, *52*, 1613-1615. (cc) Schneider, H.-J.; Güttes, D.; Schneider, U. *Angew. Chem., Int. Ed. Engl.* **1986**, *25*, 647-649. (dd) Schneider, H.-J.; Busch, R.; *Angew. Chem., Int. Ed. Engl.* **1984**, *23*, 911-912. (ee) Schneider, H.-J.; Philippi, K.; Pohlman, J.; *Angew. Chem., Int. Ed. Engl.* **1984**, *23*, 908-910.

26. Webb, T. H.; Suh, H.; Wilcox, C. S. *J. Am. Chem. Soc.* **1991**, *113*, 8554-8555.

27. (a) Murakami, Y.; Hayashida, O.; Nagai, Y. *J. Am. Chem. Soc.* **1994**, *116*, 2611-2612. (b) Araki, K.; Shimizu, H.; Shinkai, S. *Chem. Lett.* **1993**, 205-208. (b) Ikeda, A.; Shinkai, S. *Tetrahedron Lett.* **1992**, *33*, 7385-7388. (c) Murakami, Y.; Hayashida, O.; Ono, K.; Hisaeda, Y. *Pure Appl. Chem.* **1993**, *65*, 2319-2324. (d) Murakami, Y.; Hayashida, O.; Ito, T.; Hisaeda, Y. *Pure Appl. Chem.* **1993**, *65*, 551-556. (e) Murakami, Y.; Ohno, T.; Hayashida, O.; Hisaeda, Y. *Chem. Lett.* **1991**, 1595-1598. (f) Murakami, Y.; Kikuchi, J.; Ohno, T.; Hirayama, T.; Hisaeda, Y.; Nishimura, H.; Snyder, J. P.; Steliou, K. *J. Am. Chem. Soc.* **1991**, *113*, 8229-8242. (g) Murakami, Y.; Kikuchi, J.; Ohno, T.; Hayashida, O.; Kojima, M. *J. Am. Chem. Soc.* **1990**, *112*, 7672-7671. (h) Hisaeda, Y.; Ihara, T.; Ohno, T.; Murakami, Y. *Tetrahedron Lett.* **1990**, *31*, 1027-1030. (i) Murakami, Y.; Kikuchi, J.; Ohno, T.; Hirayama, T. *Chem. Lett.* **1989**, 881-884. (j) Shinmyozu, T.; Sakai, T.; Uno, E.; Inazu, T. *J. Org. Chem.* **1985**, *50*, 1959-1963.

28. Rotger, M. C.; González, J. F.; Ballester, P.; Deyá, P. M.; Costa, A.; J. Org. Chem. **1994**, *59*, 4501-4505.

29. (a) Garel, L.; Lozach, B.; Dutasta, J.-P.; Collet, A.; *J. Am. Chem. Soc.* **1993**, *115*, 11652-11653. (b) Canceill, J.; Lacombe, L.; Collet, A.; *J. Chem. Soc., Chem. Commun.* **1987**, 219-222.

30. Menger, F. M.; Catlin, K. K.; *Angew. Chem., Int. Ed. Engl.* **1995**, *34*, 2147-2150.

31. (a) Fujimoto, T.; Yanagihara, R.; Kobayashi, K.; Aoyama, Y.; *Bull. Chem. Soc. Jpn.* **1995**, *68*, 2113-2124. (b) Yanagihara, R.; Tominaga, M.; Aoyama, Y.; *J. Org. Chem.* **1994**, *59*, 6865-6867. (c) Yanagihara, R.; Aoyama, Y.; *Tetrahedron Lett.* **1994**, *35*, 9725-9728. (d) Kobayashi, K.; Tominaga, M.; Asakawa, Y.; Aoyama, Y.; *Tetrahedron Lett.* **1993**, *34*, 5121-5124. (e) Kobayashi, K.; Asakawa, Y.; Kato, Y.; Aoyama, Y.; J. Am. Chem. Soc. **1992**, *114*, 10307-10313.

32. It is important to point out that hydrogen bonding in water, while weak, has been observed in synthetic systems; most notably: (a) Jiménez-Barbero, J.; Junquera, E.; Martin-Pastor, M.; Sharma, S.; Vicent, C.; Penadés, S.; *J. Am. Chem. Soc.* **1995**, *117*, 11198-11204. (b) Kato, Y.; Conn, M. M.; Rebek, J., Jr.; *Proc. Natl. Acad. Sci. USA* **1995**, *92*, 1208-1212. (c) Kato, Y.; Conn, M. M.; Rebek, J., Jr.; *J. Am. Chem. Soc.* **1994**, *116*, 3279-3284 (see all also page 9411). (d) Rotello, V. M.; Viani, E. Z.; Deslongchamps, G.; Murray, B. A.; Rebek, J., Jr.; *J. Am. Chem. Soc.* **1993**, *115*, 797-798.

33. Ngola, S. M., Dougherty, D. A.; *Submitted.*

34. (a) Aoki, K.; Murayama, K.; Nishiyama, H.; *J. Chem. Soc., Chem. Commun.* **1995**, 2221-2222. (b) Kumpf, R. A.; Dougherty, D. A.; *Science* **1993**, *261*, 1708-1710. (c) Durell, S.R.;Guy, H. R.; *Biophys. J.* **1992**, *62*, 238-250. (d)

Heginbotham, L.; MacKinnon, R.; *Neuron* **1992**, *8*, 483-491. (e) Bogusz, S.; Boxer, A.; Busath, D. D.; *Protein Engineer.* **1992**, *5*, 285-293.

35. (a) Fujii, T.; Tokiwa, H.; Ichikawa, H.; Shinoda, H.; *J. Mol. Struct. (Theochem)* **1992**, *277*, 251-262. (b) Guo, B. C.; Purnell, J. W.; Castelman, A. W., Jr.; *Chem. Phys. Lett.* **1990**, *168*, 155-160. (c) Taft, R. W.; Anvia, F.; Gal, J.-F.; Walsh, S.; Capon, M.; Holmes, M. C.; Hosn, K.; Oloumi, G.; Vasanwala, R.; Yazdani, S.; *Pure Appl. Chem.* **1990**, *62*, 17-23. (d) Deakyne, C. A.; Moet-Ner (Mautner), M.; *J. Am. Chem. Soc.* **1985**, *107*, 474-479. (e) Moet-Ner (Mautner), M.; Deakyne, C. A.; *J. Am. Chem. Soc.* **1985**, *107*, 469-474. (f) Sunner, J.; Nishizawa, K.; Kebarle, P.; *J. Phys. Chem.* **1981**, *85*, 1814-1820.

36. Dougherty, D. A.; in *Comprehensive Supramolecular Chemistry*, Lehn, J.-M. (ed), Pergamon Press, *Submitted*, Vol. 2.

37. (a) Constable, E. C.; Smith, D.; *Chemistry Brit.* **1995**, 33-37, 41. (b) Constable, E. C.; Chem. Ind. 1994, 56-59. (c) Lehn, J. M.; *Pure. Appl. Chem.* **1994**, *66*, 1961-1966. (d) Lindsey, J. S.; *New J. Chem.* **1991**, *15*, 153-180. (e) Whitesides, G. M.; Mathias, J. P.; Seto, C. T.; *Science* **1991**, *254*, 1312-1319. (f) Lehn, J. M.; *Angew. Chem., Int. Ed. Engl.* **1990**, *29*, 1304-1319. (g) Lehn, J. M.; *Angew. Chem. Int. Ed. Engl.* **1988**, *27*, 89-112.

38. (a) Klug, A.; *Phil. Trans. R. Soc. Lond. A* **1994**, *348*, 167-178. (b) Klug, A.; *New Scientist* **1987**, *21*, 46-50. (c) Klug, A.; *Angew. Chem., Int. Ed. Engl.* **1983**, *22*, 565-636. (d) Klug, A.; *Bioscience Reports* **1983**, *3*, 395-430.

39. Tomalia, D. A.; *Adv. Mater.* **1994**, *6*, 529-539.

40. (a) Dubois, L. H.; Nuzzo, R. G.; *Annu. Rev. Phys. Chem.*; **1992**, *43*, 437-463. (b) Ulman, A.; *An Introduction to Ultrathin Organic Films: From Langmuir-Blodgett to Self-Assembly*; Academic Press; 1991. (c) Whitesides, G. M.; Laibinis, P. E.; *Langmuir*, **1990**, *6*, 87-96. (d) Whitesides, G. M.; Ferguson, G. S.; *Chemtracts-Organic Chemistry*, **1988**, *1*, 171-187.

41. Kirschner, M.; Mitchison, T.; *Cell* **1986**, *45*, 329-342.

42. (a) Symons, R. H.; *Crit. Rev. Plant Sci.* **1991**, *10*, 189-234. (b) Eiserling, F. A.; Dickson, R. C.; *Ann. Rev. Biochem.* **1972**, *41*, 467-502.

43. (a) Ashton, P. R.; Campbell, P. J.; Chrystal, E. J. T.; Glink, P. T.; Menzer, S.; Philip, D.; Spencer, N.; Stoddart, J. F.; Tasker, P. A.; Williams, D. J.; *Angew. Chem., Int. Ed. Engl.* **1995**, *34*, 1865-1869. (b) Ashton, P. R.; Ballardihi, R.; Balzani, V.; Credi, A.; Gandolfi, M. T.; Menzer, L.; Pérez-Garciá, L.; Prodii, L.; Stoddart, J. F.; Venturi, M.; White, A. J. P.; Williams, D. J.; *J. Am. Chem. Soc.* **1995**, *117*, 11171-11197. (c) Langford, S. J.; Pérez-Garciá, L.; Stoddart, J. F.; *Supramol. Chem.* **1995**, *6*, 11-27. (d) Amabilino, D. B.; Ashton, P. R.; Brown, C. L.; Córdova, E.; Godínez, L. A.; Goodnow, T. T.; Kaifer, A. E.; Newton, S. P.; Pietraszkiewicz, M.; Philip, D.; Raymo, F. M.; Reder, A. S.; Rutland, M. T.; Slawin, A. M. Z.; Spencer, N.; Stoddart, J. F.; Williams, D. J.; *J. Am. Chem. Soc.* **1995**, *117*, 1271-1293. (e) Hoss, R.; Vögtle, F.; *Angew. Chem., Int. Ed. Engl.* **1994**, *33*, 375-384. (f) Fujita, M.; Ibukuro, F.; Hagihara, H.; Ogura, K.; *Nature* **1993**, *367*, 720-723. (g) Gibson, H. W.; Bheda, M. C.; Engen, P. T.; *Prog. Polym. Sci.* **1994**, *19*, 843-945. (h) Anelli, P. L.; Ashton, P. R.; Ballardini, R.; Balzani, V.; Delgado, M.; Gandolfi, M. T.; Goodnow, T. T.; Kaifer, A. E.; Philip, D.; Pietraszkiewicz, M.; Prodi, L.; Reddington, M. V.; Slawin, A. M. Z.; Spencer, N.; Stoddart, J. F.; Vicent,

C.; Williams, D. J.; *J. Am. Chem. Soc.* **1992**, *114*, 193-218. (i) Dietrich-Buchecker, C. O.; Sauvage, J. P.; *Angew. Chem., Int. Ed. Engl.* **1989**, *28*, 189-192. (j) Dietrich-Buchecker, C. O.; Sauvage, J. P.; *Chem. Rev.* **1987**, *87*, 795-810.

44. (a) Martinus, R. D.; Ryan, M. T.; Naylor, D. J.; Herd, S. M.; Hoogenraad, N. J.; Hoj, P. B.; *FASEB J.* **1995**, *9*, 371-378. (b) Gupta, R. S.; *Mol. Microbiol.* **1995**, *15*, 1-11. (c) Randall, L. L.; Hardy, S. J. S.; *Trends Biochem. Sci.* **1995**, *20*, 65-70. (d) Groenen, P. J. T. A.; Merck, K. B.; Dejong, W. W.; Bloemendal, H.; *Eur. J. Biochem.* **1994**, *225*, 1-19. (e) Wynn, R. M.; Davie, J. R.; Cox, R. P.; Chuang, D. T.; *J. Lab. Clin. Med.* **1994**, *124*, 31-36. (f) Cueza, J. M.; Flores, A. I.; Liras, A.; Santaren, J. F.; Alconada, A.; *Biol. Cell* **1993**, *77*, 47-62. (g) Horwich, A. L.; Williamson, K. R.; *Phil. Trans. R Soc. Lond. B* **1993**, *339*, 313-326. (h) Kumamoto, C. A.; *Mol. Microbiol.* **1991**, *5*, 19-22. (i) Ellis, R. J.; Hemmingsen, S. M.; *Trends Biochem. Sci.* **1989**, *14*, 339-342.

45. (a) Orgel, L. E.; *Acc. Chem. Res.* **1995**, *28*, 109-118. (b) Sievers, D.; von Kiedrowski, G.; *Nature* **1994**, *369*, 221-224. (c) Li, T.; Nicolaou, K. C.; *Nature* **1994**, *369*, 218-221. (d) Hoffman, S.; *Angew. Chem., Int. Ed. Engl.* **1992**, *31*, 1013-1016. (e) Orgel, L. E.; *Nature* **1992**, *358*, 203-209.

46. (a) Wintner, E. A.; Tsao, B.; Rebek, J., Jr.; *J. Org. Chem.* **1995**, *60*, 7995-8001. (b) Wintner, E. A.; Conn, M. M.; Rebek, J., Jr.; *Acc. Chem. Res.* **1994**, *27*, 198-203. (c) Pieters, R. J.; Huc, I.; Rebek, J., Jr.; *Angew. Chem., Int. Ed. Engl.* **1994**, *33*, 1579-1581. (d) Conn, M. M.; Wintner, E. A.; Rebek, J., Jr.; *Angew. Chem., Int. Ed. Engl.* **1994**, *33*, 1577-1579. (e) Rebek, J., Jr.; *Chem. Brit.* **1994**, *30*, 286-290. (f) Conn, M. M.; Rebek, J. Jr.; *Curr. Opin. Struct. Biol.* **1994**, *4*, 629-635. (g) Conn, M. M.; Wintner, E. A.; Rebek, J., Jr.; *Heterocycle* **1994**, *39*, 879-889.

(h) Wintner, E. A.; Conn, M. M.; Rebek, J., Jr.; *J. Am. Chem. Soc.* **1994**, *116*, 8877-8884. (i) Conn, M. M.; Wintner, E. A.; Rebek, J., Jr.; *J. Am. Chem. Soc.* **1994**, *116*, 8823-8824. (j) Rebek, J., Jr.; *Sci. American* **1994**, *271*, 48. (k) Andreu, C.; Beerli, R.; Branda, N.; Conn, M. M.; de Mendoza, J.; Galán, A.; Huc, I.; Kato, Y.; Tymoschenko, M.; Valdez, C.; Wintner, E.; Wyler, R.; Rebek, J., Jr.; *Pure Appl. Chem.* **1993**, *65*, 2313-2318. (l) Rebek, J., Jr.; *Supramolec. Chem.* **1993**, *1*, 261-266. (m) Famulok, M.; Nowick, J. S.; Rebek, J., Jr.; *Acta Chem. Scand.* **1992**, *46*, 315-324. (n) Rebek, J., Jr.; *Chem. Ind.* **1992**, 171-174. (o) Park, T. K.; Feng, Q.; Rebek, J., Jr.; *J. Am. Chem. Soc.* **1992**, *114*, 4529-4532. (p) Feng, Q.; Park, T. K.; Rebek, J., Jr.; *Science* **1992**, *256*, 1179-1180. (q) Hong, J. I.; Feng, Q.; Rotello, V.; Rebek, J., Jr.; *Science* **1992**, *255*, 848-850. (r) Rebek, J., Jr.; *Experentia* **1991**, *47*, 1096-1104. (s) Rotello, V.; Hong, J. I.; Rebek, J., Jr.; *J. Am. Chem. Soc.* **1991**, *113*, 9422-9423. (t) Nowick, J. S.; Feng, Q.; Tjivikua, T.; Ballester, P.; Rebek, J., Jr.; *J. Am. Chem. Soc.* **1991**, *113*, 8831-8839. (u) Tjivikua, T.; Ballester, P.; Rebek, J., Jr.; *J. Am. Chem. Soc.* **1990**, *112*, 1249-1250.

47. For a critisism of some of the work reported in reference 46, see (a) Menger, F. M.; Eliseev, A. V.; Khanjin, N. A.; Sherrod, M. J.; *J. Org. Chem.* **1995**, *60*, 2870-2878. (b) Menger, F. M.; Eliseev, A. V.; Khanjin, N. A.; *J. Am. Chem. Soc.* **1994**, *116*, 3613-3614.

48. (a) Larson, D. E.; Zahradka, P.; Sells, B. H.; *Bioch. Cell Biol.* **1991**, *69*, 5-22. (b) Anderson, R. G. W.; in *Cell Biology: A Comprehensive Treatise*, Vol. 4, Prescott, D. M.; Goldstein, L. (eds); Academic Press, 1980, 393-441. (c) Nomura, M.; *Science* **1979**, *179*, 864-873.

49. (a) Kellenberger, E.; Wunderliallenspach, H.; *Micron.* **1995**, *26*, 213-245. (b) Russel, M.; *Mol. Microbiol.* **1991**, *5*, 1607-1613. (c) Thompson, R. L.; Goel, N. S.; *BioSystems* **1985**, *18*, 23-45. (d) King, J.; in *Biological Regulation and Development, Vol. 2*, Goldberger, R. F. (ed); Plenum, 1980, 101-132. (e) Wood, W. B.; in *Genetic Mechanisms of Development*, Ruddle, F. H. (ed); Academic Press, 1973, 29-46.

50. Fredericks, J.; Yang, J.; Geib, S. J.; Hamilton, A. D.; *Proc. Indian Acad. Sci. (Chem. Sci.)* **1994**, *106*, 923-935.

51. (a) Subramanian, S.; Zaworotko, M. J.; *Coord. Chem. Rev.* **1994**, *137*, 357-401. (b) Fan, E.; Vicent, C.; Geib, S. J.; Hamilton, A. D.; *Chem. Mater.* **1994**, *6*, 1113-1117. (c) Macdonald, J. C.; Whitesides, G. M.; *Chem. Rev.* **1994**, *94*, 2383-2420.

52. (a) Whitesides, G. M.; Simanek, E. E.; Mathias, J. P.; Seto, C. T.; Chin, D. N.; Mammen, M.; Gordon, D. M.; *Acc. Chem. Res.* **1995**, *28*, 37-44. (b) Cheng, X.; Gao, Q.; Smith, R. D.; Simanek, E. E.; Mammen, M.; Whitesides, G. M.; *Rapid Commun. Mass Spectrom.* **1995**, *9*, 312-316. (c) Simanek, E. E.; Mammen, M.; Gordon, D. M.; Chin, D.; Mathias, J. P.; Seto, C. T.; Whitesides, G. M.; *Tetrahedron* **1995**, *51*, 607-619. (d) Chin, D. N.; Gordon, D. M.; Whitesides, G. M.; *J. Am. Chem. Soc.* **1994**, *116*, 12033-12044. (e) Mathias, J. P.; Simanek, E. E.; Whitesides, G. M.; *J. Am. Chem. Soc.* **1994**, *116*, 4326-4340. (f) Mathias, J. P.; Simanek, E. E.; Zerkowski, J. A.; Seto, C. T.; Whitesides, G. M.; *J. Am. Chem. Soc.* **1994**, *116*, 4316-4325. (g) Mathias, J. P.; Seto, C. T.; Simanek, E. E.; Whitesides, G. M.; *J. Am. Chem. Soc.* **1994**, *116*, 1725-1736. (h) Mathias, J. P.; Simanek, E. E.; Seto, C. T.; Whitesides, G. M.; *Angew. Chem., Int. Ed. Engl.* **1993**, *32*, 1766-1769. (i) Seto, C. T.; Whitesides, G. M.; *J. Am. Chem. Soc.*

1993, *115*, 1330-1340. (j) Seto, C. T.; Mathias, J. P.; Whitesides, G. M.; *J. Am. Chem. Soc.* **1993**, *115*, 1321-1329. (k) Seto, C. T.; Whitesides, G. M.; *J. Am. Chem. Soc.* **1993**, *115*, 905-916. (l) Seto, C. T.; Whitesides, G. M.; *J. Am. Chem. Soc.* **1991**, *113*, 712-713. (m) Seto, C. T.; Whitesides, G. M.; *J. Am. Chem. Soc.* **1990**, *112*, 6409-6411.

53. (a) Russell, K. C.; Leize, E.; van Dorsselaer, A.; Lehn, J.-M.; *Angew. Chem., Int. Ed. Engl.* **1995**, *34*, 209-213. (b) Hanan, G. S.; Lehn, J.-M.; Kyritsakas, N.; Fischer, J.; *J. Chem. Soc., Chem. Commun.* **1995**, 765-766. (c) Brienne, M.-J.; Gabard, J.; Leclercq, M.; Lehn, J.-M.; Cesario, M.; Pascard, C.; Cheve, M.; Dutruc-Rosset, G.; *Tetrahedron Lett.* **1994**, *35*, 8157-8160. (d) Marsh, A.; Nolen, E. G.; Gardinier, K. M.; Lehn, J.-M.; *Tetrahedron Lett.* **1994**, *35*, 397-400. (e) Drain, C. M.; Fischer, R.; Nolen, E. G.; Lehn, J.-M.; *J. Chem. Soc., Chem. Commun.* **1993**, 243-245. (f) Gulik-Krzywicki, T.; Fouquey, C.; Lehn, J.-M.; *Proc. Natl. Acad. Sci. USA* **1993**, *90*, 163-167.

54. (a) Goodman, M. S.; Hamilton, A. D.; Weiss, J.; *J. Am. Chem. Soc.* **1995**, *117*, 8447-8455. (b) Goodman, M. S.; Weiss, J.; Hamilton, A. D.; *Tetrahedron Lett.* **1994**, *35*, 8943-8946. (c) Yang, J.; Marendaz, J.-L.; Geib, S.-J.; Hamilton, A. D.; *Tetrahedron Lett.* **1994**,*35*, 3665-3668. (d) Geib, S. J.; Vincent, C.; Fan, E.; Hamilton, A. D.; *Angew. Chem. Int. Ed. Engl.* **1993**, *32*, 119-121. (e) Yang, J.; Fan, E.; Geib, S. J.; Hamilton, A. D.; *J. Am. Chem. Soc.* **1993**, *115*, 5314-5315. (f) Tecilla, P.; Dixon, R. P.; Slobodkin, G.; Alavi, S.; Waldeck, D. H.; Hamilton, A. D.; *J. Am. Chem. Soc.* **1990**, *112*, 9408-9410.

55. (a) Grotzfeld, R. M.; Branda, N.; Rebek, J., Jr.; *Science* **1996**, *271*, 487-489. (b)

Valdes, C.; Spitz, U. P.; Kubik, S. W.; Rebek, J., Jr.; *Angew. Chem., Int. Ed. Engl.* **1995**, *34*, 1885-1887. (c) Branda, N.; Grotzfeld, R. M.; Valdes, C.; Rebek, J., Jr.; *J. Am. Chem. Soc.* **1995**, *117*, 85-88. (d) Meissner, R. S.; Rebek, J., Jr.; de Mendoza, J.; *Science* **1995**, *270*, 1485-1488. (e) Branda, N.; Wyler, R.; Rebek, J., Jr.; *Science* **1994**, *263*, 1267-1268. (f) Wyler, R.; de Mendoza, J.; Rebek, J., Jr.; *Angew. Chem., Int. Ed. Engl.* **1993**, *32*, 1699-1701. See also references 46fj.

56. (a) Bisson, A. P.; Carver, F. J.; Hunter, C. A.; Waltho, J. P.; *J. Am. Chem. Soc.* **1994**, *116*, 10292-10293. (b) Schall, O. F.; Gokel, G. W.; *J. Am. Chem. Soc.* **1994**, *116*, 6089-6100. (c) Bonar-Law, R. P.; Sanders, J. K. M.; *Tetrahedron Lett.* **1993**, *34*, 1677-1680. (d) Zimmerman, S. C.; Duerr, B. F.; *J. Org. Chem.* **1992**, *57*, 2215-2217. (e) Gallant, M.; Viet, M. T. P.; Wuest, J. D.; *J. Org. Chem.* **1991**, *56*, 2284-2286. (f) Ducharme, Y.; Wuest, J. D.; *J. Org. Chem.* **1988**, *53*, 5787-5789. (g) Kim, M. S.; Gokel, G. W.; J. Chem. Soc., Chem. Commun. 1987, 1686-1688.

57. (a) Zerkowski, J. A.; Macdonald, J. C.; Whitesides, G. M.; *Chem. Mater.* **1994**, *6*, 1250-1257. (b) Zerkowski, J. A.; Mathias, J. P.; Whitesides, G. M.; *J. Am. Chem. Soc.* **1994**, *116*, 4305-4315. (c) Zerkowski, J. A.; Whitesides, G. M.; *J. Am. Chem. Soc.* **1994**, *116*, 4298-4304. (d) Zerkowski, J. A.; Macdonald, J. C.; Seto, C. T.; Wierda, D. A.; Whitesides, G. M.; *J. Am. Chem. Soc.* **1994**, *116*, 2382-2391. (e) Zerkowski, J. A.; Seto, C. T.; Whitesides, G. M.; *J. Am. Chem. Soc.* **1992**, *114*, 5473-5475. (f) Zerkowski, J. A.; Seto, C. T.; Wierda, D. A.; Whitesides, G. M.; *J. Am. Chem. Soc.* **1990**, *112*, 9025-9026.

58. (a) Lehn, J.-M.; Mascal, M.; DeCian, A.; Fischer, J.; *J. Chem. Soc. Perkin Trans 2*

1992, 461-467. (b) Lehn, J.-M.; Mascal, M.; DeCian, A.; Fischer, J.; *J. Chem. Soc., Chem. Commun.* **1990**, 479-481.

59. (a) Fan, E. K.; Yang, J.; Geib, S. J.; Stoner, T. C.; Hopkins, M. G.; Hamilton, A. D.; *J. Chem. Soc., Chem. Commun.* **1995**, 1251-1252. (b) Garcia-Tellado, F.; Geib, S. J.; Goswami. S.; Hamilton, A. D.; *J. Am. Chem. Soc.* **1991**, *113*, 9265-9269. (c) Geib, S. J.; Hirst, S. C.; Vicent, C.; Hamilton, A. D.; *J. Chem. Soc., Chem. Commun.* **1991**, 1283-1285. (d) Garcia-Tellado, F.; Goswami, S.; Chang, S. K.; Geib, S. J.; Hamilton, A. D.; *J. Am. Chem. Soc.* **1990**, *112*, 7393-7394. (e) Goswami, S.; Van Engen, D.; Hamilton, A. D.; *J. Am. Chem. Soc.* **1989**, *111*, 3425-3426. (f) Muehldorf, A. V.; Van Engen, D.; Warner, J. C.; Hamilton, A. D.; *J. Am. Chem. Soc.* **1988**, *110*, 6561-6562. (g) Hamilton, A. D.; Van Engen, D.; *J. Am. Chem. Soc.* **1987**, *109*, 5035-5036.

60. (a) Alyea, E. C.; Ferguson, G.; Xu, Z.; *Acta Cryst. Section C* **1995**, *C51*, 353-356. (b) Karle, I. L.; Ranganathan, D.; *Biopolymers* **1995**, *36*, 323-331. (c) Toledo, L. M.; Musa, K. M.; Lauher, J. W.; Fomler, F. W.; *Chem. Mater.* **1995**, *7*, 1639-1637. (d) Mak, T. C. W.; Hing Yip, W.; Li, Q.; *J. Am. Chem. Soc.* **1995**, *117*, 11995-11996. (e) Endo, K.; Sawaki, T.; Koyanogi, M.; Kobayashi, K.; Masuda, H.; Aoyama, Y.; *J. Am. Chem. Soc.* **1995**, *117*, 8341-8352. (f) Hanessian, S.; Simard, M.; Roelens, S.; *J. Am. Chem. Soc.* **1995**, *117*, 7630-7645. (g) Sui, D.; Wang, X.; Simard, M.; Wuest, J. D.; *Supramol. Chem.* **1995**, *6*, 171-178. (h) Kyritsakas, N.; Fischer, J.; Hosseini, M. W.; Ruppert, R.; Schaeffer, P.; Decian, A.; *J. Chem. Soc., Chem. Commun.* **1994**, 2135-2136. (i) Wang, X.; Simard, M.; Wuest, J. D.; *J. Am. Chem. Soc.* **1994**, *116*, 12119-12120. (j) Hanessian, S.; Gomtsyan, A.; Simard, M.; Roelens, S.; *J. Am. Chem. Soc.* **1994**, *116*, 4495-4496. (k) Russell, V. A.; Etter, M. C.; Ward, M. D.; *J. Am. Chem. Soc.* **1994**, *116*, 1941-

1952. (l) Copp, S. B.; Subramian, S.; Zaworotko, M. J.; *Angew. Chem., Int. Ed. Engl.* **1993**, *32*, 706-709. (m) Yamanari, K.; Kida, M.; Yamamoto, M.; Fujihara, T.; Fuyuhiro, A.; Kaizaki, S.; *Chem. Lett.* **1993**, 1865-1868. (n) Copp, S. B.; Subramian, S.; Zaworotko, M. J.; *J. Chem. Soc., Chem. Commun.* **1993**, 1078-1079. (o) Soghomonian, V.; Chen, Q.; Haushalter, R. C.; Zubieta, J.; O'Connor, C. J.; *Science* **1993**, *259*, 1596-1599. (p) Chang, Y.-L.; West, M.-A.; Fowler, F. W.; Lauher, J. W.; *J. Am. Chem. Soc.* **1993**, *115*, 5991-6000. (q) Kobayashi, K.; Endo, K.; Aoyama, Y.; Masuda, H.; *Tetrahedron Lett.* **1993**, *34*, 7929-7932. (r) Simard, M.; Su, D.; Wuest, J. D.; *J. Am. Chem. Soc.* **1991**, *113*, 4696-4698. (s) Wang, Y.; Wei, B.; Wang, Q.; *J. Crystallogr. Spectrosc. Res.* **1990**, *20*, 79-84. (t) Etter, M. C.; Urbanczyck-Lipkowska, Z.; Jahn, D. A.; Frye, J. S.; *J. Am. Chem. Soc.* **1986**, *108*, 5871-5876. (u) Feibush, B.; Figueroa, A.; Charles, R.; Onan, K. D.; Feibush, P.; Kargar, B. L.; *J. Am. Chem. Soc.* **1986**, *108*, 3310-3318. (v) Shimizu, N.; Nishigaki, S.; Nakai, Y.; Osaki, K.; *Acta Cryst. Section B* **1982**, *B38*, 2309-2311. (w) Benedetti, E.; Ciajolo, M. R.; Corradini, P.; *Eur. Polym. J.* **1973**, *9*, 101-109. (x) Alcala, R.; Martinez-Carrera, S.; *Acta Cryst. Section B* **1972**, *B28*, 1671-1684. (y) Voet, D.; *J. Am. Chem. Soc.* **1972**, *94*, 8213-8222. (z) Duchamp, D. J.; Marsh, R. E.; *Acta Cryst. Section B* **1969**, *B25*, 5-19.

61. (a) Kleppinger, R.; Lillya, C. P.; Yang, C. Q.; *Angew. Chem., Int. Ed. Engl.* **1995**, *34*, 1637-1638. (b) Yang, W. S.; Chen, S. G.; Chai, X. D.; Cao, Y. W.; Lu, R.; Chai, W.-P.; Jiang, Y.-S.; Li, T.-I.; Lehn, J.-M.; *Synth. Metal* **1995**, *71*, 2107-2108. (c) Kotera, M.; Lehn, J.-M.; Vigneron, J.-P.; *Tetrahedron* **1995**, *51*, 1953-1972. (d) Kato, T.; Kihara, H.; Kumar, U.; Uryu, T. Fréchet, J.-M. J.; *Angew. Chem., Int. Ed. Engl.* **1994**, *33*, 1644-1645. (e) Kotera, M.; Lehn, J.-M.; Vigneron, J.-P.; *J. Chem. Soc., Chem. Commun.* **1994**, 197-199. (f) Kawamata, J.; Matsunaga, Y.; *Mol. Cryst. Liquid Cryst.* **1993**, *231*, 79-85. (g) Malthête, J.;

Leuelut, A.-M.; Liébert, L.; *Adv. Mater.* **1992**, *4*, 36-41. (h) Kato, T.; Adachi, H.; Fujishima, A.; Fréchet, J.-M. J.; *Chem. Lett.* **1992**, 265-268. (i) Kumar, U.; Kato, T.; Fréchet, J.-M. J.; *J. Am. Chem. Soc.* **1992**, *114*, 6630-6639. (j) Kato, T.; Kihara, H.; Uryu, T.; Fujishima, A.; Fréchet, J.-M. J.; *Macromolecules* **1992**, *25*, 6836-6841. (k) Lauher, J. W.; Chang, Y.-L.; Fowler, F. W.; *Mol. Cryst. Liquid Cryst.* **1992**, *211*, 99-109. (l) Zhao, X.; Chang, Y.-L.; Fowler, F. W.; Lauher, J. W.; *J. Am. Chem. Soc.* **1990**, *112*, 6627-6634. (m) Kato, T.; Fujishima, A.; Fréchet, J. M. J.; *Chem. Lett.* **1990**, 919-922. (n) Kato, T.; Fréchet, J.-M. J.; *J. Am. Chem. Soc.* **1989**, *111*, 8533-8534. (o) Brienne, M. J.; Gabard, J.; Lehn, J.-M.; Stibor, I.; *J. Chem. Soc., Chem. Commun.* **1989**, 1868-1870. (p) Malthête, J.; Collet, A.; Levelut, A.-M.; *Liquid Cryst.* **1989**, *5*, 123-131. (q) Goodby, J. W.; *Mol. Cryst. Liquid Cryst.* **1984**, *110*, 205-219. (r) Gray, G. W.; Jones, B.; *J. Chem. Soc.* **1954**, 683-686. (s) Gray, G. W.; Jones, B.; *J. Chem. Soc.* **1953**, 4179-4181.

62. (a) Müller, A.; Reuter, H.; Dillinger, S.; *Angew. Chem., Int. Ed. Engl.* **1995**, *34*, 2328-2361. (b) Desiraju, G. R.; *Angew. Chem., Int. Ed. Engl.* **1995**, *34*, 2311-2327. (c) Zaworotko, M. J.; *Chem. Soc. Rev.* **1994**, *23*, 283-288. (d) Desiraju, G. R.; *Crystal Engineering-The Design of Organic Solids*, Elsevier, 1989.

63. (a) Ashton, P. R.; Chrystal, E. J. T.; Glink, P. T.; Menzer, S.; Schiavo, C.; Stoddart, J. F.; Tasker, P. A.; Williams, D. J.; *Angew. Chem., Int. Ed. Engl.* **1995**, *34*, 1869-1871. (b) Ashton, P. R.; Claessens, C. G.; Hayes, W.; Menzer, S.; Stoddart, J. F.; White, A. J. P.; Williams, D. J.; *Angew. Chem., Int. Ed. Engl.* **1995**, *34*, 1862-1865. (c) Ortholand, J.-Y.; Slawin, A. M. Z.; Spencer, N.; Stoddart, J. F.; Williams, D. J.; *Angew. Chem., Int. Ed. Engl.* **1989**, *28*, 1394-1395.

64. (a) Schoentjes, B.; Lehn, J.-M.; *Helv. Chim. Acta* **1995**, *78*, 1-12. (b) Kramer, R.; Lehn, J.-M.; Decian, A.; Fischer, J.; *Angew. Chem., Int. Ed. Engl.* **1993**, *32*, 703-706. (c) Kramer, R.; Lehn, J.-M.; Marquisrigault, A.; *Proc. Natl. Acad. Sci. USA* **1993**, *90*, 5394-5398. (d) Pfeil, A.; Lehn, J.-M.; *J. Chem. Soc., Chem. Commun.* **1992**, 838-840. (e) Garrett, T. M.; Koert, U.; Lehn, J.-M.; *J. Phys. Org.* **1992**, *5*, 529-532. (f) Zarges, W.; Hall, J.; Lehn, J.-M.; Bolm, C.; *Helv. Chim. Acta* **1991**, *74*, 1843-1852. (g) Harding, M. M.; Koert, U.; Lehn, J.-M.; Marquisrigault, A.; Piguet, C.; Siegel, J.; *Helv. Chim. Acta* **1991**, *74*, 594-610. (h) Youinou, M. T.; Ziessel, R.; Lehn, J.-M.; *Inorg. Chem.* **1991**, *30*, 2144-2148. (i) Garrett, T. M.; Koert, U.; Lehn, J.-M.; Rigault, A.; Meyer, D.; Fischer, J.; *J. Chem. Soc., Chem. Commun.* **1990**, 557-558. (j) Koert, U.; Harding, M. M.; Lehn, J.-M.; *Nature* **1990**, *346*, 339-342. (k) Lehn, J.-M.; Rigault, A.; *Angew. Chem., Int. Ed. Engl.* **1988**, *27*, 1095-1097. (l) Lehn, J.-M.; Rigault, A.; Siegel, J.; Harrowfield, J.; Chevrier, B.; Moras, D.; *Proc. Natl. Acad. Sci. USA* **1987**, *84*, 2565-2569. (m) Lehn, J.-M.; Sauvage, J. P.; Ziessel, R.; Piccinni-Leopardi, C.; Germain, G.; Declerq, J. P.; Van Meerssche, M.; *Nouv. J. Chem.* **1983**, *7*, 413-420.

65. (a) Constable, E. C.; Heirtzler, F. R.; Neuburger, M.; Zehnder, M.; *Supramolec. Chem.* **1995**, *5*, 197-200. (b) Constable, E. C.; Edwards, A. J.; Hannon, M. J.; Raithby, P. R.; *J. Chem. Soc. Chem. Commun.* **1995**, 1991-1992. (c) Constable, E. C.; Hannon, M. J.; Edwards, A. J.; Raithby, P. R.; *J. Chem. Soc. Dalton Trans.* **1994**, 2669-2677. (d) Constable, E. C.; *Prog. Inorg. Chem.* **1994**, *42*, 67-138. (e) Constable, E. C.; Edwards, A. J.; Raithby, P. R.; Walker, J. V.; *Angew. Chem. Int. Ed. Engl.* **1993**, *32*, 1465-1467. (f) Constable, E. C.; Daniels, M. A. M.; Drew, M. G. B.; Tocher, D. A.; Walker, J. V.; Wood, P. D.; *J. Chem. Soc. Dalton Trans.* **1993**, 1947-1958. (g) Constable, E. C.; Hannon, M. J.; Tocher, D. A.; *J. Chem. Soc. Dalton Trans.* **1993**, 1883-1890. (h) Constable, E. C.; Hannon, M. J.; Tocher,

D. A.; *Angew. Chem., Int. Ed. Engl.* **1992**, *31*, 230-323. (i) Constable, E. C.; Walker, J. V.; *J. Chem. Soc., Chem. Commun.* **1992**, 884-886. (j) Constable, E. C.; Walker, J. V.; Tocher, D. A.; Daniels, M. A. M.; *J. Chem. Soc., Chem. Commun.* **1992**, 768-771. (k) Constable, E. C.; Chotalia, R.; *J. Chem. Soc., Chem. Commun.* **1992**, 64-66. (l) Constable, E. C.; Hannon, M. J.; Martin, A.; Raithby, P. R.; Tocher, D. A.; *Polyhedron* **1992**, *11*, 2967-2971. (m) Constable, E. C.; *Tetrahedron* **1992**, *48*, 10013-10059. (n) Constable, E. C.; *Angew. Chem., Int. Ed. Engl.* **1991**, *30*, 1450-1451. (o) Constable, E. C.; Ward, M. D.; Tocher, D. A.; *J. Chem. Soc. Dalton Trans.* **1991**, 1675-1683. (p) Constable, E. C.; Elder, S. M.; Raithby, P. R.; Ward, M. D.; *Polyhedron* **1991**, *10*, 1395-1400. (q) Constable, E. C.; Elder, S. M.; Healy, J. A.; Ward, M. D.; Tocher, D. A.; *J. Am. Chem. Soc.* **1990**, *112*, 4590-4592. (r) Constable, E. C.; Ward, M. D.; Tocher, D. A.; *J. Am. Chem. Soc.* **1990**, *112*, 1256-1258. (s) Constable, E. C.; Ward, M. D.; Drew, M. G. B.; Forsyth, G. A.; *Polyhedron* **1989**, *8*, 2551-2555. (t) Barley, M.; Constable, E. C.; Corr, S. A.; McQueen, R. C. S.; Nutkins, J. C.; Ward, M. D.; Drew, M. G. B.; *J. Chem. Soc. Dalton Trans.* **1988**, 2655-2662. (u) Constable, E. C.; Drew, M. G. B.; Ward, M. D.; *J. Chem. Soc., Chem. Commun.* **1987**, 1600-1601.

66. (a) Potts, K. T.; Keshavarz-K, M.; Tham, F. S.; Gheysen-Raiford, K. A.; Arana, C.; Abruna, H. D.; *Inorg. Chem.* **1993**, *32*, 5477-5484 (b) Potts, K. T.; Keshavarz-K, M.; Tham, F. S.; Abruna, H. D.; Arana, C. R.; *Inorg. Chem.* **1993**, *32*, 4450-4456. (c) Potts, K. T.; Keshavarz-K, M.; Tham, F. S.; Abruna, H. D.; Arana, C. R.; *Inorg. Chem.* **1993**, *32*, 4436-4449. (d) Potts, K. T.; Keshavarz-K, M.; Tham, F. S.; Abruna, H. D.; Arana, C. R.; *Inorg. Chem.* **1993**, *32*, 4422-4435. (e) Potts, K. T.; Horwitz, C. P.; Fessak, A.; Nash, K. E.; Toscano, P. J.; *J. Am. Chem. Soc.* **1993**, *115*, 10444-10445. (f) Potts, K. T.; Gheysen-Raiford, K. A.; Keshavarz-K,

M.; *J. Am. Chem. Soc.* **1993**, *115*, 2793-2807. (g) Potts, K. T.; *Bull. Soc. Chim. Belg.* **1990**, *99*, 741-768.

67. (a) Piguet, C.; Bocquet, B.; Hopfgartner, G.; *Helv. Chim. Acta* **1994**, *77*, 931-942. (b) Piguet, C.; Hopfgartner, G.; Bocquet, B.; Schaad, O.; Williams, A. F.; *J. Am. Chem. Soc.* **1994**, *116*, 9092-9102. (c) Hopfgartner, G.; Piguet, C.; Henion, J. D.; Williams, A. F.; *Helv. Chim. Acta* **1993**, *76*, 1759-1766. (d) Piguet, C.; Williams, A. F.; Bernardinelli, G.; Bunzli, J. C. G.; *Inorg. Chem.* **1993**, *32*, 4139-4149. (e) Piguet, C.; Bunzli, J. C. G.; Bermardinelli, G.; Hopfgartner, G.; Williams, A. F.; *J. Am. Chem. Soc.* **1993**, *115*, 8197-8206. (f) Piguet, C. Bernardinelli, G.; Bocquet, B.; Quattropani, A.; Williams, A. F.; *J. Am. Chem. Soc.* **1992**, *114*, 7440-7451. (g) Ruthman, S.; Piguet, C.; Bernardinelli, G.; Bocquet, B.; Williams, A. F.; *J. Am. Chem. Soc.* **1992**, *114*, 4230-4237. (h) Williams, A. F.; Piguet, C.; Bernardinelli, G.; *Angew. Chem., Int. Ed. Engl.* **1991**, *30*, 1490-1492. (i) Piguet, C.; Bernardinelli, G.; Williams, A. F.; *Inorg. Chem.* **1989**, *28*, 2920-2925.

68. (a) Ziessel, R.; Youinou, M.-T.; *Angew. Chem., Int. Ed. Engl.* **1993**, *32*, 877-880. (b) Goodgame, D. M. L.; Hill, S. P. W.; Williams, D. J.; *J. Chem. Soc., Chem. Commun.* **1993**, 1019-1021.

69. (a) Baxter, P. N. W.; Lehn, J.-M.; Fischer, J.; Youinou, M.-T.; *Angew. Chem. Int. Ed. Engl.* **1994**, *33*, 2284-2287. (b) Drain, C. M.; Lehn, J., Jr.; *J. Chem. Soc., Chem. Commun.* **1994**, 2313-2315 (correction see *J. Chem. Soc., Chem. Commun.* **1995**, 503).

70. (a) Baxter, P.; Lehn, J.-M.; Decian, A.; Fischer, J.; *Angew. Chem., Int. Ed. Engl.*

1993, *32*, 69-72. (b) Leize, E.; van Dorsselaer, A.; Kramer, R.; Lehn, J.-M.; *J. Chem. Soc., Chem. Commun.* **1993**, 990-993.

71. (a) Subramian, S.; Zaworotko, M. J.; *Angew. Chem., Int. Ed. Engl.* **1995**, *34*, 2127-2129. (b) Constable, E. C.; Cargill Thompson, A. M. W.; Macko, L.; Zehnder, M.; *Chem. Eur. J.* **1995**, *1*, 360-367. (c) Fujita, M.; Kwon, Y. J.; Sasaki, O.; Yamaguchi, K.; Ogura, K.; *J. Am. Chem. Soc.* **1995**, *117*, 7287-7288. (d) Serroni, S.; Denti, G.; Campagna, S.; Juris, A.; Ciano, M.; Balzani, V.; *Angew. Chem., Int. Ed. Engl.* **1992**, *31*, 1493-1495. (e) Robson, R.; Abrahams, B. F.; Batten, S. R.; Gable, R. W.; Hoskins, B. F.; Liu, J.; *Supramolecular Architecture*, Bein, T. (ed); ACS Symposium Series 499; American Chemical Society: Washington DC, 1992, chapter 19. (f) in *Inclusion Compounds*, Vol 1, Atwood, J. L.; Davies, J. E. D.; MacNicol, D. D. (eds); Academic Press, 1991, chapter 6, 177-212. (g) Iwamoto, T. (chapter 2); (h) Liplowski, J. (chapter 3); (i) Hanotier, J.; de Radizitzky, P. (chapter 4); Iwamoto, T.; in *Inclusion Compounds*, Vol 5, Atwood, J. L.; Davies, J. E. D.; MacNicol, D. D. (eds); Academic Press, 1984, chapters 2-4, 29-134.

72. (a) Stang, P. J.; Chen, K.; *J. Am. Chem. Soc.* **1995**, *117*, 1667-1668. (b) Fujita, M.; Nagao, S.; Ogura, K.; *J. Am. Chem. Soc.* **1995**, *117*, 1649-1650. (c) Fujita, M.; Oguro, D.; Miyazawa, M.; Oka, H.; Yamaguchi, K.; Ogura, K.; *Nature* **1995**, *378*, 469-471. (d) Goodman, M. S.; Jubian, V.; Hamilton, A. D.; *Tetrahedron Lett.* **1995**, *36*, 2551-2554. (e) Hunter, C. A.; Sarson, L. D.; *Angew. Chem., Int. Ed. Engl.* **1994**, *33*, 2313-2316. (f) Lee, J.; Schwabacher, A. W.; *J. Am. Chem. Soc.* **1994**, *116*, 8382-8383. (g) Stang, P. J.; Cao, D. H.; *J. Am. Chem. Soc.* **1994**, *116*, 4981-4982. (h) Stang, P. J.; Whiteford, J. A.; *Organometallics* **1994**, *13*, 3776-3777. (i) Jones, M. W.; Gupta, N.; Schepartz, A.; Thop, H. H.; *Inorg. Chem.*

1992, *31*, 1308-1310. (j) Schall, O. F.; Robinson, K.; Atwood, J. L.; Gokel, G. W.; *J. Am. Chem. Soc.* **1993**, *115*, 5962-5969. (k) Fujita, M.; Nagao, S.; Iida, M.; Ogata, K.; Ogura, K.; *J. Am. Chem. Soc.* **1993**, *115*, 1574-1576. (l) Schwabacher, A. W.; Lee, J.; Lei, H.; *J. Am. Chem. Soc.* **1992**, *114*, 7597-7598. (m) Schall, O. F.; Robinson, K.; Atwood, J. L.; Gokel, G. W.; *J. Am. Chem. Soc.* **1991**, *113*, 7434-7435. (n) Fujita, M.; Yazaki, J.; Ogura, K.; *Tetrahedron Lett.* **1991**, *32*, 5589-5592. (o) Maverick, A. W.; Ivie, M. L.; Waggenspack, J. W.; Fronzek, F. R.; *Inorg. Chem.* **1990**, *29*, 2403-2409. (p) Fujita, M.; Yazaki, J.; Ogura, K.; *J. Am. Chem. Soc.* **1990**, *112*, 5645-5647. (q) Schepartz, A.; McDevitt, J. P.; *J. Am. Chem. Soc.* **1989**, *111*, 5976-5977. (r) Maverick, A. W.; Buckingham, S. C.; Bradbury, J. R.; Yao, Q.; Stanly, G. G.; *J. Am. Chem. Soc.* **1986**, *108*, 7430-7431. (s) Maverick, A. W.; Klavetter, F. E.; *Inorg. Chem.* **1984**, *23*, 4129-4130.

73. (a) Ghadiri, M. R.; Case, M. A.; *Angew. Chem., Int. Ed. Engl.* **1993**, *32*, 1594-1597. (b) Ghadiri, M. R.; Soares, C.; Choi, C.; *J. Am. Chem. Soc.* **1992**, *114*, 4000-4002. (c) Ghadiri, M. R.; Soares, C.; Choi, C.; *J. Am. Chem. Soc.* **1992**, *114*, 825-831. (d) Lieberman, M.; Sasaki, T.; *J. Am. Chem. Soc.* **1991**, *113*, 1470-1471. (e) Ghadiri, M. R.; Fernholz, A. K.; *J. Am. Chem. Soc.* **1990**, *112*, 9633-9635. (f) Ghadiri, M. R.; Choi, C.; *J. Am. Chem. Soc.* **1990**, *112*, 1630-1632.

74. (a) Menger, F. M.; *Chem. Brit.* **1993**, *29*, 300-302. (b) Menger, F. M.; *Angew. Chem., Int. Ed. Engl.* **1991**, *30*, 1086-1099.

75. (a) Ciuchi, F.; Nicola, G. D.; Franz, H.; Gottarelli, G.; Mariani, P.; Bossi, M. G. P.; Spada, G. P.; *J. Am. Chem. Soc.* **1994**, *116*, 7064-7071. (b) Garbesi, A.; Gottarelli, G.; Mariani, P.; Spada, G. P.; *Pure Appl. Chem.* **1993**, *65*, 641-646. (c) Detellier, C.; Laszlo, P.; *Helv. Chim. Acta* **1979**, *62*, 1559-1565. (d) Klump, H.;

Ber. Bunsen-Gesellschaft **1976**, *80*. 121-124. (e) Gellert, M.; Lipsett, M. N.; Davies, D. R.; *Proc. Natl. Acad. Sci. USA* **1962**, *48*, 2013-2018.

76. (a) Menger, F. M.; Lee, S. S.; Tao, X.; *Adv. Mater.* **1995**, *7*, 669-671. (b) Menger, F. M.; Yamasaki, Y.; Catlin, K. K.; Nishimi, T.; *Angew. Chem., Int. Ed. Engl.* **1995**, *34*, 585-586. (c) Menger, F. M.; Lee, S. J.; *J. Am. Chem. Soc.* **1994**, *116*, 5987-5988. (d) Newkome, G. R.; Moorfield, C. N.; Baker, G. R.; Behera, R. K.; Escamillia, G. H.; Saunders, M. J.; *Angew. Chem., Int. Ed. Engl.* **1992**, *31*, 917-919. (e) Newkome, G. R.; Baker, G. R.; Arai, S.; Saunders, M. J.; Russo, P. S.; Theriot, K. J.; Moorefield, C. N.; Rogers, L. E.; Miller, J. E.; Lieux, T. R.; Murray, M. E.; Phillips, B.; Pascal, L.; *J. Am. Chem. Soc.* **1990**, *112*, 8458-8465.

77. (a) Ghadiri, M. R.; *Adv. Mater.* **1995**, *7*, 675-677. (b) Ghadiri, M. R.; Kobayashi, K.; Granja, J. R.; Chadha, R. K.; McRee, D. E.; *Angew. Chem., Int. Ed. Engl.* **1995**, *34*, 93-95. (c) Sun, X.; Lorenzi, G. P.; *Helv. Chim. Acta* **1994**, *77*, 1520-1526. (d) Granja, J. R.; Ghadiri, M. R.; *J. Am. Chem. Soc.* **1994**, *116*, 10785-10786. (e) Khazanovich, N.; Granja, J. R.; McRee, D. E.; Milligan, D. A.; Ghadiri, M. R.; *J. Am. Chem. Soc.* **1994**, *116*, 6011-6012. (f) Saviano, M.; Zaccaro, L.; Lombardi, A.; Pedone, C.; Diblasio, B.; Sun, X. C.; Lorenzi, G. P.; *J. Inclusion Phenom. Mol. Rec.* **1994**, *18*, 27-36. (g) Ghadiri, M. R.; Granja, J. R.; Buehler, L. K.; *Nature* **1994**, *369*, 301-304. (h) Ghadiri, M. R.; Granja, J. R.; Milligan, R. A.; Mcree, D. E.; Khazanovich, N.; *Nature* **1993**, *366*, 324-327 (correction see *Nature* **1994**, *372*, 709). (i) De Santis, P.; Morosetti, S.; Rizzo, R.; *Macromolecules* **1974**, *7*, 52-58.

78. (a) Laughlan, G.; Murchie, A. I. H.; Norman, D. G.; Moore, M. H.; Moody, P. C.

E.; Lilley, D. M. J.; Luisi, B.; Science 1994, 265, 520-524. (b) Gupta, G.; Garcia, A. E.; Guo, Q.; Lu, M.; Kallenbach, N. R.; *Biochemistry* **1993**, *32*, 7098-7103. (c) Wang, K. Y.; McCurdy, S.; Shea, R. G.; Swaminathan, S.; Bolton, P. H.; *Biochemistry* **1993**, *32*, 1899-1904. (d) Hardin, C. C.; Henderson, E.; Watson, T.; Prosser, J. K.; *Biochemistry* **1991**, *30*, 4460-4472. (d) Kim, J.; Cheong, C.; Moore, P. B.; *Nature* **1991**, *351*, 331-332. (e) Blackburn, E. H.; *Nature* **1991**, *350*, 569-573. (f) Sen, D.; Gilbert, W.; *Nature* **1990**, *344*, 410-414. (g) Williamson, J. R.; Raghuraman, M. K.; Cech, T. R.; *Cell* **1989**, *59*, 871-880. (h) Sundquist, W. I.; Klug, A.; *Nature* **1989**, *342*, 825-829. (i) Sen, D.; Gilbert, W.; *Nature* **1988**, *334*, 364-366.

79. (a) Jones, M. N.; Chapman, D.; *Micelles, Monolayers, and Biomembranes*, Wiley-Liss, 1995. (b) *Micelles, Membranes, Microemulsions, and Monolayers*; Gelbart, W. M.; Ben-Shaul, A.; Roux, D. (eds); Springer-Verlag, 1994. (c) N. Funasaki; *Adv. Colloid Inter. Sci.*, **1993**, *43*, 87-136. (d) Moroi, Y.; Micelles: *Theoretical and Applied Aspects*, Plenum Press, 1992. (e) Nagarajan, R.; Ruckenstein, E.; *Langmuir*, **1991**, *7*, 2934-2969. (f) Grieser, F.; Drummond, C. J.; *J. Phys. Chem.*, **1988**, *92*, 5580-5593. (g) Nagarajan, R.; *Adv. Colloid Inter. Sci.*, **1986**, *26*, 205-264. (h) *Physics of Amphiphiles: Micelles, Vesicles, and Microemulsions*, Degiorgio, V.; Corti, M; (eds), North-Holland, 1985. (i) *Physics of Amphiphiles: Micelles, Vesicles, and Microemulsions*, Degiorgio, V.; Corti, M. (eds); North Holland, 1985. (j) *Aggregation Processes in Solution*, Wyn-Jones, E.; Gormally, J; (eds), Elsevier Scientific Publishing Company, 1983. (k) Eicke, H.-F.; *Chimia*, **1982**, *36*, 241-246. (l) Menger, F. M.; *Acc. Chem. Res.* **1979**, *4*, 111-117. (m) Fendler, J. H.; Fendler, E. J.; *Catalysis in Micellar and Macromolecular Systems*, Academic Press, 1975.

Chapter 2:
Molecular Recognition with Cyclophane Hosts in Aqueous Media. Measurement of Association Constants with Circular Dichroism.

Chapter 2

Molecular Recognition with Cyclophane Hosts in Aqueous Media. Measurement of Association Constants with Circular Dichroism.[1]

2.1 Introduction

Previous studies in the Dougherty group have conclusively established the formation of 1:1 complexes between host **P** (Figure 2.1) and a number of neutral and cationic molecules in aqueous solution.[2] Quantitative estimates of the binding constants for these 1:1 complexes were established primarily through the use of ^{1}H NMR spectroscopy.[2] These studies further established that the guest molecule resides within the cavity of the host molecule in the complex, and it was shown that molecules containing no binding cavity (**1** and **2**, Figure 2.1) do not form complexes with guests in aqueous solution.[2b,3]

The NMR method used in these studies follows standard protocols for studying binding interactions in host-guest systems.[4-6] NMR is a powerful tool for use in these studies, allowing measurement of thermodynamic binding constants as well as providing information on the structure of the complexes being formed.[4-6] However, there are limitations. These limitations arise when the hosts and/or guests have low solubilities or critical aggregation concentrations (CAC) and when relaxation phenomena result in a loss of signal. For the cyclophanes studied in our laboratories, these problems limit the range of binding constants we can measure to $-\Delta G^\circ_a \leq 8.0$ kcal/mol.[1,2a]

Optical methods (UV/Vis and circular dichroism spectroscopy) are attractive alternatives to NMR due to a higher instrumental sensitivity. UV/Vis spectroscopy can be employed to overcome some of the NMR problems by allowing studies at lower concentrations. This also allows for more accurate evaluation of the equilibrium constants

since activity coefficients approach values of unity under these conditions.[7] Unfortunately, the UV spectra of cyclophane molecules (P) are often not very informative; they typically appear with multiple overlapping absorption bands. This requires guests with long wavelength (colored) absorption bands for elucidation of structural information on binding. Circular dichroism (CD) spectroscopy on the other hand provides spectra in which the overlapping absorptions are resolved for chiral molecules, but still operates at low concentration. Additionally, CD spectra are very sensitive to geometry changes in the absorbing species, allowing information about the conformation of a chiral host to be obtained in the presence of a guest.

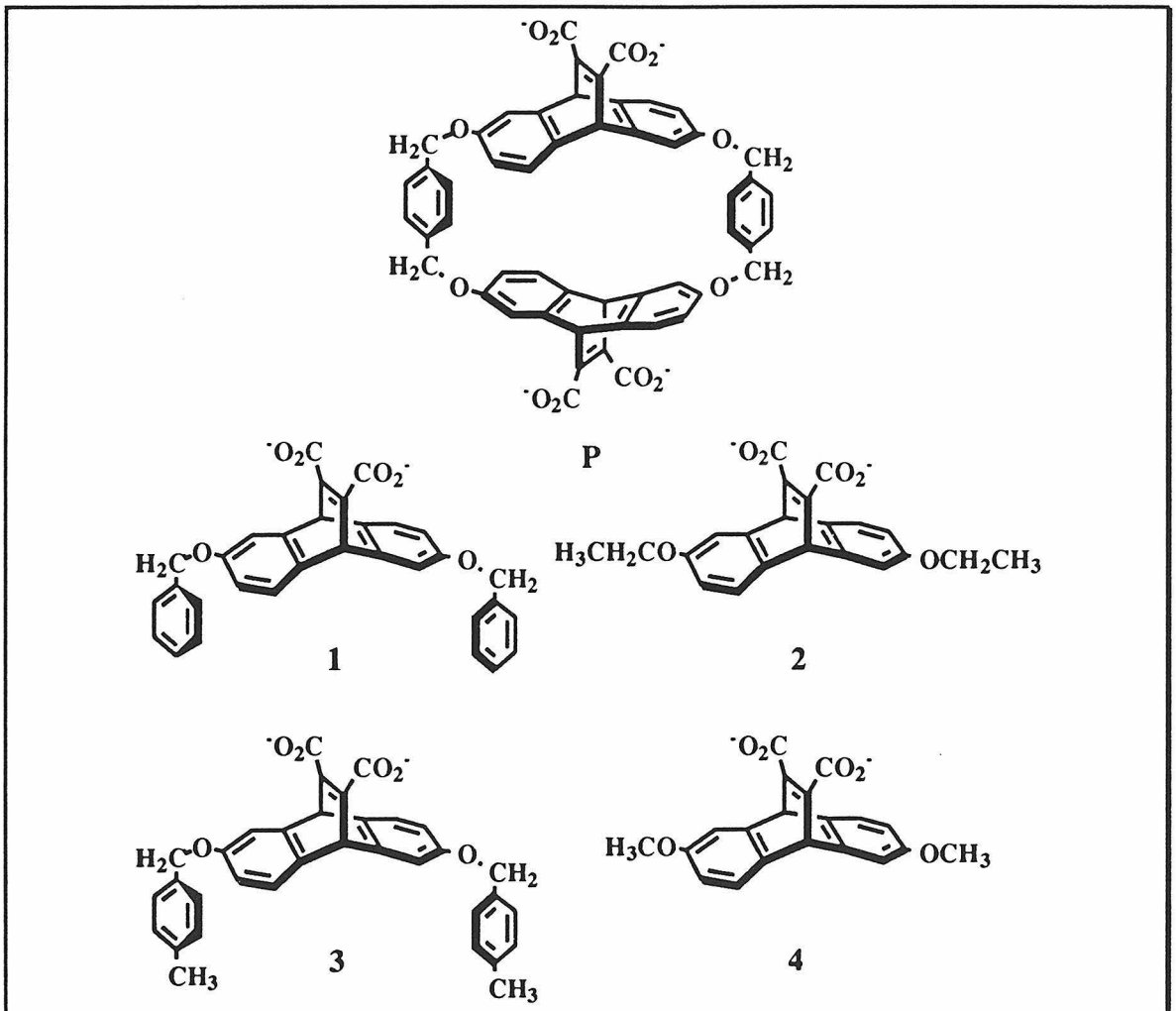

Figure 2.1. Host P and non-macrocyclic control molecules studied in this chapter.

The intrinsic chirality (D_2-symmetry) of host **P** makes circular dichroism (CD) spectroscopy a potentially powerful probe of binding interactions with this host. CD spectroscopy provides the advantages of UV concentrations as well as highly informative spectra with respect to structural information. For studies of host **P** (and analogous hosts), CD allows us to take advantage of the chirality of the system, a feature of these hosts that has been largely neglected in the previous NMR studies.[2] While CD spectroscopy has been used extensively for studying inclusion in cyclodextrin hosts[8-12] and substrate binding in biological systems,[13] its application for the study of synthetic host systems has been limited.[14-16]

2.2 Circular Dichroism (CD) Spectroscopy[16]

2.2.1 Introduction

Circular dichroism spectroscopy is a form of UV/Visible spectroscopy that employs linearly polarized light.[17] A linearly polarized beam of light can be decomposed into two circular components of equal amplitude-right circularly polarized light and left circularly polarized light (Figure 2.2).[17] These two components cancel each other to give the linearly polarized beam.[17] For an achiral molecule (in an achiral environment) the extinction coefficients, ε_l and ε_r, for the absorption of left and right circularly polarized light respectively, are equivalent.[17] For an optically active molecule, these extinction coefficients are inequivalent for any given absorption ($\varepsilon \neq o$), and the circular dichroism (in units of $M^{-1}cm^{-1}$) is defined by equation 2.1.[17]

$$\Delta\varepsilon = \varepsilon_l - \varepsilon_r \qquad (2.1)$$

The result of this differential absorption of the circularly polarized components is that the transmitted light will have a greater contribution of one of the circularly polarized

components.[17] The components no longer cancel each other, instead the transmitted light beam becomes elliptic (Figure 2.3).[17] The eccentricity (ellipticity, θ_λ, in millidegrees) of the ellipse of the transmitted light is measured at each wavelength of the spectrum and relates to the circular dichroism at a given wavelength as shown in equation 2.2,[17]

$$\theta_\lambda = g\Delta\varepsilon_\lambda lc \tag{2.2}$$

$$g = \frac{2.30259}{100} \times \frac{4500}{\pi} \times 1000 \tag{2.3}$$

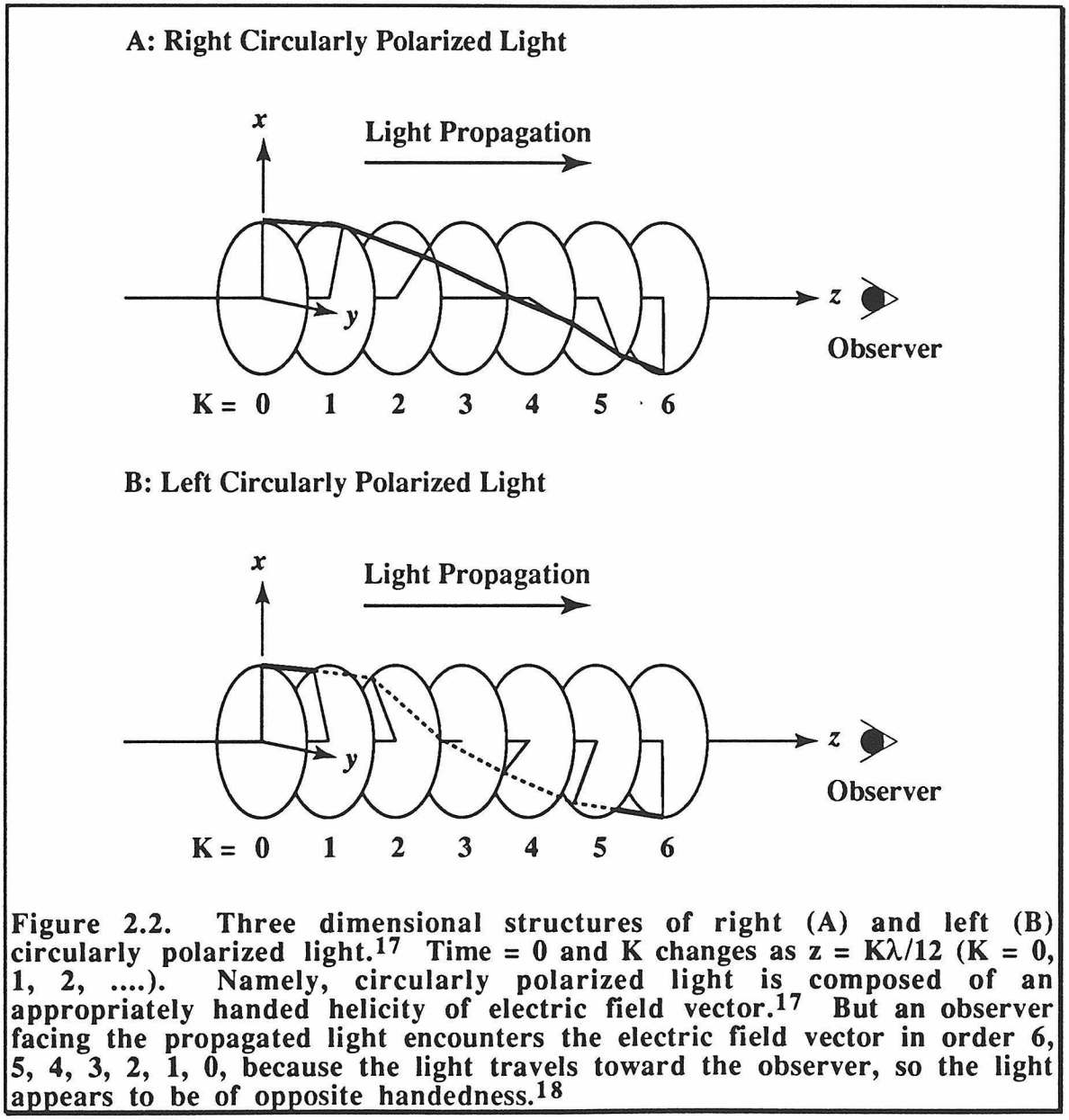

Figure 2.2. Three dimensional structures of right (A) and left (B) circularly polarized light.[17] Time = 0 and K changes as z = Kλ/12 (K = 0, 1, 2, ...). Namely, circularly polarized light is composed of an appropriately handed helicity of electric field vector.[17] But an observer facing the propagated light encounters the electric field vector in order 6, 5, 4, 3, 2, 1, 0, because the light travels toward the observer, so the light appears to be of opposite handedness.[18]

where c is the concentration of the absorbing species (M), l is the pathlength of the cell (cm), and θ_λ is measured in millidegrees. A circular dichroism active absorption band is called a Cotton effect and its rotational strength (R) is defined as the area under the curve of the absorption band.[17] Enantiomers rotate the plane of polarized light in equal amounts but opposite directions and thus CD spectra of a pair of enantiomers will have Cotton effects of equal magnitude but opposite sign (Figure 2.4).[17]

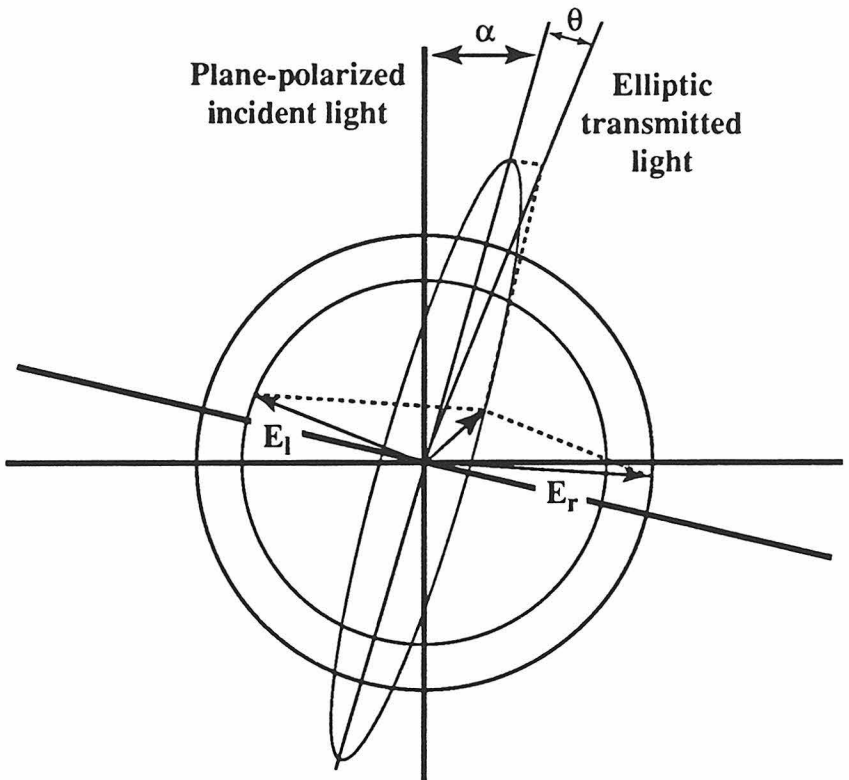

Figure 2.3. Definition of optical rotation and ellipticity.[18] The elliptic transmitted light as seen by an observer facing the direction of the propagated light (for the case of $\varepsilon_l > \varepsilon_r$).[18]

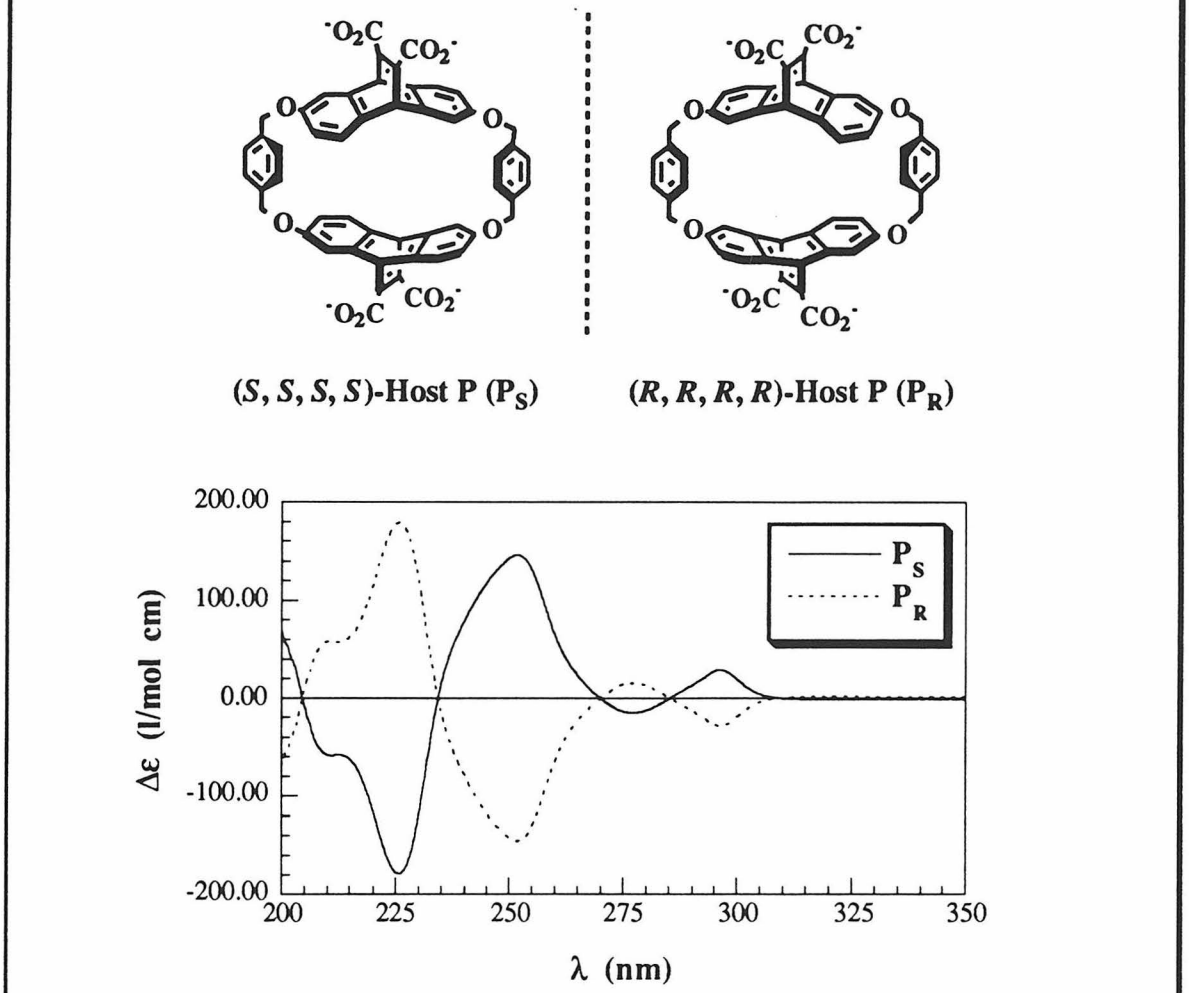

Figure 2.4. Circular dichroism spectra of the enantiomers of Host P in aqueous borate buffer (pH 9).

2.2.2 Measurement of Binding Constants with CD[1,19]

The equations and procedures described in this section (as well as in sections 2.2.3, 2.2.4, and 2.2.5) were developed in collaboration with Richard E. Barrans, Jr.

For a system containing a host (H) and guest (G) that are in equilibrium with the 1:1 host-guest complex **HG** (equation 2.4): the equilibrium constant, K, is given by

equation 2.5 and the mass balance relations for the total host ($[\mathbf{H}]_o$) and total guest ($[\mathbf{G}]_o$) are given by equations 2.6, and 2.7.[4,5]

$$\mathbf{H} + \mathbf{G} \rightleftharpoons \mathbf{HG} \tag{2.4}$$

$$K = \frac{[\mathbf{HG}]}{[\mathbf{H}][\mathbf{G}]} \tag{2.5}$$

$$[\mathbf{H}]_o = [\mathbf{H}] + [\mathbf{HG}] \tag{2.6}$$

$$[\mathbf{G}]_o = [\mathbf{G}] + [\mathbf{HG}] \tag{2.7}$$

The equilibrium concentration of **HG** can be determined from equation 2.8, when the equilibrium constant is known.

$$[\mathbf{HG}] = \frac{1}{2}\left\{[\mathbf{H}]_o + [\mathbf{G}]_o + \frac{1}{K} - \sqrt{\left([\mathbf{H}]_o + [\mathbf{G}]_o + \frac{1}{K}\right)^2 - 4[\mathbf{H}]_o[\mathbf{G}]_o}\right\} \tag{2.8}$$

The procedure for determining the equilibrium constant, K, from a set of CD spectra at different total host ($[\mathbf{H}]_o$) and total guest ($[\mathbf{G}]_o$) concentrations is similar to that for obtaining K from NMR data, as in our previously described NMRfit and EMUL programs.[4]

The basic assumption of our model is that the observed ellipticity at wavelength λ of a sample containing free host (**H**), free guest (**G**), and host-guest complex (**HG**) is given by equation 2.9,

$$\theta_\lambda = gl\left(\Delta\varepsilon_{\mathbf{H}\lambda}[\mathbf{H}] + \Delta\varepsilon_{\mathbf{G}\lambda}[\mathbf{G}] + \Delta\varepsilon_{\mathbf{HG}\lambda}[\mathbf{HG}]\right) \tag{2.9}$$

where θ_λ = the observed ellipticity at wavelength λ (millidegrees, m°), $\Delta\varepsilon_{i\lambda}$ = the molar circular dichroism of species i at wavelength λ, and [i] = the concentration of species i. Substituting the expressions for total host concentration, and total guest concentration (equations 2.6 and 2.7, respectively) into equation 2.9 results in equation 2.10:

$$\theta_\lambda = gl\{\Delta\varepsilon_{H\lambda}[H]_o + \Delta\varepsilon_{G\lambda}[G]_o + E_\lambda[HG]\} \quad (2.10')$$

where

$$E_\lambda = \Delta\varepsilon_{HG\lambda} - \Delta\varepsilon_{H\lambda} - \Delta\varepsilon_{G\lambda} \quad (2.11)$$

E_λ, an unknown quantity, is the change in molar ellipticity arising upon complexation. The value of [HG] is determined by K, $[H]_o$, and $[G]_o$ (equation 2.8). The optical constants for the free species ($\Delta\varepsilon_H$ and $\Delta\varepsilon_G$) are experimentally measured and thus represent known quantities in these equations.

The task of the fitting procedure is to find K and E_λ to minimize equation 2.12, over the N experimental samples n and L observed wavelengths λ (analogous to the estimation of K and D from NMR data).[4]

$$SSR = \sum_{n=1}^{N} \sum_{\lambda}^{L} \left(\theta_{n\lambda\ calc} - \theta_{n\lambda\ obs}\right)^2 \quad (2.12)$$

The best-fit value of E_λ corresponding to any K is immediately available by linear regression. The best-fit value of K, however, can only be found by iteration. Richard Barrans, Jr., developed a computer program (CDfit) that uses a Levenberg-Marquardt[20] procedure to accomplish this. Given the experimental data and an initial estimate of K, it returns the best-fit K and the set of best-fit E_λ. CDfit further converts the E_λ values into the best-fit CD spectrum of the pure host-guest complex (see Figure 2.5).

Although we have not applied this methodology to UV/Vis spectroscopy, the model is easily modified to accept this type of spectral data as well. In such studies absorbance (A) rather than ellipticity is measured; the constant g (equation 2.3) is replaced with a value of 1.00, and the circular dichroism optical constants ($\Delta\varepsilon$) are replaced with the appropriate extinction coefficients (ε).

2.2.3 The CD Fitting Procedure[19]

The Levenberg-Marquardt method is described in detail elsewhere.[20] For our purposes, all that is necessary to carry out the fitting is the expression for χ^2 (this is SSR as defined in equation 2.12) and the derivatives $\partial\chi^2/\partial K$ and $\partial^2\chi^2/\partial K^2$. The derivatives follow:

$$\frac{\partial \chi^2}{\partial K} = 2\sum_{n=1}^{N}\sum_{\lambda}^{L}\left(\theta_{n\lambda\,\mathrm{calc}} - \theta_{n\lambda\,\mathrm{obs}}\right)\left(\frac{\partial \theta_{n\lambda\,\mathrm{calc}}}{\partial K}\right) \tag{2.13}$$

Where

$$\frac{\partial \theta_{n\lambda\,\mathrm{calc}}}{\partial K} = g l_n\left(E_\lambda \frac{\partial [\mathrm{HG}]_n}{\partial K} + [\mathrm{HG}]_n \frac{\partial E_\lambda}{\partial K}\right), \tag{2.14}$$

$$\frac{\partial [\mathrm{HG}]_n}{\partial K} = \frac{1}{2K}\left(\frac{[\mathrm{H}]_{on} + [\mathrm{G}]_{on} + \frac{1}{K}}{\sqrt{\left([\mathrm{H}]_{on} + [\mathrm{G}]_{on} + \frac{1}{K}\right)^2 - 4[\mathrm{H}]_{on}[\mathrm{G}]_{on}}} - 1\right), \text{ and} \tag{2.15}$$

$$\frac{\partial E_\lambda}{\partial K} = \frac{1}{g\sum_{n}^{N} l_n^2[\mathrm{HG}]_n^2}\left\{\sum_{n}^{N}\left[\theta_{n\lambda\,\mathrm{calc}} - g l_n D_\lambda\right] l_n \frac{\partial [\mathrm{HG}]_n}{\partial K} - 2gE_\lambda \sum_{n}^{N} l_n^2 [\mathrm{HG}]_n \frac{\partial [\mathrm{HG}]_n}{\partial K}\right\} \tag{2.16}$$

and where

$$D_\lambda = \Delta\varepsilon_\lambda [\mathrm{H}]_{on} + \Delta\varepsilon_\lambda [\mathrm{G}]_{on} \tag{2.17}$$

The second derivative, with the destabilizing residual term omitted, is given by equation 2.18:

$$\frac{\partial^2 \chi^2}{\partial K^2} \approx 2\sum_{n}^{N}\sum_{\lambda}^{L}\left(\frac{\partial \theta_{n\lambda\,\mathrm{calc}}}{\partial K}\right)^2 \tag{2.18}$$

For completeness, the best-fit value of E_λ at an arbitrary K is given by equation 2.19:

$$E_\lambda = \frac{\sum_n^N \left[\theta_{n\lambda\,\mathrm{calc}} - g l_n\left(\Delta\varepsilon_\lambda[\mathrm{H}]_{on} + \Delta\varepsilon_\lambda[\mathrm{G}]_{on}\right)\right] l_n[\mathrm{HG}]_n}{g\sum_n^N l_n^2[\mathrm{HG}]_n^2} \qquad (2.19)$$

2.2.4 Data Handling[19]

In NMRfit, every proton is assigned a list of the samples in which it was observed. This allows for signals broadening into the baseline, crossing, disappearing under the solvent peak, and so on.[4,5] Likewise, in CDfit a given wavelength (or wavelength range) can be eliminated from one or more samples in a set of N samples (this is done by assigning the value $\theta_\lambda = 10{,}000$ for each data point to be eliminated from the fitting), while this wavelength region is kept in the remaining samples of the set. This allows for elimination of regions where UV absorbance is either strong enough to produce high noise levels and/or other spectral artifacts in more concentrated samples, or to eliminate regions of high noise in very low concentration samples. Basically, each wavelength is assigned a reference to a list of samples; in practice, many wavelengths will be referred to the same list. New lists are created only when necessary.

2.2.5 Comparison with Other CD Methods[1,19]

The method commonly used for obtaining association constants from CD spectra was developed by Rosen.[21] Rosen's method can be used for cases in which the host has an unknown number of non-interacting binding sites for the guest, but here we will only discuss its application to the case in which the host has exactly one site. Although this method was derived for cases in which the free guest has no CD over the wavelengths studied ($\Delta\varepsilon_G = 0$), it is easily extended to cases for which $\Delta\varepsilon_G \neq 0$.

This method requires measuring the CD of a set of samples in which $[H]_o$ is held constant and $[G]_o$ varies, or vice versa. Equation 2.10 rearranges to 2.20,

$$\frac{1}{[H]_{on}}\left(\frac{\theta_{n\lambda}}{gl_n} - \Delta\varepsilon_{H\lambda}[H]_{on} - \Delta\varepsilon_{G\lambda}[G]_{on}\right) = E_\lambda \frac{[HG]_n}{[H]_{on}} \qquad (2.20)$$

in which the value on the right-hand side is $E\lambda$ multiplied by the fraction of host that is bound. For convenience, let us call this B, $B \equiv E\lambda([HG]/[H]_o)$. A plot of B as a function of $[G]_o$ forms a rectangular hyperbola with an asymptote of $E\lambda$. Near the origin of the plot, where $[G]_o$ approaches zero,[22] [HG] is equal to $[G]_o$, making the response of B to $[G]_o$ the same as its response to [HG]. Thus, a tangent line drawn to the initial region of the B vs. $[G]_o$ plot is a graph of the definition of B, giving B as a function of [HG]. This definition readily inverts to yield [HG] as a function of B. Consequently, [HG], [H], and [G] are known from the measured value of B.

K is then estimated by Scatchard analysis.[23] A plot of $B/[G]$ vs. B has a slope of $-K$ and a y-intercept of $KE\lambda$, making these parameters readily available from the plot by linear regression. Weighting each point by $1/[G]_o$ corrects for transforming the experimental observations θ_{obs} to B.

For our systems, the CDfit analysis has several advantages over the Rosen/Scatchard analysis. CDfit does not require that $[H]_o$ be held constant; any combination of informative values of $[H]_o$ and $[G]_o$ may be used. No error is introduced by estimating the initial slope of the plot. The loss score χ^2 directly measures how well the experimental data are modeled, in contrast to the equation fitted in the Scatchard analysis. Furthermore, CDfit is better suited to analyze data recorded at a number of wavelengths. There is no need to estimate L initial slopes, nor does one need to reconcile L different estimates of K from L Scatchard plots. Only one estimate of K is returned, and it is the single value, in a least squares sense, most consistent with the experimental CD spectra in their entirety. Recording and fitting data at a number of wavelengths uses all of the

available information in determining K. This not only makes the fitted K more reliable, but also directly shows the effect of binding on the host and guest circular dichroism spectra.

2.2.6 Comparison with NMRfit and EMUL Results[1,19]

The accuracy of our CD method is illustrated in the comparison of binding constants measured by this method and by our ^{1}H NMR method (Table 2.1). As shown in Table 2.1, the agreement with NMR lies within the 0.2 kcal/mol error bar range, except where the binding constant lies at the outer limits of either method. In the case of cyclophane hosts like **P**, our NMR method seems best suited to the range of 3.5 kcal/mol $\leq -\Delta G^\circ \leq$ 8.0 kcal/mol. Likewise, the CD method also has its limitations for the study of **P** and its analogs: 4.5 kcal/mol $\leq -\Delta G^\circ \leq$ 10.5 kcal/mol; the lower limit of this range approaches 5.0-6.0 kcal/mol when the guest has strong UV absorbance in spectral regions that overlap with transitions in the host. These limits of these ranges arise from a combination of solubility (and aggregation) limits and instrument sensitivity. Unlike our EMUL program, CDfit does not give a statistically meaningful estimate of error bars. Based on experimental observations and reproducibility of experiments, we estimate the error bars on a typical CD result (with good fit) to be of ±0.2 kcal/mol (the same as with our NMR measurements).

In general a CD binding study is taken to be valid when 1) statistical fitting parameters show strong agreement with our model, 2) the samples used in the experiment cover a reasonable portion of the 20-80% bound range of the more dilute component in the solution, and/or 3) the results are reproducible to $-\Delta G^\circ \pm 0.2$ kcal/mol. CDfit evaluates the statistical parameters root mean square (RMS, equations 2.21 and 2.22) and SSR (equation 2.12) for individual samples and for the entire data set; the data output includes $\theta_{n\lambda\,\mathrm{calc}}$ and $(\theta_{n\lambda\,\mathrm{calc}} - \theta_{n\lambda\,\mathrm{obs}})$ for all samples. Control experiments with our ethenoanthracenes **3** and **4** (Figure 2.1) consistently gave poorly fitting, non-reproducible data sets. Binding

constants obtained from the fitted data of these control studies were either negligible ($\Delta G° > 0$) or erroneous ($-\Delta G° > 20$ kcal/mol), providing further evidence that the preorganized cavity is required for guest binding.

$$\text{rms (individual sample)} = \sqrt{\frac{SSr}{L}} \tag{2.21}$$

$$\text{RMS (entire data set)} = \sqrt{\frac{\sum_{n=1}^{N} (\text{rms})^2}{N}} \tag{2.22}$$

Guest	$-\Delta G°$ (CD)	$-\Delta G°$ (NMR)[a]
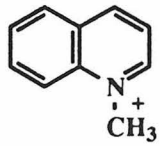 **5**	8.4 kcal/mol	(8.0) kcal/mol
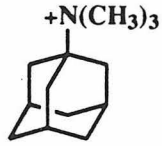 **6**	6.7	6.7
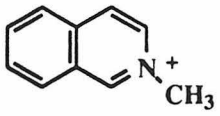 **7**	7.3	7.3
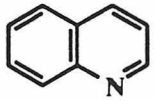 **8**	5.3	5.3
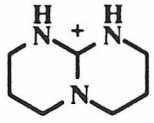 **9**	4.9	5.0

Table 2.1. Comparison of binding constants for host P measured by CD and ^{1}H NMR in pH 9 aqueous buffer.

[a]These values are considered accurate to ±0.2 kcal/mol, except for guest **5** which cannot be accurately studied with our NMR methodology.

Data which best fits the model shows the smallest values of SSR and RMS, in general RMS ≤ 0.1 and SSR ≤ 1 % of *K* are taken to be good fits. Figure 2.5 shows the output from a typical data set for guest 7 in Table 2.1.

best-fit binding constant = 214260.2689 M^{-1} ($-\Delta G°_a$ = 7.3 kcal/mol)
chi-squared (SSR) = 41.9053
geometric average deviation (RMS) = 0.0964
breakdown by spectrum:

n	*l*	$[H]_0$	$[G]_0$	%H Bound	%G Bound	ssr	rms
1	1.00	1.2×10^{-6}	1.75×10^{-6}	23.872	16.369	24.200	0.180
2	1.00	1.2×10^{-6}	3.50×10^{-6}	39.348	13.491	5.747	0.087
3	1.00	1.2×10^{-6}	5.24×10^{-6}	49.863	11.419	2.477	0.057
4	1.00	1.2×10^{-6}	6.75×10^{-6}	56.539	10.0514	2.622	0.059
5	1.00	1.2×10^{-6}	1.05×10^{-5}	67.992	7.713	4.210	0.075
6	1.00	1.2×10^{-6}	1.75×10^{-5}	78.017	5.350	2.649	0.059

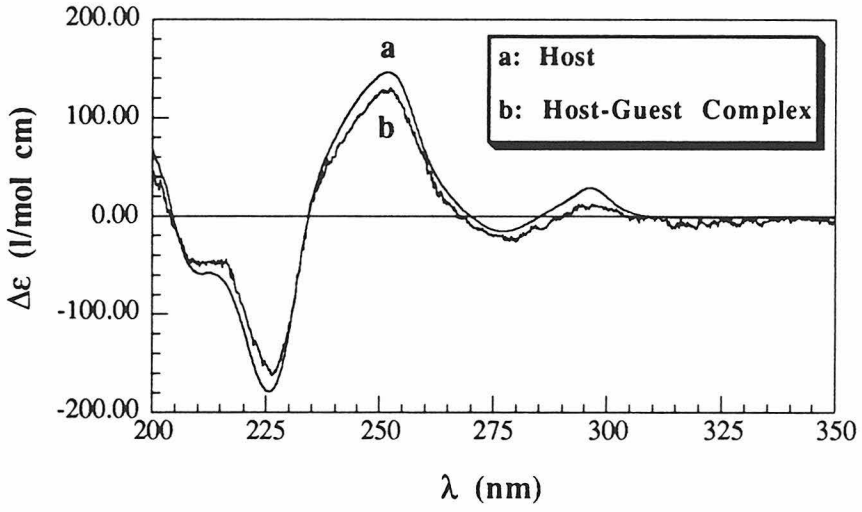

Figure 2.5. CDfit output and fitted spectrum of Host-Guest complex for guest 7 bound by host P_S in aqueous borate buffer (pH 9).

The charged guests in Table 2.1 can have a variety of counter ions. Previous work in our labs showed that counter ions have a negligible effect on binding.[2a] Of course, in the CD experiment the use of a UV/Vis-active counter ion (iodide for example) can result in erroneous data sets under conditions of low binding. When lower binding guests are used ($-\Delta G° < 6.5$ kcal/mol), the experimental conditions require guest concentrations (and thus

counter ion concentrations) to increase to levels where the counter ion absorbance becomes significant. This can result in high noise and/or spectral artifacts in the absorbing regions of the spectrum. For this reason, chloride and tetrafluoroborate are the preferred counter ions for CD studies. This susceptibility to erroneous results due to UV active achiral species is one of the major limitations of this CD methodology.

2.3 Applications of the CD Methodology[1,2a]

2.3.1 Introduction

The results described thus far in this chapter show the success of our CD methodology on systems that had already been studied by NMR. Once it had been established that we could obtain accurate and reproducible results with CD, we wished to apply the methodology to guest systems that were problematic for studies with NMR, thereby taking advantage of CD as a method that can stand on its own for studying molecular recognition. The extension of the class of guest we can study includes tightly bound, highly water soluble molecules, molecules with limited aqueous solubility, and dyes with very long wavelength absorption bands. A summary of guests studied and binding constants measured with the CD methodology is given in Figure 2.6.

2.3.2 Tightly Bound, Highly Water Soluble Molecules[1]

Guests **5** and **10-13** are highly water soluble molecules that all bind to host **P** with an affinity too large to accurately measure by NMR ($-\Delta G^\circ \geq 8.0$ kcal/mol). Guests **10** and **11** deserve special mention as these molecules have absorption bands which lie at longer wavelength than those of the host. As anticipated for the coupling of an achiral chromophore to a chiral environment (host **P**), circular dichroism can be induced into these

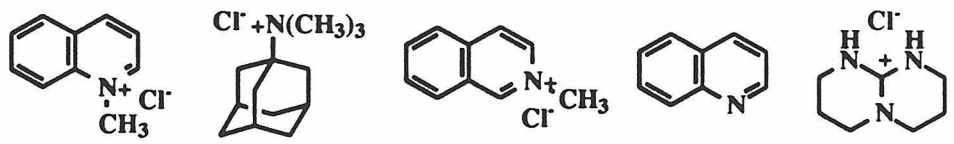

5, *8.4*

6, *6.7*

7, *7.3*

8, *5.3*

9, *4.9*

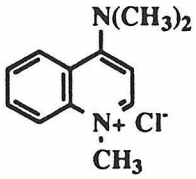

10, *8.5*

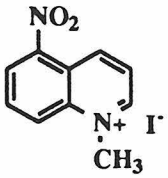

11, *8.5*

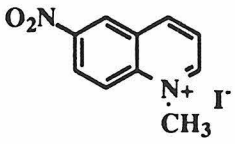

12, *8.0*

13, *8.5*

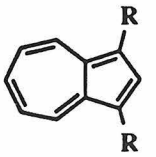

14, R = H: *9.0*

15, R = CHO: *9.4*

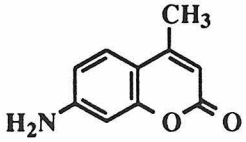

16, *6.6*

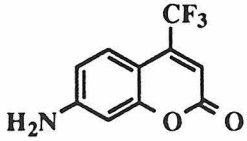

17, *9.4*

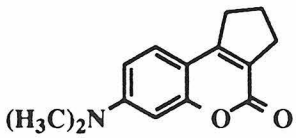

18, *9.1*

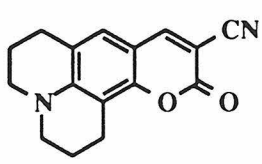

19, *9.6*

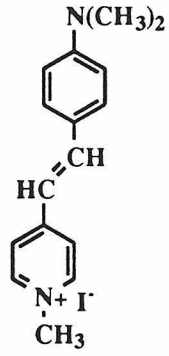

20, *7.0*

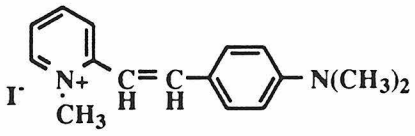

21, *7.4*

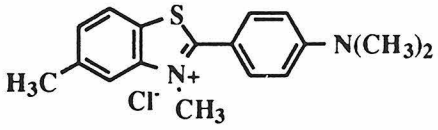

22, *7.7*

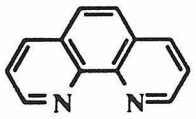

23, *6.9*

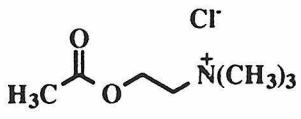

24, *6.2*

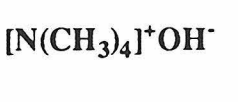

25, *5.2*

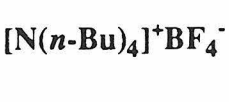

26, *5.5*

Figure 2.6. Binding constants ($-\Delta G°_a$ in kcal/mol) measured by CD with host P and a variety of guests in aqueous borate buffer (pH 9).[1]

long wavelength transitions.[24,25] Figure 2.7 shows the fitted spectrum of the host **P/10** complex, illustrating the induced negative Cotton effect ($R < 0$) centered near 350 nm. This induced CD phenomenon will be further explored in Chapter 4.

2.3.3 Sparingly Soluble Molecules[1]

The guests **14-19** represent a special class of guest for our host system. These molecules have limited aqueous solubility, with the concentration of saturated solutions near or below the NMR sensitivity limit. The high binding constants of these sparingly soluble guests can be attributed in part to strong hydrophobic forces.

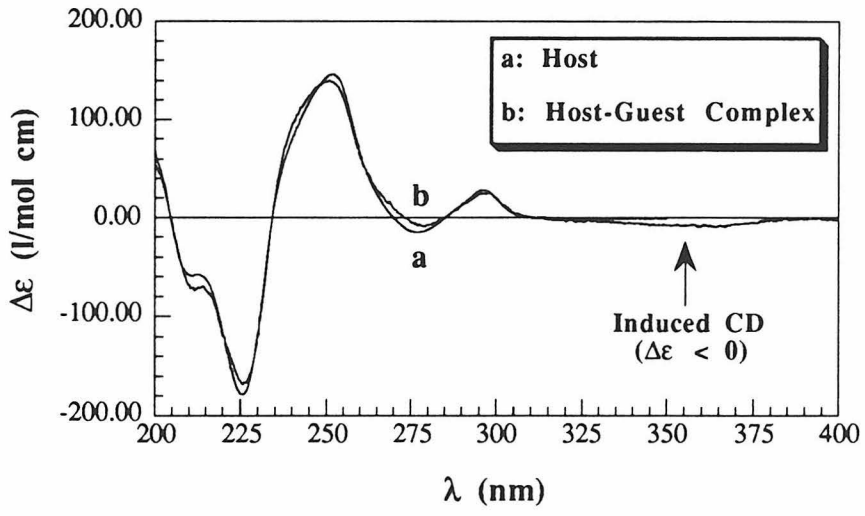

Figure 2.7. CD spectrum of host P_S and fitted spectrum of its complex with guest 10 in aqueous borate buffer (pH 9).

There are a number of interesting observations that can be made concerning guests **14-19**. First, the azulenes **14** and **15** are of interest because these molecules have a resonance structure in which the seven membered ring can be thought of as a tropylium cation (Figure 2.8).[1,2a,26] Given the strong cation-π component in the binding of guests to

host **P**, it is tempting to describe a cation-π effect with this seven membered ring. However, strong hydrophobic forces dominate the binding interaction with these guests.[1] The azulenes also show induced CD with their long-wavelength transitions;[1] **15** is particularly interesting as it shows excitonic coupling[18] (Figure 2.9) with the host.[1] These observations will be discussed in detail in Chapter 4.

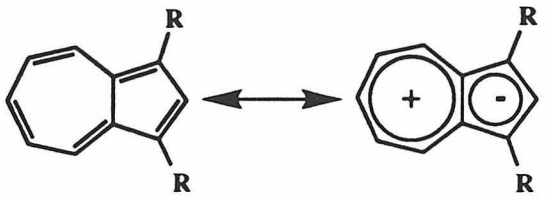

Figure 2.8. Resonance structures of azulene hydrocarbons.

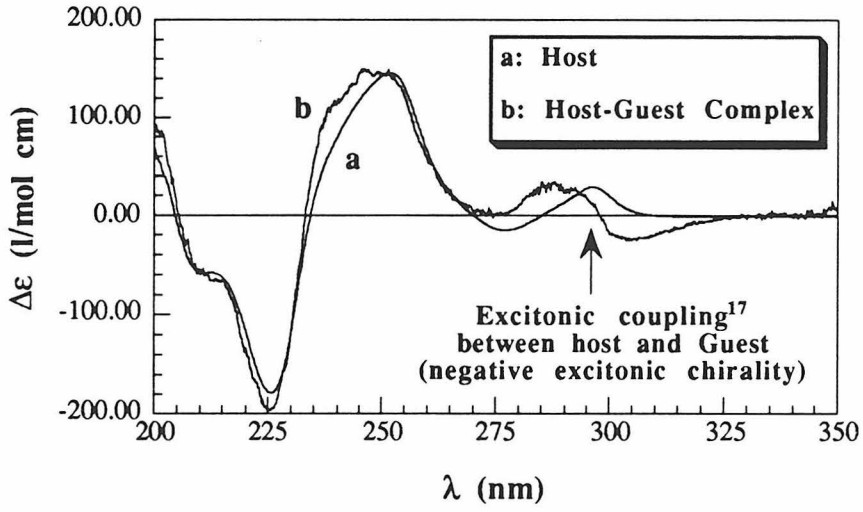

Figure 2.9. CD spectrum of host P_S and fitted spectrum of its complex with guest 15 in aqueous borate buffer (pH 9).

Guests **16** and **17** provide an interesting comparison. These two coumarins differ only by replacement of a methyl group with a trifluoromethyl group, yet their binding constants differ by a remarkable 2.8 kcal/mol.[1] One might consider this to be due to hydrophobic forces, but a comparison of octanol/water partition coefficients (log *P*)[27] for a

series of methyl and trifluoromethyl analogs (Table 2.2) shows that this substitution results in only small increases in the hydrophobic nature of the molecules.[1] We attribute the increase in binding affinity to the inductive effect of the electron withdrawing trifluoromethyl group. This leads to a stronger cation-π effect operating on the more electron deficient coumarin.[1]

Structure	Log *P*, X = CH_3	Log *P*, X = CF_3
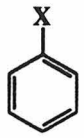 **27**	2.73	2.79
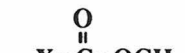 **28**	0.66	1.18
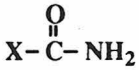 **29**	-0.13	0.12
 **30**	1.55	1.96

Table 2.2. Octanol/water partition coefficients for a series of methyl and trifluoromethyl substituted molecules.[27]

2.3.4 Dyes[1]

While the binding constants of the dye guests **20-22** do not fall outside of the range that can be measured by NMR, these guests show some interesting spectral features that would not be observed in an NMR experiment. The long wavelength charge transfer absorptions of the dyes **20-22** exhibit bathochromic shifting in the presence of host **P** as in Figure 2.10 and tabulated in Table 2.3. Such behavior is consistent with the dye moving into an environment of different polarity than the solvent (the host cavity);[28] this

observation further supports guest inclusion in the host cavity (no bathochromic shifting is observed with the dyes and non-macrocyclic molecules **3** and **4**). Strong induced circular dichroism was also observed with these guests (Figure 2.10).

	Free Guest		Bound Guest[a]		
Guest	λ_{max} (nm)	ε^b ($M^{-1}cm^{-1}$)	λ_{max} (nm)	ε^b ($M^{-1}cm^{-1}$)	$\Delta\lambda$ (nm)
20	452	2.6×10^4	482	2.8×10^4	+30
21	439	2.8×10^4	473	2.0×10^4	+34
22	412	1.8×10^4	424	1.9×10^4	+12

Table 2.3. Bathochromic shifting of guest absorption bands observed on binding to host P in aqueous borate buffer.

[a]Data was obtained by fitting from known binding constants, equilibrium concentrations, and optical constants. [b]Approximate value.

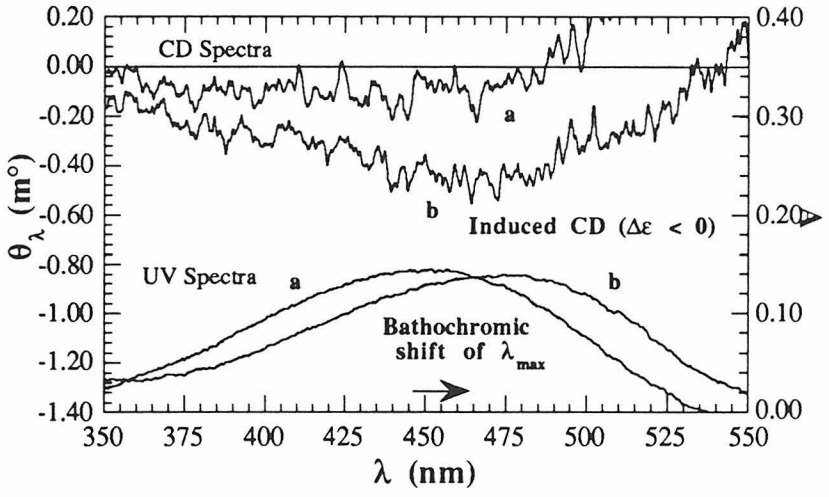

Figure 2.10. CD and UV/visible spectra of Guest 20 (5.75×10^{-6} M) in the absence (a) and in the presence (b) of host P_S (2.00×10^{-5} M) in aqueous borate buffer (pH 9).

2.3.5 Other Host-Guest Systems

The CD methodology has been successfully applied to host **P** and its guests. Its extension to other host-guest systems has also been realized. Additional work to be described later in this manuscript (Chapters 5 and 6) and studies by Pat Kearney[2a,29] and Sarah Ngola[30] have established that this methodology can be successfully applied to other hosts. The most notable of these hosts are the higher oligomers of host **P** (**31** and **32**, Chapters 5 and 6, Figures 2.11 and 2.12)[1] and the tetrabromo derivative of **P**, **TBP** (Figure 2.13).[2a,29] These hosts all have critical aggregation concentrations that prohibit study at NMR concentrations in purely aqueous solvents.

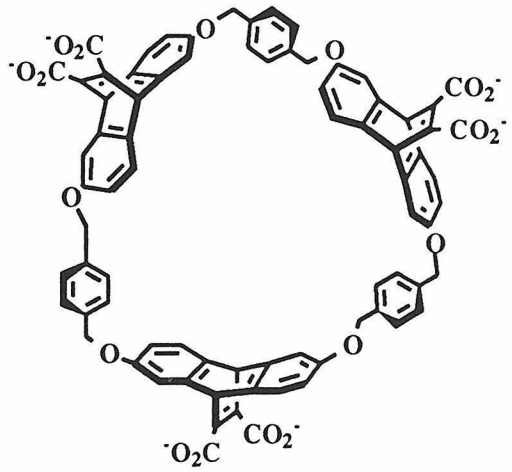

31

Figure 2.11. Host P trimer (31).[1,2b]

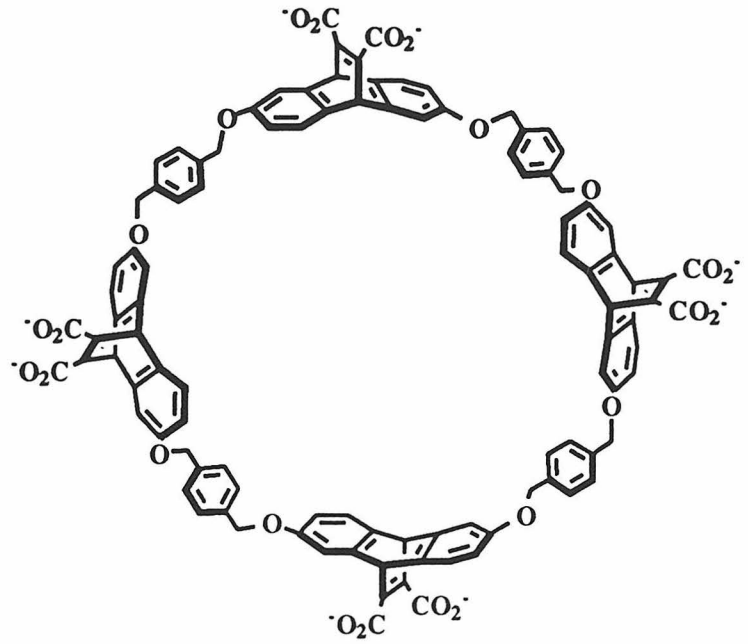

32

Figure 2.12. Host P tetramer (32).[1,2b]

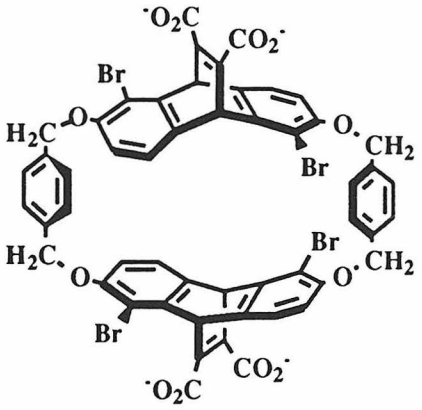

TBP

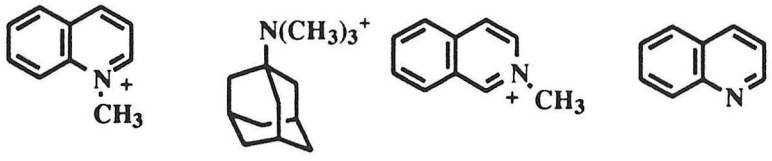

5, *8.1* 6, *9.3* 7, *7.8* 8, *8.8*

Figure 2.13. Host TBP and representative binding constants measured by CD in aqueous borate buffer (pH 9).[2a,29]

2.4 Conclusions

Circular dichroism (CD) spectroscopy has been used to develop methodology for measuring binding constants of guests with cyclophane hosts in aqueous media.[1] While the use of CD to measure binding constants is not novel,[8,13] this work represents the first use of a non-linear least-squares fitting procedure (CDfit) that fits every data point from a series of spectra to generate an estimate of the binding constant.[1] Another novel feature of the CDfit program is that it also generates a best-fit CD spectrum of the pure host-guest complex; this has the advantage of allowing quantitative changes in the CD to be observed between the free and bound states (see Chapters 3 and 4). This methodology complements our previously reported NMR methodology,[4,5] expanding the range of binding constants that can be measured and providing another means by which structural information on the host-guest complex can be obtained. Figure 2.6 is a summary of all the binding constants measured for host **P** by the CD method; the data in this figure nicely illustrates the range of binding constants that can be covered using this methodology.

2.5 Experimental Section[1]

2.5.1 General Methods

CD spectra were recorded on a JASCO J-600 Spectropolarimeter with either 1.0 or 0.5 cm pathlength quartz cells. A standard set of measurement parameters was used in all quantitative experiments: Band Width 1.0 nm, Sensitivity 50 m°/cm, Time Constant 1.0 Sec., Scan Speed 50 nm/min., Step Width 0.2 nm/point, and a minimum of 4 accumulations. Quantitative UV/Vis spectra were recorded on a CARY 2200 or Beckman DU-640 spectrophotometer; UV/Vis spectra used for qualitative purposes for CD studies were taken from the J-600. ^{1}H NMR spectra were recorded on a Bruker AM-500

spectrometer; routine spectra were referenced to the residual proton signals of the solvents and are reported in ppm downfield of 0.0 as δ values. NMR spectra in borate-*d* were referenced to the 1.09 ppm peak of 3,3-dimethylglutarate (DMG) as internal standard. Preparation of solutions used for NMR binding studies and the protocols for such studies have been described previously.[2ab]

All solvents used in spectroscopy were spectrophotometric or HPLC grade. Aqueous cesium borate buffer (pH 9) was prepared by dissolving 0.25 g high purity boric oxide in 800 g water and adding 3.74 ml of 1 M CsOH followed by thorough mixing. The water used in these preparations was passed through a Milli-Q purification system.

All reactions, unless otherwise noted, were stirred magnetically under nitrogen atmosphere. Solvents were distilled from drying agents under argon atmosphere; acetonitrile, CaH_2; THF, sodium benzophenone ketyl. Ion exchange for NH_4^+ was carried out with Dowex® 50w-x2 cation exchange resin (the resin was treated with concentrated ammonium carbonate then washed with Milli-Q purified water before use). Unless otherwise noted reagents obtained from commercial sources were used without further purification.

2.5.2 CD Binding Studies[1,2a]

Stock solutions of guests were prepared by weighing out solutes on a Sartorius microbalance followed by dilution to appropriate volumes. Further dilutions of stock solutions gave the desired concentrations. For sparingly soluble guests **14**, **15**, **16**, **17**, **18**, and **19**, saturated solutions in cesium borate buffer were prepared. Aliquots of these saturated solutions were diluted with acetonitrile and the concentrations determined by fitting to UV/Vis calibration curves of the guest in mixed acetonitrile/cesium borate solvent systems. Stock solutions of guest were prepared fresh for all studies with the sparingly

soluble guests and with guests **22** and **24** (these guests decompose upon prolonged standing in cesium borate).

Solutions of host **P** were prepared by dissolving lyophilized samples of the tetraacid in cesium borate buffer.[2ab] Concentrations were determined from CD spectroscopy by fitting to standardized $\Delta\varepsilon$ data (See Appendix 2, Section 2.7).

Standardized $\Delta\varepsilon$ values for hosts were determined from a series of 5-6 solutions of the host in the 10^{-7} - 10^{-5} M concentration range. The data at each wavelength in the 200-350 nm range was fitted to the Beer-Lambert law to give the best fit $\Delta\varepsilon$ data used in the binding studies. For host **P** these calibration studies used stock solutions prepared and standardized for NMR studies.[2ab]

Fitting CD data from acetonitrile solutions of **P** tetraacid to $\Delta\varepsilon$ values for the 230-350 nm region of $\mathbf{P_E}$ in CH_3CN provided estimates of purity of samples of the tetraacid. Calibration studies with **P** stock solutions in cesium borate prepared by weighing out samples of the tetraacid (with "known purity") produced nearly identical $\Delta\varepsilon$ values to the studies with NMR standardized stock solutions. This method of $\Delta\varepsilon$ determination was used for **3**, and **4** using the corresponding esters.

In a typical CD binding study, 5-6 spectra of solutions with a fixed concentration of one component (usually host) but varying concentration of the other component (usually guest) were used. The spectra and the $\Delta\varepsilon$ values of the host were fit to an association constant with the CDfit program. In general, host concentrations were kept between 1-5 μM. All cases of guest induced CD in fitted $\Delta\varepsilon_{HG}$ spectra were confirmed in solutions where [Host]:[Guest] ratios were alternately very high and very low (high % bound guest and high % bound host).

The ε and λ_{max} values for the bathochromic shifts of guest absorptions in host **P** complexes (Table 2.3) come from spectra of solutions containing known amounts of host and guest. Using previously measured binding constants and extinction coefficients, the host-guest complex spectrum was calculated from the measured spectrum using equation

2.23 and fitting over all wavelengths in the spectrum (comes from the resultant plotted spectrum).

$$\varepsilon_{HG\lambda} = \frac{A_\lambda}{l\,[HG]} - \frac{[H]\varepsilon_{H\lambda} + [G]\varepsilon_{G\lambda}}{[HG]} \qquad (2.23)$$

Where A_λ is the total solution absorption at wavelength λ; [H], [G], and [HG] are equilibrium concentrations of host, guest and host-guest complex; l is the pathlength of the cell (cm); and $\varepsilon_{i\lambda}$ is the extinction coefficeint for species i at wavelength λ. For dyes **20-22**, the wavelength range of interest covered only wavelengths where the host had no absorption ($\varepsilon_{H\lambda} = 0$).

2.5.3 Synthesis of Ethenoanthracene-based Molecules[1]

Compounds **P**, **3**, and **4** were prepared by procedures described previously.[2b]

(9*R*, 10*R*)-2, 6-Bis(*p*-methylbenzyloxy)-9,10-dihydro-11, 12-dicarboxyethenoanthracene (3_R-diacid). In a 50 ml flask 0.018 g (3.38×10^{-5} mol) **3-dimethyl ester** (preparation below) was dissolved in 10 ml THF, followed by addition of 0.049 g (3.27×10^{-4} mol) cesium hydroxide and 2.5 ml water. The mixture was allowed to stir in the dark at room temperature overnight, after which the THF was removed by rotary evaporation. The aqueous mixture was frozen at -78 °C and lyophilized to give a white powder that was dissolved in water and ion-exchanged for NH_4^+. The ion-exchanged solution was frozen at -78 °C and lyophilized to give 0.020 g of a white powder (78.3% pure by CD; impurities were inorganic salts and water). ^{1}H NMR (Borate-*d*) δ (ppm) 7.34 (d, 4H, J = 6.0 Hz), 7.32 (d, 4H, J = 5.6 Hz), 7.25 (d, 2H, J = 7.9 Hz), 7.11 (d, 2H, J = 1.8 Hz), 6.62 (dd, 2H), 5.28 (s, 2H), 4.98 (S, 4H), 2.33 (s, 6H).

(9*R*, 10*R*)-2, 6-Bis(*p*-methylbenzyloxy)-9,10-dihydro-11, 12-dicarbomethoxyethenoanthracene (3_R-dimethyl ester). A 25 ml oven dried flask

was charged with 0.012 g (3.40×10^{-5} mol) **(9*R*, 10*R*)-2,6-dihydroxyethenoanthracene,**[2b] 0.020 g (1.08×10^{-4} mol) α-bromo-p-xylene, and 0.054 g (1.65×10^{-4} mol) cesium carbonate. After addition of 10 ml acetonitrile, the mixture was heated to 55 °C and allowed to stir in the dark. After 18 hours TLC (silica gel, 3:1 ether:pet ether) indicated completion of the reaction. The mixture was filtered and purified by flash chromatography (material placed on silica gel plug, 1:1 ether:pet ether). Obtained 0.0176 g (98%) of product. ^{1}H NMR ($CDCl_3$) δ (ppm) 7.21 (d, 4 H), 7.16 (d, 4 H), 7.05 (d, 2H), 7.02 (d, 2H), 6.54 (dd, 2H), 5.30 (s, 2H), 4.93 (s, 4H), 3.76 (s, 6H), 2.33 (s, 6H). CD [(9*R*, 10*R*)-enantiomer, CH_3CN] λ (Δε) [nm ($M^{-1}cm^{-1}$)], 318 (+2.3), 301 (-0.8), 286 (+17.6), 250 (-53.1), 230 (+102.4), 216 (-2.5), 207 (+52.1).

(9*R*, 10*R*)-2, 6-Bis(methoxy)-9,10-dihydro-11, 12-dicarboxy-ethenoanthracene (4_R-diacid). In a 10 ml flask 0.015 g (3.94×10^{-5} mol) **4_R-dimethyl ester** (preparation below) was dissolved in 4 ml THF, followed by addition of 0.06 g (3.96×10^{-4} mol) cesium hydroxide and 1.0 ml water. The mixture was allowed to stir in the dark at room temperature overnight, after which the THF was removed by rotary evaporation. The aqueous mixture was frozen at -78 °C and lyophilized to give a white powder that was dissolved in water and ion-exchanged for NH_4^+. The ion-exchanged solution was frozen at -78 °C and lyophilized to give 0.022 g of an off-white powder (69.1% pure by CD; impurities were inorganic salts and water). ^{1}H NMR (Borate-*d*) δ (ppm) 7.36 (d, 2H, J = 7.6 Hz), 7.13 (d, 2H, J = 2.3 Hz), 6.63 (dd, 2H, J = 2.4, 7.4 Hz), 5.31 (s, 2H), 3.77 (s, 6H).

(9*R*, 10*R*)-2, 6-Bis(methoxy)-9,10-dihydro-11, 12-dicarbomethoxy-ethenoanthracene (4_R-dimethylester). A 25 ml oven dried flask was charged with 0.051 g (1.45×10^{-5} mol) **(9*R*, 10*R*)-2,6-dihydroxyethenoanthracene,**[2b] and 0.234 g (7.46×10^{-4} mol) cesium carbonate. After addition of 10 ml acetonitrile, methyl iodide (0.1 ml, 0.228 g 1.60×10^{-3} mol) was added dropwise. The mixture was heated to 50 °C and allowed to stir in the dark. After six hours TLC (silica gel, 1:1 ether:pet ether)

indicated completion of the reaction. The mixture was filtered and purified by flash chromatography (material placed on silica gel plug, 1:1 ether:pet ether). Obtained 0.06 g (quantitative yield) of product. ^{1}H NMR ($CDCl_3$) δ (ppm) 7.23 (d, 2 H), 6.95 (d, 2H,), 6.47 (dd, 2H), 5.31 (s, 2H), 3.79 (s, 6H), 3.76 (s, 6H). CD [(9*R*, 10*R*)-enantiomer, CH_3CN] λ (Δε) [nm ($M^{-1}cm^{-1}$)], 318 (+2.6), 302 (-1.4), 285 (+16.2), 250 (-46.6), 229 (+71.0), 217 (-1.1), 205 (+72.6).

2.5.4 Guests[1]

Guests **7**, **14**, **16**, **17**, **18**, **19**, **20**, **21**, **22**, **23**, **24**, **25**, and **26** were obtained from commercial sources. Guests **9**[31] and **15**[32] were prepared as described in the literature. Guests **5**, **6**, **7**, **10**, **11**, **12**, and **13** were prepared through alkylation of the appropriate amine, quinoline, or isoquinoline with methyl iodide. Guest **8** was distilled under vacuum prior to use. Chloride salts were obtained by ion exchange of the appropriate iodide or bromide salt using Dowex® 1X8-400 ion exchange resin. Guest purity of hydroscopic guests (all the chloride salts) was ascertained by elemental analysis. Guests were used as is unless elemental analysis, NMR, or UV/Vis spectroscopy indicated the presence of organic impurities; in such cases further ion exchange, recrystallization, or other appropriate means of purification were employed and the samples checked by elemental analysis.

2.5.5 CD Data for Previously Reported Compounds[1]

2, 6-Dihydroxyethenoanthracene.[2b] [(9*R*, 10*R*)-enantiomer, CH_3CN] λ (Δε) [nm ($M^{-1}cm^{-1}$)], 302 (-3.5), 285 (+16.4), 250 (-41.9), 229 (+61.3), 217 (-9.0), 206 (+59.8).

P-Tetramethyl Ester.[2b] [(9*S*, 10*S*, 9'*S*, 10'*S*)-enantiomer, CH_3CN] λ (Δε) [nm ($M^{-1}cm^{-1}$)], 297 (+14.0), 283 (-2.8), 251 (+144), 227 (-272), 208 (-85.6).

P.[2b] [(9*S*, 10*S*, 9'*S*, 10'*S*)-enantiomer, pH 9 borate buffer] λ (Δε) [nm ($M^{-1}cm^{-1}$)], 296 (-35.0), 277 (+15.7), 252 (-151), 226 (+168), 211 (sh) (+50.6).

2.6 Appendix 1: Creating CDfit Input files[19]

The input file for CDfit must contain the following information: concentrations and pathlengths of each sample, the range of wavelengths being covered with the known optical constants for each solution component for each of the wavelengths in the range, and the observed θ_λ at each wavelength for each sample. If it is desired to eliminate some wavelengths from the fitting for a given sample, setting θ_λ = 10,000 at the given wavelength will alert the computer to ignore that data point. Using a program like Kaleidagraph[33] or Excel,[34] the wavelength, optical constant, and ellipticity data can be compiled into columns and saved in a text format.

In the text file (which should have no column headings for the data), the following information is added at the top of the page, for each solution: host concentration, guest concentration, and pathlength. Each solution gets its own line with each piece of information separated by a single space.

As an illustrative example, consider a study in which three solutions containing a chiral host and an achiral guest are to be fitted over the wavelength range from 250-240 nm with data taken with a 1 nm step width.

Solution	$[H]_0$	$[G]_0$	l
1	1×10^{-6} M	1×10^{-6} M	1 cm
2	1×10^{-6} M	2×10^{-6} M	1 cm
3	1×10^{-6} M	3×10^{-6} M	1 cm

The input file should appear as follows:

```
1e-6 1e-6 1
1e-6 2e-6 1
1e-6 3e-6 1

250.00  100.00  0  1.500  1.510  1.520
249.00  98.00   0  1.480  1.490  1.500
248.00  97.00   0  1.460  1.470  1.480
247.00  95.00   0  1.400  1.410  1.420
246.00  80.00   0  1.350  1.360  1.370
245.00  75.00   0  1.340  1.350  1.360
244.00  60.00   0  1.240  1.250  1.260
243.00  50.00   0  1.200  1.210  1.220
242.00  45.00   0  1.150  1.160  1.170
241.00  44.00   0  1.140  1.150  1.160
240.00  43.00   0  1.130  1.140  1.150
```

At the top of the page is the information on each solution being fitted–all information separated by a single space, and each solution on a separate line; the first line is solution number 1, the second line solution number 2, and so on. A single blank line separates the solution information, which is seen as the six vertical columns of data. Reading from left to right, these columns of data are (1) wavelengths, (2) host optical constants ($\Delta\varepsilon_{\mathbf{H}\lambda}$), (3) guest optical constants ($\Delta\varepsilon_{\mathbf{G}\lambda}$, all are zero because the guest is achiral), (4) θ_λ from solution 1, (5) θ_λ from solution 2, and (6) θ_λ from solution 3. If there had been more than three solutions, the θ_λ columns for solution 4 and on would go on the right of the solution 3 data. The row of data for the final wavelength (240 nm in the above example) is the terminal line of the text file; any characters or blank lines beyond this will cause CDfit to give an error message.

The input file should be given the extension ".in", thus for the above case we can call the file "example.in". To run CDfit off of the Dougherty group Silicon Graphics machine, type "CDfit" and follow the instructions. There are two output files with extensions ".cdf" and ".tab". The .cdf file contains the output summary (see Figure 2.5), and the .tab file contains all the input data with the quantities E_λ, $\Delta\varepsilon_{\mathbf{HG}\lambda}$, and $\theta_{\lambda\text{calc}}$. It also contains the residuals $\theta_{\lambda\text{calc}}$ - $\theta_{\lambda\text{obs}}$.

2.7 Appendix 2: Measurement of Δε values and Estimation of Concentrations

Standardized sets of Δε values are obtained by fitting data to the Beer-Lambert law at each wavelength over the desired range from N solutions of known concentration. Mathematically, this is performed for the N data points at each wavelength using equation 2.24,

$$\Delta\varepsilon_\lambda = \frac{\sum_{n=1}^{N} c_n l_n \theta_{\lambda n}}{g \sum_{n=1}^{N} (c_n l_n)^2} \tag{2.24}$$

where c is the concentration (M), l is the pathlength of the cell (cm), the constant g is defined by equation 2.3, and θ_λ is measured in millidegrees. Concentrations of solutions can be estimated by plotting θ_λ vs $gl\Delta\varepsilon$. The plotted data is fitted to a straight line with an intercept of zero, the slope is the molar concentration of the unknown solution.

2.8 References and Footnotes

1. Forman, J. E.; Barrans, R. E., Jr.; Dougherty, D. A.; *J. Am. Chem. Soc.* **1995**, *117*, 9213-9228.

2. (a) Kearney, P. C.; Mizoue, L. S.; Kumpf, R. A.; Forman, J. E.; McCurdy, A.; Dougherty, D. A. *J. Am. Chem. Soc.* **1993**, *115*, 9907-9919. (b) Petti, M. A.; Shepodd, T. J.; Barrans, R. E., Jr.; Dougherty, D. A. *J. Am. Chem. Soc.* **1988**, *110*, 6825-6840. (c) Shepodd, T. J.; Petti, M. A.; Dougherty, D. A. *J. Am. Chem. Soc.* **1988**, *110*, 1983-1985. (d) Shepodd, T. J.; Petti, M. A.; Dougherty, D. A. *J.*

Am. Chem. Soc. **1986**, *108*, 6085-6087. (e) Petti, M. A.; Shepodd, T. J.; Dougherty, D. A.; *Tetrahedron Lett.* **1986**, *27*, 807-810.

3. The NMR methodology used in these studies cannot accurately measure binding interactions with $-\Delta G^{\circ}_{a} \leq 3.5$ kcal/mol,[1,2a] thus any weak interaction between **1** or **2** and a guest would not be detectable. Also, the spectral changes observed in these experiments are negligible, and this infers that the control molecules **1** and **2** do not bind guests in aqueous solution to a significant extent.

4. Barrans, R. E., Jr.; Dougherty, D. A. *Supramolecular Chem.* **1994**, *4*, 121-130.

5. Barrans, R. E., Jr.; California Institute of Technology, Ph.D. Thesis, 1993.

6. (a) Wang, T. M.; Bradshaw, J. S.; Izatt, R. M. *J. Heterocyclic Chem.* **1994**, *31*, 1097-1114. (b) Wilcox, C. S. In *Frontiers in Supramolecular Organic Chemistry and Photochemistry*, Schneider, H.-J., Dürr, H., Eds.; VCH, 1990. (c) Horman, I.; Dreux, B. *Anal. Chem.* **1983**, *55*, 1219-1221. (d) Creswell, C. J.; Allred, A. L. *J. Phys. Chem.* **1962**, *66*, 1469-1472.

7. Alberty, R. A.; *Physical Chemistry*, John Wiley and Sons, 1987.

8. Estimation of binding constants with CD: (a) Engle, A. R.; Purdie, N.; Hyatt, J. A.; *Carbohydr. Res.* **1994**, *265*, 181-195. (b) Wulff, G.; Kubik, S. *Carbohydr. Res.* **1992**, *237*, 1-10. (c) Suzuki, M.; Kajtar, M.; Szejtli, J.; Vikmon, M.; Fenyvesi, E. *Carbohydr. Res.* **1992**, *223*, 71-80. (d) Schuette, J. M.; Ndou, T. T.; Warner, I. M.; *J. Phys. Chem.*, **1992** *96*, 5309-5314. (e) Suzuki, M.; Kajtar, M.; Szejtli, J.; Vikmon, M.; Fenyvesi, E.; Szente, L. *Carbohydr. Res.* **1991**, *214*, 25-33. (f)

Patonay, G.; Warner, I. M. *J. Inclusion Phenom. Mol. Recognit. Chem.* **1991**, *11*, 313-322. (g) Barra, M.; Bohne, C.; Scaiano, J. C. *J. Am. Chem. Soc.* **1990**, *112*, 8075-8079. (h) Ishizuka, Y.; Nagawa, Y.; Nakanishi, H.; Akira, K. *J. Inclusion Phenom. Mol. Recognit. Chem.* **1990**, *9*, 219-225. (i) Breslow, R.; Greenspoon, N.; Guo, T.; Zarzycki, R. *J. Am. Chem. Soc.* **1989**, *111*, 8296-8297. (j) Hirai, H.; Toshima, N.; Hayashi, S.; Fuji, Y. *Chem. Lett.* **1983**, 643-646. (k) Yorozu, T.; Hoshino, M.; Imamura, M.; Shizuka, H., *J. Phys. Chem.* **1982**, *86*, 4422-4426.

9. Determining guest orientations and conformations from analysis of CD curves: (a) Hamai, S.; *J. Phys. Chem.* **1995**, *99*, 12179-12114. (b) Marcomi, G.; Monti, S.; Mayer, B.; Kohler, G.; *J. Phys. Chem.* **1995**, *99*, 3943-3950. (c) Yoshida, N.; Yamaguchi, H.; Higashi, M.; *J. Chem. Soc. Perkin 2* **1994**, 2507-2513. (d) Sakurai, T.; Saitou, E.; Hayashi, N.; Hirasawa, N.; Inoue, H. *J. Chem. Soc. Perkin 2* **1994**, 1929-1935. (e) Kajtar, M.; Szejtli, J.; Vikman, M.; Suzuki, M.; Ohmori, H.; *J. Inclusion Phenom. Mol. Recognit. Chem.* **1994**, *18*, 219-225. (f) Hamai, S.; Ikeda, T.; Nakamura, A.; Ikeda, H.; Ueno, A.; Toda, F. *J. Am. Chem. Soc.* **1992**, *114*, 6012-6016. (g) Buss, V.; Reichardt, C. *J. Chem. Soc., Chem. Commun.* **1992**, 1636-1638. (h) Kano, K; Yoshiyasu, K.; Yasouka, H.; Hata, S.; Hashimoto, S. *J. Chem. Soc., Perkin Trans. 2,* **1992**, 1265-1259. (i) Buss, V. *Angew. Chem., Int. Ed. Engl.* **1991**, *30*, 869-870. (j) Kano, K.; Tatsumi, M.; Hashimoto, S. *J. Org. Chem.* **1991**, *56*, 6579-6585. (k) Kodaka, M. *J. Phys. Chem.* **1991**, *95*, 2110-2112. (l) Kobayashi, N.; Opallo, M. *J. Chem. Soc., Chem. Commun.* **1990**, 477-479. (m) Ata, M.; Kubozono, Y.; Suzuki, Y.; Aoyagi, M.; Gondo, Y. *Bull. Chem. Soc. Jpn.* **1989**, *62*, 3706-3708. (n) Ueno, A.; Moriwaki, F.; Osa, T.; Hamada, F.; Murai, K. *J. Am. Chem. Soc.* **1989**, *111*, 6391-6397. (o) Komiyama, M.; Takeshige, Y. *J. Org. Chem.* **1989**, *54*, 4936-4939. (p) Ueno, A.; Suzuki, I.; Osa, T. *J. Am. Chem. Soc.* **1988**, *110*, 4323-4328. (q) Kobayashi, N. *J. Chem.*

Soc., Chem. Commun. **1988**, 918-919. (r) Kobayashi, N.; Zao, X.; Osa, T.; Kato, K.; Hanabusa, K.; Imoto, T.; Shirai, H. *J. Chem. Soc., Dalton Trans.* **1987**, 1801-1803. (s) Le Bas, G.; de Rango, C.; Rysanek, N.; Tsoucaris, G. *J. Inclusion Phenom. Mol. Recognit. Chem.* **1984**, *2*, 861-867. (t) Yamaguchi, H. *J. Inclusion Phenom. Mol. Recognit. Chem.* **1984**, *2*, 747-753. (u) Kobayashi, N.; Hino, Y.; Uneo, A.; Osa, T. *Bull. Chem. Soc. Jpn.* **1983**, *56*, 1849-1850. (v) Kobayashi, N.; Hino, H.; Hino, Y.; Uneo, A.; Osa, T. *J. Chem. Soc., Perkin Trans. 2* **1983**, 1031-1035. (w) Shimizu, H.; Kaito, A.; Hatano, M. *J. Am. Chem. Soc.* **1982**, *104*, 7059-7065. (x) Shimizu, H.; Kaito, A.; Hatano, M. *Bull Chem. Soc. Jpn.* **1981**, *54*, 513-519. (y) Shimizu, H.; Kaito, A.; Hatano, M. *Bull Chem. Soc. Jpn.* **1979**, *52*, 2678-2684. (z) Ikeda, N.; Yamaguchi, H. *Chem. Phys. Lett.* **1978**, *56*, 167-169. (aa) Yamaguchi, H.; Ikeda, N.; Hirayama, F.; Uekama, K. *Chem. Phys. Lett.* **1978**, *55*, 75-76. (bb) Harata, K.; Uedaira, H.; *Bull Chem. Soc. Jpn.* **1975**, *48*, 375-378. See also references 7d and 7h.

10. Determination of polarization directions of electronic transitions from analysis of induced CD curves: (a) Yamaguchi, M.; Higashi, M.; Oda, M. *Spectrochim. Acta* **1988**, *44A*, 547-548. (b) Kobayashi, N.; Minato, S.; Osa, T. *Makromol. Chem.* **1983**, *184*, 2123-2132. (c) Shimizu, H.; Kaito, A.; Hatano, M. *J. Am. Chem. Soc.* **1982**, *104*, 7059-7065.

11. Extent of guest association with substituted cyclodextrins: (a) Kuwabara, T.; Nakamura, A.; Ueno, A.; Toda, F. *J. Phys. Chem.* **1994**, *98*, 6297-6303. (b) Yamaguchi, H.; Higashi, M. *J. Inclusion Phenom. Mol. Recognit. Chem.* **1987**, *5*, 725-728. (c) Kobayashi, N.; Osa, T. *Chem. Lett.* **1986**, 421-424. (d) Hira, H.; Toshima, N.; Uenoyama, S. *Bull. Chem. Soc. Jpn.* **1985**, *58*, 1156-1164.

12. Solvent effects on the complex from CD data: Opallo, M.; Kobayashi, N.; Osa, T. *J. Inclusion Phenom. Mol. Recognit. Chem.* **1989**, *6*, 413-422.

13. For Example: (a) Huggins, J. P.; Ganzhom, A. J.; Saudek, V.; Pelton, J. T.; Atkinson, R. A. *Eur. J. Biochem.* **1994**, *221*, 581-593. (b) Gassner, G. T.; Ballou, D. P.; Landrum, G. A.; Whittaker, J. W. *Biochemistry* **1993**, *32*, 4820-4825. (c) Allen, B.; Blum, M.; Cunningham, A.; Tu, G. C.; Hofmann, T. *J. Biol. Chem.* **1990**, *265*, 5060-5065. (d) Reed, J.; Kinzel, V.; Kemp, B. E.; Cheng, H. C.; Walsh, D. A. *Biochemistry* **1985**, *24*, 2967-2973. (e) Kimura, T.; Bicknell-Brown, E.; Lim, B. T.; Nakamura, S,; Hasumi, H.; Koga, K.; Yoshizumi, H. *Dev. Biochem.* **1982**, *21*, 695-698. (f) Hofler, J. G.; Burns, R. O. *J. Biol. Chem.* **1978**, *253*, 1245-1251. (g) Orengo, A.; Patenia, D. M. Int. *J. Biochem.* **1976**, *7*, 423-432.

14. Calixarenes: (a) James, T. D.; Samankumara Sandanayake, K. R. C.; Shinkai, S.; *Supramol. Chem.* **1995**, *6*, 141-157. (b) Morozumi, T.; Shinkai, S.; *Chem. Lett.* **1994**, 1315-1518. (c) Morozumi, T.; Shinkai, S.; *J. Chem. Soc. Chem. Commun.* **1994**, 1219-1220. (d) Arimura, T.; Shinkai, S. *Bull. Chem. Soc. Jpn.* **1991**, *64*, 1896-1900. (e) Arimura, T.; Kawabata, H.; Matsuda, T.; Muramatsu, T.; Satoh, H.; Fujio, K.; Manabe, O.; Shinkai, S. *J. Org. Chem.* **1991**, *56*, 301-306. (f) Arimura, T.; Kawabata, H.; Edamitsu, S.; Shinkai, S.; Manabe, O.; Muramatsu, T.; Tashiro, M. *Chem. Lett.* **1987**, 2269-2272. (g) Shinkai, S.; Arimura, T.; Satoh, H.; Manabe, O. *J. Chem. Soc., Chem. Commun.* **1987**, 1495-1496.

15. Cyclophane Hosts: (a) Murakami, Y.; Hayashida, O.; Nagai, Y. *J. Am. Chem. Soc.* **1994**, *116*, 2611-2612. (b) Kobayashi, K.; Asakawa, Y.; Kikuchi, Y.; Toi, H.; Aoyama, Y.; *J. Am. Chem. Soc.* **1993**, *115*, 2648-2654. (c) Murakami, Y.; Hayashida, O.; Ono, K.; Hisaeda, Y. *Pure Appl. Chem.* **1993**, *65*, 2319-2324. (d)

Murakami, Y.; Hayashida, O.; Ito, T.; Hisaeda, Y. *Pure Appl. Chem.* **1993**, *65*, 551-556. (e) Kikuchi, Y.; Kobayashi, K.; Aoyama, Y.; *J. Am. Chem. Soc.* **1992**, *114*, 1351-1358. (f) Murakami, Y.; Ohno, T.; Hayashida, O.; Hisaeda, Y. *Chem. Lett.* **1991**, 1595-1598. (g) Murakami, Y.; Kikuchi, J.; Ohno, T.; Hayashida, O.; Kojima, M. *J. Am. Chem. Soc.* **1990**, *112*, 7672-7671.

16. Crown Ethers: (a) Gu, D.; Kenney, B. D.; Brown, B. W. *Tetrahedron Lett.* **1994**, *35*, 681-684. (b) Mack, M. P.; Hendrixson, R. P.; Palmer, R. A.; Ghirardelli, R. G. *J. Org. Chem.* **1983**, *48*, 2029-2035. (c) Malpass, G. D., Jr.; Palmer, R. A.; Ghirardelli, R. G. *Tetrahedron Lett.* **1980**, *21*, 1489-1492. (c) Kaneko, O.; Matsuura, N.; Kimura, K.; Shono, T. *Chem. Lett.* **1979**, 369-372. (d) Mack, M. P.; Hendrixson, R. P.; Palmer, R. A.; Ghirardelli, R. G. *J. Am. Chem. Soc.* **1976**, *98*, 7830-7832.

17. (a) Nakanishi, K.; Berova, N.; Woody, R. W. (eds); *Circular Dichroism-Principles and Applications*, VCH, 1994. (b) Charney, E.; *The Molecular Basis of Optical Activity-Optical Rotatory Dispersion and Circular Dichroism*, Robert E. Krieger Publishing Company: Malabar, Fl, 1985. (c) Mason, S. F. *Molecular Optical Activity and the Chiral Discriminations*, Cambridge University Press: Cambridge, 1982. (d) Crabbé, P. *Optical Rotary Dispersion and Circular Dichroism in Chemistry and Biochemistry*, Academic Press, 1972. (e) Crabbé, P. *Optical Rotary Dispersion and Circular Dichroism in Organic Chemistry*, Holden-Day, 1965. (f) Velluz, L.; Legrand, M.; Grosjean, M. *Optical Circular Dichroism: Principles, Measurements, and Applications*, Verlag Chemie, 1965. (g) Mislow, K. *Introduction to Stereochemistry*, W. A. Benjamin Inc., 1965.

18. Harada, N.; Nakanishi, K.; *Circular Dichroic Spectroscopy-Exciton Coupling in*

Organic Stereochemistry, University Science Books: Mill Valley, CA, 1983.

19. Barrans, R. E., Jr.; *Personal Communication.*

20. Press, W. H.; Flannery, D. P.; Teukolsky, S. A.; Vetterling, W. T. *Numerical Recipes: the Art of Scientific Computing*; Cambridge University: New York, 1986, 521-528.

21. Rosen, A. *Biochem. Pharmacol.* **1970**, *19*, 2075-2081.

22. The rigorous condition is $K([H]_o - [G]_o) >> 1$.

23. (a) Wyman, J.; Gill, S. J. *Binding and Linkage*, University Science Books: Mill Valley, CA, 1990, p 36. (b) Scatchard, G. *Ann. N.Y. Acad. Sci.* **1949**, *51*, 660-672.

24. (a) Norden, B.; Kubista, M. *NATO ASI ser., ser. C, 242*, 1988, 133-165. (b) Hatano, M. *Induced Circular Dichroism in Biopolymer-Dye Systems*, Springer-Verlag, 1986.

25. (a) Tinoco, I., Jr. *Adv. Chem. Phys.* **1962**, *4*, 113-160. (b) Rosini, C.; Zandomeneghi, M.; Salvadori, P. *Tetrahedron Asymmetry* **1993**, *4*, 545-554.

26. Dougherty, D. A.; Kearney, P. C.; Mizoue, L. S.; Kumpf, R. A.; Forman, J. E.; McCurdy, A.; in *Computational Approaches in Supramolecular Chemistry*, G. Wipff (ed), NATO ASI Series, 1994.

27. Leo, A.; Hansch, C.; Elkins, D. *Chem. Rev.* **1971**, *71*, 525-616.

28. (a) Silverstein, R. M.; Bassler, G. C.; Morrill, T. C. *Spectrometric Identification of Organic Compounds*, John Wiley and Sons: New York, 1974. (b) Reichardt, C. *Chem. Rev.* **1994**, *94*, 2319-2358.

29. Kearney, P. C.; California Institute of Technology, Ph.D. Thesis, 1994.

30. Ngola, S. M.; Dougherty, D. A.; *Submitted.*

31. Schmidtchen, F. P. *Chem. Ber.* **1980**, *113*, 2175-2182.

32. Hafnex, K.; Bernhard, C. *Ann.* **1959**, *625*, 108-123.

33. Version 3.02, Abelbeck Software, © 1993.

34. Version 4.0, Microsoft Corp., © 1985-1992.

Chapter 3:
Stereochemical Assignments and Molecular Conformations of Cyclophane Host Molecules.

Chapter 3

Stereochemical Assignments and Molecular Conformations of Cyclophane Host Molecules.

3.1 Introduction

One of the questions of primary interest in the study of host-guest complexes is that of the host structure in both the free and bound states. The previous studies of host **P** (Figure 3.1) and similar ethenoanthracene hosts relied primarily on ^{1}H NMR spectroscopy, and to a lesser extent on molecular mechanics calculations to infer important structural information about the hosts.[1] The studies in this chapter describe the application of methodology other than ^{1}H NMR to experimentally address these structural issues. These studies have employed circular dichroism (CD) spectroscopy (see Chapter 2) to address issues of stereochemistry (section 3.2) and solution structure (section 3.3).[2] In addition, x-ray crystallography has been used to address the structure of the host binding site (section 3.4).[3]

3.2 Stereochemical Assignments of 2,6-Dihydroxyethenoanthracenes

3.2.1 Background

One of the important issues that had not been conclusively established in previous studies was the assignment of absolute stereochemistry of the samples of our molecules. In earlier work the absolute stereochemistry of the hosts had been assigned based on indirect observations and empirical models.[1b] Two dimensional ^{1}H-^{1}H correlated NMR (NOESY) was used to confirm the identities of the *syn* and *anti* diastereomers (**2** and **3**)

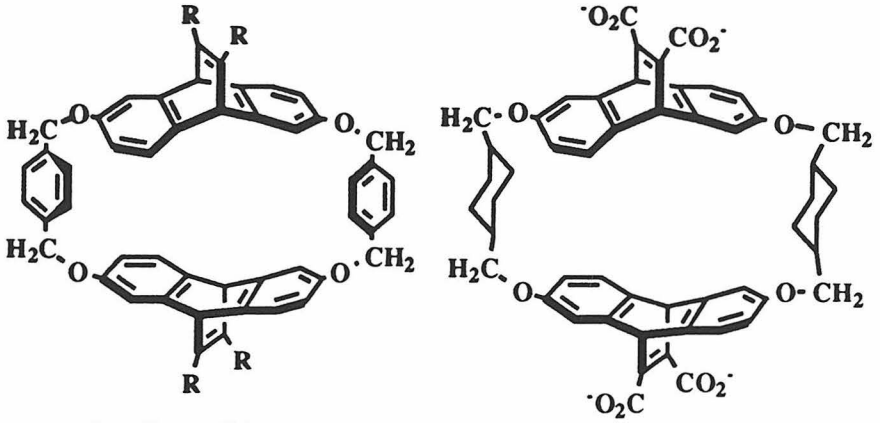

P, R = $-CO_2^-$

P_E, R = $-CO_2CH_3$

C

[(*S*, *S*, *S*, *S*)-Enantiomers shown]

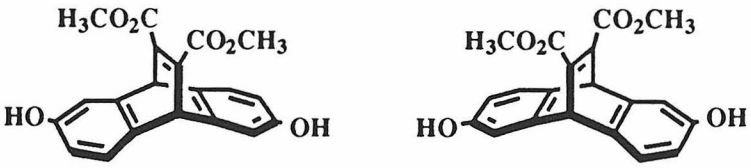

(*S*, *S*)-**1** (**1**$_S$)

(*R*, *R*)-**1** (**1**$_R$)

Figure 3.1. Hosts P, P_E, and C and their 2,6-dihydroxyethenoanthracene building blocks (1$_S$, 1$_R$).

used for the preparation of ethenoanthracene building block **1** (Figure 3.2).[1b] The absolute stereochemistry of these samples was then inferred by the known olefin-facial selectivity of the asymmetric Diels-Alder reaction between TBS protected 2,6-dihydroxyanthracene (**5**) and (+) or (-)-dimenthylfumarate (Figure 3.2).[1] The final evidence for correct assignment came from data on a variety of C_2-symmetric bridged anthracenes.[1b] These molecules show a consistent relationship between the sign of the optical rotation ($[\alpha]_D$) and the absolute configuration.[1b,4] Positive optical rotation is expected for the absolute stereochemistry of **1**$_R$ and negative optical rotation is expected for the absolute stereochemistry of **1**$_S$.[1b,4] The measured optical rotations complemented the NOESY re-

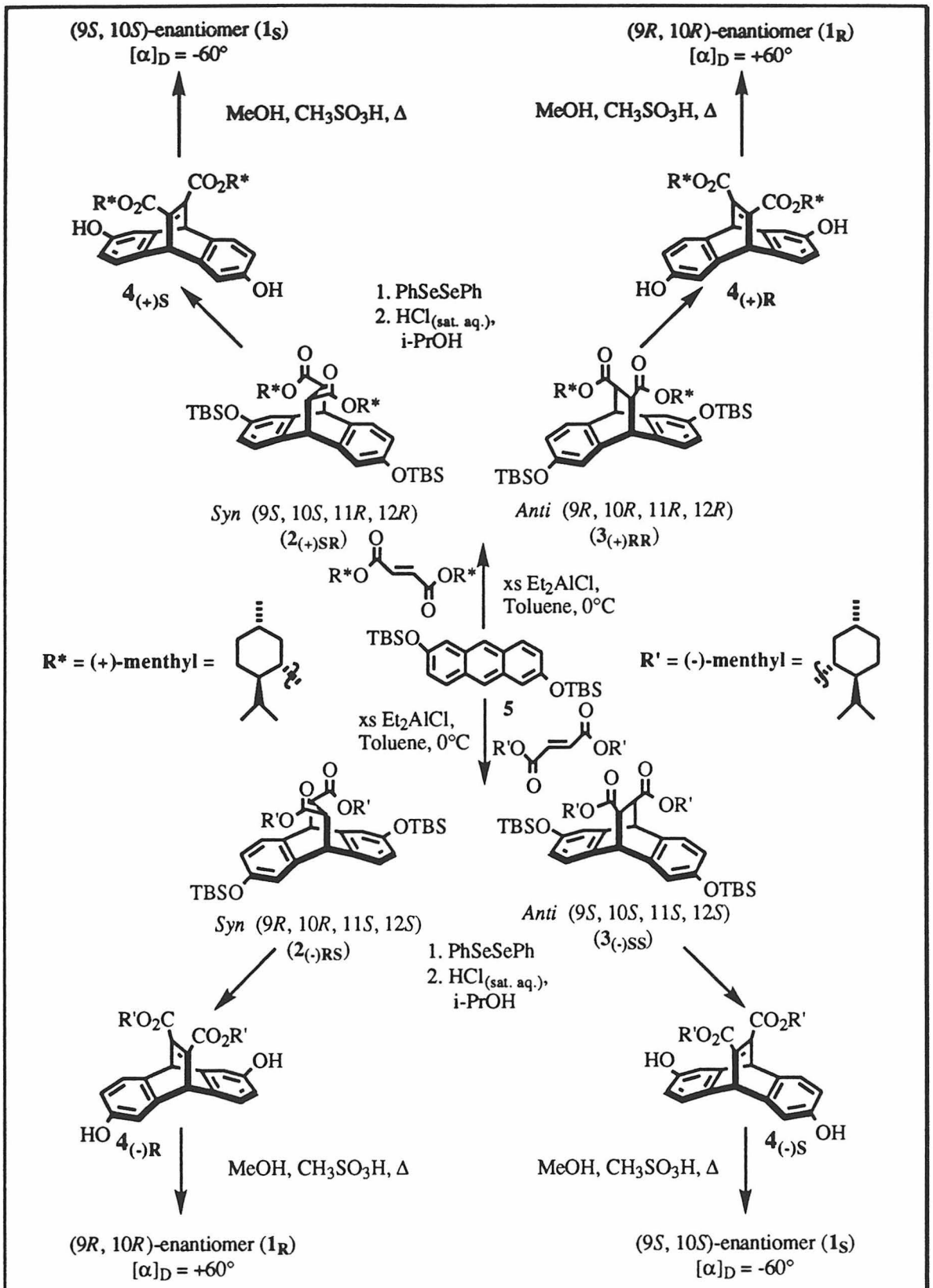

Figure 3.2. Olefin-facial selectivities in the Diels-Alder reaction that leads to the preparation of 2,6-dihydroxyethenoanthracenes 1_S and 1_R.[1b]

sults and the inferred olefin-facial selectivity, leading to the assignments.[1b] Although the evidence strongly suggested that the stereochemistry of the samples had been correctly assigned, more direct proof was desirable.

In multichromophoric systems, the positions in space of the chromophores with respect to one another (and hence absolute stereochemistry) can be deduced from the CD spectra.[5-8] As expected the chirooptical properties of our hosts appear to be dominated by the coupling of the component chromophores (exciton optical activity) and thus the spectra could reveal the spatial relations of these chromophores.[5,6] However, complete interpretation of the host spectra (Figures 3.3 and 3.4) is complicated by a number of overlapping transitions between the component chromophores of the molecules (**6** and **7** Figure 3.5). Semi-empirical calculations (INDO/S, to be discussed more fully in Chapter 4) indicate that there are at least seventeen $\pi \rightarrow \pi^*$ transitions associated with the diprotonated form of **6** (Figure 3.5) in the 200-315 nm region of the CD spectrum. Calculations on α, α'-dimethoxy-*p*-xylene (**7**, a model for the linker chromophore, Figure 3.5) indicate two additional $\pi \rightarrow \pi^*$ transitions occur in the 200-250 nm region, further complicating the direct analysis of the host **P** CD curves.

While the interpretation of the host CD spectra is quite complex, circular dichroism spectra of exciton coupled C_2-symmetric systems has been used to assign absolute stereochemistry.[6-8] The ethenoanthracene building block **1** is a C_2-symmetric chromophore and is thus suited for this type of analysis. Assignment of the absolute configuration of **1** establishes the absolute stereochemistry of the host prepared from the known sample. Exciton-coupled CD has been addressed in much detail by Harada and Nakanishi,[6] from which the introduction in section 3.2.2 is adapted.

3.2.2 Excitonic Chirality[6]

For a binary system composed of two chromophores (*a* and *b*) that are either identi-

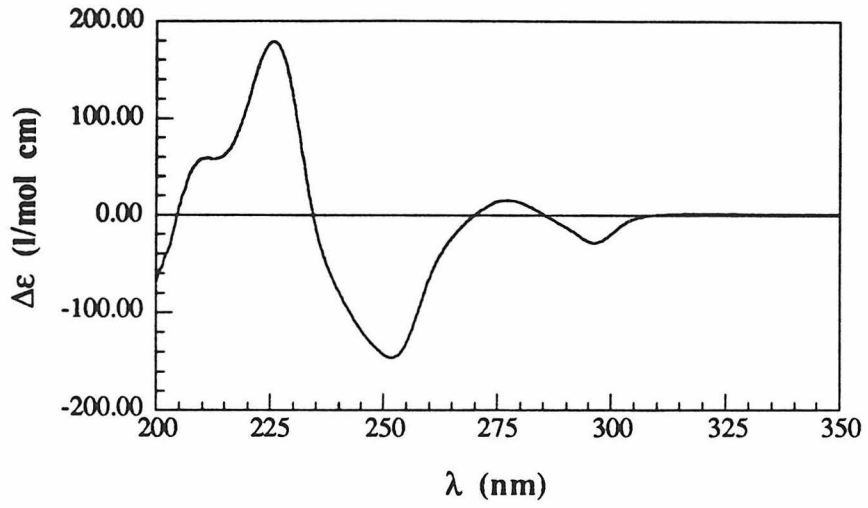

Figure 3.3. Circular dichroism spectra of host P_R in aqueous borate buffer (pH 9).[2]

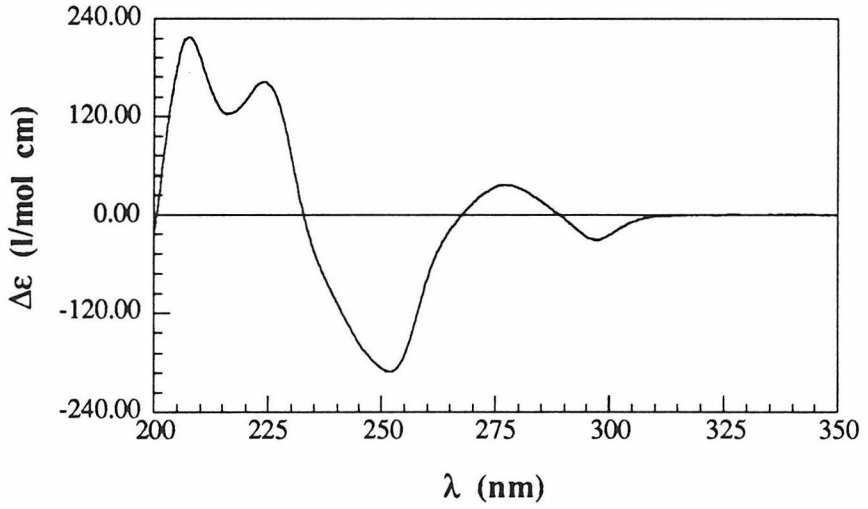

Figure 3.4. Circular dichroism spectra of host C_R in aqueous borate buffer (pH 9).[2]

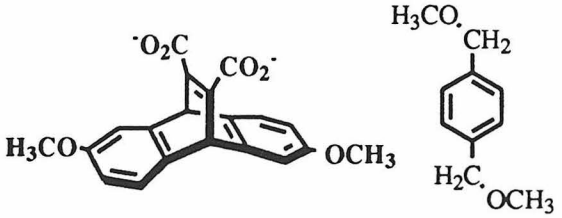

6 **7**

Figure 3.5. Model chromophores for host P.

cal or have similar λ_{max} positions for a particular absorption band, and where *a* and *b* are brought to an excited state at the same probability, the two states can mix to give the excited state of the whole system (Figure 3.6).[6] This results in a splitting of the absorption band into two components.[6] In the UV/vis spectrum the splitting is not experimentally observed, but if the chromophores are in chiral positions with respect to one another, a CD spectrum can exhibit a split Cotton effect (Figure 3.7).[6] As illustrated in Figure 3.7, the split Cotton effect shows positive and negative components with equal rotational strength (the area under the curve).[6] The wavelength midway between the minimum and maximum points passes through $\Delta\varepsilon = 0$ and corresponds to the λ_{max} of the chiral absorption band.[6]

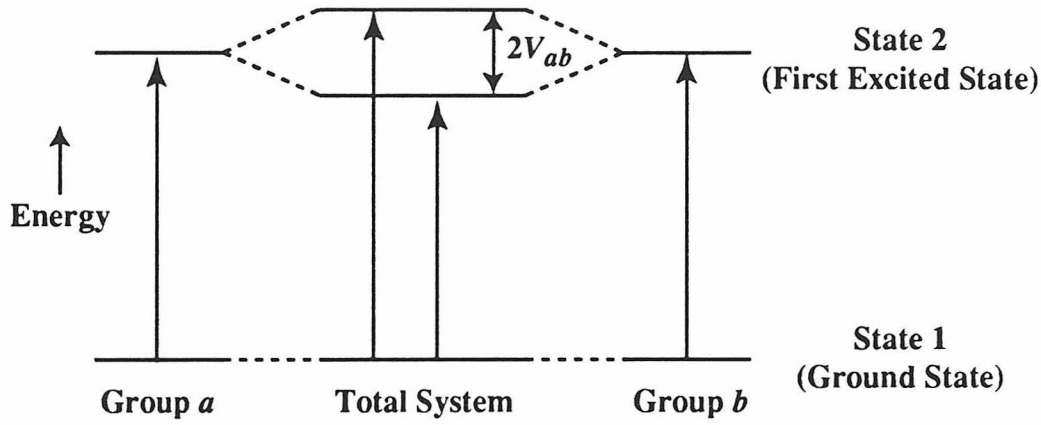

Figure 3.6. By exciton interaction between the two chromophores *a* and *b*, the excited state splits into two energy levels.[6] The energy gap $2V_{ab}$ is called the Davydov splitting.[6a]

The splitting pattern of the Cotton effect directly correlates with the relative positions of the electronic transition moments of the two chromophores, thus allowing unambiguous determination of their positions in space with respect to one another (that is the chirality of the system, Figure 3.8).[6] Harada and Nakanishi have presented a thorough theoretical discussion of this phenomenon; interested readers are referred to reference 6.

Mathematically, the chirality of a C_2-symmetric molecule that contains the two identical chromophores a and b, separated from one another through space, can be determined by evaluating the sign of expression 3.1,

$$\mathbf{R}_{ab} \cdot (\mu_{a12} \times \mu_{b12}) V_{ab} \qquad (3.1)$$

where $\mathbf{R}_{ab}$ is the interchromophoric distance vector between the midpoints of the transition moments of a and b, μ_{a12} and μ_{b12} are the electronic transition dipole moments of the excitation from the ground state to the first excited state (State 1 → State 2) for groups a and b, and V_{ab} is the interaction energy of the two chromophores.

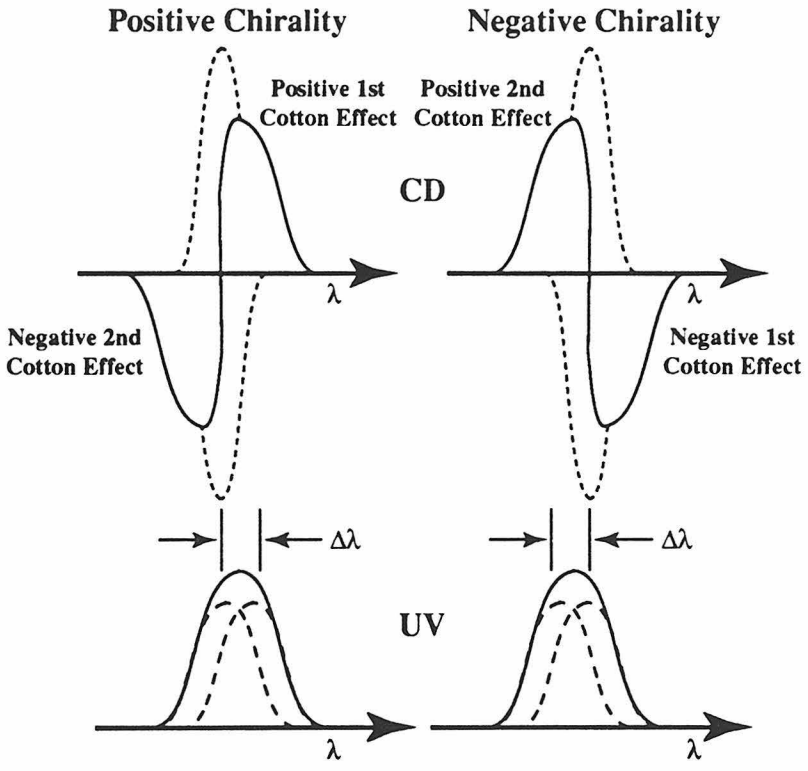

Figure 3.7. Summation curves (CD and UV, solid lines) of two component absorption bands (dotted lines) separated by Davydov splitting Δλ.[6a]

If the sign of expression 3.1 is negative, the system has negative chirality (negative long-wavelength, positive short-wavelength splitting pattern, Figure 3.7).[6] If the sign is

positive, the system has positive chirality (positive long-wavelength, negative short-wavelength splitting pattern, Figure 3.7).[6] To evaluate the sign one must know the handedness of the system, the polarization directions of the interacting transitions, and the relative positions in space of the atoms that make up the interacting chromophores.[6] The cross product of the electronic transition dipoles can be assigned a positive value by taking an in phase combination of the two vectors; the correct result will be obtained as long as the vector directions are consistent in all calculations.[6] The sign of equation 3.1 thus depends only on the sign of V_{ab}. The interaction energy can be evaluated by equation 3.2:[6]

$$V_{ab} = \frac{\mu_{a12} \cdot \mu_{b12}}{R_{ab}^3} - \frac{3(\mu_{a12} \cdot \mathbf{R}_{ab})(\mu_{b12} \cdot \mathbf{R}_{ab})}{R_{ab}^5} = \frac{\mu_{a12}\mu_{b12}\{\mathbf{e}_a \cdot \mathbf{e}_b - 3(\mathbf{e}_a \cdot \mathbf{e}_{ab})(\mathbf{e}_b \cdot \mathbf{e}_{ab})\}}{R_{ab}^3} \qquad (3.2)$$

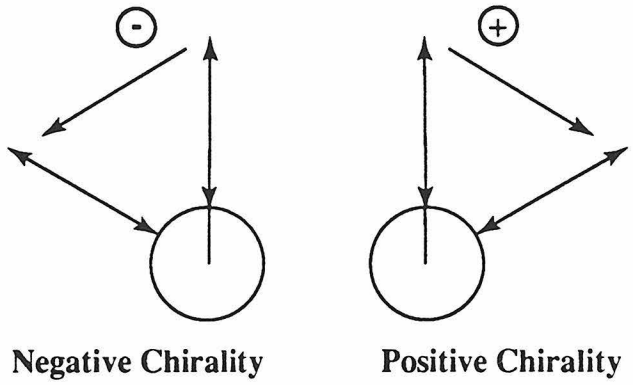

Figure 3.8. Spacial relationship between transition moments (double-headed arrows) showing excitonic chirality.[6a]

In equation 3.2, $\mathbf{e}_a$, $\mathbf{e}_b$, and $\mathbf{e}_{ab}$ are unit vectors along the directions of μ_{a12}, μ_{b12}, and $\mathbf{R}_{ab}$, while R_{ab}, μ_{a12}, and μ_{b12} are scalar, not directional quantities. The sign comes from the dot products of the unit vectors, which are

$$\mathbf{e}_a \cdot \mathbf{e}_b = \text{Cos } \theta_{ab} \qquad (3.3)$$

$$\mathbf{e}_a \cdot \mathbf{e}_{ab} = \text{Cos } \theta_{\mu_a R_{ab}} \qquad (3.4)$$

$$\mathbf{e}_b \cdot \mathbf{e}_{ab} = \text{Cos } \theta_{\mu_b R_{ab}} \qquad (3.5)$$

These angles are the angles between the transition dipole moment and distance vectors on the molecule in question.

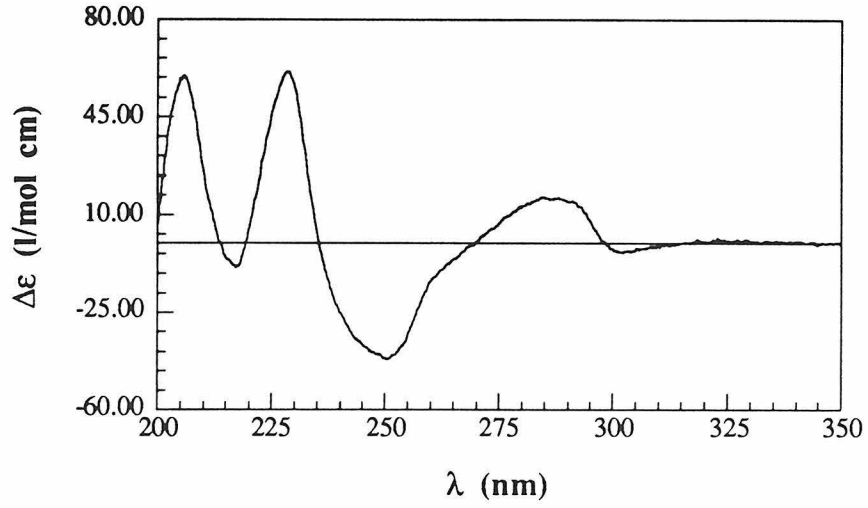

Figure 3.9. CD Spectrum of 1_R in acetonitrile.

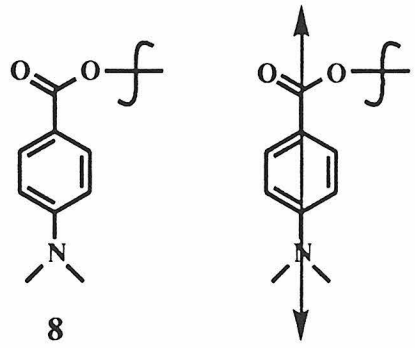

8

Figure 3.10. The *p*-(dimethylamino)benzoate chromophore (8); the arrow indicates the direction of the electronic transition moment.[6a]

3.2.3 Application to the Dougherty Group System

Ethenoanthracene **1** does not show a strong, easily assignable excitonic coupling in its CD spectrum despite the presence of the phenolic rings (Figure 3.9). So, two strongly

interacting chromophores needed to be placed onto the phenolic oxygens. Following Nakanishi's protocol, we chose the *p*-(dimethylamino)benzoate chromophore (**8**, Figure 3.10).[6a] The bis[*p*-(dimethylamino)benzoate] derivative of **1**, compound **9**, was prepared as shown in Figure 3.11.[6a]

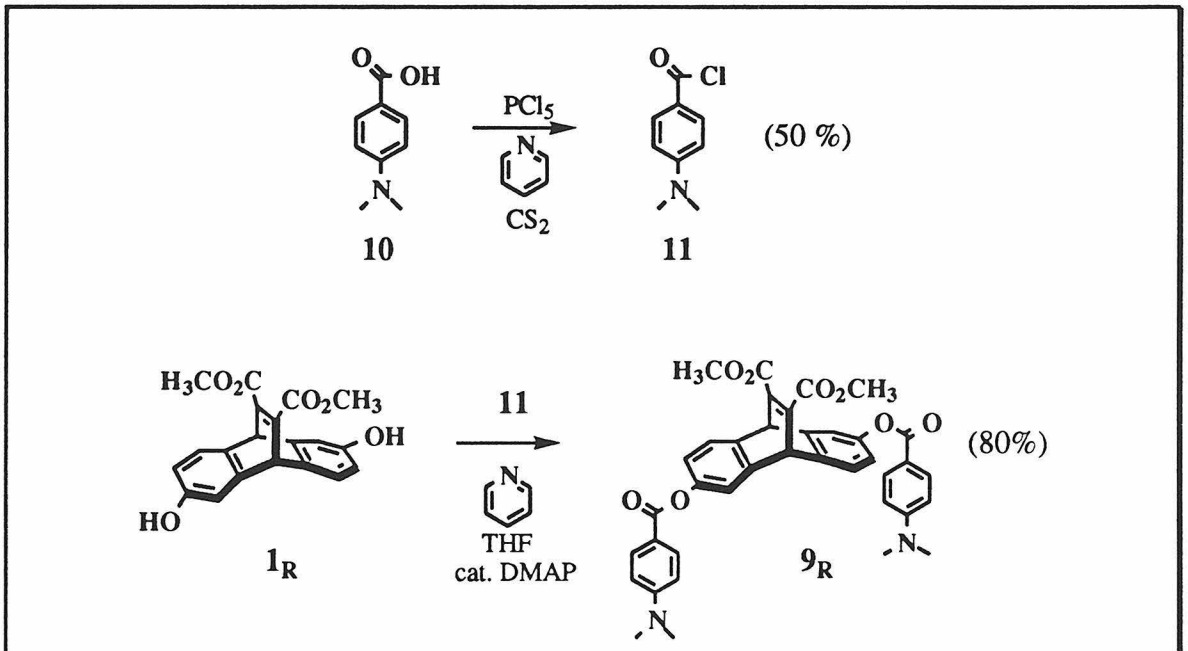

Figure 3.11. Synthesis of the bis[*p*-(dimethylamino)benzoate] derivative of 1_R.[6a]

3.2.4 Expected Excitonic Chirality of the 2,6-Dihydroxyetheno-anthracene System

In order to assess the meaning of the bisignate signal from **9**, a calculation to evaluate the expected sign of the excitonic chirality for a given enantiomer is required. The atomic coordinates for $\mathbf{9_R}$ were obtained from molecular mechanics calculations on the (R, R)-enantiomer using BIOGRAF[9] with the AMBER[10] force field. To obtain the best sampling of possible conformations, a usage-directed Monte Carlo search[11] was performed in which the torsion angles *A-B-C-D*, *B-C-D-E*, *C-D-E-F*, *G-H-I-J*, *H-I-J-K*, and *I-J-K-L* (Figure 3.12) were varied from 0-180°. After minimization and duplicate elimination, 64

low energy conformations (all within 1.2 kcal) were obtained. The lowest energy conformer is shown in Figure 3.13 and the (R, R)-enantiomer has a right-handed (clockwise) sense of screw as indicated by the arrow. AMBER[10] is not parameterized for an $N_{(amine)}$-$C_{(aromatic)}$ bond, so for purposes of calculation the dimethylamino group was replaced with an isopropyl group.

To calculate the sign of equation 3.1 for $\mathbf{9_R}$, the following must be defined. First, since $\mathbf{9_R}$ has clockwise-handedness (Figure 3.13)

$$\mathbf{R}_{ab} > 0 \tag{3.6}$$

Defining the directions of the transition moment vectors as "in-phase" for all calculations makes[6a]

$$(\mu_{a12} \times \mu_{b12}) > 0 \tag{3.7}$$

Thus only the sign of V_{ab} needs to be evaluated. From equation 3.2, the sign of V_{ab} depends only on the term with the unit vectors (expression 3.8).[6a]

$$\{\mathbf{e}_a \bullet \mathbf{e}_b - 3(\mathbf{e}_a \bullet \mathbf{e}_{ab})(\mathbf{e}_b \bullet \mathbf{e}_{ab})\} \tag{3.8}$$

Substituting equations 3.3, 3.4, and 3.5 into expression 3.8, the following expression for the sign of V_{ab} is obtained:

$$\text{sign of } V_{ab} = \text{sign of } \left\{\text{Cos } \theta_{ab} - 3\left(\text{Cos } \theta_{\mu_a \mathbf{R}_{ab}} \text{Cos } \theta_{\mu_b \mathbf{R}_{ab}}\right)\right\} \tag{3.9}$$

The desired angles can be found by creating lines that are superimposed onto the points in space that define the actual distance and transition moment vectors, then finding the angles between these lines. The atoms which define these points in space are defined in Figure 3.13.

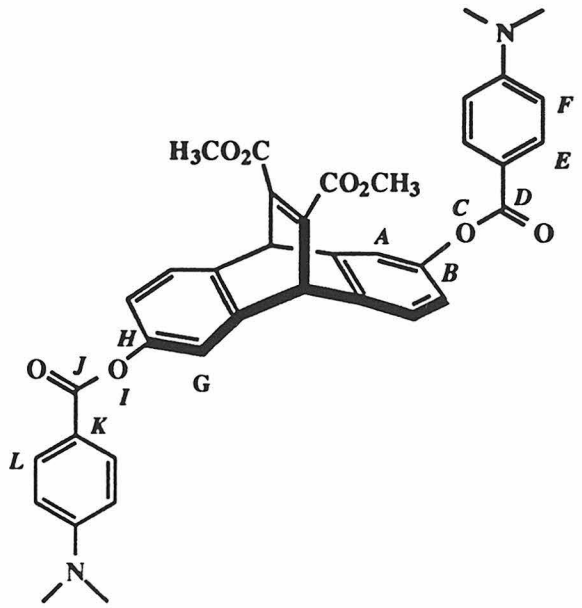

Figure 3.12. Atoms defining torsion angles for the (9*R*, 10*R*)-enantiomer of 9.

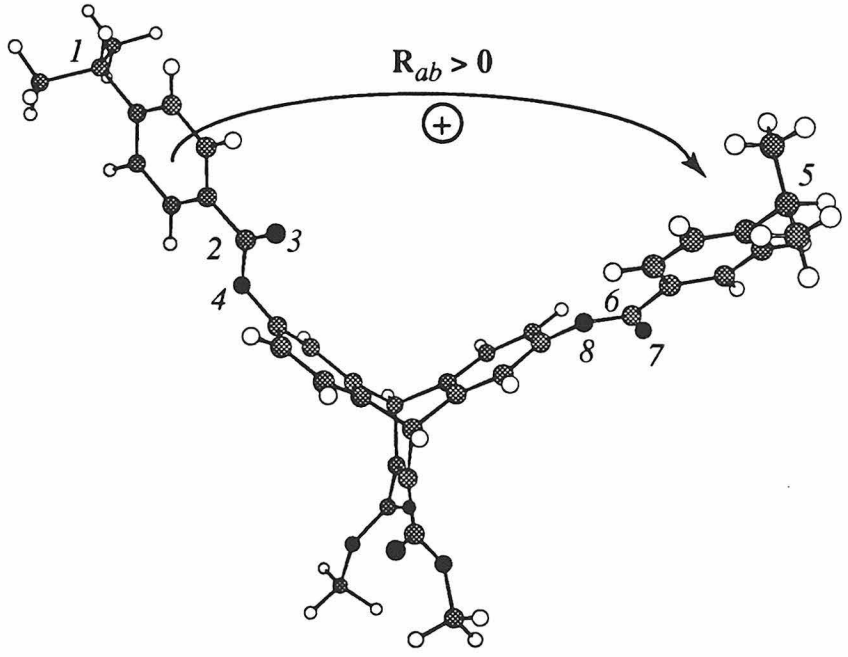

Figure 3.13. Lowest energy conformer of 9_R, the arrow indicates the right-handed sense of screw. The atoms that define the directions of the transition moments are also indicated.[6a]

To define the electronic moment vectors, two lines on each chromophore must be defined. These lines are from atoms *2* to *1* and from *3* to *4* on the left side, and the analogous lines on the right side from atoms *6* to *5* and *8* to *7* (Figure 3.13) For four points in space, two lines can be found using the general relationships 3.10 and 3.11[12]

$$\mathbf{L} = \langle x_2 - x_1, y_2 - y_1, z_2 - z_1 \rangle \tag{3.10}$$

$$\mathbf{L}' = \langle x_4 - x_3, y_4 - y_3, z_4 - z_3 \rangle \tag{3.11}$$

Once these lines are defined the points of intersection between lines *2-1* and *3-4* (point **A**) and between *6-5* and *8-7* (point **B**) are needed. These intersections can be found from the equations for a line in space. For the two lines, the following equations can be written[12]

$$x = x_1 + (x_2 - x_1)t, \; x' = x_3 + (x_4 - x_3)s \tag{3.12, 3.13}$$

$$y = y_1 + (y_2 - y_1)t, \; y' = y_3 + (y_4 - y_3)s \tag{3.14, 3.15}$$

$$z = z_1 + (z_2 - z_1)t, \; z' = z_3 + (z_4 - z_3)s \tag{3.16, 3.17}$$

where s and t are parameters for each line. At the intersection of the two lines

$$x = x', \; y = y', \; z = z' \tag{3.18}$$

The following expressions can be written for the unknown parameters s and t

$$s = \frac{x_1 + (x_2 - x_1)t - x_3}{(x_4 - x_3)}, \; t = \frac{x_3 + (x_4 - x_3)s - x_1}{(x_2 - x_1)} \tag{3.19, 3.20}$$

$$s = \frac{y_1 + (y_2 - y_1)t - y_3}{(y_4 - y_3)}, \; t = \frac{y_3 + (y_4 - y_3)s - y_1}{(y_2 - y_1)} \tag{3.21, 3.22}$$

$$s = \frac{z_1 + (z_2 - z_1)t - z_3}{(z_4 - z_3)}, \; t = \frac{z_3 + (z_4 - z_3)s - z_1}{(z_2 - z_1)} \tag{3.23, 3.24}$$

Solving for s and t in terms of x and y gives equation 3.25:

$$s = \frac{(y_2 - y_1)(x_3 - x_1) + (x_2 - x_1)(y_1 - y_3)}{(x_2 - x_1)(y_4 - y_3) - (y_2 - y_1)(x_4 - x_3)} \tag{3.25}$$

From equation 3.25 it is possible to obtain values of s and t and then to find the points of intersection of the lines using the Cartesian coordinates of the atoms in Figure 3.13.

The transition moment vector of the left chromophore (call it *a*) in Figure 3.13 is defined by the vector from point **A** to atom *1*,[6a] i.e.,

$$\mathbf{R}_{A1} = \mu_a = \langle (x_1 - x_A), (y_1 - y_A), (z_1 - z_A) \rangle = \langle x_a, y_a, z_a \rangle \tag{3.26}$$

The transition dipole moment for the right chromophore (call it *b*) is defined by the vector from point **B** to atom *5*,[6] i.e.,

$$\mathbf{R}_{B5} = \mu_b = \langle (x_5 - x_B), (y_5 - y_B), (z_5 - z_B) \rangle = \langle x_b, y_b, z_b \rangle \tag{3.27}$$

Defining the midpoints of the transition moment vectors as points **C** and **D** allows the distance vector to be defined[6a]

$$\mathbf{R}_{CD} = \mathbf{R}_{ab} = \langle (x_D - x_C), (y_D - y_C), (z_D - z_C) \rangle = \langle x_{ab}, y_{ab}, z_{ab} \rangle \tag{3.28}$$

Using equations 3.26, 3.27, and 3.28, the following expressions can be defined

$$\text{Cos } \theta_{ab} = \frac{\mu_{a12} \bullet \mu_{b12}}{|\mu_{a12}||\mu_{b12}|} = \frac{[(x_a)(x_b) + (y_a)(y_b) + (z_a)(z_b)]}{\sqrt{(x_a^2 + y_a^2 + z_a^2)}\ \sqrt{(x_b^2 + y_b^2 + z_b^2)}} \tag{3.29}$$

$$\text{Cos } \theta_{\mu_b \mathbf{R}_{ab}} = \frac{\mu_{b12} \bullet \mathbf{R}_{ab}}{|\mu_{b12}||\mathbf{R}_{ab}|} = \frac{[(x_b)(x_{ab}) + (y_b)(y_{ab}) + (z_b)(z_{ab})]}{\sqrt{(x_b^2 + y_b^2 + z_b^2)}\ \sqrt{(x_{ab}^2 + y_{ab}^2 + z_{ab}^2)}} \tag{3.30}$$

$$\text{Cos } \theta_{\mu_a \mathbf{R}_{ab}} = \frac{\mu_{a12} \bullet \mathbf{R}_{ab}}{|\mu_{a12}||\mathbf{R}_{ab}|} = \frac{[(x_a)(x_{ab}) + (y_a)(y_{ab}) + (z_a)(z_{ab})]}{\sqrt{(x_a^2 + y_a^2 + z_a^2)}\ \sqrt{(x_{ab}^2 + y_{ab}^2 + z_{ab}^2)}} \tag{3.31}$$

Equation 3.9 allows evaluation of the sign of V_{ab} and thus determination of the chirality of the system.

Evaluation of V_{ab} for all 64 conformers gave a positive value, indicating that the (R, R)-enantiomer of **9** should show a split Cotton effect with positive long-wavelength and negative short-wavelength components. The Cotton effect is expected to be centered near 310 nm (λ_{max} for chromophore **8**).[6]

3.2.5 Results and Other Applications

Figure 3.14 shows the CD spectrum in acetonitrile of a sample assigned from the synthesis as $\mathbf{9_R}$. As expected, there is a split Cotton effect centered at 307 nm with positive long-wavelength and negative short-wavelength components. However, the two component curves should be of approximately the same rotational strength, and as observed in Figure 3.14 this is not the case; the rotational strength of the long wavelength (first) Cotton effect is about six times that of the shorter wavelength (second) Cotton effect. It appears that the reason for this is the overlapping of the shorter-wavelength component of the split Cotton effect with a Cotton effect from the phenolic rings of **1** (Figure 3.9). The difference spectrum[13] (subtraction of the $\mathbf{1_R}$ spectrum from the $\mathbf{9_R}$ spectrum) does show a split Cotton effect with a ratio of about 2:1 for the rotational strengths of the component curves (Figure 3.15), thus confirming that the chirality assignment of the sample was correct. Likewise, the sample assigned from the synthesis as $\mathbf{9_S}$ showed negative excitonic chirality.

Once the sample assignments had been confirmed, the CD spectra of all intermediates in the synthesis of **1** were obtained, and these can be used to assign the stereochemistry of synthetic samples. These spectra are available in Appendix 1 (section 3.7) of this chapter. The excitonic chirality approach has also been used to confirm the stereochemistry of the dibromo ethenoanthracene (**12**) used in our laboratories to prepare host **TBP** (Figure 3.16).[1a,14]

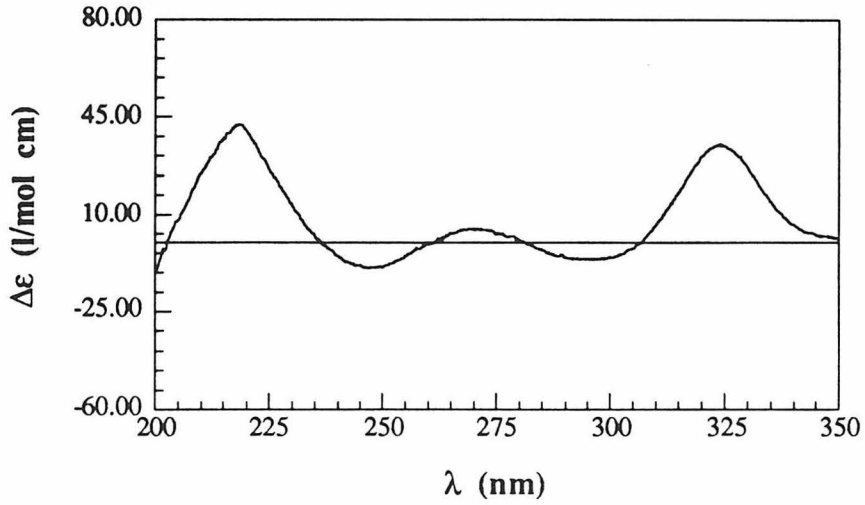

Figure 3.14. CD Spectrum of 9_R in acetonitrile.

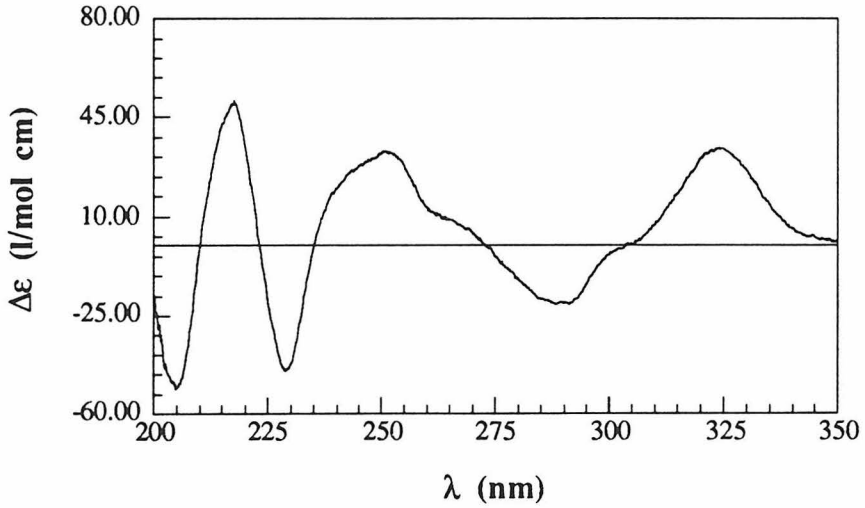

Figure 3.15. CD difference spectrum of 9_R and 1_R in acetonitrile.

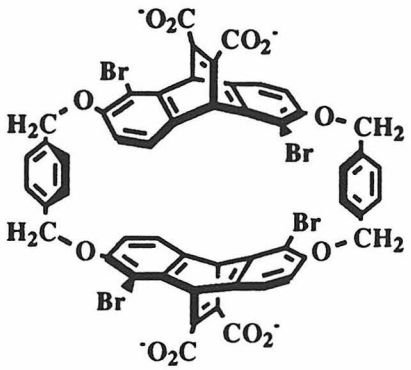

TBP [(*R*, *R*, *R*, *R*)-Enantiomer]

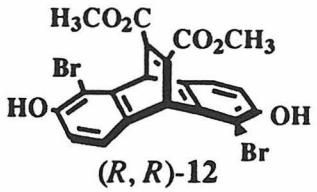

(*R*, *R*)-**12**
Bis(*p*-dimethylamino)benzoate
shows Negative Chirality

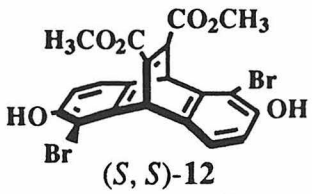

(*S*, *S*)-**12**
Bis(*p*-dimethylamino)benzoate
shows Positive Chirality

Figure 3.16. Host TBP and its ethenoanthracene building block (12).[1a,14]

3.3 Solution Conformations of Cyclophane Host Molecules

3.3.1 Introduction - Conformations of Host P

On the basis of modeling studies, it had been proposed that host **P** has two preferred conformations capable of encapsulating a guest molecule (Figure 3.17).[1b,2] These are a D_2-symmetric toroid conformation (Figure 3.17A) and a C_2-symmetric rhomboid conformation (Figure 3.17B).[1b,2] The toroid is thought to be preferred only for guests with a three-dimensionally spherical structure; the prototypical guest of this type being adamantyltrimethylammonium (ATMA) ion (**13**, Figure 3.18).[1b,2] The rhomboid conformation is best suited for binding guests that have a naphthalene-like shape; the prototypical guest for this conformation is N-methylquinolinium (NMQ) ion (**14**, Figure 3.18).[1b,2] Figure 3.19 illustrates how well these prototypical guests fit into the optimized cavities of the two conformations.

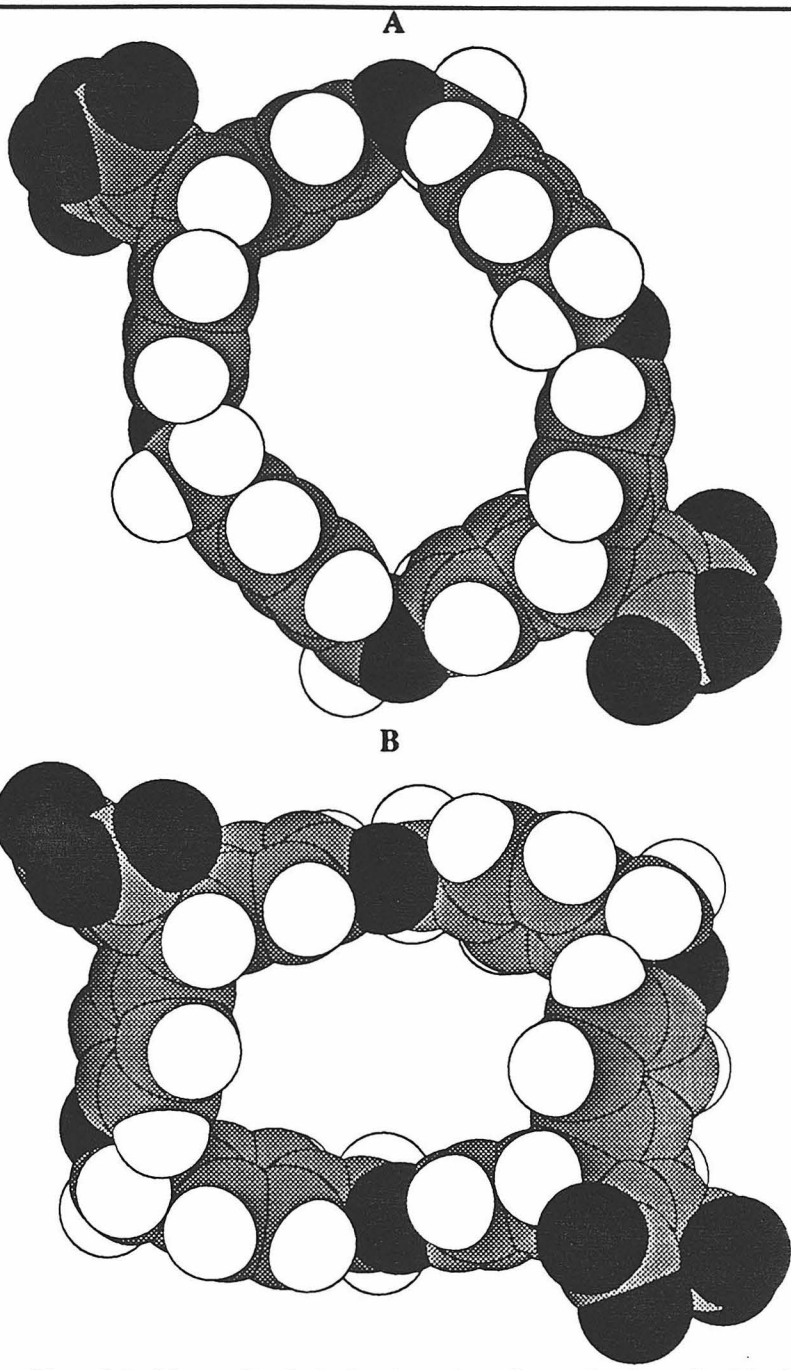

Figure 3.17. Toroid (A, calculated structure) and rhomboid (B, structure adopted from crystal structure of P tetramethyl ester[3]) conformations of host P.[1b,2]

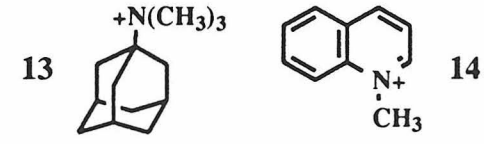

Figure 3.18. Prototypical toroid- and rhomboid-binding guests.

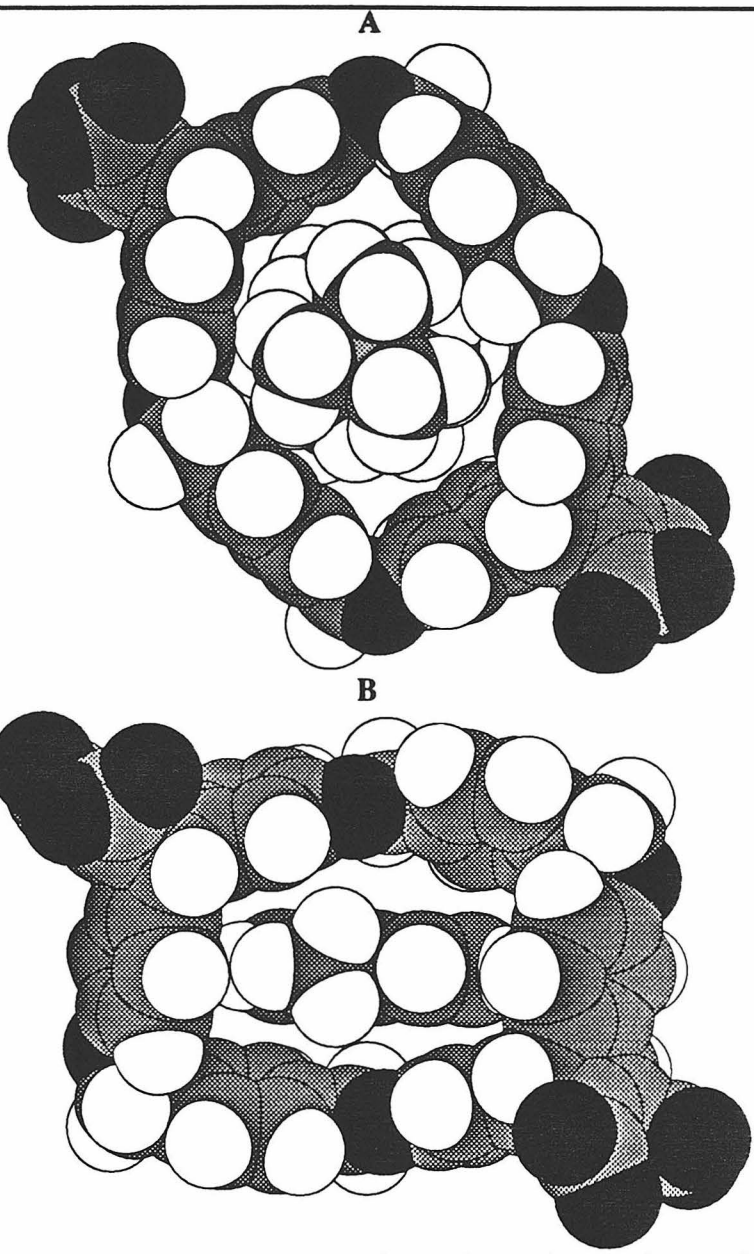

Figure 3.19. Toroid (A) and rhomboid (B) conformations of host P with docked prototypical guests.[1b,2]

NMR studies with host **P** and the guests of Figure 3.18, support the two-state binding model proposed in Figure 3.19.[1b] The shifting of host proton peaks is quite small in these NMR studies,[1b] and more conclusive experimental evidence for this binding model was desired. It was thought that the two conformations should be readily detectable from the CD spectra of the bound complexes.

3.3.2 Circular Dichroism Studies[2]

Figures 3.20 and 3.21 show the best-fit CD spectra of complexes of host **P** with ATMA chloride (**13**) and NMQ chloride (**14**) in aqueous borate buffer compared to the CD spectrum of uncomplexed host.[2] The spectra show very striking qualitative differences. The CD spectra provide strong experimental support for our two-state model. The changes associated with the rhomboid are very subtle, the CD curve showing a general decrease in magnitude of all Cotton effects (Figure 3.21). This is consistent with the host preferring the rhomboid conformation and thus being preorganized to bind NMQ-like guests. The toroid form is characterized by increasing intensity of lower wavelength Cotton effects (Figure 3.21); the changes observed in the spectrum are consistent with the host undergoing a significant conformational change in order to bind guest **13**. This pattern persists throughout the series of guests studied (see Chapter 2). Only two guests showed the toroid binding spectral changes, **13** and tetrabutylammonium ion. All other guests show the rhomboid binding spectrum, and CPK models show that all of these other guests fit well into the rhomboid binding site.

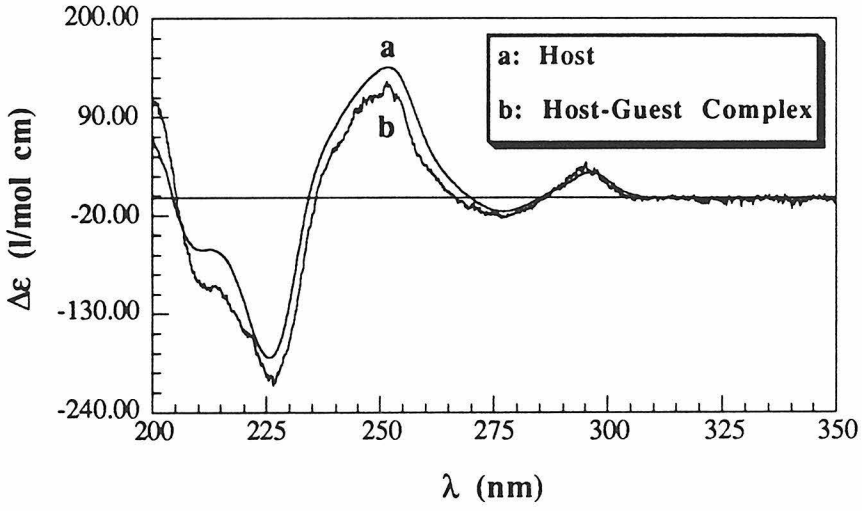

Figure 3.20. CD spectrum of host P_S and best-fit spectrum of its complex with guest 13 in aqueous borate buffer (pH 9).

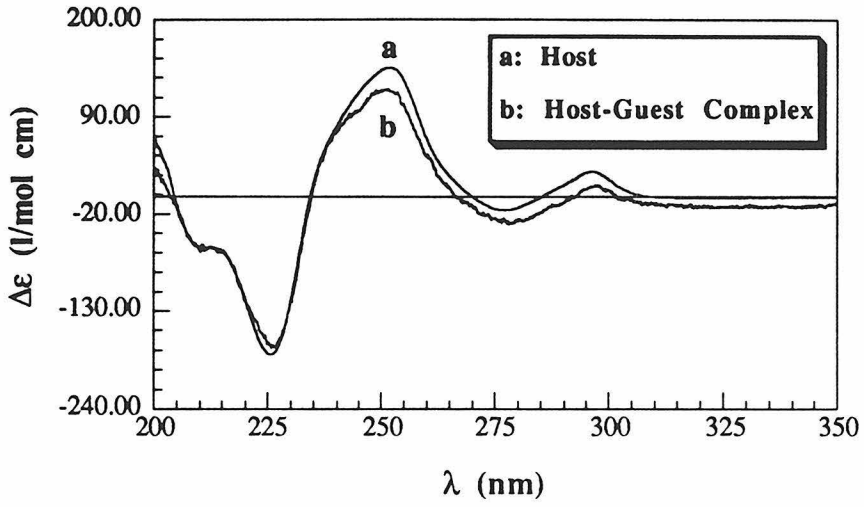

Figure 3.21. CD spectrum of host P_S and best-fit spectrum of its complex with guest 14 in aqueous borate buffer (pH 9).

3.3.3 Other Hosts

Another host of interest is the saturated linker analog of host **P**, host **C** (Figure 3.1).[1b,15] Modeling suggests that host **C** has binding conformations and behavior nearly identical to host **P**.[16] Host **C** is also thought to have a cavity of approximately the same dimensions as host **P**.[16] As a result, spectral behavior similar to that observed for host **P** was expected.

Figures 3.22 and 3.23 show the CD spectra of host **C** and its complexes with ATMA chloride (**13**) and NMQ chloride (**14**) in aqueous borate buffer. The differences between the spectra of the two conformations are very subtle (Figures 3.22 and 3.23). This data suggests that it is the repositioning of the linkers (CD active in **P**, non-contributing to CD spectrum in **C**) which are responsible for the observed CD changes accompanying host conformational changes. This assumption is consistent with the calculated conformations of the hosts.

CD studies of other hosts derived from **P** have also shown the rhomboid vs toroid binding conformations with appropriate guests when the linkers are CD active.[14,17]

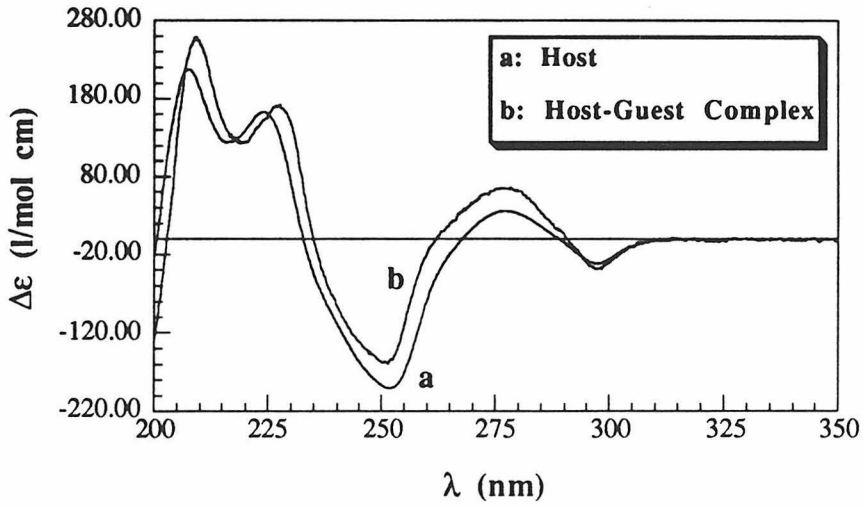

Figure 3.22. CD spectrum of host C_R and fitted spectrum of its complex with guest 13 in aqueous borate buffer (pH 9).

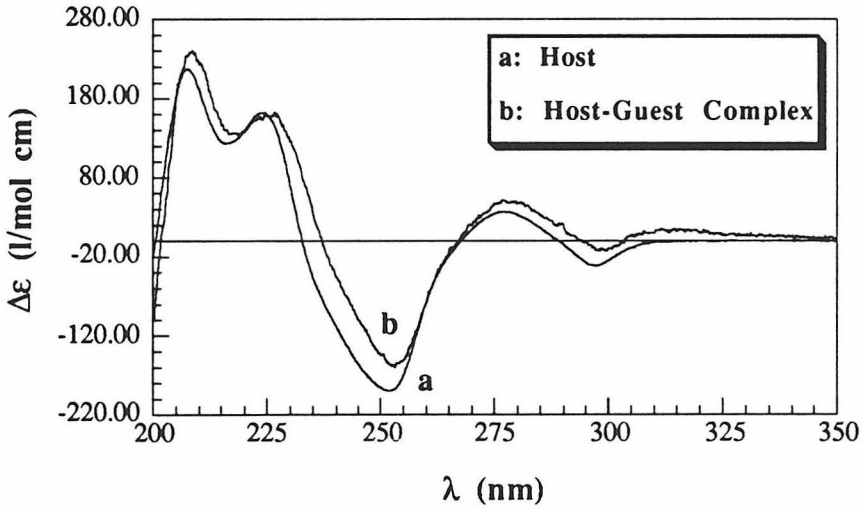

Figure 3.23. CD spectrum of host C_R and fitted spectrum of its complex with guest 14 in aqueous borate buffer (pH 9).

3.4 X-Ray Crystallography[3]

3.4.1 Introduction

A number of attempts were made to obtain solid-state structures of hosts from our laboratories with and without bound guests. The only success from these experiments was obtained with the tetramethyl ester of host **P** ($\mathbf{P_E}$, Figure 3.1). $\mathbf{P_E}$ was crystallized by a combination of slow evaporation of and water vapor diffusion into an acetonitrile solution of the host. Crystals of $\mathbf{P_E}$ as a mono-acetonitrile solvate were obtained from solutions containing no guests and from solutions containing guests **13** or **14**. The binding constants for these guests with $\mathbf{P_E}$ in pure acetonitrile are expected to be negligible,[18] but it was hoped that the water vapor would serve to increase hydrophobic binding forces and thus allow for crystals of host-guest complexes to form. Unfortunately, no guest binding was obtained in the crystal. However, esters from neighboring host molecules in the crystal were bound in the cavity. Thus the crystal structure of $\mathbf{P_E}$ is believed to represent a true binding conformation.[3]

3.4.2 Crystal Structure of $\mathbf{P_E \cdot CH_3CN}$[3]

Table 3.1 summarizes the crystal data for the orthorhombic crystals obtained of the (*S*,*S*,*S*,*S*)-enantiomer of $\mathbf{P_E \cdot CH_3CN}$. The final heavy atom parameters are give in Table 3.2. Figure 3.24 shows an ORTEP[19] drawing of the molecule, including the numbering system. The cavity is in the rhomboid conformation, consistent with this being the more energetically favorable of the two preferred solution conformations.[1b,2,3] The cavity has an effective size of approximately 4.0×7.6 Å, as illustrated in Figure 3.25. Table 3.3 lists selected trans-cavity distances.[3]

Interestingly, the acetonitrile molecule of solvation was not associated with the cavity. Rather, the cavity is filled with the ester moieties from two adjacent $\mathbf{P_E}$ molecules, one entering from either side.[3] Figure 3.26 illustrates two views of this arrangement. The ester moieties ("guests") are packed quite snugly into the cavity: O•••C distances to the aromatic atoms in the walls (from oxygen atoms involved in the ester linkage) range down to 3.28(1) Å, and C•••C distances (from the terminal methyl groups) down to 3.56(1) Å.[3] Although none of the ester groups penetrate completely into the center of the cavity, it is still perhaps best to think of the observed conformation of $\mathbf{P_E}$ as a binding conformation, rather than as a conformation of free host.[3] It is important to point out that the preferred gas-phase conformation of the host cavity without any guest present is thought to be collapsed on itself.[16,20] It should be noted that the single ester grouping that enters the cavity from the right-hand side in Figure 3.26B is disordered between two conformations; only the major orientation is shown in Figures 3.24-3.26.[3] The alternative orientation, with population 0.16(1), is rotated by -102° about the C-C bond. In this orientation, the terminal methyl group C46B lies outside the cavity.[3] It is worth noting that the positions of the ester grouping atoms in the cavity are less certain than the other atoms in the structure, as illustrated by the large thermal ellipsoids for these atoms (Figure 3.24).

The cavity shows approximate C_2-symmetry. Disregarding the central linker groupings (rings *B* and *B'*, Figure 3.25), corresponding atoms in the two halves of the molecule map onto one another to within 0.2 Å.[3] Some atoms of *B* and *B'* show mismatches of about 0.5 Å, representing significantly different tilts of these rings relative to the central axis.[3] The walls of the cavity are only approximately vertical. Rings *C* and *C'* are inclined (from the vertical) by about 10°, and rings *A* and *A'* by about 30°, while ring *B'* is inclined by only 12°, and ring *B* is inclined by 34°.[3] Opposite walls are inclined in opposite directions, so that the two openings into the cavity have quite different shapes.[3] In the present case, one side of the opening accommodates much of two methyl esters, while the other side accommodates but one.[3] Despite the deviations from perfect C_2-symmetry, the

structure agrees quite well with the calculated rhomboid structure. The rhomboids of Figures 3.17 and 3.19 are derived from this crystal structure, and as seen in Figure 3.19. The cavity size is ideally suited to encapsulation of our prototypical rhomboid binding guest **(14)**.

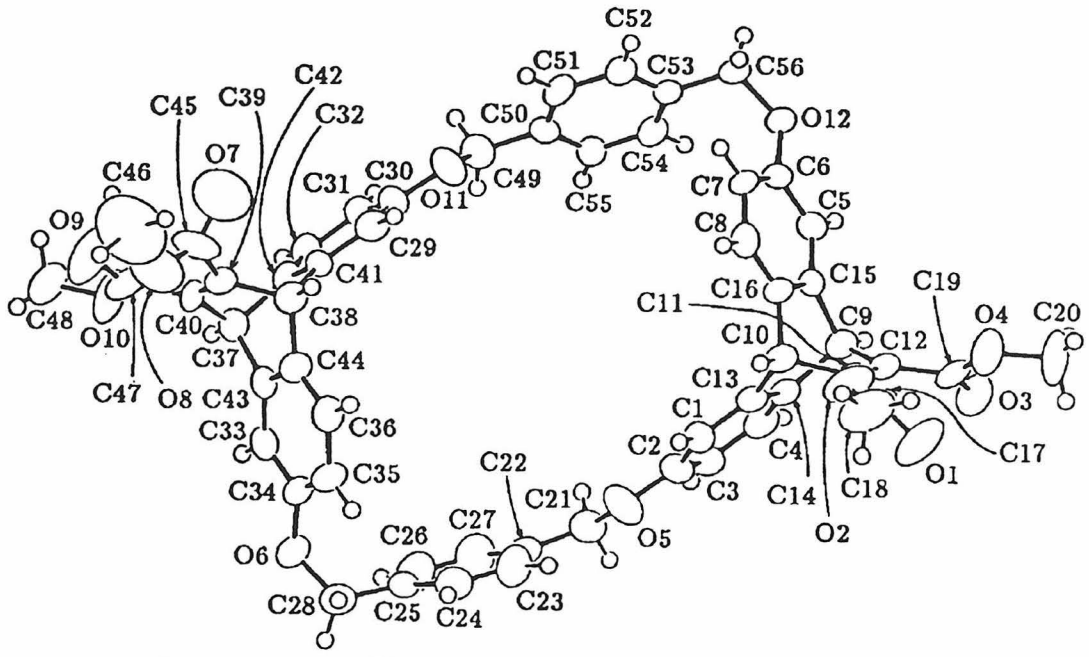

Figure 3.24.[3] An ORTEP[19] view of P_{ES}, with the atom numbering. Heavy atoms are shown as their 50% probability ellipsoids and H atoms as spheres of arbitrary, small dimension. C11 is hidden behind O2.

Space Group	orthorhombic, $P2_12_12_1$
a	11.741(6) Å
b	16.155(5) Å
c	25.895(7) Å
V	4912 Å^3
Z	4
D_x	1.28
***F*(000)**	2020e$^-$
Radiation	Mo *Kα*
λ	0.7107 Å
μ	0.84 cm^{-1}
R	0.0538 (for 2410 independent reflections with I > 0)
S	2.29 (for 2610 total reflections)

Table 3.1. Crystal data for P_{ES}•CH_3CN.[3]

	x, y, z, and $U_{eq}{}^{a} \times 10^4$								
Atom	x	y	z	U_{eq}	Atom	x	y	z	U_{eq}
O1	7798(6)	41(4)	2690(3)	919(25)	C25	5024(8)	4866(7)	-394(4)	605(30)
O2	6257(5)	-344(4)	2270(3)	750(21)	C26	4928(9)	5478(6)	-37(5)	786(34)
O3	7532(6)	1559(4)	3884(3)	777(21)	C27	5227(9)	5337(6)	479(5)	789(34)
O4	7033(5)	242(4)	3737(3)	816(21)	C28	4639(8)	4991(6)	-945(4)	746(33)
O5	5895(5)	3572(4)	1288(2)	694(20)	C29	-738(7)	3372(5)	548(4)	474(24)
O6	3486(5)	5304(4)	-961(2)	744(22)	C30	-943(7)	3831(6)	996(3)	469(26)
O7	-2563(9)	2610(6)	-766(3)	1498(35)	C31	-1107(7)	4660(5)	969(3)	467(25)
O8	-2040(7)	3002(5)	-1514(3)	1133(28)	C32	-1015(7)	5074(5)	503(3)	455(22)
O9	-2927(7)	2610(6)	-766(3)	1498(35)	C33	1579(8)	5146(5)	-735(3)	522(26)
O10	-2149(6)	5790(5)	-1042(3)	984(26)	C34	2625(8)	4753(7)	-828(3)	569(32)
O11	-955(5)	3382(3)	1449(2)	617(18)	C35	2727(7)	3915(6)	-808(4)	583(31)
O12	1481(4)	1786(3)	3764(2)	507(18)	C36	1778(8)	3441(5)	-685(3)	548(27)
C1	5616(7)	2441(5)	1824(3)	446(24)	C37	-530(7)	4973(5)	-470(3)	446(22)
C2	5853(7)	3271(6)	1783(4)	494(26)	C38	-366(7)	3391(5)	-430(3)	455(23)
C3	5997(7)	3752(5)	2229(4)	502(25)	C39	-1288(7)	3708(6)	-802(3)	429(25)
C4	5925(7)	3378(6)	2708(3)	482(26)	C40	-1353(7)	4523(6)	-825(3)	453(26)
C5	3391(8)	1889(5)	3529(3)	405(23)	C41	-648(7)	3767(5)	87(3)	385(24)
C6	2311(7)	1590(5)	3402(3)	417(25)	C42	-744(7)	4630(5)	64(3)	393(24)
C7	2121(7)	1144(5)	2954(3)	438(27)	C43	659(7)	4659(5)	-614(3)	418(25)
C8	3042(8)	986(5)	2628(3)	457(25)	C44	741(7)	3800(5)	-589(3)	443(25)
C9	5493(7)	2029(5)	3237(3)	436(23)	C45	-2046(10)	3086(7)	-1049(5)	867(40)
C10	5193(7)	1190(5)	2412(3)	421(23)	C46	-2870(15)	2409(8)	-1735(5)	1969(65)
C11	6119(6)	856(5)	2766(3)	427(24)	C47	-2172(8)	5002(70	-1127(4)	611(34)
C12	6258(7)	1265(5)	3203(3)	427(25)	C48	-2946(8)	6344(6)	-1286(4)	967(39)
C13	5529(6)	2093(5)	2303(3)	384(22)	C49	-932(7)	3835(5)	1916(3)	575(25)
C14	5703(7)	2550(5)	2749(3)	379(22)	C50	-622(7)	3287(5)	2357(3)	427(24)
C15	4277(7)	1723(5)	3196(3)	363(22)	C51	-1076(7)	2502(6)	2392(3)	560(28)
C16	4113(7)	1265(5)	2744(3)	370(23)	C52	-780(7)	1976(5)	2799(3)	545(25)
C17	6830(9)	141(6)	2592(4)	512(29)	C53	-17(7)	2254(5)	3169(3)	438(26)
C18	6869(8)	-1031(6)	2047(4)	919(36)	C54	413(7)	3040(6)	3132(3)	489(25)
C19	7025(7)	1046(7)	3635(4)	544(35)	C55	129(7)	3542(5)	2721(4)	460(23)
C20	7770(10)	-41(8)	4162(4)	1172(40)	C56	300(7)	1694(6)	3607(3)	531(28)
C21	5857(8)	4437(5)	1202(4)	622(27)	C57	2204(14)	2428(9)	4988(5)	1486(54)
C22	5642(7)	4594(6)	640(4)	532(27)	C58	1019(13)	2337(8)	5175(5)	952(43)
C23	5798(8)	3993(6)	270(4)	711(30)	N	192(11)	2278(9)	5332(6)	1036(44)
C24	5501(8)	4126(6)	-247(4)	672(30)					

Table 3.2. Final heavy atom parameters (Å, U_{eq} in Å^2) for $P_{ES}\cdot CH_3CN$.[3]

[a] $U_{eq} = \frac{1}{3}\sum_i \sum_j \left[U_{ij}(\mathbf{a}_i^* \mathbf{a}_j^*)(\vec{\mathbf{a}}_i \cdot \vec{\mathbf{a}}_j)\right]$

	Distance (Å)		Distance (Å)		Distance (Å)		Distance (Å)
C1-C51	7.994(12)	O5-O11	8.060(8)	C27-C31	7.624(13)	C6-C43	11.683(12)
C1-C55	7.075(12)	C21-C49	7.624(13)	C8-C33	11.133(12)	C6-C44	11.087(12)
C2-C50	7.745(12)	C23-C29	7.624(13)	C8-C36	9.567(12)	C7-C43	10.980(12)
C3-C51	8.557(12)	C23-C31	8.376(13)	C5-C33	12.414(12)	C7-C44	10.256(12)
C3-C55	7.014(12)	C27-C29	7.624(13)	C5-C36	11.355(12)		

Table 3.3. Selected distances (Å) across the cavity in $P_{ES}\cdot CH_3CN$.[3]

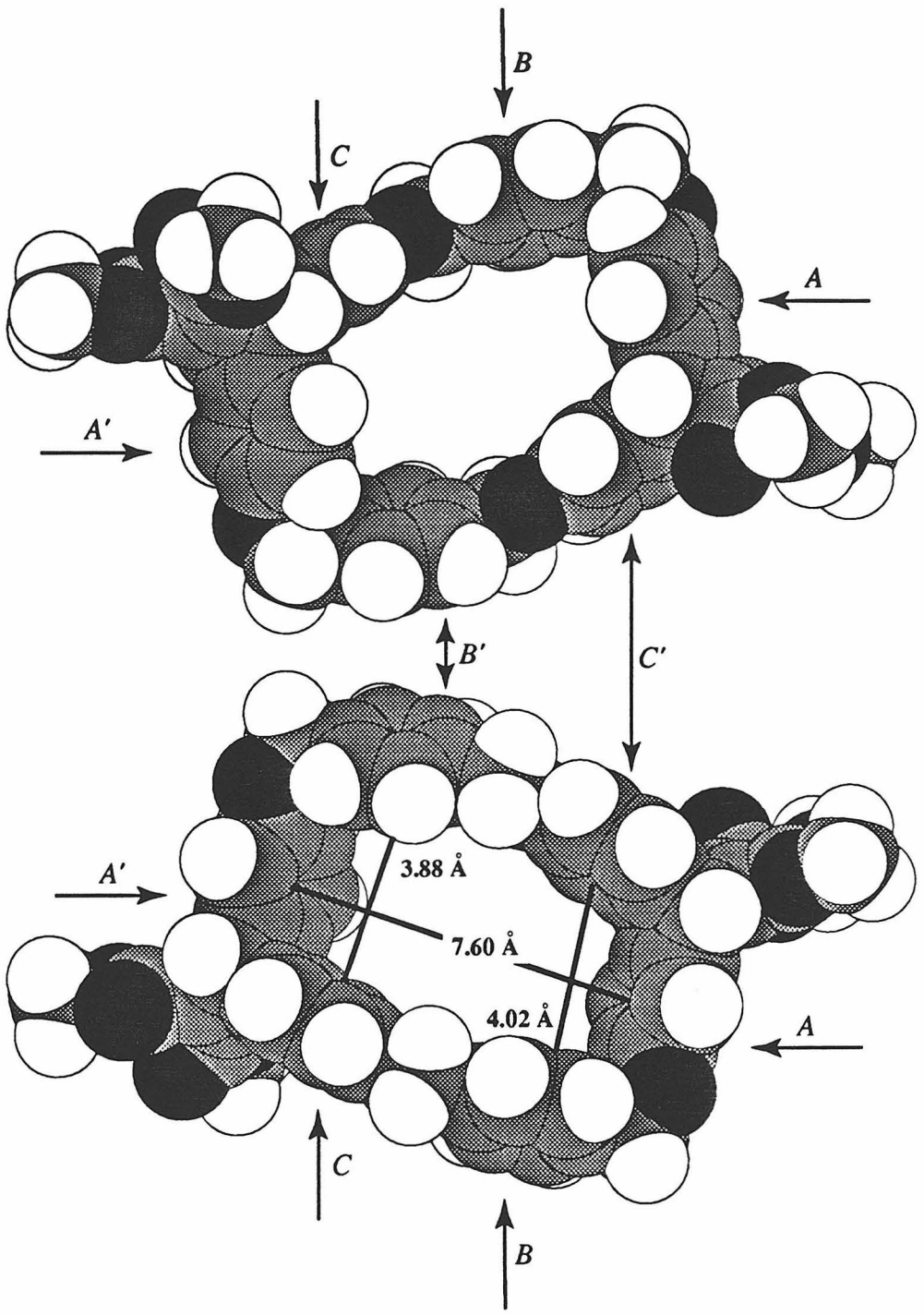

Figure 3.25.[3] Two views of P_{ES} in space-filling representation, showing the dimensions of the cavity. The top view is the orientation of Figure 3.24, and the bottom view is the back, *i.e.* rotated by 180° about the horizontal axis. The six aromatic rings of the cavity are labeled *A*-*C*.

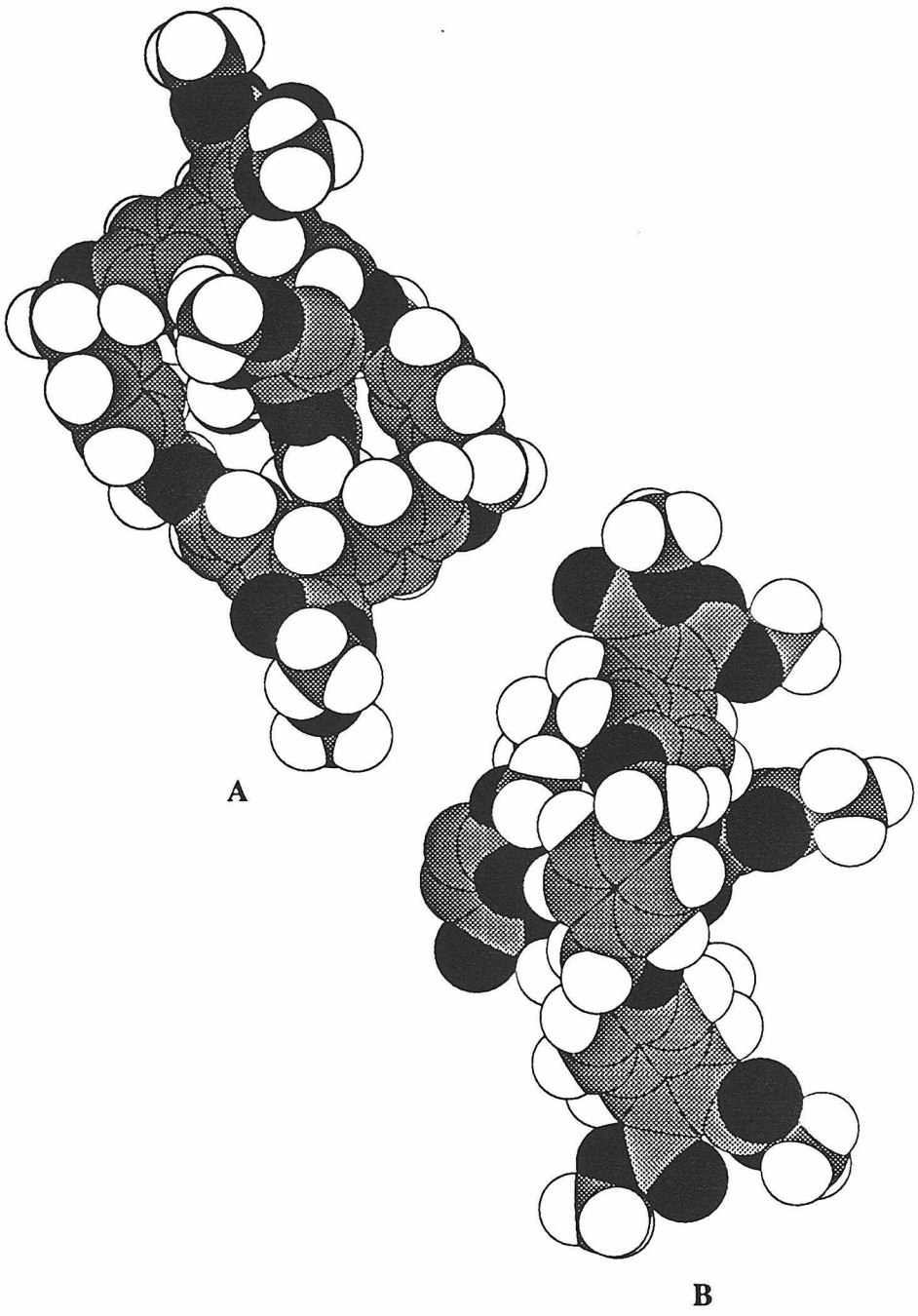

Figure 3.26. View of P_{ES} (A) perpendicular to the cavity and (B) 90° from (A) showing ester groupings of adjacent molecules entering from both sides of the cavity.

Bond lengths and angles are, in general, normal (Table 3.4), but it is worth noting the following: the CH_2-O bond lengths between rings *A* and *B*, and between A' and B', are

significantly longer [1.443(6) vs 1.1415(6) Å] than those between *B* and *C* (and *B'*, *C'*), reflecting a lack of conjugation due to the sharp bend in the molecule.[3] The two adjacent bonds show similar but smaller effects, the differences bordering on insignificance.[3]

Bond Type	Number of Bonds	Average Lengths[b]	Expected Lengths[21,b]
C-C(aromatic)	36	1.381(16)	1.380(13)
C(aromatic)-C(sp^3)	4	1.500(8)	1.510(9)
C(sp^3)-O(ether)	4	1.432(20)	1.424(12)
C(aromatic)-O(ether)	4	1.383(9)	1.370(11)
C(bridgehead)-C(aromatic)	8	1.524(13)	1.515(11)
C(bridgehead)-C(sp^3)	4	1.527(8)	1.510(14)
C(sp^2)-C(sp^2)	2	1.320(1)	1.317(13)
C(sp^2)-C(carbonyl)	4	1.480(15)	1.488(14)
C(carbonyl)-O(carbonyl)	4	1.206(21)	1.196(10)
C(carbonyl)-O(ester)	3[a]	1.315(19)	1.336(14)
O(ester)-C(sp^3)	4	1.459(21)	1.448(10)

Table 3.4. Average bond distances (Å) for P_{ES}.[3]
[a]C45-O8, 1.212(14) Å, not included. [b]Quantities in parentheses are sample standard deviations.

Lists of distances and angles not involving hydrogen (Tables 3.5 and 3.6), assigned hydrogen parameters (Table 3.7), distances and angles involving hydrogen (Tables 3.8 and 3.9), and anisotropic displacement parameters (Table 3.10) are given in appendices 2-5 (Sections 3.8-3.11).

3.5 Conclusions

Through a combination of experiments using circular dichroism (CD) spectroscopy and x-ray crystallography, several important features of the structures of hosts **P**, P_E, and **C** have been probed. Exciton coupled CD spectroscopy has established the absolute stereochemistry of samples of the chiral ethenoanthracene building blocks (**1**) used in the preparation of these hosts.[1,2] CD spectroscopy has also provided direct experimental evidence of the proposed two-state binding model of host **P** in solution.[2] Finally, an x-ray crystal structure of P_E has confirmed the rhomboid binding conformation proposed as one

of the two favored solution conformations.[3] In this solid-state structure, ester groupings from neighboring hosts in the crystal act as guests bound in the cavity.[3] These studies serve to confirm earlier studies in which the structures were inferred from indirect experimental evidence and computation.[1]

3.6 Experimental Section

3.6.1 General Methods[1]

CD spectra were recorded on a JASCO J-600 Spectropolarimeter with a 1.0 cm pathlength quartz cell. A standard set of measurement parameters was used in all quantitative experiments: Band Width 1.0 nm, Sensitivity 50 m°/cm, Time Constant 1.0 Sec., Scan Speed 50 nm/min., Step Width 0.2 nm/point, and a minimum of 4 accumulations. IR spectra were recorded on a Perkin-Elmer 1600 FT-IR. GC/MS data was obtained on a Hewlett-Packard 5890/5970 GC/MS. ^{1}H NMR spectra were recorded on a Bruker AM-500 spectrometer; routine spectra were referenced to the residual proton signals of the solvents and are reported in ppm downfield of 0.0 as δ values.

All solvents used in spectroscopy were spectrophotometric or HPLC grade. Aqueous cesium borate buffer (pH 9) was prepared by dissolving 0.25 g high purity boric oxide in 800 g water and adding 3.74 ml of 1 M CsOH followed by thorough mixing. The water used in these preparations was passed through a Milli-Q purification system.

All reactions, unless otherwise noted, were stirred magnetically under a nitrogen atmosphere. Solvents were distilled from drying agents under argon atmosphere; acetonitrile, CaH_2; THF, sodium benzophenone ketyl. Ion exchange for NH_4^+ was carried out with Dowex® 50w-x2 cation exchange resin (the resin was treated with concentrated ammonium carbonate then washed with Milli-Q purified water before use).

Unless otherwise noted, reagents obtained from commercial sources were used without further purification.

Compounds **1, 2, 3, 4, 5, 13, 14, P, P_E,** and **C** were prepared by procedures described previously.[1,2] Circular dichroism binding studies are described in Chapter 2 of this manuscript.

The $\Delta\varepsilon$ values for the host **C** complexes (Figures 3.22 and 3.23) come from single spectra of solutions containing known amounts of host and guest; using previously measured binding constants and extinction coefficients ($-\Delta G°_a$ = 5.5 kcal/mol for **13**, $-\Delta G°_a$ = 6.3 kcal/mol for **14**);[1b] the host-guest complex spectrum was calculated from the measured spectrum using equations 3.32 and 3.33.

$$\Delta\varepsilon_{HG\lambda} = \frac{\theta_\lambda}{gl\,[HG]} - \frac{[H]\Delta\varepsilon_{H\lambda} + [G]\Delta\varepsilon_{G\lambda}}{[HG]} \tag{3.32}$$

$$g = \frac{2.30259}{100} \times \frac{4500}{\pi} \times 1000 \tag{3.33}$$

Where θ_λ is the total solution ellipticity at wavelength λ; [H], [G], and [HG] are equilibrium concentrations of host, guest and host-guest complex; l is the pathlength of the cell (cm), and $\Delta\varepsilon_{i\lambda}$ is the extinction coefficeint for species i at wavelength λ.

3.6.2 Synthesis

(9*R*, 10*R*)-2, 6-Bis[*p*-(dimethylamino)benzoyloxy]-9,10-dihydro-11, 12-di-carbomethoxyethenoanthracene (9_R). A 25 ml oven dried flask was charged with 0.024 g (6.81 x 10^{-5} mol) $\mathbf{1}_R$, 0.065 g (3.54 × 10^{-4} mol) *p*-(dimethylamino)benzoyl chloride (**11**, preparation below), 50 µl (0.05 g, 6.18 × 10^{-4} mol) pyridine, and a catalytic amount of 4-dimethylaminopyridine. The mixture was dissolved in 5 ml THF and heated to 55 °C with stirring in the dark. After 19 hours TLC (silica gel, 7:3 CH_2Cl_2:ether) indicated completion of reaction. The mixture was filtered and the filtrate rotary evaporated

to give a yellowish residue. Two consecutive purifications by flash chromatography (Si gel, 7:3 CH_2Cl_2:ether) provided 0.035 g (80%) of 9_R. ^1H NMR (CD_3CN) δ (ppm) 8.12 (d, 4H, J = 8.6 Hz), 7.48 (d, 2H, J = 8.3 Hz), 7.38 (d, 4H, J = 8.6 Hz), 7.33 (d, 2H, J = 2.2 Hz), 6.91 (dd, 2H, J = 8.3, 2.3 Hz), 5.63 (s, 2H), 3.75 (s, 6H), 3.09 (s, 12H). FAB-MS, *m/e* 647 (MH^+), 312, 180, 166, 148, 122; HRMS, 664.2659 (M + NH_4^+), calculated for $C_{38}H_{34}N_2O_8$ + NH_4^+ 664.2660. CD [(9*R*, 10*R*)-enantiomer, CH_3CN] λ ($\Delta\varepsilon$) [nm ($M^{-1}cm^{-1}$)], 324 (+35.0), 295 (-6.2), 270 (+4.9), 247 (-9.4), 218 (+42.3).

***p*-(Dimethylamino)benzoyl Chloride (11).**[6] A suspension of phosphorous pentachloride (12.61 g, 0.061 mol) in 225 ml carbon disulfide was added slowly over a one hour period to a stirring suspension of 10.04 g (0.061 mol) *p*-(dimethylamino)benzoic acid (**10**) and 5.4 ml (5.28 g, 0.067 mol) pyridine in 100 ml carbon disulfide. Upon complete addition the mixture was heated at reflux until all the white solid dissolved, after which the mixture was filtered (CAUTION-CS_2 is very flammable) and allowed to cool. The white crystals that formed on cooling were collected and dried under vacuum in a desiccator to yield 5.52 g (50%). ^1H NMR ($CDCl_3$) δ (ppm) 7.95 (d, 2H, J = 9.12 Hz), 6.71 (d, 2H, J = 9.4 Hz), 3.15 (s, 6H). IR (KBr) 1737 cm^{-1} (COCl). GC/MS 21 min. *m/e* 120 (M - COCl).

3.6.3 CD Data for Previously Reported Compounds

C. [(9*R*, 10*R*, 9'*R*, 10'*R*)-enantiomer, aqueous borate buffer] λ ($\Delta\varepsilon$) [nm ($M^{-1}cm^{-1}$)], 297 (-30.9), 277 (+36.6), 252 (-190), 224 (+163), 208 (+218).

3.6.4 Computational Studies[2]

Excitonic chirality calculations were set up and executed using Excel.[22] The atomic coordinates for $\mathbf{9_R}$ were obtained from molecular mechanics calculations using BIOGRAF[9] with the AMBER[10] force field.

Conformational Searching. The six torsion angles involving the benzoates were varied from 0°-180°using a 1000-step Monte Carlo search with 200 minimizations at each step. A total of 1000 possible structures were searched by a usage-directed method[11] and all structures within 6 kcal of the lowest energy conformation were saved. In an effort to save computational time, energy was checked after the first 100 minimizations, and if the best structure was 12 kcal above the previous best structure, it was discarded. This gave 553 low energy structures, which were resubmitted for further minimization, and duplicates were identified and eliminated by superimposing of heavy atoms resulting in deviations in overlap of less than 0.25 Å. This resulted in 64 structures within 1.2 kcal of one another. The excitonic chirality calculations (as described in section 3.2.4)[6] on these 64 structures all predicted positive excitonic chirality (positive first Cotton effect, negative second Cotton effect). This observation was experimentally confirmed.

3.6.5 X-Ray Crystallography[3]

The crystal structure was solved by R. E. Marsh and W. P. Schaefer at the Caltech X-ray Facility. The crystal examined was obtained from an acetonitrile solution that contained a 1:1 mole ratio of $\mathbf{P_{ES}}$:**13** (as iodide salt), by a combination of vapor diffusion of water and evaporation of acetonitrile. After a preliminary photographic survey, the crystal was mounted on an Enraf-Nonius CAD-4 diffractometer (Mo $K\alpha$ radiation). The unit-cell dimensions and orientation matrix were obtained from the setting angles of 25 reflections having $20° < 2\theta < 26°$. Intensities were collected, by ω scans, for four octants

(h, ± k, ± l) to $2\theta = 40°$, at $4°min^{-1}$ over a range of 1.5°; backgrounds were collected for five seconds at each extremum. The backgrounds measured for the very weak reflections were averaged in regions of 2θ and these averages were substituted for the measured backgrounds for *all* reflections, to increase precision and reduce truncation losses.[23] Three check reflections showed no significant variations.

There resulted 9882 intensities, which were averaged according to Laue symmetry *mmm* to yield 2610 independent observations; the goodness-of-fit for merging was 0.95, with variances σ^2_I including, besides counting statistics, a term $0.014I^2$. An additional lack-of-confidence term $0.014\hat{I}^2$ was then added to the final variances $\sigma\hat{I}^2$. An *E* map calculated from the best *MULTAN*[24] solution showed two small fragments (five and seven atoms) of the molecule; the remaining C, N, and O atoms were recovered gradually from a series of factor-Fourier cycles. All hydrogen atoms were placed in assumed positions (with the help of a difference section for the acetonitrile group). Refinement was by least-squares minimization of $\Sigma\omega(F_o^2 - F_c^2)^2$ with weights ω equal to the reciprocals of the variances $\sigma_{F^2}^2$. Initial convergence was reached at R = 0.063, S = 2.7; however, a difference map showed two peaks at about $0.5e^-Å^{-3}$ in positions that strongly suggested alternative orientations of the two ester groups at C45 and C47. Eventually, three of the oxygen atoms and one methyl group (O7, O8, O9, C46) were represented as disordered between two distinct sites, with a refinable population parameter; the remaining pair of atoms O10 and C48 seemed content in single sites, with their U_{ij}'s (and those of the central carbon atom C47) being able to compensate for the necessary disorder. The four atoms in the minor sites, with final population 0.16(1), were refined as isotropic, and their hydrogen atoms were ignored; all other C, N, and O atoms were anisotropic. The full-matrix cycles now involved 641 parameters (including a secondary-extinction coefficient; final value, $0.19(4) \times 10^{-6}$); at the end, the most significant shift was at 0.12σ, involving the minor site C46B. A final difference map had no feature as large as $0.3e^-Å^{-3}$. Final indicators: S = 2.3 for 2610 total reflections and 641 parameters; R = 0.054 for 2410 reflections with $I >$

0.0; $R = 0.050$ for 2293 reflections with $I > 3.0\sigma_I$. Incomplete modeling of the disorder can surely be blamed for at least some of its overruns.

Calculations were made on a VaxStation 3100 under the *CRYM* Crystallographic Computing System,[25] using scattering factors from the International Tables;[26] the secondary extinction coefficient was that of Larson.[27] Final coordinates are in Table 3.2; they correspond to the (9*S*, 10*S*, 9'*S*, 10'*S*)-enantiomer as required by the synthesis,[1b] which we did not attempt to confirm by crystallography.

3.7 Appendix 1: CD Spectra of Intermediates in the Synthesis of Ethenoanthracene Building Blocks 1 and 12

3.7.1 Introduction

This appendix contains circular dichroism (CD) spectra of a number of etheno- and ethano-anthracene-based building blocks used in the Dougherty labs to prepare hosts and self-assembling molecules. The purpose of this appendix is to aid in the assignment of the sample's absolute stereochemistry during synthesis. The CD spectra were taken in spectrograde acetonitrile using the standard measurement parameters for the J-600 Spectropolarimeter (see Section 3.6.1). The $\Delta\varepsilon$ values reported here were determined from analyses of a single spectra, and as such they are only approximate values and should not be used quantitatively. In addition, baseline corrections for CD drift were employed as needed. For purposes of qualitative analysis, use the following relationship as a guide to preparing solutions of appropriate concentration for study:

$$\theta_\lambda = g l \Delta\varepsilon_\lambda c \tag{3.34}$$

where θ_λ is the observed ellipticity at wavelength λ (in millidegrees, m°), l is the pathlength of the cell (cm), $\Delta\varepsilon_\lambda$ is the molar circular dichroism of the species being

examined at wavelength λ ($M^{-1}cm^{-1}$), c is the concentration of the species being examined (M), and g is defined by equation 3.33.

3.7.2 2,6-Dihydroxyethenoanthracene (1)

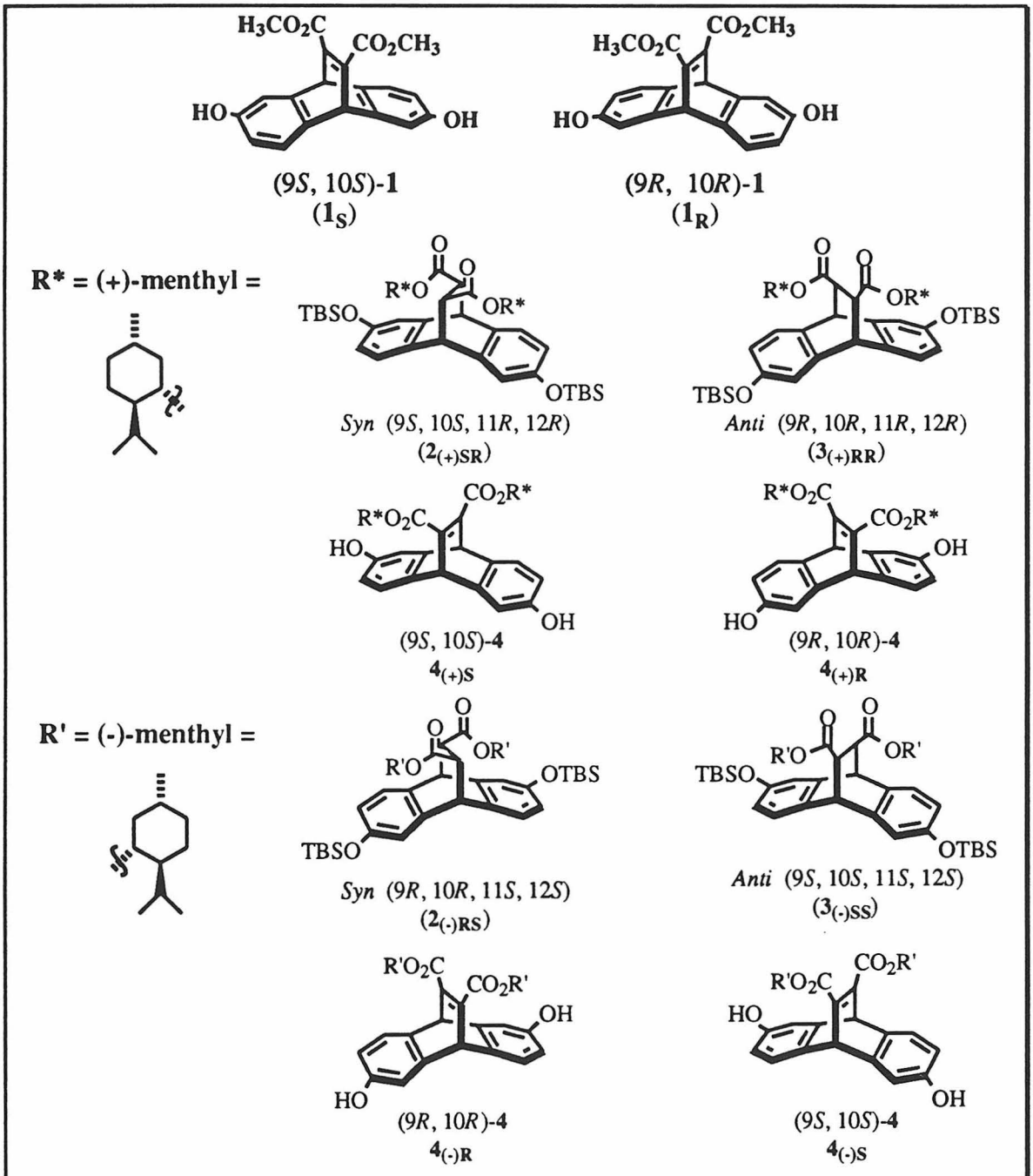

Figure 3.27. Structures and stereochemistry of 2,6-dihydroxyethenoanthracene (1) and the intermediates in its synthesis.

Figure 3.27 shows the structures and stereochemistry of the intermediates in the synthesis of 2,6-dihydroxyethenoanthracene (**1**). Figures 3.28-3.32 show the spectra.

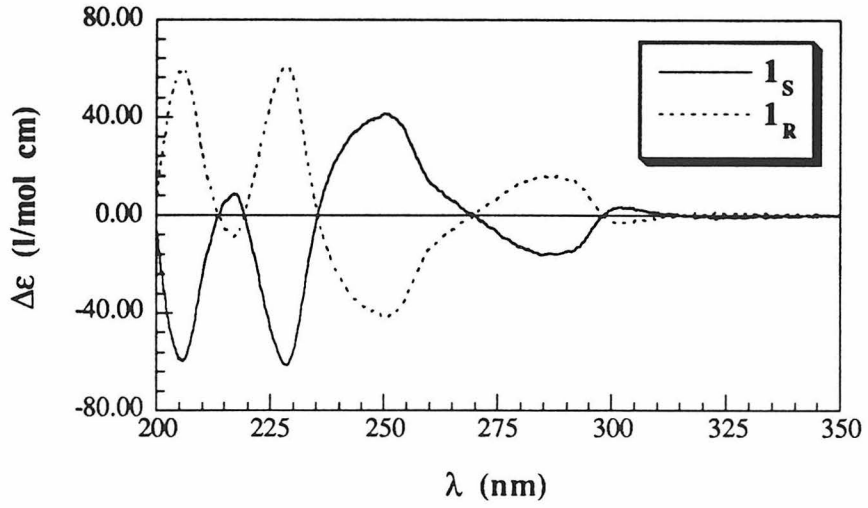

Figure 3.28. CD spectra of 1 in acetonitrile.

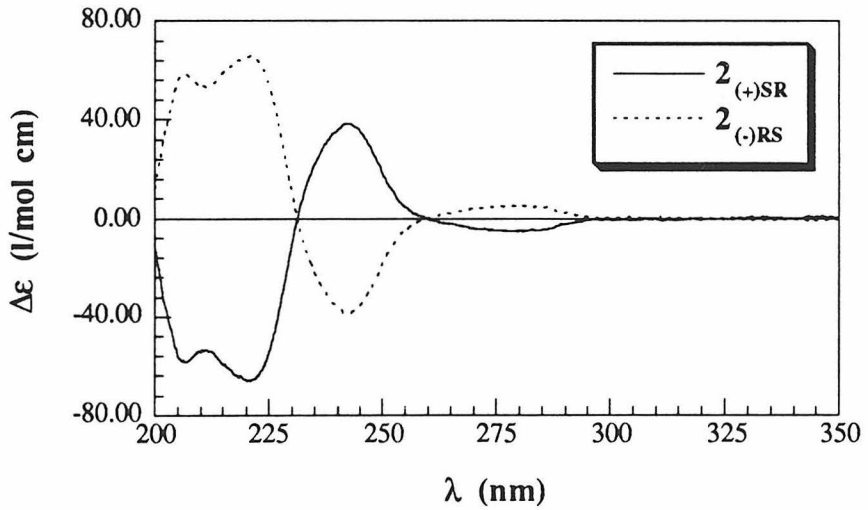

Figure 3.29. CD spectra of 2 in acetonitrile.

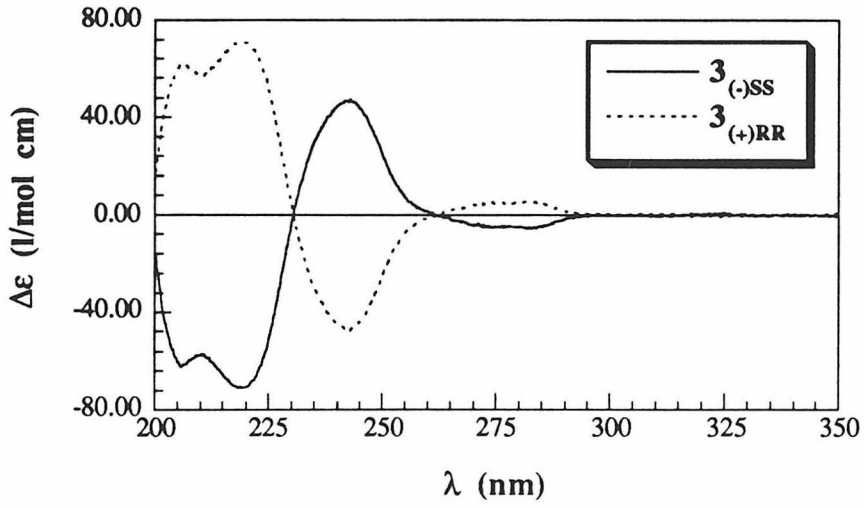

Figure 3.30. CD spectra of 3 in acetonitrile.

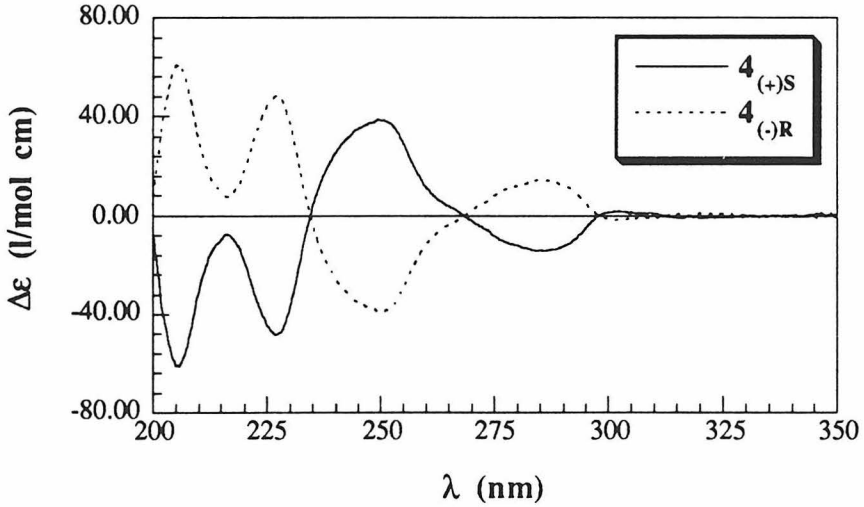

Figure 3.31. CD spectra of 4 in acetonitrile (first set of enantiomers).

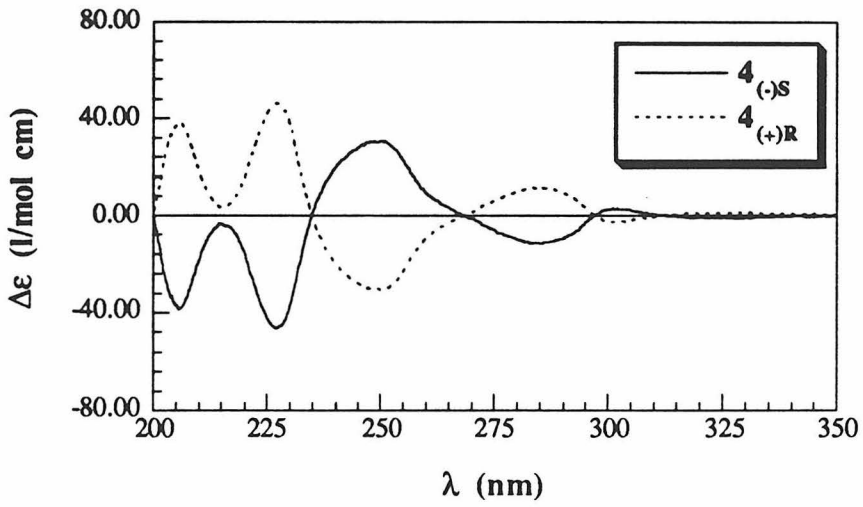

Figure 3.32. CD spectra of 4 in acetonitrile (second set of enantiomers).

3.7.3 1,5-dibromo-2,6-dihydroxyethenoanthracene (12)

Th spectra of the enantiomers of the dibromo ethenoanthracene derivative (**12**) are shown in Figure 3.33. The Diels-Alder reaction used to prepare **12** (Figure 3.34) produces a single diastereomer (**13**),[1a,14] whose spectra are shown in Figure 3.35.

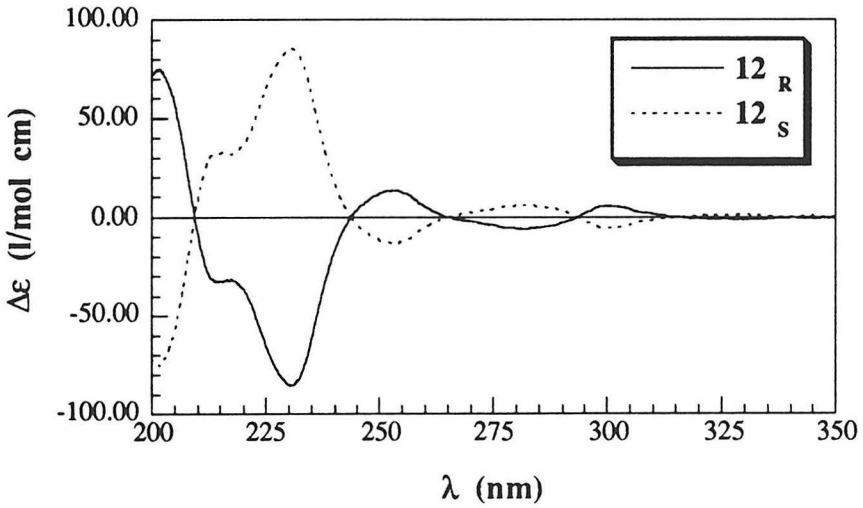

Figure 3.33. CD spectra of 12 in acetonitrile.

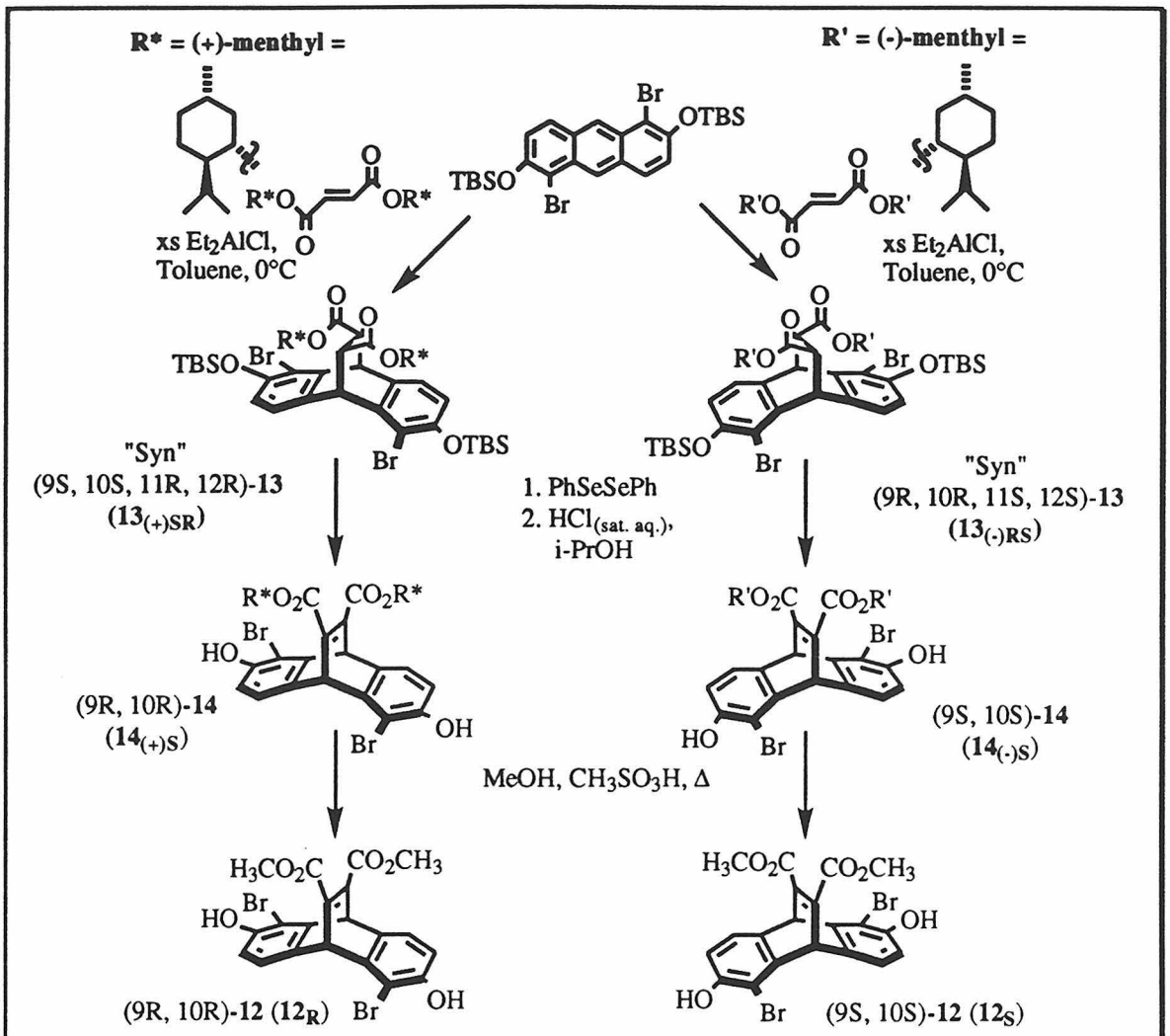

Figure 3.34. Synthesis of 12.[1a,14]

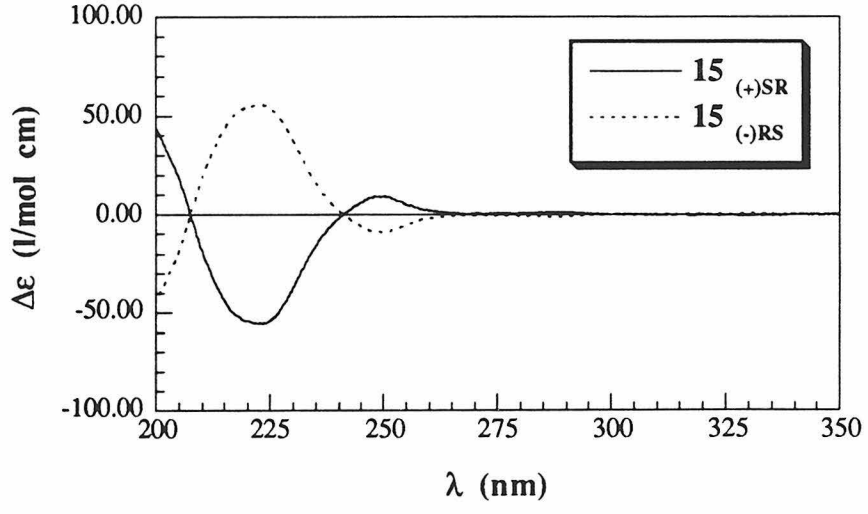

Figure 3.35. CD spectra of 15 in acetonitrile.

3.7.4 Ethanoanthracenes

Figure 3.36 shows the structures and stereochemistry of a number of 2,6-dihydroxyethanoanthracenes. Figures 3.37-3.40 show the spectra.

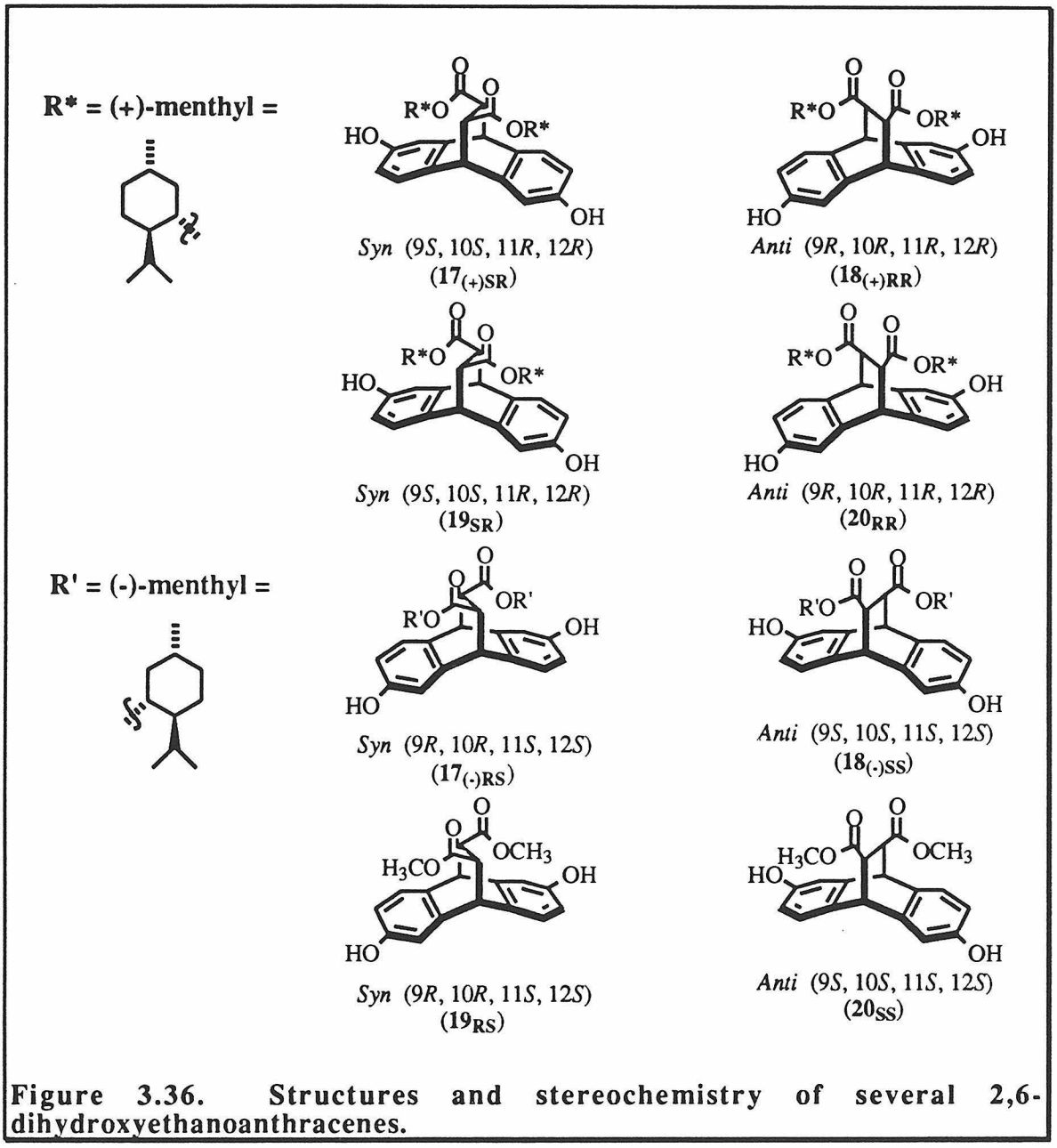

Figure 3.36. Structures and stereochemistry of several 2,6-dihydroxyethanoanthracenes.

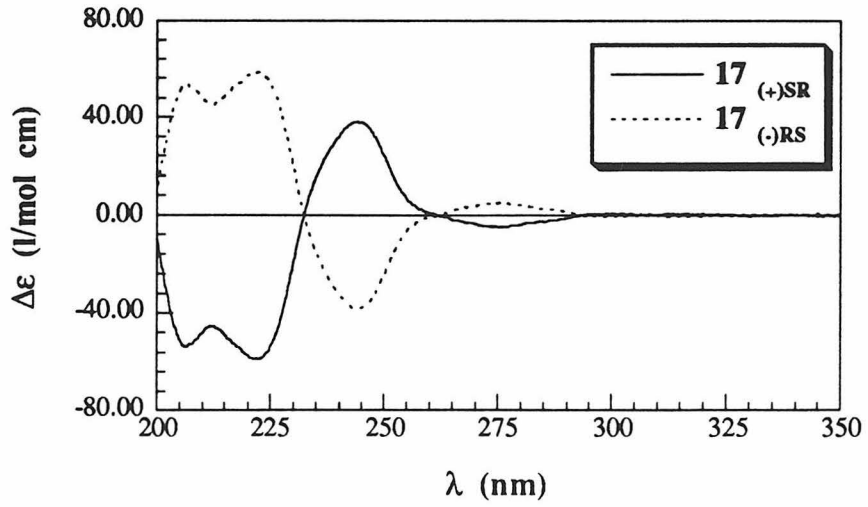

Figure 3.37. CD spectra of 17 in acetonitrile.

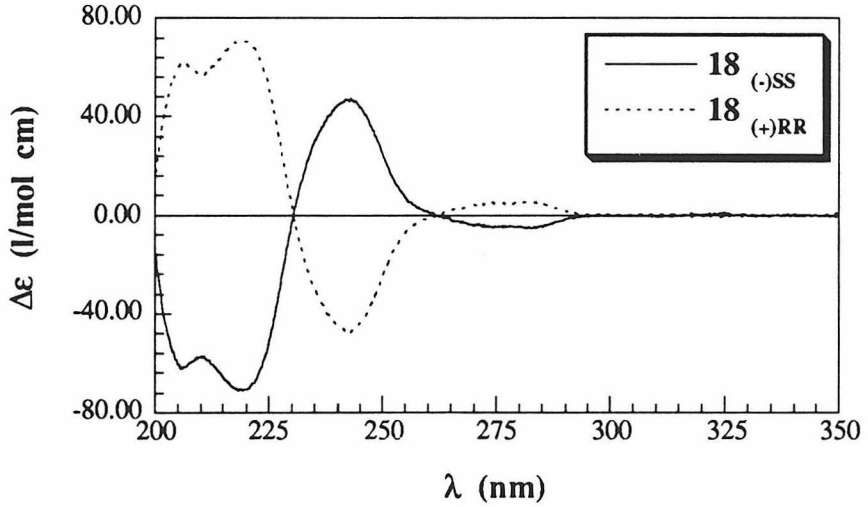

Figure 3.38. CD spectra of 18 in acetonitrile.

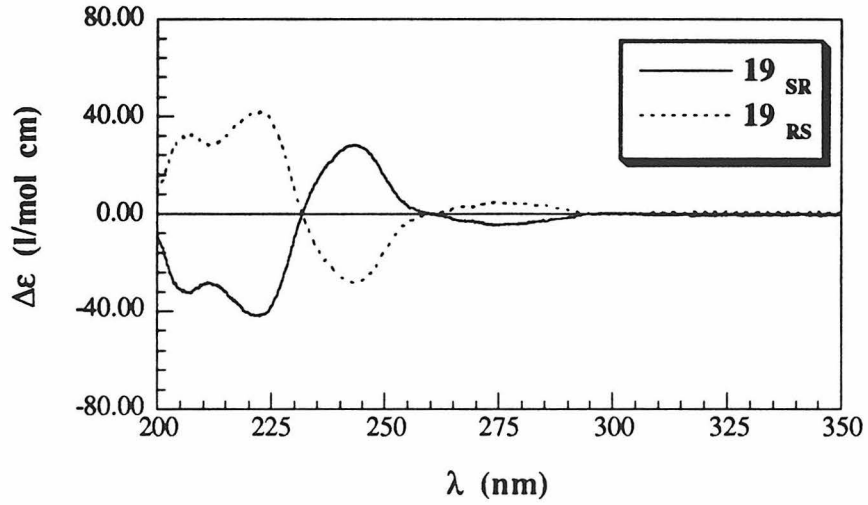

Figure 3.39. CD spectra of 19 in acetonitrile.

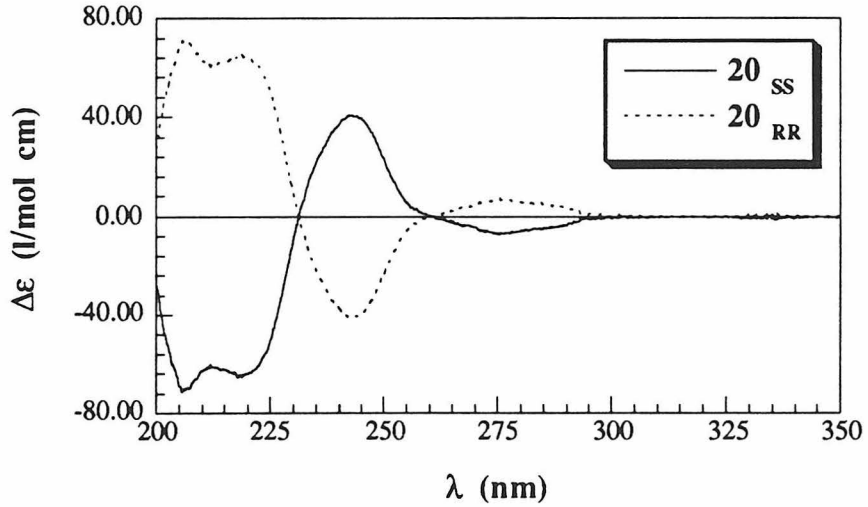

Figure 3.40. CD spectra of 20 in acetonitrile.

3.8 Appendix 2: Distances and Angles Not Involving Hydrogen for the P_{ES} Crystal Structure

	Distance (Å)		Distance (Å)		Distance (Å)		Distance (Å)
O1-C17	1.176(12)	C1-C2	1.372(12)	C15-C16	1.397(11)	C37-C42	1.510(11)
O2-C17	1.327(11)	C1-C13	1.365(11)	C21-C22	1.499(13)	C37-C43	1.531(11)
O2-C18	1.442(12)	C2-C3	1.401(12)	C22-C23	1.375(14)	C38-C39	1.537(12)
O3-C19	1.207(12)	C3-C4	1.382(12)	C22-C27	1.361(14)	C38-C41	1.508(11)
O4-C19	1.324(12)	C4-C14	1.366(12)	C23-C24	1.400(14)	C38-C44	1.515(11)
O4-C20	1.473(13)	C5-C6	1.396(11)	C24-C25	1.374(14)	C39-C40	1.320(12)
O5-C2	1.373(11)	C5-C15	1.378(11)	C25-C26	1.359(15)	C39-C45	1.487(14)
O5-C21	1.416(11)	C6-C7	1.384(12)	C25-C28	1.510(14)	C40-C47	1.460(13)
O6-C28	1.446(11)	C7-C8	1.395(12)	C26-C27	1.400(15)	C41-C42	1.400(11)
O6-C34	1.390(11)	C8-C16	1.369(11)	C29-C30	1.397(12)	C43-C44	1.394(12)
O7-C45	1.225(15)	C9-C12	1.530(11)	C29-C41	1.357(11)	C49-C50	1.491(12)
O8-C45	1.212(14)	C9-C14	1.539(11)	C30-C31	1.355(12)	C50-C51	1.378(12)
O8-C46	1.481(17)	C9-C15	1.515(11)	C31-C32	1.385(11)	C50-C55	1.355(12)
O9-C47	1.217(13)	C10-C11	1.521(11)	C32-C42	1.380(11)	C51-C52	1.398(12)
O10-C47	1.293(12)	C10-C13	1.538(11)	C33-C34	1.404(13)	C52-C53	1.387(12)
O10-C48	1.440(12)	C10-C16	1.537(11)	C33-C43	1.372(12)	C53-C54	1.369(12)
O11-C30	1.378(10)	C11-C12	1.319(11)	C34-C35	1.360(13)	C53-C56	1.499(12)
O11-C49	1.413(10)	C11-C17	1.494(12)	C35-C36	1.389(13)	C54-C55	1.380(12)
O12-C6	1.390(10)	C12-C19	1.480(13)	C36-C44	1.372(12)	C57-C58	1.48(2)
O12-C56	1.452(10)	C13-C14	1.386(11)	C37-C40	1.520(12)	C58-N	1.058(19)

Table 3.5. Distances not involving hydrogen for the P_{ES} crystal structure.

	Angle (°)		Angle (°)		Angle (°)
C18-O2-C17	117.0(7)	C16-C15-C5	121.5(7)	C44-C38-C39	106.7(6)
C20-O4-C19	117.2(8)	C16-C15-C9	111.2(7)	C44-C38-C41	104.7(6)
C21-O5-C2	119.8(7)	C10-C16-C8	127.5(7)	C40-C39-C38	113.7(7)
C34-O6-C28	116.7(7)	C15-C16-C8	119.0(7)	C45-C39-C38	117.8(8)
C46-O8-C45	116.9(10)	C15-C16-C10	113.3(7)	C45-C39-C40	128.3(9)
C48-O10-C47	121.6(8)	O2-C17-O1	122.9(9)	C39-C40-C37	114.4(8)
C49-O11-C30	117.1(6)	C11-C17-O1	125.6(9)	C47-C40-C37	119.3(8)
C56-O12-C6	117.2(6)	C11-C17-O2	111.3(7)	C47-C40-C39	126.2(8)
C13-C1-C2	119.1(8)	O4-C19-O3	124.4(9)	C38-C41-C29	127.5(7)
C1-C2-O5	115.2(8)	C12-C19-O3	122.6(8)	C42-C41-C29	120.0(7)
C3-C2-O5	124.6(8)	C12-C19-O4	112.9(8)	C42-C41-C38	112.4(7)
C3-C2-C1	120.2(8)	C22-C21-O5	108.9(7)	C37-C42-C32	127.0(7)
C4-C3-C2	119.3(8)	C23-C22-C21	122.3(8)	C41-C42-C32	120.0(7)
C14-C4-C3	120.6(8)	C27-C22-C21	120.4(9)	C41-C42-C37	113.1(7)
C15-C5-C6	118.1(7)	C27-C22-C23	117.2(9)	C37-C43-C33	125.7(7)
C5-C6-O12	113.5(7)	C24-C23-C22	121.6(9)	C44-C43-C33	121.9(8)
C7-C6-O12	124.9(7)	C25-C24-C23	120.0(9)	C44-C43-C37	112.4(7)
C7-C6-C5	121.6(8)	C26-C25-C24	118.6(9)	C38-C44-C36	128.8(8)
C8-C7-C6	118.5(8)	C28-C25-C24	120.1(9)	C43-C44-C36	118.3(8)
C16-C8-C7	121.3(7)	C28-C25-C26	121.3(9)	C43-C44-C38	112.8(7)
C14-C9-C12	107.4(6)	C27-C26-C25	120.6(10)	O8-C45-O7	121.8(11)
C15-C9-C12	106.6(6)	C26-C27-C22	121.8(10)	C39-C45-O7	117.6(10)
C15-C9-C14	105.7(6)	C25-C28-O6	110.7(7)	C39-C45-O8	120.0(10)
C13-C10-C11	105.3(6)	C41-C29-C30	119.6(8)	O10-C47-O9	121.1(9)
C16-C10-C11	106.3(6)	C29-C30-O11	115.4(7)	C40-C47-O9	123.5(9)
C16-C10-C13	103.9(6)	C31-C30-O11	124.2(8)	C40-C47-O10	114.7(9)
C12-C11-C10	115.3(7)	C31-C30-C29	120.4(8)	C50-C49-O11	110.7(7)
C17-C11-C10	119.4(7)	C32-C31-C30	120.7(8)	C51-C50-C49	120.2(7)
C17-C11-C12	125.2(8)	C42-C32-C31	119.1(7)	C55-C50-C49	120.7(7)
C11-C12-C9	112.4(7)	C43-C33-C34	118.0(8)	C55-C50-C51	119.1(8)
C19-C12-C9	120.4(7)	C33-C34-O6	112.9(8)	C52-C51-C50	120.9(8)
C19-C12-C11	127.2(8)	C35-C34-O6	125.7(8)	C53-C52-C51	118.9(8)
C10-C13-C1	125.2(7)	C35-C34-C33	121.3(9)	C54-C53-C52	119.4(8)
C14-C13-C1	121.8(7)	C36-C35-C34	119.2(8)	C56-C53-C52	119.2(7)
C14-C13-C10	112.9(7)	C44-C36-C35	121.4(8)	C56-C53-C54	121.3(7)
C9-C14-C4	129.1(7)	C42-C37-C40	105.8(6)	C55-C54-C53	120.6(8)
C13-C14-C4	118.9(7)	C43-C37-C40	105.9(6)	C54-C55-C50	121.0(8)
C13-C14-C9	111.7(7)	C43-C37-C42	104.7(6)	C53-C56-O12	112.8(7)
C9-C15-C5	127.1(7)	C41-C38-C39	105.6(6)	N-C58-C57	176.4(16)

Table 3.6. Angles not involving hydrogen for the P_{ES} crystal structure.

3.9 Appendix 3: Assigned Hydrogen Atom Parameters for the P_{ES} Crystal Structure

	x, y, and $z \times 10^4$								
Atom	***x***	***y***	***z***	***B***	**Atom**	***x***	***y***	***z***	***B***
H1	5515	2110	1523	5.0	H32	-1135	5655	485	5.0
H3	6137	4329	2203	5.0	H33	1511	5734	-755	5.0
H4	6035	3703	3009	5.0	H35	3443	3655	-878	5.0
H5	3511	2198	3838	4.0	H36	1851	2855	-670	5.0
H7	1372	954	2869	4.0	H37	-616	5558	-489	5.0
H8	2923	668	2321	4.0	H38	-319	2800	-423	5.0
H9	5628	2335	3545	4.0	H46A	-2761	2405	-2098	20.0
H10	5094	858	2110	4.0	H46B	-2704	1883	-1596	20.0
H18A	6380	-1337	1830	10.0	H46C	-3599	2584	-1649	20.0
H18B	7501	-832	1859	10.0	H48A	-2797	6892	-1172	10.0
H18C	7135	-1383	2321	10.0	H48B	-2872	6308	-1646	10.0
H20A	7704	-623	4196	10.0	H48C	-3699	6191	-1185	10.0
H20B	8539	99	4085	10.0	H49A	-392	4273	1888	6.0
H20C	7546	222	4473	10.0	H49B	-1669	4068	1976	6.0
H21A	6566	4679	1301	6.0	H51	-1600	2316	2137	5.0
H21B	5264	4676	1403	6.0	H52	-1098	1432	2821	5.0
H23	6122	3474	367	6.0	H54	908	3244	3396	5.0
H24	5636	3706	-495	6.0	H55	465	4080	2697	5.0
H26	4661	6012	-141	6.0	H56A	174	1136	3506	5.0
H27	5136	5770	724	6.0	H56B	-177	1819	3896	5.0
H28A	4675	4478	-1123	7.0	H57A	2302	2993	4915	15.0
H28B	5134	5379	-1108	7.0	H57B	2243	2103	4684	15.0
H29	-661	2786	564	5.0	H57C	2671	2234	5248	15.0
H31	-1292	4962	1275	5.0					

Table 3.7. Assigned hydrogen atom parameters (Å) for the P_{ES} crystal structure.

3.10 Appendix 4: Distances and Angles Involving Hydrogen for the P_{ES} Crystal Structure

	Distance (Å)		Distance (Å)		Distance (Å)		Distance (Å)
C1--H1	0.953	C20-H20C	0.946	C33-H33	0.955	C49-H49B	0.956
C3-H3	0.950	C21-H21A	0.954	C35-H35	0.957	C51-H51	0.951
C5-H5	0.955	C21-H21B	0.951	C36-H36	0.951	C52-H52	0.955
C7-H7	0.957	C23-H23	0.954	C37-H37	0.952	C54-H54	0.955
C8-H8	0.956	C24-H24	0.947	C38-H38	0.956	C55-H55	0.956
C9-H9	0.952	C26-H26	0.956	C46-H46A	0.950	C56-H56A	0.951
C10-H10	0.956	C27-H27	0.952	C46-H46B	0.943	C56-H56B	0.956
C18-H18A	0.943	C28-H28A	0.949	C46-H46C	0.928	C57-H57A	0.938
C18-H18B	0.943	C28-H28B	0.952	C48-H48C	0.928	C57-H57B	0.946
C18-H18C	0.962	C29-H29	0.953	C48-H48B	0.939	C57-H57C	0.924
C20-H20A	0.947	C31-H31	0.954	C48-H48C	0.955		
C20-H20B	0.953	C32-H32	0.951	C49-H49A	0.952		

Table 3.8. Distances involving hydrogen for the P_{ES} crystal structure.

	Angle (°)		Angle (°)		Angle (°)
H1-C1-C2	120.7	H21B-C21-H21A	109.1	H46C-C46-O8	108.4
H1-C1-C13	120.2	H23-C23-C22	119.4	H46B-C46-H46A	110.1
H3-C3-C2	120.4	H23-C23-C24	119.0	H46C-C46-H46A	111.4
H3-C4-C3	120.3	H24-C24-C23	119.8	H46C-C46-H46B	112.0
H4-C4-C3	119.2	H24-C24-C25	120.2	H48A-C48-O10	108.9
H4-C4-C14	120.8	H26-C26-C25	119.6	H48B-C48-O10	109.7
H5-C5-C6	120.8	H26-C26-C27	119.8	H48C-C48-O10	108.7
H5-C5-C15	121.1	H27-C27-C22	119.0	H48B-C48-H48A	110.4
H7-C7-C6	120.4	H27-C27-C26	119.2	H48C-C48-H48A	109.1
H7-C7-C8	121.0	H28A-C28-O6	109.5	H48C-C48-H48B	110.0
H8-C8-C7	119.2	H28B-C28-O6	109.3	H49A-C49-O11	109.5
H8-C8-C16	119.6	H28A-C28-C25	109.1	H49B-C49-O11	109.0
H9-C9-C12	111.7	H28B-C28-C25	108.9	H49A-C49-C50	109.6
H9-C9-C14	112.2	H28B-C28-H28A	109.4	H49B-C49-C50	109.2
H9-C9-C15	112.7	H29-C29-C30	120.6	H49B-C49-H49A	108.8
H10-C10-C11	112.4	H29-C29-C41	119.8	H51-C51-C50	119.6
H10-C10-C13	114.4	H31-C31-C30	119.7	H51-C51-C52	119.5
H10-C10-C16	113.7	H31-C31-C32	119.6	H52-C52-C51	120.4
H18A-C18-O2	109.8	H32-C32-C31	120.5	H52-C52-C53	120.7
H18B-C18-O2	109.7	H32-C32-C42	120.5	H54-C54-C53	119.7
H18C-C18-O2	108.7	H33-C33-C34	120.8	H54-C54-C55	119.7
H18B-C18-H18A	110.6	H33-C33-C43	121.2	H55-C55-C50	120.0
H18C-C18-H18A	109.0	H35-C35-C34	120.4	H55-C55-C54	119.0
H18C-C18-H18B	109.0	H35-C35-C36	120.4	H56A-C56-O12	108.9
H20A-C20-O4	109.3	H36-C36-C35	119.1	H56B-C56-O12	108.7
H20B-C20-O4	109.0	H36-C36-C44	119.5	H56A-C56-C53	108.9
H20C-C20-O4	109.5	H37-C37-C40	112.1	H56B-C56-C53	108.6
H20B-C20-H20A	109.4	H37-C37-C42	113.2	H56B-C56-H56A	108.9
H20C-C20-H20A	110.1	H37-C37-C43	114.4	H57A-C57-C58	106.1
H20C-C20-H20B	109.6	H38-C38-C39	112.7	H57B-C57-C58	105.2
H21A-C21-O5	109.5	H38-C38-C41	113.5	H57C-C57-C58	106.6
H21B-C21-O5	109.7	H38-C38-C44	113.0	H57B-C57-H57A	111.5
H21A-C21-C22	109.8	H46A-C46-O8	107.3	H57C-C57-H57A	113.8
H21B-C21-C22	109.8	H46B-C46-O8	107.5	H57C-C57-H57B	113.0

Table 3.9. Angles involving hydrogen for the P_{ES} crystal structure.

3.11 Appendix 5: Anisotropic Displacement Parameters for the P_{ES} Crystal Structure

The form of the displacement factor is given by expression 3.35.

$$\exp[-2\pi^2(U_{11}h^2a^{*2} + U_{22}k^2b^{*2} + U_{33}l^2c^{*2} + 2U_{12}hka^*b^* + 2U_{13}hla^*c^* + 2U_{23}klb^*c^*)] \quad (3.35)$$

	$U_{ij} \times 10^4$					
Atom	U_{11}	U_{22}	U_{33}	U_{12}	U_{13}	U_{23}
O1	467(44)	928(54)	1361(62)	213(43)	-143(47)	-422(47)
O2	452(39)	519(41)	1279(56)	22(35)	92(43)	-311(41)
O3	614(47)	918(52)	799(52)	-66(44)	-222(40)	-48(42)
O4	766(51)	710(50)	971(52)	69(42)	-321(44)	138(42)
O5	995(54)	508(42)	579(43)	24(39)	179(40)	118(33)
O6	379(41)	844(48)	1008(52)	-34(40)	-73(36)	399(42)
O7	1611(92)	1666(88)	1216(74)	-781(76)	-82(70)	-75(64)
O8	1370(74)	1391(69)	639(51)	-592(58)	21(56)	-186(54)
O9	837(58)	1434(71)	1206(63)	410(55)	-441(55)	-500(54)
O10	820(57)	692(52)	1441(68)	-20(47)	-648(51)	2689(51)
O11	891(50)	485(37)	474(38)	-65(37)	47(38)	56(35)
O12	293(36)	785(44)	443(35)	67(32)	83(32)	130(33)
C1	457(56)	465(63)	415(59)	82(51)	43(48)	14(48)
C2	495(62)	463(64)	525(67)	57(52)	156(54)	67(54)
C3	461(59)	418(55)	627(64)	-30(46)	85(53)	35(57)
C4	390(55)	488(66)	567(64)	42(50)	-8(50)	-138(53)
C5	421(61)	428(57)	365(51)	19(48)	44(51)	-1(44)
C6	328(61)	495(58)	427(61)	63(51)	96(50)	99(50)
C7	237(53)	552(60)	524(63)	-30(46)	14(51)	101(51)
C8	551(66)	344(53)	477(58)	35(49)	-83(55)	23(44)
C9	379(57)	522(56)	406(54)	-13(51)	-3(46)	-101(47)
C10	353(53)	438(58)	472(57)	28(46)	42(46)	-57(44)
C11	288(52)	418(57)	574(60)	50(47)	111(51)	-12(54)
C12	294(53)	477(59)	511(60)	38(48)	57(51)	5(51)
C13	314(50)	365(53)	474(57)	42(43)	65(49)	-18(52)
C14	293(47)	460(58)	383(54)	-13(46)	-3(45)	-58(52)
C15	341(57)	399(52)	348(53)	-23(46)	-33(51)	89(46)
C16	275(57)	385(51)	449(56)	-14(43)	11(47)	33(46)
C17	372(62)	431(64)	734(71)	29(58)	11(55)	0(52)
C18	698(73)	588(66)	1471(101)	123(62)	169(71)	-399(67)
C19	227(56)	786(85)	620(73)	35(58)	8(56)	-62(64)
C20	1033(96)	1414(108)	1069(89)	321(83)	-473(84)	448(88)
C21	548(61)	562(66)	756(72)	-48(53)	68(57)	143(52)
C22	361(56)	579(67)	655(70)	-101(54)	-10(53)	127(62)
C23	685(71)	572(68)	877(81)	115(60)	-118(68)	98(66)
C24	571(67)	749(78)	696(73)	-65(64)	43(58)	66(64)
C25	362(56)	680(75)	774(78)	9(58)	75(59)	412(71)
C26	638(72)	612(75)	1109(96)	211(61)	-32(72)	93(76)
C27	812(82)	648(78)	907(86)	55(64)	-91(70)	-3(67)
C28	454(68)	811(74)	973(84)	-110(56)	19(59)	415(68)

Table 3.10. Anisotropic displacement parameters for the P_{ES} crystal structure (continued on next page).

	$U_{ij} \times 10^4$					
Atom	U_{11}	U_{22}	U_{33}	U_{12}	U_{13}	U_{23}
C29	465(57)	372(51)	584(62)	-110(48)	-7(52)	-41(53)
C30	499(62)	488(63)	421(62)	12(51)	29(49)	73(53)
C31	522(60)	459(63)	421(58)	-2(51)	15(48)	2(50)
C32	495(58)	398(52)	471(53)	-10(48)	-89(51)	-26(53)
C33	531(68)	523(65)	513(58)	-114(59)	-115(51)	187(49)
C34	321(63)	728(79)	658(69)	-95(61)	-76(51)	243(59)
C35	349(60)	516(70)	883(77)	20(54)	46(54)	187(56)
C36	576(69)	439(59)	629(65)	-7(61)	-92(55)	94(50)
C37	491(59)	426(52)	420(52)	54(49)	-19(52)	-49(47)
C38	440(59)	457(53)	467(56)	-45(48)	-10(50)	-80(47)
C39	360(56)	511(66)	415(57)	-106(52)	22(48)	-91(50)
C40	352(57)	657(72)	350(54)	86(55)	-84(47)	25(50)
C41	347(50)	522(65)	285(54)	-15(46)	18(44)	42(46)
C42	458(54)	288(54)	434(58)	-15(46)	-94(48)	-38(47)
C43	483(65)	423(63)	347(53)	14(54)	-65(47)	28(44)
C44	412(63)	493(69)	425(55)	-3(53)	2(48)	-103(45)
C45	832(91)	1233(105)	535(79)	-480(81)	272(73)	-20(82)
C46	2818(209)	1714(136)	1374(121)	-1668(148)	-625(127)	-379(103)
C47	302(60)	789(83)	743(74)	-27(66)	-15(59)	-244(69)
C48	506(68)	905(79)	1489(106)	-17(64)	-213(74)	450(74)
C49	605(64)	612(60)	509(61)	65(54)	66(53)	31(56)
C50	386(54)	525(63)	371(56)	-38(52)	63(52)	49(50)
C51	341(54)	748(74)	590(66)	-95(56)	-130(49)	12(56)
C52	377(55)	628(63)	630(61)	-84(52)	-45(57)	173(57)
C53	281(53)	537(65)	497(59)	28(49)	66(50)	138(52)
C54	357(55)	557(63)	552(61)	-1(54)	-38(49)	50(53)
C55	397(53)	441(55)	541(57)	1(47)	-1(53)	105(53)
C56	288(54)	748(65)	556(61)	-22(49)	57(46)	167(55)
C57	1690(154)	1851(139)	918(92)	-166(130)	34(104)	-381(91)
C58	1103(121)	787(90)	967(104)	106(105)	113(101)	-103(74)
N	819(97)	833(91)	1457(127)	81(88)	370(95)	-45(83)

Table 3.10 (continued). Anisotropic displacement parameters for the P_{ES} crystal structure.

3.12 Appendix 7: IUPAC Name for P_{ES}[3]

(3*S*, 18a*S*, 21*S*, 36a*S*)-Tetramethyl 3,8,13,18a,21,26,31,36a-octahydro-4,6:9, 12:22,24:27,30-tetraetheno-15,18,21:33,36,39-diethenylylidenedibenzo-[*k*,*a*1][1,8,17, 24]-tetraoxacyclodotriacontene-1,2,19,20-tetracarboxylate.

3.13 References and Footnotes

1. (a) Kearney, P. C.; Mizoue, L. S.; Kumpf, R. A.; Forman, J. E.; McCurdy, A.;

Dougherty, D. A. *J. Am. Chem. Soc.* **1993**, *115*, 9907-9919. (b) Petti, M. A.; Shepodd, T. J.; Barrans, R. E., Jr.; Dougherty, D. A. *J. Am. Chem. Soc.* **1988**, *110*, 6825-6840.

2. Forman, J. E.; Barrans, R. E., Jr.; Dougherty, D. A.; *J. Am. Chem. Soc.* **1995**, *117*, 9213-9228.

3. Forman, J. E.; Marsh, R. E.; Schaefer, W. P.; Dougherty, D. A.; *Acta. Cryst. Section B*, **1993** *B49*, 892-896.

4. Hagishita, S.; Kuriama, K.; *Tetrahedron* **1972**, *28*, 1435-1467.

5. (a) Nakanishi, K.; Berova, N.; Woody, R. W. (eds); *Circular Dichroism-Principles and Applications*, VCH, 1994. (b) Rosini, C.; Zandomeneghi, M.; Salvadori, P. *Tetrahedron Asymmetry* **1993**, *4*, 545-554. (c) Charney, E.; *The Molecular Basis of Optical Activity-Optical Rotatory Dispersion and Circular Dichroism*, Robert E. Krieger Publishing Company: Malabar, Fl, 1985. (d) Mason, S. F. *Molecular Optical Activity and the Chiral Discriminations*, Cambridge University Press: Cambridge, 1982. (e) Tinoco, I., Jr. *Adv. Chem. Phys.* **1962**, *4*, 113-160.

6. (a) Harada, N.; Nakanishi, K.; *Circular Dichroic Spectroscopy-Exciton Coupling in Organic Stereochemistry*, University Science Books: Mill Valley, CA, 1983. (b) Nakanishi, K.; Berova, N.; Chapter 13 in reference 5a, pages 361-398.

7. (a) Humpf, H.-U.; Berova, N.; Nakanishi, K.; Jarstfer, M. B.; Poulter, C. D.; *J. Org. Chem.* **1995**, *60*, 3539-3542. (b) Gargiulo, D.; Ikemoto, N.; Odingo, J.; Bozhkova, N.; Iwashita, Takashi; Berova, N.; Nakanishi, K.; *J. Am. Chem. Soc.*

1994, *116*, 3760-3767. (c) Humpf, H.-U.; Zhao, N.; Berova, N.; Nakanishi, K.; Schreier, P.; *J. Nat. Prod.*, **1994**, *57*, 1761-1765. (d) Gargiulo, D.; Cai, G.; Ikemoto, N.; Bozhkova, N.; Odingo, J.; Berova, N.; Nakanishi, K.; *Angew. Chem., Int. Ed. Engl.* **1993**, *32*, 888-981. (e) Cai, G.; Bozhkova, N.; Odingo, J.; Berova, N.; Nakanishi, K.; *J. Am. Chem. Soc.* **1993**, *115*, 7192-7198. (f) Gargiulo, D.; Derguini, F.; Berova, N.; Nakanishi, K.; Harada, N.; *J. Am. Chem. Soc.* **1991**, *113*, 7046-7047. (g) Zhou, P.; Berova, N.; Nakanishi, K.; Knani, M.; Rohmer, M.; *J. Am. Chem. Soc.* **1991**, *113*, 4040-4042. (h) Zhou, P.; Berova, N.; Nakanishi, K.; Rohmer, M.; *J. Chem. Soc., Chem. Commun.* **1991**, 256-258. (i) Wiesler, W. T.; Nakanishi, K.; *Croat. Chem. Acta* **1989**, *62*, 211-226. (j) Takeda, R.; Park, M. H.; Nakanishi, K.; *Isr. J. Chem.* **1989**, *29*, 239-242. (k) Wiesler, W. T.; Nakanishi, K.; *J. Am. Chem. Soc.* **1989**, *111*, 9205-9213. (l) Wiesler, W. T.; Nakanishi, K.; *J. Am. Chem. Soc.* **1989**, *111*, 3446-3447. (m) Chang, M.; Vazquez, J. T.; Nakanishi, K.; Cataldo, F.; Estrada, D. M.; Fernandez, J.; Gallardo, A. M.; Julio, D.; Norte, M.; Perez, R.; Rodriguez, M. L.; *Phytochemistry* **1989**, *28*, 1417-1424. (n) Chang, M.; Meyers, H. V.; Nakanishi, K.; Ojika, M.; Park, J. H.; Park, M. H.; Takeda, R.; Vazquez, J. T.; Wiesler, W. T.; *Pure Appl. Chem.* **1989**, *61*, 1193-1200. (o) Wiesler, W. T.; Vazquez, J. T.; Nakanishi, K.; *J. Am. Chem. Soc.* **1987**, *109*, 5586-5592. (p) Verdine, G. L.; Nakanishi, K.; *J. Chem. Soc., Chem. Commun.* **1985**, 1093-1095. (q) Nakanishi, K.; Kuroyanagi, M.; Nambu, H.; Oltz, E. M.; Takeda, R.; Verdine, G. L.; Zask, A.; *Pure Appl. Chem.* **1984**, *56*, 1031-1048. (r) Stonard, R. J.; Trainor, D. A.; Nakatani, M.; Nakanishi, K.; *J. Am. Chem. Soc.* **1983**, *105*, 130-131.

8. (a) Bernart, M. W.; Hallock, Y. F.; Cardellina, J. H., II; Boyd, M. R.; *Tetrahedron Lett.* **1994**, *35*, 993-994. (b) Gaffield, W.; in *Bioactive Natural Products*, Colegate, S. M.; Molyneux, R. J. (eds); CRC Press: Boca Raton, Fl.; 1993, 147-157. (c)

Harada, N.; Saito, A.; Ono, H.; Gawronski, J.; Gawronski, K.; Sugioka, T.; Uda, H.; Kuriki, T.; *J. Am. Chem. Soc.* **1991**, *113*, 3842-3850. (d) Harada, N.; Ono, H.; Nishiwaki, T.; Uda, H.; *J. Chem. Soc., Chem. Commun.* **1991**, 1753-1755. (e) Harada, N.; Tamai, Y.; Uda, H.; *J. Org. Chem.* **1984**, *49*, 4266-4271. (f) Harada, N.; Iwabuchi, J.; Yokota, Y.; Uda, H.; Okamoto, Y.; Yuki, H.; Kawada, Y.; *J. Chem. Soc. Perkin Trans. 1* **1985**, 1845-1848.

9. Version 2.2, Biodesign Inc., 1990.

10. (a) Weiner, S. J.; Kollman, P. A.; Case, D. A.; Singh, U. C.; Ghio, C.; Algona, G.; Profeta Jr., S.; Weiner, P. *J. Am. Chem. Soc.* **1984**, *106*, 765-784. (b) Weiner, S. J.; Kollman, P. A.; Nguyen, D. T.; Case, D. A. *J. Comput. Chem.* **1986**, *7*, 230-252.

11. Saunders, M.; Houk, K. M.; Wu, Y-D.; Still, W. C.; Liptin, M.; Chang, G.; Guida, W. C. *J. Am. Chem. Soc.* **1990**, *112*, 1419-1427.

12. Larson, R. E.; Hostetler, R. P.; *Calculus*, D. C. Heath and Co., 1986.

13. Ishitsuka, M. O.; Kusami, T.; Kakisawa, H.; *Tetrhedron Lett.* **1991**, *32*, 6595-6596.

14. Kearney, P. C.; California Institute of Technology, Ph.D. Thesis, 1994.

15. (a) McCurdy, A.; Jimenez, L.; Stauffer, D. A.; Dougherty, D. A. *J. Am. Chem. Soc.* **1992**, *114*, 10314-10321. (b) Stauffer, D. A.; Barrans, R. E., Jr.; Dougherty, D. A. *Angew. Chem., Int. Ed. Engl.* **1990**, *29*, 915-918. (c) Stauffer, D. A.; Barrans, R. E., Jr.; Dougherty, D. A. *J. Org. Chem.* **1990**, *55*, 2762-2767.

16. Kumpf, R. A.; Dougherty, D. A.; *Personal Communication.*

17. Ngola, S. M.; Dougherty, D. A.; *Unpublished Results.*

18. Stauffer, D. A.; Dougherty, D. A.; *Unpublished Results.*

19. Johnson, C. K.; *ORTEP*. Report ORNL-3794, Oak Ridge National Laboratory, Tennessee, USA, 1965.

20. Kearney, P. C.; *Personal Communication.*

21. Allen, F. H.; Kennard, O.; Watson, D. G.; Brammer, L.; Orpen, A. G.; Taylor, R.; *J. Chem. Soc. Perkin Trans. 2* **1987**, S1-S19.

22. Version 4.0, Microsoft Corp., © 1985-1992.

23. Destro, R.; Marsh, R. E.; *Acta Cryst. Section A* **1987**, *A43*, 711-718.

24. Debaerdemaeker, T.; Germain, G.; Main, P.; Refaat, L. S.; Tate, C.; Woolfson, M. M.; *Multan 88: A System of Computer Programs for the Automatic Solution of Crystal Structures from X-Ray Diffraction Data*, Universities of York, U.K. and Louvain, Belgium; 1988.

25. Duchamp, D. J.; *CRYM Crystallographic Computing System.* Am. Crystallogr. Assoc. Meeting, Bozeman, Montana, Paper B14, page 29, 1964.

26. Hahn, T. (ed); *International Tables for Crystallography*, Kluwer Academic publishers,

1983.

27. Equation 3 from: Larson, A. C.; *Acta. Cryst.* **1967**, *23*, 664-665.

Chapter 4:
Bound Guest Orientations in Chiral Cyclophane Hosts From Induced Circular Dichroism Data.

Chapter 4

Bound Guest Orientations in Chiral Cyclophane Hosts From Induced Circular Dichroism Data.

4.1 Introduction

The studies in Chapter 3 described the structure of the host in both free and bound states, but the issue of guest orientation in the bound complex was not addressed. This issue is the subject of this chapter. Guest orientations are determined through a combination of experimentally observed induced circular dichroism (ICD) data with computational analysis.

In previous studies with hosts **P** and **C** (Figure 4.1), the strongest evidence for bound guest orientations came from ^{1}H NMR *D* values.[1] These values represent the maximum upfield shift that an NMR signal for a guest proton exhibits upon being bound in the host. The shifts are generally in the upfield direction as a result of the shielding effect of the aromatic rings of the cavity on the guest protons. The largest *D* value for a given guest proton corresponds to a proton (and thus a portion of the guest) more preferentially bound within the host cavity.[1] The *D* values come from comparison of an observed chemical shift (δ_{obs}) for the guest proton in the presence of host, with the chemical shift of the free guest (δ_{free}). The δ_{obs} comes from a weighted average of free and multiple bound states arising through complexation events; thus the *D* values do not come from observations resulting exclusively from the bound guests.

In circular dichroism (CD) studies with hosts **P** and **C**,[2] it was observed that circular dichroism could be induced in achiral guests with longer wavelength electronic absorption bands (Figure 4.2). A specific example is shown in Figures 4.3, where a negative Cotton effect is observed in the spectrum of the host-guest complex for the long-

wavelength absorption band of guest **4**. This is not unexpected as circular dichroism induced in an achiral chromophore by complexation to a chiral receptor is well known from studies of cyclodextrins[3] and biological molecules;[4] as well as other synthetic host systems.[5-8]

However, this observation of ICD is very significant in light of our NMR studies, as these ICD signals result exclusively from specific orientations of the bound guest, unlike the NMR studies where the *D* value is determined from an averaged signal of free and bound guests.[1b] Additionally, the observed ICD results from complexation of the guest within the host binding cavity. This has been established with chiral non-macrocyclic control molecules **1** and **2** (Figure 4.1) which do not induce CD in achiral chromophoric guests.[2,9]

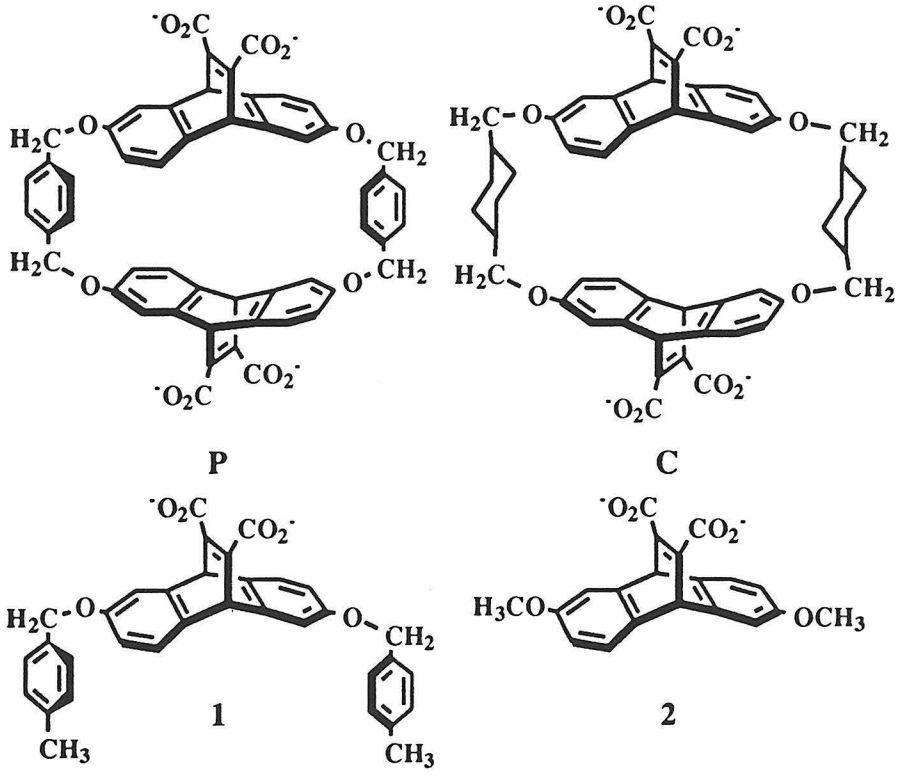

[(*S*, *S*)-Stereochemistry of ethenoanthracene units shown]

Figure 4.1. Hosts P and C and non-macrocyclic control molecules.

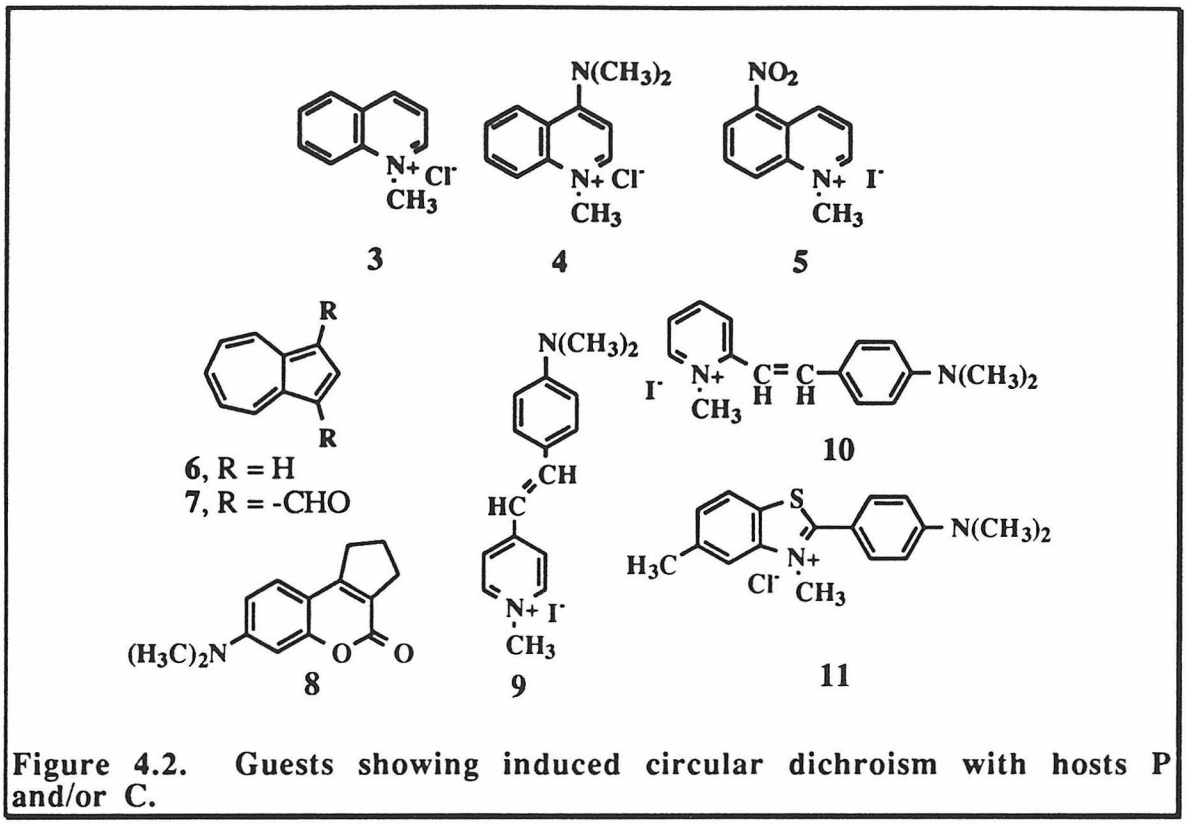

Figure 4.2. Guests showing induced circular dichroism with hosts P and/or C.

With the exception of guest **5**, the ICD data with host **P** did not appear very informative for the determination of orientations of bound guests, as the ICD showed the same sign with all guests ($\Delta\varepsilon < 0$ with $\mathbf{P_S}$, $\Delta\varepsilon > 0$ with $\mathbf{P_R}$).[2] However, control experiments with host **C** (which we believe exhibits bound guest orientations very similar to those of host **P**)[10] revealed some interesting differences from host **P**.[2] Guests **9**, **10**, and **11** exhibit opposite signs of ICD with **P** and **C** (Figures 4.4 and 4.5), while guests such as **4**, **6**, and **7** show the same sign of ICD with **P** and **C**.[2] These discrepancies provided the impetus for the calculations of binding orientations described in Sections 4.2 and 4.3. Table 4.1 lists the observed ICD with the guests shown in Figure 4.3.

One final observation of the data in Table 4.1 is that the ICD observed with our host systems is larger than that normally induced by cyclodextrin hosts. This is thought to be the result of strong $\pi \rightarrow \pi^*$ transitions in the host coupling with $\pi \rightarrow \pi^*$ transitions in the guest by a coupled-oscillator mechanism,[12,13] a phenomenon expected for systems with

strong $\pi \rightarrow \pi^*$ absorptions.[12,13] Not surprisingly, host **P** appears to induce larger rotational strengths (*R*) in achiral chromophores than does host **C** (a host with fewer $\pi \rightarrow \pi^*$ transitions).

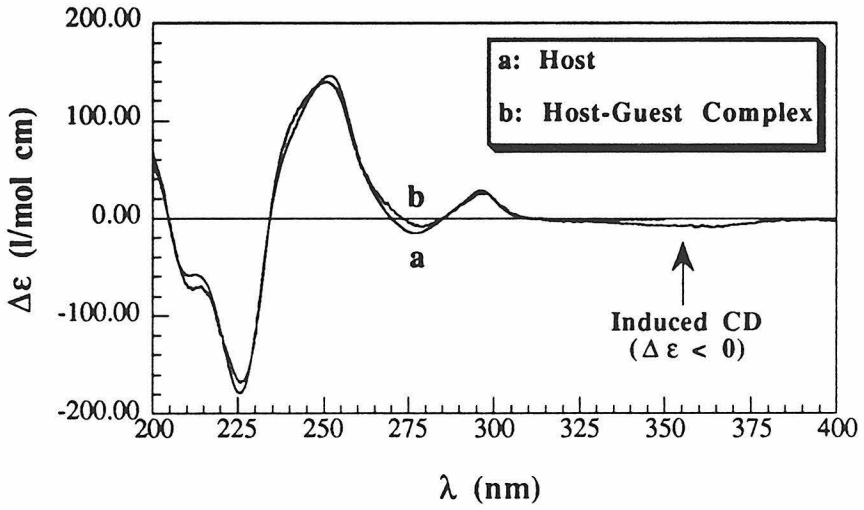

Figure 4.3. CD spectrum of host P_S and best-fit spectrum of its complex with guest 4 in aqueous borate buffer (pH 9).

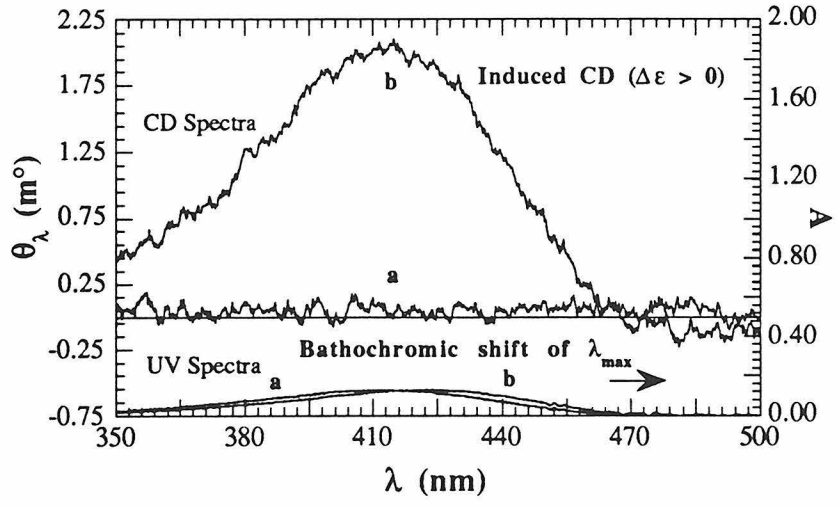

Figure 4.4. CD and UV/visible spectra of Guest 11 (7.18×10^{-6} M) in the absence (a) and in the presence (b) of host P_R (1.26×10^{-5} M) in aqueous borate buffer (pH 9).

Guest	Host	λ_{max} free guest	λ_{max} for induced CD	$\Delta\varepsilon$ ($M^{-1}cm^{-1}$)	Rotational Strength (cgs)
3	C_R[a]	318 nm	315 nm	+14.6	$+2.6 \times 10^{-39}$
4	P_S	355 nm	357 nm	-8.0	-2.2×10^{-39}
4[b]	C_R	355 nm	356 nm	$\Delta\varepsilon > 0$	$R > 0$
5	P_R[c]	323 nm[d]	341 nm 309 nm	+1.5 -8.8	$+9.1 \times 10^{-41}$ -1.1×10^{-39}
6	P_R	570 nm 337 nm	ICD not observed[d] 340 nm	N/A[e] +0.74	N/A[e] $+1.5 \times 10^{-40}$
6[b]	C_R	570 nm 337 nm	ICD not observed[d] 321 nm	N/A[e] $\Delta\varepsilon > 0$	N/A[e] $R > 0$
7	P_S	467 nm 376 nm 292 nm	ICD not observed[d] 379 nm 299 nm	N/A[e] -5.6 shows excitonic coupling with host transitions	N/A[e] -1.5×10^{-39} negative excitonic chirality
7[b]	C_R	467 nm 376 nm 292 nm	ICD not observed[d] 379 nm 297 nm	N/A[e] $\Delta\varepsilon > 0$ shows excitonic coupling with host transitions	N/A[e] $R > 0$ positive excitonic chirality
8[b]	C_R[a]	366 nm	376 nm	$\Delta\varepsilon > 0$	$R > 0$
9	P_S	452 nm	456 nm	-4.7	-3.5×10^{-39}
9[b]	C_R	452 nm	470 nm	$\Delta\varepsilon < 0$	$R < 0$
10	P_S	439 nm	449 nm	-11.6	-7.8×10^{-39}
10[b]	C_R	439 nm	470 nm	$\Delta\varepsilon < 0$	$R < 0$
11	P_S	412 nm	422 nm	-18.8	-3.5×10^{-39}
11[b]	C_R	412 nm	427 nm	$\Delta\varepsilon < 0$	$R < 0$

Table 4.1. Induced circular dichroism (ICD) observed in aqueous borate buffer with hosts P and C.

[a]No ICD was detectable for this guest with Host P. [b]A binding constant was not obtained for this host-guest system, thus ICD is qualitative only. [c]No ICD was detectable for this guest with Host C. [d]This data comes from the observed UV band of free guest; unfortunately, the band was too broad to pick out the true λ_{max} for both of the transitions. [e]While it is tempting to assume this transition has $\Delta\varepsilon \approx 0$ and $R \approx 0$, it should be noted that the ICD may have been undetectable under the conditions of our studies.

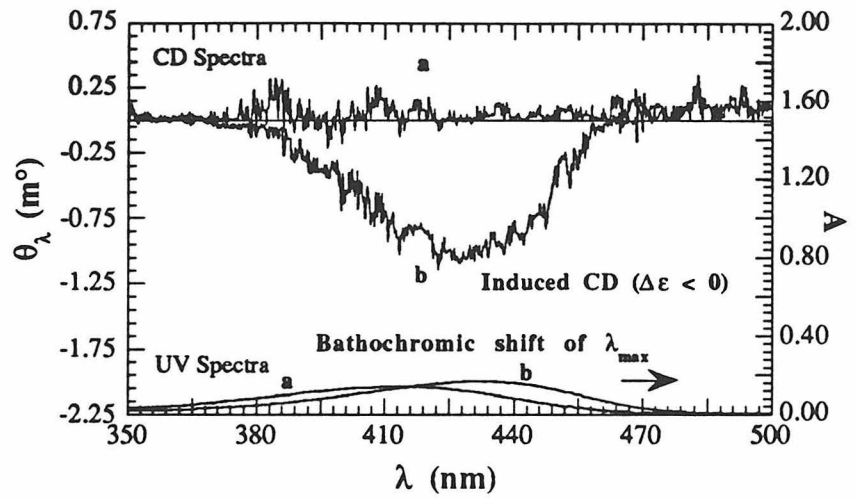

Figure 4.5. CD and UV/visible spectra of Guest 11 (7.50×10^{-6} M) in the absence (a) and in the presence (b) of host C_R (1.40×10^{-5} M) in aqueous borate buffer (pH 9). A larger bathochromic shift is observed with the guest visible absorption band than occurs with host P; this is consistent with cavities of differing polarity for the two hosts.[11]

This chapter describes how the ICD observed in the guests of Figure 4.3 can be used to determine the bound orientations of the guest. These studies were carried out using coupled-oscillator calculations[12,13] with INDO/S[14] calculated spectral data. Before such studies can be described, a brief introduction into the theoretical basis of optical activity is required.

4.2 Modeling Optical Activity

4.2.1 Mechanisms of Optical Activity

Optical activity arises in a molecule through a number of additive mechanisms. For a system of chromophores (*a*, *b*, ...) with transitions from the ground state (State 1) to

excited states (States A, B, ...), the rotational strength (R) of the system has the general mathematical form[13b]

$$R = \sum_{a} \mathrm{Im}\mu_{a1A}\bullet\mathbf{m}_{a1A} \tag{4.1.1}$$

$$+ 2\sum_{b\neq a}\sum_{\mathrm{B}\neq\mathrm{A}} \frac{\mathrm{Im}V_{a1\mathrm{A},b1\mathrm{B}}(\mu_{a1\mathrm{A}}\bullet\mathbf{m}_{b\mathrm{B}1}\nu_{\mathrm{A}} + \mu_{b\mathrm{B}1}\bullet\mathbf{m}_{a1\mathrm{A}}\nu_{\mathrm{B}})}{h(\nu_{\mathrm{B}}^2 - \nu_{\mathrm{A}}^2)} \tag{4.1.2}$$

$$-\sum_{a\neq b}\sum_{\mathrm{B}\neq\mathrm{A}} \frac{\mathrm{Im}V_{a\mathrm{AB},b11}(\mu_{a1\mathrm{A}}\bullet\mathbf{m}_{a\mathrm{B}1} + \mu_{a1\mathrm{B}}\bullet\mathbf{m}_{a\mathrm{A}1})}{h(\nu_{\mathrm{B}} - \nu_{\mathrm{A}})} \tag{4.1.3}$$

$$-\sum_{b\neq a}\sum_{\mathrm{B}\neq\mathrm{A}} \frac{\mathrm{Im}V_{a1\mathrm{B},b11}(\mu_{a1\mathrm{A}}\bullet\mathbf{m}_{a\mathrm{AB}} + \mu_{a\mathrm{AB}}\bullet\mathbf{m}_{a\mathrm{A}1})}{h\nu_{\mathrm{B}}} \tag{4.1.4}$$

$$-\sum_{b\neq a} \frac{\mathrm{Im}V_{a1\mathrm{A},b11}(\mu_{a\mathrm{AA}} - \mu_{a11})\bullet\mathbf{m}_{a\mathrm{A}1}}{h\nu_{\mathrm{A}}} \tag{4.1.5}$$

$$-\frac{2\pi}{c}\sum_{b\neq a}\sum_{\mathrm{B}\neq\mathrm{A}} \frac{V_{a1\mathrm{A},b1\mathrm{B}}\nu_{\mathrm{A}}\nu_{\mathrm{B}}\mathbf{R}_{ba}\bullet(\mu_{b1\mathrm{B}}\times\mu_{a1\mathrm{A}})}{h(\nu_{\mathrm{B}}^2 - \nu_{\mathrm{A}}^2)} \tag{4.1.6}$$

where $\mu_{i1\mathrm{I}}$ and $\mathbf{m}_{i1\mathrm{I}}$ are the electronic transition and magnetic transition moments respectively, for the transition from State 1 $\rightarrow$ State I for chromophore i, $\mathbf{R}_{ij}$ is the interchromophoric distance vector between the midpoints of the transition moments for chromophores i and j, ν_I is the frequency of excitation for the transition from State 1 $\rightarrow$ State I for chromophore i (in cm^{-1}), h is Planck's constant (6.26176×10^{-27} erg•sec), and c is the velocity of light (2.99792458×10^{10} cm•sec^{-1}).[13ab] The interaction energies (V) are defined as the coulombic interaction energy between the charge densities of the transition State 1 $\rightarrow$ State I in chromophore i and the transition State 1 $\rightarrow$ J in chromophore j ($V_{i1\mathrm{I}j1\mathrm{J}}$) or between the ground-state charge density in chromophore j and the transition charge density for the transition State 1 $\rightarrow$ State I in chromophore i ($V_{i1\mathrm{I}j11}$).[13a] Each of the terms in equation 4.1 represents a specific mechanism of optical activity.[13ab]

The first term (4.1.1) represents the contribution of electronic and magnetic transitions within the same chromophore to the rotational strength.[13] This is the familiar

Rosenfeld equation that describes an intrinsically dissymmetric chromophore.[13] If the electronic and magnetic moments are perpendicular to one another, the chromophore is achiral and the contribution to *R* from this term is zero.[13]

Term 4.2.1 is Schnellman's, $\mu \cdot m$ mechanism.[13] The contribution to *R* arises from the mixing of the electronic and magnetic states on different chromophores.[13] This term corresponds to an asymmetrically perturbed inherently achiral chromophore.[13]

Terms 4.1.3 and 4.1.4 represent the mixing of excited states within individual chromophores due to the static field of the rest of the system (molecule).[13] These terms correspond to the one-electron theory of optical activity.[13]

The fifth term (4.1.5) represents a change in the electronic transition moment upon excitation.[13b] The contribution from this term is generally negligible and is often ignored in modeling studies.[13b]

The final term (4.1.6) represents the mixing of electronic transition moments (dipolar coupling) in different chromophores.[13] This corresponds to the Coupled Oscillator theory.[12,13] For molecules with strong $\pi \rightarrow \pi^*$ electronic transitions, such as hosts **P** and **C** (and control molecules **1** and **2**), the major contribution to the optical activity comes from this coupled-oscillator term (Figures 4.6 and 4.7).[13a,15] Furthermore, ICD in an achiral $\pi \rightarrow \pi^*$ absorption band (guest) bound in a chiral environment (host) arises primarily through this type of dipolar coupling,[2,3,12,13] where the guest transition moment couples with all of the $\pi \rightarrow \pi^*$ transition moments in the chiral environment to which it is bound.[2,3,12,13]

4.2.2 Coupled-Oscillator Calculations

As noted in the previous section, in highly chromophoric systems such as our hosts, optical activity arises predominantly through the coupled-oscillator mechanism (dipolar coupling).[12,13] The theoretical rotational strength from the dipolar coupling (R_D)

comes from term 6 of equation 4.1; in terms of transitions in host (H) and guest (G) chromophores, 4.1.6 can be rewritten as equation 4.2.

$$R_D = -\frac{2\pi}{hc} \sum_{B \neq A} \frac{V_{H1A,G1B} \nu_A \nu_B R_{GH} (\mu_{G1B} \times \mu_{H1A})}{(\nu_B^2 - \nu_A^2)} \qquad (4.2)$$

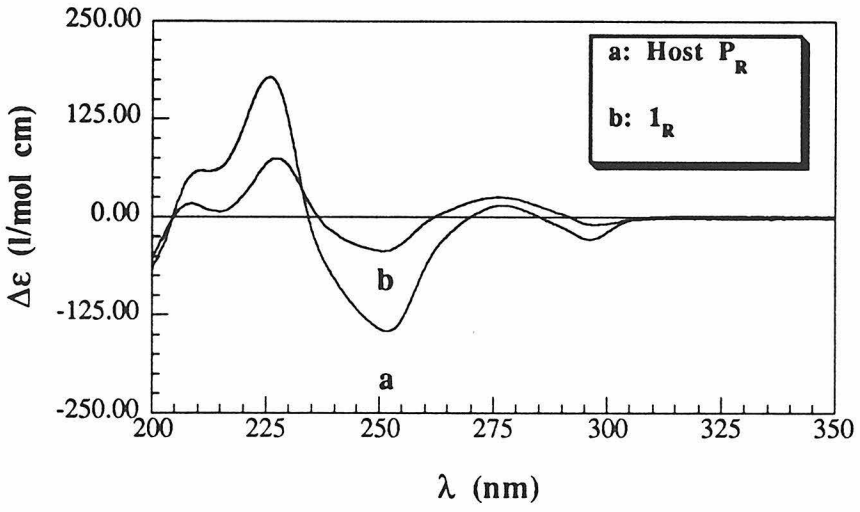

Figure 4.6. Circular dichroism spectra of host P_R and control molecule 1_R in aqueous borate buffer (pH 9).

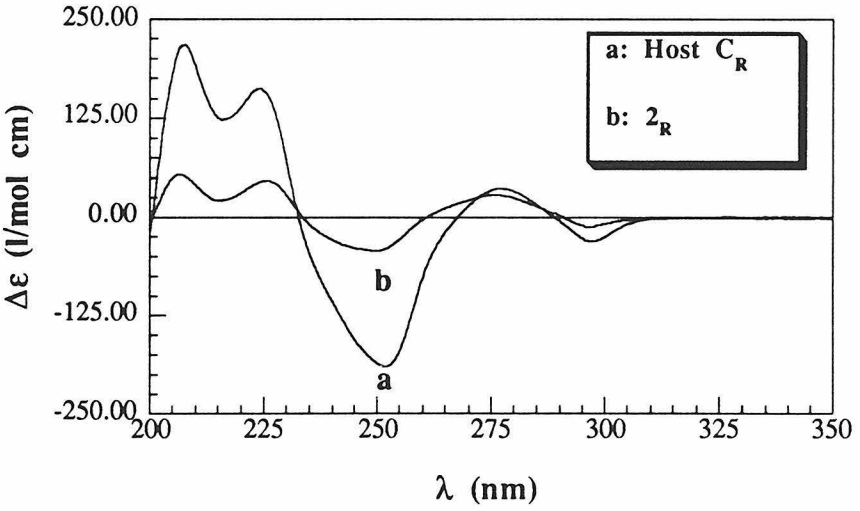

Figure 4.7. Circular dichroism spectra of host C_R and control molecule 2_R in aqueous borate buffer (pH 9).

In this equation, excited State A corresponds to an excited state in the host chromophore and excited State B corresponds to an excited state in the guest chromophore. The interaction potential, $V_{H1A,G1B}$, can be approximated using the point-dipole approximation and is defined by equation 4.3.[13b]

$$V_{H1A,G1B} = \frac{\mu_{H1A} \cdot \mu_{G1B}}{R_{HG}^3} - \frac{3(\mu_{H1A} \cdot R_{GH})(\mu_{G1B} \cdot R_{GH})}{R_{HG}^5} \qquad (4.3)$$

The denominator terms, R_{HG}, represent the magnitude of the interchromophoric distance vector.

The use of equations 4.2 and 4.3 require knowledge of the magnitudes and directions of all the $\pi \rightarrow \pi^*$ transition moments in the system. These quantities can be obtained by calculation. Determining the rotational strengths of ICD from experimentally observable data, however, requires linear dichroism[16] to obtain the directions of the transition moments and polarizabilities to obtain the magnitudes; using this experimental approach R_D is available through equation 4.4.[13b]

$$R_D = -\frac{2\pi}{hc} \sum_{B \neq A} \frac{\nu_A \nu_B}{(\nu_B^2 - \nu_A^2)} \cdot \frac{1}{6 R_{HG}^2} \alpha_H \alpha_G \beta_H \beta_G (\cos \theta_{HG} - 3 \cos \phi_H \cos \phi_G) \cos X_{HG} \sin \theta_{HG} \qquad (4.4)$$

In equation 4.4, θ_{HG} is the angle between the transition moments in the host and guest chromophores (the sign is determined by the right-hand rule), X_{HG} is the angle formed between the cross product $\mu_H \times \mu_G$ and the interchromophoric distance vector (R_{HG}), ϕ_H is the angle between μ_H and R_{GH}, and ϕ_G is the angle between μ_G and R_{GH}.[13b] α_i and β_i are the mean anisotropic polarizabilities and are defined, respectively, by equations 4.5 and 4.6.[13b]

$$\alpha_i = \frac{1}{3}\left(\alpha_{xx}^{(i)} + \alpha_{yy}^{(i)} + \alpha_{zz}^{(i)}\right) \qquad (4.5)$$

$$\beta_i = \frac{\alpha_{xx}^{(i)} - \frac{1}{2}\left(\alpha_{yy}^{(i)} + \alpha_{zz}^{(i)}\right)}{\alpha_i} \qquad (4.6)$$

The coupled-oscillator approach to calculating ICD (and thus determining binding orientations) has seen much application in studies of cyclodextrin-based systems.[3,17] The general approach has been to treat each bond in the host (cyclodextrin) as a chromophore with a single transition moment. Each of these transitions are then coupled with the transition of interest in the guest using a combination of equations 4.2 and 4.4.[3k,17c,18]

Another approach to the use of equations 4.2 and 4.4 is to break up the interacting molecules into their component $\pi \rightarrow \pi^*$ chromophores. Experiments with the component chromophores or semi-empirical calculations (INDO/S[14]) can then be used to determine all the transition moments of each individual chromophore. The individual transition moments can then be superimposed onto the framework of the host-guest system and equation 4.2 or 4.4 can be applied directly for the calculation of ICD of a given guest transition coupled to the host transitions. For our host-guest system, it was decided to follow this "component chromophore" approach using semi-empirical calculations to obtain the required spectral data.

We chose to use this computational approach for several reasons. First, the facilities for linear dichroism were not immediately available to us, and linear dichroism has seen its most successful applications with planar chromophores,[16] not the three-dimensional chromophores that make up the host framework (see section 4.3). Additionally, polarizabilities (α_{xx}, α_{yy}, and α_{zz}) are not available for our host chromophores and guests. Some attempts to calculate the polarizability tensors using Gaussian92[19] at 6-31G, 6-31G*, and 6-31G** levels of theory failed to give results that reproduced known experimental polarizabilities. Given these difficulties, it seemed reasonable to proceed with an INDO/S approach to determine the transition moments. We feel our approach using component chromophores is a more accurate approximation of ICD

data than the cyclodextrin approach.[3k,17c,18] Our goal, however, was to obtain qualitative agreement of calculation with experimental data.

4.2.3 Electronic Transition Moments and the INDO/S Method

In the preceding discussion (and in Chapter 3) the term *electronic transition moment* has been used repeatedly, but it has never been fully defined. A transition moment (μ_{1A}) is the dipole moment of the overlap charge density (ρ_{1A}) between the initial and final states in an electronic transition (Figure 4.8).[16] The electronic transition moment can be calculated from the wavefunctions of the initial and final states [$\Psi_1(\mathbf{q}, \mathbf{Q})$ and $\Psi_A(\mathbf{q}, \mathbf{Q})$ respectively] by integration over the coordinates of all electrons ($\mathbf{q}$) and all nuclei ($\mathbf{Q}$), as shown in equation 4.7.[16]

$$\mu_{1A} = \int \Psi_1(\mathbf{q}, \mathbf{Q}) \hat{\mu} \Psi_A(\mathbf{q}, \mathbf{Q})\, d\mathbf{q} d\mathbf{Q} \tag{4.7}$$

Where the electric dipole moment operator, $\hat{\mu}$, has the form[16]

$$\hat{\mu} = -|e| \sum_{l=1}^{n} \mathbf{r}_l + |e| \sum_{k=1}^{N} \mathbf{Z}_k \mathbf{R}_k \tag{4.8}$$

in equation 4.8, e is the charge of an electron ($4.80324238 \times 10^{-10}$ cgs•esu), $\mathbf{Z}_k$ is the atomic number of nucleus k, n is the number of electrons, N is the number of nuclei, $\mathbf{r}_l$ is the position vector of the l-th electron, with coordinates (x_l, y_l, z_l), and $\mathbf{R}_k$ is the position of the k-th nucleus, with coordinates (x_k, y_k, z_k).[16] Equations 4.7 and 4.8 can be written in terms of their x, y, and z components to give expressions for the three coordinates that define the transition moment in an appropriate principle axis system, as illustrated for the x component in equations 4.9 and 4.10.[16]

$$\mu_{x1A} = \int \Psi_1(q, Q)\hat{\mu}_x\Psi_A(q, Q)\, dq dQ \tag{4.9}$$

$$\hat{\mu}_x = -|e|\sum_{l=1}^{n} x_l + |e|\sum_{k=1}^{N} Z_k x_k \tag{4.10}$$

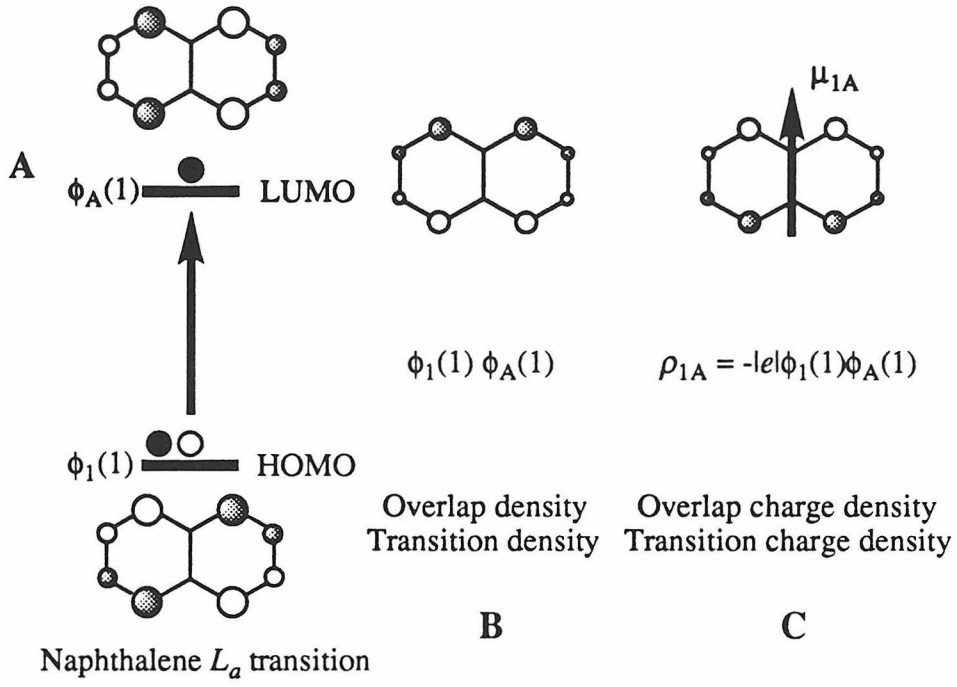

Figure 4.8.[16a] Illustration of an electronic transition moment using the L_a transition of naphthalene. (A) Coefficients of the highest occupied (HOMO) and lowest unoccupied (LUMO) molecular orbitals. (B) The transition density for the HOMO → LUMO transition. (C) The transition charge density (ρ_{1A}) and its dipole moment (μ). The circles indicate the sign (white = positive, dark = negative) and magnitude (proportional to radius) of the contributions from the individual carbon $2p_z$ orbitals. Although shown as a one directional arrow, transition moments are generally written as two-headed arrows or straight lines to indicate the oscillation (see Figure 4.13).[15b]

Semi-empirical calculations using INDO/S (Intermediate Neglect of Differential Overlap parametrized for Spectroscopy) Hamiltonians have been quite successful in reproducing the spectral properties of $\pi \rightarrow \pi^*$ chromophores,[14] and thus provide a method for obtaining the transition moments needed for the coupled-oscillator calculations. INDO/S calculations include all valence electrons to predict the spectral properties of a

compound.[14] The calculation consists of two parts: first the ground state is calculated, providing molecular orbital coefficients and eigenvalues, and then a configuration interaction calculation is preformed to provide the excited states.[14]

4.3 Application to Hosts P and C

4.3.1 Calculation Coordinate System

Spectral changes observed in the CD spectra together with size complementarity suggest that the guests of Figure 4.2 are all bound in the rhomboid conformation of the host cavity (Chapter 3). The crystal structure of host P_S tetramethyl ester represents a rhomboid binding conformation;[20] thus it serves as an ideal framework in which guests can be oriented and coupled-oscillator calculations undertaken.

The coordinate system chosen for these calculations was based on the crystal structure with the esters optimized as acids (Figures 4.9 and 4.10). We set the origin of our coordinate system as the center of mass of the six aromatic rings that form the host cavity. The *z*-axis is defined as the axis coming directly out of the cavity, and we define the angle θ as the angle of inclination with respect to the *z*-axis (Figure 4.10). A general orientation of a transition moment in the *xz*-plane (as defined in Figure 4.10) will have θ varied from 0° (aligned on *z*-axis) through 360° by rotation of the transition moment counter-clockwise about the *y*-axis. A full listing of the atomic coordinates of host atoms in this coordinate system is given in Appendix 1 (Section 4.8).

4.3.2 Host Chromophores

Host **P** can be thought of as being made up of four independent chromophores: the two *p*-xylyl linkers and the two ethenoanthracene units (Figure 4.11). While the average

conformation of the individual chromophores should be the same for each set (linkers and ethenoanthracenes) based on C_2-symmetry in the host rhomboid binding conformation, the crystal structure of **Ps** tetramethyl ester (Chapter 3) shows slight asymmetry between the two units of each set.[20] We felt that this asymmetry might also be typical of the host in solution, and so the calculations were carried out using the four distinct chromophores implied by the crystal structure (Figure 4.12). The most significant difference between the two units in a set of chromophores is seen with the ethenoanthracenes: where the carboxylic acid moieties show different degrees of twisting (Figure 4.12, Tables 4.2 and 4.3). This slight degree of asymmetry between otherwise equivalent structures, however, produced only very small perturbations in the calculated transitions of the chromophores (Tables 4.4 and 4.5).

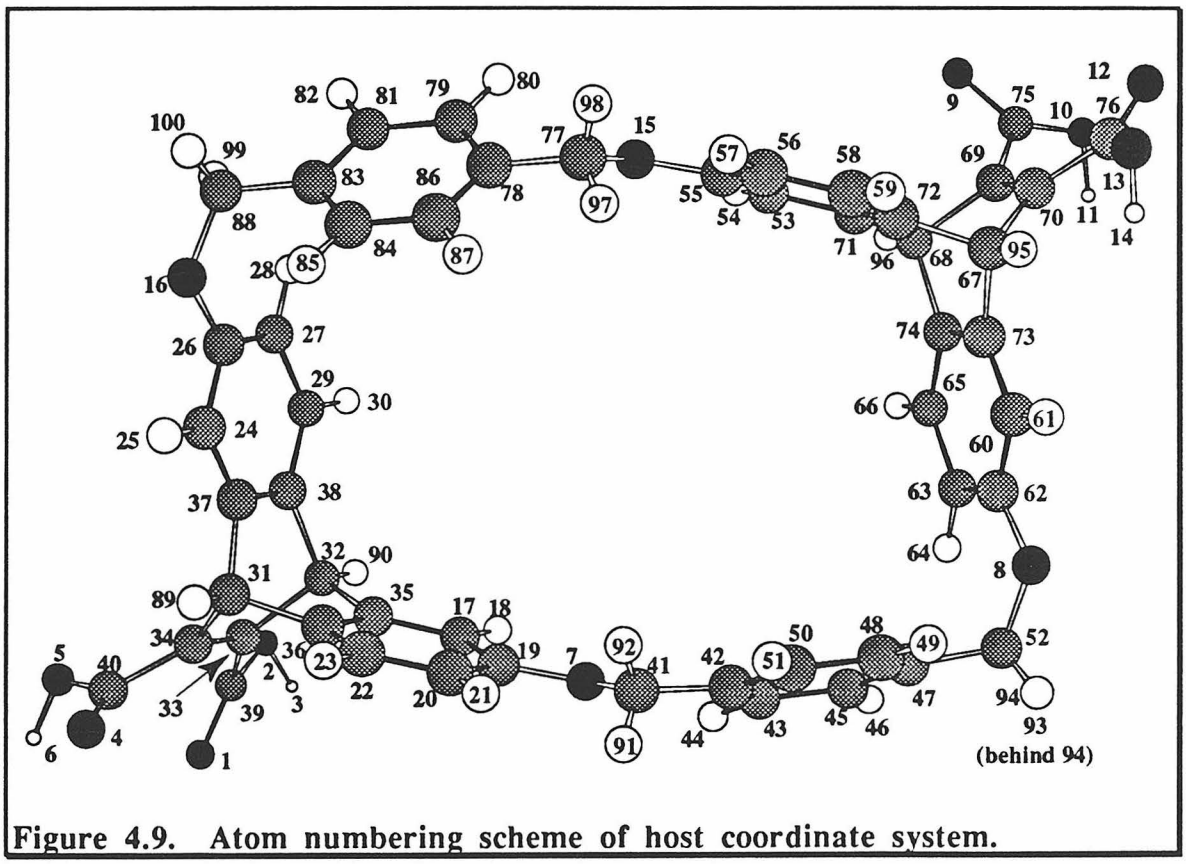

Figure 4.9. Atom numbering scheme of host coordinate system.

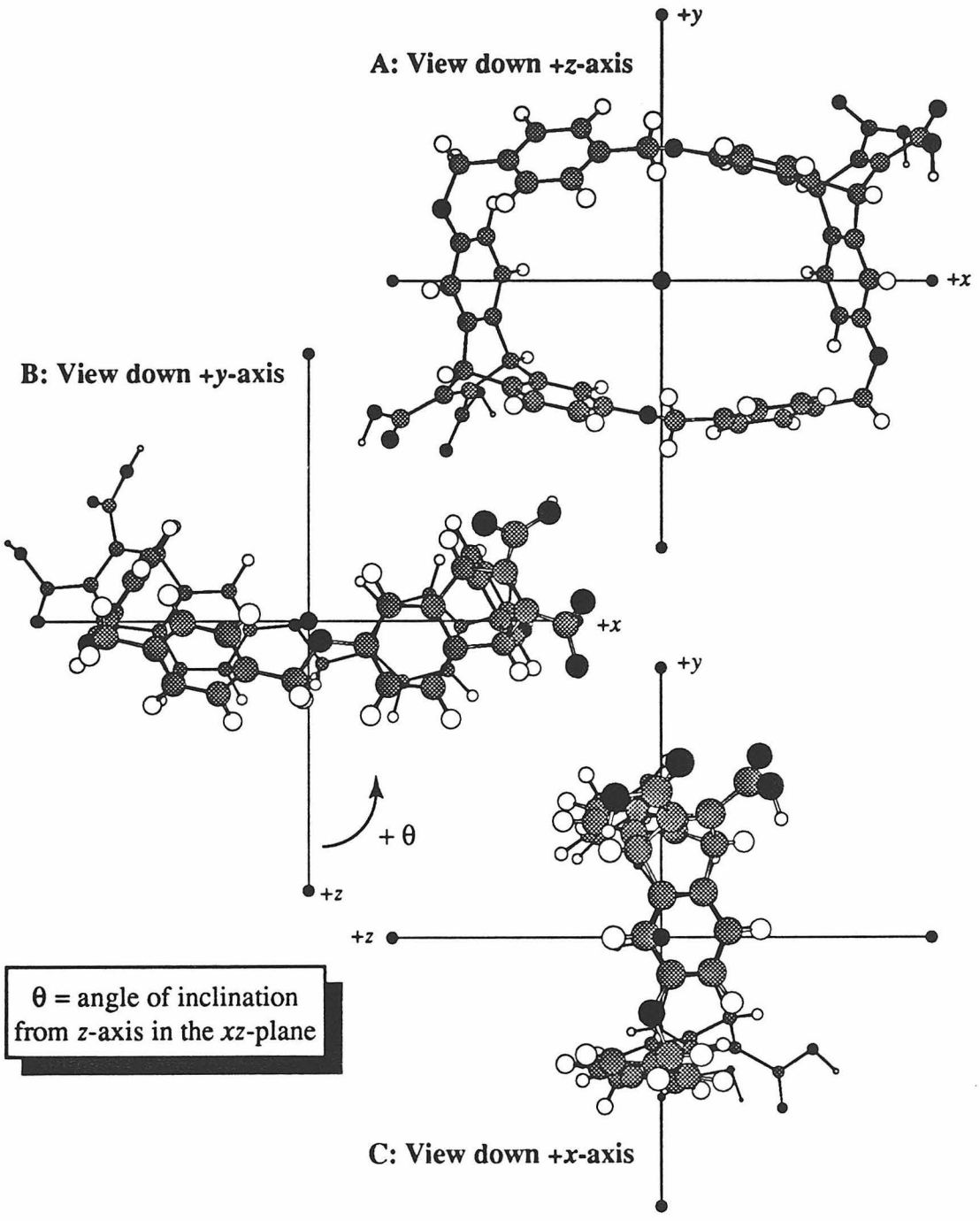

Figure 4.10. Host coordinate system showing views down *x*, *y*, and *z*-axes (A, B, and C respectively).[2]

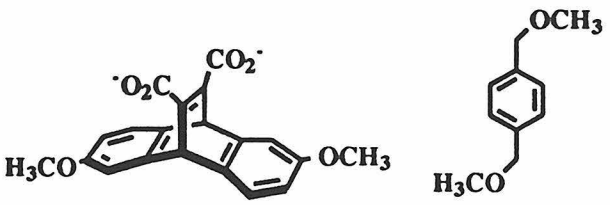

Ethenoanthracene Linker

Figure 4.11. Component chromophores of host P.

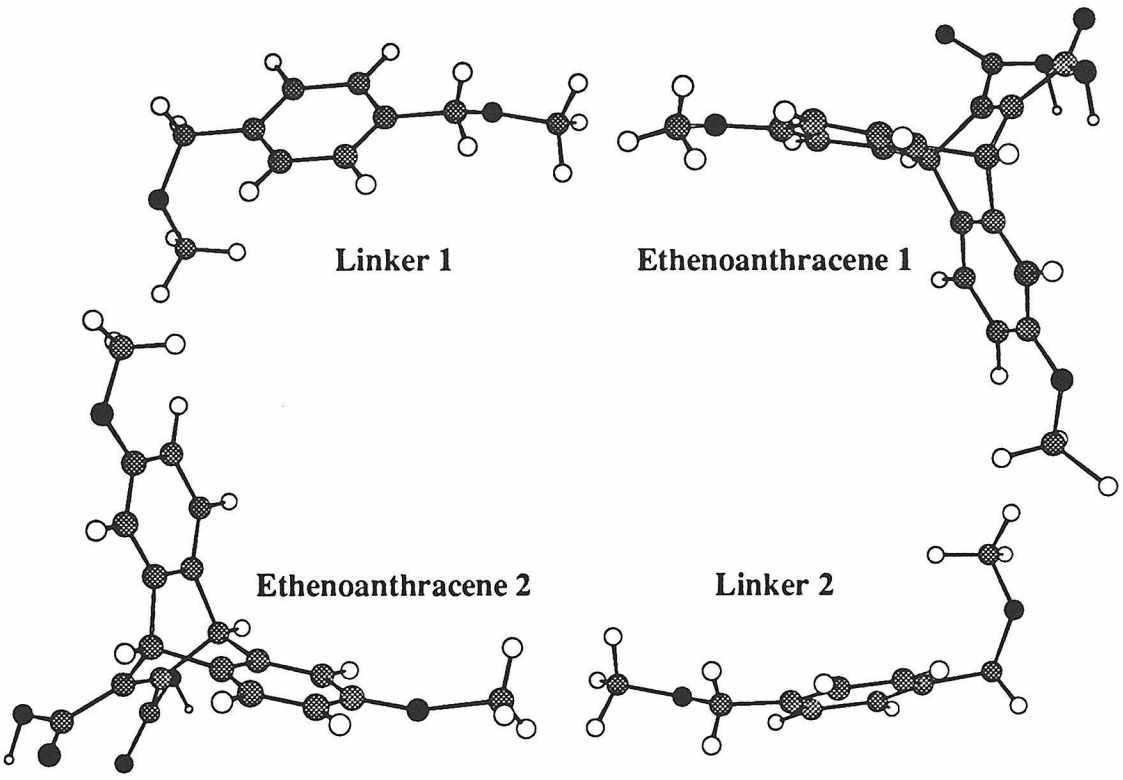

Figure 4.12. Component chromophores of host P_S (taken from the P_{SE} crystal structure).[20]

Semi-empirical methods do not lend themselves to the calculation of anionic species with high accuracy,[21] so we approximated the host as the tetraacid (as opposed to tetracarboxylate). Experimental data show that the tetraester and tetraacid of host **P** and related structures have nearly identical CD and UV spectra.[22] Thus, we felt that using the crystal structure of our tetraester with replacement of esters by acids was justified. In addition,

INDO/S calculations are expected to be reliable only for $\pi \rightarrow \pi^*$ transitions, so only states predominated by $\pi \rightarrow \pi^*$ contributions were considered for the actual calculation.[23] This exclusion of states predominated by $n \rightarrow \pi^*$ and $\sigma \rightarrow \pi^*$ is not expected to affect the reliability of the calculations, as the low oscillator strengths of these transitions should not significantly contribute to calculated rotational strengths. An additional constraint of the calculations was the limitation of transitions to only those above 180 nm (the energy gap between shorter wavelength host transitions and longer wavelength guest transitions results in insignificant contributions to the rotational strength of the induced transition). Comparison of the calculated wavelengths for the transitions with actual spectra showed good agreement in general, thus the calculated wavelengths were not corrected to approximate experimental observations.

In the work described here, the INDO/S Hamiltonian with the Zerner parameter set and the closed-shell RHF method for SCF calculations was employed. In addition, CI was limited to singly excited states and considered only excitations from the 10 highest occupied to the 10 lowest unoccupied orbitals (for the ethenoanthracene chromophores, excitations from the 14 highest occupied to the 14 lowest unoccupied orbitals were considered). Tables 4.2-4.9 list the principle axis coordinates and INDO/S calculated transition moments for the component chromophores of Figure 4.12. The $\pi \rightarrow \pi^*$ transition moments in the framework of the chromophore are shown pictorially in Appendix 2 (Section 4.9).

4.3.3 Guests

INDO/S calculations[14] on guest molecules were handled in the same manner as for the host chromophores (Section 4.3.2). The guest geometries come from AM1 calculations.[24] The transition moments corresponding to the absorption bands of interest are given in Table 4.10 and pictorially illustrated in Figure 4.13. All calculations with guests **9**

and **10** assume the *trans*-isomer.[25] Complete listing of the guest INDO/S spectral data and the principle axis coordinates for each guest are given in Appendix 3 (Section 4.10).

Atom	*x*	*y*	*z*	Atom	*x*	*y*	*z*
O(8)	-4.53377	2.00240	0.61578	C(65)	-1.97029	0.92024	-1.80409
O(9)	1.74989	-2.81254	-2.02612	H(66)	-1.75723	0.94012	-2.87280
O(10)	-0.13942	-3.75439	-1.73743	C(67)	-0.25718	-0.33326	1.24263
H(11)	-1.00673	-3.33966	-2.10702	C(68)	0.25509	-0.32331	-1.27092
O(12)	0.20520	-4.00830	1.16958	C(69)	0.24105	-1.72317	-0.63588
O(13)	-0.23455	-2.60539	2.78763	C(70)	-0.04321	-1.71771	0.65345
H(14)	-1.03125	-1.96258	2.90056	C(71)	1.25915	0.47008	-0.47517
O(15)	4.04675	2.73920	-0.64876	C(72)	0.98272	0.45788	0.89681
C(52)	-5.33704	2.91705	-0.16385	C(73)	-1.37185	0.30813	0.41069
C(53)	2.28791	1.21686	-0.95279	C(74)	-1.08071	0.31456	-0.95233
H(54)	2.49711	1.24143	-2.02217	C(75)	0.65356	-2.87402	-1.48292
C(55)	3.07672	1.95344	-0.06535	C(76)	-0.07770	-2.88228	1.53418
C(56)	2.86180	1.87399	1.27042	C(77)	4.68353	3.69267	0.17691
H(57)	3.52067	2.40853	1.95465	H	-4.73165	3.84157	-0.29603
C(58)	1.81487	1.12132	1.77621	H	5.12844	4.45582	-0.50009
H(59)	1.65047	1.05402	2.85155	H(93)	-5.46897	2.50989	-1.01182
C(60)	-2.51414	0.87834	0.90963	H(94)	-6.17652	2.98958	0.27899
H(61)	-2.73296	0.85586	1.97722	H(95)	-0.43346	-0.36473	2.17742
C(62)	-3.39421	1.49255	0.00321	H(96)	0.44421	-0.34573	-2.20760
C(63)	-3.13702	1.50869	-1.33162	H(97)	4.00143	4.10153	0.69846
H(64)	-3.83749	1.97747	-2.02278	H(98)	5.26924	3.20722	0.75601

Table 4.2. Principle axis coordinates (Å) for ethenoanthracene chromophore 1 using full host atom numbering scheme (Figure 4.9).

Atom	*x*	*y*	*z*	Atom	*x*	*y*	*z*
O(1)	0.94007	-3.92696	-1.00620	C(38)	-1.01353	0.41272	-0.90705
O(2)	0.23439	-2.72052	-2.70497	C(39)	0.45875	-2.93467	-1.41482
O(3)	-0.19000	-2.98765	2.66951	C(40)	-0.50900	-2.91137	1.50903
O(5)	-1.23400	-3.81570	0.87093	C(41)	5.07421	3.29357	0.11418
O(7)	4.35236	2.31218	-0.60567	C(88)	-4.97018	3.46732	-0.18057
O(16)	-4.29661	2.45062	0.60876	H(3)	0.48035	-3.48068	-3.35502
C(17)	2.45823	1.00382	-0.87849	H(6)	-1.49054	-4.66632	1.39205
C(19)	3.28089	1.68529	-0.01682	H(18)	2.65557	0.96283	-1.80987
C(20)	2.97954	1.74050	1.35081	H(21)	3.53189	2.23560	1.94437
C(22)	1.86366	1.07714	1.82399	H(23)	1.66829	1.10443	2.75250
C(24)	-2.42208	1.10836	0.93609	H(25)	-2.63570	1.10319	1.86570
C(26)	-3.21587	1.80501	0.02316	H(28)	-3.46286	2.32470	-1.93690
C(27)	-2.91785	1.82409	-1.32878	H(30)	-1.60250	1.10595	-2.71111
C(29)	-1.80457	1.11452	-1.77684	H(89)	-0.48632	-0.33952	2.19309
C(31)	-0.28495	-0.31973	1.26219	H(90)	0.48589	-0.38614	-2.16142
C(32)	0.28605	-0.34249	-1.22714	H	5.72810	3.83856	-0.56673
C(33)	0.14324	-1.72119	-0.60092	H(91)	5.60062	2.87229	0.78907
C(34)	-0.19688	-1.72945	0.67359	H(92)	4.46768	3.89876	0.52694
C(35)	1.34998	0.37901	-0.38290	H	-4.26186	4.26426	-0.40671
C(36)	1.05201	0.38455	0.97157	H(99)	-5.28494	3.07253	-0.98550
C(37)	-1.32609	0.42363	0.45402	H(100)	-5.71733	3.79523	0.31679

Table 4.3. Principle axis coordinates (Å) for ethenoanthracene chromophore 2 using full host atom numbering scheme (Figure 4.9).

State	λ (nm)	Predominate Transition	f^a	Transition Moment Vectors (atomic units) R_x	R_y	R_z
2	378.6	$n \rightarrow \pi^*$	0.00050	0.07721	-0.00396	0.01607
3	359.9	$n \rightarrow \pi^*$	0.00307	-0.15103	0.03580	0.11088
4	314.9	$\pi \rightarrow \pi^*$	0.03191	-0.27134	-0.45437	0.22516
5	300.0	$\pi \rightarrow \pi^*$	0.11570	0.90534	-0.09235	0.56078
6	287.6	$\pi \rightarrow \pi^*$	0.00811	-0.07667	0.26131	0.05106
7	272.8	$\pi \rightarrow \pi^*$	0.01522	-0.00744	0.36872	-0.02676
8	244.2	$\pi \rightarrow \pi^*$	0.00169	-0.03447	0.10280	-0.04310
9	238.5	$\pi \rightarrow \pi^*$	0.09115	-0.59985	-0.46784	0.37000
10	238.0	$\pi \rightarrow \pi^*$	0.22410	-1.13727	-0.19890	0.65028
11	233.6	$\pi \rightarrow \pi^*$	0.19849	0.08520	0.80826	-0.93051
12	229.0	$\pi \rightarrow \pi^*$	0.07922	-0.52338	-0.52348	-0.22198
13	225.5	$\pi \rightarrow \pi^*$	0.55924	2.02298	-0.07136	0.23268
14	216.7	$\pi \rightarrow \pi^*$	0.00172	-0.08786	-0.06764	-0.00129
15	215.9	$\pi \rightarrow \pi^*$	0.04347	-0.52975	0.15388	-0.06800
16	214.1	$\pi \rightarrow \pi^*$	0.03434	0.12343	-0.43239	0.19961
17	211.0	$\pi \rightarrow \pi^*$	0.12206	-0.28479	-0.84668	-0.22337
18	206.8	$\pi \rightarrow \pi^*$	0.24151	-1.20081	-0.44301	-0.07927
19	205.0	$\pi \rightarrow \pi^*$	0.03250	-0.29915	0.34010	0.11883
20	202.5	$\pi \rightarrow \pi^*$	0.10426	-0.54443	0.36596	-0.51460
21	198.8	$\pi \rightarrow \pi^*$	0.01397	0.24206	0.01501	-0.18059
22	196.0	$\pi \rightarrow \sigma^*$	0.07034	-0.15144	0.13694	-0.64200
23	195.2	$n \rightarrow \pi^*$	0.05684	-0.22011	-0.21535	-0.52001
24	193.6	$\pi \rightarrow \pi^*$	0.27318	-0.78946	0.73423	-0.76058
25	193.5	$\pi \rightarrow \pi^*$	0.19087	0.46745	0.24448	0.96820
26	192.7	$\pi \rightarrow \pi^*$	0.13010	-0.89461	-0.13952	-0.07493
27	190.4	$\pi \rightarrow \pi^*$	0.26965	0.67771	0.28297	-1.07258
28	189.6	$\pi \rightarrow \sigma^*$	0.12872	-0.44262	0.31508	0.71278
29	188.8	$\pi \rightarrow \pi^*$	0.44196	-0.66693	1.44268	0.47057
30	187.2	$\pi \rightarrow \pi^*$	0.12553	-0.22819	-0.09883	0.84363
31	186.6	$\pi \rightarrow \sigma^*$	0.04706	0.07341	-0.43861	0.30216

Table 4.4. INDO/S calculated transition moments for ethenoanthracene chromophore 1 (Figure 4.12).

[a]Oscillator strength from transition dipole moments.

State	λ (nm)	Predominate Transition	f^a	Transition Moment Vectors (atomic units) R_x	R_y	R_z
2	353.3	$n \rightarrow \pi^*$	0.00445	-0.02861	-0.08107	0.21064
3	348.2	$n \rightarrow \pi^*$	0.00180	0.12847	-0.05617	-0.03068
4	315.4	$\pi \rightarrow \pi^*$	0.01421	0.26779	-0.11626	-0.24959
5	300.3	$\pi \rightarrow \pi^*$	0.09960	0.83115	-0.02876	0.54145
6	288.6	$\pi \rightarrow \pi^*$	0.01409	-0.08630	-0.35098	-0.05675
7	273.6	$\pi \rightarrow \pi^*$	0.00547	0.02042	0.22073	-0.01261
8	243.7	$\pi \rightarrow \pi^*$	0.00844	-0.03632	0.25759	-0.00132
9	238.5	$\pi \rightarrow \pi^*$	0.08362	-0.59201	-0.08183	0.54724
10	233.3	$\pi \rightarrow \pi^*$	0.29167	0.76568	-0.19020	-1.27201
11	227.9	$\pi \rightarrow \pi^*$	0.22850	-0.89728	0.93329	-0.19488
12	223.9	$\pi \rightarrow \pi^*$	0.69330	-2.21670	-0.39250	-0.20593
13	219.4	$\pi \rightarrow \pi^*$	0.02507	-0.41935	-0.04096	0.05970
14	218.3	$\pi \rightarrow \pi^*$	0.12505	0.78090	-0.46496	-0.26980
15	211.2	$\pi \rightarrow \pi^*$	0.01286	-0.18782	-0.21359	0.09234
16	208.9	$\pi \rightarrow \pi^*$	0.06995	-0.06240	0.65883	-0.20769
17	207.0	$\pi \rightarrow \pi^*$	0.16415	-1.03310	-0.19185	-0.12106
18	204.1	$\pi \rightarrow \pi^*$	0.01929	-0.02204	0.33744	-0.12343
19	201.5	$\pi \rightarrow \pi^*$	0.01672	-0.10347	-0.05032	-0.31257
20	197.3	$\pi \rightarrow \sigma^*$ $n \rightarrow \pi^*$	0.05743	-0.02444	-0.51933	-0.32041
21	195.3	$n \rightarrow \pi^*$	0.01667	0.11499	-0.25065	0.17641
22	194.8	$n \rightarrow \pi^*$	0.18653	0.60166	0.25568	0.87672
23	192.2	$\pi \rightarrow \pi^*$	0.21091	0.33913	-0.88383	0.66204
24	191.5	$\pi \rightarrow \pi^*$	0.28556	-1.15275	0.09355	-0.68042
25	190.7	$\pi \rightarrow \pi^*$	0.23366	0.04269	-0.63438	-1.03089
26	188.5	$\pi \rightarrow \pi^*$	0.25891	-0.20130	1.22747	0.24457
27	188.1	$\pi \rightarrow \pi^*$	0.52647	0.80321	0.00689	-1.61706
28	187.3	$\pi \rightarrow \sigma^*$	0.21469	-0.31418	-0.94115	0.58225
29	183.7	$\pi \rightarrow \pi^*$	0.00389	0.13645	-0.06787	-0.01712
30	183.2	$\pi \rightarrow \pi^*$	0.29480	-0.82351	0.16042	1.03652
31	182.2	$\pi \rightarrow \sigma^*$	0.00854	0.02915	-0.08897	-0.20610

Table 4.5. INDO/S calculated transition moments for ethenoanthracene chromophore 2 (Figure 4.12).

[a]Oscillator strength from transition dipole moments.

Atom	*x*	*y*	*z*	Atom	*x*	*y*	*z*
O(15)	3.35978	0.07332	-0.58526	H(80)	1.53356	1.89042	-0.42438
O(16)	-3.73505	-0.37416	-0.08866	C(81)	-0.56042	1.44550	-0.16918
C(26)	-3.49147	-1.03742	-1.28389	H(82)	-0.89999	2.37827	-0.61935
H	-4.18587	-1.90664	-1.31456	C(83)	-1.47628	0.51631	0.30009
H	-2.44443	-1.41162	-1.23440	C(84)	-1.02522	-0.63741	0.88258
H	-3.75852	-0.33126	-2.10171	H(85)	-1.74042	-1.35123	1.29123
C(59)	4.62536	-0.43302	-0.78675	C(86)	0.32733	-0.90553	0.95745
H	4.97765	-0.03394	-1.76416	H(87)	0.66442	-1.85259	1.37878
H	4.51912	-1.53825	-0.86369	C(88)	-2.94188	0.81142	0.18642
H	5.26700	-0.02254	0.02472	H(97)	2.83115	-1.22923	0.76503
C(77)	2.70069	-0.30050	0.60738	H(98)	3.07360	0.19101	1.33772
C(78)	1.24160	-0.00932	0.51514	H(99)	-3.07683	1.44025	-0.51300
C(79)	0.80496	1.16799	-0.05638	H(100)	-3.24010	1.19452	1.00956

Table 4.6. Principle axis coordinates (Å) for linker chromophore 1 using full host atom numbering scheme (Figure 4.9).

Atom	*x*	*y*	*z*	Atom	*x*	*y*	*z*
O(7)	3.34727	0.55819	-0.04284	H	4.94100	1.77030	-0.29777
O(8)	-3.67043	0.01441	-0.46403	H	5.29289	0.03164	-0.15499
C(19)	4.60156	0.76918	-0.56255	H(91)	3.10965	-1.35477	0.27589
C(41)	2.69718	-0.68016	-0.25800	H(92)	2.76790	-0.92397	-1.17458
C(42)	1.25383	-0.54386	0.12163	H(44)	1.41770	1.10138	1.28649
C(43)	0.79310	0.49238	0.90017	H(46)	-0.85957	1.37957	1.71053
C(45)	-0.57167	0.67083	1.15216	H(49)	-1.66274	-1.90337	-0.43530
C(47)	-1.49205	-0.18736	0.59656	H(51)	0.62257	-2.16606	-0.87166
C(48)	-1.03901	-1.25547	-0.11135	H(93)	-3.09401	0.90047	1.20589
C(50)	0.32938	-1.42143	-0.35522	H(94)	-3.31536	-0.62618	1.37017
C(52)	-2.96816	0.05132	0.79873	H	-2.41170	1.16100	-1.57521
C(62)	-3.47005	1.08968	-1.32287	H	-4.05147	0.94134	-2.23317
H	4.56665	0.67240	-1.64781	H	-3.78984	2.01032	-0.83354

Table 4.7. Principle axis coordinates (Å) for linker chromophore 2 using full host atom numbering scheme (Figure 4.9).

				Transition Moment Vectors (atomic units)		
State	λ (nm)	Predominate Transition	f^a	R_x	R_y	R_z
2	267.5	$\pi \rightarrow \pi^*$	0.01222	0.15436	0.26381	-0.11908
3	210.2	$\pi \rightarrow \pi^*$	0.05647	0.55159	-0.24735	0.15936
4	186.5	$\pi \rightarrow \pi^*$	1.10946	-2.57219	0.41025	-0.16466
5	185.5	$\pi \rightarrow \pi^*$	0.88425	-0.42957	-2.05130	1.00309

Table 4.8. INDO/S calculated transition moments for linker chromophore 1 (Figure 4.12).

[a]Oscillator strength from transition dipole moments.

State	λ (nm)	Predominate Transition	f^a	Transition Moment Vectors (atomic units) R_x	R_y	R_z
2	267.5	$\pi \rightarrow \pi^*$	0.00844	-0.10195	-0.21095	-0.13953
3	209.6	$\pi \rightarrow \pi^*$	0.01288	0.29224	-0.05850	-0.00200
4	188.1	$\pi \rightarrow \pi^*$	1.09376	2.58623	-0.11585	-0.26747
5	187.3	$\pi \rightarrow \pi^*$	0.86197	-0.10826	-1.91555	-1.27804

Table 4.9. INDO/S calculated transition moments for linker chromophore 2 (Figure 4.12).

[a]Oscillator strength from transition dipole moments.

Guest	State	λ (nm) INDO/S	λ (nm) Experiment	Predominate Transition	f^b	Transition Moment Vector (atomic units) R_X	R_Y	R_Z
3	2	329.9	318	$\pi \rightarrow \pi^*$	0.12855	-0.95750	0.69220	-0.00028
4	2	337.0	355	$\pi \rightarrow \pi^*$	0.35896	1.89165	0.63533	0.00404
5	2	589.3	not observed	$n \rightarrow \pi^*$	0.00111	-0.14144	0.03783	0.00769
	3	530.1	not observed	$n \rightarrow \pi^*$	0.00049	0.01445	0.09149	0.00753
	4	313.3	323[c]	$\pi \rightarrow \pi^*$	0.13569	1.13598	0.32958	0.02228
	5	308.2		$\pi \rightarrow \pi^*$	0.13795	0.45616	-1.08923	-0.07288
6	2	618.6	570	$\pi \rightarrow \pi^*$	0.01691	0.00011	-0.58680	0.00001
	3	353.0	340	$\pi \rightarrow \pi^*$	0.03038	-0.59421	0.00021	0.00004
7	2	515.3	467	$\pi \rightarrow \pi^*$	0.02292	0.62336	0.01458	0.00036
	3	434.7	not observed	$n \rightarrow \pi^*$	0.00000	0.00028	0.00017	0.00224
	4	431.9	not observed	$n \rightarrow \pi^*$	0.00008	-0.00005	0.00018	-0.03381
	5	362.6	376	$\pi \rightarrow \pi^*$	0.22150	-0.00569	-1.62597	-0.00029
	6	301.8	292	$\pi \rightarrow \pi^*$	0.12011	-1.09238	-0.00021	0.00098
8	2	366.5	not observed	$n \rightarrow \pi^*$	0.00072	0.01469	-0.00751	0.09186
	3	340.0	366	$\pi \rightarrow \pi^*$	0.64682	2.51389	-0.95928	-0.00787
9	2	486.7	452	$\pi \rightarrow \pi^*$	1.44654	-4.81355	-0.09670	0.00077
10	2	482.5	439	$\pi \rightarrow \pi^*$	1.16405	4.29969	-0.06427	-0.00361
11	2	430.9	412	$\pi \rightarrow \pi^*$	0.95693	-3.67980	0.18417	0.02033

Table 4.10. INDO/S Calculated Parameters for Longer Wavelength Transitions in AM1[24] Optimized Guests.[a]

[a]State 2 up to shortest wavelength state for which ICD was experimentally observed. [b]Oscillator strength from transition dipole moments. [c]Only one broad absorption band observed experimentally (λ_{max} = 323 nm), but ICD shows two transitions at 341 and 309 nm (see Table 4.1).

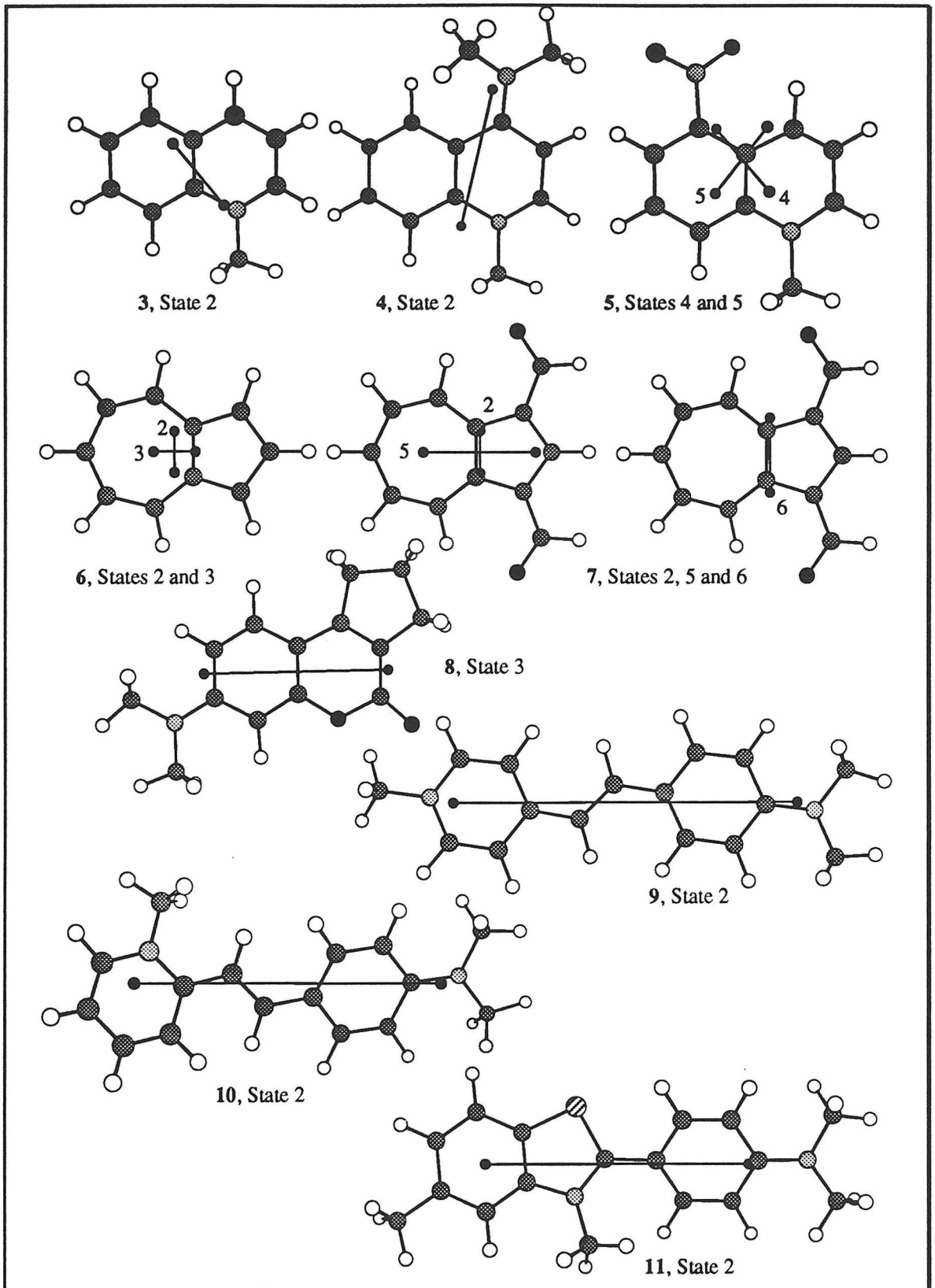

Figure 4.13. AM1[24] optimized guests with the transition moments of interest.[2]

4.3.4 Calculation Setup

Once the host transition moments were known, they needed to be superimposed onto the host coordinate system of Section 4.3.1. From the calculations all the host chromophores and their transition moments are obtained in a principle axis coordinate system specific to the component chromophore. In addition, the coordinates for each atom in the host framework are also known, but the coordinates of the transition moments are unknown in the host coordinate system. The positions of the endpoints of the transition moments (μ_1 and μ_2) can be obtained from their relation in space (from the principle axis coordinate system) to six atoms in the host framework (Figure 4.14). Tables 4.4, 4.5, 4.8, 4.9, and 4.10 list μ_1 only (this endpoint defines the direction of the dipole); the coordinates of the second endpoint are obtained by reflecting μ_1 through the origin of the principle axis coordinate system.

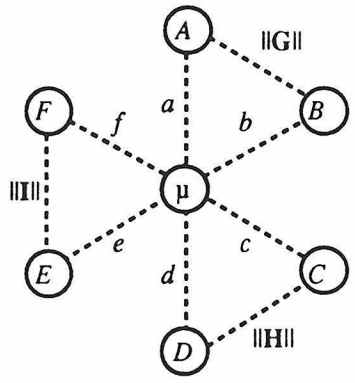

Figure 4.14. Relationship in space between a transition moment endpoint (μ) and six atoms (*A*-*F*) with known positions in the host coordinate system. The vectors G, H, and I are defined by equations 4.11-4.13.

With reference to Figure 4.14, the six known atoms can be labeled *A*-*F*, and the distances from these atoms to an endpoint, μ, are labeled *a*-*f*, where *a* is the distance from atom *A* to μ, and so on. It is also useful to define three vectors **G**, **H**, and **I**.

$$\mathbf{G} = \mathbf{R}_{BA} \tag{4.11}$$

$$\mathbf{H} = \mathbf{R}_{DC} \tag{4.12}$$

$$\mathbf{I} = \mathbf{R}_{FE} \tag{4.13}$$

Where $\mathbf{R}_{IJ}$ denotes the distance vector from atom *J* to atom *I*. From the six known points in space (atoms) and the six known distances (*a-f*), the following relationships are obtained:

$$a^2 = (\mu_x - A_x)^2 + (\mu_y - A_y)^2 + (\mu_z - A_z)^2 \tag{4.14}$$

$$b^2 = (\mu_x - B_x)^2 + (\mu_y - B_y)^2 + (\mu_z - B_z)^2 \tag{4.15}$$

$$c^2 = (\mu_x - C_x)^2 + (\mu_y - C_y)^2 + (\mu_z - C_z)^2 \tag{4.16}$$

$$d^2 = (\mu_x - D_x)^2 + (\mu_y - D_y)^2 + (\mu_z - D_z)^2 \tag{4.17}$$

$$e^2 = (\mu_x - E_x)^2 + (\mu_y - E_y)^2 + (\mu_z - E_z)^2 \tag{4.18}$$

$$f^2 = (\mu_x - F_x)^2 + (\mu_y - F_y)^2 + (\mu_z - F_z)^2 \tag{4.19}$$

In expressions 4.14-4.19, the *x*, *y*, and *z* subscripts refer to *x*, *y*, and *z* coordinates in the host coordinate system. The only unknown variables in these expressions are μ_x, μ_y, and μ_z. Subtracting equation 4.15 from equation 4.14 and rearranging the terms gives the following expression:

$$\frac{a^2 - b^2 - A_x^2 - A_y^2 - A_z^2 + B_x^2 + B_y^2 + B_z^2}{2} = \mu_x(B_x - A_x) + \mu_y(B_y - A_y) + \mu_z(B_z - A_z) \tag{4.20}$$

In equation 4.20, the terms on the left are all known and thus a constant for a given μ; this constant can arbitrarily be defined as g_1. Substituting the expression for **G** (equation 4.11) into equation 4.20 gives:

$$g_1 = \mu_x \mathbf{G}_x + \mu_y \mathbf{G}_y + \mu_z \mathbf{G}_z \tag{4.21}$$

where g_1 is defined as:

$$g_1 = \frac{a^2 - b^2 - A_x^2 - A_y^2 - A_z^2 + B_x^2 + B_y^2 + B_z^2}{2} \tag{4.22}$$

Analogously, equations 4.23 and 4.24 can be derived and are defined in terms of atom set (C, D) for 4.23 and atom set (E, F) for 4.24.

$$g_2 = \mu_x H_x + \mu_y H_y + \mu_z H_z \tag{4.23}$$

$$g_3 = \mu_x I_x + \mu_y I_y + \mu_z I_z \tag{4.24}$$

Where

$$g_2 = \frac{c^2 - d^2 - C_x^2 - C_y^2 - C_z^2 + D_x^2 + D_y^2 + D_z^2}{2} \tag{4.25}$$

$$g_3 = \frac{e^2 - f^2 - E_x^2 - E_y^2 - E_z^2 + F_x^2 + F_y^2 + F_z^2}{2} \tag{4.26}$$

Equations 4.21, 4.23, and 4.24 provide three expressions to solve for the three unknown quantities μ_x, μ_y, and μ_z. Solving the system as a 3×3 determinant[26] gives the following relationships for the unknown quantities:

$$\mu_x = \frac{\begin{vmatrix} g_1 & G_y & G_z \\ g_2 & H_y & H_z \\ g_3 & I_y & I_z \end{vmatrix}}{\begin{vmatrix} G_x & G_y & G_z \\ H_x & H_y & H_z \\ I_x & I_y & I_z \end{vmatrix}} = \frac{g_1 H_y I_z + G_y H_z g_3 + G_z g_2 I_y - G_z H_y g_3 - g_1 H_z I_y - G_y g_2 I_z}{G_x H_y I_z + G_y H_z I_x + G_z H_x I_y - G_z H_y I_x - G_x H_z I_y - G_y H_x I_z} \tag{4.27}$$

$$\mu_y = \frac{\begin{vmatrix} G_x & g_1 & G_z \\ H_x & g_2 & H_z \\ I_x & g_3 & I_z \end{vmatrix}}{\begin{vmatrix} G_x & G_y & G_z \\ H_x & H_y & H_z \\ I_x & I_y & I_z \end{vmatrix}} = \frac{G_x g_2 I_z + g_1 H_z I_x + G_z H_x g_3 - G_z g_2 I_x - G_x H_z g_3 - g_1 H_x I_z}{G_x H_y I_z + G_y H_z I_x + G_z H_x I_y - G_z H_y I_x - G_x H_z I_y - G_y H_x I_z} \tag{4.28}$$

$$\mu_z = \frac{\begin{vmatrix} G_x & G_y & g_1 \\ H_x & H_y & g_2 \\ I_x & I_y & g_3 \end{vmatrix}}{\begin{vmatrix} G_x & G_y & G_z \\ H_x & H_y & H_z \\ I_x & I_y & I_z \end{vmatrix}} = \frac{G_xH_yg_3 + G_yg_2I_x + g_1H_xI_y - g_1H_yI_x - G_xg_2I_y - G_yH_xg_3}{G_xH_yI_z + G_yH_zI_x + G_zH_xI_y - G_zH_yI_x - G_xH_zI_y - G_yH_xI_z} \quad (4.29)$$

Using Excel,[27] a spreadsheet was set up to solve equations 4.27-4.29 given appropriate input atoms and their coordinates in both principle axis and host coordinate systems. In this manner the coordinates of all endpoints for the transition moments (and thus the transition moments themselves) were obtained in the host coordinate system. Given appropriate aligning of axes or planes in a guest molecule, this spreadsheet could also be used to locate positions of guest transition moments and atoms in the host coordinate system as well. The complete listing of transformed coordinates for the host $\pi \rightarrow \pi^*$ transitions are given in Appendix 1 (Section 4.8).

Once all the transition moments are translated into the host coordinate system, calculations using equation 4.2 can be carried out. The transition moments from Tables 4.4, 4.5, 4.8, 4.9, and 4.10 give directions, but not magnitudes. The magnitude of the transition moment (in cgs units, esu•cm) is given by equation 4.30[13b]

$$\|\mu\| = 1.46 \times 10^{-15} \sqrt{\frac{f}{\nu}} \quad (4.30)$$

In this equation f is the oscillator strength of the transition and ν is the frequency of the transition (cm^{-1}). This requires that all transition moment coordinates be multiplied by a constant, m, in order to calculate dot and cross vector products; m is defined by equation 4.31 and always has the value shown.[13b]

$$m = \frac{\sqrt{(\mu_{1x} - \mu_{2x})^2 + (\mu_{1y} - \mu_{2y})^2 + (\mu_{1z} - \mu_{2z})^2}}{\|\mu\|} = 1.27 \times 10^{-18} \text{ cm•esu•Å}^{-1} \quad (4.31)$$

For the calculations, guests were oriented in the cavity based on reasonable binding geometries (specific to the type of guest; see Section 4.4) and rotated about the *y*-axis in 10° increments. The rotated coordinates ($\mu_{x+\theta}$, $\mu_{y+\theta}$, $\mu_{z+\theta}$) are obtained from multiplying the initial coordinates (μ_x, μ_y, μ_z) by the rotation matrix shown in equation 4.32.

$$\begin{vmatrix} \cos\theta & 0 & \sin\theta \\ 0 & 1 & 0 \\ -\sin\theta & 0 & \cos\theta \end{vmatrix} \times \begin{vmatrix} \mu_x \\ \mu_y \\ \mu_z \end{vmatrix} = \begin{vmatrix} \mu_{x+\theta} \\ \mu_{y+\theta} \\ \mu_{z+\theta} \end{vmatrix} = \begin{vmatrix} \mu_x \cos\theta + \mu_z \sin\theta \\ \mu_{y1} \\ -\mu_x \sin\theta + \mu_z \cos\theta \end{vmatrix} \qquad (4.32)$$

Unless otherwise specified in Section 4.4, the initial orientation ($\theta = 0°$) was alignment of the transition dipole under consideration with the *z*-axis. Rotational strength (R) was calculated at each 10° increment. The value of R was calculated for the given orientation of the transition moment and was not modified for "impossible" orientations, i.e., guest atoms and host atoms sitting at the same locations in space. Calculation of ICD with host $\mathbf{C_S}$ was done analogously to the case of host $\mathbf{P_S}$, but the contributions from transition moments in the linkers were neglected from the coupling.[28]

4.4 Calculation Results and Bound Guest Orientations

4.4.1 Long-Axis Dyes

Guests **9**, **10**, and **11** can be thought of as control molecules. CPK and molecular mechanics calculations show that these guests can only orient themselves in the host cavity with the long-axis having a less than 90° (and probably much less than 90°) inclination from the *z*-axis in the *xz*-plane. For purposes of calculation, the starting orientation placed the guest long axis transition moment in the *xz*-plane, aligned along the *z*-axis with the midpoint of the transition moment coincident with the origin. The ICD vs θ curves are shown in Figures 4.15 and 4.16. The host **P** calculations (Figure 4.15) are relatively

uninformative, as $R < 0$ for all values of θ, but the host **C** data (Figure 4.16) confirm what the models have shown. Experimentally, host C_S induces CD with $R > 0$ for all three of the long axis guests.[29] According to the calculations this places the transition moments at $140° \leq \theta \leq 185°$ ($\pm$ n180°), or up to 40° off perfect alignment with the *z*-axis for guests **9** and **10**. Guest **11** has a slightly broader range, $135° \leq \theta \leq 190°$ ($\pm$ n180°). Based on the size of the guests, θ approaching 90° should be impossible to attain, and this is confirmed by the calculation. The host **C** cavity is thought to be slightly narrower than host **P**, thus a guest in host **P** may have a slightly broader range of allowed θ's.

Another feature of the curves showing the expected ICD (Figures 4.15 and 4.16) is that a larger R is to be expected for CD induced by host **P** than by host **C**. This is the result of the contribution to R from the transitions associated with the linkers (particularly the transition to State 4; see Tables 4.8 and 4.9). This larger R for ICD in host **P** complexes is predicted for all the guests studied in these coupled-oscillator calculations.

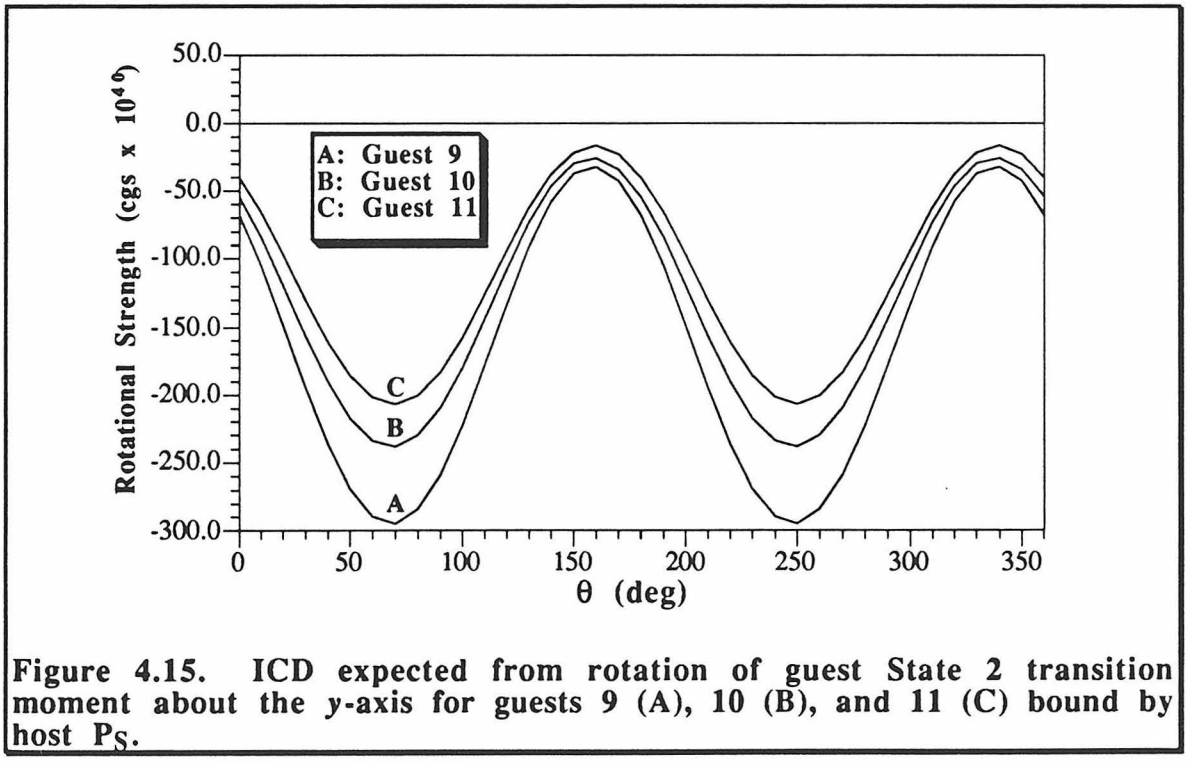

Figure 4.15. ICD expected from rotation of guest State 2 transition moment about the *y*-axis for guests 9 (A), 10 (B), and 11 (C) bound by host P_S.

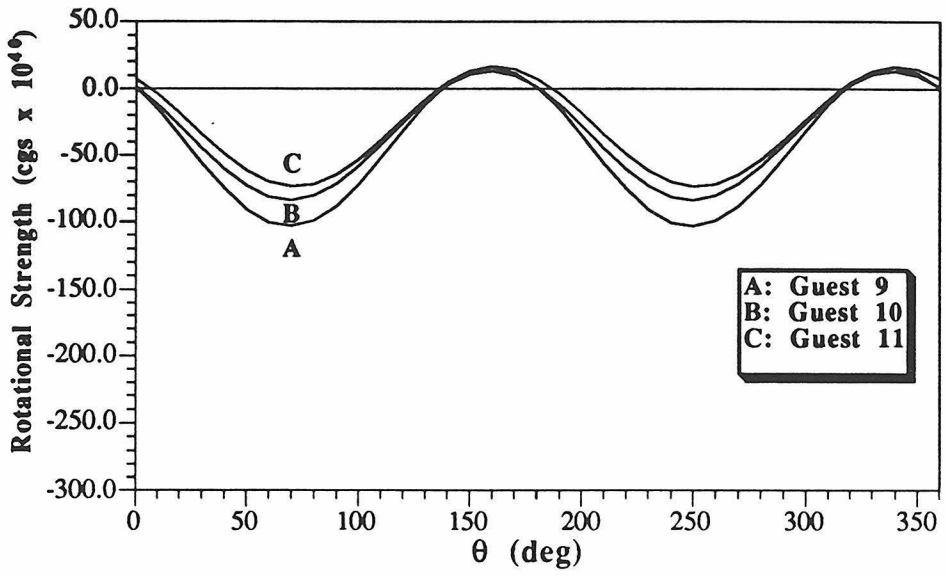

Figure 4.16. ICD expected from rotation of guest State 2 transition moment about the *y*-axis for guests 9 (A), 10 (B), and 11 (C) bound by host C_S.

The binding orientation suggests that these guests may twist in order to better fill the cavity and to push their aromatic rings into the aromatic cavity walls. In each of the three guests, one ring is electron deficient, and we believe that it is the electron-poor ring that pushes up to the electron-rich face of a cavity aromatic ring. One intriguing aspect of the calculations is the preference for two of four possible binding orientations (Figure 4.17). The difference in sign of ICD for these seemingly equivalent orientations suggests that the interaction of wavefunctions of cavity walls and guest differ significantly. The difference is apparently strong enough to result in a preference for a clockwise inclination from the *z*-axis (Figure 4.17). This preference for the "clockwise" twisted bound guest is a very subtle aspect of the bound complex that would not be detectable in an NMR study (the *D* values are expected to be similar for either conformation). AM1 calculations show that guest **9** is ideally planar, but there is a low energy barrier to conformations in which the aromatic rings are twisted relative to the plane of the ethylene bridge;[30] AM1 optimized **10** and **11** are twisted (and thus chiral) in their lowest energy conformations.[31] We propose

that the chirality of the host induces a subtle preference for the rings of guests **9**, **10**, and **11** to be twisted to cause a better fit (and thus better cation-π stabilization) at one side of the cavity.[32] These data suggest that there is some directionality in the cation-π effect acting as a stabilizing force in molecular recognition.

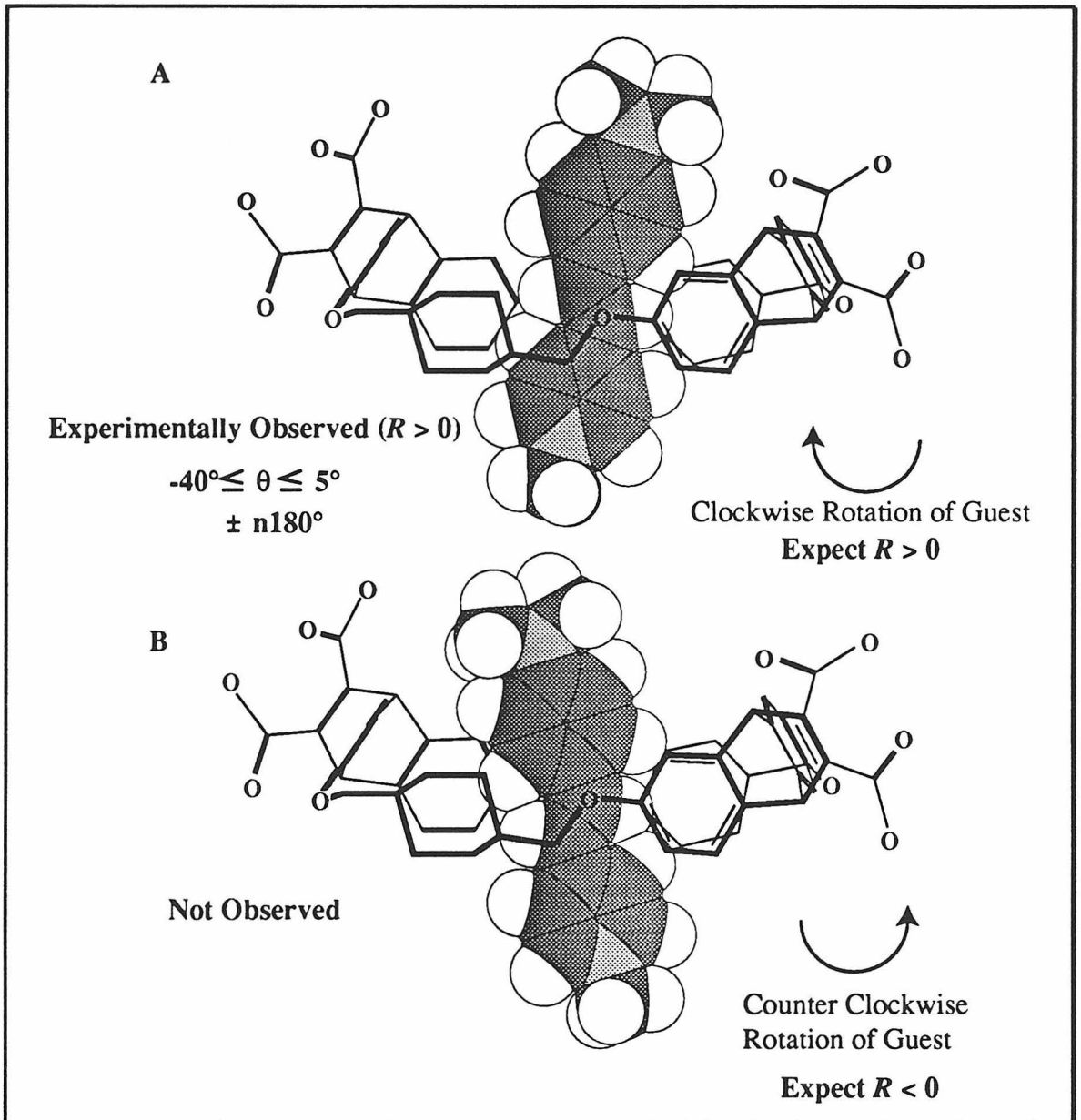

Figure 4.17. Observed (A) and non-observed (B) binding orientations for long-axis guests with host C_S (illustrated with guest 9). The view is down the +*y*-axis, and the guest lies in the *xz*-plane and is positioned with the long-axis transition moment at an angle midway through the range of allowed θ's off the *z*-axis. Note that each of the two orientations shown generates an equivalent orientation by adding 180° to the value of θ.

4.4.2 Azulenes

Guests **6** and **7** were chosen for study because each has a pair of well-defined, mutually perpendicular long wavelength transition moments (oriented along the long and short axes of the molecule; see Figure 4.13). It was also of interest to determine if a cation-π effect is operative with the seven-membered "cationic" ring of the guest.[1a,33] As with the long-axis guests, the starting orientation put the guest transition moment in the *xz*-plane, aligned along the *z*-axis with the midpoint of the transition moment coincident with the origin.

Figures 4.18 and 4.19 show the expected rotational strength for bound conformations of azulene (**6**) with hosts **P** and **C**. Only the transition to State 3 was experimentally observed (with both hosts), this transition being polarized along the long axis of the guest (Figure 4.13). The expected $R < 0$ places the binding orientation from 0°-140° (± n180°) for host **P** and from 30°-130°(± n180°) for host **C** (Figure 4.20). This suggests the guest is most likely to be near the 90° orientation. That is, the guest prefers to be nearly fully encapsulated in the host–a binding conformation consistent with a strong hydrophobic effect contributing to the binding. Models show that the host cavity is long enough to accommodate the long axis. We were unable to experimentally see ICD for State 2 (short axis transition, 90° inclination from State 3). The calculations indicate that, in general, the magnitude of $\Delta\varepsilon$ should be smaller for State 2 than for State 3. If we assume our observation is not an experimental artifact, but rather indicates that $\Delta\varepsilon \approx 0$, Figure 4.18 suggests the binding orientations for host **C** to be in the range of 140°-175°(± n180°). This would imply 50-85°(± n180°) for State 3 (Figure 4.21), a result consistent with the direct analysis of State 3. Host **P** is expected to have a similar binding orientation.

Figures 4.22 and 4.23 show the expected rotational strength for bound conformations of guest **7** with hosts **P** and **C**. ICD is observed in State 5 (long-axis transition) for both hosts and State 2 (short-axis transition) is not observed under our

experimental conditions. Based on an analysis analogous to that of the rotational strength curves for guest **6**, it can be shown that the most likely orientation for guest **7** with host **C** (and presumably host **P**) is 50°-80° (± n180°) for the long axis of the guest (Figure 4.24). Again we see a preference for greater encapsulation of guest surface area and strong hydrophobic binding contributions.

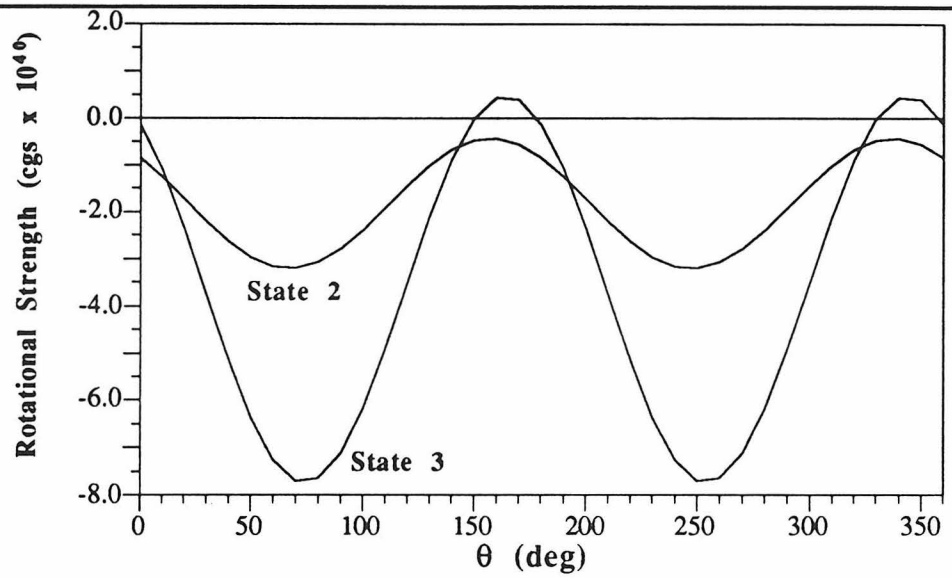

Figure 4.18. ICD expected from rotation of guest States 2 and 3 transition moments about the *y*-axis for guest 6 bound by host P_S.

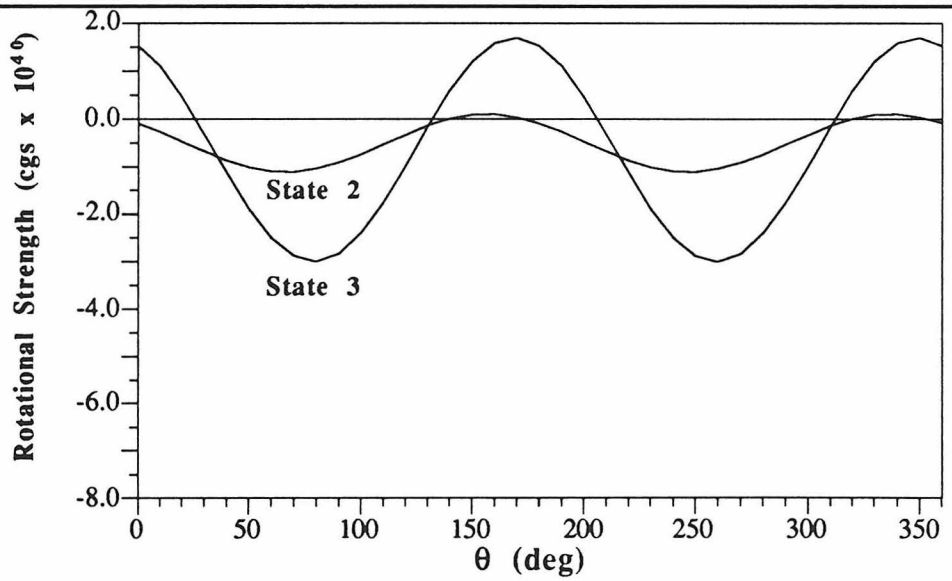

Figure 4.19. ICD expected from rotation of guest States 2 and 3 transition moments about the *y*-axis for guest 6 bound by host C_S.

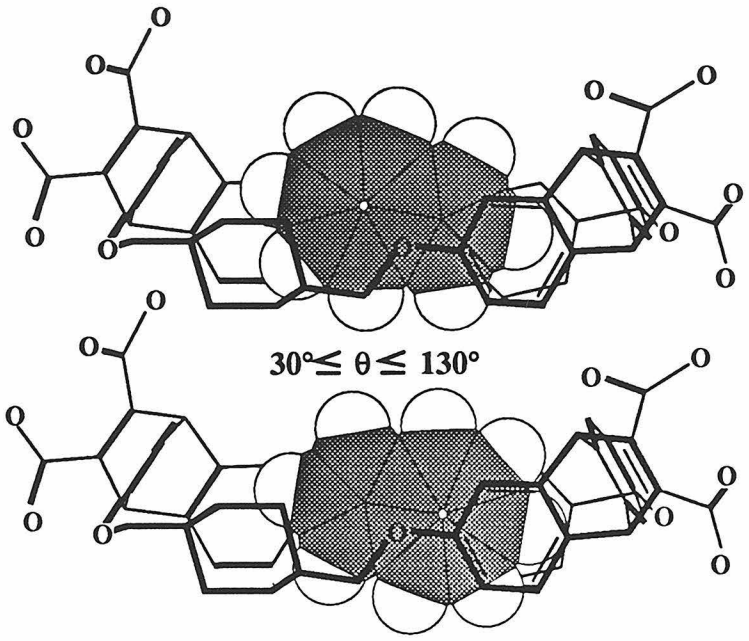

30°≤ θ ≤ 130°

210°≤ θ ≤ 310°

Figure 4.20. Binding orientations predicted for guest 6 with host C_S based on ICD observed in guest long-axis (State 3) transition. The view is the same as that of Figure 4.17.

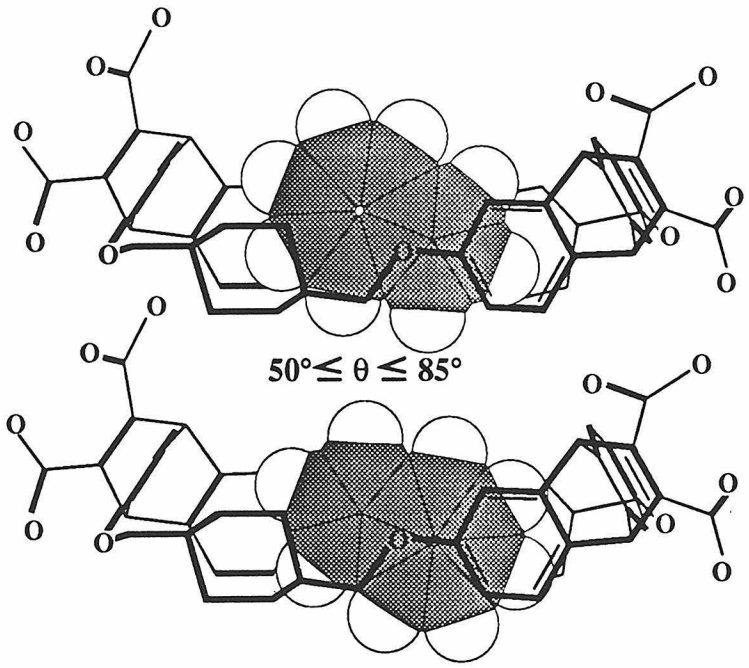

50°≤ θ ≤ 85°

230°≤ θ ≤ 265°

Figure 4.21. Binding orientations predicted for guest 6 with host C_S based on ICD observed in guest long-axis (State 3) transition when $\Delta\varepsilon$ for ICD in short-axis (State 2) transition is approximately zero. The view is the same as that of Figure 4.17.

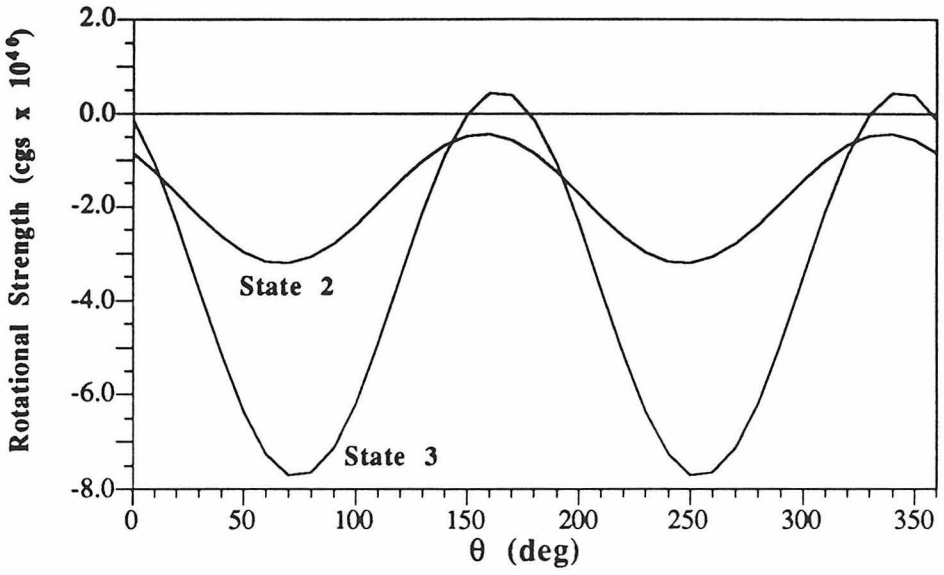

Figure 4.22. ICD expected from rotation of guest States 2 and 5 transition moments about the *y*-axis for guest 7 bound by host P_S.

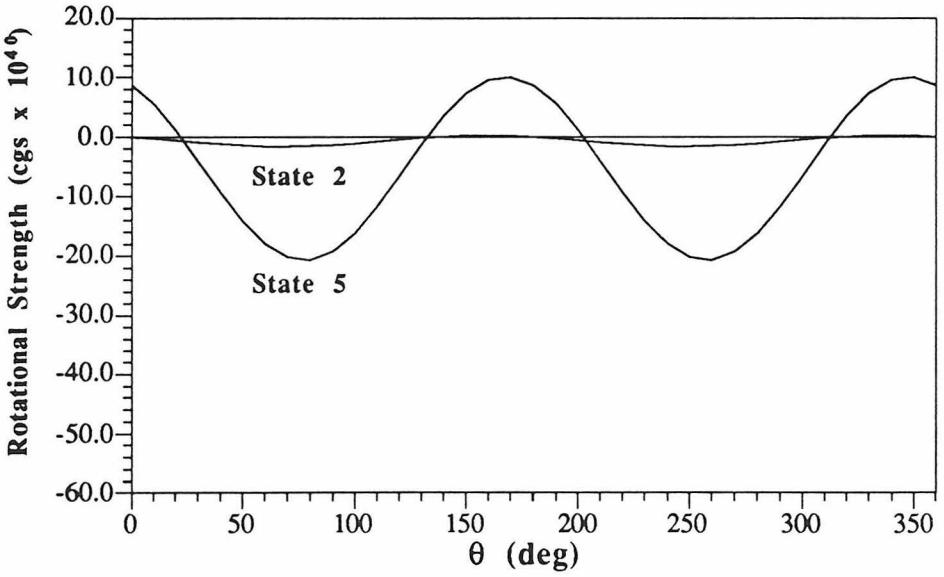

Figure 4.23. ICD expected from rotation of guest States 2 and 5 transition moments about the *y*-axis for guest 7 bound by host C_S.

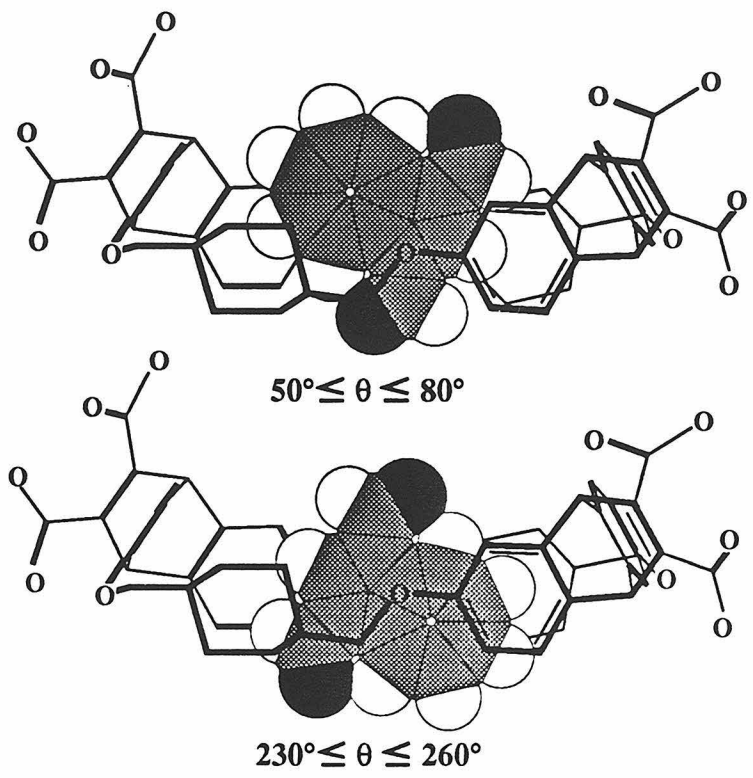

Figure 4.24. Binding orientations predicted for guest 7 with host C_S based on ICD observed in guest long-axis (State 5) transition when $\Delta\varepsilon$ for ICD in short-axis (State 2) transition is approximately zero. The view is the same as that of Figure 4.17.

Guest **7** also shows an interesting spectral feature in its host-guest complex with both hosts **P** and **C** (data for host **P** shown in Figure 4.25). It appears that the transition to State 6 (short-axis, near 300 nm) shows an excitonic coupling[15] (split Cotton effect centered near 300 nm) to State 5 of the ethenoanthracene chromophores of the host. To our knowledge, this is the first example of an excitonic coupling between host and guest chromophores in a host-guest complex; Previous reports of excitonic coupled CD spectra in host-guest complexes have shown excitonic coupling between bound guests[3i] or between component chromophores in the host itself.[5ab,6be]

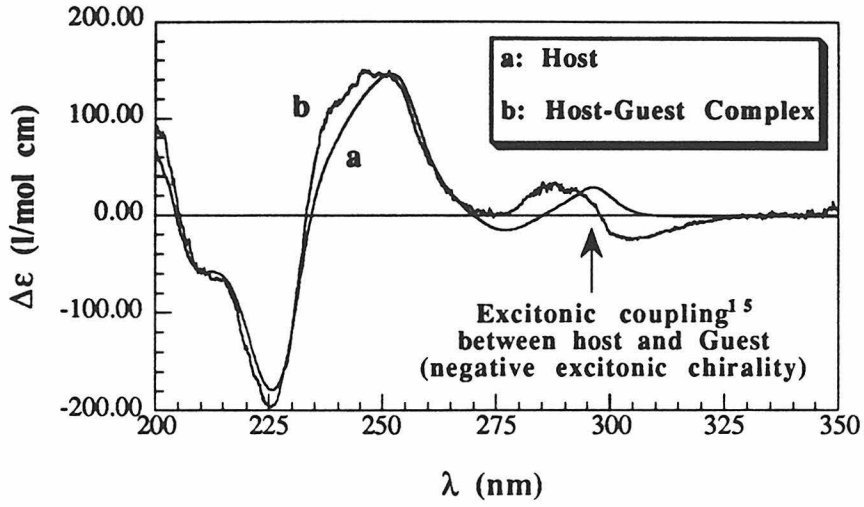

Figure 4.25. CD spectrum of host P_S and fitted spectrum of its complex with guest 7 in aqueous borate buffer (pH 9).

The general form of the equation describing excitonic coupling of chromophores (see Chapter 3, Section 3.2.2) is[15]

$$\sum_{a \neq b} \mathbf{R}_{ab} \cdot (\mu_{a1A} \times \mu_{b1B}) V_{a1A,b1B} \tag{4.33}$$

where the interaction energy ($V_{a1A,b1B}$) between the interacting transitions is defined by the point-dipole approximation and has the form of equation 4.3.[15] The expected sign of the excitonic chirality for the host P_S/C_S-guest **7** complex was computed for the binding orientations of Figures 4.22 and 4.23; the result is shown in Figure 4.26. Using these binding orientations, the relationship of the three transition moments in space shows a left-handed sense of screw in our host coordinate system (Figure 4.27). This requires that the sign of $\mathbf{R}_{ab} < 0$ for purposes of calculation.[15] Based on the observed negative chirality for **7**-P_S complex (negative first Cotton effect, positive second Cotton effect; as expected C_R gives opposite chirality), the calculation gives a short-axis binding orientation in the range 115°-240° (± n180°); this is 25°-150° (± n180°) for the guest long-axis. While broad, the range of θ is consistent with the data obtained from Figures 4.22 and 4.23 and guest **6**; it

also rules out the orientation where the seven membered "cationic" ring is exclusively bound (0° with respect to the long-axis of the guest).

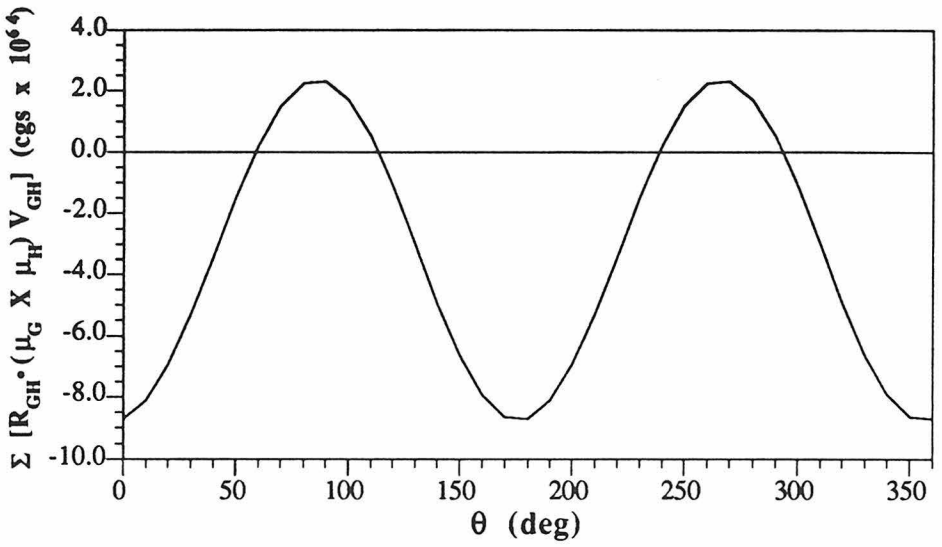

Figure 4.26. Calculated sign of excitonic coupling between guest 7 State 6 and ethenoanthracene chromophores State 5 in complexes with hosts P_S and C_S.

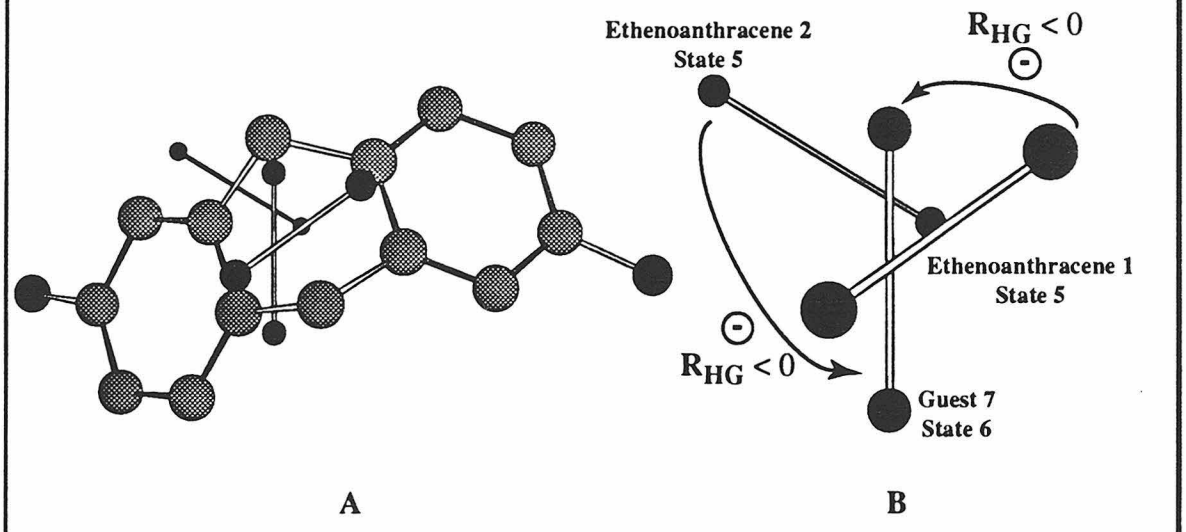

Figure 4.27. Relationship in space of guest 7 State 6 and ethenoanthracene State 5 transition moments for the θ = 0° orientation of the guest long-axis, illustrating the left-handed sense of screw for the system. Viewed through anthracene framework of ethenoanthracene chromophore 1 (A) and in relation to one another (B).

4.4.3 Quinolines and Coumarins

While convienient for our analysis, the dyes and azulenes previously described do not represent typical guests studied with our hosts. The most prototypical guests that exhibited ICD were the quinoliniums **3**, **4**, and **5**. These guests have transition moments that do not lie perfectly along a long or short-axis in the guest framework (Figure 4.13). As a result, using a $\theta = 0°$ based on the transition moment (as in the previous cases) provides bound guest orientations that are unlikely to occur (given NMR data and cavity dimensions).[1,20] In order to approximate a more realistic binding orientation, the guests were oriented in the *xz*-plane so that the C(9)-C(10) bond of the quinoline ring was coincident with the *z*-axis, and the midpoint of this bond was placed at the origin. The midpoints of the C(2)-C(3) and C(6)-C(7) bonds were bisected by the *x*-axis. Beginning

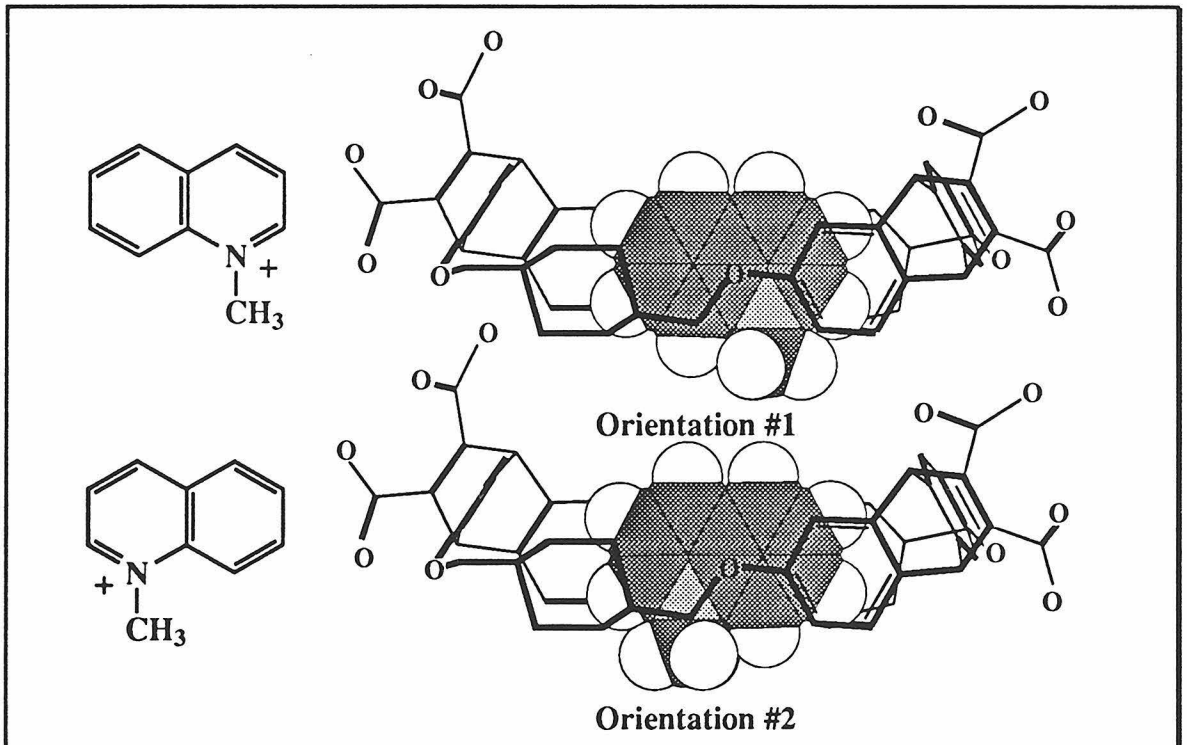

Figure 4.28. $\theta = 0°$ orientations for quinoline based guests in the host coordinate system (illustrated with host C_S and guest 3). The view is down the +*y*-axis, and the guest lies in the *xz*-plane with the C(9)-C(10) bond aligned with the *z*-axis and centered at the origin.

with this orientation, the guest was rotated about the *y*-axis to give the *R* vs θ curves. Unlike the previous guests, whose orientations were determined by the transition moments, the three quinolines each have two initial orientations that need to be considered (Figure 4.28).

Experimentally, guest **3** shows ICD only with host **C**. In the case of host **P**, the ICD band is thought to be buried under the tail of the host longer wavelength Cotton effects. Figure 4.29 shows the expected rotational strength for guest **3** interacting with host **C**. The data (C_S, $R < 0$) puts θ at 0°-100° (± n180°) for orientation #1 and 80°-185° (± n180°) for orientation #2. In each case the guest appears to rotate in such a way as to place the N-methyl group towards the interior of the cavity (Figure 4.30). Since the methyl group carries a large fraction of the positive charge in such a structure, this finding is consistent with the cation-π interaction influencing binding orientations.[34]

NMR experiments with guest **3** and host **P** show that the protons in the 2, 6, and 7 positions on the quinoline ring experience greater upfield shifting on complexation than do other guest protons (Figure 4.31).[35] We believe that these protons are therefore more deeply buried in the host cavity than are the remaining (more exposed) guest protons. The

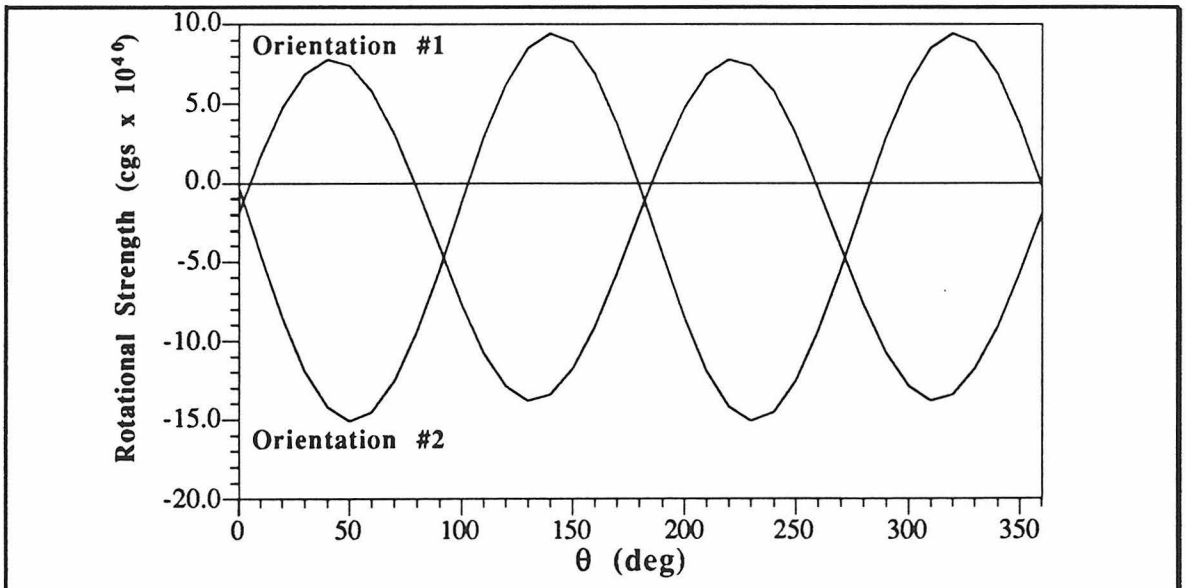

Figure 4.29. ICD expected for guest State 2 transition from rotation of guest C(9)-C(10) bond about the *y*-axis for guest 3 bound by host C_S.

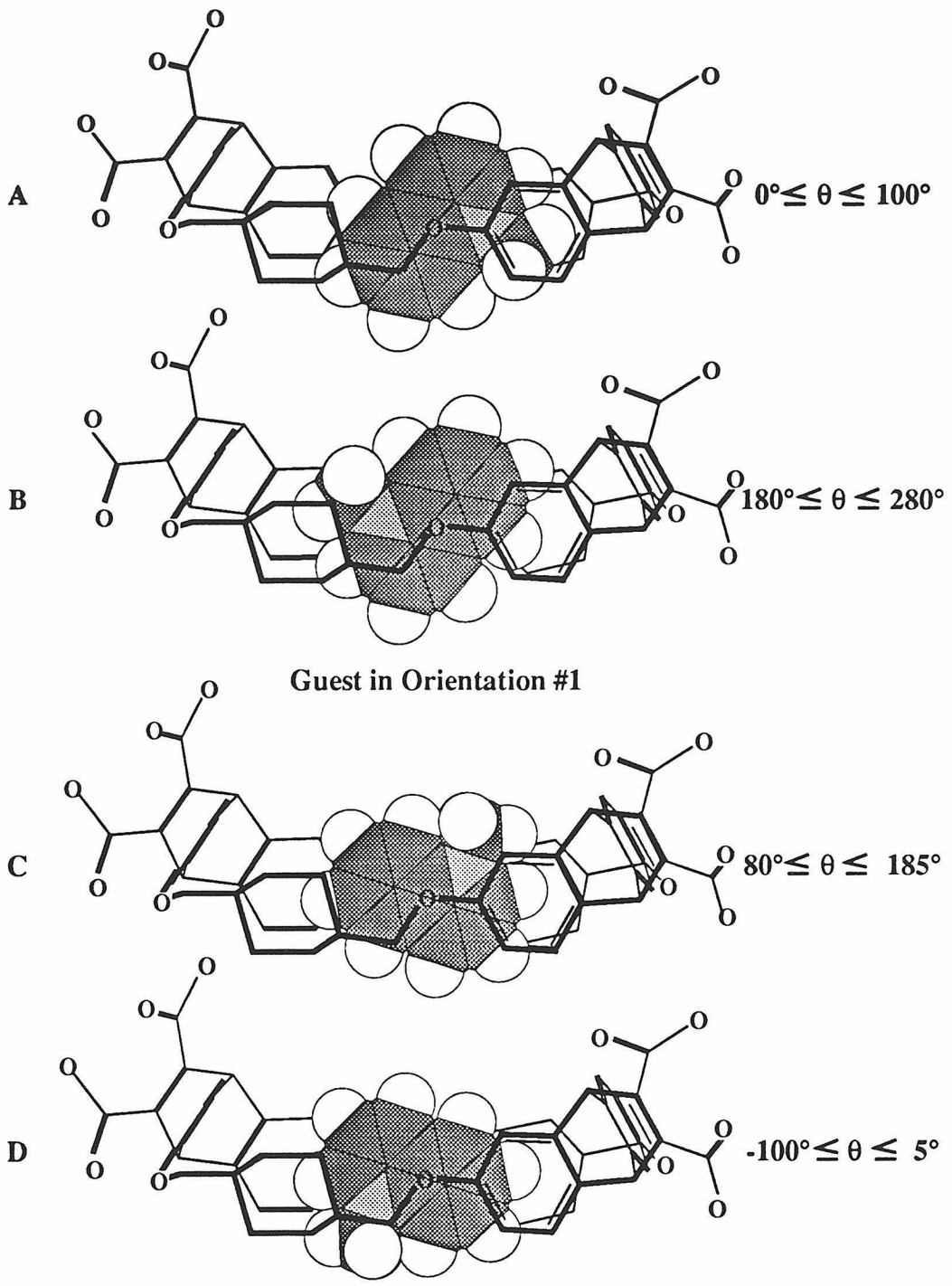

Figure 4.30. Binding orientations predicted for guest 3 with host C_S based on ICD observed in the guest State 2 transition. The view is down the $+y$-axis, and the guest lies in the xz-plane and is positioned with the C(9)-C(10) bond at an angle midway through the range of allowed θ's off the z-axis.

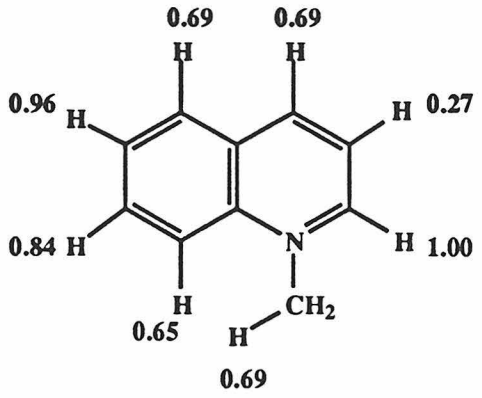

Figure 4.31. Relative *D* values from NMR experiments for guest protons in guest 3 bound by host P.[35,36]

binding orientations shown in Figure 4.30 are consistent with these NMR observations. In particular the proton at the 2-position is shown to be near the cavity walls in all four of the Figure 4.30 binding orientations, and this proton is upfield shifted to the greatest extent in the NMR studies (Figure 4.31).[36] As expected, we observe binding orientations for host **P** that are similar to those of host **C** with a given guest.

Similar calculations were performed for guest **4**. The R vs θ curves are shown in Figures 4.32 and 4.33. With host $\mathbf{P_S}$ ($R < 0$), the data places θ at 10°-140° (± n180°) for orientation #1 and at -25°-125° (± n180°) for orientation #2 (Figure 4.32). The host **C** data narrows the range of θ, giving ranges of 35°-125° (± n180°) for orientation #1 and 30°-115° (± n180°) for orientation #2 (where $\mathbf{C_S}$ is expected to produce $R < 0$, Figure 4.33). Again the data for the two systems are consistent and indicate that the guest rotates in such a way as to place one substituent towards the inside of the cavity (Figure 4.34). In this case there are two substituents, the N-methyl and 4-dimethylamino groups. We expect the preferred orientation would place the hydrophilic dimethylamino group more exposed to solvent and the hydrophobic methyl group in the cavity (Figure 4.34 orientions A and B). This also puts the formal positive charge in the cavity, where it can experience cation-π interactions.

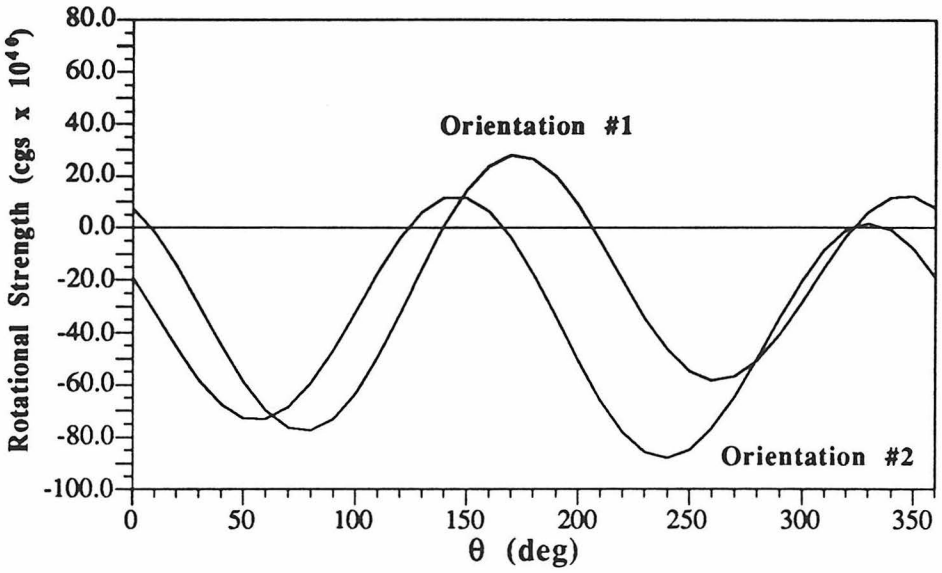

Figure 4.32. ICD expected for guest State 2 transition from rotation of guest C(9)-C(10) bond about the *y*-axis for guest 4 bound by host P_S.

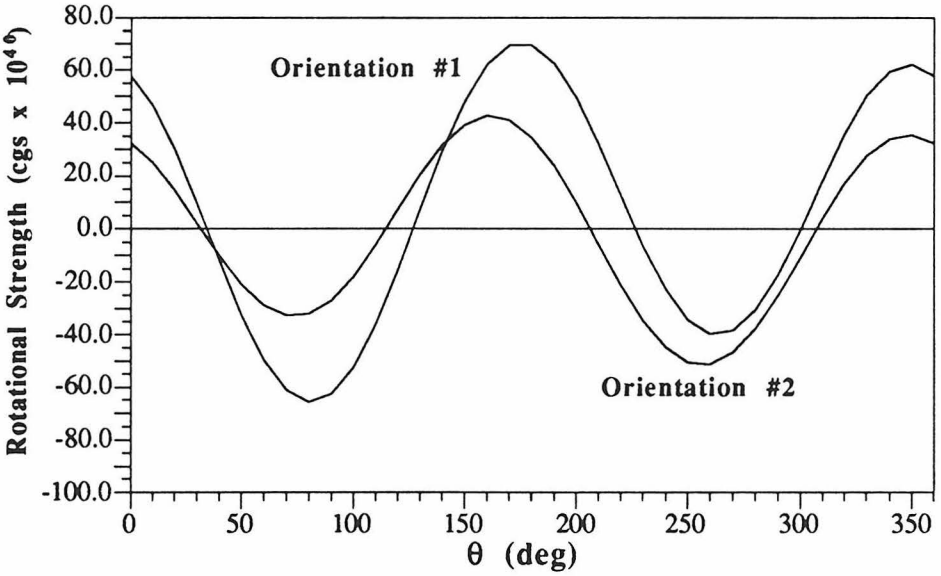

Figure 4.33. ICD expected for guest State 2 transition from rotation of guest C(9)-C(10) bond about the *y*-axis for guest 4 bound by host C_S.

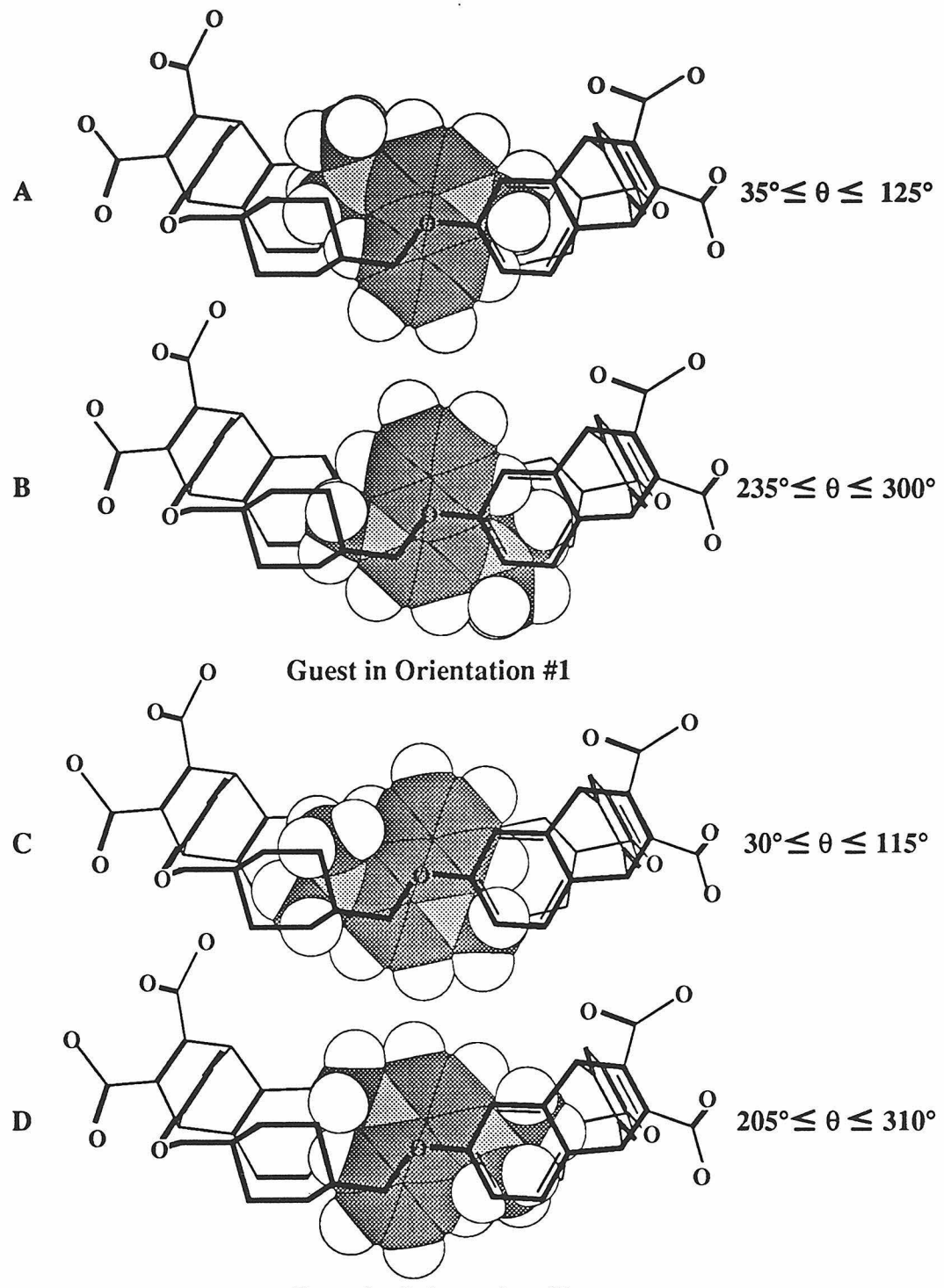

Figure 4.34. Binding orientations predicted for guest 4 with host C_S based on ICD observed in guest State 2 transition. The view is the same as that of Figure 4.30.

For guest **5**, induced CD was observed only with host P_S (Figure 4.35). The expected rotational strength is shown in Figures 4.36 and 4.37. This guest was of particular interest, as the ICD was observed for two nearly in-plane transitions separated through an angle of 83.5° (States 4 and 5, see Figure 4.13). The θ range satisfying the observed ICD (State 4 $R > 0$, State 5 $R < 0$) for host P_S is 80° - 150° (± n180°) for orientation #1 and 0°-70° (± n180°) for orientation #2. This indicates a preference for binding orientations in which both substituents are outside the cavity (Figure 4.38). This places the hydrophilic nitro group in a solvent-exposed environment. This is in contrast to the preferred orientations of guests **3** and **4** where a substituent is pushed towards the interior of the cavity. It may be that a 1,5 substitution pattern does not allow a comfortable fit in the cavity unless both substituents are outside. Alternatively, a high desolvation penalty for the hydrophilic nitro group may dictate that this group remain exposed to solvent.

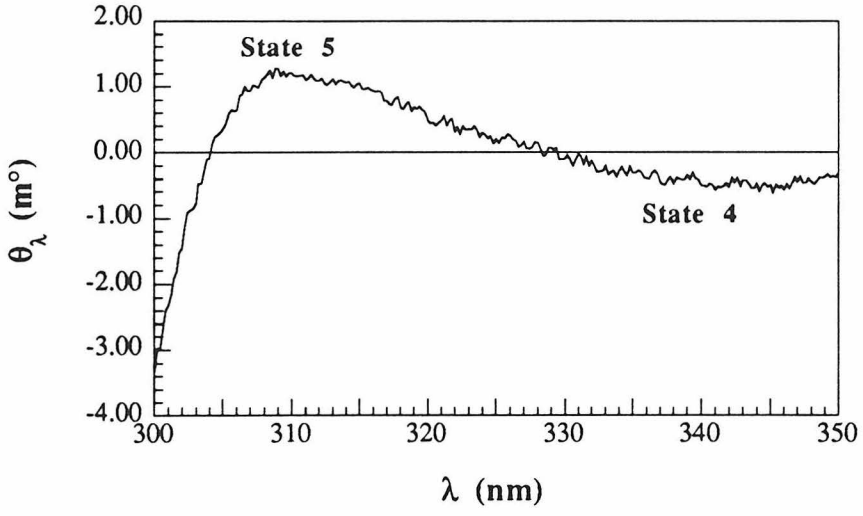

Figure 4.35. CD spectrum of an aqueous borate buffer (pH 9) solution 1.08×10^{-5} M in guest 5 and 1.06×10^{-5} M in host P_R.

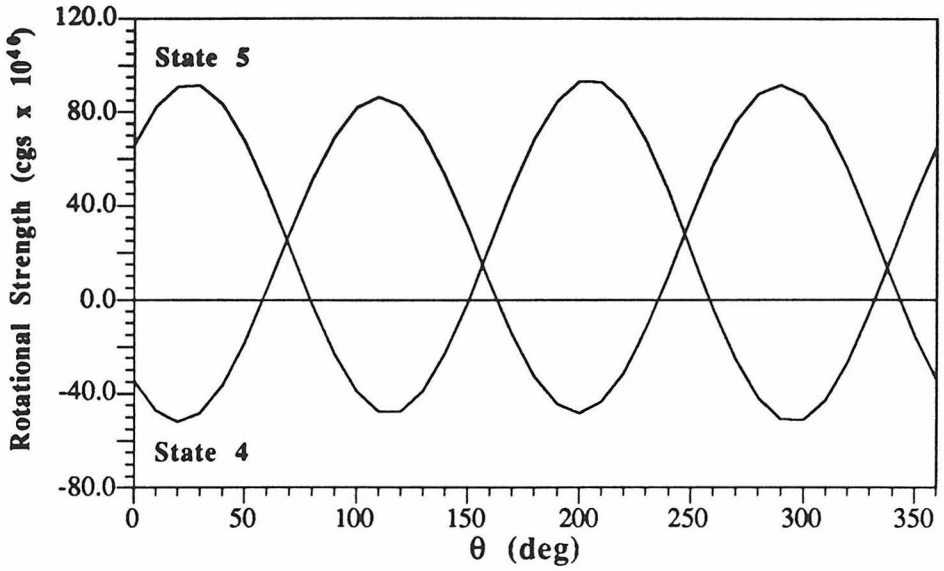

Figure 4.36. ICD expected for guest State 4 and 5 transitions from rotation of guest C(9)-C(10) bond about the *y*-axis for guest 5 (in θ = 0° orientation #1) bound by host P_S.

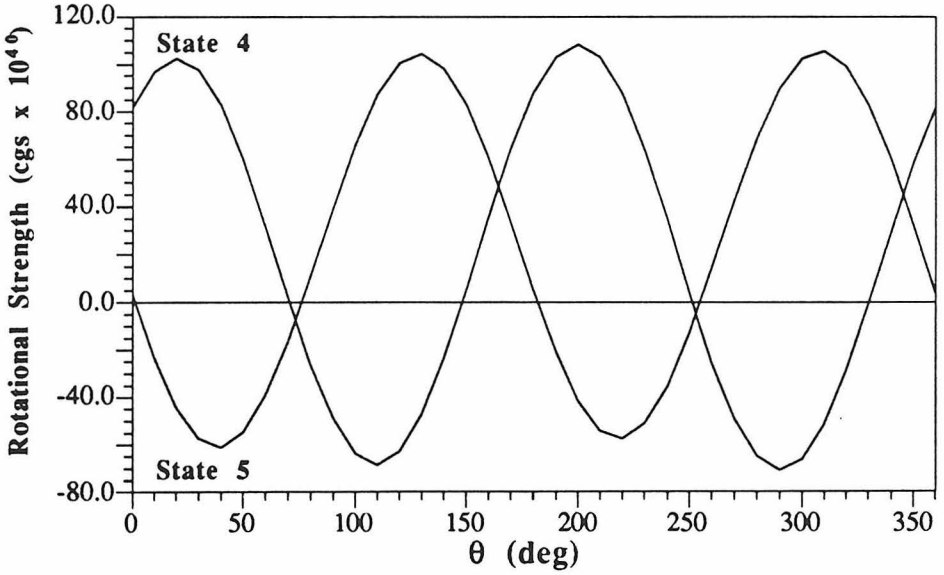

Figure 4.37. ICD expected for guest State 4 and 5 transitions from rotation of guest C(9)-C(10) bond about the *y*-axis for guest 5 (in θ = 0° orientation #2) bound by host P_S.

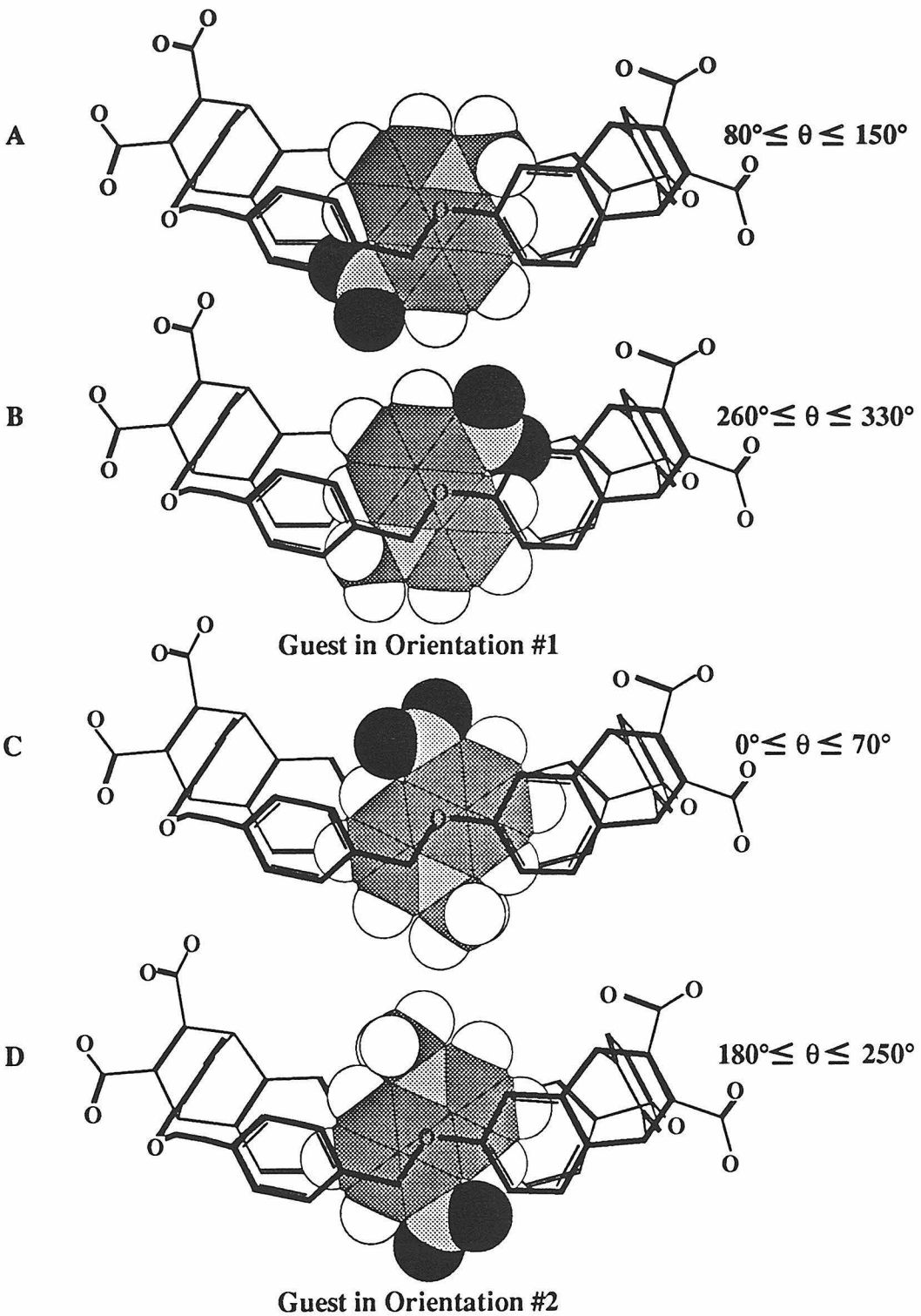

Figure 4.38. Binding orientations predicted for guest 5 with host P_S based on ICD observed in guest State 4 and 5 transitions. The view is the same as that of Figure 4.30.

It was hoped that by looking at chromophoric guests with a naphthalene-like topology, we could learn about the binding orientations of more protoypical guests than the dyes and azulenes. For these studies, we looked at several coumarin based-dyes (**8**, **12**-**14**), but only **8** gave detectable ICD and only in studies with host **C**. Calculation by orienting the guest with its transition moment coincident with the *z*-axis and the midpoint of the transition moment at the origin, places θ in the range 30° - 130° (± 180°) for the expected $R < 0$ with host C_S (Figure 4.40) As seen with guests **6** and **7**, this puts the guest in an orientation that allows most of its surface area to be placed in the cavity (Figure 4.41). The data suggests hydrophobic forces dominate the binding of this guest.

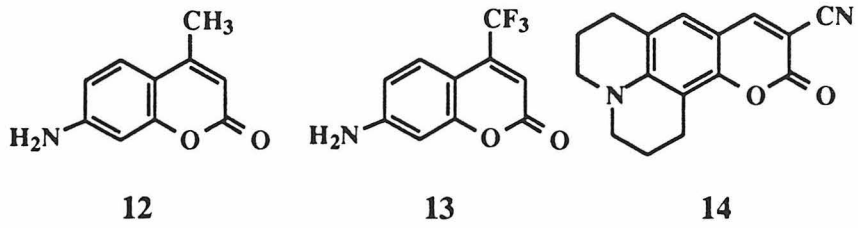

12 **13** **14**

Figure 4.39. Coumarin dyes.

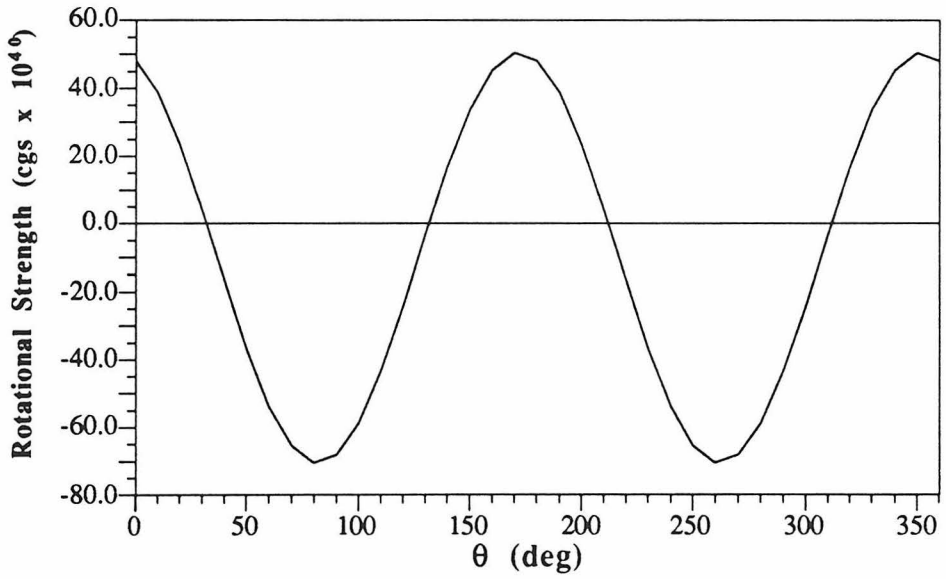

Figure 4.40. ICD expected from rotation of guest State 3 transition moment about the *y*-axis for guest 8 bound by host C_S.

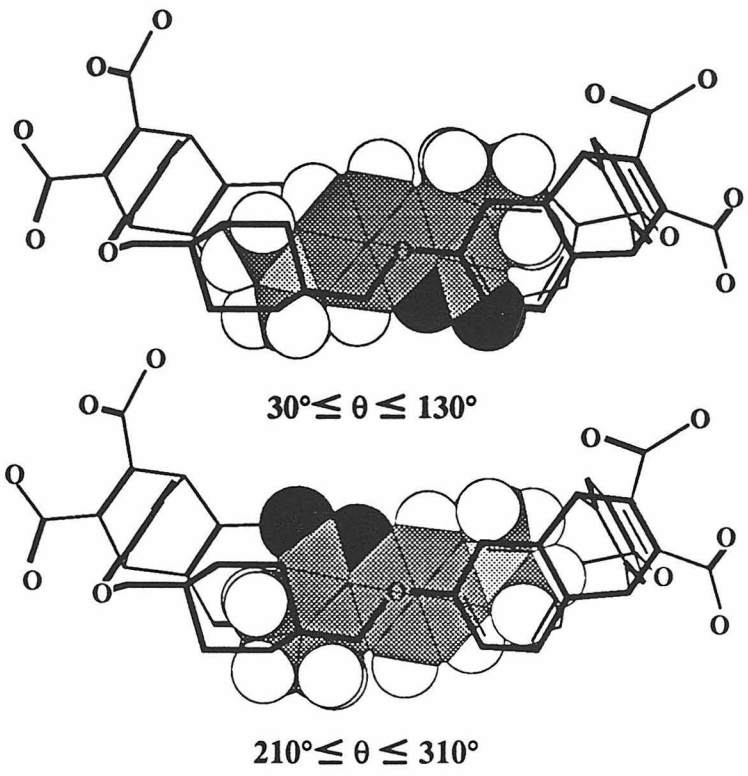

Figure 4.41. Binding orientations predicted for guest 8 with host C_S based on ICD observed in guest long-axis (State 3) transition. The view is the same as that of Figure 4.17.

4.5 Calculation Control Studies

4.5.1 Approaches to Coupled-Oscillator Calculations

As previously noted, our approach towards coupled-oscillator calculations (described in Sections 4.2-4.4) differs from more commonly applied approaches[3k,12,17c,18] in the way we define the chromophores. It is the general practice to treat each bond in the host (usually a non-chromophoric system) as a chromophore and then couple the resultant transition moments with $\pi \rightarrow \pi^*$ transition moments in the guest.[3k,12,17c,18] This immediately brings into question the validity of our approach, since others do not use it. We believe that our approach to defining actual chromophores is

more realistic, but we needed to demonstrate this in light of the literature precedence for the bond chromophore approach.

As a test of our method, we chose to calculate the expected CD in (+)-2-methylenebenzonorbornene (**15**, Figure 4.42). As for our guest molecules, the INDO/S calculation was carried out on AM1[24] optimized **15** (Table 4.11, Figure 4.43), with the calculation subject to the same computational constraints as described in Section 4.3.2 (with the exception that $\pi \rightarrow \pi^*$ transitions below 180 nm were included). Structure **15** has component chromophores **16** and **17** (Figure 4.42), the INDO/S[14] calculated spectral data for these component chromophores and principle axis coordinates are presented in Tables 4.12 and 4.13; the $\pi \rightarrow \pi^*$ transition moments are shown pictorially in Figure 4.44.

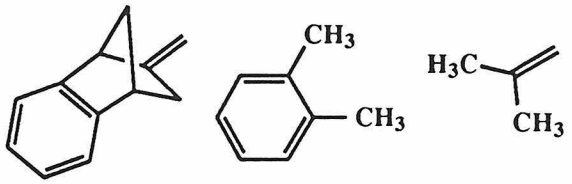

15 **16** **17**

Figure 4.42. (+)-2-Methylenebenzonorbornene (15) and its component chromophores (16 and 17).

Atom	*x*	*y*	*z*	Atom	*x*	*y*	*z*
C(1)	-1.390915	0.008896	-1.705215	H(13)	-0.310425	1.999329	1.253159
C(2)	-0.553894	0.138870	-0.599609	C(14)	0.286194	-0.135071	1.564804
C(3)	-0.865067	-0.489639	0.599518	H(15)	0.028625	-0.235474	2.635788
C(4)	-2.014893	-1.264496	0.720108	H(16)	0.958252	1.744720	-1.054886
C(5)	-2.861252	-1.399826	-0.384933	C(17)	1.941100	-0.067291	-0.159241
C(6)	-2.550171	-0.765427	-1.594086	H(18)	1.423981	1.794754	1.579514
H(7)	-1.143036	0.497833	-2.635773	C(19)	1.643906	-0.791489	1.153992
H(8)	-2.245193	-1.756348	1.653625	H(20)	1.555252	-1.886353	1.020538
H(9)	-3.756943	-1.999313	-0.306427	H(21)	2.436676	-0.605591	1.903305
H(10)	-3.206741	-0.876404	-2.445145	C(22)	2.988785	-0.263824	-0.962067
C(11)	0.768951	0.899155	-0.367111	H(23)	3.756943	-0.995071	-0.707855
C(12)	0.547028	1.309448	1.101028	H(24)	3.094650	0.302400	-1.888107

Table 4.11. Atomic coordinates of AM1[24] optimized 15, using the atom numbering scheme of Figure 4.43.

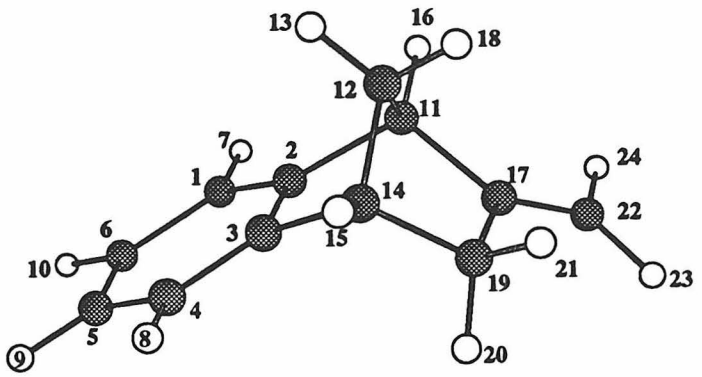

Figure 4.43. AM1[24] optimized 15 showing calculation numbering scheme.

Atom	x	y	z	Atom	x	y	z
Chromophore 16							
C(1)	0.72998	1.40503	-0.00394	H(10)	2.87580	1.25014	-0.00921
C(2)	-0.46482	0.68934	0.00028	C(11)	-1.94702	1.11953	0.00648
C(3)	-0.45595	-0.69978	0.00700	C(12)	-2.35570	1.09203	-1.02838
C(4)	0.74431	-1.40439	0.00512	H(13)	-2.54049	0.43110	0.64883
C(5)	1.94869	-0.69363	0.00149	C(14)	-1.93999	-1.12428	-0.00966
C(6)	1.94174	0.70682	-0.00339	H(15)	-2.04207	-2.15809	0.37008
H(7)	0.71735	2.48494	-0.01145	H(16)	-2.04094	2.14778	0.40364
H(8)	0.74224	-2.48437	0.00215	H	-2.53854	-0.44124	0.63367
H(9)	2.88837	-1.22728	-0.00124	H	-2.33728	-1.07889	-1.04833
Chromophore 17							
C(11)	0.83312	1.17329	-0.00137	H(21)	0.45209	-1.86096	-0.90134
H	1.69976	0.93439	0.65485	H(20)	0.47060	-1.86325	0.90028
H	1.20069	1.35046	-1.03683	C(22)	-1.50039	0.08297	-0.00154
H(16)	0.34599	2.09573	0.36696	H(23)	-2.10742	-0.82309	-0.00593
C(17)	-0.16786	0.01182	0.00831	H(24)	-2.00640	1.04906	-0.00719
C(19)	0.68240	-1.25876	-0.00206	H	1.76323	-0.99337	-0.01066

Table 4.12. Atomic coordinates of component chromophores of AM1[24] optimized 15 in their principle axis coordinate systems, using the atom numbering scheme of Figure 4.43.

				Transition Moment Vectors (atomic units)		
State	λ (nm)	Predominate Transition	f^a	R_x	R_y	R_z
Chromophore 16						
2	271.5	$\pi \rightarrow \pi^*$	0.00349	0.17649	-0.00131	0.00941
3	215.3	$\pi \rightarrow \pi^*$	0.00745	-0.01788	-0.22894	0.00792
4	209.3	$\pi \rightarrow \pi^*$	0.18557	-1.13061	-0.02212	-0.00188
5	199.7	$\pi \rightarrow \pi^*$	0.19819	0.04915	-1.14032	0.00865
6	189.7	$\sigma \rightarrow \pi^*$	0.49319	-0.22902	-1.74003	0.00569
7	188.7	$\pi \rightarrow \pi^*$	0.82651	2.25973	-0.16370	0.03559
Chromophore 17						
2	175	$\pi \rightarrow \pi^*$	0.57175	-1.81081	0.11784	0.01130

Table 4.13. INDO/S[14] calculated data for component chromophores of 15.
[a]Oscillator strength from transition dipole moments.

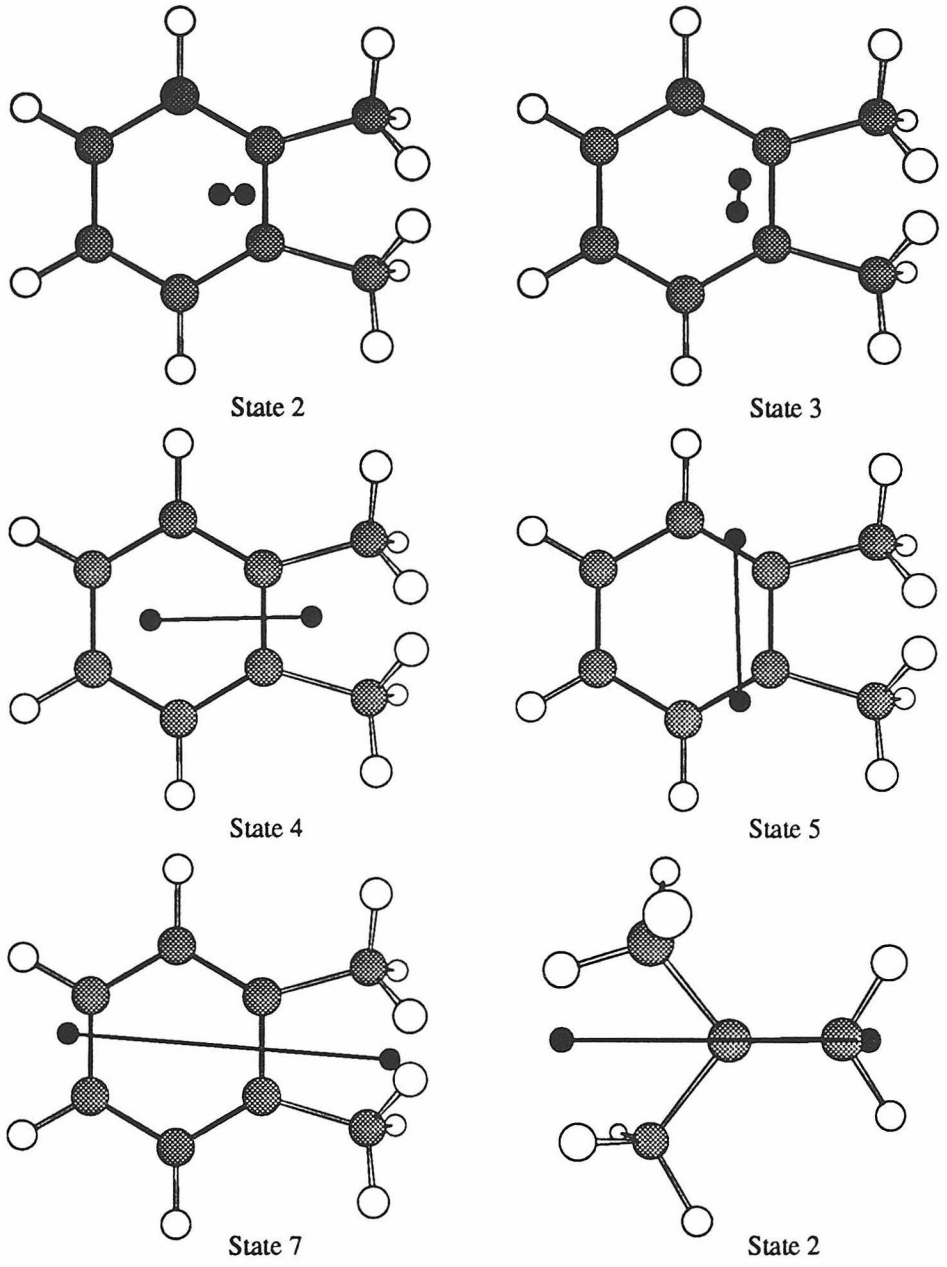

Figure 4.44. Component chromophores of AM1[24] optimized 15 and their π → π* transition moments.

The calculation results are compared with experiment in Table 4.14 and agree quite well with experimental observations[37] in terms of sign, but not in magnitude of R. Experimentally, two Cotton effects are observed at 265 nm ($R > 0$) and 224 nm ($R > 0$). Additionally, a third Cotton effect is detected through a fitting procedure and is thought to

be at about 207 nm with $R < 0$.[37] Computationally, we predict a Cotton effect at about 272 nm ($R > 0$), corresponding to the experimental 265 nm Cotton effect. A second Cotton effect is predicted at about 215 nm with $R < 0$, but this is not seen experimentally; however, the experimentally observed Cotton effect at 224 nm with $R > 0$ is calculated to occur at about 209 nm, a greater $|R|$ than the 215 nm transition. Experimentally, the larger R transition should hide the 215 nm Cotton effect. Additionally the Cotton effect expected at 207 nm with $R < 0$ is predicted computationally at about 200 nm. The results of a previously reported calculation[38] of CD in **15** that used the approach of coupling the benzene $\pi \rightarrow \pi^*$ transitions with each bond in the rest of the molecule are also reported in Table 4.14. This calculation predicts two Cotton effects at 275 nm ($R > 0$) and 220 nm ($R < 0$).[38] While these transitions are also predicted by our calculation (271 nm, 224 nm), they certainly do not represent the experimental observations without also predicting the large $R > 0$ transition below 220 nm.

While the data of Table 4.14 shows some discrepancy in the calculated magnitude of R with experiment, we see strong qualitative agreement with the sign of R, and our results explain the observed spectrum. A coupled-oscillator calculation using the more common bond as chromophore approach,[38] however, fails to rationalize the experimental CD spectrum of **15**. This example nicely illustrates the utility of our component chromophore approach to carrying out coupled-oscillator calculations.

Experiment[37]		Calculated[38] (Coupling of bond transitions with benzene ring)		Calculated in this work	
λ (nm)	R (cgs × 10^{-40})	λ (nm)	R (cgs × 10^{-40})	λ (nm)	R (cgs × 10^{-40})
265	small > 0	275	0.1	271.5	0.26
		220	-17.0	215.3	-7.0
224	43.5			209.3	30.6
207	-20.0			199.7	-7.1
				175.0	4.1

Table 4.14. Experimental and calculated CD spectral data for 15.

4.5.2 Guest Binding Orientations

Another important question that arises from these calculations concerns the choice of the $\theta = 0°$ orientation of the guest. The $\theta = 0°$ orientations employed within the calculations are based on ideal fits (supported by NMR data and CPK models) for the guest within the host cavity, but how valid are they and how would the calculated results differ with slight perturbations of these $\theta = 0°$ orientations? A series of calculations in which the $\theta = 0°$ orientations were systematically varied was undertaken in order to address these questions. These calculations and their implications are discussed in this section.

The first issue addressed was that of the guest transition moment not lying in the *xz*-plane. All the guests, except the quinoliniums **3-5**, were oriented such that their transition moments lie in the *xz*-plane. Quinoliniums **3-5** were placed so that the quinoline ring actually lies in the *xz*-plane. In order to address the effect of non-planarity, a "generic" transition moment (with a constant magnitude of 2.54×10^{-18} esu•cm at wavelengths from 350-700 nm)[39] was placed with the standard $\theta = 0°$ orientation (in *xz*-plane, aligned along *z*-axis, centered on origin). Then the transition moment was rotated in 10° increments counter-clockwise about the *x*-axis (this is done as in *y*-axis rotation calculations using the rotation matrix of equation 4.34), the results are shown in Figures 4.45 and 4.46.

$$\begin{vmatrix} 1 & 0 & 0 \\ 0 & \cos\theta & \sin\theta \\ 0 & -\sin\theta & \cos\theta \end{vmatrix} \times \begin{vmatrix} \mu_x \\ \mu_y \\ \mu_z \end{vmatrix} = \begin{vmatrix} \mu_{x+\theta} \\ \mu_{y+\theta} \\ \mu_{z+\theta} \end{vmatrix} = \begin{vmatrix} \mu_x \\ \mu_y \cos\theta - \mu_z \sin\theta \\ \mu_y \sin\theta + \mu_z \cos\theta \end{vmatrix} \qquad (4.34)$$

In Figures 4.45 and 4.46, the sign at $\theta = 0°$ represents the in plane transition moment as implied in our calculations. From the *R* vs θ curves, it can be seen that it requires an *x*-axis rotation of at least 20° to change the sign of *R*. Given the dimensions of the host cavity and the fit of the guest in the cavity (from CPK models), such a rotation of

the guest out of the *xz*-plane would require the guest actually leave the cavity, so such a perturbation shouldn't represent a bound-guest orientation.

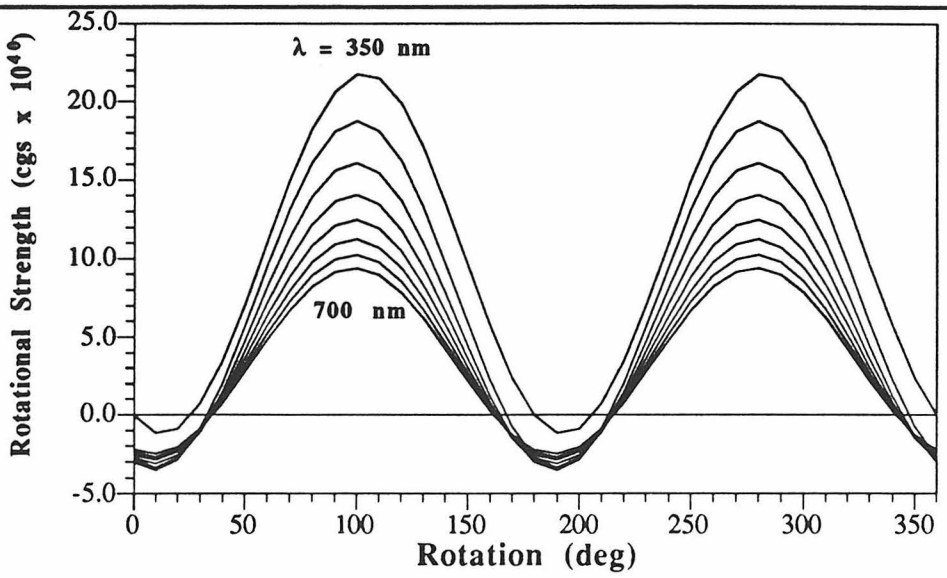

Figure 4.45. ICD expected from rotation of a transition moment about the *x*-axis for a guest bound by host P_S. ($|\mu| = 2.54 \times 10^{-18}$ esu·cm; f = 0.0867, 0.0759, 0.0675, 0.0607, 0.0552, 0.0506, 0.0467, and 0.0434 at λ = 350, 400, 450, 500, 550, 600, 650, and 700 nm).[39]

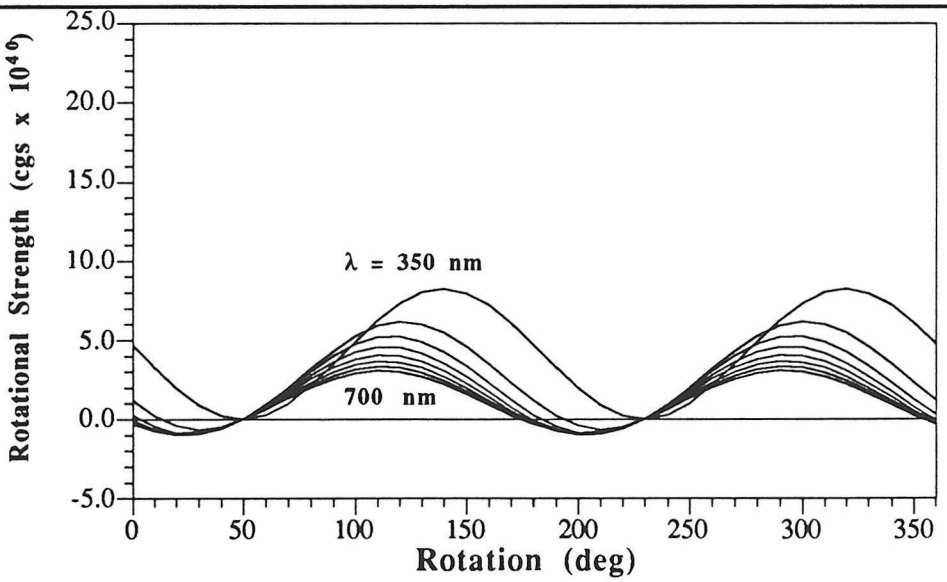

Figure 4.46. ICD expected from rotation of a transition moment about the *x*-axis for a guest bound by host C_S. ($|\mu| = 2.54 \times 10^{-18}$ esu·cm; f = 0.0867, 0.0759, 0.0675, 0.0607, 0.0552, 0.0506, 0.0467, and 0.0434 at λ = 350, 400, 450, 500, 550, 600, 650, and 700 nm).[39]

Following a similar protocol, the "generic" transition moment was placed in the *xz*-plane, centered at the origin, and aligned with the *x*-axis. This time the transition moment was rotated about the *z*-axis, and the results are shown in Figures 4.47 and 4.48; the rotation matrix is given in equation 4.35.

$$\begin{vmatrix} \cos\theta & -\sin\theta & 0 \\ \sin\theta & \cos\theta & 0 \\ 0 & 0 & 1 \end{vmatrix} \times \begin{vmatrix} \mu_x \\ \mu_y \\ \mu_z \end{vmatrix} = \begin{vmatrix} \mu_{x+\theta} \\ \mu_{y+\theta} \\ \mu_{z+\theta} \end{vmatrix} = \begin{vmatrix} \mu_x \cos\theta + \mu_y \sin\theta \\ -\mu_x \sin\theta + \mu_y \cos\theta \\ \mu_z \end{vmatrix} \qquad (4.35)$$

These *R* vs θ curves also show that an out of plane rotation of at least 20° is required to change the sign of the ICD. Since such an out-of-plane rotation precludes the guest from fitting into the rhomboid binding site, it appears that our choice of θ = 0° orientations are reasonable for the host-guest complexes of interest.

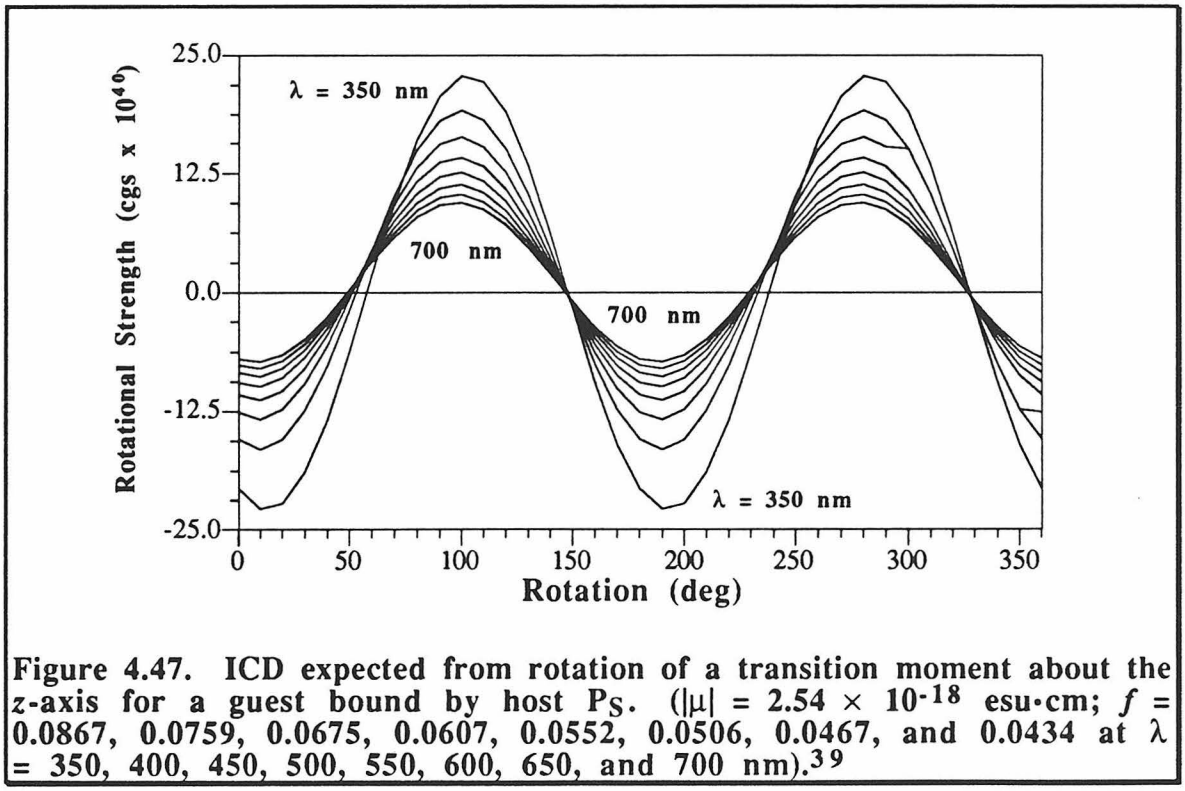

Figure 4.47. ICD expected from rotation of a transition moment about the *z*-axis for a guest bound by host P_S. ($|\mu| = 2.54 \times 10^{-18}$ esu·cm; f = 0.0867, 0.0759, 0.0675, 0.0607, 0.0552, 0.0506, 0.0467, and 0.0434 at λ = 350, 400, 450, 500, 550, 600, 650, and 700 nm).[39]

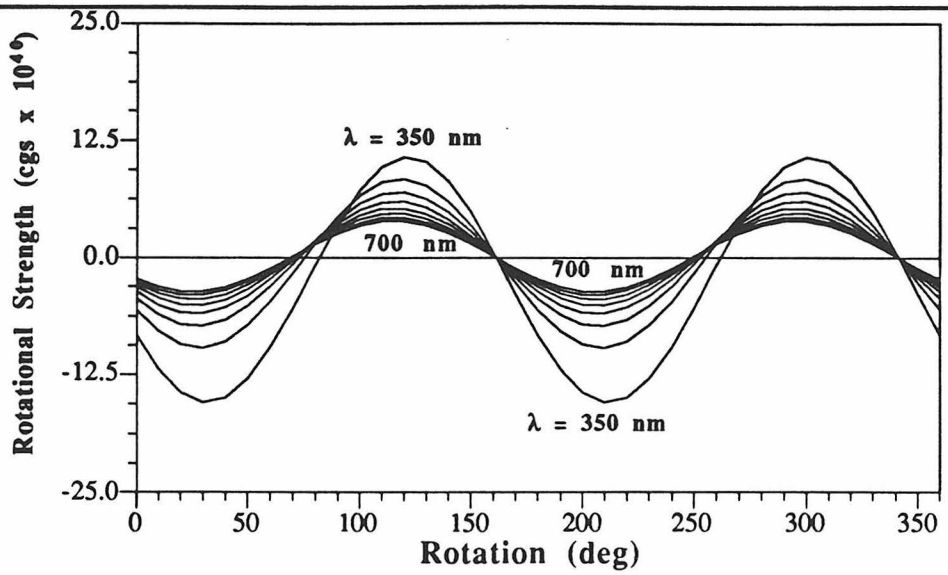

Figure 4.48. ICD expected from rotation of a transition moment about the *z*-axis for a guest bound by host C_S. ($|\mu|$ = 2.54 × 10^{-18} esu•cm; f = 0.0867, 0.0759, 0.0675, 0.0607, 0.0552, 0.0506, 0.0467, and 0.0434 at λ = 350, 400, 450, 500, 550, 600, 650, and 700 nm).[39]

With the exception of the quinolinium guests (**3**-**5**), all of the calculations were carried out with the transition moments centered at the origin. However, given the degrees of freedom of the system and the *xz*-plane dimensions of the binding site compared to the size of some guests, it seems likely that perturbations of these ideal binding conformations should occur. To examine the effects of in-plane translation of the θ = 0° orientation, a generic transition moment was studied (2.54 × 10^{-18} esu•cm at 350 nm with f = 0.0867). Translating the transition moment along either *x* or *z*-axes followed by *y*-axis rotation provided the *R* vs θ curves of Figures 4.49-4.52. Offsetting along the *y*-axis was not considered as the cavity dimensions prohibit any significant translation of a guest along this axis.

Figures 4.49 and 4.50 show the effect of translation on the *x*-axis, that is moving the transition moment from the cavity center towards the cavity walls. The host **P** calculation (Figure 4.49) suggests that only as the transition gets very close to the cavity walls (3 Å translation) is a change in the sign of the ICD observed (although differences in magnitude are predicted even for small offsets). Such an offset towards the cavity walls is

not expected to occur, as this puts the transition moment itself about 1.3 Å from the cavity wall (see Chapter 3 for cavity dimensions). This short distance should result in some of the atoms that make up the guest framework being at even closer distances to the atoms in the cavity walls; the close contact of these guest and host atoms should result in severe repulsions and thus suggests that such a binding orientation is unlikely. Similarly, for host **C** (Figure 4.50) the data suggest no significant effects on the sign of the ICD for x-axis offsets up to 3 Å.

Figures 4.51 and 4.52 show the effects of z-axis offsetting. This is essentially the moving of the guest transition moment away from the origin towards the outside of the cavity. As in the case of *x*-axis offsetting, host **P** is more affected than host **C** (Figure 4.51 vs Figure 4.52). However, only at larger displacements is the sign of the ICD significantly affected. This means that the guest is expected to be outside the cavity for a sign change to occur, and since this does not represent a bound conformation, such a θ = 0° orientation should not be considered for the ICD in a bound complex.

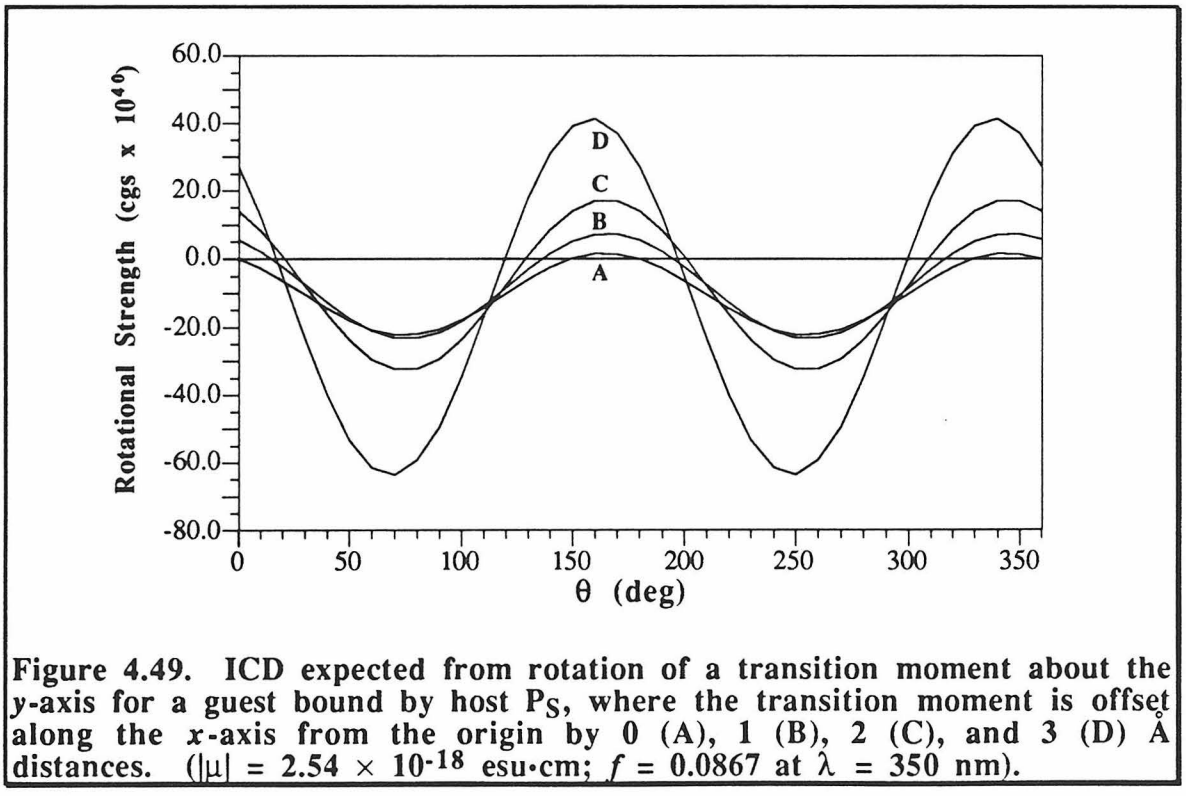

Figure 4.49. ICD expected from rotation of a transition moment about the *y*-axis for a guest bound by host P_S, where the transition moment is offset along the *x*-axis from the origin by 0 (A), 1 (B), 2 (C), and 3 (D) Å distances. ($|\mu| = 2.54 \times 10^{-18}$ esu·cm; $f = 0.0867$ at $\lambda = 350$ nm).

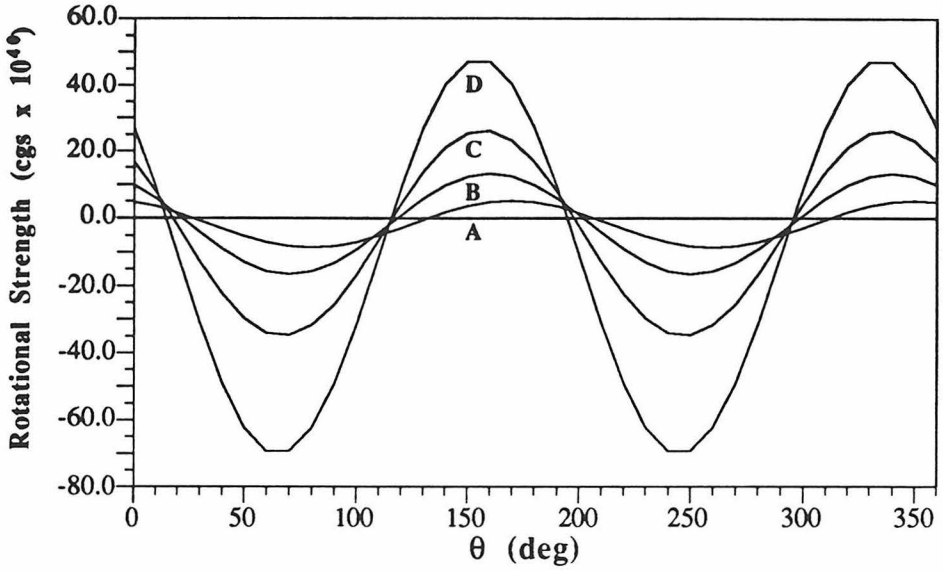

Figure 4.50. ICD expected from rotation of a transition moment about the *y*-axis for a guest bound by host C_S, where the transition moment is offset along the *x*-axis from the origin by 0 (A), 1 (B), 2 (C), and 3 (D) Å distances. ($|\mu| = 2.54 \times 10^{-18}$ esu·cm; $f = 0.0867$ at $\lambda = 350$ nm).

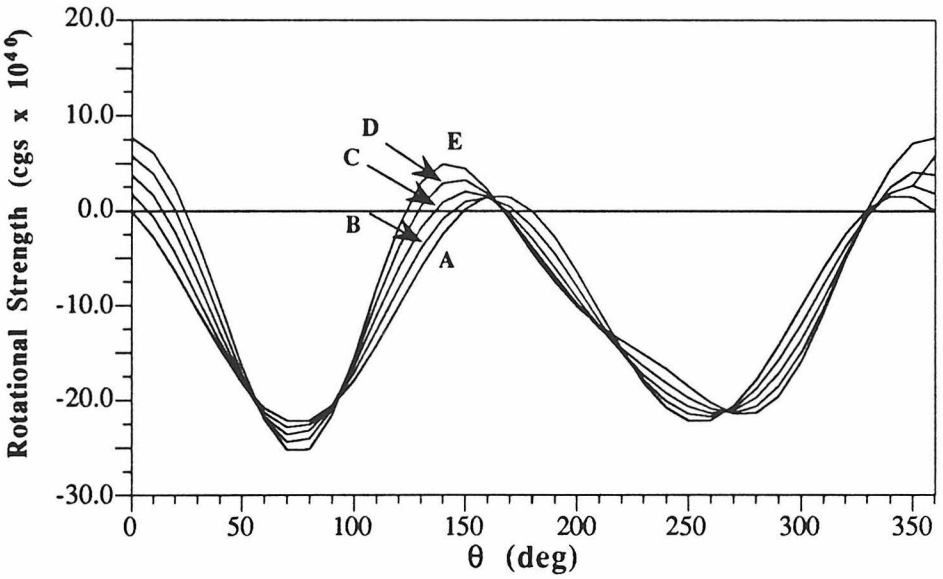

Figure 4.51. ICD expected from rotation of a transition moment about the *y*-axis for a guest bound by host P_S, where the transition moment is offset along the *x*-axis from the origin by 0 (A), 0.25 (B), 0.50 (C), 0.75 (D), and 1 (E) Å distances. ($|\mu| = 2.54 \times 10^{-18}$ esu·cm; $f = 0.0867$ at $\lambda = 350$ nm).

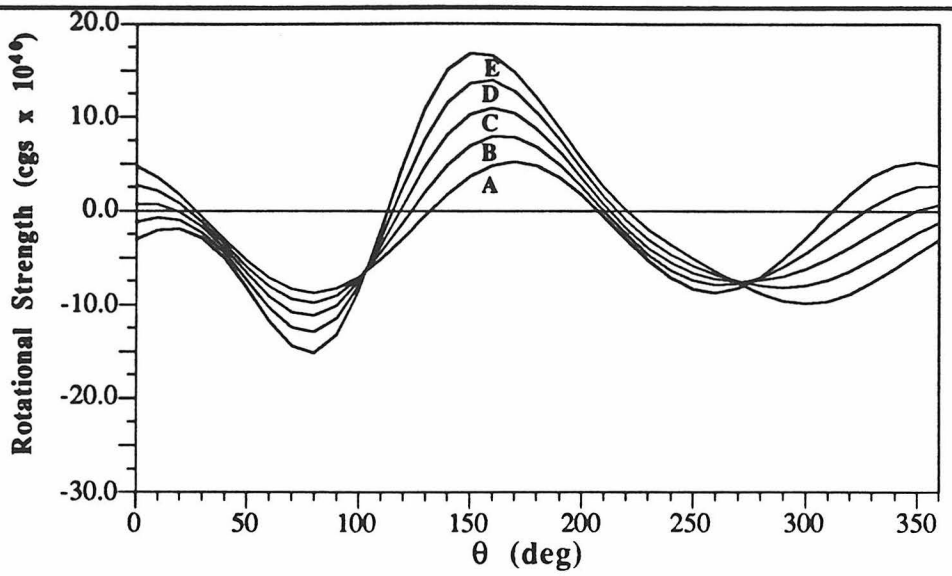

Figure 4.52. ICD expected from rotation of a transition moment about the *y*-axis for a guest bound by host C_S, where the transition moment is offset along the *x*-axis from the origin by 0 (A), 0.25 (B), 0.50 (C), 0.75 (D), and 1 (E) Å distances. ($|\mu| = 2.54 \times 10^{-18}$ esu·cm; $f = 0.0867$ at $\lambda = 350$ nm).

The factor that appears to have the most significant effect on the sign (and magnitude) of ICD is the wavelength of the guest transition, where longer wavelength absorptions are more likely to show $R < 0$ with (*S*, *S*, *S*, *S*)-host stereochemistry. This is seen with transition moments having constant magnitude across the 350-700 nm range (decreasing *f* with increasing λ,[39] Figures 4.53 and 4.54) and with transition moments having constant oscillator strength across the 350-700 nm region (increasing |μ| with increasing λ,[40] Figures 4.55 and 4.56). Given that longer wavelength transitions are required in order to observe ICD, Figures 4.53-4.56 predict that *x* and *z*-axis offsets for the transitions at longer wavelengths should show less propensity for a change in the sign of ICD than the short wavelength (350 nm) transition moment chosen to generate Figures 4.49-4.52. It is also worth noting, especially for Figures 4.49-4.52, that the increase in magnitudes of the ICD as a result of off-setting is due to a decrease in the distance between the guest transition moments and some of the host transition moments. In many cases the

higher magnitude portion of the ICD curve is the result of an orientation that places guest atoms at sub van der Waals radii distances from host atoms (impossible orientations).

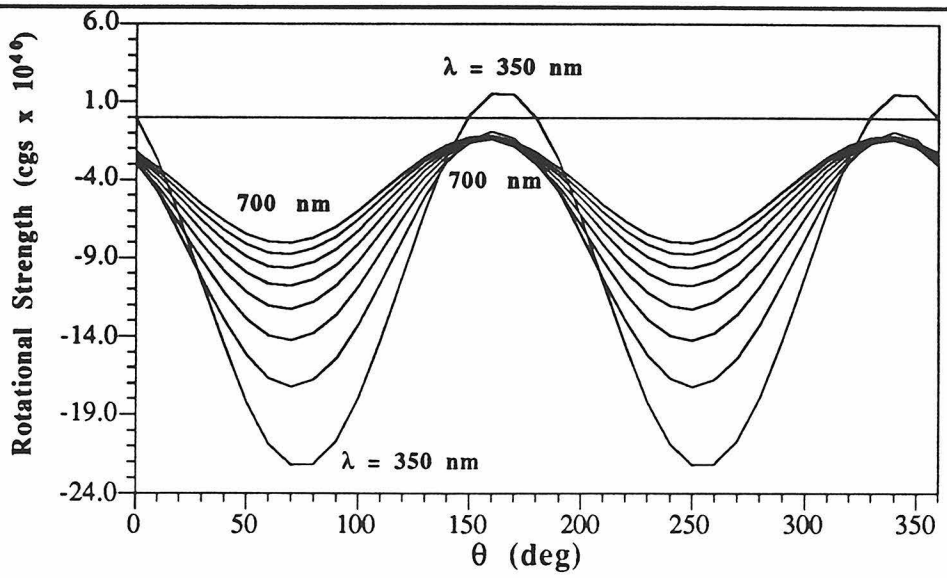

Figure 4.53. ICD expected from rotation of a transition moment about the *y*-axis for a guest bound by host P_S. ($|\mu| = 2.54 \times 10^{-18}$ esu·cm; f = 0.0867, 0.0759, 0.0675, 0.0607, 0.0552, 0.0506, 0.0467, and 0.0434 at λ = 350, 400, 450, 500, 550, 600, 650, and 700 nm).[39]

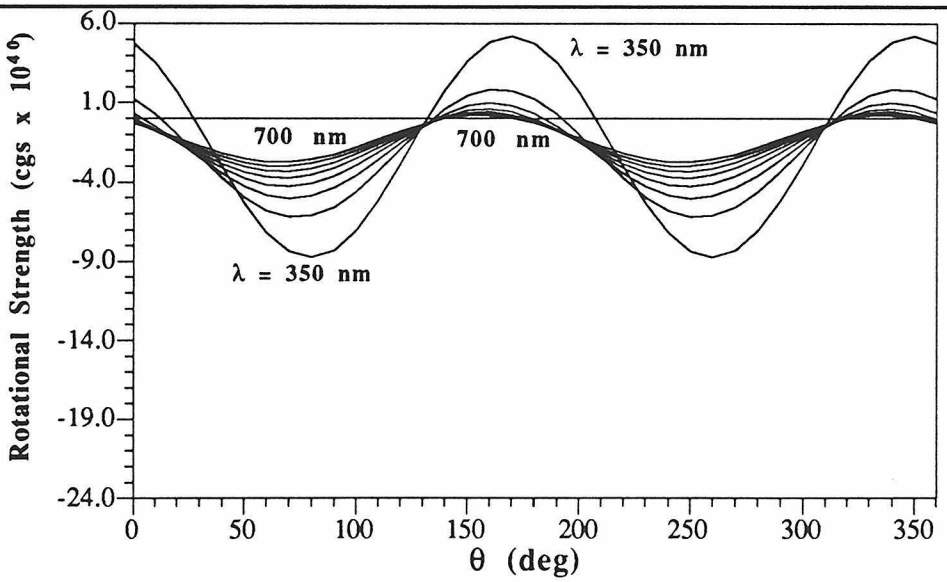

Figure 4.54. ICD expected from rotation of a transition moment about the *y*-axis for a guest bound by host C_S. ($|\mu| = 2.54 \times 10^{-18}$ esu·cm; f = 0.0867, 0.0759, 0.0675, 0.0607, 0.0552, 0.0506, 0.0467, and 0.0434 at λ = 350, 400, 450, 500, 550, 600, 650, and 700 nm).[39]

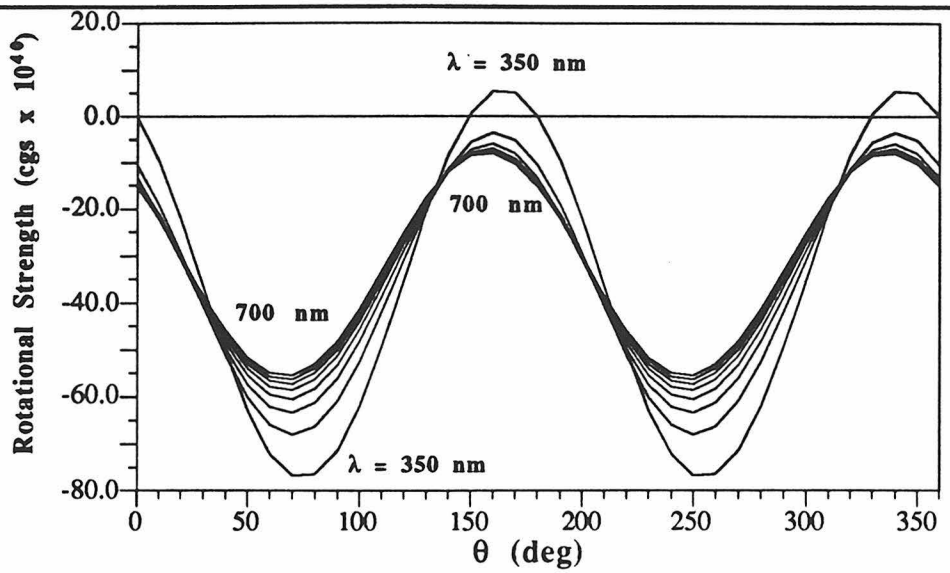

Figure 4.55. ICD expected from rotation of a transition moment about the *y*-axis for a guest bound by host P_S. (f = 0.30; $|\mu|$ = 4.731 × 10^{-18}, 5.058 × 10^{-18}, 5.364 × 10^{-18}, 5.655 × 10^{-18}, 5.931 × 10^{-18}, 6.194 × 10^{-18}, 6.447 × 10^{-18}, and 6.691 × 10^{-18} esu·cm at λ = 350, 400, 450, 500, 550, 600, 650, and 700 nm).[40]

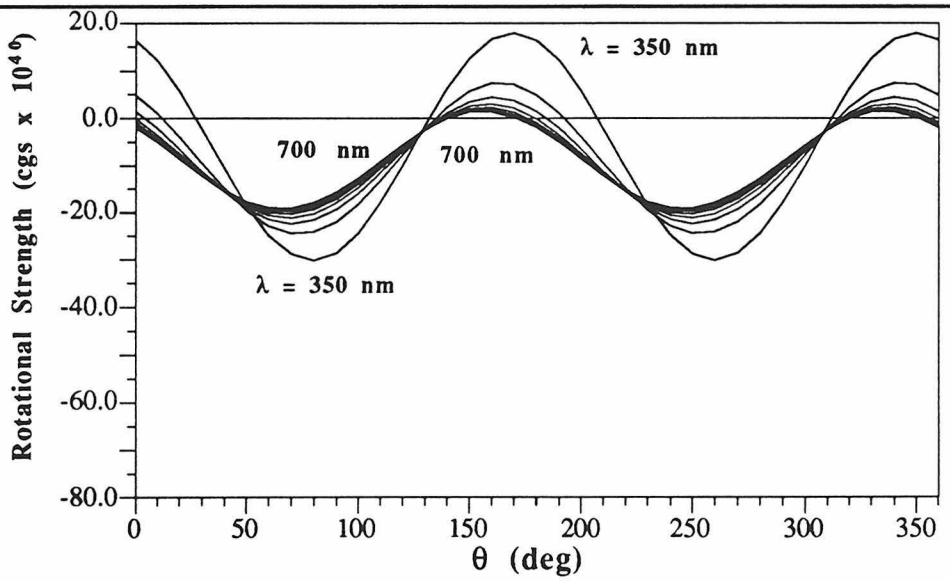

Figure 4.56. ICD expected from rotation of a transition moment about the *y*-axis for a guest bound by host C_S. (f = 0.30; $|\mu|$ = 4.731 × 10^{-18}, 5.058 × 10^{-18}, 5.364 × 10^{-18}, 5.655 × 10^{-18}, 5.931 × 10^{-18}, 6.194 × 10^{-18}, 6.447 × 10^{-18}, and 6.691 × 10^{-18} esu·cm at λ = 350, 400, 450, 500, 550, 600, 650, and 700 nm).[40]

Surprisingly, increasing the oscillator strength for a given transition (Figures 4.57 and 4.58) only serves to increase the magnitude of the observed ICD in regions where $R \neq$

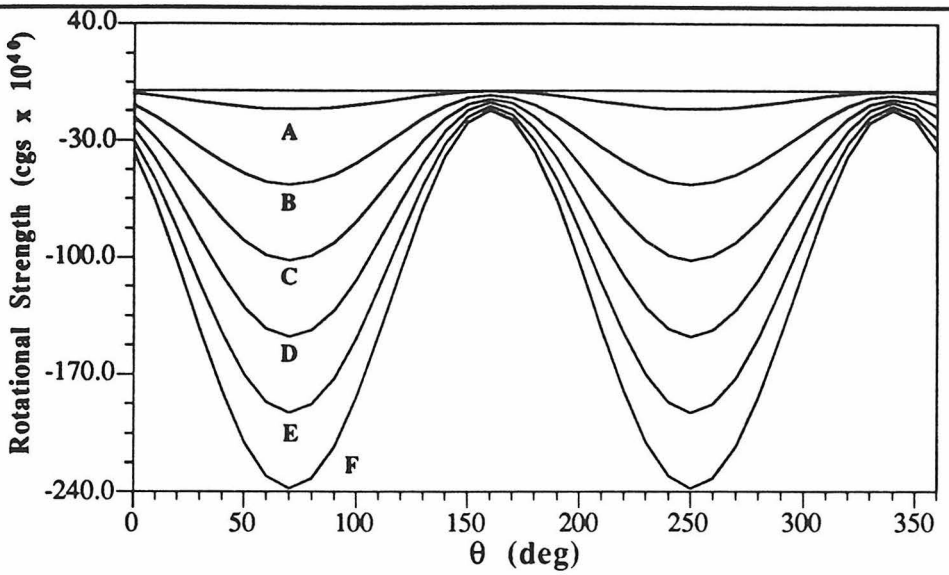

Figure 4.57. ICD expected from rotation of a transition moment about the *y*-axis for a guest bound by host P_S. [*f* = 0.05 (A), 0.25 (B), 0.45 (C), 0.65 (D), 0.85 (E), and 1.05 (F) with $|\mu|$ = 2.065 × 10^{-18}, 4.617 × 10^{-18}, 6.194 × 10^{-18}, 7.445 × 10^{-18}, 8.513 × 10^{-18}, and 9.462 × 10^{-18} esu·cm at λ = 400].[40]

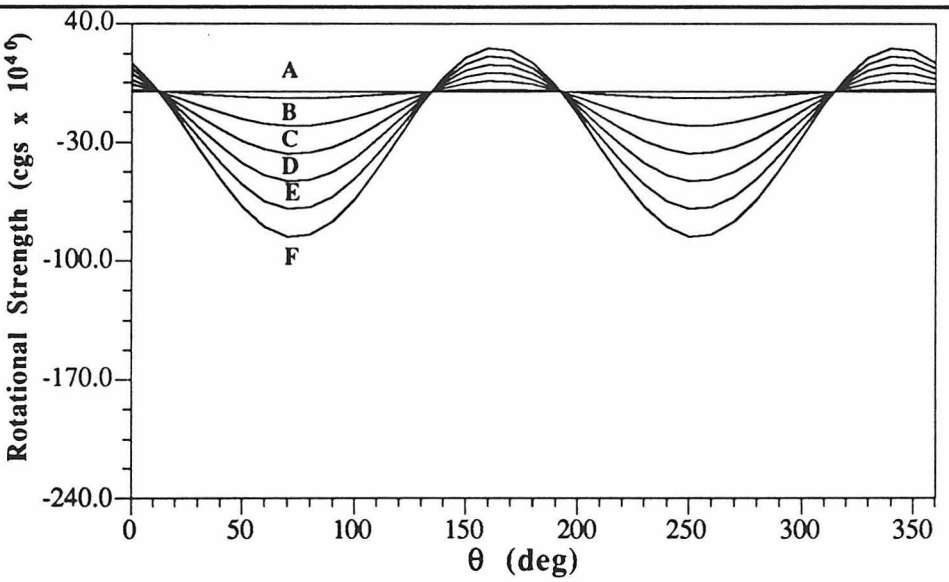

Figure 4.58. ICD expected from rotation of a transition moment about the *y*-axis for a guest bound by host C_S. [*f* = 0.05 (A), 0.25 (B), 0.45 (C), 0.65 (D), 0.85 (E), and 1.05 (F) with $|\mu|$ = 2.065 × 10^{-18}, 4.617 × 10^{-18}, 6.194 × 10^{-18}, 7.445 × 10^{-18}, 8.513 × 10^{-18}, and 9.462 × 10^{-18} esu·cm at λ = 400].[40]

0. However, as shown in Figures 4.57 and 4.58, the value of θ where $R = 0$ remains constant. Given this data and the data of Figures 4.55 and 4.56, it appears that oscillator

strength has only a small effect on the sign of the observed ICD with our host-guest system.

The control calculations described here suggest that only the more extreme cases of perturbation from the ideally chosen $\theta = 0°$ orientation of a bound guest should produce different results than what we have based our bound orientations on in Section 4.4. The extent of these deviations are furthermore likely to decrease as the guest transition moves to longer wavelength. For these reasons we believe that our choice of in-plane and origin centered $\theta = 0°$ orientations are valid and produce results that qualitatively agree with experimental observations.

4.6 Conclusions

Using INDO/S transition moments[14] combined with appropriately optimized geometries, a series of coupled-oscillator calculations[12,13] were carried out. These calculations were used to analyze experimental induced circular dichroism (ICD) spectra and to infer bound guest orientations in cyclophane hosts **P** and **C**. In general, the calculations suggest that the guests fit in the host cavity in such a way as to maximize both cation-π and hydrophobic interactions.

The ICD observed in achiral guests with hosts **P** and **C** complements *D* values obtained from NMR experiments for providing information on the bound guest orientation. In addition, the ICD analysis can provide information too subtle to be picked up from the NMR experiment, as seen with dyes **9**, **10**, and **11** (see Figure 4.17).

Control calculations have shown the applicability of our coupled-oscillator calculation method to qualitative interpretation of CD spectra and suggest that our approach is more realistic than that of previous studies where actual bonds are treated as chromophore groups. In addition, control calculations in which guest orientations are slightly perturbed in a number of ways suggest that the types of deviations expected in the

actual host-guest geometry from the ideal orientations used in our calculations should not affect our results and conclusions.

The method developed here for analysis of ICD data, while specific to hosts **P** and **C**, is easily applicable to other host-guest systems with strong $\pi \rightarrow \pi^*$ absorptions. Calculations are easily carried out provided that transition moments and optimized geometries are available for the host and guest and their component chromophores. Applications to other hosts derived from host **P** have already been undertaken in the Dougherty labs.[41]

4.7 Experimental Section

4.7.1 General Methods[1,2]

Circular dichroism binding studies (from which quantitative values of $\Delta\varepsilon$ and R were obtained) are described in Chapter 2 of this manuscript. Qualitative detection of induced CD was done using excess concentrations of the appropriate host and/or control molecule with the guest of interest. For these studies the standard measurement parameters were often varied to provide conditions with the highest sensitivity. All solvents used in spectroscopy were spectrophotometric or HPLC grade. Aqueous cesium borate buffer (pH 9) was prepared by dissolving 0.25 g high purity boric oxide in 800 g water and adding 3.74 ml of 1 M CsOH followed by thorough mixing. The water used in these preparations was passed through a Milli-Q purification system. Assessment of purity of samples of **3** and **4** was done from the corresponding esters using the method described in Chapter 2.

Compounds **3**, **4**, **5**, **P**, and **C** were prepared by procedures described previously.[1,2] The synthesis of control molecules **1** and **2** is described in Chapter 2.[2] All other compounds were obtained commercially, except guest **7** which was synthesized according to published procedure.[42]

4.7.2 Experimental Measurement of *R*

Quantitative rotational strengths (R) can be obtained from experimental CD spectra (plotted as $\Delta\varepsilon$ vs ν) in cgs units using equation 4.36[15]

$$R = \frac{2.296 \times 10^{-39}}{\nu_0} \int_{\nu_i}^{\nu_f} \Delta\varepsilon(\nu) d\nu \qquad (4.36)$$

where the value of the integral of $\Delta\varepsilon(\nu)$ is obtained from the area under the curve of the Cotton effect; ν_0 is the wavenumber of the extremum of the Cotton effect (in cm^{-1}); and ν_i and ν_f are the beginning and ending wavenumbers (cm^{-1}), respectively, of the Cotton effect.[15]

4.7.3 Computational Studies[2]

Coupled-oscillator calculations were set up and executed (as described in Section 4.3 and 4.5) using Excel.[27] Geometry optimizations with AM1 were done in InsightII.[43] Semi-empirical calculations of spectroscopic observables were set up and executed using the DZDO program[44] using the Zerner parameter set for an INDO/S model Hamiltonian with the SCF calculations using the closed shell RHF method (the Hamiltonian was an INDO/2 with /S). CI was limited to singly excited states and considered transitions from the ten highest occupied to the ten lowest unoccupied orbitals for all chromophores except the ethenoanthracenes. For the ethenoanthracenes, transitions from the 14 highest occupied to the 14 lowest unoccupied orbitals were considered. A complete description of the DZDO input commands employed for the calculations and the use of the program is given in Appendix 4 (Section 4.11).

4.8 Appendix 1: Host Coordinates in Calculation Coordinate System

Atom	*x*	*y*	*z*	Atom	*x*	*y*	*z*
O(1)	-6.396836	-5.090683	-3.579025	H(51)	2.508117	-3.775925	2.858124
O(2)	-5.406434	-3.347122	-4.483841	C(52)	5.962310	-3.525391	-0.247879
H(3)	-5.011582	-4.009201	-5.166931	C(53)	2.393905	3.465485	-0.467728
O(4)	-8.073594	-4.759186	-0.008591	H(54)	1.873321	3.512528	-1.424133
O(5)	-8.539887	-3.947403	-2.041718	C(55)	1.708038	3.733780	0.719635
H(6)	-8.924027	-4.851486	-2.351395	C(56)	2.366150	3.741119	1.904343
O(7)	-0.398316	-4.036133	0.113678	H(57)	1.831466	4.008225	2.815857
O(8)	6.424118	-2.262405	0.282410	C(58)	3.710266	3.413284	1.970444
O(9)	5.247283	5.359436	-2.906754	H(59)	4.237365	3.428055	2.924347
O(10)	7.150543	4.456680	-3.226975	C(60)	6.144485	0.043655	0.463791
H(11)	7.233596	3.483612	-3.554245	H(61)	6.668670	-0.012482	1.417831
O(12)	8.159927	5.165314	-0.559937	C(62)	5.900543	-1.111786	-0.297104
O(13)	7.978912	4.129822	1.356964	C(63)	5.263565	-1.047409	-1.496353
H(14)	8.026123	3.122391	1.565811	H(64)	5.094696	-1.951996	-2.080567
O(15)	0.358108	3.973145	0.581573	C(65)	4.830429	0.185639	-1.968247
O(16)	-6.532029	2.156754	0.682403	H(66)	4.311065	0.238648	-2.925049
C(17)	-2.357407	-3.321045	-0.898346	C(67)	5.801330	2.594269	0.685882
H(18)	-1.793000	-3.205566	-1.823548	C(68)	4.600050	2.749985	-1.575348
C(19)	-1.742539	-3.781174	0.239059	C(69)	5.845993	3.643021	-1.460571
C(20)	-2.471955	-3.922455	1.427444	C(70)	6.467300	3.539719	-0.300141
H(21)	-1.980576	-4.265320	2.337936	C(71)	3.713058	3.145798	-0.423279
C(22)	-3.820650	-3.622238	1.432144	C(72)	4.371750	3.067444	0.809112
H(23)	-4.396546	-3.739838	2.350082	C(73)	5.703201	1.243820	-0.030090
C(24)	-6.268250	-0.140793	0.410094	C(74)	5.043136	1.338181	-1.254028
H(25)	-6.867402	-0.274109	1.310821	C(75)	6.133941	4.580231	-2.578995
C(26)	-5.979889	1.134827	-0.078232	C(76)	7.642181	4.298920	0.119888
C(27)	-5.212632	1.318375	-1.215958	C(77)	-0.416474	3.984406	1.763260
H(28)	-4.986100	2.320969	-1.578659	C(78)	-1.867524	3.868530	1.441818
C(29)	-4.735840	0.193665	-1.887985	C(79)	-2.400071	4.570618	0.380371
H(30)	-4.132660	0.322907	-2.786621	H(80)	-1.756989	5.222809	-0.210663
C(31)	-5.884232	-2.685516	0.110351	C(81)	-3.754380	4.455689	0.053650
C(32)	-4.492966	-2.398834	-2.012222	H(82)	-4.170594	5.014496	-0.784485
C(33)	-5.709595	-3.297516	-2.172989	C(83)	-4.560227	3.620087	0.811767
C(34)	-6.465821	-3.420517	-1.099121	C(84)	-4.019577	2.946625	1.873840
C(35)	-3.686188	-3.010131	-0.854599	H(85)	-4.658005	2.321823	2.498474
C(36)	-4.439118	-3.179703	0.297775	C(86)	-2.673020	3.051254	2.161484
C(37)	-5.773362	-1.227692	-0.279877	H(87)	-2.251893	2.467331	2.979919
C(38)	-5.011475	-1.070221	-1.439575	C(88)	-6.014650	3.497330	0.468963
C(39)	-5.924790	-4.019516	-3.464020	H(89)	-6.414216	-2.818741	0.890716
C(40)	-7.757569	-4.136307	-0.991638	H(90)	-4.002457	-2.301407	-2.827423
C(41)	0.396377	-4.200531	1.272796	H(91)	0.201965	-5.042511	1.676926
C(42)	1.842330	-4.146438	0.882522	H(92)	0.203857	-3.506561	1.894134
C(43)	2.258941	-4.305131	-0.418762	H(93)	6.018295	-3.509659	-1.195999
H(44)	1.527023	-4.566482	-1.182861	H(94)	6.511962	-4.226013	0.088455
C(45)	3.598968	-4.139221	-0.785980	H(95)	6.259796	2.564377	1.519440
H(46)	3.902801	-4.290405	-1.821747	H(96)	4.172317	2.822296	-2.427124
C(47)	4.533035	-3.785431	0.159927	H(97)	-0.154831	3.260544	2.321823
C(48)	4.141586	-3.700287	1.458679	H(98)	-0.262558	4.804504	2.229950
H(49)	4.881500	-3.498581	2.233185	H(99)	-6.137650	3.732254	-0.443436
C(50)	2.797470	-3.869156	1.811355	H(100)	-6.508698	4.106232	1.015259

Table 4.15. Host coordinates in calculation coordinate system (Å) using atom numbering scheme of Figure 4.9.

State	μ_{1x}	μ_{1y}	μ_{1z}	μ_{2x}	μ_{2y}	μ_{2z}
Ethenoanthracene 1						
4	5.536940	2.556975	-0.303320	4.398392	2.396499	-0.336934
5	4.696623	3.304482	0.299484	5.238710	1.648963	-0.939797
6	4.842162	2.263661	-0.195163	5.093170	2.689804	-0.445109
7	4.695861	2.246337	-0.221276	5.239471	2.707132	-0.418989
8	4.898458	2.383353	-0.330348	5.036874	2.570112	-0.309925
9	5.792689	2.318752	-0.220137	4.142643	2.634726	-0.420110
10	6.015937	1.758118	0.054696	3.919395	3.195331	-0.695000
11	4.002766	1.967365	-0.899874	5.932541	2.986097	0.259490
12	5.577878	2.355309	-0.778547	4.357454	2.598166	0.138295
13	3.902837	4.145899	0.161190	6.032495	0.807547	-0.801501
14	5.068209	2.447667	-0.356788	4.867123	2.505799	-0.283484
15	5.146205	1.957582	-0.407003	4.789127	2.995884	-0.233269
16	5.278032	2.854196	-0.263224	4.657300	2.099271	-0.377046
17	5.669792	2.738812	-0.855130	4.265540	2.214669	0.214888
18	5.971698	1.783770	-0.715389	3.963633	3.169731	0.075188
19	4.941026	2.046470	-0.137274	4.994306	2.906992	-0.503005
20	4.843253	1.774887	-0.752654	5.092080	3.178557	0.112340
21	4.749370	2.642025	-0.448399	5.185962	2.311437	-0.191879
24	4.634860	1.335088	-0.891848	5.300425	3.618366	0.251525
25	4.856820	2.794267	0.729792	5.078513	2.159156	-1.370150
26	5.572225	1.844260	-0.564892	4.363106	3.109218	-0.075354
27	3.981309	2.739343	-1.125039	5.954026	2.214031	0.484583
29	4.486001	1.125570	0.510436	5.449332	3.827868	-1.150765
30	5.473298	2.437304	0.398271	4.462036	2.516094	-1.038677
Ethenoanthracene 2						
4	-4.767160	-2.535743	-1.056866	-5.181840	-2.142562	-0.543484
5	-4.666560	-3.135788	-0.294837	-5.282434	-1.542428	-1.305629
6	-5.227956	-2.467473	-1.030733	-4.721045	-2.210831	-0.569620
7	-4.817539	-2.219030	-0.698997	-5.131461	-2.459275	-0.901354
8	-4.836634	-2.157923	-0.674359	-5.112367	-2.520380	-0.925994
9	-5.643229	-2.105376	-0.406678	-4.305768	-2.572890	-1.193723
10	-4.061963	-2.653125	-1.944588	-5.887024	-2.024973	0.343969
11	-4.902765	-1.054575	-0.556945	-5.046226	-3.623595	-1.043580
12	-6.601022	-0.856056	-1.315538	-3.347964	-3.822036	-0.285089
13	-5.302099	-2.067582	-0.795812	-4.646902	-2.610729	-0.804530
14	-4.637932	-3.121443	-1.216737	-5.311069	-1.556871	-0.383603
15	-5.270609	-2.353186	-0.839602	-4.678391	-2.325116	-0.760752
16	-4.517331	-1.838677	-0.652754	-5.431664	-2.839558	-0.947687
17	-5.727779	-1.646004	-1.066403	-4.221222	-3.032302	-0.533946
18	-4.726744	-2.085257	-0.738744	-5.222255	-2.593030	-0.861630
19	-4.945335	-2.200469	-1.101667	-5.003664	-2.477816	-0.498709
23	-5.577256	-3.313329	-0.651219	-4.371727	-1.364718	-0.949466
24	-5.397118	-1.222904	-1.413219	-4.551890	-3.455507	-0.186994
25	-4.917821	-2.448237	-2.005243	-5.031172	-2.229962	0.404756
26	-4.439812	-1.527747	0.013968	-5.509184	-3.150495	-1.614400
27	-3.771198	-2.462860	-2.140834	-6.177796	-2.215345	0.540353
29	-4.919714	-2.476641	-0.840348	-5.029287	-2.201667	-0.759998
30	-5.846656	-1.930744	0.122264	-4.102337	-2.747443	-1.722767

Table 4.16. Host ethenoanthracene chromophore $\pi \rightarrow \pi^*$ transition moment coordinates in calculation coordinate system (Å).

State	μ_{1x}	μ_{1y}	μ_{1z}	μ_{2x}	μ_{2y}	μ_{2z}
Linker 1						
2	-2.863665	3.598406	0.671322	-3.111431	3.160689	1.092545
3	-2.436054	3.353772	1.175204	-3.539064	3.405405	0.588726
4	-5.527383	3.084248	0.359230	-0.448206	3.676667	1.406042
5	-3.215936	1.886330	2.647355	-2.759139	4.872690	-0.883546
Linker 2						
2	3.056555	-3.466185	0.599505	2.839620	-3.587949	0.114146
3	2.673770	-3.616811	0.431171	3.222408	-3.437341	0.282482
4	0.410286	-3.937823	0.762064	5.486143	-3.117956	-0.048228
5	3.137892	-3.153452	2.623769	2.758162	-3.899898	-1.910205

Table 4.17. Host linker chromophore $\pi \rightarrow \pi^*$ transition moment coordinates in calculation coordinate system (Å).

4.9 Appendix 2: Transition Moments of Host Chromophores

4.9.1 $\pi \rightarrow \pi^*$ Transition Moments for Ethenoanthracene Chromophore 1.

The following views are looking at the anthracene ring from the face opposite the bridge. Hydrogen atoms have been omitted for clarity.

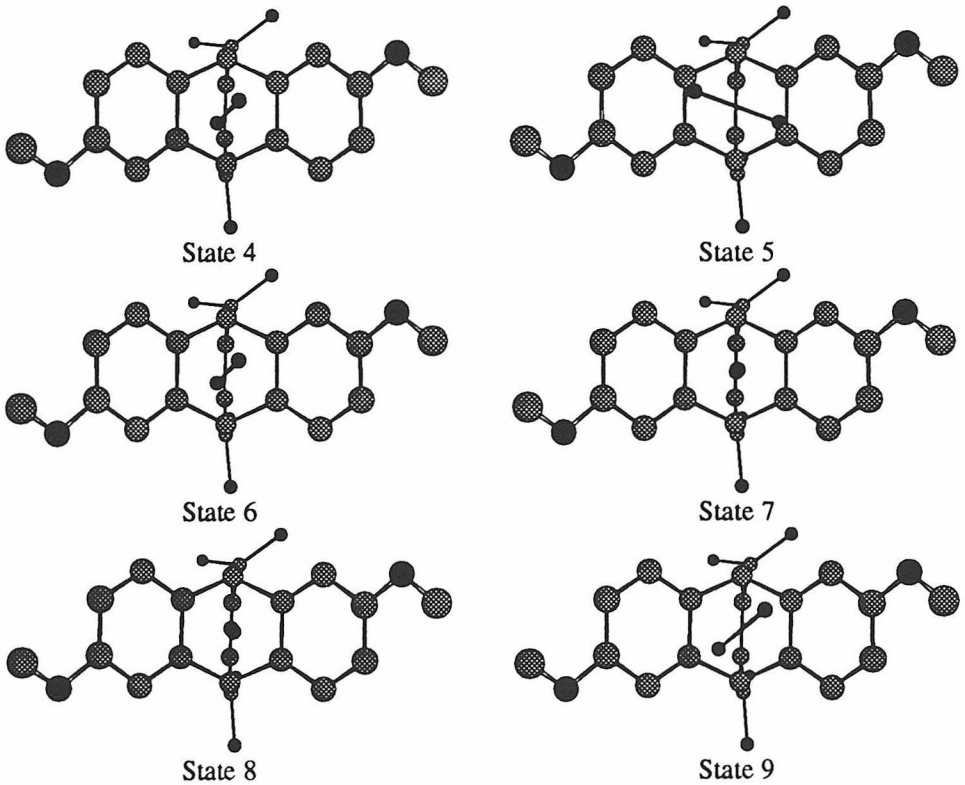

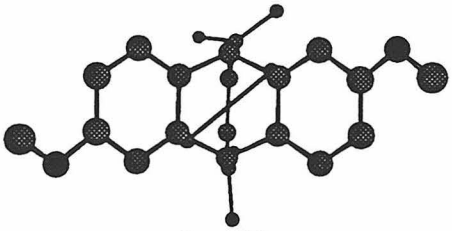

State 10

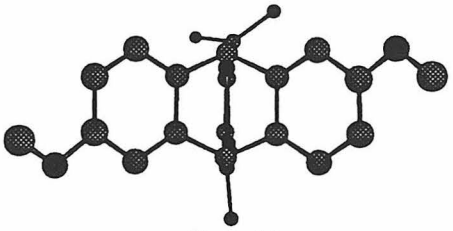

State 11

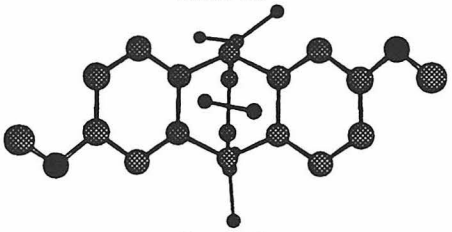

State 12

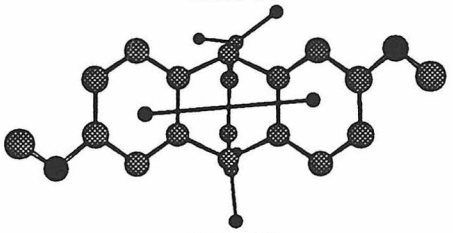

State 13

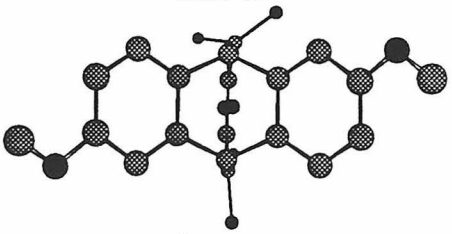

State 14

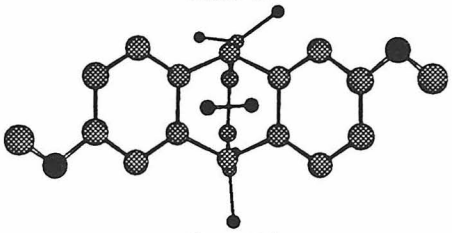

State 15

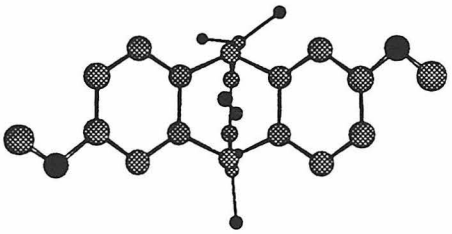

State 16

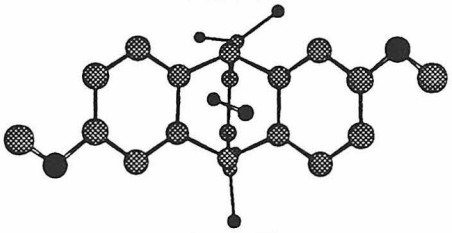

State 17

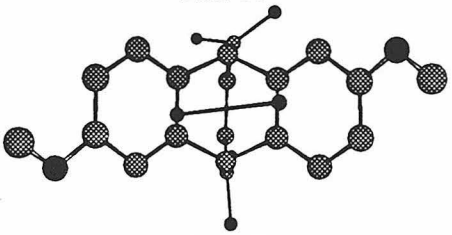

State 18

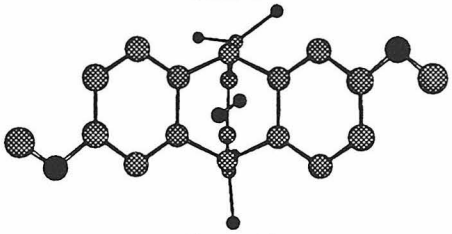

State 19

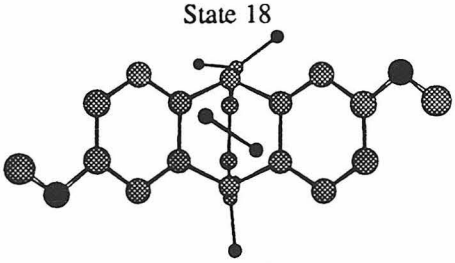

State 20

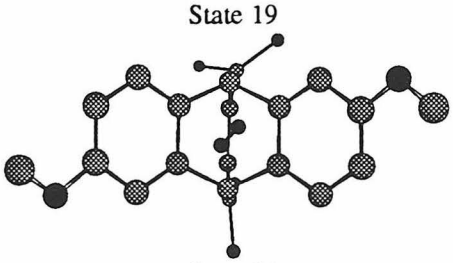

State 21

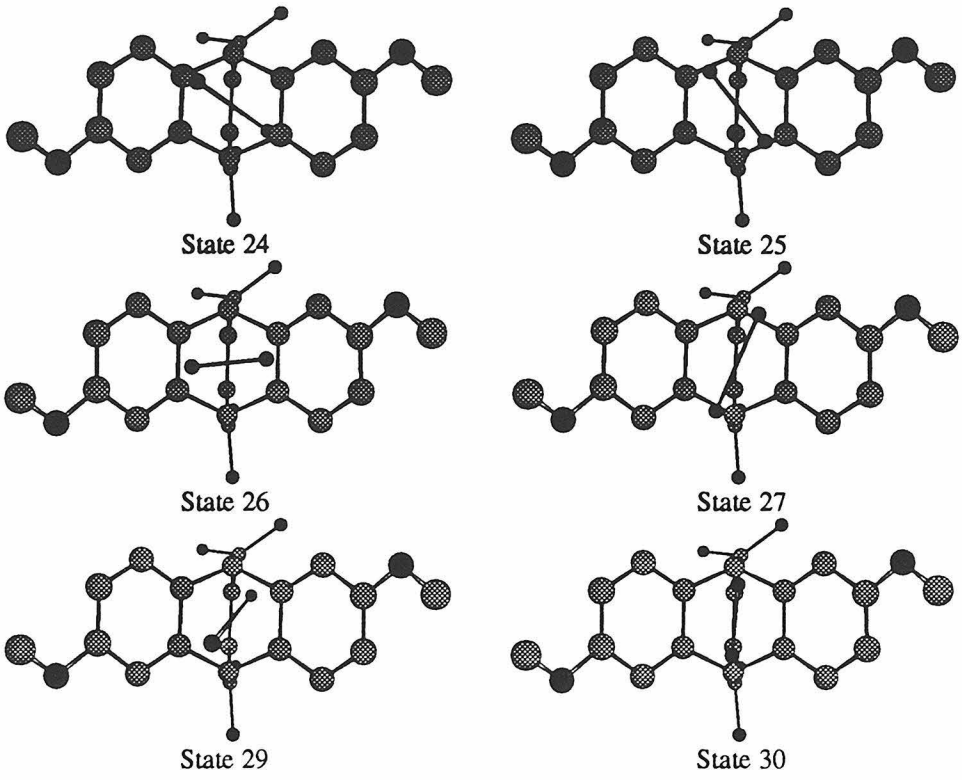

4.9.2 $\pi \rightarrow \pi^*$ Transition Moments for Ethenoanthracene Chromophore 2.

The following views are looking at the anthracene ring from the face opposite the bridge. Hydrogen atoms have been omitted for clarity.

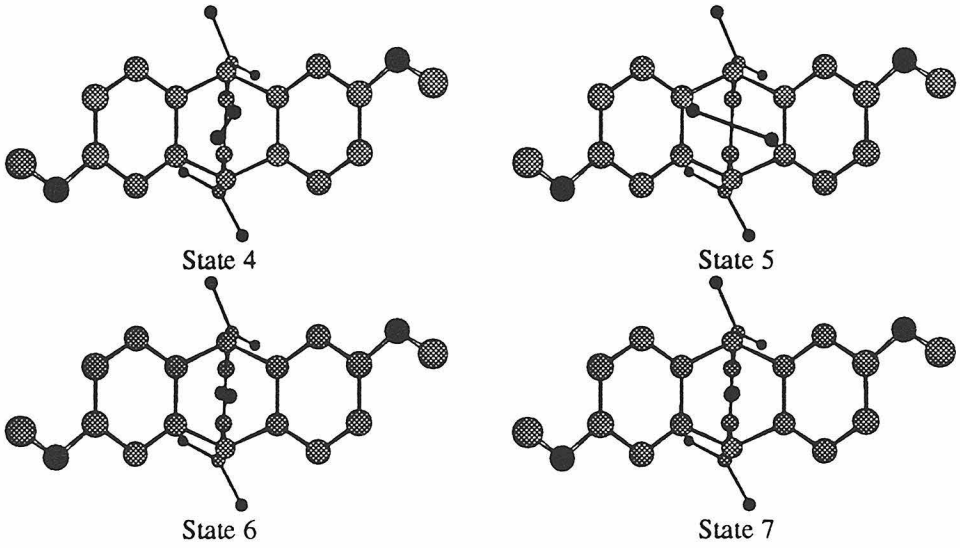

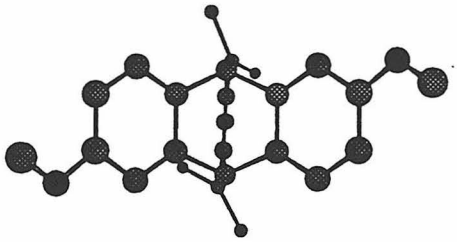

State 8

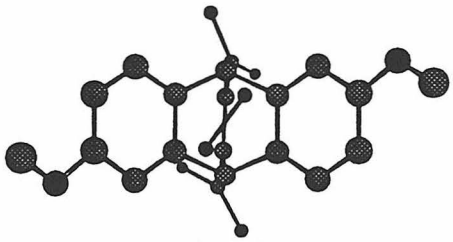

State 9

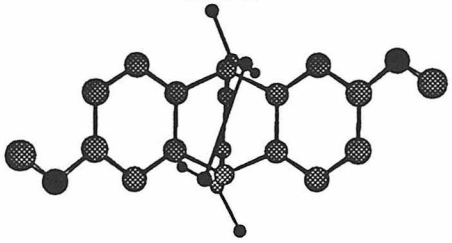

State 10

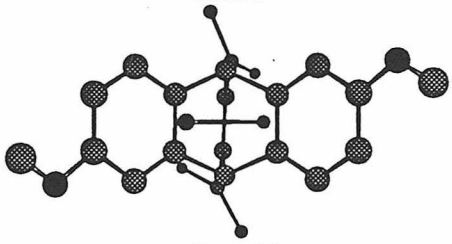

State 11

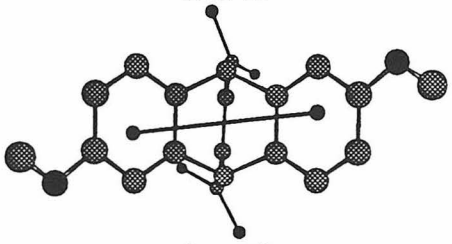

State 12

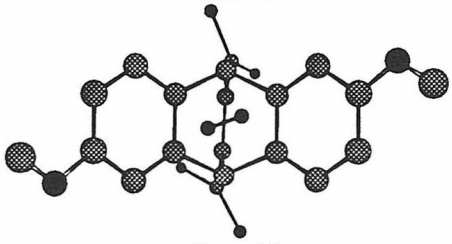

State 13

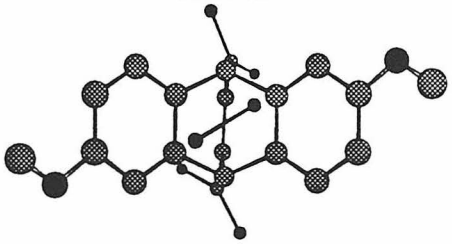

State 14

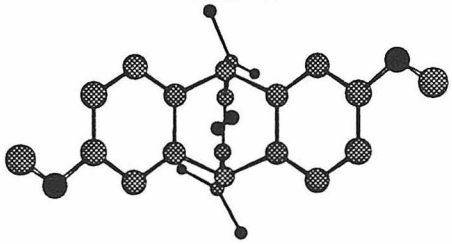

State 15

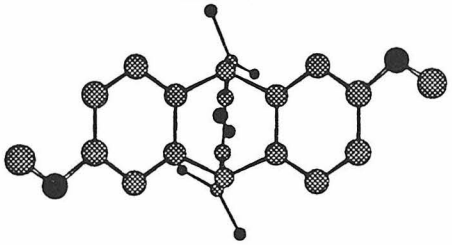

State 16

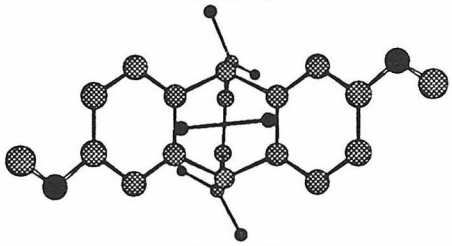

State 17

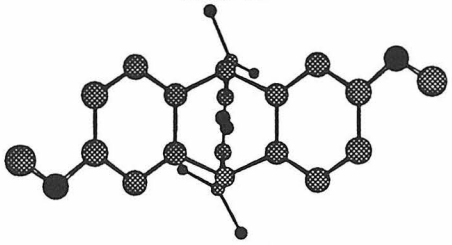

State 18

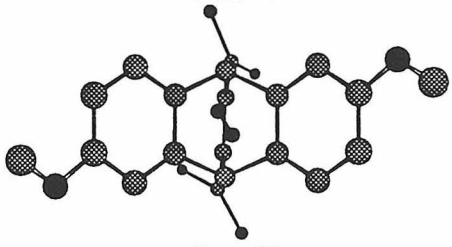

State 19

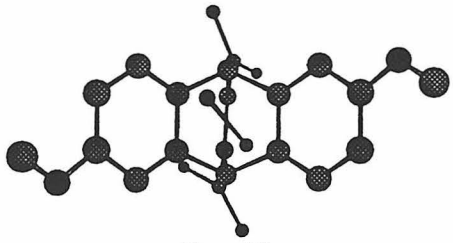

State 23

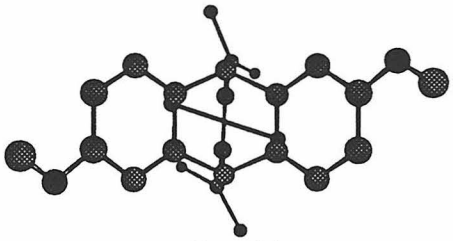

State 24

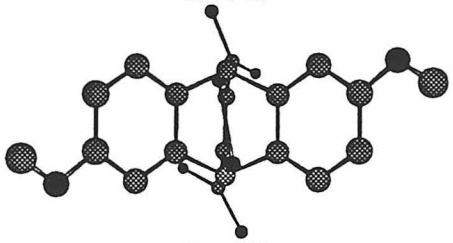

State 25

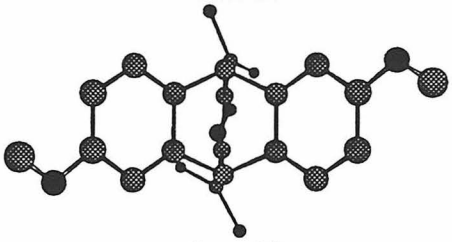

State 26

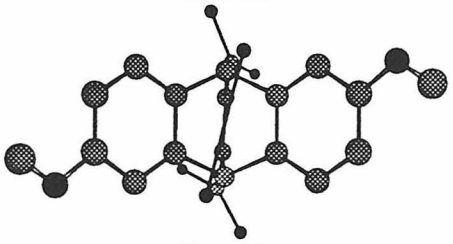

State 27

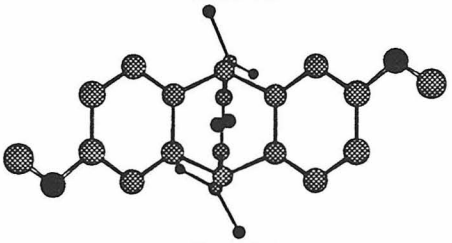

State 29

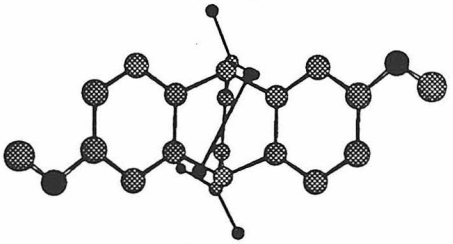

State 30

4.9.3 $\pi \rightarrow \pi^*$ Transition Moments for Linker Chromophore 1

In the following views hydrogen atoms have been omitted for clarity.

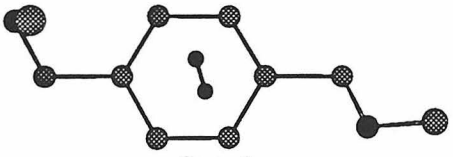

State 2

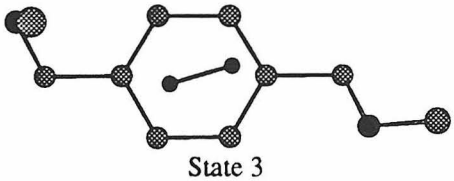

State 3

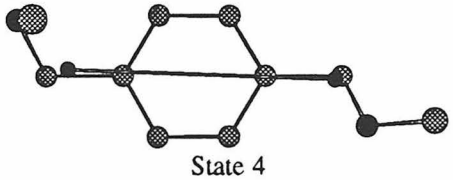

State 4

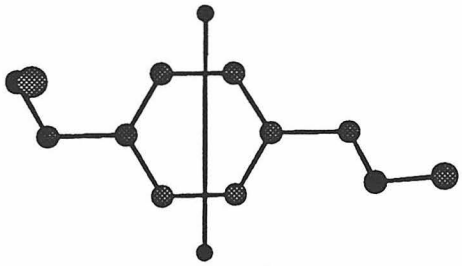

State 5

4.9.4 $\pi \rightarrow \pi^*$ Transition Moments for Linker Chromophore 2

In the following views hydrogen atoms have been omitted for clarity.

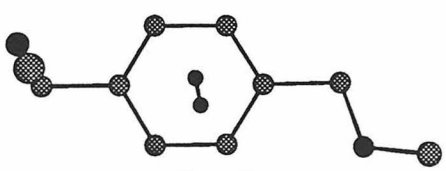

State 2

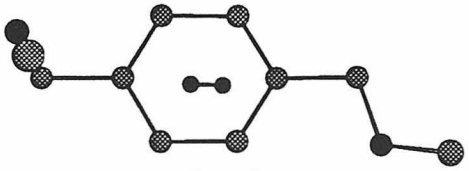

State 3

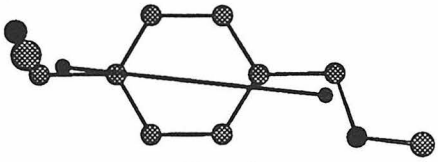

State 4

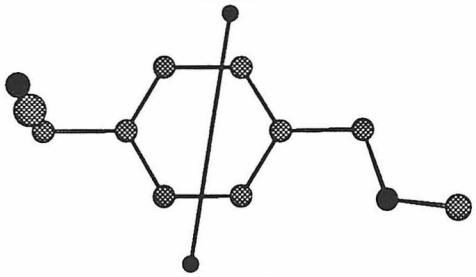

State 5

4.10 Appendix 3: AM1 optimized Geometries and INDO/S Spectral Data for Guest Molecules

4.10.1 Long-Axis dyes

Atom	x	y	z	Atom	x	y	z
Guest 9							
N(1)	5.47109	-0.05924	-0.00244	C(20)	-3.93356	-0.00830	0.00344
C(2)	4.64325	-1.15580	-0.00672	C(21)	-3.06763	1.12746	0.00074
C(3)	3.26158	-1.03091	-0.01203	C(22)	-1.69711	0.97359	-0.00146
C(4)	2.67142	0.25915	-0.00730	C(23)	-1.09308	-0.30075	-0.00381
C(5)	3.54092	1.38375	-0.00412	C(24)	-1.94931	-1.42950	-0.00353
C(6)	4.91354	1.20005	-0.00030	H(25)	-3.94002	-2.20867	0.00317
H(7)	5.13453	-2.14916	-0.00768	H(26)	-3.48717	2.14497	0.00135
H(8)	2.64418	-1.94172	-0.01838	H(27)	-1.06547	1.87742	-0.00305
H(9)	3.13066	2.40645	-0.00473	H(28)	-1.50508	-2.43862	-0.00475
H(10)	5.61786	2.05618	0.00499	N(29)	-5.29973	0.13348	0.00628
C(11)	6.91175	-0.22822	0.02689	C(30)	-6.15490	-1.02219	0.00756
H(12)	7.26417	-0.24439	1.09424	H(31)	-5.95621	-1.65418	0.91526
H(13)	7.19312	-1.19335	-0.47260	H(32)	-7.23235	-0.70735	0.02161
H(14)	7.40551	0.62266	-0.51591	H(33)	-5.97577	-1.64287	-0.91267
C(15)	1.26653	0.47995	-0.00784	C(34)	-5.89466	1.44302	-0.00007
C(16)	0.31737	-0.50242	-0.00532	H(35)	-5.57634	2.01109	-0.91692
H(17)	0.95231	1.53875	-0.00746	H(36)	-7.01338	1.36134	-0.00092
H(18)	0.63466	-1.56448	-0.00624	H(37)	-5.57966	2.01958	0.91199
C(19)	-3.31839	-1.30017	0.00256				
Guest 10							
N(1)	-3.87004	0.96389	-0.18768	C(20)	1.41446	0.85057	0.28965
C(2)	-2.93287	-0.01837	0.08444	C(21)	2.77966	1.04222	0.32133
C(3)	-3.39463	-1.33572	0.37300	C(22)	3.68106	-0.02077	0.00429
C(4)	-4.74452	-1.63353	0.38374	C(23)	3.10371	-1.27466	-0.36296
C(5)	-5.67522	-0.61252	0.10965	C(24)	1.73705	-1.44562	-0.39005
C(6)	-5.21316	0.66460	-0.16503	H(25)	0.75673	1.69396	0.55368
H(7)	-2.64725	-2.10914	0.61144	H(26)	3.16875	2.03143	0.60712
H(8)	-5.09621	-2.65555	0.61215	H(27)	3.75094	-2.12609	-0.62922
H(9)	-6.75867	-0.81524	0.11431	H(28)	1.32517	-2.42858	-0.67435
H(10)	-5.91094	1.49994	-0.38070	N(29)	5.04217	0.15599	0.05059
C(11)	-3.44607	2.31962	-0.49004	C(30)	5.59816	1.44023	0.38171
H(12)	-3.02097	2.79564	0.43557	H(31)	5.30445	1.73410	1.42688
H(13)	-2.66013	2.29335	-1.29398	H(32)	6.71796	1.40544	0.32215
H(14)	-4.31881	2.92613	-0.85105	H(33)	5.22674	2.22361	-0.33421
C(15)	-1.52801	0.30037	0.09638	C(34)	5.92876	-0.93207	-0.25867
C(16)	-0.55572	-0.63324	-0.10463	H(35)	6.99581	-0.61364	-0.12316
H(17)	-1.24658	1.34965	0.28525	H(36)	5.72729	-1.80348	0.42233
H(18)	-0.84472	-1.67770	-0.34438	H(37)	5.78550	-1.26252	-1.32474
C(19)	0.85032	-0.39261	-0.06540				

Table 4.18. Principle axis atomic coordinates (Å) of AM1[24] optimized geometry long-axis dye guests 9, 10, and 11 (continued on next page).

Atom	x	y	z	Atom	x	y	z
Guest 11							
N(1)	1.22914	0.87074	0.17774	H(21)	-3.62001	2.03920	-0.98230
C(2)	0.32933	-0.14834	0.02999	H(22)	-1.19532	1.91450	-0.94986
S(3)	1.05618	-1.65892	-0.21366	C(23)	6.22787	1.27749	0.07939
C(4)	2.61158	-1.01347	-0.13469	H(24)	6.04721	2.35461	0.31581
C(5)	2.55904	0.39923	0.06540	H(25)	6.89829	0.84932	0.86733
C(6)	3.85239	-1.64169	-0.24780	H(26)	6.76156	1.21513	-0.90318
C(7)	5.01383	-0.88676	-0.17219	N(27)	-5.31869	0.13698	0.01923
C(8)	4.96058	0.51176	0.01496	C(28)	-6.08436	-1.07100	0.20912
C(9)	3.73473	1.16159	0.13522	H(29)	-6.20482	-1.27684	1.30730
H(10)	3.90697	-2.73240	-0.39954	H(30)	-7.10271	-0.94692	-0.24845
H(11)	5.99571	-1.38008	-0.26182	H(31)	-5.58109	-1.94809	-0.27864
H(12)	3.69073	2.25239	0.27776	C(32)	-6.07281	1.30730	-0.34708
C(13)	-1.87749	-1.09421	0.53926	H(33)	-6.89995	1.45009	0.40254
C(14)	-3.25007	-1.03723	0.54269	H(34)	-5.44555	2.23411	-0.32520
C(15)	-3.94864	0.09317	-0.00176	H(35)	-6.53080	1.17785	-1.36532
C(16)	-3.14913	1.15659	-0.52209	C(36)	0.92463	2.23528	0.51704
C(17)	-1.77223	1.08807	-0.50205	H(37)	-0.09676	2.29493	0.98268
C(18)	-1.09985	-0.02866	0.03019	H(38)	1.68603	2.61145	1.25378
H(19)	-1.37147	-1.97563	0.97149	H(39)	0.95734	2.87247	-0.40829
H(20)	-3.81712	-1.87496	0.98015				

Table 4.18 (Continued). Principle axis atomic coordinates (Å) of AM1[24] optimized geometry long-axis dye guests 9, 10, and 11.

State	λ (nm)	Predominate Transition	f^a	Transition Moment Vectors (atomic units) R_x	R_y	R_z
Guest 9						
2	486.7	$\pi \rightarrow \pi^*$	1.44654	-4.81355	-0.09670	0.00077
3	323.5	$\pi \rightarrow \pi^*$	0.00458	-0.02057	0.21987	0.00238
4	310.5	$\pi \rightarrow \pi^*$	0.00331	-0.02372	-0.18240	0.00154
5	286.3	$\pi \rightarrow \pi^*$	0.07410	0.83275	-0.06990	-0.00905
6	279.1	$\pi \rightarrow \pi^*$	0.08682	-0.88795	-0.09603	-0.00578
7	268.3	$\pi \rightarrow \pi^*$	0.12094	0.38147	0.96051	0.00013
8	255.7	$\pi \rightarrow \pi^*$	0.13331	0.21726	1.03686	0.00276
9	234.5	$\pi \rightarrow \pi^*$	0.03066	-0.34067	0.34722	-0.00445
10	211.2	$\pi \rightarrow \pi^*$	0.10354	0.11626	-0.84031	-0.00927
11	209.4	$\pi \rightarrow \pi^*$	0.05214	-0.33025	-0.50030	0.00687
Guest 10						
2	482.5	$\pi \rightarrow \pi^*$	1.16405	4.29969	-0.06427	-0.00361
3	335.6	$\pi \rightarrow \pi^*$	0.12431	-1.04851	-0.50011	0.15423
4	309.0	$\pi \rightarrow \pi^*$	0.00666	-0.06533	0.23934	0.07849
5	288.7	$\pi \rightarrow \pi^*$	0.02531	-0.38973	0.29590	0.03372
6	275.3	$\pi \rightarrow \pi^*$	0.12662	-1.05185	0.14545	-0.14184
7	264.8	$\pi \rightarrow \pi^*$	0.12953	-0.40420	0.94388	0.27339
8	238.8	$\pi \rightarrow \pi^*$	0.02613	-0.42024	-0.05335	0.16133
9	228.0	$\pi \rightarrow \pi^*$	0.02315	0.25665	0.32393	0.05410
10	219.0	$\pi \rightarrow \pi^*$	0.00293	-0.00748	0.13139	-0.06176
Guest 11						
2	430.9	$\pi \rightarrow \pi^*$	0.95693	-3.67980	0.18417	0.02033
3	319.7	$\pi \rightarrow \pi^*$	0.05127	-0.57350	-0.44803	-0.10047
4	306.5	$\pi \rightarrow \pi^*$	0.00550	0.03942	0.22012	-0.07381
5	292.2	$\pi \rightarrow \pi^*$	0.01677	0.23091	0.32557	0.04545
6	276.1	$\pi \rightarrow \pi^*$	0.00594	-0.14565	-0.17795	-0.03379
7	264.6	$\pi \rightarrow \pi^*$	0.12304	-0.03086	0.90979	-0.49292
8	256.3	$\pi \rightarrow \pi^*$	0.12023	0.99830	0.13086	-0.02548
9	235.6	$\pi \rightarrow \pi^*$	0.10602	-0.15313	-0.88544	-0.12157
10	227.0	$\pi \rightarrow \sigma^*$	0.00077	-0.02944	-0.06053	0.03511
11	214.6	$\pi \rightarrow \pi^*$	0.06879	-0.69667	0.02691	-0.00634

Table 4.19. INDO/S[14] calculated spectral data for AM1[24] optimized long-axis dye guests 9, 10, and 11.

[a]Oscillator strength from transition dipole moments.

4.10.2 Azulenes

Atom	x	y	z	Atom	x	y	z
Guest 6							
C(1)	0.52884	-0.71021	0.00006	C(10)	-2.47098	-0.00005	-0.00007
C(2)	1.86256	-1.13105	0.00004	C(11)	-1.88669	-1.24250	-0.00002
C(3)	2.67810	-0.00001	-0.00004	H(12)	2.20809	-2.15519	0.00010
C(4)	1.86258	1.13105	-0.00007	H(13)	3.75917	-0.00002	-0.00005
C(5)	0.52884	0.71023	0.00001	H(14)	2.20815	2.15519	-0.00015
C(6)	-0.55747	-1.57608	0.00002	H(15)	-0.34239	2.63639	0.00016
H(7)	-0.34242	-2.63637	-0.00005	H(16)	-2.57363	2.07775	0.00010
C(8)	-0.55749	1.57612	0.00006	H(17)	-3.55239	-0.00011	-0.00012
C(9)	-1.88674	1.24252	0.00002	H(18)	-2.57358	-2.07773	-0.00004
Guest 7							
C(1)	0.02495	3.13345	-0.00027	H(12)	-0.01904	-3.18092	0.00062
H(2)	0.03243	4.24312	-0.00099	H(13)	-2.66981	0.97657	-0.00044
C(3)	1.14270	-1.27651	0.00073	H(14)	-2.08595	3.25745	-0.00279
C(4)	-0.01415	-2.09041	0.00076	H(15)	2.14074	3.22562	0.00145
C(5)	-1.16216	-1.26620	0.00042	H(16)	2.68102	0.93337	0.00271
C(6)	-0.73564	0.10662	0.00036	C(17)	-2.51785	-1.77052	0.00013
C(7)	0.73188	0.09770	0.00085	O(18)	-3.53775	-1.07018	-0.00033
C(8)	-1.57883	1.20675	-0.00068	H(19)	-2.59540	-2.88337	-0.00014
C(9)	-1.23209	2.54797	-0.00161	C(20)	2.49135	-1.79965	-0.00046
C(10)	1.27473	2.53080	0.00134	O(21)	3.52064	-1.11324	-0.00202
C(11)	1.59463	1.18387	0.00156	H(22)	2.55517	-2.91351	-0.00017

Table 4.20. Principle axis atomic coordinates (Å) of AM1[24] optimized geometry azulene guests 6 and 7.

				Transition Moment Vectors (atomic units)		
State	λ (nm)	Predominate Transition	f^a	R_x	R_y	R_z
Guest 6						
2	618.6	$\pi \rightarrow \pi^*$	0.01691	0.00011	-0.58680	0.00001
3	353.0	$\pi \rightarrow \pi^*$	0.03038	-0.59421	0.00021	0.00004
4	282.6	$\pi \rightarrow \pi^*$	0.15014	0.00056	1.18198	-0.00004
5	259.5	$\pi \rightarrow \pi^*$	1.67658	-3.78488	0.00014	0.00000
6	223.3	$\pi \rightarrow \pi^*$	0.00003	-0.00023	0.01597	0.00005
7	210.8	$\pi \rightarrow \sigma^*$	0.00013	0.00004	-0.00007	-0.02961
8	204.5	$\pi \rightarrow \pi^*$	0.01753	-0.34358	0.00006	0.00003
9	199.7	$\pi \rightarrow \pi^*$	0.00038	-0.00009	0.04966	-0.00009
Guest 7						
2	515.3	$\pi \rightarrow \pi^*$	0.02292	0.62336	0.01458	0.00036
3	434.7	$n \rightarrow \pi^*$	0.00000	0.00028	0.00017	0.00224
4	431.9	$n \rightarrow \pi^*$	0.00008	-0.00005	0.00018	-0.03381
5	362.6	$\pi \rightarrow \pi^*$	0.22150	-0.00569	-1.62597	-0.00029
6	301.8	$\pi \rightarrow \pi^*$	0.12011	-1.09238	-0.00021	0.00098
7	283.9	$\pi \rightarrow \pi^*$	0.78641	2.68454	-0.37731	0.00010
8	282.7	$\pi \rightarrow \pi^*$	0.77279	-0.38026	-2.65493	-0.00026
9	255.9	$n \rightarrow \pi^*$	0.00007	-0.00051	-0.00407	0.02324
10	254.6	$n \rightarrow \pi^*$	0.00000	0.00262	-0.00075	-0.00469
11	230.1	$\pi \rightarrow \pi^*$	0.20375	-0.00493	-1.24231	0.00077

Table 4.21. INDO/S[14] calculated spectral data for AM1[24] optimized azulene guests 6 and 7.

[a]Oscillator strength from transition dipole moments.

4.10.3 Quinolines and Coumarins

Atom	x	y	z	Atom	x	y	z
Guest 3							
C(1)	-2.27830	-0.25659	0.00046	H(12)	-0.25538	-3.01732	-0.00160
C(2)	-1.90729	-1.61555	-0.00006	H(13)	2.10388	-2.31976	0.00101
C(3)	-0.56861	-1.95701	-0.00068	H(14)	3.82114	-0.49159	-0.00143
C(4)	0.41890	-0.93961	0.00046	H(15)	3.11589	1.88550	0.00351
C(5)	0.00511	0.43291	-0.00014	H(16)	0.72237	2.51370	0.00062
C(6)	1.80498	-1.25820	0.00058	N(17)	-1.36150	0.73711	0.00027
C(7)	2.74332	-0.25376	-0.00067	C(18)	-1.78564	2.12870	-0.00047
C(8)	2.33816	1.10040	0.00028	H(19)	-1.38054	2.64086	0.91494
C(9)	1.00512	1.44826	-0.00027	H(20)	-1.39299	2.63559	-0.92410
H(10)	-3.35161	0.03474	0.00284	H(21)	-2.90666	2.19342	0.00659
H(11)	-2.70237	-2.38051	-0.00004				
Guest 4							
C(1)	-0.03798	-1.87844	-0.33153	N(16)	1.41337	1.52196	0.07217
C(2)	1.09727	-2.65710	-0.27673	C(17)	2.70822	2.13914	0.28007
C(3)	2.34691	-2.06819	-0.01328	H(18)	2.60135	3.25680	0.30090
C(4)	2.44758	-0.70115	0.14397	H(19)	3.40438	1.85337	-0.55495
C(5)	1.29118	0.12533	0.05117	H(20)	3.13455	1.79541	1.26165
C(6)	0.00619	-0.48179	-0.10507	N(21)	-2.44650	-0.11449	0.07305
C(7)	0.31102	2.28655	-0.15738	C(22)	-2.75719	-1.38266	0.69105
C(8)	-0.96178	1.76056	-0.26290	H(23)	-3.04222	-2.13650	-0.09244
C(9)	-1.18563	0.35682	-0.09791	H(24)	-3.63078	-1.24182	1.38652
H(10)	-0.98969	-2.36331	-0.60418	H(25)	-1.88939	-1.76076	1.29444
H(11)	1.03586	-3.74365	-0.45315	C(26)	-3.58260	0.73880	-0.20944
H(12)	3.24807	-2.70015	0.05331	H(27)	-4.51743	0.11566	-0.23509
H(13)	3.43908	-0.25424	0.32286	H(28)	-3.45728	1.23190	-1.21136
H(14)	0.46156	3.38719	-0.20668	H(29)	-3.68987	1.52603	0.58504
H(15)	-1.79484	2.45972	-0.43558				
Guest 5							
C(1)	-1.24695	-0.39946	-0.02193	C(13)	1.17957	2.27829	0.09969
C(2)	-1.29709	-1.78066	-0.06402	H(14)	1.22568	3.38057	0.14366
C(3)	-0.10028	-2.53122	-0.10447	C(15)	0.13982	1.69341	0.09870
C(4)	1.12489	-1.90933	-0.08774	H(16)	-0.75224	2.35130	0.11568
C(5)	1.19717	-0.49306	-0.01504	H(17)	-2.26906	-2.31524	-0.07898
C(6)	0.00517	0.27727	0.03030	H(18)	-0.16592	-3.63398	-0.15346
N(7)	2.44183	0.14224	0.02395	H(19)	2.04383	-2.51851	-0.12829
C(8)	3.72028	-0.64228	0.01559	H(20)	3.35261	2.07243	0.09701
H(9)	4.59531	0.04565	0.16967	N(21)	-2.55659	0.33569	-0.01325
H(10)	3.82851	-1.16632	-0.97337	O(22)	-2.61287	1.55575	-0.50328
H(11)	3.70574	-1.39737	0.84834	O(23)	-3.60269	-0.29713	0.47361
C(12)	2.39125	1.53843	0.07262				

Table 4.22. Principle axis atomic coordinates (Å) of AM1[24] optimized geometry quinoline and coumarin guests 3, 4, 5, and 8 (continued on next page).

Atom	x	y	z	Atom	x	y	z
Guest 8							
C(1)	-0.19528	-0.62495	0.01520	C(17)	4.00187	1.63276	-0.09039
C(2)	0.31653	0.69276	0.01877	C(18)	3.99284	0.09524	0.00154
C(3)	-0.60894	1.75266	0.01548	H(19)	2.25335	2.75871	-0.82777
C(4)	-1.96739	1.51420	0.00958	H(20)	2.36534	2.65415	0.97693
C(5)	-2.48874	0.18430	0.01324	H(21)	4.43402	1.95966	-1.06648
C(6)	-1.57466	-0.88931	0.01402	H(22)	4.61954	2.07446	0.72793
H(7)	-0.22911	2.78746	0.01650	H(23)	4.48710	-0.25720	0.94047
H(8)	-2.65602	2.37277	0.01918	H(24)	4.52224	-0.37142	-0.86420
H(9)	-1.90052	-1.93929	0.01264	C(25)	-4.77665	1.05099	-0.00402
N(10)	-3.85521	-0.04815	0.02811	H(26)	-5.83152	0.67250	0.03118
C(11)	1.73623	0.83506	0.01388	H(27)	-4.61001	1.72173	0.88262
C(12)	2.54641	-0.26508	0.00923	H(28)	-4.64388	1.65476	-0.94283
C(13)	2.00794	-1.60443	0.00905	C(29)	-4.35404	-1.38881	-0.07391
O(14)	2.55225	-2.70626	0.00676	H(30)	-4.03751	-1.98631	0.82518
O(15)	0.61143	-1.74166	0.01191	H(31)	-5.47410	-1.38455	-0.13103
C(16)	2.53894	2.09212	0.02363	H(32)	-3.94854	-1.89419	-0.99319

Table 4.22 (Continued). Principle axis atomic coordinates (Å) of AM1[24] optimized geometry quinoline and coumarin guests 3, 4, 5, and 8.

State	λ (nm)	Predominate Transition	f^a	Transition Moment Vectors (atomic units) R_x	R_y	R_z
Guest 3						
2	329.9	$\pi \rightarrow \pi^*$	0.12855	-0.95750	0.69220	-0.00028
3	314.9	$\pi \rightarrow \pi^*$	0.08378	-0.84741	-0.38779	-0.00009
4	248.8	$\pi \rightarrow \pi^*$	0.65193	-2.16374	-0.81054	0.00023
5	217.7	$\pi \rightarrow \pi^*$	0.13628	-0.92976	0.33510	-0.00014
6	208.4	$\pi \rightarrow \pi^*$	0.04357	0.49412	0.23399	0.00135
7	204.9	$\pi \rightarrow \pi^*$	0.71098	1.96595	0.96547	-0.00108
8	194.4	$\pi \rightarrow \pi^*$	0.95490	0.69395	-2.37278	0.00049
Guest 4						
2	337.0	$\pi \rightarrow \pi^*$	0.35896	1.89165	0.63533	0.00404
3	311.7	$\pi \rightarrow \pi^*$	0.01030	0.03491	-0.32231	0.02473
4	280.4	$\pi \rightarrow \pi^*$	0.31801	-1.51312	0.78965	0.14989
5	250.8	$\pi \rightarrow \pi^*$	0.45909	-0.32676	1.91586	-0.11666
6	244.1	$\pi \rightarrow \pi^*$	0.15993	-0.11441	1.12747	-0.02667
7	221.0	$\pi \rightarrow \pi^*$	0.13513	0.81493	-0.56271	0.05100
8	210.3	$\pi \rightarrow \pi^*$	0.14293	-0.99454	-0.02463	0.00363
9	203.7	$\pi \rightarrow \pi^*$	0.09396	0.62868	-0.45868	0.15613
10	199.9	$\pi \rightarrow \sigma^*$	0.04828	0.35558	-0.43323	0.06026
11	193.0	$\pi \rightarrow \pi^*$	0.47194	0.63108	1.59928	0.20492
Guest 5						
2	589.3	$n \rightarrow \pi^*$	0.00111	-0.14144	0.03783	0.00769
3	530.1	$n \rightarrow \pi^*$	0.00049	0.01445	0.09149	0.00753
4	313.3	$\pi \rightarrow \pi^*$	0.13569	1.13598	0.32958	0.02228
5	308.2	$\pi \rightarrow \pi^*$	0.13795	0.45616	-1.08923	-0.07288
6	279.6	$\pi \rightarrow \pi^*$	0.20280	-1.36198	-0.09665	-0.05016
7	273.2	$\pi \rightarrow \pi^*$	0.01567	-0.20637	0.23106	-0.21211
8	255.6	$\pi \rightarrow \pi^*$	0.10392	-0.17883	-0.88782	-0.23262
9	249.5	$n \rightarrow \pi^*$	0.09703	0.52595	0.58876	-0.41662
10	239.2	$\pi \rightarrow \pi^*$	0.07880	0.31585	0.62127	0.36718
11	230.6	$\pi \rightarrow \pi^*$	0.62173	-1.09988	-1.79119	0.54965
Guest 8						
2	366.5	$n \rightarrow \pi^*$	0.00072	0.01469	-0.00751	0.09186
3	340.0	$\pi \rightarrow \pi^*$	0.64682	2.51389	-0.95928	-0.00787
4	314.0	$\pi \rightarrow \pi^*$	0.08119	0.90331	0.15288	-0.00823
5	254.6	$\pi \rightarrow \pi^*$	0.09036	0.64634	0.58259	-0.00843
6	244.4	$\pi \rightarrow \pi^*$	0.18105	-0.16095	-1.19612	0.00175
7	226.2	$\pi \rightarrow \pi^*$	0.19306	-0.59869	-1.03888	0.01076
8	217.2	$\pi \rightarrow \pi^*$	0.66664	1.60870	-1.47619	-0.00484
9	206.8	$\pi \rightarrow \sigma^*$	0.00065	-0.03896	-0.01781	-0.05080
10	205.4	$\pi \rightarrow \pi^*$	0.19062	0.74005	0.86101	0.00205

Table 4.23. INDO/S[14] calculated spectral data for AM1[24] optimized quinoline and coumarin guests 3, 4, 5, and 8.

[a]Oscillator strength from transition dipole moments.

4.11 Appendix 4: Using the DZDO Program[44]

4.11.1 Input Files

Unless otherwise noted for a specific calculation, the switches of Table 4.24 were set in the input files, and all other input settings were left at the DZDO defaults.[44] Switch settings were only varied when the calculation output came up with error messages or if the molecule had special requirements for its calculation.

Switch	Setting	Description	Notes
IRHYB	1	Hybridization calculations are performed.	
MULTI	1	Multiplicity to be used for LHP open shell SCF method.	
ISYMM	1	Classifies point group symmetry of SCF MO's.	
IPRTY	1	Output contains details of symmetry analysis.	
INTRNL	0	Geometries are put in Cartesian coordinates.	
ETOL	1.D-10	Tolerance of SCF convergence for SCF energy.	
PTOL	1.D-10	Tolerance for SCF convergence for bond order matrix.	
MXIT	100	Maximum number of SCF iterations.	
IRHF	1	SCF is carried out using closed shell RHF method.	
NSTPRT	10	Number of CI states printed in output.	For ethenoanthracenes this was set to 30.[45]
ISTOXP	0	STO exponents are used with modifications.	
LORTH	0	MO's are deorthoganalized before transforming AO operator matrixes (this requires operator matrix elements be calculated explicitly from an STO basis).	
IZPARM	1	Zerner parameter set specified for an INDO/S Hamiltonian.	
ISPEC	1	Specifies a spectroscopic (/S) modal Hamiltonian.	
NDOTYP	2	Specifies a /2 type Hamiltonian.	
ICNDO	2	Specifies an INDO Hamiltonian.	
IDOCI	1	CI calculation is done on basis of the MO's produced by SCF method.	
KPRCI	1	CI eigenvalues and eigenvectors printed in output.	
ICISC	1	CI is limited to singly excited states.	
IOBS	1	Spectroscopic observables are calculated.	
MCLFY	1	Orbitals are classified as π, σ, or n depending on composition in terms of hybrid orbitals.	
HRBNDL	1.650	Atoms further apart than this distance (in Å) will not be treated as bonded for hybridization calculations.	In most input files this switch was not specified (1.650 is a default), but for guest **11** the switch had to be specified as 1.700.[46]

Table 4.24. Input switches for INDO/S[14] calculations with DZDO.[44]

A sample input file is shown on the following page for linker 1 (Figure 4.12). The first part of the input file is the calculation set up. The first line is for notes (file name), the second line separates the control switches and is denoted by "&CTL". The switches specified in the calculation follow, each on its own line with the "=" symbol preceding the switch setting (no spaces between characters). The switches are separated from the rest of the input file by the final line "&END".

The second part (molecule input) begins on the line immediately below the "&END" statement. First is the molecular charge of the ground-state; the "+" sign is not used for positive charges. Only the number is written. Immediately below this is the input coordinates (from the optimized geometry used for the calculation, in Å); each atom is on a separate line that contains the following information (each number separated by at least one space): atomic number of the atom, *x*-coordinate, *y*-coordinate, *z*-coordinate. Note that DZDO will take the input coordinates and convert them into the principle axis coordinates, used in the calculation; thus any set of input coordinates can be used for the input file.

The line below the final atom is left blank. However, the final line of the file (no blank lines below this) lists two numbers separated by a space; these are the number of highest occupied orbitals to consider for CI and the number of lowest unoccupied orbitals to consider for CI (this value is written as a negative number). As shown in the sample file, for excitation from the 10 highest occupied to the 10 lowest unoccupied molecular orbitals, the final line is written: 10 -10.

```
LINKER1
&CTL
IRHYB=1,
MULTI=1,
ISYMM=1,
IPRTY=1,
INTRNL=0,
ETOL=1.D-10,
PTOL=1.D-10,
MXIT=100,
IRHF=1,
NSTPRT=10,
ISTOXP=0,
LORTH=0,
IZPARM=1,
ISPEC=1,
NDOTYP=2,
ICNDO=2,
IDOCI=1,
KPRCI=1,
ICISC=1,
IOBS=1,
MCLFY=1
&END
0
8   2.541000   -0.964294   -0.056015
8  -4.288437    1.070877   -0.038620
6  -3.923584    1.288971    1.283173
1  -4.416885    2.235275    1.599136
1  -2.820297    1.435486    1.290421
1  -4.345093    0.445587    1.874634
6   3.882904   -0.813370    0.218170
1   4.129990   -1.545441    1.019241
1   4.013962    0.217606    0.616470
1   4.432068   -1.091705   -0.709000
6   1.991440   -0.129044   -1.054459
6   0.502808   -0.125122   -0.975784
6  -0.181885   -1.300842   -0.747223
1   0.371277   -2.234116   -0.641403
6  -1.576309   -1.309631   -0.649734
1  -2.112518   -2.241684   -0.471497
6  -2.267059   -0.114853   -0.783051
6  -1.573181    1.039078   -1.029648
1  -2.114594    1.973450   -1.177505
6  -0.193756    1.030640   -1.092941
1   0.342728    1.968094   -1.239349
6  -3.763153   -0.119522   -0.684692
1   2.318939    0.756866   -0.943527
1   2.259796   -0.451035   -1.913727
1  -4.037674   -0.883438   -0.190826
1  -4.126160   -0.173889   -1.567032

10 -10
```

4.11.2 Execution of Program

DZDO is run from the Dougherty Group SGI machine. All input files must have the extension ".zdo", while the output file can have any extension desired. The command to run the program is as follows (each string of characters is separated by a single space):

dzdo <infile-name.zdo >outfile-name

The time required for a calculation is proportional to the number of heavy atoms; generally DZDO calculations take several minutes, with larger molecule calculations taking up to 30 minutes.

4.12 References and Footnotes

1. (a) Kearney, P. C.; Mizoue, L. S.; Kumpf, R. A.; Forman, J. E.; McCurdy, A.; Dougherty, D. A. *J. Am. Chem. Soc.* **1993**, *115*, 9907-9919. (b) Petti, M. A.; Shepodd, T. J.; Barrans, R. E., Jr.; Dougherty, D. A. *J. Am. Chem. Soc.* **1988**, *110*, 6825-6840.

2. Forman, J. E.; Barrans, R. E., Jr.; Dougherty, D. A.; *J. Am. Chem. Soc.* **1995**, *117*, 9213-9228.

3. (a) Hamai, S.; *J. Phys. Chem.* **1995**, *99*, 12109-12114. (b) Marconi, G.; Monti, S.; Mayer, B.; Kohler, G.; *J. Phys. Chem.* **1995**, *99*, 3943-3950. (c) Yoshida, N.; Yamaguchi, H.; Higashi, M.; *J. Chem. Soc. Perkin Trans. 2* **1994**, 2507-2513. (d) Sakurai, T.; Saitou, E.; Hayashi, N.; Hirasawa, Y.; Inoue, H.; *J. Chem. Soc. Perkin Trans. 2* **1994**, 1929-1935. (e) Hamai, S.; Ikeda, T.; Nakamura, A.; Ikeda, H.;

Ueno, A.; Toda, F. *J. Am. Chem. Soc.* **1992**, *114*, 6012-6016. (f) Buss, V.; Reichardt, C. *J. Chem. Soc., Chem. Commun.* **1992**, 1636-1638. (g) Kano, K; Yoshiyasu, K.; Yasouka, H.; Hata, S.; Hashimoto, S. *J. Chem. Soc., Perkin Trans. 2*, **1992**, 1265-1259. (h) Schuette, J. M.; Ndou, T. T.; Warner, I. M.; *J. Phys. Chem.*, **1992** *96*, 5309-5314. (i) Buss, V. *Angew. Chem., Int. Ed. Engl.* **1991**, *30*, 869-870. (j) Kano, K.; Tatsumi, M.; Hashimoto, S. *J. Org. Chem.* **1991**, *56*, 6579-6585. (k) Kodaka, M. *J. Phys. Chem.* **1991**, *95*, 2110-2112. (l) Kobayashi, N.; Opallo, M. *J. Chem. Soc., Chem. Commun.* **1990**, 477-479. (m) Ishizuka, Y.; Nagawa, Y.; Nakanishi, H.; Akira, K. *J. Inclusion Phenom. Mol. Recognit. Chem.* **1990**, *9*, 219-225. (n) Ata, M.; Kubozono, Y.; Suzuki, Y.; Aoyagi, M.; Gondo, Y. *Bull. Chem. Soc. Jpn.* **1989**, *62*, 3706-3708. (o) Ueno, A.; Moriwaki, F.; Osa, T.; Hamada, F.; Murai, K. *J. Am. Chem. Soc.* **1989**, *111*, 6391-6397. (p) Komiyama, M.; Takeshige, Y. *J. Org. Chem.* **1989**, *54*, 4936-4939. (q) Ueno, A.; Suzuki, I.; Osa, T. *J. Am. Chem. Soc.* **1988**, *110*, 4323-4328. (r) Kobayashi, N. *J. Chem. Soc., Chem. Commun.* **1988**, 918-919. (s) Kobayashi, N.; Zao, X.; Osa, T.; Kato, K.; Hanabusa, K.; Imoto, T.; Shirai, H. *J. Chem. Soc., Dalton Trans.* **1987**, 1801-1803. (t) Le Bas, G.; de Rango, C.; Rysanek, N.; Tsoucaris, G. *J. Inclusion Phenom. Mol. Recognit. Chem.* **1984**, *2*, 861-867. (u) Yamaguchi, H. *J. Inclusion Phenom. Mol. Recognit. Chem.* **1984**, *2*, 747-753. (v) Kobayashi, N.; Hino, Y.; Uneo, A.; Osa, T. *Bull. Chem. Soc. Jpn.* **1983**, *56*, 1849-1850. (w) Kobayashi, N.; Hino, H.; Hino, Y.; Uneo, A.; Osa, T. *J. Chem. Soc., Perkin Trans. 2* **1983**, 1031-1035. (x) Shimizu, H.; Kaito, A.; Hatano, M. *Bull Chem. Soc. Jpn.* **1981**, *54*, 513-519. (y) Shimizu, H.; Kaito, A.; Hatano, M. *Bull Chem. Soc. Jpn.* **1979**, *52*, 2678-2684. (z) Ikeda, N.; Yamaguchi, H. *Chem. Phys. Lett.* **1978**, *56*, 167-169. (aa) Yamaguchi, H.; Ikeda, N.; Hirayama, F.; Uekama, K. *Chem. Phys. Lett.* **1978**, *55*, 75-76. (bb) Harata, K.; Uedaira, H.; *Bull Chem. Soc. Jpn.* **1975**, *48*, 375-378.

4. (a) Okabe, N.; Hashizuma, N.; *Biol. Pharm. Bull.* **1994**, *17*, 16-21. (b) Pal, M. K.; Ghosh, J. K.; *Spectrochim. Acta* **1994**, *50A*, 199-126. (c) Kishore, S.; Maruthamuthu, M.; *Proc. Indian Acad. Sci. (Chem. Sci.)* **1993**, *105*, 279-285. (d) Norden, B.; Kubista, M. *NATO ASI ser., ser. C, 242*, 1988, 133-165. (e) Hatano, M. *Induced Circular Dichroism in Biopolymer-Dye Systems*, Springer-Verlag: Berlin, 1986.

5. Studies of calixarenes: Morozumi, T.; Shinkai, S.; *Chem. Lett.* **1994**, 1515-1518. (b) Morozumi, T.; Shinkai, S.; *J. Chem. Soc., Chem. Commun.* **1994**, 1219-1220. (c) Arimura, T.; Shinkai, S. *Bull. Chem. Soc. Jpn.* **1991**, *64*, 1896-1900. (d) Arimura, T.; Kawabata, H.; Matsuda, T.; Muramatsu, T.; Satoh, H.; Fujio, K.; Manabe, O.; Shinkai, S. *J. Org. Chem.* **1991**, *56*, 301-306. (e) Arimura, T.; Kawabata, H.; Edamitsu, S.; Shinkai, S.; Manabe, O.; Muramatsu, T.; Tashiro, M. *Chem. Lett.* **1987**, 2269-2272. (f) Shinkai, S.; Arimura, T.; Satoh, H.; Manabe, O. *J. Chem. Soc., Chem. Commun.* **1987**, 1495-1496.

6. Studies of cyclophane hosts: (a) Murakami, Y.; Hayashida, O.; Nagai, Y. *J. Am. Chem. Soc.* **1994**, *116*, 2611-2612. (b) Kobayashi, K.; Asakawa, Y.; Kikuchi, Y.; Toi, H.; Aoyama, Y.; *J. Am. Chem. Soc.* **1993**, *115*, 2648-2654. (c) Murakami, Y.; Hayashida, O.; Ono, K.; Hisaeda, Y. *Pure Appl. Chem.* **1993**, *65*, 2319-2324. (d) Murakami, Y.; Hayashida, O.; Ito, T.; Hisaeda, Y. *Pure Appl. Chem.* **1993**, *65*, 551-556. (e) Kikuchi, Y.; Kobayashi, K.; Aoyama, Y.; *J. Am. Chem. Soc.* **1992**, *114*, 1351-1358. (f) Murakami, Y.; Ohno, T.; Hayashida, O.; Hisaeda, Y. *Chem. Lett.* **1991**, 1595-1598. (g) Murakami, Y.; Kikuchi, J.; Ohno, T.; Hayashida, O.; Kojima, M. *J. Am. Chem. Soc.* **1990**, *112*, 7672-7671.

7. Studies of crown ethers: (a) Gu, D.; Kenney, B. D.; Brown, B. W. *Tetrahedron Lett.*,

1994 *35*, 681-684. (b) Mack, M. P.; Hendrixson, R. P.; Palmer, R. A.; Ghirardelli, R. G. *J. Org. Chem.* **1983**, *48*, 2029-2035. (c) Malpass, G. D., Jr.; Palmer, R. A.; Ghirardelli, R. G. *Tetrahedron Lett.* **1980**, *21*, 1489-1492. (c) Kaneko, O.; Matsuura, N.; Kimura, K.; Shono, T. *Chem. Lett.* **1979**, 369-372. (d) Mack, M. P.; Hendrixson, R. P.; Palmer, R. A.; Ghirardelli, R. G. *J. Am. Chem. Soc.* **1976**, *98*, 7830-7832.

8. Jansen, J. F. G. A.; de brabander-van den Berg, E. M. M.; Meijer, E. W.; *Rec. Trav. Chim.* **1995**, *114*, 225-230.

9. The only exception occurring when the control molecule is aggregated and the guest encapsulated inside the resultant micelle. This type of ICD is observed in general with solubilization of achiral chromophores by chiral surfactant aggregates; see for example: (a) Nakashima, N.; Ando, R.; Muramatsu, T.; Kunitake, T.; *Langmuir* **1994**, *10*, 232-234. (b) Nakashima, N.; Fukushima, H.; Kunitake, T.; *Chem. Lett.* **1981**, 1207-1210.

10. Kumpf, R. A.; Dougherty, D. A.; *Unpublished Results*.

11. (a) Silverstein, R. M.; Bassler, G. C.; Morrill, T. C. *Spectrometric Identification of Organic Compounds*, John Wiley and Sons: New York, 1974. (b) Reichardt, C. *Chem. Rev.* **1994**, *94*, 2319-2358.

12. (a) Tinoco, I., Jr. *Adv. Chem. Phys.* **1962**, *4*, 113-160. (b) Rosini, C.; Zandomeneghi, M.; Salvadori, P. *Tetrahedron Asymmetry* **1993**, *4*, 545-554.

13. (a) Volosov, A.; Woody, R. W.; in *Circular Dichroism-Principles and Applications*,

Nakanishi, K.; Berova, N.; Woody, R. W. (eds); VCH, 1994, 59-84. (b) Charney, E.; *The Molecular Basis of Optical Activity-Optical Rotatory Dispersion and Circular Dichroism*, Robert E. Krieger Publishing Company: Malabar, Fl, 1985. (c) Mason, S. F. *Molecular Optical Activity and the Chiral Discriminations*, Cambridge University Press: Cambridge, 1982.

14. (a) Zerner, M. C.; Loew, G. H.; Kirchner, R. F.; Mueller-Westerhoff, U. T.; *J. Am. Chem. Soc.* **1980**, *102*, 589-599. (b) Bacon, A. D.; Zerner, M. C.; *Theoret. Chim. Acta* **1979**, *53*, 21-54. (c) Ridley, J. E.; Zerner, M. C.; *J. Mol. Spectrosc.* **1974**, *50*, 457-473. (d) Ridley, J. E.; Zerner, M. C.; *Theoret. Chim. Acta* **1973**, *32*, 111-134.

15. (a) Nakanishi, K.; Berova, N.; in *Circular Dichroism-Principles and Applications*, Nakanishi, K.; Berova, N.; Woody, R. W. (eds); VCH, 1994, 361-398. (b) Harada, N.; Nakanishi, K.; *Circular Dichroic Spectroscopy-Exciton Coupling in Organic Stereochemistry*, University Science Books: Mill Valley, CA, 1983.

16. (a) Thulstrup, E. W.; Michl, J.; *Elementary Polarization Spectroscopy*, VCH, 1989. (b) Michl, J.; Thulstrup, E. W.; *Spectroscopy with Polarized Light. Solute Alignment by Photoselection, in Liquid Crystals, Polymers, and Membranes*, VCH, 1986.

17. (a) Yamaguchi, M.; Higashi, M.; Oda, M. *Spectrochim. Acta* **1988**, *44A*, 547-548. (b) Kobayashi, N.; Minato, S.; Osa, T. *Makromol. Chem.* **1983**, *184*, 2123-2132. (c) Shimizu, H.; Kaito, A.; Hatano, M. *J. Am. Chem. Soc.* **1982**, *104*, 7059-7065.

18. Kodaka, M. *J. Am. chem. Soc.* **1993**, *115*, 3702-3705.

19. Gaussian 92, Revision Frisch, C. M. J.; Trucks, G. W.; Head-Gordon, M.; Gill, P. M. W.; Wong, M. W.; Foresman, J. B.; Johnson, B. G.; Schlegel, H. B.; Robb, M. A.; Replogle, E. S.; Gomperts, R.; Andres, J. L.; Raghavachari, K.; Binkley, J. S.; Gonzalez, C.; Martin, R. L.; Fox, D. J.; Defrees, D. J.; Baker, J.; Stewart, J. J. P.; Pople, J. A.; Gaussian, Inc.; Pittsburgh, PA, 1992.

20. Forman, J. E.; Marsh, R. E.; Schaefer, W. P.; Dougherty, D. A.; *Acta. Cryst. Section B*, **1993** *B49*, 892-896.

21. Dougherty, D. A.; *Personal Communication.*

22. It is important to note that many of the experimental hosts were of (*R*, *R*, *R*, *R*) stereochemistry (Table 4.1), while the calculations were performed on hosts of (*S*, *S*, *S*, *S*) stereochemistry. When such a discrepancy exists, the calculations are interpreted based on the opposite sign of the data in Table 4.1.

23. Michl, J.; *Personal Communication.*

24. Dewar, M. J. S.; Zoebisch, E. G.; Healy, E. F.; Stewart, J. J. P.; *J. Am. Chem. Soc.* **1985**, *107*, 3902-3909.

25. A control calculation using the *cis*-isomer of **10** gave essentially identical results.

26. Damiano, D. B.; Little, J. B.; *A Course in Linear Algebra*, Harcourt Brace Jovanovich, Publishers; 1988.

27. Version 4.0, Microsoft Corp., © 1985-1992.

28. For the creation of a number of Figures in this Chapter, a host **C** coordinate system was required. This was created by converting the linkers of host **P** into cyclohexyl groups and optimizing the geometry without allowing any non-linker atoms to change position, thus creating an identical coordinate system.

29. Experimentally, host $\mathbf{C_R}$ shows induced CD with $R < 0$ for these guests.

30. Ponterini, G.; Momicchioli, F. *Chem. Phys.* **1991**, *151*, 111-126.

31. For thoroughness, calculations were done using the enantiomers of the guest structures used for guests **10** and **11**. As expected, the outcome of the binding orientation analysis was unchanged.

32. Similarly, a recent molecular dynamics study on host **P** with acetylcholine as guest showed that the guest prefers to reside at one side of the cavity. Axelson, P. H. *Israel J. Chem.* **1994**, *34*, 159-163.

33. Dougherty, D. A.; Kearney, P. C.; Mizoue, L. S.; Kumpf, R. A.; Forman, J. E.; McCurdy, A.; in *Computational Approaches in Supramolecular Chemistry*, G. Wipff (ed), NATO ASI Series, 1994.

34. As shown in electrostatic potential maps calculated in our laboratories.[35]

35. Kearney, P. C. California Institute of Technology, Ph.D. Thesis, 1994.

36. The relative *D* values are upfield shifts observed in ^{1}H NMR signals of guest protons

under conditions of excess host (so that a high percentage of the guest is bound); these values have been scaled relative to the highest observed shift (which is assigned a value of 1.0.).

37. Sandman, D. J.; Mislow, K.; *J. Am. Chem. Soc.*, **1969**, *70*, 645-648.

38. Inskeep, W. H.; Miles, D. W.; Eyring, H.; *J. Am. Chem. Soc.*, **1970**, *71*, 3866-3881.

39. This requires *f* to decrease as λ increases in order for the magnitude to remain constant (equation 4.30).[13b]

40. This requires |μ| to increase as λ increases in order for *f* to remain constant (equation 4.30).[13b]

41. Ngola, S. M.; Dougherty, D. A.; *Submitted.*

42. Hafnex, K.; Bernhard, C. *Ann.* **1959**, *625*, 108-123.

43. Version 2.3, BioSym Technologies, 1993.

44. Version 4.01, 1990. This semi-empirical package was obtained as a gift from Professor Josef Michl.

45. Although the first 10 excited states (first 30 for ethenoanthracenes) were obtained from

the calculations, only data up to the highest $\pi \rightarrow \pi^*$ state above 180 nm has been presented in the tabulated INDO/S data for guests and host chromophores in this chapter.

46. This was necessary due to the length of the AM1[24] optimized C-S bonds in guest **11** (1.686 and 1.694 Å).

Chapter 5:
Larger Hosts and Higher Order Stoichiometries.

Chapter 5
Larger Hosts and Higher Order Stoichiometries.

5.1 Introduction

The studies in Chapters 2-4 have focused primarily on host **P**, a cyclophane made up of two ethenoanthracene units linked together by *p*-xylylene units.[1,2] Host **P** is prepared from its tetramethyl ester ($\mathbf{P_E}$), a molecule formed from the macrocyclization of 2,6-dihydroxyethenoanthracene **1** with α, α'-dibromo-*p*-xylene (**2**, Figure 5.1).[1b] In addition to providing $\mathbf{P_E}$, this macrocyclization yields a number of higher order oligomeric by-products; the most notable of these are the trimer $\mathbf{3_E}$ and tetramer $\mathbf{4_E}$ (Figure 5.1).[1b] The properties of the hosts formed by hydrolysis of these esters (**3** and **4**) were not initially investigated due to low quantities of material and very low critical aggregation concentrations (CAC's) prohibiting study by ^{1}H NMR methodology. However, the development of circular dichroism methodology for the study of molecular recognition (Chapters 2-4) provides a convenient means to overcome the problems faced in NMR studies.[2] This chapter focuses on the investigations of the larger macrocycles **3** and **4** as host molecules in aqueous media.

One interesting property of the large macrocycles is a propensity for forming 1:2 and/or higher order host:guest complexes with appropriate guests. While not unexpected, given the size of the macrocycles, guests capable of forming such non 1:1 stoichiometries have been avoided in studies with host **P**. This has been mainly due to the difficulties associated with quantitative studies of such systems. The studies with hosts **3** and **4** have brought to light some of the spectral features expected when such higher order complexes are forming. These spectral changes associated with higher order complexes have also been observed with certain guests and host **P**,[2] details of which are also presented.

5.2 Circular Dichroism Studies of Hosts 3 and 4

5.2.1 Spectral Features

The circular dichroism spectra of hosts **P**, **3** and **4** are shown in Figure 5.2.[2] The spectra are all qualitatively similar in appearance, but quantitatively the optical constants ($\Delta\varepsilon$) do not increase in a linear fashion. As described for host **P** in Chapter 4, the spectra of these molecules appears to be dominated by the coupled-oscillator mechanism of optical activity.[3]

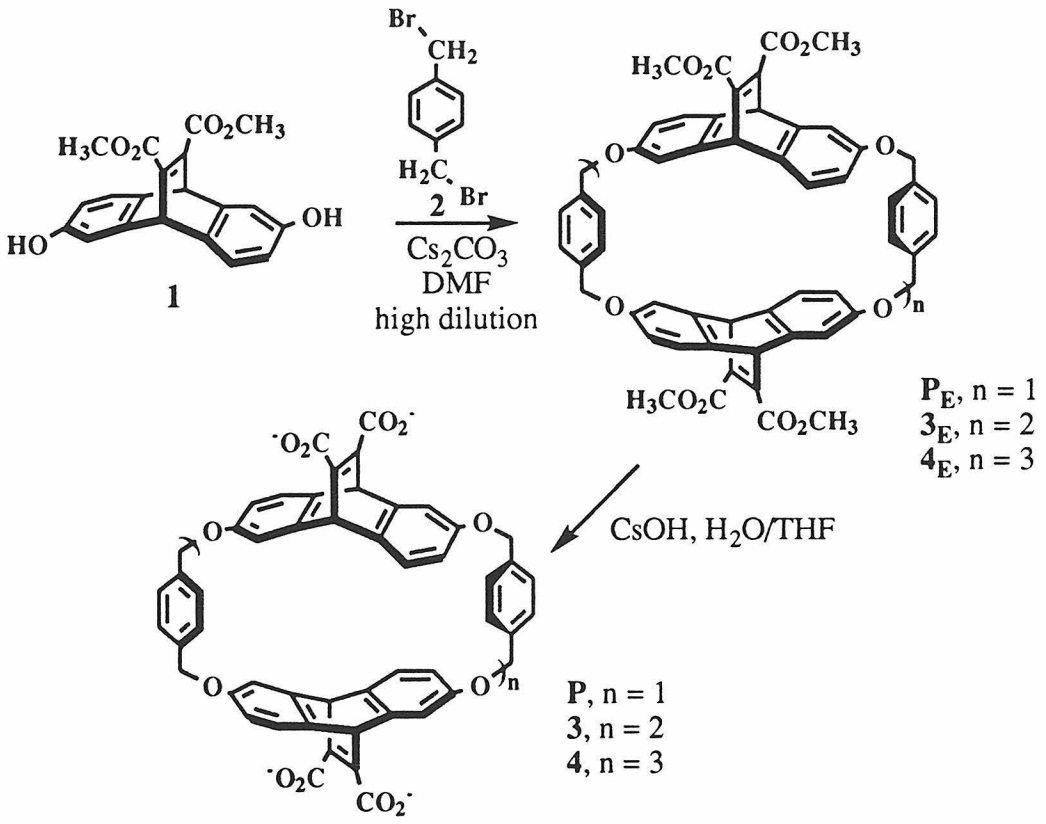

Figure 5.1. Preparation of host P and its higher oligomers.[1b]

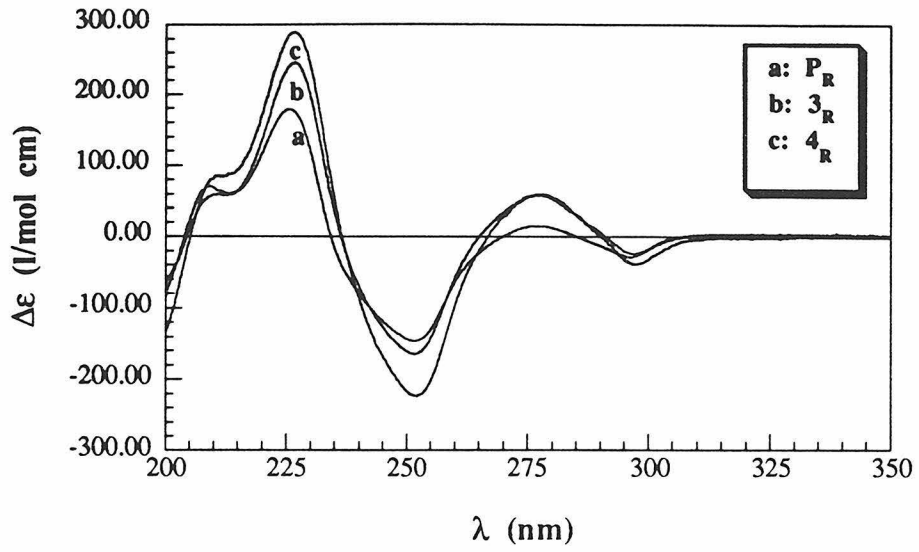

Figure 5.2. CD spectra of P_R, 3_R, and 4_R in aqueous borate buffer (pH 9).[2]

5.2.2 Bound Guests and Binding Conformations.

Figures 5.3 and 5.4 present the guests studied and their binding constants with hosts **3** and **4** (with comparisons to host **P** where appropriate). The CD studies with hosts **3** and **4** generally show rhomboid-like changes (based on host **P** observations; see Chapter 3) on binding guests, but there is some evidence for a toroid-like conformation with **3** (see Chapter 6). There is a general decrease in binding affinity on moving from **1** to the less conformationally restricted **3** and **4**. Both **3** and **4** are expected to exist in aqueous solution as highly collapsed structures. Also in both **3** and **4** the ethenoanthracene units can twist so that the carboxylates can enter the cavity, thus allowing electrostatic contributions to the binding that are much stronger than in host **P**. This enhancement of electrostatic contributions to binding is thought to be more significant for **4** as this host is much less conformationally restricted than host **3** (from CPK models). This effect can be observed by the large binding constant for the highly positively charged guest **7**.

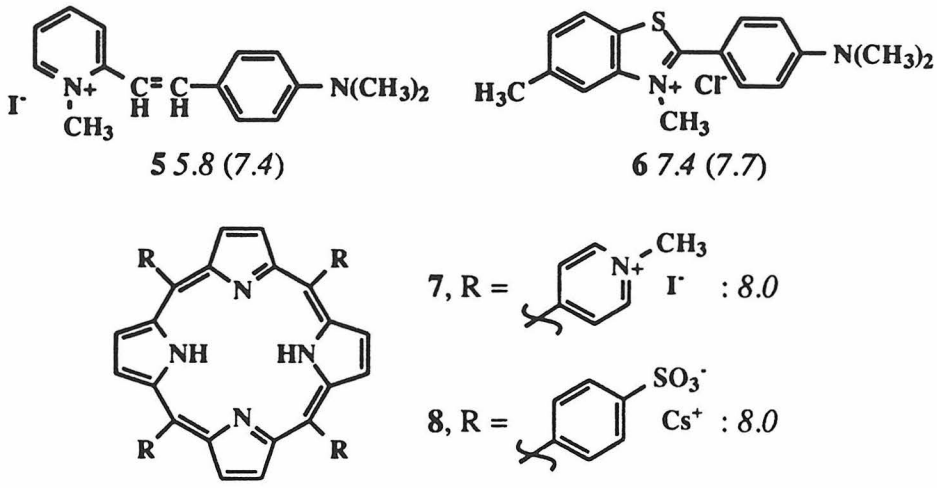

Figure 5.3. Binding constants ($-\Delta G°_a$ in kcal/mol) for guests bound by host 3 in aqueous borate buffer (pH 9). Binding constants for the guest with host P are given in parentheses.[2]

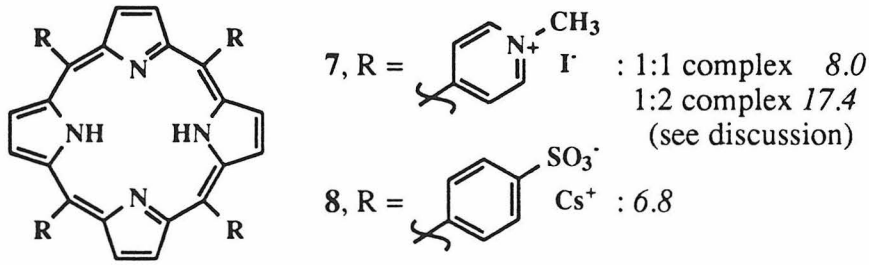

Figure 5.4. Binding constants ($-\Delta G°_a$ in kcal/mol) for guests bound by host 4 in aqueous borate buffer (pH 9).[2]

CPK models indicate that the structures of **3** and **4** have considerably more degrees of freedom than host **P**. A result of this is that there should be numerous possible preferred binding conformations, not the two-state model as proposed for host **P** itself. Given the complexity of these structures and the large number of heavy atoms, no attempts were made to quantitatively address the issue of preferred conformations by molecular dynamics calculations. Despite many attempts, no crystal structures were obtained for **3** and **4** or for their ester precursors ($\mathbf{3_E}$ and $\mathbf{4_E}$). Thus the studies of **3** and **4** are lacking in quantitative structural data.

5.2.3 Spectral Changes Associated with Guest Binding.

As with host **P**, some guests show bathochromic shifting on binding to **3** and **4**. Red shifting of absorption bands for guests **5** and **6** with host **3** is much larger than what is observed for host **P** (Table 5.1). Additionally, the apparent extinction coefficients for these absorptions in the complex show an increase in magnitude compared to the free guest (hyperchromic shifting). This is inconsistent with what has been observed for host **P** (**6** shows a hyperchromic shift, but **5** exhibits a hypochromic shifting, Table 5.1) and is thought to be the result of significantly different binding conformations occurring with the two hosts. In support of this claim the two guests exhibit opposite signs for their respective ICD with host **3** (both guests have long axis transition moments, Table 5.2, Figures 5.5 and 5.6). In addition, we observe sign reversals in the ICD of **5** when binding studies are carried out with excess guest (Figure 5.7). Such spectral changes are thought to be the result of additional guest molecules entering the cavity to produce HG_2 and/or higher order complexes. The large hyperchromic shift reported for the **3/5** complex in Table 5.1 may be due in part to the presence of higher order complexes effecting the fitting procedure used to obtain the data. Guest **6** with host **3** does not show this behavior.

Given the size of the guest compared to the size of the host, it is not surprising to observe the formation of 2:1 and/or higher order complexes. The most notable examples are the **3/5** and **4/7** systems.[2] For the other host-guest systems (**3/6**; **3/7**; **3/8**; and **4/8**), control studies with excess host reveal no unusual spectral changes–these complexes are thought to be exclusively 1:1 host:guest.[2]

The dipolar coupling mechanism of ICD[3] is evident in examination of the rotational strengths in Table 5.2. In general, **3** induces greater rotational strengths than **P**, and **4** induces greater rotational strengths than **3**. This is expected from the coupling of a greater number of host transitions with the guest transition in the higher oligomers. Unfortunately,

due to the absence of rigorous conformational data, no induced CD calculations of bound-guest orientations (Chapter 4) could be attempted for hosts **3** and **4** and their guests.

		Free Guest		Bound Guest[a]		
Guest	Host	λ_{max} (nm)	ε^b ($M^{-1}cm^{-1}$)	λ_{max} (nm)	ε^b ($M^{-1}cm^{-1}$)	$\Delta\lambda$ (nm)
5	**P**	439	2.8×10^4	473	2.0×10^4	+34
5	**3**	439	2.8×10^4	527	6.6×10^4	+88
6	**P**	412	1.8×10^4	424	1.9×10^4	+12
6	**3**	412	1.8×10^4	440	2.9×10^4	+28
7	**P**	423	1.9×10^5	c	c	$\Delta\lambda > 0$
7	**3**	423	1.9×10^5	436	1.4×10^5	+13
7	**4**	423	1.9×10^5	1:1 complex 439 1:2 complex 432	1:1 complex 2.0×10^5 1:2 complex 2.8×10^5	1:1 complex +16 1:2 complex +9
8	**P**	414	4.6×10^5	c	c	$\Delta\lambda > 0$
8	**3**	414	4.6×10^5	414	4.4×10^5	±0
8	**4**	414	4.6×10^5	423	4.4×10^5	+9

Table 5.1. Bathochromic shifting of guest absorption bands observed on binding to hosts P, 3, and 4 in aqueous borate buffer.
[a]Data was obtained by fitting from known binding constants, equilibrium concentrations, and optical constants. [b]Approximate value. [c]A binding constant was not obtained for this host-guest system, thus UV/Visible spectral changes are qualitative only.

5.2.4 Porphyrins as Guests.

The tetracationic porphyrin **7** shows significant CD changes on binding to **3** and **4**. For the **3/7** system a strong Cotton effect is observed at 439 nm (red shifted 15 nm from the UV Soret λ_{max}), and a weaker Cotton effect is observed at 419 nm (5 nm blue shift from UV Soret λ_{max}) as shown in Figure 5.8. We believe this results from induced CD in the two mutually perpendicular component transitions in the Soret band (the long wavelength B_x transition lies along a line connecting the H atoms of opposing pyrrole groups, Figure 5.9).[4] This observation of a split Cotton effect in induced CD for **7** has been observed in the intercalation of helical peptides and polymers.[4,5] In the case of the **3/7** complex, the two Cotton effects are not equivalent in rotational strength (Figure 5.8). Guest **8** also does not show the split induced CD for the Soret bands with either host **3** or

4 (Figures 5.10 and 5.11). We believe these observations to be the result of a much less specific binding orientation, where all guest orientations average to give a single induced CD band. The single induced CD band might also result from the host causing the porphyrin ring to bend out of the plane.

Guest	Host	λ_{max} free guest	λ_{max} for induced CD	$\Delta\varepsilon$ ($M^{-1}cm^{-1}$)	Rotational Strength (cgs)
5	P_S	439 nm	449 nm	-11.6	-7.8×10^{-39}
5	3_S	439 nm	ca 450 nm	$\Delta\varepsilon < 0$[a]	$R < 0$[a]
6	P_S	412 nm	422 nm	-18.8	-3.5×10^{-39}
6	3_R	412 nm	448 nm	-3.4	-7.4×10^{-40}
7[b]	P_R	424 nm	ca 432 nm	when $[P_R] > [7]$ $\Delta\varepsilon < 0$ when $[7] > [P_R]$ $\Delta\varepsilon > 0$	when $[P_R] > [7]$ $R < 0$ when $[7] > [P_R]$ $R > 0$
7	3_S	424 nm[c]	439 nm 419 nm	-145 +15.6	-1.5×10^{-38} $+2.0 \times 10^{-40}$
7	4_R	424 nm[c]	1:1 complex 447 nm 429 nm 1:2 complex 438 nm 419 nm	-18[d] +7[d] +96[d] -71[d]	-1×10^{-38} [d] $+5 \times 10^{-40}$ [d] $+7 \times 10^{-39}$ [d] -9×10^{-39} [d]
8[b]	P_R	424 nm	e	e	e
8	3_S	414 nm	418 nm	-38.9	-2.5×10^{-39}
8	4_R	414 nm	421 nm	+153	$+9.2 \times 10^{-39}$

Table 5.2. Induced circular dichroism (ICD) observed in aqueous borate buffer with hosts P, 3, and 4.

[a]Consistent data is only obtained when [3] > [5]; under conditions of excess guest there is evidence for the formation of complexes of the general form HG_n where $n \geq 2$. [b]A binding constant was not obtained for this host-guest system, thus ICD is qualitative only. [c]Soret band of porphyrin, ICD resolves it into the two component bands. [d]Given the inaccuracy in the binding constants for this host-guest system (see discussion), the values given here are approximate. [e]No ICD was detectable for this guest with Host **P**; while it is tempting to assume this transition has $\Delta\varepsilon \approx 0$ and $R \approx 0$, it should be noted that the ICD may have been undetectable under the conditions of our studies. Bathochromic shifting of the guest absorption band is, however, observed (Table 5.1).

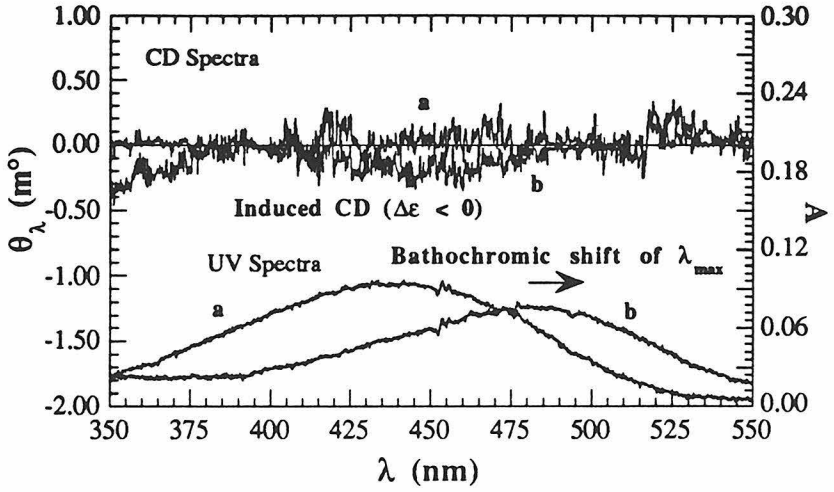

Figure 5.5. CD and visible spectra of guest 5 (3.69×10^{-6} M) in the absence (a) and in the presence (b) of host 3_S (2.14×10^{-5} M) in aqueous borate buffer (pH 9).

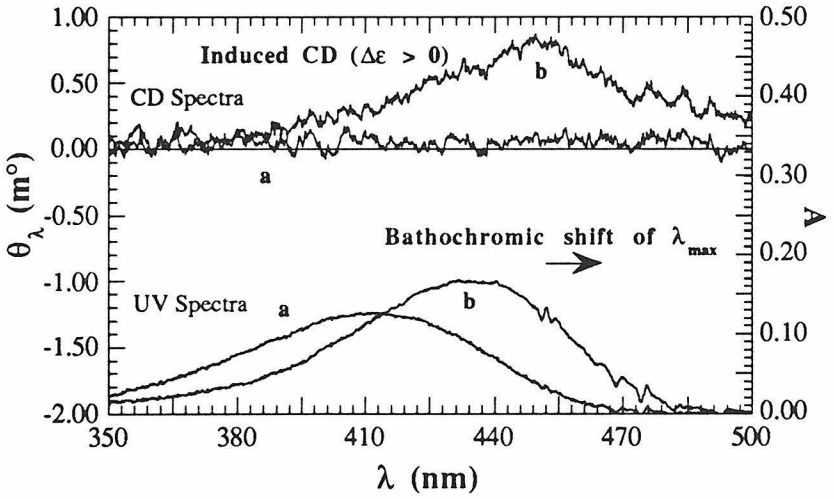

Figure 5.6. CD and UV/visible spectra of guest 6 (7.18×10^{-6} M) in the absence (a) and in the presence (b) of host 3_S (1.53×10^{-5} M) in aqueous borate buffer (pH 9).

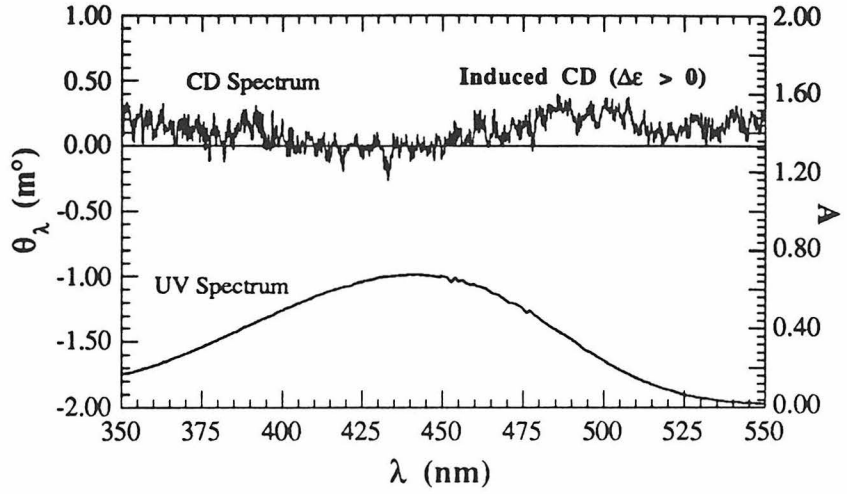

Figure 5.7. CD and visible spectra of guest **5** (7.64×10^{-7} M) in the presence of a limiting concentration of host 3_S (1.26×10^{-5} M) in aqueous borate buffer (pH 9).

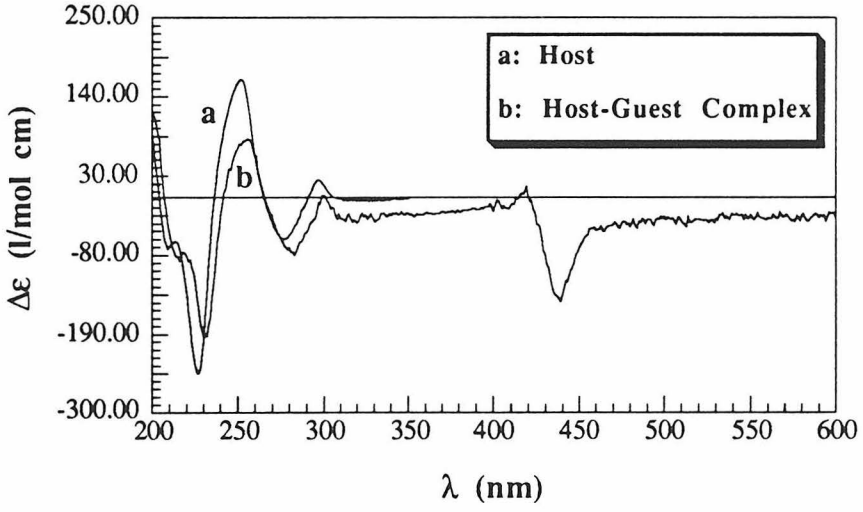

Figure 5.8. CD spectrum of host 3_S and fitted spectrum of its complex with guest **7** in aqueous borate buffer (pH 9).

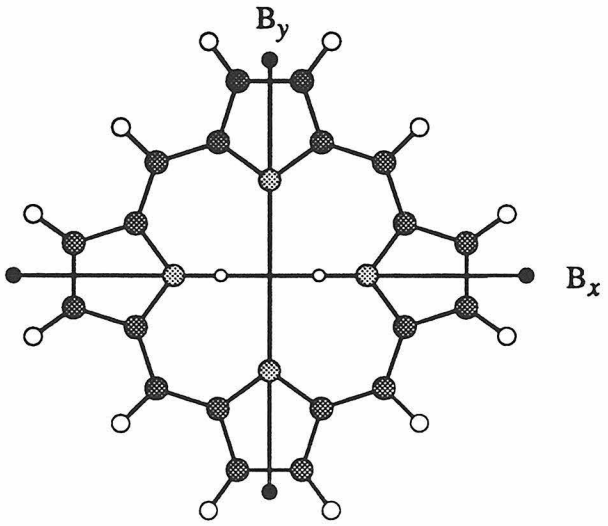

Figure 5.9. Transition moments for the porphyrin Soret band. The transition moments shown were obtained from an INDO/S[6] calculation of AM1[7] optimized porphyrin.

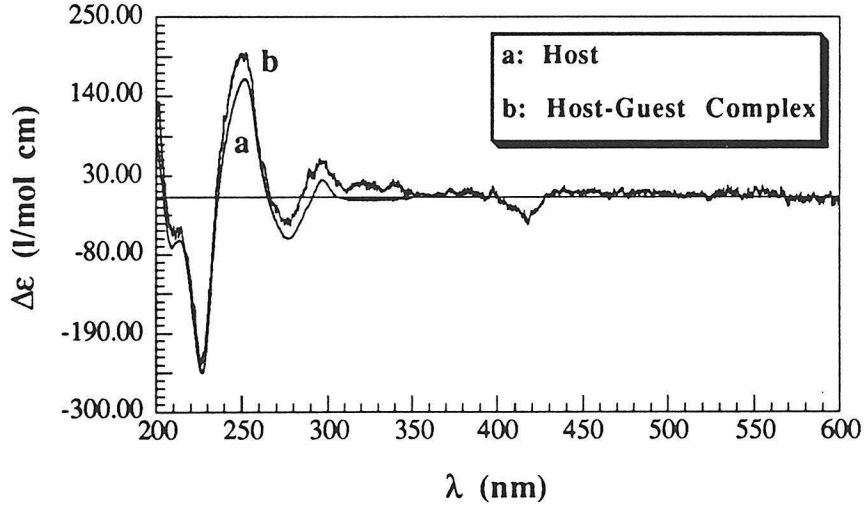

Figure 5.10. CD spectrum of host 3_S and fitted spectrum of its complex with guest 8 in aqueous borate buffer (pH 9).

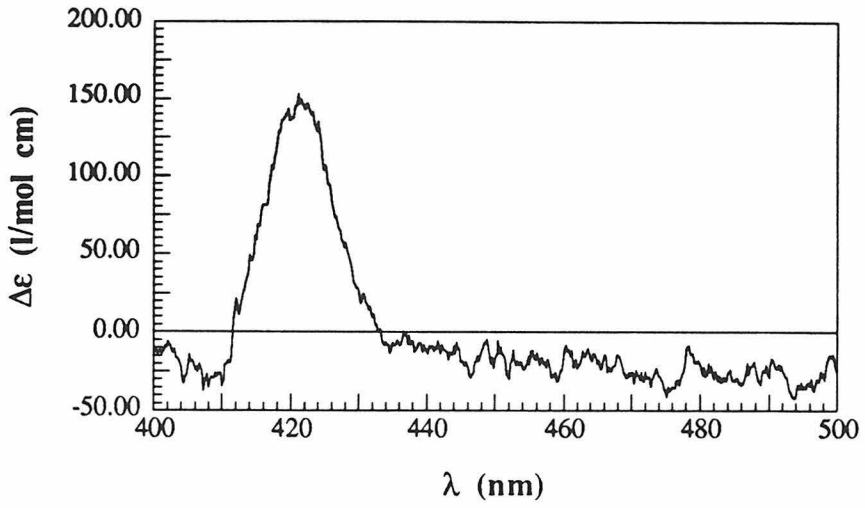

Figure 5.11. Fitted CD spectrum of the host 4_R complex with guest 8 in aqueous borate buffer (pH 9).

With the **4/7** system two distinct spectral patterns are observed, depending on whether one is under conditions of excess host or excess guest (Figure 5.12).[2] In the case of excess host, the expected split Cotton effect is observed as with **3**, but the rotational strengths of the two bands are more equally matched. Under conditions of excess guest, the Cotton effect changes sign and is blue shifted relative to the excess host induced CD bands. Mol ratio and Job plots[8] of this data suggest a 1:2 host:guest complex is forming (Figures 5.13 and 5.14). The discreet signals between 1:1 and 1:2 complexes suggest a specific orientation for the porphyrins in the cavity of **4**.[2]

The binding constants given for the **4/7** complex in Figure 5.4 are only approximate. The 1:1 number comes from data fitting (using CDfit)[2] a series of solutions in which only the spectral features of curve a in Figure 5.12 were evident. Starting from the 1:1 complex and assuming all host was initially present as the complex, a series of solutions for which the spectral features of curve b were evident were then fitted assuming formation of a 2:1 complex. The fitting gave $-\Delta G^\circ$ = 8.8 kcal/mol for the second association. This gives an overall formation constant of 17.4 kcal/mol for the 2:1 complex. Given the approximations involved in the analysis, however, these values should be

considered as only estimates. The results do indicate a cooperative process is occurring in the formation of the higher order complex.

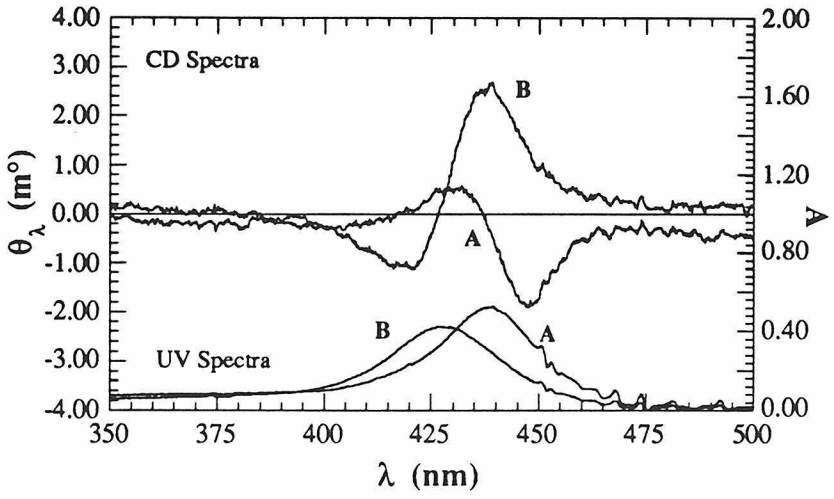

Figure 5.12. CD and visible spectra of guest 7 (2.97×10^{-6} M) in the presence of 8.01×10^{-6} M host 4_R (A, 1:1 complex) and in the presence of 8.90×10^{-5} M host 4_R (B, 2:1 complex) in aqueous borate buffer (pH 9).

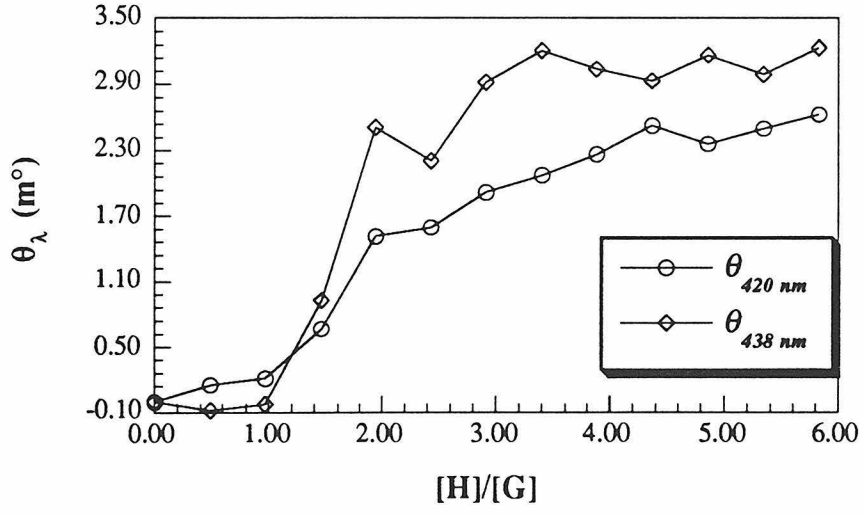

Figure 5.13. Mol ratio plot for binding of guest 7 by host 4_R in aqueous borate buffer (pH 9).

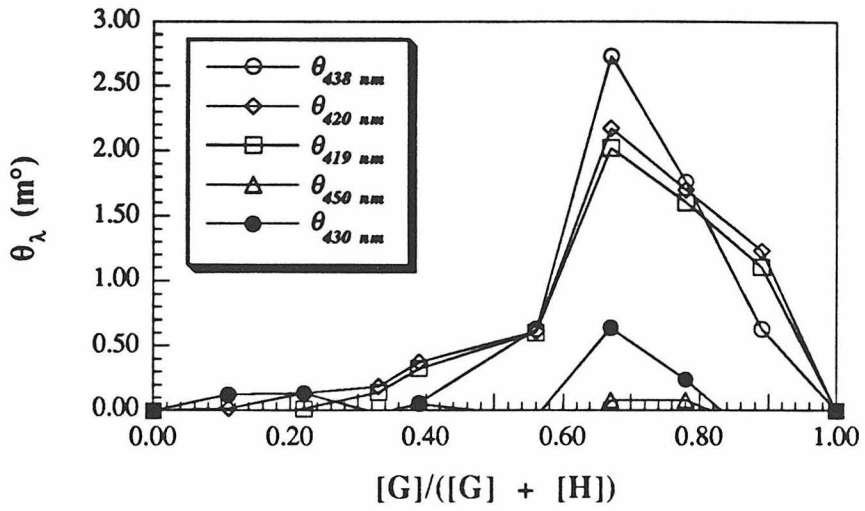

Figure 5.14. Job plot[8] for binding of guest 7 by host 4_R in aqueous borate buffer (pH 9). ([G] + [H] = 4.00 × 10^{-6} M)

It should be noted that the aggregation state of guest **7** in aqueous solution is not clear. The literature contains several conflicting reports in regard to this porphyrin, with different authors claiming it exists exclusively as monomer,[9] exclusively as dimer,[10] or as monomer in equilibrium with dimer[11] under the concentration range we studied. CDfit is unable to account for this aggregation, but our data shows good agreement with our model. This leads us to believe that the monomer predominates under our experimental conditions. Consideration of a monomer-dimer equilibrium (using a dimerization constant of $K_D = 1 \times 10^5$ M^{-1})[11] and data fitting by the Benesi-Hildebrand method[12] gives $-\Delta G° = 6.9$ kcal/mol for the **3/35** complex. Benesi-Hildebrand treatment of the **3/7** data without accounting for the monomer-dimer equilibrium gives a value of 7.3 kcal/mol. Guest **8** has also been reported to dimerize ($K_D = 6 \times 10^3$ M^{-1}).[11] These observations may result in additional error in the reported binding constants for **7** and **8** with host **4**.

Like **3/8** the **4/8** system shows only a single induced CD band (Figure 5.11). With **8** host **4** is certainly capable of binding two guests (as per guest **7**), but electrostatic repulsions from the high number of negative charges present in both host and guest are thought to keep the complex at a 1:1 stoichiometry.

Guest **8** is significant because our hosts, as a rule, do not bind anionic species. We rationalize the binding of **8** to host **3** and **4** by a cation-π effect with the electron deficient (positive) face of the porphyrin ring. This binding of the porphyrin, but not the phenylsulfonate substituents, is supported by NMR experiments in 10% CD_3CN/90% Borate-*d* (a solvent that decreases aggregation)[1a] involving **3/8**. These studies have shown weak downfield shifting of the phenylsulfonate protons–not the strong upfield shifting expected for encapsulation in an aromatic rich cavity. The interaction of host with the electron deficient region of an anionic guest represents a novel cation-π effect previously unobserved in our studies of this phenomena. The relative *D* values for guest **8** from these NMR experiments are given in Figure 5.15.

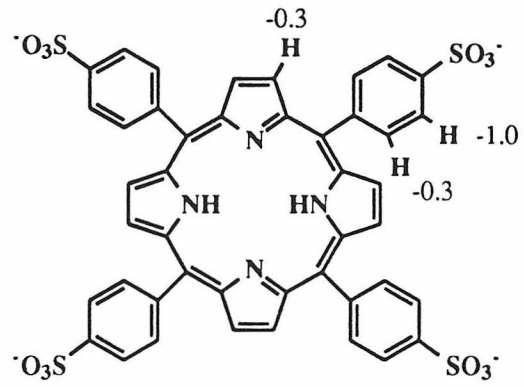

Figure 5.15. Relative *D* values from ^1H NMR studies of guest 8 with host 4_R in 10% CD_3CN/90% borate-*d*.[13] *D* < 0 represents a down-field shift of the NMR signal on binding.

The porphyrin guests are also unusual in that they show an extremely high propensity not only for self-association, but also for association into tightly bound ion-pairs with certain oppositely charged ions.[14] The prototypical ion-pair of this type is the porphyrin dimer formed from a cationic and an anionic porphyrin (such as between **7** and **8**).[14] This overall neutral **7/8** ion-pair is believed to be very stable in aqueous solution.[14] Given the highly favorable formation of a 1:2 complex with host **4** and guest **7**, several attempts were made at complexation of a neutral **7/8** dimer. In these experiments, host was

added to solutions containing 1:1 mixtures of the two porphyrins, which were expected to exist primarily as neutral dimers;[14] Figure 5.16 and 5.17 illustrate the visible spectra associated with these porphyrins in the presence and absence of host. Guest **7** appears to interact much more strongly with host **4** than with guest **8**; as seen in Figure 5.17 the visible absorption band associated with the **7/8** dimer begins to break up into the component **7** and **8** absorptions as host is added. The observed ICD in these experiments also supports the preferential formation of the **4/7** complex, not the encapsulation of the neutral porphyrin dimer (Figure 5.17).

Likewise, anions such as host **P** and the non-macrocyclic **9** (Figure 5.18) also show strong interaction with these porphyrins (Figures 5.19 and 5.20). With host **P**, the sign of the induced CD is inconsistent at high and low host:guest ratios (Table 5.2). This is thought to be the result of non 1:1 stoichiometric complexes forming under conditions of excess host. Such 2:1 host:guest complexes have been observed with tetracationic porphyrins and cyclodextrin hosts; in some instances the complexes are stable enough to

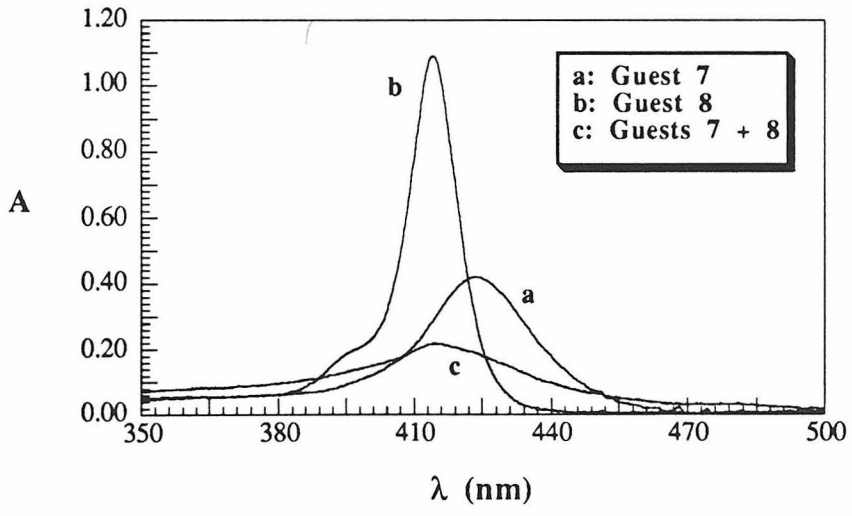

Figure 5.16. Visible absorption spectra of solutions 2.26 × 10^{-6} M in guest 7 (a), 2.26 × 10^{-6} M in guest 8 (b), and 1.13 × 10^{-6} M in both guests (c) in aqueous borate buffer (pH 9).

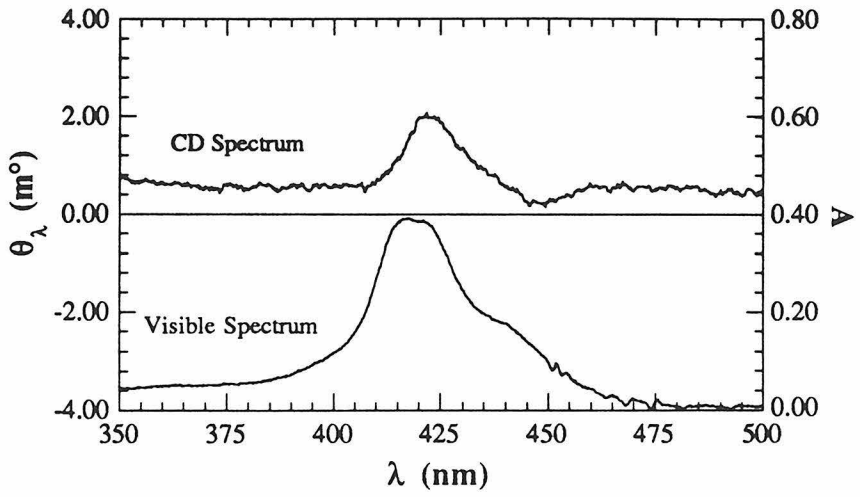

Figure 5.17. CD and visible absorption spectra of a solution containing 7 (1.13×10^{-6} M), 8 (1.13×10^{-6} M), and host 4_R (6.75×10^{-6} M) in aqueous borate buffer (pH 9).

isolate by chromatography.[15] With **9**, a molecule that normally shows no interaction with the guests bound by host **P**, a split Cotton effect is observed for the induced CD. Again this is thought to be the result of non 1:1 stoichiometries. The sign of this split signal remains the same at both high and low ratios of **9**:**7**. Given the difficulties associated with the quantitation of such complexes, further studies were not pursued.

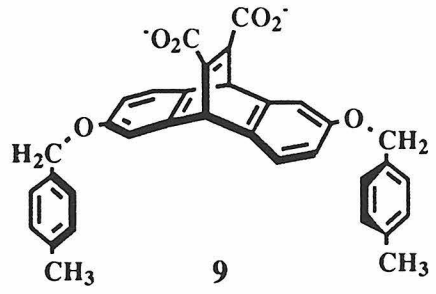

9

[(*R*, *R*)-Stereochemistry of ethenoanthracene unit shown]

Figure 5.18. Non-macrocyclic molecule that normally shows no interaction with the guests bound by host P.

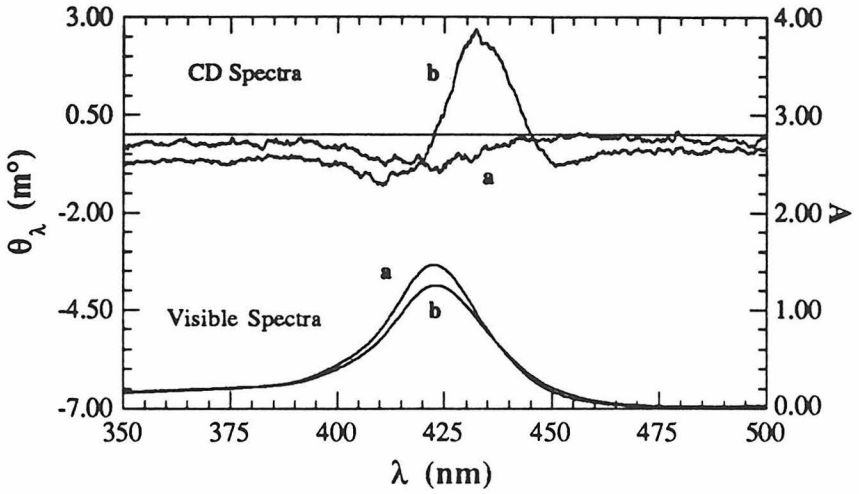

Figure 5.19. CD and visible absorption spectra of guest 7 (7.20×10^{-6} M) in the absence (a) and in the presence (b) of host P_R (1.26×10^{-6} M) in aqueous borate buffer (pH 9).

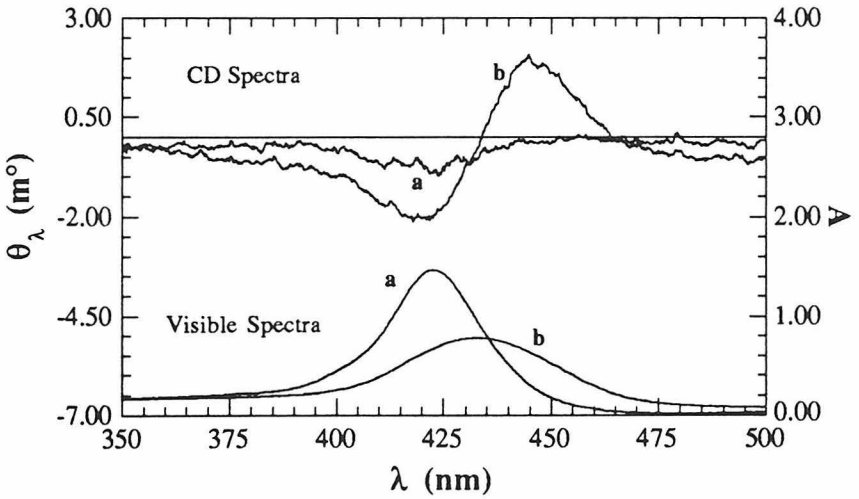

Figure 5.20. CD and visible absorption spectra of guest 7 (7.18×10^{-6} M) in the absence (a) and in the presence (b) of 9_R (1.60×10^{-5} M) in aqueous borate buffer (pH 9).

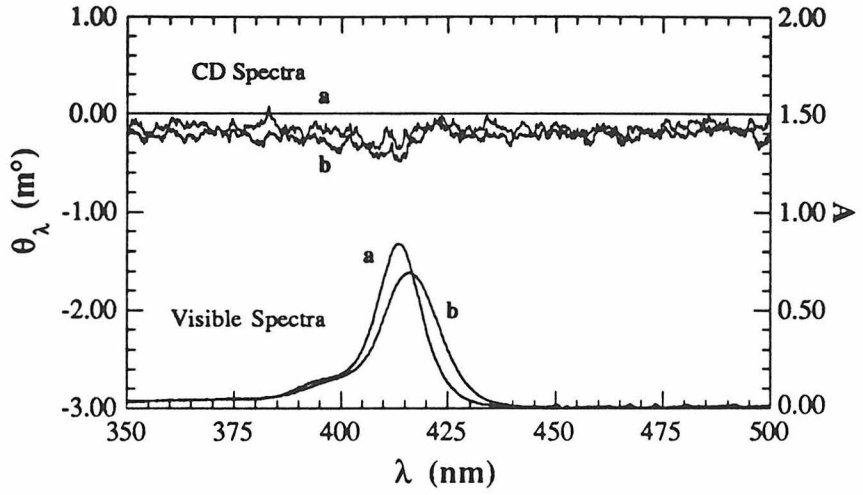

Figure 5.21. CD and visible absorption spectra of guest 8 (1.68×10^{-6} M) in the absence (a) and in the presence (b) of host P_R (1.77×10^{-5} M) in aqueous borate buffer (pH 9).

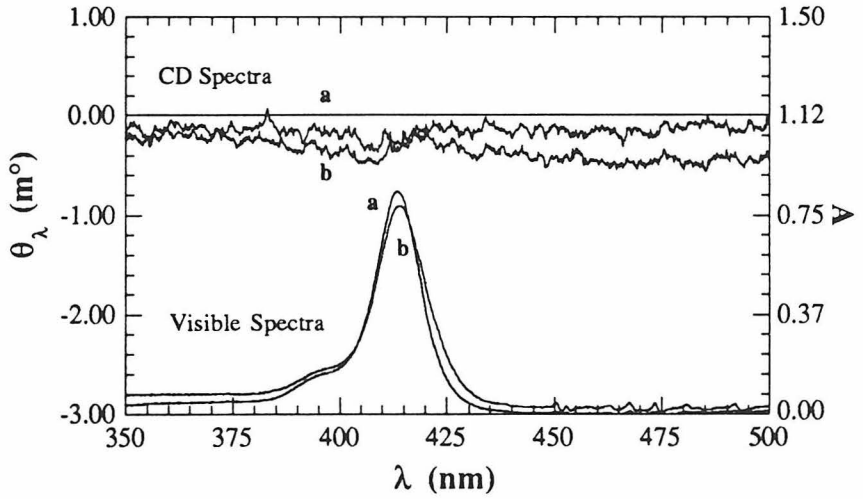

Figure 5.22. CD and visible absorption spectra of guest 8 (1.68×10^{-6} M) in the absence (a) and in the presence (b) of 9_R (1.28×10^{-5} M) in aqueous borate buffer (pH 9).

Guest **8** also shows interaction with both **P** and **9** (Figures 5.21 and 5.22). No ICD was detected in either interaction, but changes in the visible absorption bands of the guest are clearly evident in the presence of both **P** and **9**. Given the absence of ICD, these interactions appear to be much weaker than those with guest **8**.

5.3 Guests Showing Unusual Behavior with Host P

5.3.1 Introduction

In Chapters 2-4 the host-guest complexes of host **P** exhibited exclusively 1:1 stoichiometries. However, the host is capable of forming higher order complexes, as has been described with the porphyrin guest **8**. A number of studies carried out with host **P** gave inconclusive data, and some of these studies appear to illustrate the formation of complexes with non 1:1 stoichiometries. The observations of higher order complexes, with the larger hosts **3** and **4**, brought to light some of the spectral changes to be expected from the formation of such higher order complexes, and many of these spectral changes were observed with the guests shown in Figure 5.23 on interaction with host **P**. This section describes observations of the formation of non 1:1 stoichiometries with host **P**.

5.3.2 Picrate Anion

Given the observations of anionic hosts binding the electron deficient anionic guest **8**, it appeared that the picrate anion (**10**, a highly electron deficient anion) might be bound by host **P**. Preliminary studies with **P** and **10** gave no detectable ICD in the guest long-wavelength absorption band, but increased magnitude in the host shorter-wavelength Cotton effects was observed (Figure 5.24). Several experiments were run, but in no case was data obtained that gave good fitting results with CDfit. This may be due in part to a

very low binding constant ($-\Delta G°_a < 4.5$ kcal/mol) or to a non 1:1 stoichiometry. A non 1:1 complex is supported by the increase in magnitude of host lower wavelength Cotton effects, a spectral change characteristic of the toroid conformation of the host (Chapter 3). CPK models indicate that such a conformation is capable of binding two picrate anions, while a 1:1 complex is expected to occur with the rhomboid conformation of the host. Alternatively, the spectral changes could arise from ICD in shorter wavelength guest absorptions. In either case, the data support the observation of a cation-π effect with a highly electron deficient anionic guest.

Binding a picrate dimer is a distinct possibility for explaining the observed results, as guest **10** is known to dimerize in both aqueous and organic media.[16] However, the data obtained in these studies have not allowed quantitative interpretation.

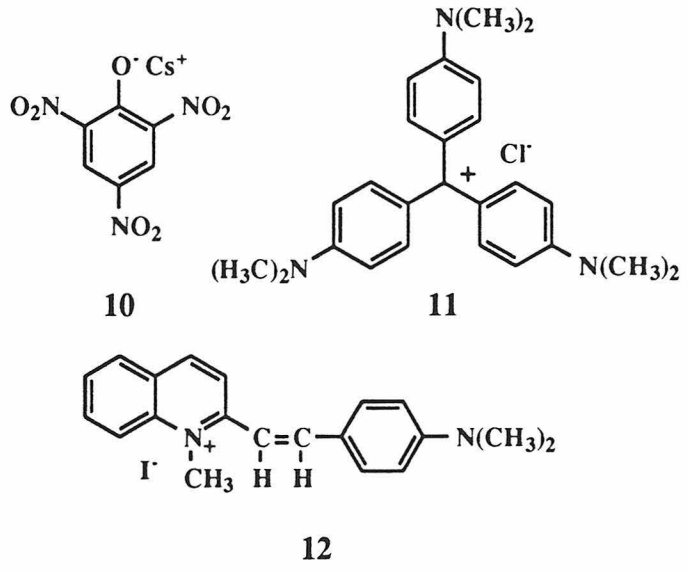

10 **11**

12

Figure 5.23. Guests showing unusual behavior with host P.

5.3.3 Cationic Dyes

Dyes **11** and **12** show bathochromic shifting of absorption bands and ICD ($\Delta\varepsilon < 0$ with P_S) on interaction with host **P**, as expected for dye guests (Figures 5.25 and 5.26).

Contrary to what is observed with other dyes in the presence of excess host, however, guests **11** and **12** show decreasing magnitudes of ICD bands relative to conditions of equivalent and excess guest concentrations (Figure 5.27). The data from studies of crystal violet (**11**) were most amenable to interpretation; Figure 5.27 shows a mol ratio plot of this data. Examining the data up to the point where the largest observed ICD magnitude occurs, it appears that a 2:1 host:guest complex is forming. A similar stoichiometry is thought to occur with **12**, although the data are not as clear.

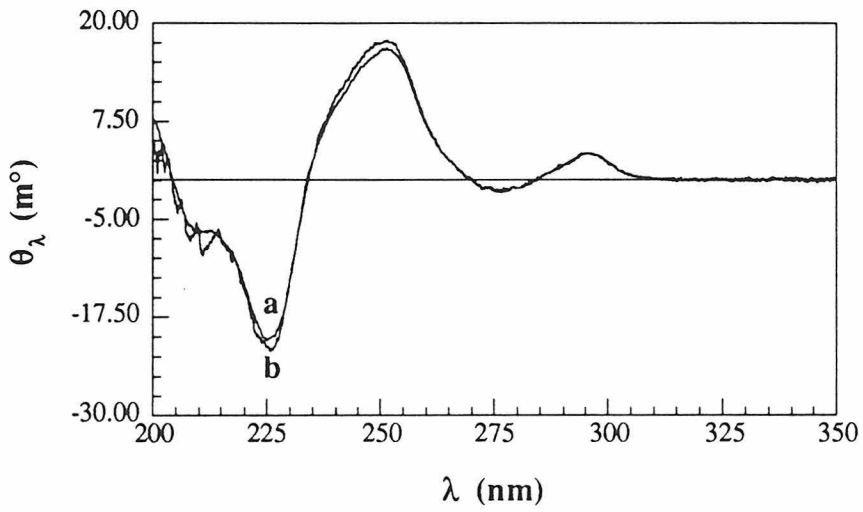

Figure 5.24. CD spectra of host P_S (3.3×10^{-6} M) in the absence (a) and in the presence (b) of guest 10 (1.17×10^{-4} M) in aqueous borate buffer (pH 9).

An interesting effect is noticed with solutions of **11** and **P**. In borate buffer, dye **11** decomposes over the course of a few days as evidenced by a loss of color and formation of a precipitate. When the solution contains host **P** though (the host does not need to be in excess), the dye remains stable in solution for a prolonged period of time (as of this writing a five year old solution is still vividly purple in color). The fading of the crystal violet dye is believed to occur through formation of the more photosensitive carbinol

(13, Figure 5.28).[17] Even under conditions of fast-exchange, it appears that encapsulation by host **P** helps to prevent this reaction from occurring.

Additionally, studies with **9** show interaction with dye 12 (Figure 5.29). The ICD signal is weak and bisignate, indicative of multiple dye chromophores.[18] Aggregation of

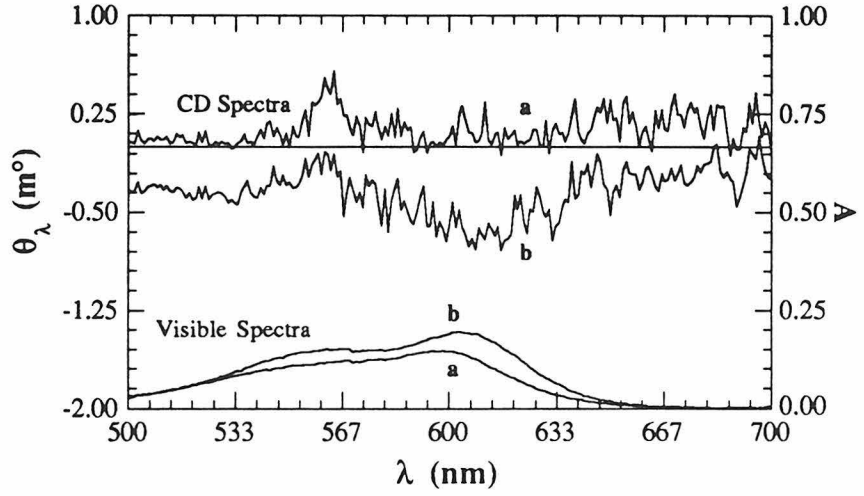

Figure 5.25. CD and visible absorption spectra of guest 11 (3.27×10^{-6} M) in the absence (a) and in the presence (b) of host P_S (4.00×10^{-6} M) in aqueous borate buffer (pH 9).

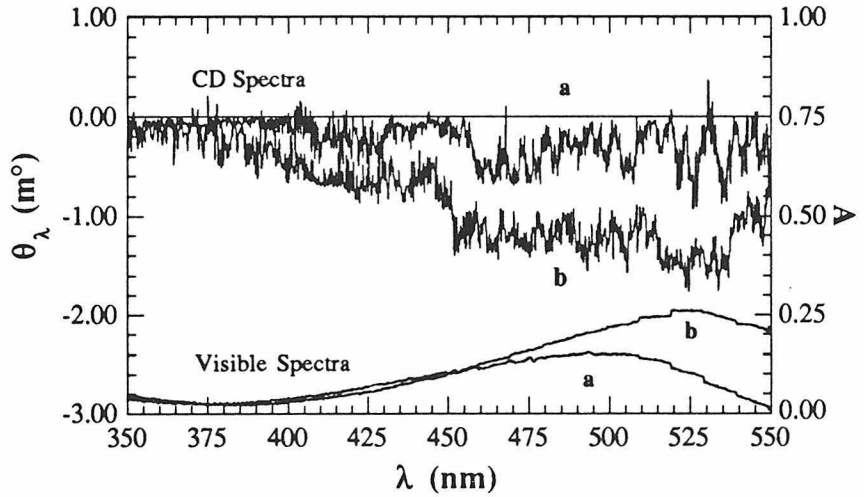

Figure 5.26. CD and visible absorption spectra of guest 12 (5.89×10^{-6} M) in the absence (a) and in the presence (b) of host P_S (6.40×10^{-6} M) in aqueous borate buffer (pH 9).

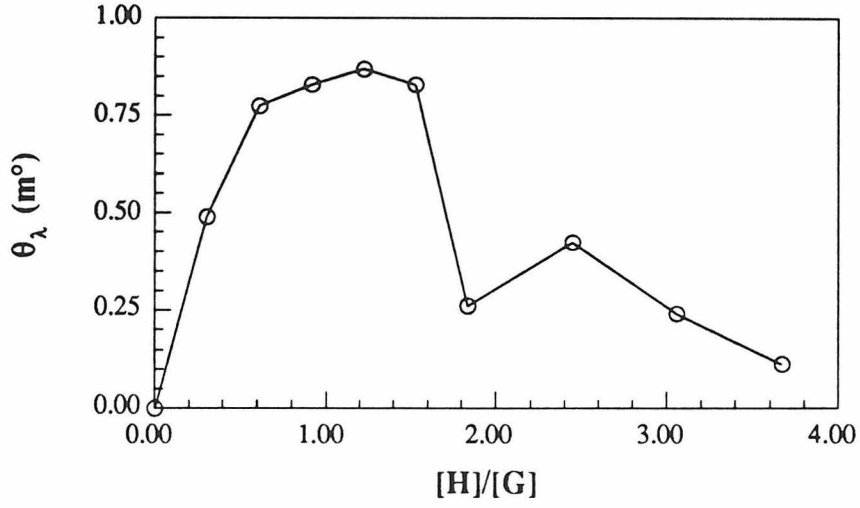

Figure 5.27. Mol ratio plot for binding of guest 11 by host P_S in aqueous borate buffer (pH 9).

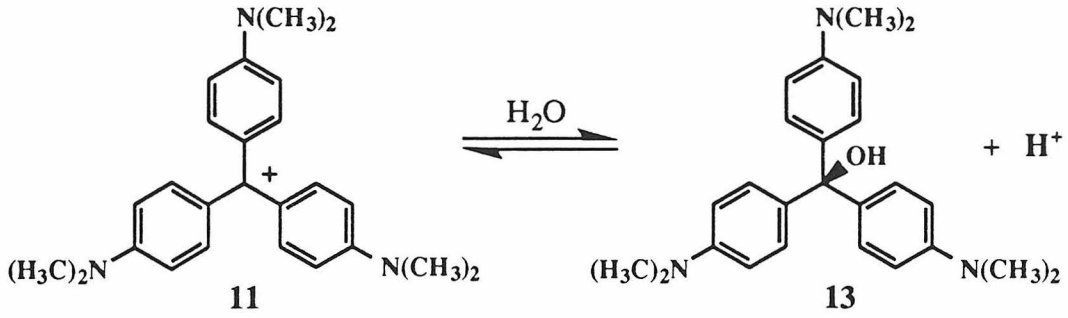

Figure 5.28. Carbinol formation from guest 11.[17] The carbinol is much more prone to photobleaching than 11 itself.[17]

dyes like **11** and **12** is known to occur at low concentrations in aqueous media, but reported CAC's suggest that this is most likely to occur only at concentrations above 10 μM.[17] Our studies suggest that for guest **12** our hosts may help to induce dye aggregation at lower concentrations, possible as a result of the formation of complexes with non 1:1 stoichiometries.

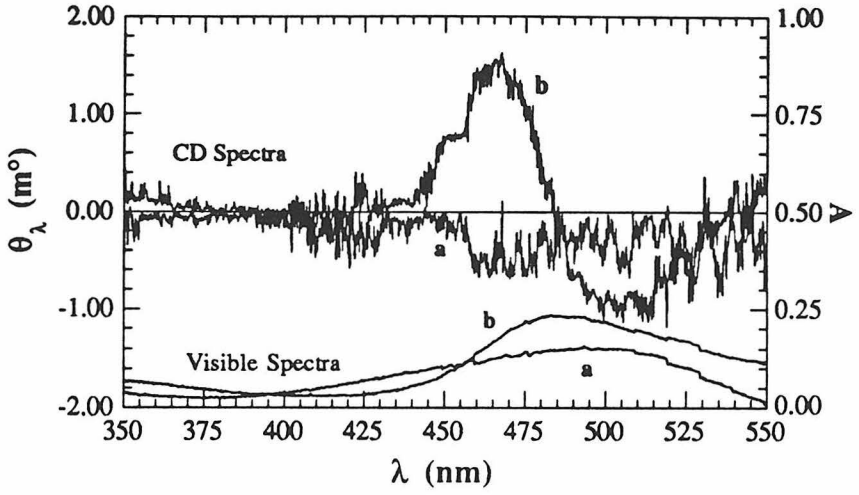

Figure 5.29. CD and visible absorption spectra of guest 12 (5.89×10^{-6} M) in the absence (a) and in the presence (b) of 9_R (4.60×10^{-5} M) in aqueous borate buffer (pH 9).

5.4 Conclusions

The studies of oligomers of host **P** demonstrate the application of our circular dichroism methodology to hosts other than **P** itself. It was shown that the larger, less conformationally restricted hosts **3** and **4**, are capable of binding guests but tend to show lower affinities for these guests than host **P**. The larger cavities of these hosts also provide the ability to bind several guests allowing the formation of higher order complexes. The spectral changes associated with the appearance of these higher order complexes are often associated with reversal of sign of induced circular dichroism signals. Several guests have also shown such anomalous spectral behavior (and higher order complex formation) with host **P** itself.

The studies described here also illustrate the first examples of anion binding by the Dougherty group anionic cyclophane hosts. These hosts normally bind electron deficient neutral and cationic molecules, but studies with guests **8** and **10** illustrate that given a

sufficiently electron poor anion binding interactions will occur. Guest **10** is interesting because it appears that a 1:2 host:guest complex may occur with host **P**.

5.5 Experimental Section

5.5.1 General Methods

CD spectra were recorded on a JASCO J-600 Spectropolarimeter with a 1.0 cm pathlength quartz cell. A standard set of measurement parameters was used in all quantitative experiments: Band Width 1.0 nm, Sensitivity 50 m°/cm, Time Constant 1.0 Sec., Scan Speed 50 nm/min., Step Width 0.2 nm/point, and a minimum of 4 accumulations. Electrospray mass spectrometry was performed at the UC Berkeley mass spectrometry center. ^{1}H NMR spectra were recorded on a Bruker AM-500 spectrometer; routine spectra were referenced to the residual proton signals of the solvents and are reported in ppm downfield of 0.0 as δ values.

All solvents used in spectroscopy were spectrophotometric or HPLC grade. Aqueous cesium borate buffer (pH 9) was prepared by dissolving 0.25 g high purity boric oxide in 800 g water and adding 3.74 ml of 1 M CsOH followed by thorough mixing. The water used in these preparations was passed through a Milli-Q purification system.

Circular dichroism binding studies are described in Chapter 2 of this manuscript.[2] Qualitative detection of induced CD was done using excess concentrations of the appropriate host and/or control molecule with the guest of interest. For these studies the standard measurement parameters were often varied to provide conditions with the highest sensitivity.

Fitting CD data from acetonitrile solutions of **P** tetraacid to $\Delta\varepsilon$ values for the 230-350 nm region of $\mathbf{P_E}$ in CH_3CN provided estimates of purity of samples of the tetraacid. Calibration studies with **P** stock solutions in cesium borate prepared by weighing out

samples of the tetraacid (with "known purity") produced nearly identical $\Delta\varepsilon$ values to the studies with NMR standardized stock solutions. This method of $\Delta\varepsilon$ determination was used for **3**, and **4**. The method was also used to determine purity of samples of **9**.

The ε values for the UV/Visible absorption spectra of host-guest complexes come from spectra of solutions containing known amounts of host and guest; using previously measured binding constants. The host-guest complex spectrum was calculated from the measured spectrum, as described in the experimental section of Chapter 2.

Some binding constants reported in this chapter were determined from the Benesi-Hildebrand method.[12] In such cases, an intial guess of the binding constant was used to estimate the equilibrium concentrations of the free species and this number optimized by repeated iterations until the best fitting plot was obtained. The application of the Benesi-Hildebrand method is given in Appendix 1 (Section 5.6).

All reactions, unless otherwise noted, were stirred magnetically under nitrogen atmosphere. Solvents were distilled from drying agents under argon atmosphere; acetonitrile, CaH_2; THF, sodium benzophenone ketyl. Ion exchange for NH_4^+ was carried out with Dowex® 50w-x2 cation exchange resin (the resin was treated with concentrated ammonium carbonate then washed with Milli-Q purified water before use). Unless otherwise noted reagents obtained from commercial sources were used without further purification.

Compounds **P**, **1**, **2**, $\mathbf{3_E}$, and $\mathbf{4_E}$ were prepared by procedures described previously.[1] The synthesis of control molecule **9** is described in Chapter 2.[2] All other compounds were obtained commercially and used as obtained, except **8** which was purified by ion-exchange (Dowex® 50w-x2 cation exchange resin, H^+ form), and **10** which was prepared in our laboratories.[19]

5.5.2 Synthesis

(9*S*, 10*S*, 9'*S*, 10'*S*, 9''*S*, 10''*S*)-3-Hexaacid. In a 25 ml flask 0.016 g (1.17×10^{-5} mol) $\mathbf{3_{SE}}$ was dissolved in 8 ml THF, followed by addition of 0.057 g (3.79×10^{-4} mol) cesium hydroxide and 2 ml water. The mixture was allowed to stir in the dark at room temperature overnight and the THF removed by rotary evaporation. The aqueous mixture was frozen to -78 °C and lyophilized to give an off-white powder that was dissolved in water and ion-exchanged for NH_4^+. The ion-exchanged solution was frozen at -78 °C and lyophilized to give 0.026 g of an off-white powder (59.7% pure by CD, impurities were inorganic salts and water). ^{1}H NMR (10% CD_3CN/90% Borate-*d*) δ (ppm) 7.32 (s, 12H), 7.19 (d, 6H), 7.03 (d, 6H), 6.55 (dd, 6H), 5.20 (s, 6H), 5.09 (s, 12H). CD [(9*S*, 10*S*, 9'*S*, 10'*S*, 9''*S*, 10''*S*)-enantiomer, pH 9 borate buffer] λ (Δε) [nm ($M^{-1}cm^{-1}$)], 297 (+24.6), 277 (-57.5), 252 (+165), 227 (-245), 209 (+70.5).

(9*R*, 10*R*, 9'*R*, 10'*R*, 9''*R*, 10''*R*, 9'''*R*, 10'''*R*)-4-Octaacid. In a 25 ml flask 0.016 g (1.17×10^{-5} mol) $\mathbf{4_{RE}}$ was dissolved in 12 ml THF, followed by addition of 0.057 g (3.79×10^{-4} mol) cesium hydroxide and 3 ml water. The mixture was allowed to stir in the dark at room temperature overnight and the THF removed by rotary evaporation. The aqueous mixture was frozen to -78 °C and lyophilized to give an off-white powder that was dissolved in water and ion-exchanged for NH_4^+. The ion-exchanged solution was frozen at -78 °C and lyophilized to give 0.030 g of an off-white powder (67.2% pure by CD, impurities were inorganic salts and water). ESMS (anion mode, material in borate buffer) *m/e* 212 (M^{8-}). CD [(9*R*, 10*R*, 9'*R*, 10'*R*, 9''*R*, 10''*R*, 9'''*R*, 10'''*R*)-enantiomer, pH 9 borate buffer] λ (Δε) [nm ($M^{-1}cm^{-1}$)], 297 (-39.1), 277 (+60.0), 252 (-224), 227 (+289), 211 (+85.0).

5.5.3 CD Data for Previously Reported compounds

3_E. [(9*R*, 10*R*, 9'*R*, 10'*R*, 9"*R*, 10"*R*)-enantiomer, CH_3CN] λ (Δε) [nm ($M^{-1}cm^{-1}$)], 320 (+4.6), 298 (-11.4), 285 (+23.7), 251 (-207), 228 (+360), 207 (+145).

4_E. [(9*S*, 10*S*, 9'*S*, 10'*S*, 9"*S*, 10"*S*, 9"'*S*, 10"'*S*)-enantiomer, CH_3CN] λ (Δε) [nm ($M^{-1}cm^{-1}$)], 319 (-12.0), 300 (+2.3), 285 (-52.7), 251 (+224), 229 (-406), 207 (-167).

5.6 Appendix 1: Determination of 1:1 Binding Constants by the Benesi-Hildebrand Method

If the equilibrium concentration of unbound guest is known for a given spectrum, a Benesi-Hildebrand plot can be used to determine the 1:1 equilibrium constant, *K*, from circular dichroism data at a given wavelength using equation 5.1,[12]

$$\frac{l}{\Delta\theta_\lambda} = \frac{1}{[H]_o K \Delta\varepsilon_{11}[G]} + \frac{1}{[H]_o \Delta\varepsilon_{11}} \qquad (5.1)$$

where *l* is the pathlength of the cell; $\Delta\theta_\lambda$ is the change in observed ellipticity at wavelength λ, for a solution containing guest (G) with total host concentration, $[H]_o$ (M) compared to a solution containing only host at concentration $[H]_o$; [G] is the equilibrium concentration (M) of free guest; and $\Delta\varepsilon_{11}$ is defined by equation 5.2 (the difference between the host-guest complex optical constant, $\Delta\varepsilon_{HG\lambda}$, and the free component optical constants).[12]

$$\Delta\varepsilon_{11} = \Delta\varepsilon_{HG\lambda} - \Delta\varepsilon_{H\lambda} - \Delta\varepsilon_{G\lambda} \qquad (5.2)$$

A plot of $l/\Delta\theta_\lambda$ vs 1/[G] provides a straight line with *K* equal to the ratio *y*-intercept/slope and $\Delta\varepsilon_{11}$ = 1/($[H]_o$*y*-intercept).[12] Equations 5.1 and 5.2 describe the situation where the

concentration of host is held constant over a range of guest concentrations, where $[G]_o > [H]_o$ in each solution.[20] Experiments run with guest as the minor component and $[G]_o$ held constant over a range of host concentrations require appropriate rewriting of the equations. The equations can be used with UV/Visible absorption data as well by replacing θ_λ with A_λ and $\Delta\varepsilon_i$ with ε_i.

5.7 Appendix 2: Estimation of Equilibrium Concentrations

In the studies described in this Chapter, there was no immediate way to obtain the equilibrium concentrations of free species from the spectra. In order to apply the Benesi-Hildebrand analysis,[12] a binding constant had to be assumed and the equilibrium concentrations calculated. Repeated iterations were then used to obtain the best-fit binding constant.

In addition, a number of similar treatments were applied to the higher order equilibria described in the Chapter. Although the treatments of higher order complexes were generally unsuccessful, their applications resulted in the derivations of equations that can be used to estimate equilibrium concentrations of solution components from assumed or known binding constants. Excel[21] was used in the applications of these equilibria relationships, and spreadsheets were created that computed the concentrations from the input total host and guest concentrations and equilibrium constants.

This appendix lists the mathematical relationships that can be used for the estimation of equilibrium concentrations based on known or assumed equilibrium constants. They are given here for reference if studies of the non 1:1 stoichiometries are pursued in future work. All relationships are derived from the determination of the concentration of free guest (G), and in all cases $[H]_o$ and $[G]_o$ represent the total host and total guest concentrations respectively, where at equilibrium

$$[H]_o = [H] + \sum_{n=1}^{n=N} [HG_n] \tag{5.3}$$

$$[G]_o = [G] + \sum_{n=1}^{n=N} n\,[HG_n] \tag{5.4}$$

In the case of guest self-association (only dimerization, m = 2, is considered in this appendix), equation 5.4 becomes

$$[G]_o = \sum_{m=1}^{m=M} m\,[G_m] + \sum_{n=1}^{n=N} n\,[HG_n] \tag{5.5}$$

For a system containing host and guest that form complexes up to HG_n and where the guest self-associates into dimers (G_2), the equilibrium relationships are

$$K_n = \frac{[HG_n]}{[HG_{n-1}][G]} \tag{5.6}$$

$$K_D = \frac{[G_2]}{[G]^2} \tag{5.7}$$

The equilibrium free guest concentration, [G], is obtained from the solution of the polynomial equation,

$$0 = [G]_o + \sum_{n=1}^{n=N} \beta_n[G]_o - n\beta_n[H]_o - \beta_{n-1} - 2K_D\beta_{n-2} \tag{5.8}$$

where β_n is defined by equation 5.9 (for $n \geq 1$), with $\beta_0 = 1$ and $\beta_{-1} = 0$.

$$\beta_n = \prod_{n=1}^{n=N} K_n \tag{5.9}$$

For the case where the highest order complex is HG ($K_n = 0$, $n > 1$) and guest self-association is negligible ($K_D = 0$), equation 5.8 reduces to the quadratic

$$0 = (K_1[G]_o - K_1[H]_o - 1)[G] - K_1[G]^2 + [G]_o \tag{5.10}$$

Quadratic equations are easily solved, but for higher order equilibria equation 5.8 has the general form

$$0 = x_1[G] + x_2[G]^2 + x_3[G]^3 + ...+ x_N[G]^N + [G]_o \qquad (5.11)$$

which can be solved iteratively using Newton's method,[22]

$$[G]_{n+1} = [G]_n - \frac{f([G]_n)}{f'([G]_n)} = [G]_n - \frac{x_1[G] + x_2[G]^2 + x_3[G]^3 + ...+ x_N[G]^N + [G]_o}{x_1 + 2x_2[G] + 3x_3[G]^2 + ...+ Nx_N[G]^{N-1} + [G]_o} \qquad (5.12)$$

basically after an initial guess of $[G]_n$, equation 5.16 is applied until $[G]_{n+1}$ and $[G]_n$ differ by an insignificant amount ($\pm$ 0.001%).

Once the equilibrium concentration of free guest is known, this can be used to find the equilibrium concentrations of the various host-guest complexes using equations 5.13 and 5.14, the mass balance relations (equations 5.3-5.5) can be used to determine the equilibrium values of [H] and [G_2].

$$[HG] = \frac{K_1[H]_o[G]}{1 + \sum_{n=1}^{n=N} \beta_n[G]^n} \qquad (5.13)$$

$$[HG_n] = \frac{\beta_n[HG][G]^{n-1}}{K_1} \qquad (5.14)$$

5.8 References and Footnotes

1. (a) Kearney, P. C.; Mizoue, L. S.; Kumpf, R. A.; Forman, J. E.; McCurdy, A.; Dougherty, D. A. *J. Am. Chem. Soc.* **1993**, *115*, 9907-9919. (b) Petti, M. A.; Shepodd, T. J.; Barrans, R. E., Jr.; Dougherty, D. A. *J. Am. Chem. Soc.* **1988**, *110*, 6825-6840.

2. Forman, J. E.; Barrans, R. E., Jr.; Dougherty, D. A.; *J. Am. Chem. Soc.* **1995**, *117*, 9213-9228.

3. (a) Volosov, A.; Woody, R. W.; in *Circular Dichroism-Principles and Applications*, Nakanishi, K.; Berova, N.; Woody, R. W. (eds); VCH, 1994, 59-84. (b) Rosini, C.; Zandomeneghi, M.; Salvadori, P. *Tetrahedron Asymmetry* **1993**, *4*, 545-554. (c) Charney, E.; *The Molecular Basis of Optical Activity-Optical Rotatory Dispersion and Circular Dichroism*, Robert E. Krieger Publishing Company: Malabar, FL, 1985. (d) Mason, S. F. *Molecular Optical Activity and the Chiral Discriminations*, Cambridge University Press: Cambridge, 1982. (e) Tinoco, I., Jr. *Adv. Chem. Phys.* **1962**, *4*, 113-160.

4. Nezu, T.; Ikeda, S. *Bull. Chem. Soc. Jpn.* **1993**, *66*, 18-24.

5. (a) Bustamonte, C.; Gurrieri, S.; Pasternack, R. F.; Purrello, R.; Rizzarelli, E. *Biopolymer*. **1994**, *34*, 1099-1104. (b) Nezu, T.; Ikeda, S. *Bull. Chem. Soc. Jpn.* **1993**, *66*, 25-31. (c) Pasternack, R. F.; Bustamonte, C.; Collings, P. J.; Giannetto, A.; Gibbs, E. J. J. *J. Am. Chem. Soc.* **1993**, *115*, 5393-5399. (d) Pasternack, R. F.; Gibbs, E. J. *Inorg. Organometal. Polym.* **1993**, *3*, 77-88. (e) Pasternack, R. F.; Giannetto, A.; Pagano, P.; Gibbs, E. J. *J. Am. Chem. Soc.* **1991**, *113*, 7799-7800. (f) Pancoka, P.; Urbanová, M.; Bednárová, L.; Vacek, K.; Paschenko, V. Z.; Vasiliev, S.; Malon, P.; Král, M. *Chem. Phys.* **1990**, *147*, 401-413. (g) Pasternack, R. F.; Brigandi, R. A.; Abrams, M. J.; Williams, A. P.; E. J. *Inorg. Chem.* **1990**, *29*, 4483-4486. (h) Pasternack, R. F.; Gibbs, E. J.; Gaudemer, A.; Bassner, A. A. S.; De Poy, L.; Turner, D. H.; Laplace, A. W. F.; Lansard, M. H.; Merienne, C.; Perrée-Fauvet, M. *J. Am. Chem. Soc.* **1985**, 8179-8186. (i) Pasternack, R. F.; Gibbs, E. J.; Villafranca, J. J. *Biochem.* **1983**, *22*, 2406-2414.

6. (a) Zerner, M. C.; Loew, G. H.; Kirchner, R. F.; Mueller-Westerhoff, U. T.; *J. Am. Chem. Soc.* **1980**, *102*, 589-599. (b) Bacon, A. D.; Zerner, M. C.; *Theoret. Chim. Acta* **1979**, *53*, 21-54. (c) Ridley, J. E.; Zerner, M. C.; *J. Mol. Spectrosc.* **1974**, *50*, 457-473. (d) Ridley, J. E.; Zerner, M. C.; *Theoret. Chim. Acta* **1973**, *32*, 111-134.

7. Dewar, M. J. S.; Zoebisch, E. G.; Healy, E. F.; Stewart, J. J. P.; *J. Am. Chem. Soc.* **1985**, *107*, 3902-3909.

8. Job, P.; *Ann.* **1928**, *9*, 113-203.

9. (a) Pasternack, R. F.; Francesconi, L.; Raff, D.; Spiro, E. *Inorg. Chem.* **1973**, *12*, 2606-2611. (b) Pasternack, R. F.; Huber, P. R.; Boyd, P.; Engasser, G.; Francesconi, L.; Gibbs, E.; Fasella, P.; Venturo, C. G.; Hinds, L. deC. *J. Am. Chem. Soc.* **1972**, *94*, 4511-4517. (c) Das, R. R.; Pasternack, R. F.; Plane, R. A. *J. Am. Chem. Soc.* **1970**, *92*, 3312-3316. See also reference 5h.

10. (a) Kano, K.; Takei, M.; Hashimoto, S. *J. Phys. Chem.* **1990**, *94*, 2181-2187. (b) Kano, K.; Hashimoto, S. *Bull. Chem. Soc. Jpn.* **1990**, *63*, 633-635. (c) Kano, K.; Nakajima, T.; Hashimoto, S. *Bull Chem. Soc. Jpn.* **1987**, *60*, 1281-1287. (d) Kano, K.; Miyake, K.; Uomoto, T.; Sato, T.; Ogawa, T.; Hashimoto, S.; *Chem. Lett.* **1983**, 1867-1870.

11. Kemnitz, K.; Sakaguchi, T. *Chem. Phys. Lett.* **1992**, *196*, 497-503.

12. Connors, K. A. *Binding Constants*, Wiley: New York, 1987.

13. The relative *D* values are upfield shifts observed in ^{1}H NMR signals guest protons under conditions of excess host (so that a high percentage of the guest is bound), these values have been scaled relative to the highest observed shift (which is assigned a value of 1.0.).

14. (a) Vergeldt, F. J.; Koehorst, R. B. M.; Schaafsma, T. J.; Lambry, J.-C.; Martin, J.-L.; Johnson, D. G.; Wasielewski, M. R.; *Chem. Phys. Lett.* **1991**, *182*, 107-113. (b) Hofstra, U.; Koehorst, R. B. M.; Schaafsma, T. J.; *Chem. Phys. Lett.* **1986**, *130*, 555-558. (c) van Willigen, H.; Das, U.; Ojadi, E.; Linschitz, H.; *J. Am. Chem. Soc.* **1985**, *107*, 7784-7785. (d) Ojadi, E.; Selzer, R.; Linschitz, H.; *J. Am. Chem. Soc.* **1985**, *107*, 7783-7784. (e) Shimidzu, T.; Iyoda, T.; *Chem. Lett.* **1981**, 853-856.

15. (a) Jiang, T.; Lawrence, D. S.; *J. Am. Chem. Soc.* **1995**, *117*, 1857-1858. (b) Dick, D.; Rao, T. V. S.; Sukumaran, D.; Lawrence, D. S.; *J. Am. Chem. Soc.* **1992**, *114*, 2664-2669. (c) Manka, J. S.; Lawrence, D. S.; *J. Am. Chem. Soc.* **1990**, *112*, 2440-2442.

16. (a) Shamim, M.; Seng, C. E.; *Z. Phys. Chem.* **1981**, *128*, 221-224. (b) Ives, D. J. G.; Moseley, P. G. N.; *J. Chem. Soc. B* **1966**, 757-761.

17. Zollinger, H.; *Color Chemistry-Syntheses, Properties, and Applications of Organic Dyes and Pigments*, VCH, 1987.

18. (a) Nakanishi, K.; Berova, N.; in *Circular Dichroism-Principles and Applications*,

Nakanishi, K.; Berova, N.; Woody, R. W. (eds); VCH, 1994, 361-398. (b) Harada, N.; Nakanishi, K.; *Circular Dichroic Spectroscopy-Exciton Coupling in Organic Stereochemistry*, University Science Books: Mill Valley, CA, 1983.

19. Barrans, R. E., Jr.; California Institute of Technology, Ph.D. Thesis, 1993.

20. Barrans, R. E., Jr.; *Personal Communication.*

21. Version 4.0, Microsoft Corp., © 1985-1992.

22. Larson, R. E.; Hostetler, R. P.; *Calculus*, D. C. Heath and Co., 1986.

Chapter 6:
Chiral Recognition of Inorganic Metal Complexes by Cyclophane Host Molecules.

Chapter 6

Chiral Recognition of Inorganic Metal Complexes by Cyclophane Host Molecules.

6.1 Introduction

The previous chapters have described cyclophane hosts that bind cationic guests in aqueous media (Figure 6.1).[1] One of the important binding forces that operates in these host-guest interactions is the cation-π effect - the interaction of a cation with the face (quadrupole) of an aromatic ring (Figure 6.2).[2] The cationic guests described in the earlier chapters have all been quaternary ammonium ions and imminium ions. Previous studies have established that our hosts do not bind the more strongly solvated alkali metal cations or ammonium ion in solution,[1i] but these hosts form insoluble salts with alkaline earth and transition metal cations.[3] However, water-soluble transition metal complexes with chelating ligands offer a means to study the binding of metal cations while attenuating any strong interactions with the host carboxylates (precipitation). These metal complexes should also have lower solvation energies than the corresponding naked metal ions, resulting in smaller desolvation penalties for binding. The ligand provides a handle from which ^{1}H NMR signals can be monitored. The metal center allows for variation of the charge of the ion and the ligands can be varied to alter hydrophobic and/or electrostatic contributions to the binding.

Figure 6.3 illustrates the metal complexes chosen for study. The complexes are all stable to racemization,[4,5] and ligand dissociation is negligible so that interactions of the metal center with the carboxylates shouldn't occur. The metal complexes of Figure 6.3 are all chiral, providing the additional aspect of chiral recognition with our enantiomerically

pure hosts. Chiral recognition has been observed in earlier studies of the ethenoanthracene based hosts in our labs with certain chiral organic cations,[1di] although the preference for a

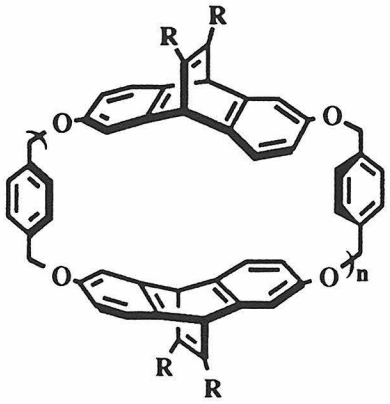

P_E, n = 1, R = $-CO_2CH_3$
2_E, n = 2, R = $-CO_2CH_3$
3_E, n = 3, R = $-CO_2CH_3$
P, n = 1, R = $-CO_2^-Cs^+$
2, n = 2, R = $-CO_2^-Cs^+$
3, n = 3, R = $-CO_2^-Cs^+$

[(*R*, *R*)-Stereochemistry of ethenoanthracene units shown]

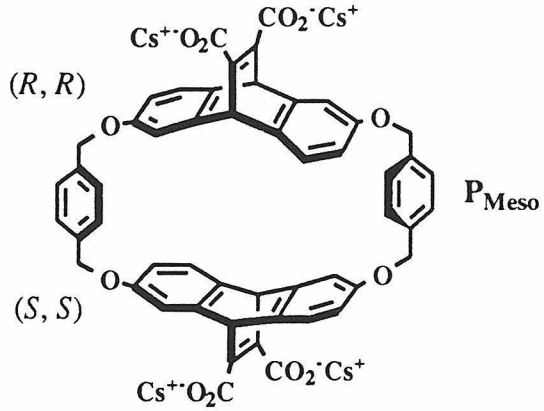

Figure 6.1. Cyclophane hosts studied in this chapter.

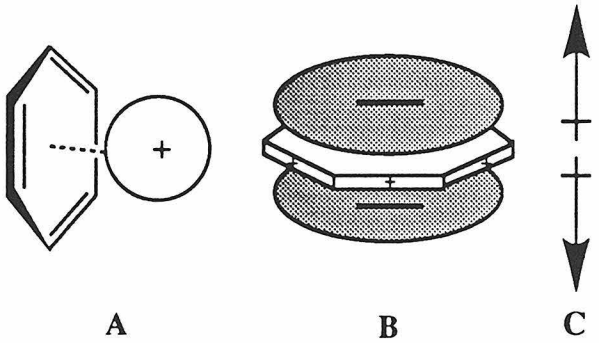

Figure 6.2. The cation-π effect (A) and the quadrupole moment of benzene (B); quadrupole moments can be thought of as being derived from two dipole moments arranged in such a way as to create no net dipole (C).[2b]

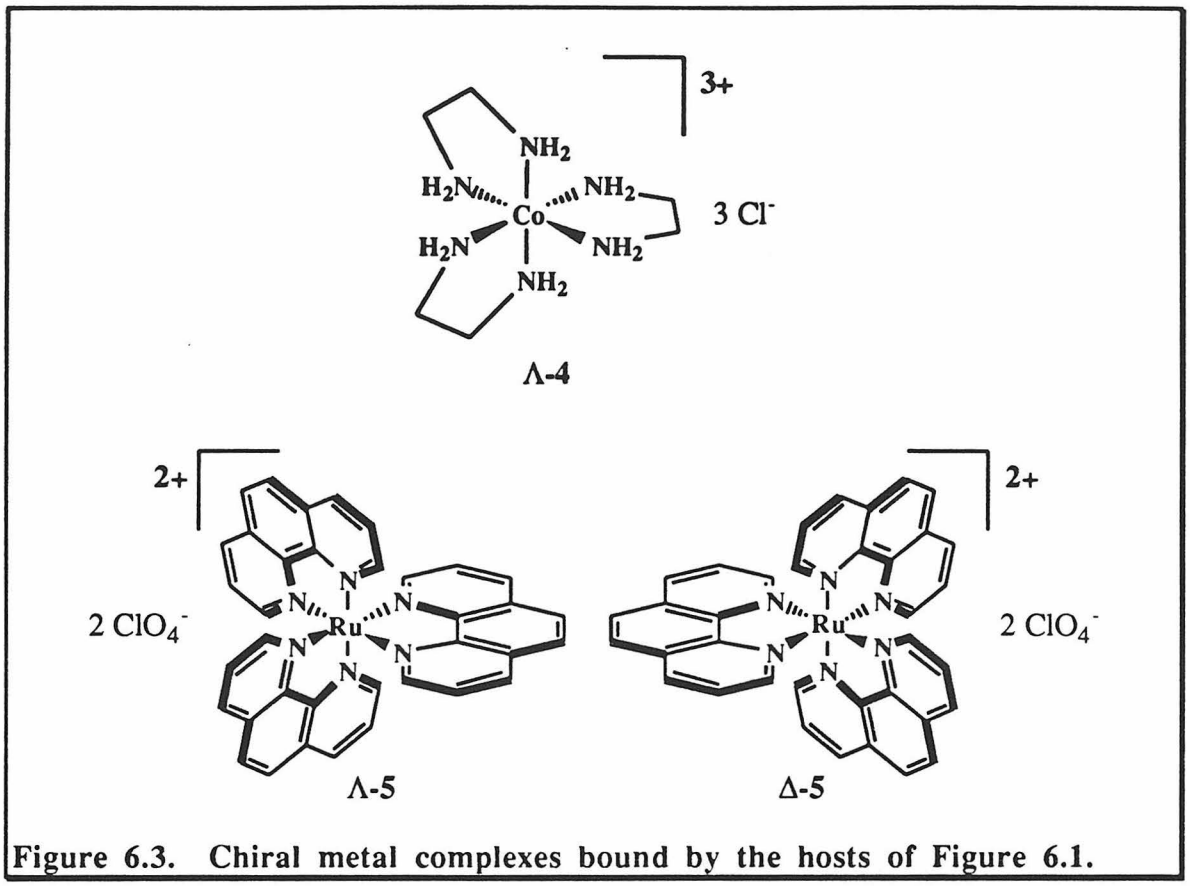

Figure 6.3. Chiral metal complexes bound by the hosts of Figure 6.1.

given guest enantiomer tends to be small (1 kcal/mol > $\Delta\Delta G°_a$).[1di] It was hoped that with higher charges on the cations, stronger cation-π interactions would lead to higher binding constants, which in turn might lead to larger enantioselectivity.

6.2 Λ-$Co(en)_3^{3+}$

6.2.1 General

The first guest we chose to look at was the $Co(en)_3^{3+}$ ion (**4**). This guest has CH_2 and NH_2 protons that can be followed by ^1H NMR. CPK models suggest that **4** can fit snugly into the toroid conformation of host **P**[1ai] with the CH_2 groups sticking partially outside the cavity and NH_2 groups fully encapsulated (Figure 6.4). This model suggests

that in an ^1H NMR experiment large upfield shifts should be observed for NH_2 protons relative to the CH_2 protons. For these reasons **4** was thought to be an ideal guest for study.

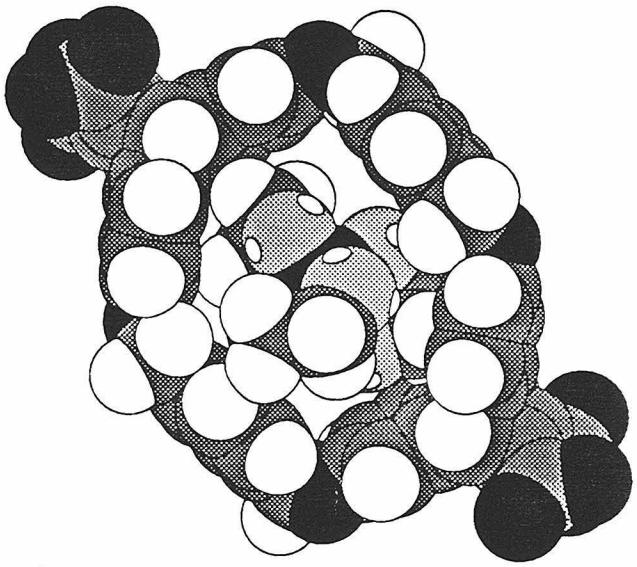

Figure 6.4. Crystal structure of guest 4^6 docked in optimized toroid conformation of host P_S.[1i]

6.2.2 Binding Results

^1H NMR experiments with host **P** and **4** in borate-*d* provided poor data for analysis, due to extreme broadening of proton signals for both host and guest. In an attempt to decrease this peak broadening (by decreasing the binding constant), several experiments were carried out in DMSO-d_6 using both the tetracaroxylate host and the tetraacid of the host. The data from these studies were still unquantifiable; however, the guest proton NH_2 signals were observed to shift in the upfield ($D > 0$) direction in the presence of the host. The observation of upfield shifting of the guest protons is significant as it suggests encapsulation within the host cavity,[1] not association at the carboxylates (hydrogen bonding of the carboxylate to the guest NH_2 protons would be expected to

produce down-field shifting).[7] Additional experiments with P_E in DMSO-d_6 also resulted in the observation of upfield shifting of guest NH_2 protons in the presence of the host (Figure 6.5), suggesting a strong cation-π interaction as the driving force for the binding of guest **4** and down playing the presence of a strong electrostatic attraction. In all cases, guest CH_2 protons exhibited only very slight upfield shifts in the presence of host ($\Delta\delta <$ 0.05 ppm). These shifts are consistent with guest encapsulation as depicted in Figure 6.4.

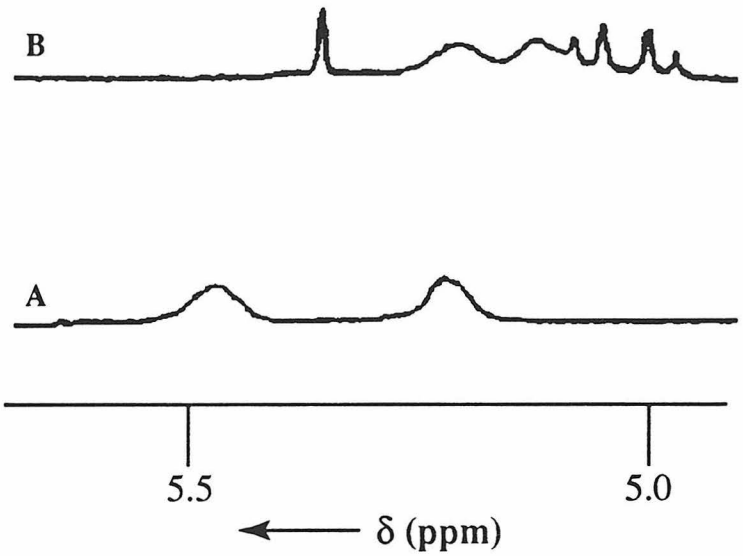

Figure 6.5. ^{1}H NMR spectra showing guest NH_2 proton signals of DMSO-d_6 solutions containing (A) free guest **4** (2.56×10^{-3} M) and (B) guest **4** (5.20×10^{-4} M) with host P_{ES} (4.86×10^{-4} M).

Given the difficulties experienced with the NMR studies, the binding interactions were further probed using circular dichroism methods (Chapter 2);[1a] the results of these studies are shown in Table 6.1. The data show a larger preference for guest **4** by the (*S*, *S*, *S*, *S*)-host compared to the (*R*, *R*, *R*, *R*)-host. Although small (0.7 kcal/mol), such a selectivity is quite remarkable given the spherical structure of the guest (and thus a very subtle difference between the enantiomers of this guest). The spectral changes associated

with the host Cotton effects don't agree with either a rhomboid or a toroid binding conformation for both P_S and P_R (Figure 6.6, P_S data shown). A large decrease in magnitude of the Cotton effects relative to the free host is observed, rhomboid binding is observed by small decreases, toroid binding by large increases at shorter wavelengths (see Chapter 3).[1a] This unusual type of spectral change may be due in part to the additivity of the guest CD absorptions to the host in the complex. Based on guest size (CPK models) a toroid conformation is still assumed.

	Host		
	P_S	P_R	P_{Meso}
$-\Delta G°_a$ (kcal/mol)	7.2	6.5	8.6

Table 6.1. Binding constants measured in aqueous borate buffer for guest 4.

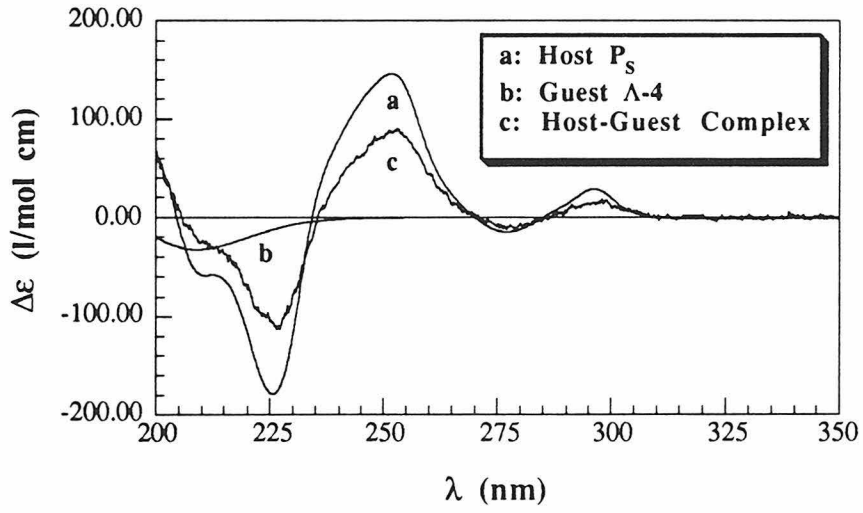

Figure 6.6. CD spectra of host P_S (a) and guest 4 (b) and fitted spectrum of the complex they form (c) in aqueous borate buffer (pH 9).

An interesting observation from table 6.1 is the significantly larger binding of guest **4** by the achiral form of the host (P_{Meso}). The achiral host binds **4** with a greater than 1.4 kcal/mol enhanced affinity compared to both enantiomers of the chiral form of host **P**. One

possible explanation for this is that with the chiral host, the twisting of the ethenoanthracene units creates a more collapsed cavity and thus provides a higher energy barrier to assuming the fully open D_2-symmetric toroid conformation. With the achiral host, the C_{2h}-symmetric toroid may be much more accessible due to the absence of the helicity that results in the twisting of the subunits in the chiral host. Studies with the prototypical toroid binding guest **6** (Figure 6.7), in pD 7.5 buffer, also show a much higher preference for binding with $\mathbf{P_{Meso}}$ than with enantiomerically pure $\mathbf{P_S}$ and $\mathbf{P_R}$ (8.1 vs 6.9 kcal/mol).[1i,8] These observations further support this assumption about toroid conformation preference between the two diastereomeric forms of host **P**, but further studies would be required to confirm this.

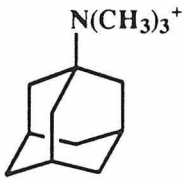

6

Figure 6.7. The prototypical toroid-binding guest, adamantyltrimethylammonium ion (6).

The data in Table 6.1 also illustrates applications of the CDfit[1a] protocol not previously exploited with studies of host **P**. The binding constants for **4** with $\mathbf{P_S}$ and $\mathbf{P_R}$ come from fitting with a guest that does not have $\Delta\varepsilon = 0$ at all wavelengths. This is the first example of the use of CDfit for a host-guest system where both species are CD active in the unbound states (as described in Chapter 2, the ability to handle this type of data is one of the advantages that CDfit has over other CD fitting procedures).[1a] The studies with $\mathbf{P_{Meso}}$ represent the first use of CDfit for a host that is not CD active with a CD active guest. In the studies with $\mathbf{P_{Meso}}$, no induced CD was observed for the host transitions; using a chiral guest with strong $\pi \rightarrow \pi^*$ transitions is, however, expected to induce CD in this host (see Chapter 8).

Given the observation of a strong cation-π interaction with guest **4**, it was postulated that a cation such as $Co(NH_3)_6^{3+}$ might also be bound by the host cavity in both aqueous and organic media. Studies with this guest are described in the following section.

6.2.3 $Co(NH_3)_6^{3+}$

In aqueous ^1H NMR and CD studies with hexaamminecobalt (III) ion and host **P**, precipitate formation occurred immediately upon adding solutions of host and guest. NMR studies in DMSO-d_6 showed down-field shifting of the guest NH_3 protons, a result consistent with hydrogen bond formation at the carboxylates.[7] Identical observations were made in studies with $\mathbf{P_E}$ (in $CDCl_3$ and DMSO-d_6). Again hydrogen bond formation, this time with the ester carbonyl oxygen, is postulated. These results were disappointing, but should not have been unexpected. In aqueous media the hexaammine ion is expected to be much more strongly solvated than a guest like **4**, thus having a much greater energy barrier for complex formation (a process in which at least part of the solvation shell of the guest must be removed).[9] In organic media, hydrogen bonding interactions can be quite strong, resulting in the preferred formation of these bonds over cation-π stabilization in the host cavity. The hydrogen-bond forming NH_3 ligands are much more accessible in the hexaammine ion than are the NH_2 groups in guest **4**.

Despite the apparent absence of guest binding in the host cavity, CD experiments with $Co(NH_3)_6^{3+}$ did show an interesting effect. Induced CD was observed with studies of the guest in the presence of an excess of the enantiomeric forms of host **P** (Figure 6.8). The guest has two weak d-d transitions at 335 nm ($^1A_{1g} \rightarrow {}^1T_{2g}$, electronically allowed)[10] and 469 nm ($^1A_{1g} \rightarrow {}^1T_{1g}$, magnetically allowed)[10] in borate buffer. The ICD illustrated in Figure 6.7 arises exclusively from the electronically allowed transition; this observation nicely supports the assumptions made in Chapter 4 of the coupling of electronic transition moments being responsible for the induction of CD active absorptions in achiral guests.

The result also contrasts what has been observed in other studies of $Co(NH_3)_6^{3+}$ with chiral anions.[11] In these studies ICD was observed only in the magnetically allowed transition.[11] Initially, this ICD was thought to be the result of encapsulation in the host cavity, a notion later dispelled by the NMR studies described in the preceding paragraph.

A series of control experiments with non-macrocyclic molecules **7** and **8** (Figure 6.9) failed to show detectable induced CD. The observation of ICD with **P** appears to simply be the result of a larger number of transitions coupling with the guest transition and

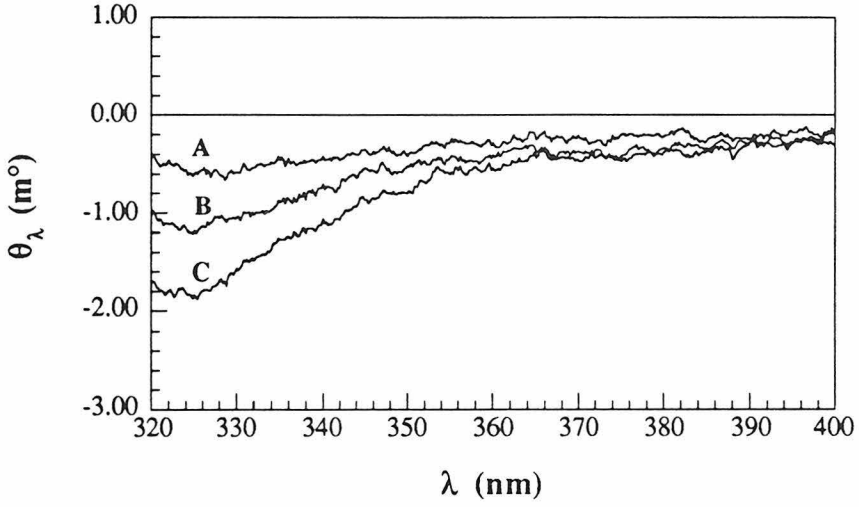

Figure 6.8. CD spectra of solutions containing 2.53×10^{-5} M $Co(NH_3)_6^{3+}$ in the presence of (A) 3.0×10^{-5} M host P_S, (B) 3.9×10^{-5} M host P_S, and (C) 5.7×10^{-5} M host P_S in aqueous borate buffer (pH 9).

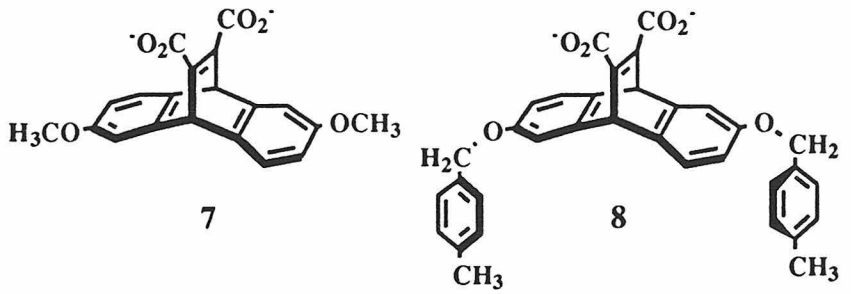

[(*R*, *R*)-Stereochemistry of ethenoanthracene units shown]

Figure 6.9. Non-macrocyclic control molecules.

leading to a larger rotational strength. Precipitation of insoluble salts with these anions was, however, observed.

6.3 $Ru(phen)_3^{2+}$

6.3.1 General

CPK models indicate that the enantiomers of guest **5** fits snugly into the fully open cavity of host **2**, likewise the guest can be fully encapsulated by host **3** as well. In the case of host **P**, the guest is too large for full encapsulation. However, the phenanthroline rings of metal complex **5** have a propensity to partially intercalate between stacked base-pairs in nucleic acids;[12] a similar mode of binding should also be possible with host **P**. Since the guest can interact with all three hosts (-4, -6, and -8 charged anions), it is ideal for probing the importance of electrostatic attractions in the binding event.

6.3.2 Binding Results

Binding constants for guest **5** in borate buffer were ultimately obtained from CD studies and are listed in Table 6.2. Enantioselectivity is observed for host **P** and **2**, but not with the much less conformationally restricted host **3**. While host **2** is less conformationally restricted than **P**, it remarkably shows almost identical enantioselectivity (but with reversed guest preference for the same ethenoanthracene stereochemistry). As with the guest **4** studies, the spherical nature of the guests was not expected to produce high enantioselectivity with our hosts, yet the hosts do recognize these very subtle changes in handedness of the guest. For host **2**, the equivalent enantioselectivity to **P** suggests a conformationally restricted binding conformation. Examination of the CD spectra of the **2**$_S$/Δ-**5** host-guest complex (Figure 6.10) illustrates spectral changes in shorter wavelength

host Cotton effects similar to what is observed with host **P** taking a toroid conformation (increase in magnitude relative to free host, Chapter 3).[1a] Such a D_3-symmetric conformation of host **2**, while possible and certainly restrictive enough for the observed enantioselectivity, should be highly entropically unfavorable. It may be the increased electrostatic attractions with a hexaanionic host help to offset this entropy loss. Studies with Λ-**5** produce similar results.

Similar spectral changes are observed with host **3** on binding guest **5**, again suggesting full encapsulation of the guest (Figure 6.11 shows the spectrum of the $\mathbf{3}_R$/Λ-**Ru** complex). However, CPK models suggest that the larger host **3** can encapsulate the guest without assuming a fully open D_4-symmetric cavity. In contrast to the observations with hosts **2** and **3**, CD spectra for the **P**/**5** complexes suggest rhomboid-like conformational changes (small decreases in magnitude of all Cotton effects relative to free host,[1a] Figure 6.12 shows the $\mathbf{P}_S$/Λ-**5** complex spectrum). This observation, however, is not expected due to the different binding modes by which the guest would be predicted to take with **P** (insertion of a phenanthroline ligand into the cavity) vs **2** or **3** (full encapsulation of guest).

	Guest	
Host	Λ-**5**	Δ-**5**
$\mathbf{P}_S$	9.0	8.4
$\mathbf{P}_{Meso}$	8.1	a
$\mathbf{2}_S$	8.3	9.0
$\mathbf{3}_R$	8.7	8.6

Table 6.2. Binding constants ($-\Delta G°_a$, kcal/mol) measured in aqueous borate buffer for guest 5.

[a]This binding study was not carried out; the achiral host presumably binds both guest enantiomers with equal affinity.

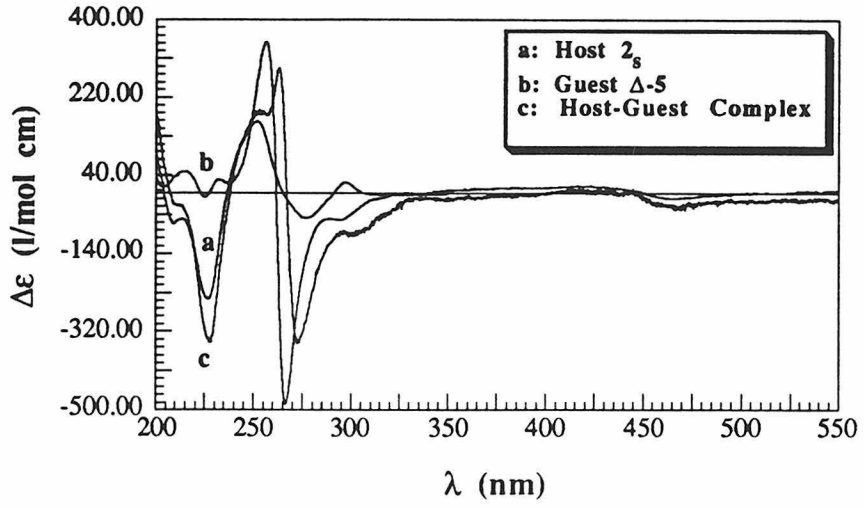

Figure 6.10. CD spectra of host 2_S (a) and guest Δ-5 (b) and fitted spectrum of the complex they form (c) in aqueous borate buffer (pH 9).

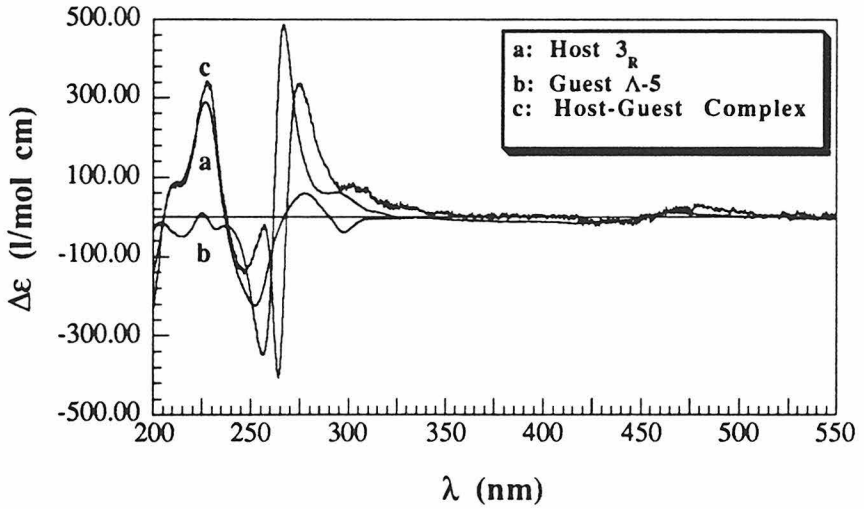

Figure 6.11. CD spectra of host 3_R (a) and guest Λ-5 (b) and fitted spectrum of the complex they form (c) in aqueous borate buffer (pH 9).

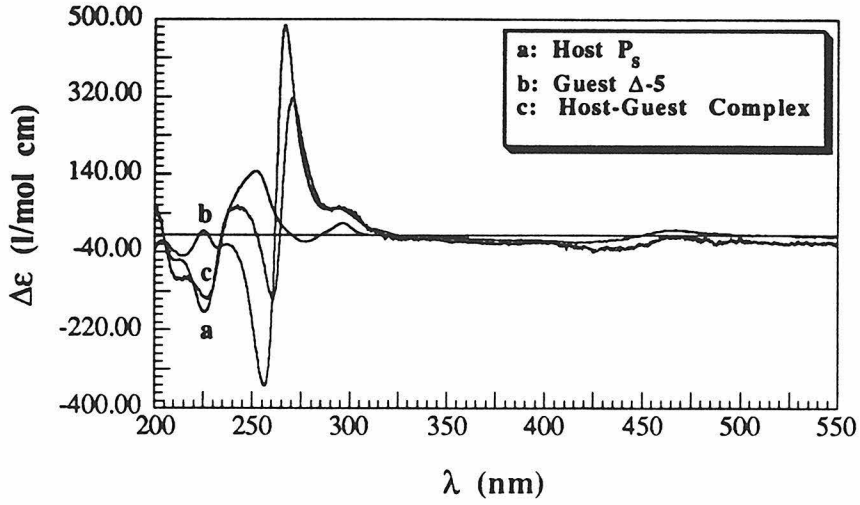

Figure 6.12. CD spectra of host P_S (a) and guest Λ-5 (b) and fitted spectrum of the complex they form (c) in aqueous borate buffer (pH 9).

Like guest **4**, ^{1}H NMR experiments with guest **5** and hosts **P**, **2**, and **3** were quantitatively unsuccessful (not unexpected given the large binding constants in Table 6.2). In borate-*d*, interaction of **5** with host **P** showed very large upfield shifts and broadening of all protons. In 10% CD_3CN/90% borate-*d*, signals were easier to follow, but only qualitative data was obtained. The enantioselectivity of hosts **P** and **2** is strong enough to allow the hosts to act as chiral shift reagents for mixtures of Λ- and Δ-**5**, as illustrated in Figure 6.13. The relative *D* values of the guest protons are given in Table 6.3.[13] With all three hosts, upfield shifting was observed supporting binding within the host cavity. Unlike guest **4**, however, studies in DMSO-d_6 with **P**, **2**, and **3** and studies in CD_2Cl_2 with the esters $\mathbf{P_E}$, $\mathbf{2_E}$, and $\mathbf{3_E}$ failed to detect any interaction, suggesting hydrophobic and electrostatic attractions control the binding of guest **5**.

The relative *D* values of Table 6.3 reveal some interesting comparisons. The shift patterns for host **P** differ significantly from the larger hosts. With **P** H_2 is shifted the farthest upfield, with **2** and **3** H_4 experiences the greatest shifting. This is consistent with

the larger hosts fully encapsulating the guest, while host **P** must exhibit a distinctly different interaction orientation. The shift patterns of the Λ- and Δ-enantiomers also show slight variations with each host, as expected for the observed enantioselectivity (that is slightly different binding orientations with the two enantiomers). The observed preferences are not obvious from examination of CPK models; again the hosts show a remarkable selectivity given the very subtle differences between the guest enantiomers.

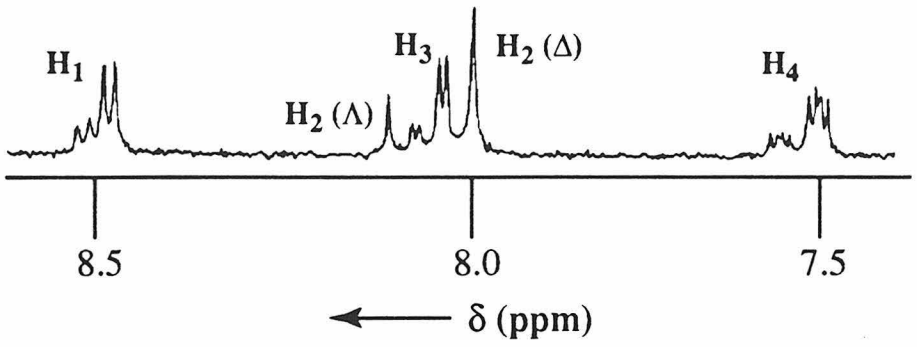

Figure 6.13. ^{1}H NMR spectrum of a solution containing host P_R (6.89×10^{-5} M), Λ-5 (5.91×10^{-5} M) and Δ-5 (1.74×10^{-4} M) in 10% CD_3CN/90% borate-*d* (for proton numbering scheme see Figure 6.14).

	Λ-5 Protons				Δ-5 protons			
Host	H_1	H_2	H_3	H_4	H_1	H_2	H_3	H_4
P_R	0.62	1.00	0.36	0.59	0.49	1.00	0.34	0.53
2_S	0.74	0.81	0.67	1.00	0.54	0.31	0.91	1.00
3_R	0.67	0.49	0.76	1.00	0.46	0.32	0.75	1.00

Table 6.3. Relative *D* values (ppm)[13] for protons of guest **5** in 10% CD_3CN/90% borate-*d* (using proton numbering scheme of Figure 6.14).

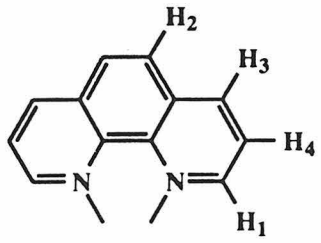

Figure 6.14. Proton numbering scheme for phenanthroline rings of guest **5**.

6.4 Control Studies

In order to asses the importance of cavity encapsulation vs electrostatic attraction, the guests of Figure 6.3 were studied with control molecules **7** and **8**. In no case was a significant interaction observed (as determined by a lack of significant spectral changes and by non-fitting CDfit results). These studies suggest forces other than pure electrostatic attractions make a significant contribution to binding. For guest **4**, the data suggest strong cation-π interactions. With guest **5**, hydrophobic forces appear to dominate the binding.

6.5 Conclusions and Future Directions

The studies described in this chapter show strong interactions of several chiral metal complexes with hosts **P**, **2**, and **3** in aqueous media. Guest **4** is bound in the cavity of host **P** through a strong cation-π interaction. The effect is observed in organic media with the neutral analog of the host ($\mathbf{P_E}$) as well. With guest **5**, strong binding interactions occur with all three hosts, but in the absence of aqueous solvent the binding is negligible, suggesting a strong hydrophobic interaction. These results are consistent with **5** being thought of as a somewhat hydrophobic cation.[14] Enantioselectivity is also observed with the chiral hosts and the chiral guests for hosts **P** and **2**. Host **4**, a conformationally unrestricted molecule, shows negligible enantioselectivity.

These studies are somewhat incomplete; a more quantitative analysis of the importance of electrostatic binding forces in these interactions could provide better insights into the data. Additional studies using the same ligands, but different metal centers, would allow variation of the charge on the cation. Alternatively, neutral analogs of the hosts could be employed in an aqueous environment.[15]

It has been shown that the neutral host $\mathbf{P_E}$ can bind cations in organic media through strong cation-π interactions.[1k] These observations were further confirmed by the

studies of guest **4**. Cation-π binding in organic media could be assessed using crown ethers to solubilize alkali metal, alkaline earth, and possibly other metal cations in organic media. The crown ether acts as a ligand for the ion that can be followed by ^{1}H NMR. In this manner a variety of cations could be studied and bound by the cyclophane host. CPK models suggest the cavity of $\mathbf{P_E}$ is large enough to accommodate complexes of 15-crown-5 and 12-crown-4. Such studies may provide further insights into the nature of solution-phase cation-π interactions.

6.6 Experimental Section

CD spectra were recorded on a JASCO J-600 Spectropolarimeter with a 1.0 cm pathlength quartz cell. A standard set of measurement parameters was used in all quantitative experiments: Band Width 1.0 nm, Sensitivity 50 m°/cm, Time Constant 1.0 Sec., Scan Speed 50 nm/min., Step Width 0.2 nm/point, and a minimum of 4 accumulations. ^{1}H NMR spectra were recorded on a Bruker AM-500 spectrometer.

All solvents used in spectroscopy were spectrophotometric or HPLC grade. Aqueous cesium borate buffer (pH 9) was prepared by dissolving 0.25 g high purity boric oxide in 800 g water and adding 3.74 ml of 1 M CsOH followed by thorough mixing. The water used in these preparations was passed through a Milli-Q purification system.

Circular dichroism binding studies are described in Chapter 2 of this manuscript.[1a] Qualitative detection of induced CD was done using excess concentrations of the appropriate host and/or control molecule with the guest of interest. For these studies the standard measurement parameters were often varied to provide conditions with the highest sensitivity.

Fitting CD data from acetonitrile solutions of **P** tetraacid to $\Delta\varepsilon$ values for the 230-350 nm region of $\mathbf{P_E}$ in CH_3CN provided estimates of purity of samples of the tetraacid. Calibration studies with **P** stock solutions in cesium borate prepared by weighing out

samples of the tetraacid (with "known purity") produced nearly identical $\Delta\varepsilon$ values to the studies with NMR standardized stock solutions. This method of $\Delta\varepsilon$ determination was used for **3**, and **4**, **7**, and **8**. Standardized $\Delta\varepsilon$ values for chiral guests were determined from a series of 5-6 solutions of the appropriate guest in the 10^{-7}-10^{-5} M concentration range. The data at each wavelength scanned was fitted to the Beer-Lambert law to give the best fit $\Delta\varepsilon$ data used in the binding studies.

Protocols for NMR binding studies in aqueous media have been described previously.[1di,16] Host concentrations of borate-*d* solutions were determined using circular dichroism spectroscopy and fitting to known calibration curves (as described in Chapter 2). For studies in DMSO-d_6 with the anionic forms of the host, samples of the host acids were weighed out, dissolved in DMSO-d_6 and mixed with quantitative amounts of cesium carbonate. Dilution to appropriate volume provided a stock solution of known concentration. For studies in organic solvents, stock solutions were prepared by weighing out solutes on a Sartorius microbalance followed by dilution to appropriate volumes. Spectra in organic solvents were referenced to the residual proton signals of the solvents and are reported in ppm downfield of 0.0 as δ values.

Compounds $\mathbf{P_{ES/R}}$, $\mathbf{P_{S/R}}$, $\mathbf{P_{Meso}}$, $\mathbf{2_E}$, and $\mathbf{3_E}$ were prepared as previously reported. The preparation of **7** and **8** is described in Chapter 2.[1a] The preparation of **2** and **3** are described in Chapter 5.[1a]

Guest **4** was prepared by the literature method and recrystallized and isolated as pure [Λ-$Co(en)_3Cl_3]_2$•NaCl•6 H_2O.[4] Samples of the enantiomers of guest **5** (as chloride salts) were gifts from the laboratories of Professor J. K. Barton at the California Institute of Technology.[17] For purification, **5** was precipitated from aqueous solution as a perchlorate salt and recrystallized from water prior to use (purity was assessed from elemental analysis). $Co(NH_3)_6Cl_3$ was obtained from commercial sources, counter ions were exchanged by precipitation from aqueous solution [ClO_4^-, BF_4^-, and/or $B(phen)_4^-$ were used for studies in non-aqueous solvents] and samples purified by recrystallization

from water (purity was assessed from elemental analysis prior to use). The tetraphenyl borate salt of $Co(NH_3)_6^{3+}$ was found to decompose on standing in air at room temperature; other salts of this trication were indefinitely stable.

6.7 References and Footnotes

1. (a) Forman, J. E.; Barrans, R. E., Jr.; Dougherty, D. A.; *J. Am. Chem. Soc.* **1995**, *117*, 9213-9228. (b) Dougherty, D. A.; Kearney, P.C.; Mizoue, L. S.; Kumpf, R. A.; Forman, J. E.; McCurdy, A.; in *Computational Approaches in Supramolecular Chemistry*, G. Wipff (ed), NATO ASI Series, 1994. (c) Forman, J. E.; Marsh, R. E.; Schaefer, W. P.; Dougherty, D. A.; *Acta. Cryst. Section B*, **1993** *B49*, 892-896. (d) Kearney, P. C.; Mizoue, L. S.; Kumpf, R. A.; Forman, J. E.; McCurdy, A.; Dougherty, D. A. *J. Am. Chem. Soc.* **1993**, *115*, 9907-9919. (e) McCurdy, A.; Jimenez, L.; Stauffer, D. A.; Dougherty, D. A. *J. Am. Chem. Soc.* **1992**, *114*, 10314-10321. (f) Stauffer, D. A.; Barrans, R. E., Jr.; Dougherty, D. A. *Angew. Chem., Int. Ed. Engl.* **1990**, *29*, 915-918. (g) Stauffer, D. A.; Barrans, R. E., Jr.; Dougherty, D. A. *J. Org. Chem.* **1990**, *55*, 2762-2767. (h) Stauffer, D. A.; Dougherty, D. A. *Science* **1990**, *250*, 1558-1560. (i) Petti, M. A.; Shepodd, T. J.; Barrans, R. E., Jr.; Dougherty, D. A. *J. Am. Chem. Soc.* **1988**, *110*, 6825-6840. (j) Shepodd, T. J.; Petti, M. A.; Dougherty, D. A. *J. Am. Chem. Soc.* **1988**, *110*, 1983-1985. (k) Stauffer, D. A.; Dougherty, D. A. *Tetrahedron Lett.* **1988**, *29*, 6039-6042. (l) Shepodd, T. J.; Petti, M. A.; Dougherty, D. A. *J. Am. Chem. Soc.* **1986**, *108*, 6085-6087. (m) Petti, M. A.; Shepodd, T. J.; Dougherty, D. A.; *Tetrahedron Lett.* **1986**, *27*, 807-810.

2. (a) Mecozzi, S.; West, A. P., Jr.; Dougherty, D. A.; *Submitted.* (b) Dougherty, D. A.; *Science* **1996**, *271*, 163-168.

3. Forman, J. E.; Dougherty, D. A.; *Unpublished Results.*

4. Broomhead, J. A.; Dwyer, F. P.; Hogarth, J. W.; *Inorg. Synth.* **1960**, *6*, 183-186.

5. Brandt, W. W.; Dwyer, F. P.; Gyarfas, E. C.; *Chem. Rev.* **1954**, *54*, 959-1017.

6. The crystal structure of the iodide salt of **4**. Whuler, A.; Spinat, P.; Brouty, C.; *Acta Cryst. B* **1980**, *B36*, 1086-1091.

7. (a) Vinogradov, S. N.; Linnell, R. H.; *Hydrogen Bonding*, van Nostrand Reinhold Company, 1971. (b) Pimentel, G. C.; McClellan, A. L.; *The Hydrogen Bond*, Freeman and Company, 1960.

8. Shepodd, T. J.; California Institute of Technology, Ph.D. Thesis, 1988.

9. Diederich, F.; *Cyclophanes*; The Royal Society of Chemistry: Cambridge, UK, 1991.

10. Ballhausen, C. J.; *Introduction to Ligand Field Theory*, MacGraw-Hill, 1962.

11. (a) Rodger, A.; *Inorg. Chim. Acta* **1986**, 122, 25-30. (b) Schipper, P. E.; Rodger, A.; *J. Am. Chem. Soc.* **1985**, *107*, 3459-3465. (c) Jonás, I.; Nordén, B.; *Acta Chem. Scand.* **1974**, *28A*, 289-293.

12. (a) Barton, J. K.; Goldberg, J. M.; Kumar, C. V.; Turro, N. J.; *J. Am. Chem. Soc.* **1986**, *108*, 2081-2088. (b) Barton, J. K.; *Science* **1986**, *233*, 727-734. (c) Kumar, C. V.; Barton, J. K.; Turro, N. J.; *J. Am. Chem. Soc.* **1985**, *107*, 5518-

5523. (d) Barton, J. K.; Danishefsky, A. T.; Goldberg, J. M.; *J. Am. Chem. Soc.* **1984**, *106*, 2172-2176.

13. The relative *D* values are upfield shifts observed in ^{1}H NMR signals of guest protons under conditions of excess host (so that a high percentage of the guest is bound); these values have been scaled relative to the highest observed shift (which is assigned a value of 1.0.).

14. Blandamer, M. J.; Burgess, J.; *Transition. Met. Chem.* **1988**, *13*, 1-18.

15. Mecozzi, S.; Dougherty, D. A.; *Unpublished Results*.

16. Barrans, R. E., Jr.; Dougherty, D. A. *Supramolecular Chem.* **1994**, *4*, 121-130.

17. See reference 12 for methods of preparation and purification.

Chapter 7:
Progress Toward Self-Assembling Systems in Aqueous Media.

Chapter 7

Progress Toward Self-Assembling Systems in Aqueous Media.

7.1 Introduction

The molecular recognition studies described in the previous chapters were inspired by a desire to probe complex binding interactions in a simple system.[1] The non-covalent interactions probed are the same as those in the more complex biological receptors. Another important aspect of biological receptors is that many assemble from component subunits to form the functional receptor.[2] With the intention of gaining insights into the self-assembly of more complex biological molecules, we set out to design and study simpler molecules that would spontaneously assemble into organized structures with discreet stoichiometries under appropriate conditions. This chapter describes observations from studies aimed toward understanding the rules governing spontaneous self-assembly in an aqueous environment.

The studies focus on C_2-symmetric molecules capable of adopting a "U-shaped" conformation. Figure 7.1 illustrates two designs for such molecules: The "type A" design has aromatic side chains appended onto an ethenoanthracene core through ether linkages. The design allows for a variety of non-U conformations, but has the advantage of synthetic accessibility from molecules already available in the Dougherty laboratories. The "type B" molecule offers the advantage of a preorganized "U-shape," but requires more complex synthesis.

The U-shape provides a concave hydrophobic surface complementary to itself. The structures are further modified with hydrophilic functional groups placed at the ends of the arms of the "U" and exterior to the concave surface. Non-directional hydrophobic forces should bring the two surfaces together, with directional forces between complementary

hydrophilic groups providing a means by which the two molecules are held in a 1:1 stoichiometry. Both homomolecular and heteromolecular systems can be envisioned (Figure 7.2). In the case of a heteromolecular system, the dimers themselves are self-complimentary, and under appropriate conditions higher order assemblies may be envisioned (Figure 7.2C).

The studies described in this chapter focus mainly on molecules of the "type A" design, as self-assembling monomers based on simple modifications of the ethenoanthracene units used in building the cyclophane host molecules studied in our laboratories.[1]

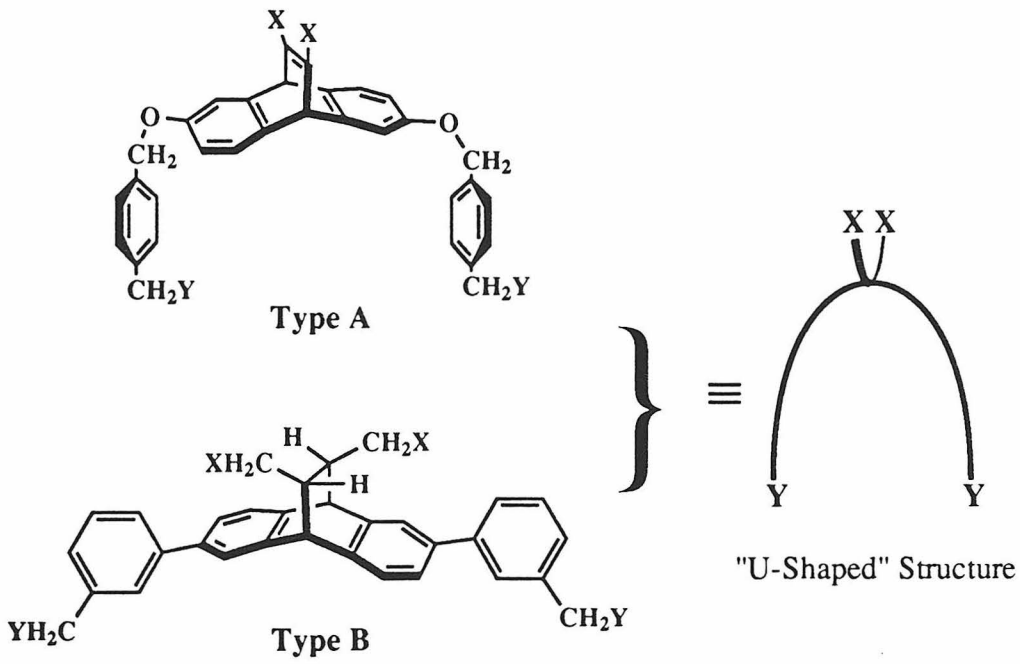

Figure 7.1. Designs for molecules capable of taking on a "U-shaped" conformation.

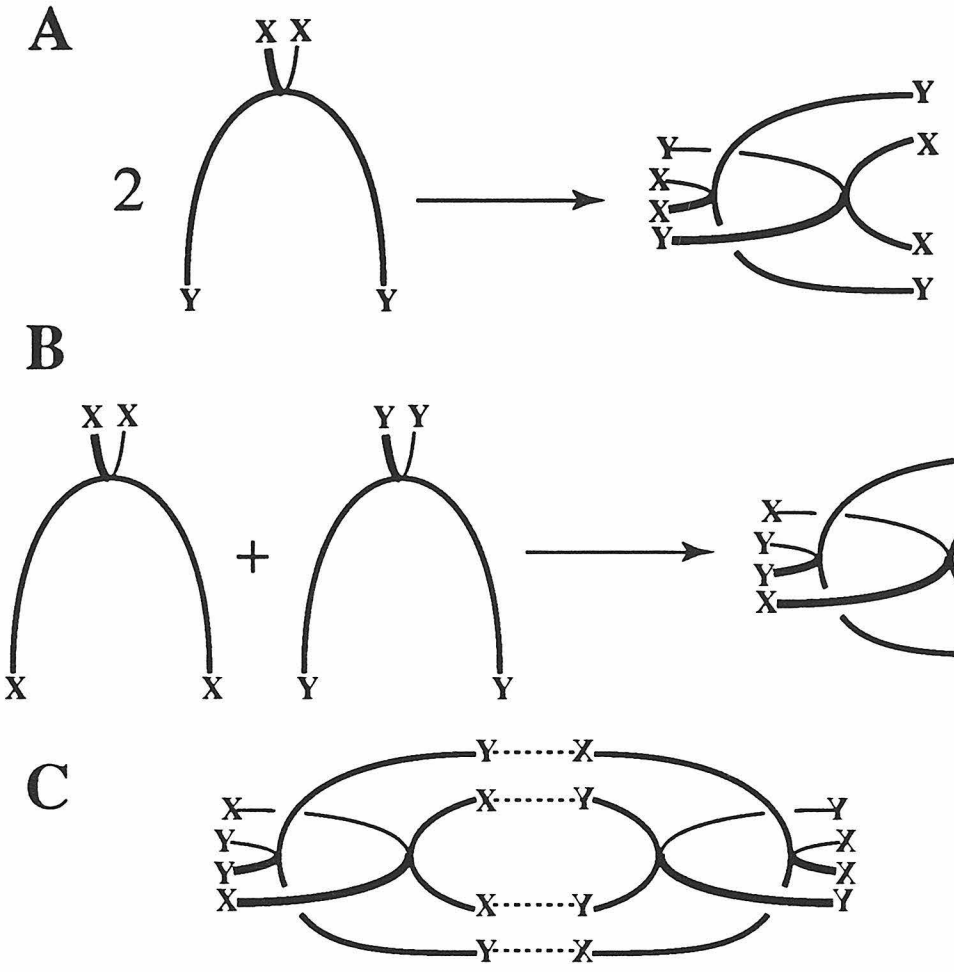

X, Y = Charged or polar functional groups that are complementary to each other.

Figure 7.2. Schematic of the self-assembly resulting from appropriate designed U-shaped molecules. (A) Homomolecular self-assembly, (B) heteromolecular self-assembly, and (C) an illustration of the self-complimentarity of heteromolecular dimers.

7.2 Initial Designs and Results

7.2.1 Homomolecular Self-Assembly

A simple application of the type A design of Figure 7.1 is the dicarboxylate/diammonium appended structure **1** (Figure 7.3). The molecule is highly

charged, yet overall neutral. The carboxylate and ammonium functional groups are self-complimentary and allow for the formation of salt-bridges or hydrogen bonds to hold the assembly in a dimeric stoichiometry. Examination of CPK models suggests a preferred conformation may be that shown in Figure 7.4. Figure 7.4 illustrates a dimeric assembly of **1**, in which hydrogen bonds form between the polar groups. The structure also places the aromatic side chains in such a position as to place the bridgehead proton (striped atom in Figure 7.4) of the ethenoanthracene unit directly under the face of an aromatic ring (see Figure 7.5 for proton designations). This positioning is significant because it predicts that in an ^1H NMR experiment, upfield shifting of the signal for the bridgehead proton from its monomeric position should be observed on formation of a dimeric assembly. Another feature of this model is the localization of hydrophobic surface area to the interior of the dimer, with polar hydrophilic functionality on the exterior of the dimer exposed to solvent. This type of segregation of hydrophobic/hydrophilic portions of a structure is a common motif in biological systems.[3]

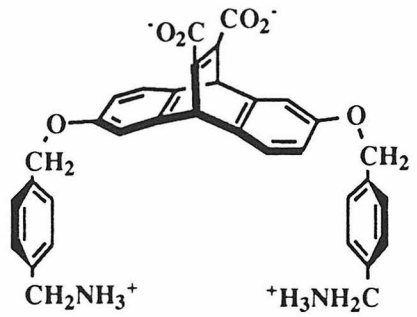

1

[(*R*, *R*)-Stereochemistry of Ethenoanthracene unit shown]

Figure 7.3. Simple application of the type A design for a self-assembling monomer.

Figure 7.6 illustrates the synthetic route used for preparation of **1**. Ethenoanthracene building block **2** is alkylated with α,α'-dibromo-*p*-xylene (**3**). Ammoniolysis provides diamine **5**, and ester hydrolysis affords the target molecule. An

alternate synthesis involved the preparation of **5** by borane reduction of dinitrile **6**; however, purification of **5** from this reaction proved troublesome; thus the ammoniolysis procedure was preferred.

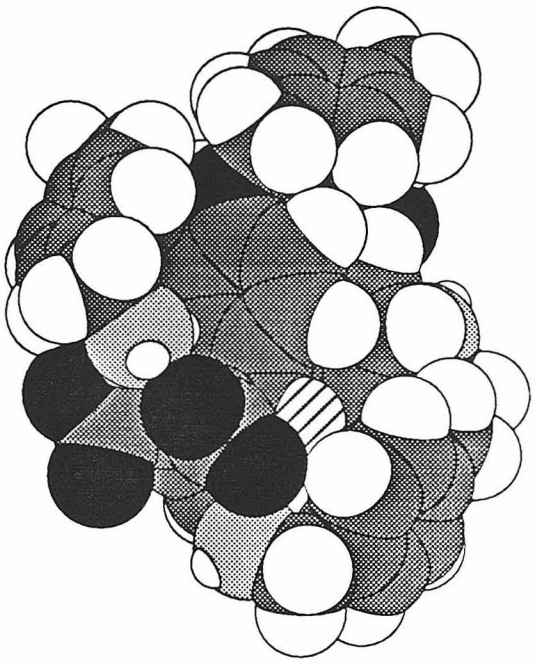

Figure 7.4. CPK representation of a possible structure for the dimer formed by 1_R. The bridgehead proton is stripped for identification.

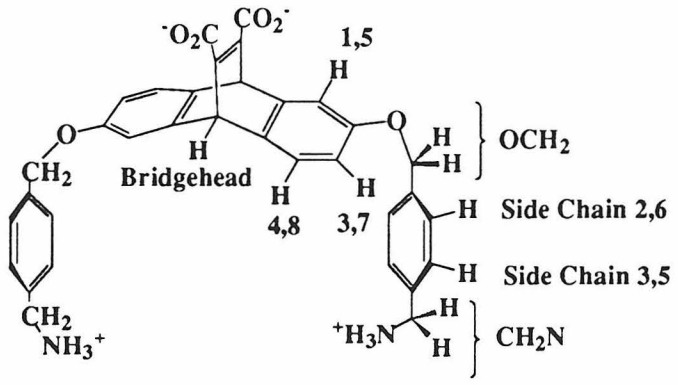

Figure 7.5. Proton designations for ethenoanthracene and ethanoanthracene building blocks used in the preparation of self-assembling molecules.

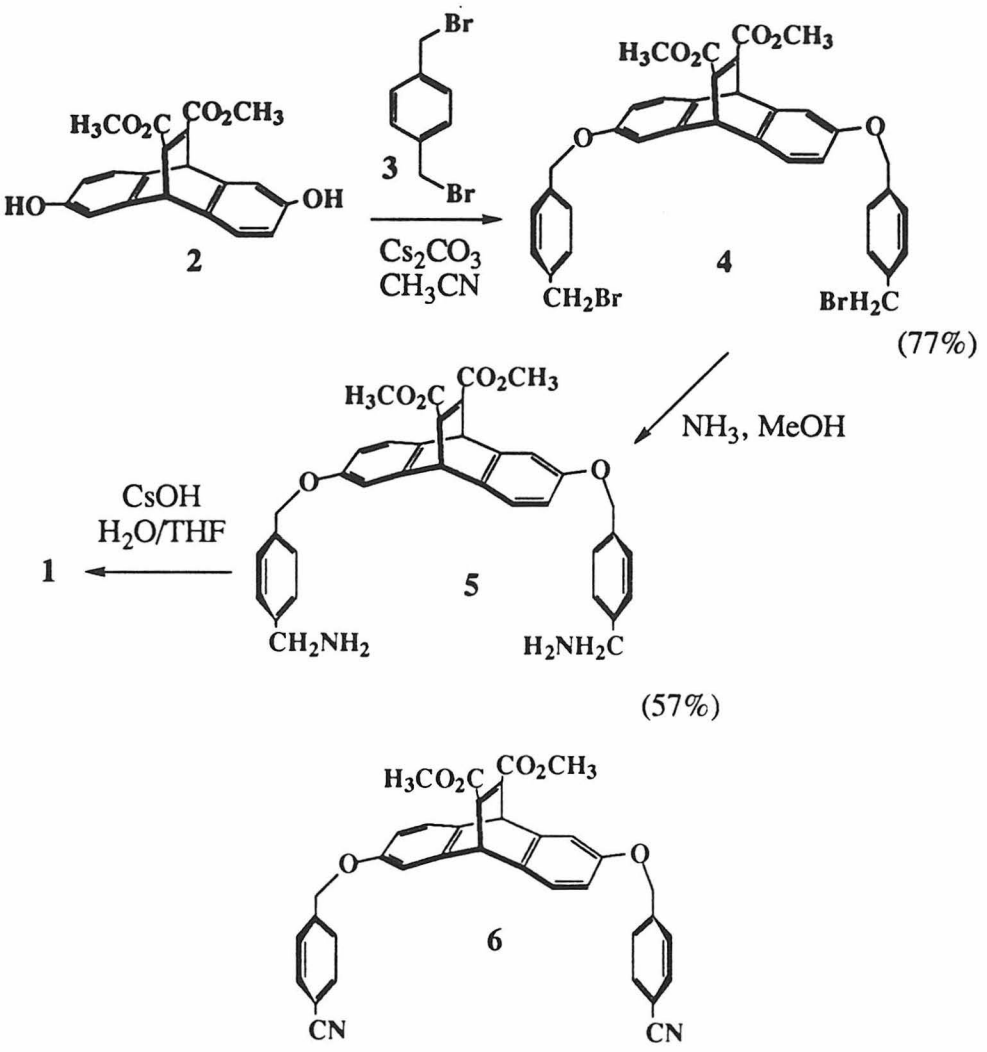

[(*R*, *R*)-Stereochemistry of Ethenoanthracene units shown]

Figure 7.6. Synthesis of 1.

Homomonomer **1** was found to be highly soluble in aqueous solutions only at low (pH ≤ 4) and high (pH ≥ 9) pH; additionally, it appeared to show negligible aggregation behavior at these pH's. At intermediate pH, the compound was observed to precipitate out of solution. Based on model compounds **7** and **8** (Figure 7.7), it was predicted that the isoelectric point of **1** should be near pH 7, a pH where the molecule was clearly aggregated and sparingly soluble at best.[4] Circular dichroism data of solutions of **1** suggest a critical

aggregation concentration of $\leq 5 \times 10^{-6}$ M at pH 7. Quantitative data were not obtained from the studies of **1**, but the molecule was soluble enough to allow some of the ^{1}H NMR signals to be followed as a function of pH.

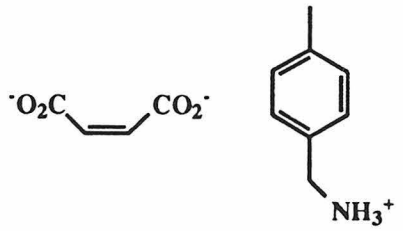

7 **8**

$pK_a = 1.910, 6.33$ $pK_a = 9.36$

$$\mathbf{1} \equiv \mathbf{7} + 2 \times \mathbf{8}$$

Isoelectric Point pH = $(pK_{a1} + pK_{a2} + pK_{a3} + pK_{a4})/4$

Isoelectric Point pH = 6.7

Figure 7.7. Estimation of the isoelectric point of 1,[5] from the pK_a's of its component ionizable groups.[6,7]

As the pH (pD) approaches 7, the NMR signals of the protons in **1** broaden and shift away from monomeric positions (high and low pH positions). These shifts are illustrated in Figure 7.8. The shift of NMR peak positions include a weak upfield shifting of the bridgehead proton signal, and a large upfield shift of the signal of the 3,7-proton. Although the model (Figure 7.4) predicts the most significant upfield shift should be observed for the bridgehead, the dimeric structure has many degrees of freedom and a slight twisting of one of the ethenoanthracene units could potentially place the aromatic ring of the side chain over any proton on the edge of the ethenoanthracene unit (such as the 3,7-proton).

These initial observations from studies of **1** are highly encouraging, but far from quantitative. The observed NMR shifting patterns, while not true to the model of Figure

7.4, may be consistent with a similar structure. The next approach was to look at a heteromolecular system. In this case, the component molecules are soluble at the pH desired for study, possibly providing data more conducive to quantitative analysis.

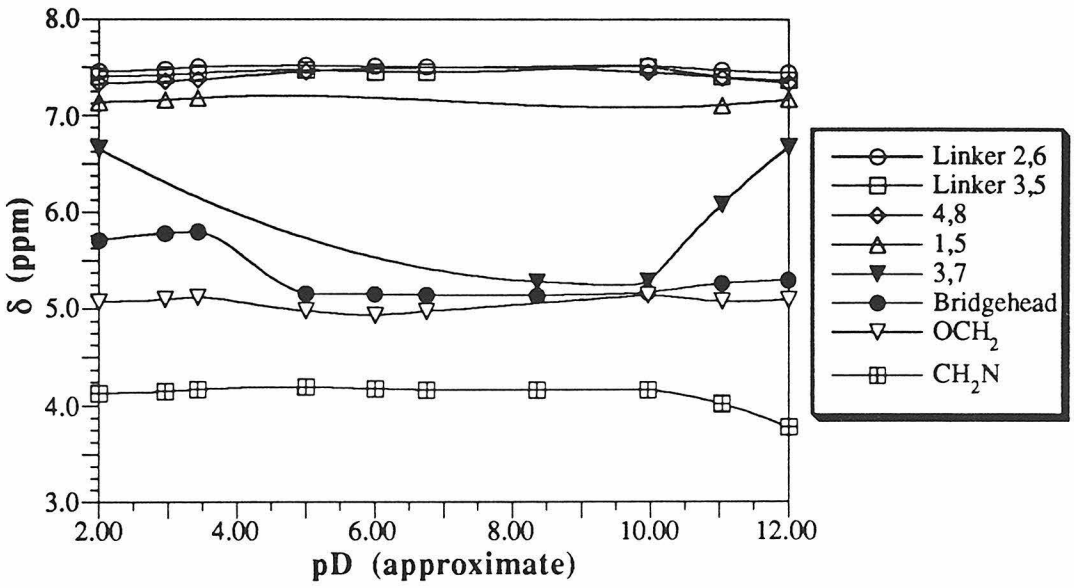

Figure 7.8. Variation of ^{1}H NMR chemical shift with pH for the protons of $\mathbf{1}_R$.

7.2.2 Heteromolecular Self-Assembly

Using the type A design and a similar dimerization model to Figure 7.4, monomers **9-12** were proposed (Figure 7.9). The tetraanion **9** is designed to be able to interact with any of the three tetracations **10-12**. The preparation of these structures (except **9**) is, however, more complex than preparation of **1**. This resulted in some difficulties in the early stages of this project.

Tetracarboxylate **9**, is synthesized in two steps from ethenoanthracene building block **2** as shown in Figure 7.10. The intermediate tetraester (**13**) provides the starting point for the synthesis of the tetracationic molecules **10-12** (Figures 7.11-7.12). For **10**, the tetraester can be converted to tetraamide **15** by ammoniolysis; unfortunately, all

attempts at the reduction of this amide failed (Figure 7.11). An alternate attempt starting from the dinitrile **6** again smoothly under went ammoniolysis to give diamide/dinitrile **16** (Figure 7.11), but all reduction attempts of **16** also failed (Figure 7.11). A similar tetrafunctionalization approach was tried for the preparation of **11** and **12** as well (Figure

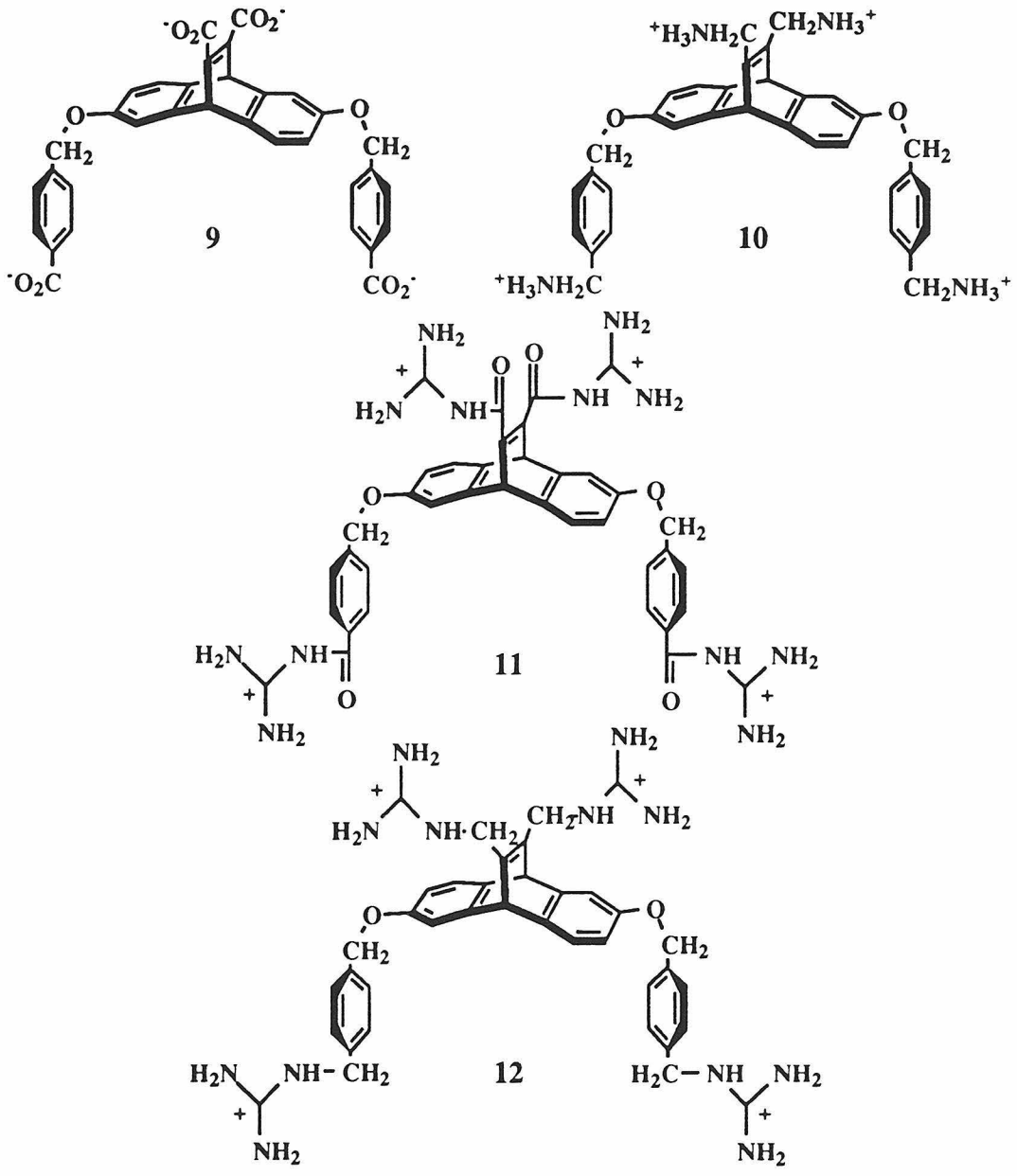

[(*R*, *R*)-Stereochemistry of Ethenoanthracene units shown]

Figure 7.9. Monomers capable of forming heteromolecular dimers.

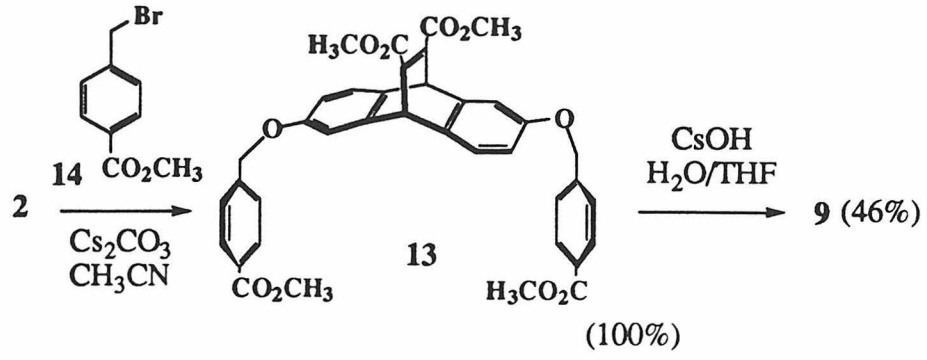

[(*R*, *R*)-Stereochemistry of Ethenoanthracene units shown]

Figure 7.10. Synthesis of 9.

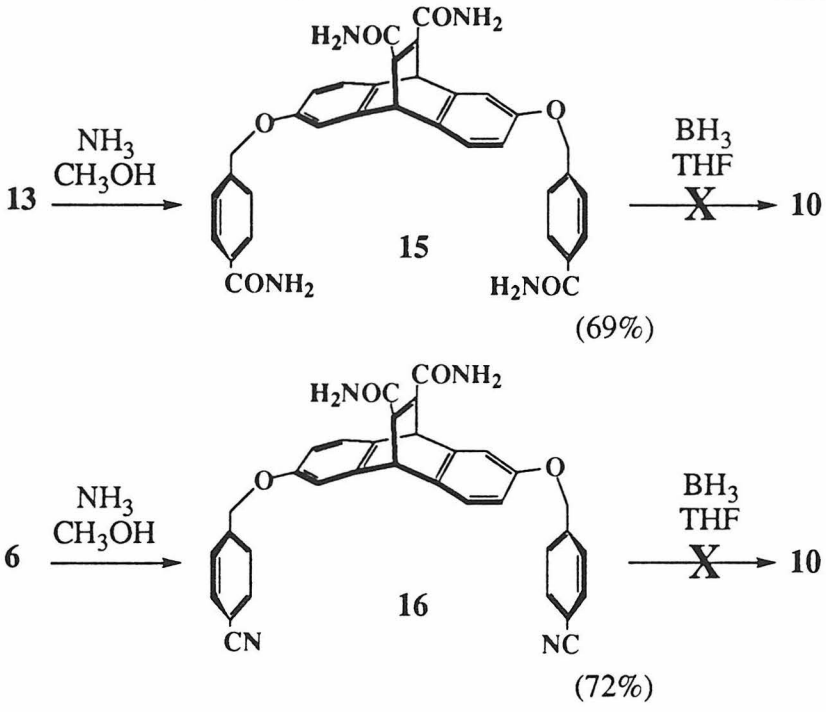

[(*R*, *R*)-Stereochemistry of Ethenoanthracene units shown]

Figure 7.11. Attempted synthesis of 10.

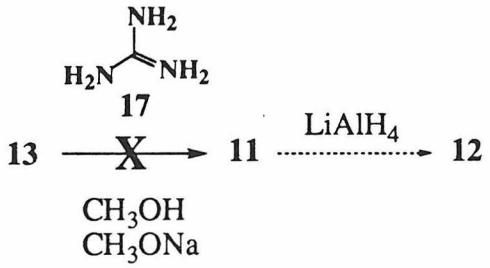

Figure 7.12. Attempted synthesis of 11 and 12.

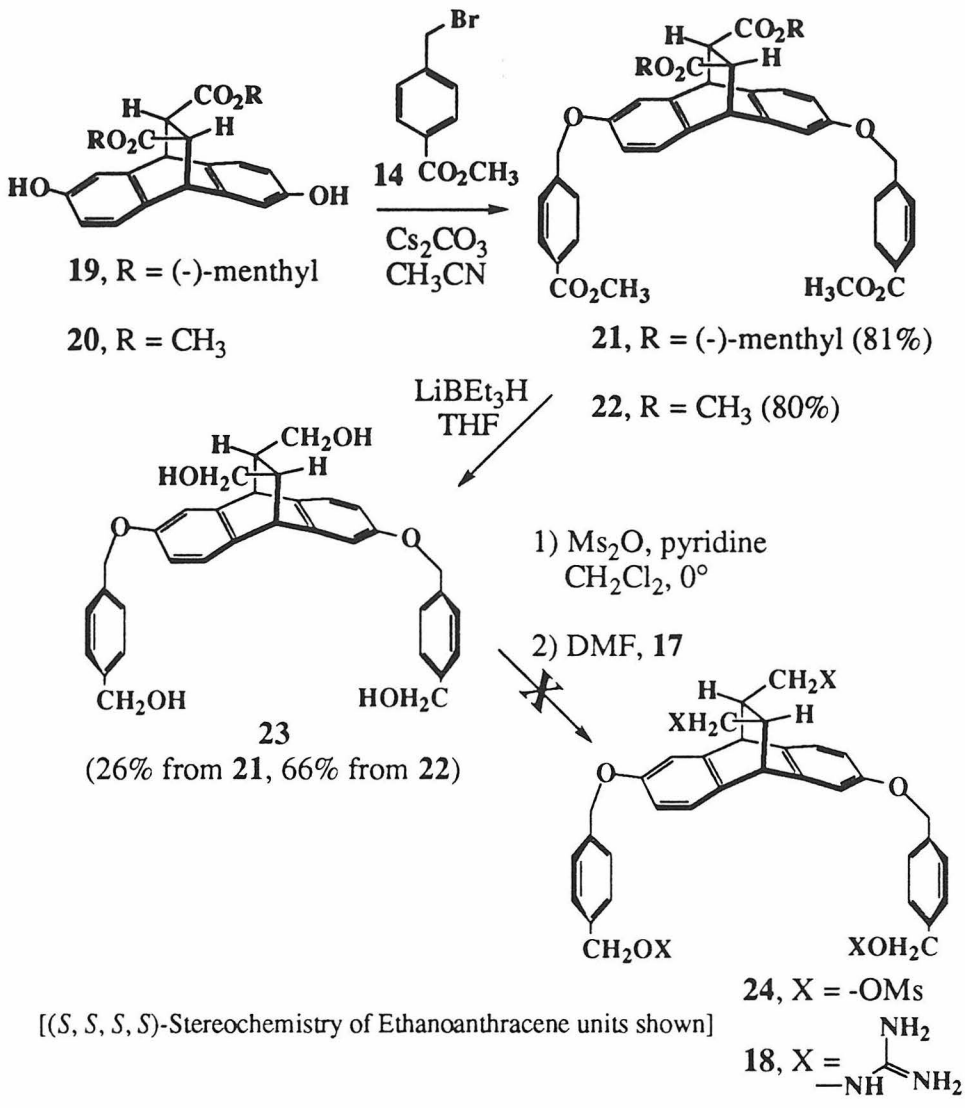

Figure 7.13. Attempted synthesis of an alternate tetraguanidine (18).

7.12). Reaction of **13** with guanidine free base (**17**), however, failed to give a structure that could be assigned as **11**.

Using an alternate approach that did not involve an acylguanidine intermediate, tetraguanidine **18** was proposed (Figure 7.13). Starting with either ethanoanthracene building block **19** or **20**, a tetraester (**21**, **22**) is prepared analogously to **13**. Reduction affords the tetra alcohol **23**. The attempted conversion to **18** without isolating the intermediate mesylate **24** was unsuccessful.

The syntheses of the tetracationic molecules **10-12** and **18** suffer from the attempts at tetrafunctionalizing the precursors to go directly to the desired product. Unfortunately, alternate syntheses in which the cationic functional groups are introduced sequentially or two at a time would require significantly lengthier syntheses (obtaining the etheno- and ethanoanthracene building blocks themselves already involves non-trivial synthetic procedures).[1bc]

At the point where attempts at the preparation of **10-12** were being abandoned, Jennifer Ma successfully prepared the type B tetracation **25** (Figure 7.14).[8] This type B structure was predicted by CPK models to interact with a tetraanion like **9** by a similar model to the two type A molecule interaction (Figure 7.15). Again it is predicted that the bridgehead protons should experience a shielding effect due to the close proximity of an aromatic ring, resulting in an upfield shift of the bridgehead proton NMR signal upon interaction with **9**. The initial heterodimerization studies were carried out with tetracation **25**.

When pD 7 (phosphate-*d* buffer) solutions of $\mathbf{9_R}$ and $\mathbf{25_{RS}}$ were mixed, immediate precipitation was observed. After the addition of a slight stoichiometric excess of $\mathbf{9_R}$ to a solution of **25**, only weak NMR signals for the protons of $\mathbf{9_R}$ were observed (Figure 7.16). Likewise prior to addition of an excess of $\mathbf{9_R}$, only NMR signals for $\mathbf{25_{RS}}$ were observed. The precipitate, however, could be resolubilized on changing pH, as shown in Figure 7.16. If the solution is made acidic (by addition of DCl), the tetraamine $\mathbf{25_{RS}}$ is redissolved, but $\mathbf{9_R}$ remains a solid (the protonated form of $\mathbf{9_R}$ is not soluble at acidic pH). If base is added, the precipitate completely dissolves and signals for both $\mathbf{9_R}$ and $\mathbf{25_{RS}}$ are observed by NMR. This is significant because $\mathbf{25_{RS}}$ is normally not soluble at high pH; it appears that some type of complex is forming in which the tetraanionic $\mathbf{9_R}$ solubilizes the deprotonated form of $\mathbf{25_{RS}}$. These observations are not unexpected as carboxylates are known to be better solubilizing groups than protonated amines.[9] Addition of organic solvents had little effect on the precipitate, CD_3CN did not solubilize the complex and

DMSO-d_6 brought the chemical shifts back to non-interacting values. The precipitate itself was found to have a 1:1 composition of $\mathbf{9_R}$:$\mathbf{25_{RS}}$, as determined by ^{1}H NMR of a DMSO-d_6 solution of the precipitate. Analogous results were obtained when $\mathbf{25_{RS}}$ was allowed to interact with $\mathbf{9_S}$ and the ethanoanthracene based tetracarboxylates **26** and **27** (Figure 7.17).[10]

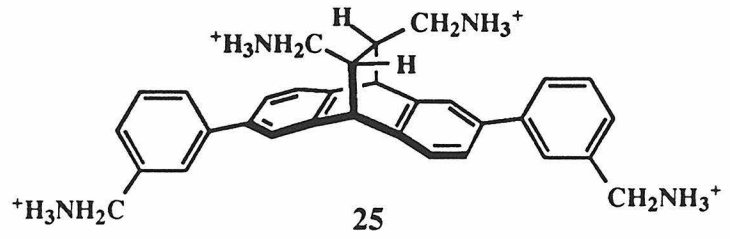

25

[(*R*, *R*, *S*, *S*)-Stereochemistry of Ethanoanthracene Unit Shown]

Figure 7.14. Type B tetracation capable of forming heterodimers with 9.[8]

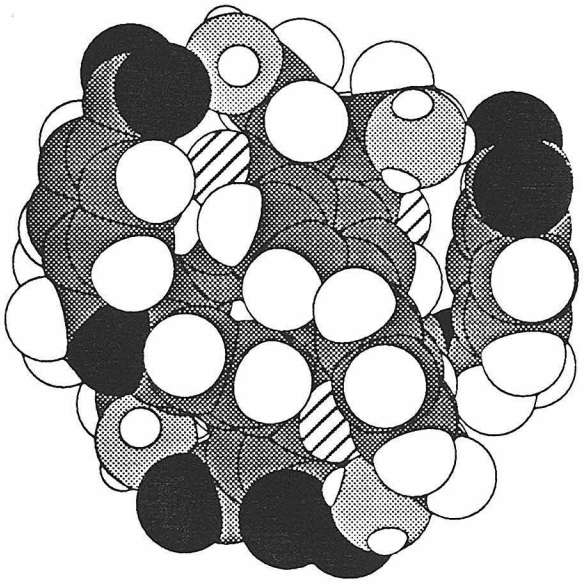

Figure 7.15. CPK representation of a possible structure for the dimer formed by $\mathbf{9_R}$ and $\mathbf{25_{RS}}$. The bridgehead protons are stripped for identification.

Especially important in Figure 7.16 is that in the high pD solution (7.16D), all the proton signals of both compounds were shifted upfield from their lower pH non-interacting

positions. Most significantly shifted are the signals for bridgehead and CH_2N protons of $\mathbf{25_{RS}}$. The signal for the CH_2N protons is expected to be shifted, due to the adjacent amine group being deprotonated at the higher pH, but the bridgehead proton signal is not expected to show significant shifting at the higher pH in the absence of complexation.

The results obtained here, along with those of the previous section, are highly encouraging and show some support for the dimer models proposed in Figures 7.4 and 7.15. The results, however, are far from definitive and bring up a number of questions and new directions for study. The most important relates to the ^1H NMR spectral changes associated with dimerization vs micelle-like aggregation.

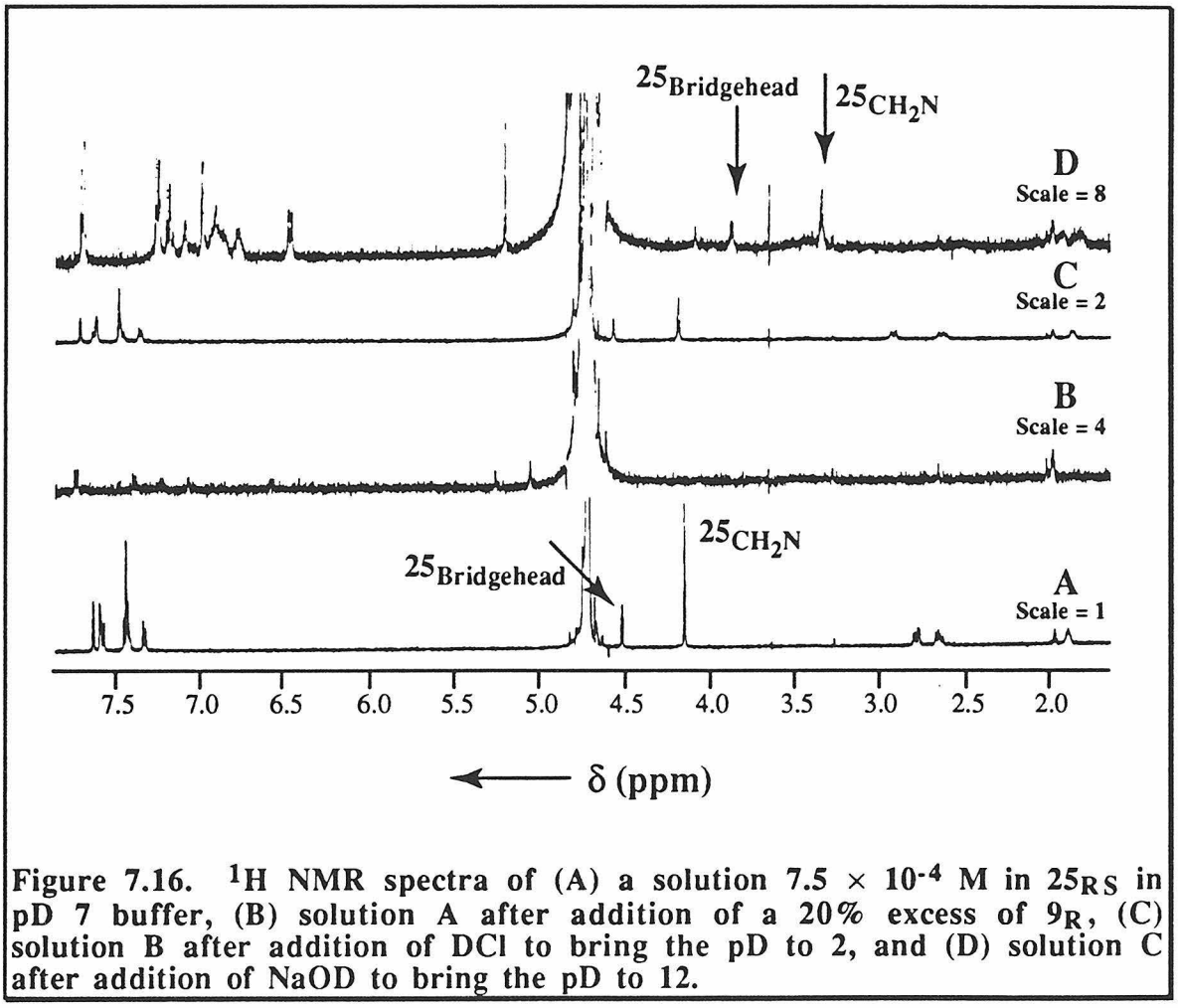

Figure 7.16. ^1H NMR spectra of (A) a solution 7.5×10^{-4} M in 25_{RS} in pD 7 buffer, (B) solution A after addition of a 20% excess of 9_R, (C) solution B after addition of DCl to bring the pD to 2, and (D) solution C after addition of NaOD to bring the pD to 12.

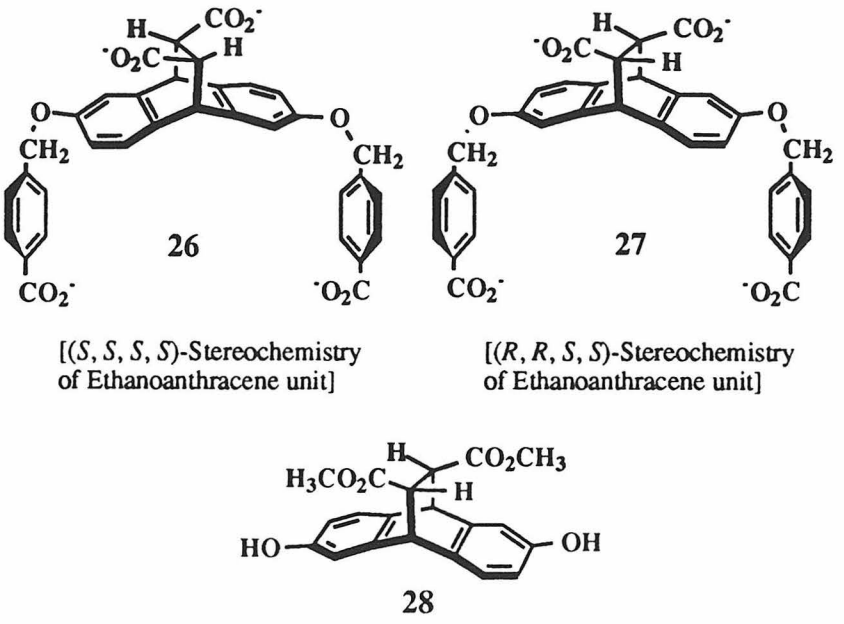

Figure 7.17. Ethanoanthracene based tetracarboxylates observed to interact with 25_{RS}.[10]

7.2.3 Control Studies

In assuming the observed upfield shifting of bridgehead and 3,7-proton NMR signals described in sections 7.2.1 and 7.2.2 are meaningful, it needed to be established that the NMR shift patterns associated with aggregation of similar molecules not self-complimentary to one another are different than what is observed for the **1** and **9/25** systems. Figure 7.18 shows several molecules based on the ethenoanthracene structure that are not self-complimentary, and hence should not assemble into dimeric assemblies.

The molecules of Figure 7.18 were studied in borate-*d* (pD 9 buffer), concentrated (aggregated) solutions were prepared and diluted while being followed with ^{1}H NMR. Spectra of **29** show broad peaks at higher concentrations, that on dilution sharpen up but do not show significant shifting ($\Delta\delta > 0.05$ ppm) of peak positions in either the upfield or downfield directions. Solutions of **30** and **31** at high concentrations showed large down-field shifts of the bridgehead proton signal relative to low concentration solutions, while

other peaks showed insignificant shifting (Figures 7.19 and 7.20). The aggregation behavior of **32** followed the same pattern of downfield shifting of the bridgehead proton signal at high concentration. Similar behavior was observed with tetracarboxylate **9** under conditions of aggregation in borate-*d* (Figure 7.21); large downfield shifting of the bridgehead proton signal occurs on aggregation.

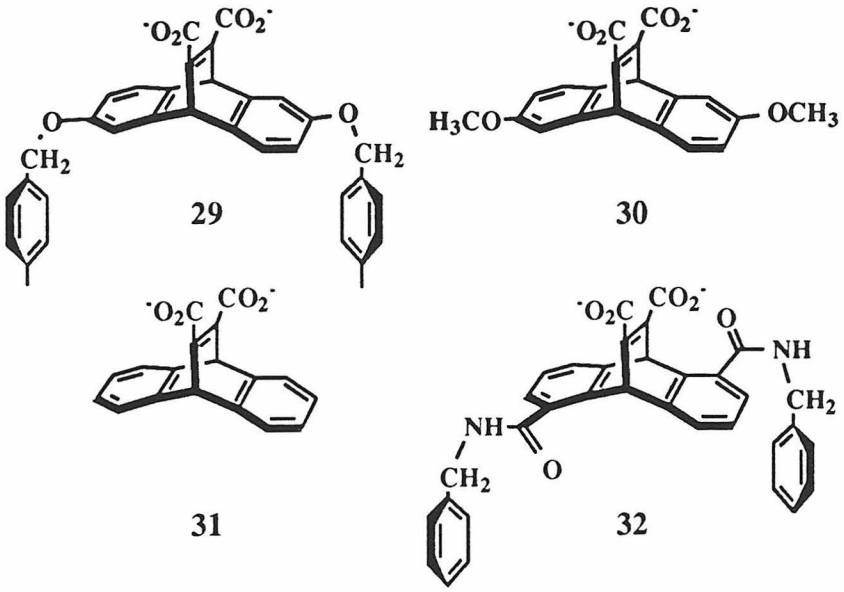

[(*R*, *R*)-Stereochemistry of Ethenoanthracene units shown]

Figure 7.18. Ethanoanthracene based molecules that are not expected to aggregate in an ordered manner.

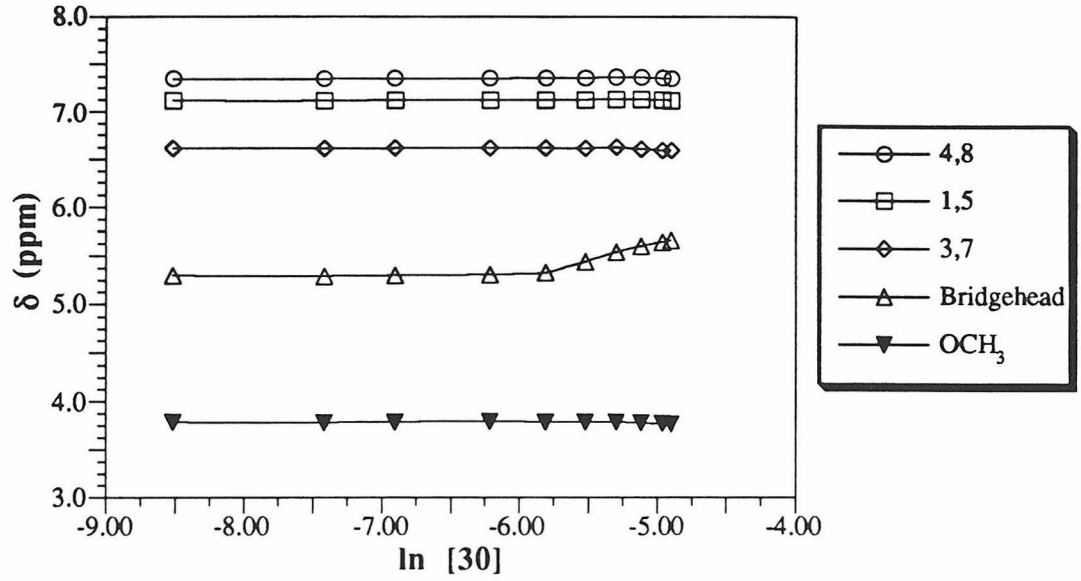

Figure 7.19. Variation of ^{1}H NMR chemical shift with concentration for the protons of 30_R in borate-*d* (pD 9 buffer).

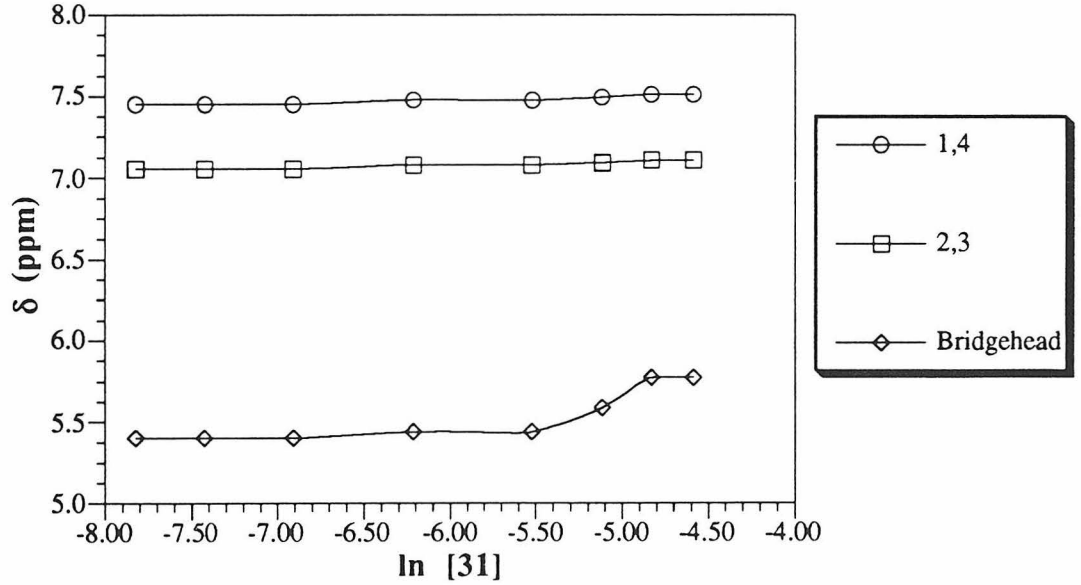

Figure 7.20. Variation of ^{1}H NMR chemical shift with concentration for the protons of 31 in borate-*d* (pD 9 buffer).

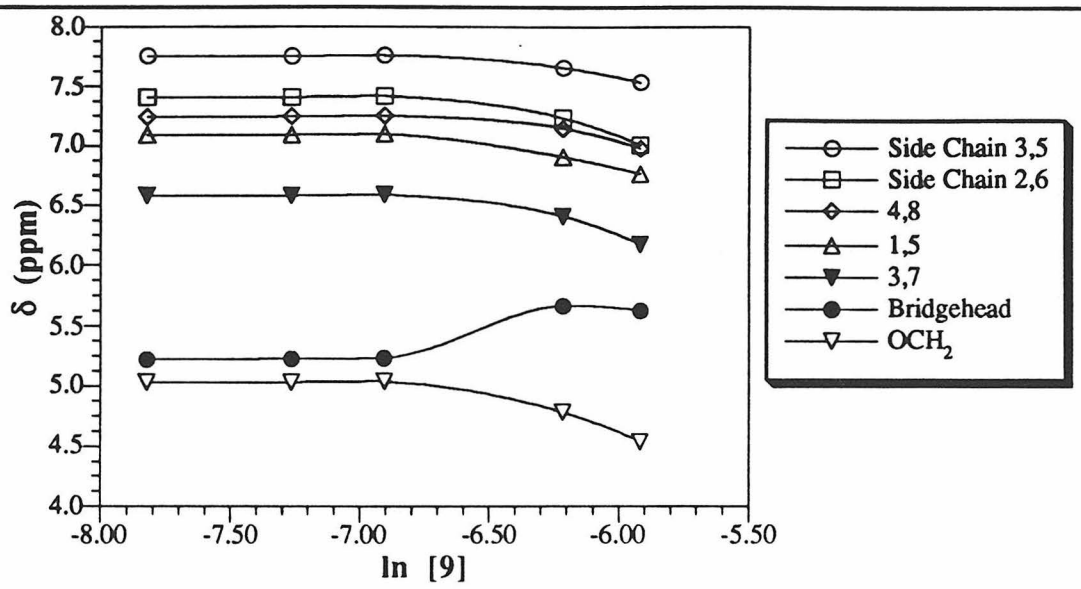

Figure 7.21. Variation of ^{1}H NMR chemical shift with concentration for the protons of 9_R in borate-*d* (pD 9 buffer).

In all of these control studies, the shift patterns clearly do not mimic those observed with studies of **1** and **9/25**. None of the molecules in Figure 7.18 are expected to form ordered assemblies; the NMR shift patterns that emerge are thought to be those of micelle-like aggregate formation. Given the dissimilarity between the observations here and those of the studies of **1** and **9/25**, it is proposed that the molecules **1** and **9/25** assemble in an ordered manner; however, the degree of order and exact structure is not known.

7.2.4 Implications of the Initial Studies

The studies described in this section have established certain ^{1}H NMR spectral shift patterns that are associated with some as of yet undetermined form of self-association that differs from micelle-like aggregation. This assembly is detected by strong upfield shifts of 3,7-proton NMR signals for assemblies formed by type A structures and by upfield shifts of the bridgehead proton signal for assemblies formed from a combination of type A and type B structures. Micelle-like aggregation, on the other hand, is indicated by downfield shifting of bridgehead proton signals.

Due to problems associated with complex solubility, quantitative studies of these self-assembling systems have not been possible; however, the observations suggest two directions for future study. The first alteration of the initial molecule designs should address the overall charge of the assembly that is forming. At the pH of interest (pH 7), the component monomers are expected to interact to form complexes with an overall neutral charge. Perhaps having a net charge on the complex may keep the assembly soluble and thus allow quantitative studies to be undertaken.

The second direction for future study involves the choice of the complimentary polar groups. The molecules studied thus far have the ability to form strong hydrogen bonds between the complimentary polar groups. The 1:1 stoichiometries observed for precipitates in these studies may not be dimers, but instead may be infinite hydrogen bonded networks. The application of complimentary groups incapable of hydrogen bonding may help to keep the aggregates soluble by not allowing these large hydrogen bonded networks to form.

Applications of these new directions are described in the following sections of this chapter.

7.3 Charge Mismatching in Aggregation Studies

7.3.1 General

In an effort to keep the molecular assemblies soluble, a number of molecules incorporating non-equivalent charge matching was desired. Figure 7.22 illustrates four structures derived from the initial type A molecules, that are suited to this task. Molecules **33**-**35** were proposed to interact with tetracations such as **25**, while **36** is designed to be a homomonomer analogous to **1**. In the case of **34**, the molecule was proposed so that its overall charge can be controlled by pH. At pH 7 the phenols should be protonated, while

the carboxylates are deprotonated (overall charge -2); at pH > 10 the molecule should be fully deprotonated with an overall charge of -4.

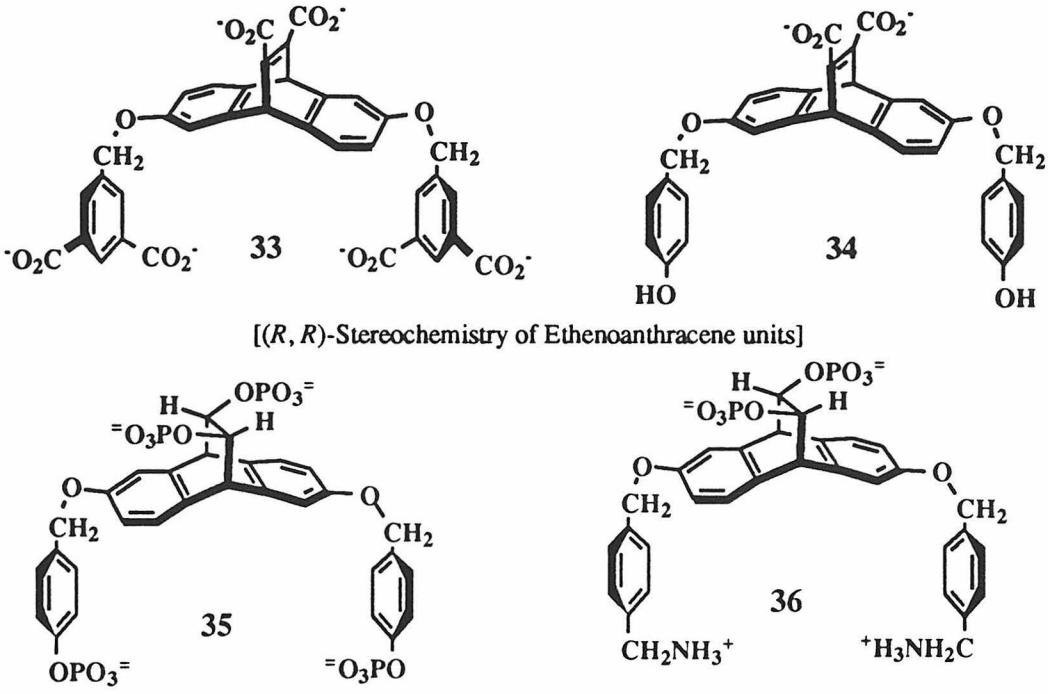

Figure 7.22. Molecules proposed to form dimers with net charge.

Due to synthetic difficulties, only **33** was successfully prepared and studied. The following section describes these results. Section 7.3.3 describes the synthetic approaches toward **34-36**.

7.3.2 Hexacarboxylate (33)

Hexaanion **33** was prepared by appending ethenoanthracene building block **2** with isophthalic ester side chains derived from 5-methylisophthalic acid (**37**) as shown in Figure 7.23.[11,12] Hydrolysis of hexaester **40** provides **33**.

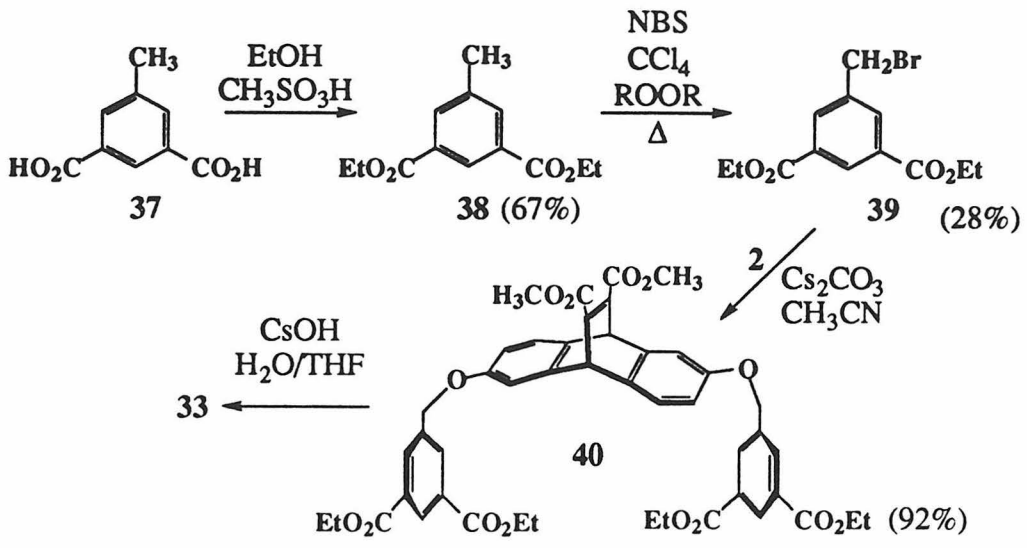

[(*R*, *R*)-Stereochemistry of Ethenoanthracene unit shown]

Figure 7.23. Synthesis of 33.

Studies of the interaction of **33** with **25** were carried out analogously to those described for **9** and **25**. The results were almost identical to the **9/25** results (precipitation, precipitate redissolves at high pD). NMR signals for **33** could be detected in the presence of an excess of **25**; however, these signals were very weak. The experiments suggest only a very slight increase in the solubility of the complex is obtained with the increased charge of the anionic component. It appears that the ability of the interacting molecules to hydrogen bond to one another is a more significant factor in complex formation than electrostatic forces.

7.3.3 Other Designs

A number of problems were encountered in attempts to prepare **34-36**, and none of these species was successfully prepared. In light of the results obtained with **33/25**, the synthesis of **34-36** was not considered a high priority. These molecules are still of interest, however, as they can be used in future work, particularly **34** and **35** for studies of

non-hydrogen bonding heteromolecular systems (see Section 7.5). This section describes the initial strategies and attempts at these preparations.

The synthesis proposed for **34** (Figure 7.24) failed in the alkylation step (preparation of **43**). The acetyl protecting groups do not withstand the reaction conditions, resulting in a competition for phenolic oxygens and a variety of products. Similar problems have been encountered in attempts to prepare cyclophane hosts with phenolic oxygen atoms in our laboratories.[13] For future attempts at **34**, the results of these other studies should prove useful.[13]

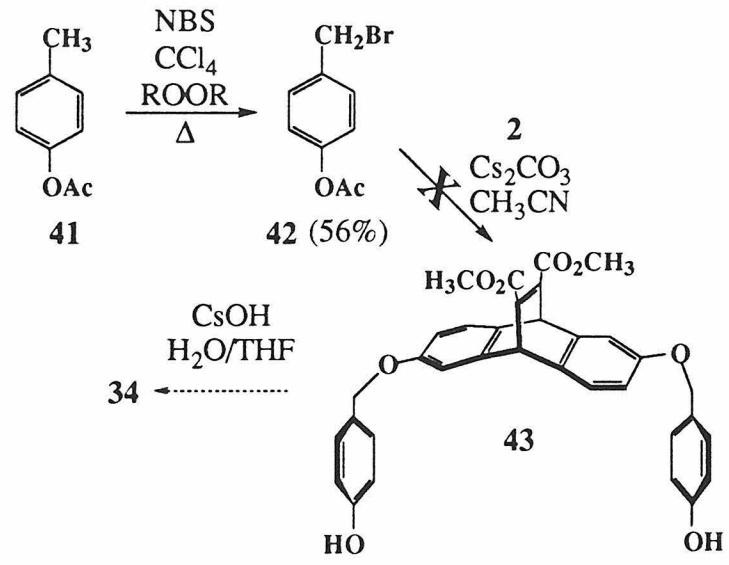

[(*R*, *R*)-Stereochemistry of Ethenoanthracene unit shown]

Figure 7.24. Attempted synthesis of 34.

Several attempts were made at preparation of the tetraphosphate **35** (Figure 7.25). Initially, a tetrafunctionalization of tetraol **23** using standard nucleic acid chemistry techniques for introducing phosphates was attempted.[14] No product was isolated from the attempted tetra-functionalization to prepare **44**. In an attempt to assemble **34** convergently, the synthesis of the ethanoanthracene **48** and benzyl halide **49** was attempted. **48** was obtained in three steps from precursor **50**, but all attempts at preparing protected phosphate

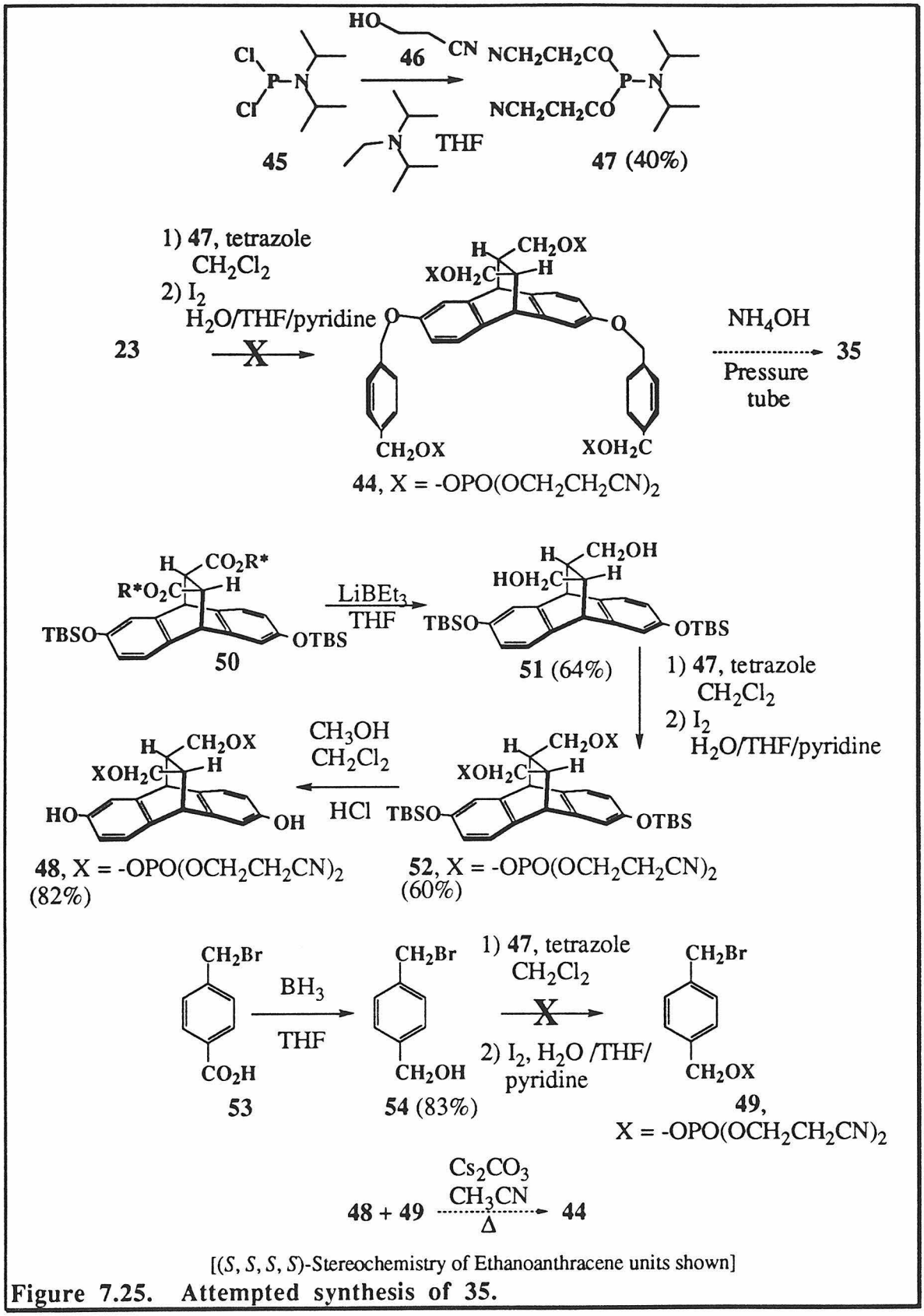

[(*S*, *S*, *S*, *S*)-Stereochemistry of Ethanoanthracene units shown]

Figure 7.25. Attempted synthesis of 35.

49 failed. It appeared that the phosphate ester was cleaving under conditions of purification (Si gel, neutral and basic). Since benzyl phosphates tend to be labile,[15] an alternate tetraphosphate **55** was proposed (Figure 7.26). Unfortunately, benzyl bromide **55** was never successfully converted to phosphate ester **58**. While the convergent approach to **35** and **55** seemed logical, attempts to alkylate **48** in order to prepare homomonomer **36** were unsuccessful. This suggests that even if **49** and **58** had been prepared, the alkylation of **48** would have failed.

Further attempts at the preparation of these compounds was abandoned, in favor of pursuing the studies described in Sections 7.4 and 7.5. Their attempted synthesis is included for reference for future studies on these types of systems.

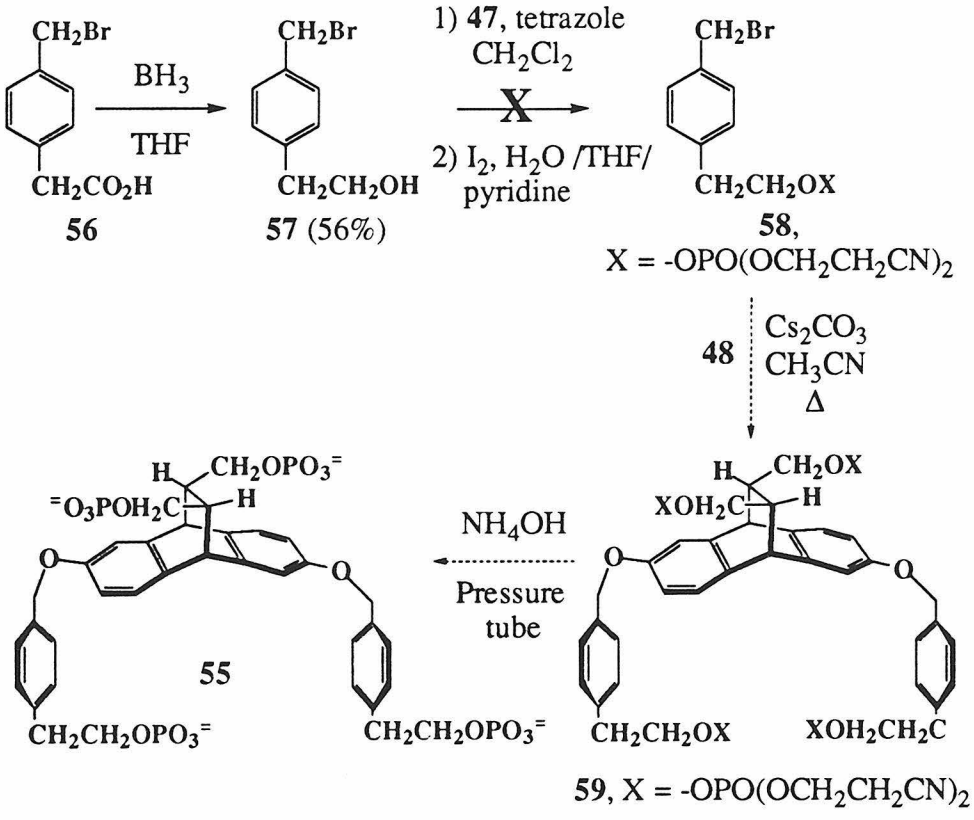

Figure 7.26. Attempted synthesis of 55.

7.3.4 Studies in Mixed Solvents

The tetraamide intermediate (**15**) from the failed synthesis of **10** was found to have limited solubility in aqueous media. It also could potentially form a weakly hydrogen bonded aggregate with either itself or **9** under appropriate conditions. Aggregation in aqueous solutions of **15** was evident by cloudiness and limited solubility, precluding any dilution studies. It was found that addition of 10% DMSO-d_6 (by volume) does solubilize **15** and in this solvent system self-association appears to be negligible. Given this observation study of the interaction of **15** with the tetraanion **9** in the mixed solvent system 10% DMSO-d_6/90% 0.01 M CsOD was investigated. In this system two type A molecules interact to form a dimer with an overall charge of -4.

^{1}H NMR spectra showed only very small changes on interaction (Figure 7.27). In general, the chemical shifts of the tetracarboxylate **9** showed no significant change in position, but upfield shifting of the signals for **15** were observed on addition of **9**. Initially these small changes were thought to be insignificant. Figure 7.27, however, shows a nearly 0.20 ppm upfield shift for the 3,7-protons of **15**-a small shift, but one that is consistent with the model proposed for the type A systems (see Section 7.2.1). Another interesting observation is that the curves saturate around a composition of 2:1 **9**:**15**; Figure 7.27 was not obtained under mol ratio conditions, and this stoichiometry requires additional testing.

Small spectral changes are to be expected from this system; in general, the addition of an organic cosolvent (CD_3CN in particular) has been found to decrease hydrophobic associations with systems studied in our laboratories.[1b] Such conditions, however, impart additional solubility to sparingly soluble molecules without negating strong intermolecular interactions.[1b] There is clearly some type of interaction between **15** and **9**; however, the association constant appears small under the given conditions. No further studies were attempted with this **9**/**15** heteromolecular system.

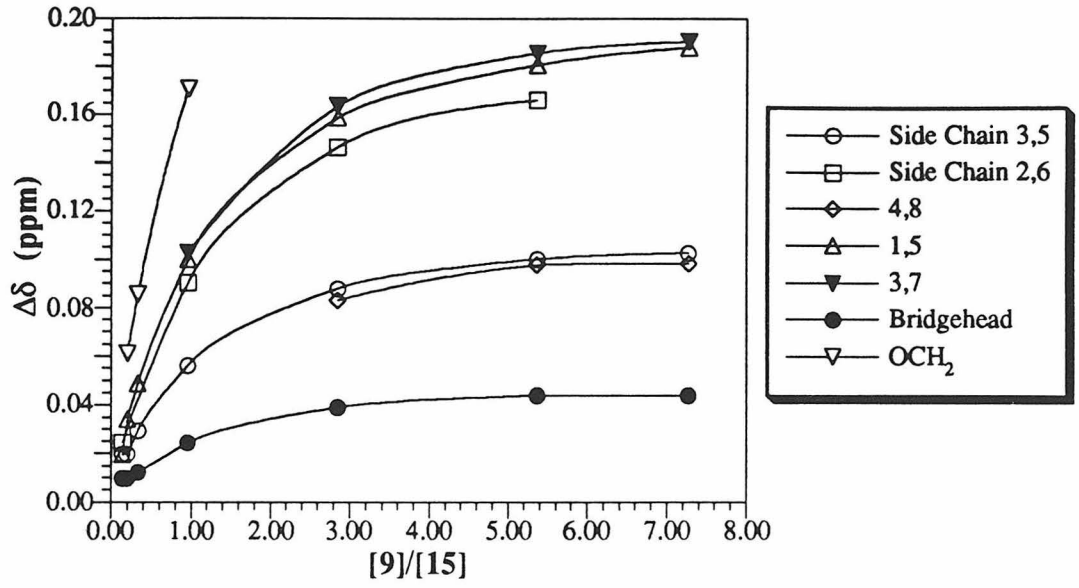

Figure 7.27. Variation of ^{1}H NMR chemical shift with addition of 9_R for the protons of 15_R in 10% DMSO-d_6/90% 0.01 M CsOD.

7.3.5 Conclusions

The addition of additional charge to the monomer units creates a number of synthetic challenges. The additional charge also does not appear to significantly help solubilize the assembly formed from the monomer units. From these initial results, it was thought that keeping the monomer units from hydrogen bonding to one another was more likely to provide results than simply changing the overall charge of the assembly.

7.4 Ion-Pairing vs Hydrogen Bonding in a Homomolecular System

7.4.1 General

In an effort to use electrostatic attractions as the directional functionality, and eliminate the ability of the monomers to hydrogen bond to one another, the molecules of Figure 7.28 were proposed. The dicarboxylate/diquaternary ammonium ion **60** is simply a

methylated analog of **1**, while the dicarboxylate/dipyridinium ion **61** represents a slight alteration of the initial designed type A systems. Both of these molecules are designed to maximize hydrophobic interactions in aggregation while using salt-bridges to hold the stoichiometry as a dimer (analogous to the model of Figure 7.4).

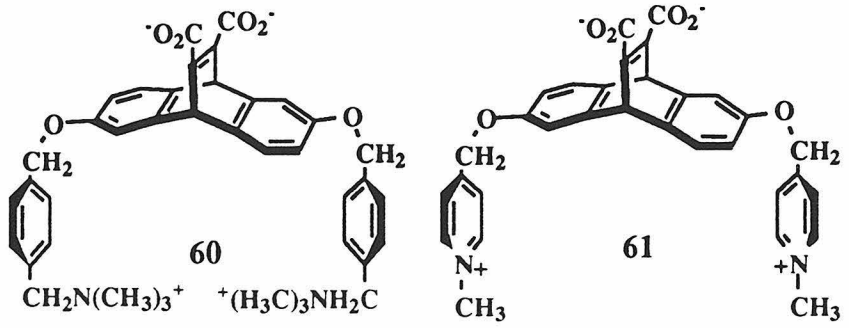

[(*R*, *R*)-Stereochemistry of Ethenoanthracene units shown]

Figure 7.28. Homomonomers proposed to form dimers incapable of hydrogen bonding together.

7.4.2 Synthesis

Following a protocol analogous to scheme of Figure 7.6, **60** was prepared by alkylation of bis(benzyl bromide) **4** with trimethyl amine to give diquaternary ammonium salt **62** (Figure 7.29). Hydrolysis of the esters of **62** provides the target molecule. Several preparations of **60** were undertaken. In the case where the product was isolated by precipitation from acidic solution, the material was found to decompose over time; this was evidenced by an initial observation of two ^{1}H NMR signals for the NCH_3 protons and, after several weeks, the observation of double signals for all protons. The results obtained from samples of **60** isolated from neutral or basic solutions are described in the following section.

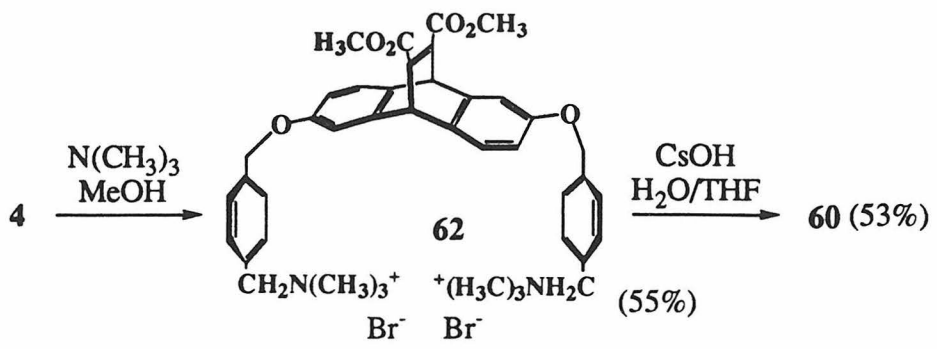

[(*R*, *R*)-Stereochemistry of Ethenoanthracene units shown]

Figure 7.29. Synthesis of 60.

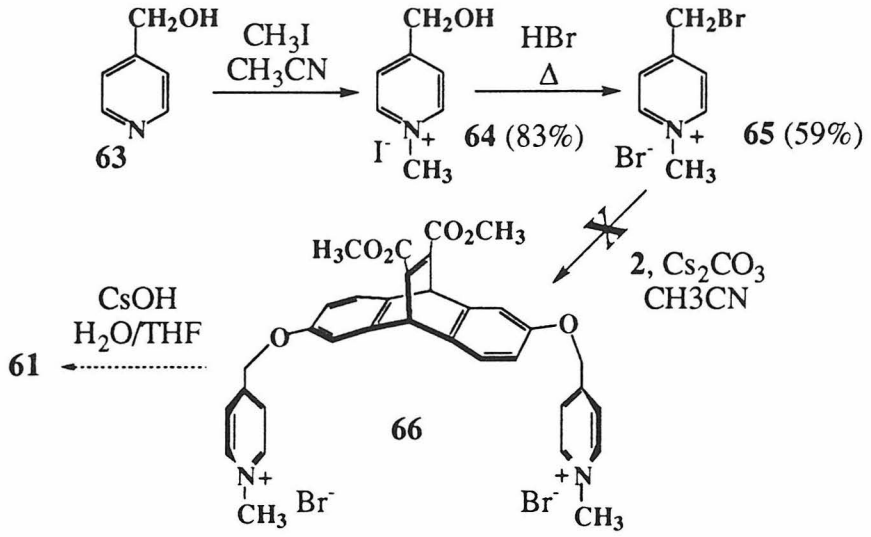

[(*R*, *R*)-Stereochemistry of Ethenoanthracene units shown]

Figure 7.30. Attempted synthesis of 61.

The proposed synthesis of **61** involves the alkylation of ethenoanthracene **2** with bromomethylpyridinium salt **62**,[16] followed by hydrolysis of ester precursor **65** (Figure 7.30). However, under the alkylation conditions the pyridinium ion decomposes to produce a bright red colored material of unknown structure (most likely a polyene dye-like structure). Pyridinium ions are known to undergo ring opening in the presence of base;[17] the alkylation conditions appear to be basic enough to bring about this rearrangement as

well. No further attempts were made to prepare **61**, as **60** was readily available for studies.

7.4.3 Experimental Observations

The aggregation behavior of **60** was found to be highly pH dependent. Figure 7.31 shows ^{1}H NMR spectra of **60** in solutions of varying pD. At pD ≥ 9, sharp signals for all protons are observed; but as the pD is lowered just below 7, the peaks begin to broaden and downfield shifting of the bridgehead proton signal is observed. As the pD is further lowered, the downfield shifting of the bridgehead proton signal continues and some peaks become so broad that they disappear into the baseline. These low pH spectral changes are consistent with the formation of a micelle-like aggregate (particularly the downfield shifting of the bridgehead proton signal as described in Section 7.2.3). The sharp peaks at basic pH on the other hand, do not represent monomeric **60** either. The positions at which these signals appear are all upfield of the positions at which they are expected for a monomeric molecule of the type A structure. Studies on large numbers of molecules that have the type A structure of Figure 7.1 have established that the ^{1}H NMR peak positions for protons in these molecules are similar across a wide variety of substitutions in both aqueous and organic solvents.[18] Table 7.1 presents typical ^{1}H NMR spectral data for several ethenoanthracene-based structures under non-aggregated conditions and compares it to the observed data of **60**.

Of particular importance was the observation of the 3,7-protons chemical shift being shifted the most upfield from the expected monomeric position. This is the same spectral shift observed in studies of **1**, a system for which there is some evidence for the dimer model in Figure 7.4. Dilution of the pD 9 solutions of **60** results in a slight downfield shifting of the proton signals toward expected monomeric positions, but the peaks are still at non-monomeric positions as the NMR detection limits approached (Figure 7.32). Addi-

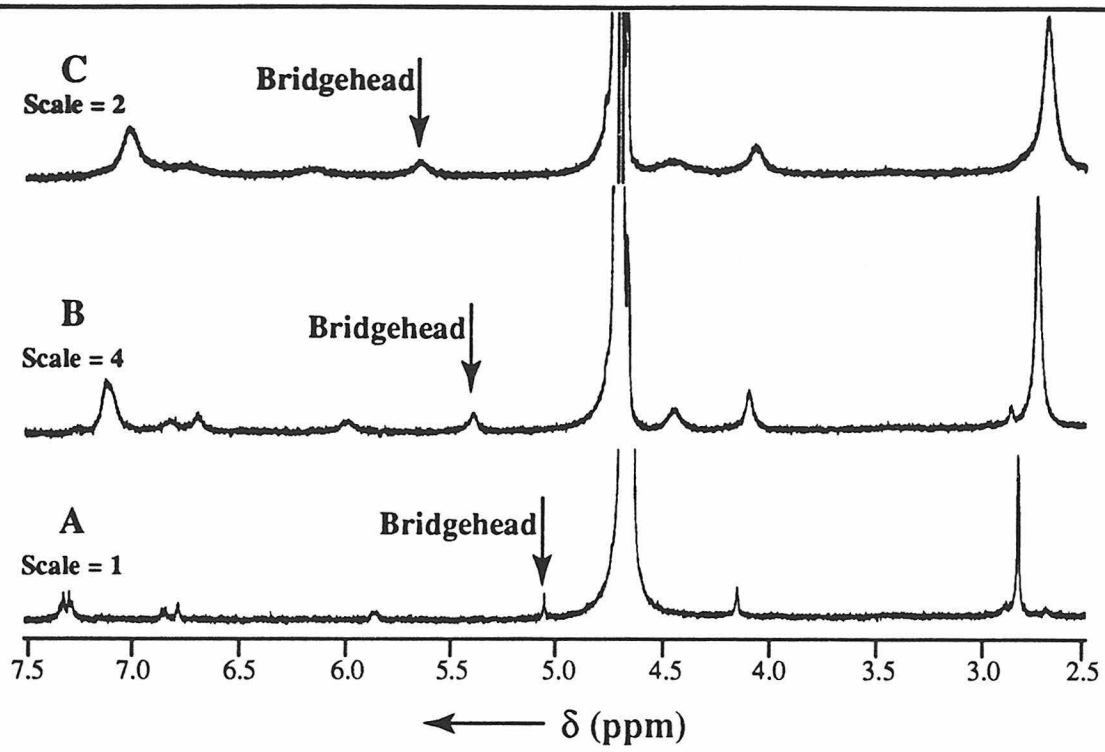

Figure 7.31. ^{1}H NMR Spectra of aqueous solutions of 60_R (1×10^{-3} M) at (A) pD 10, (B) pD 7, and (C) pD 5.

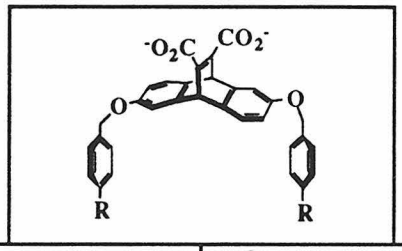

R =	-$CH_2N(CH_3)_3^+$ (60)[a]	-CH_2NH_2 (1)	-CH_3 (29)[c]	-CH_3[d]
Solvent =	pD 9	pD 12[b]	pD 9	$CDCl_3$
$\delta_{side\ chain}$ (d,d)	7.24	7.44, 7.37	7.34, 7.32	7.21, 7.16
$\delta_{4,8}$ (d)	6.80	7.34	7.25	7.05
$\delta_{1,5}$ (d)	6.74	7.16	7.11	7.02
$\delta_{3,7}$ (dd)	5.76	6.67	6.62	6.54
$\delta_{bridgehead}$ (s)	5.04	5.29	5.28	5.30
δ_{OCH2} (s)	(under solvent peak)	5.09	4.98	4.93
δ_{CO2CH3} (s)				3.77
δ_{NCH2} (s)	4.08	3.78		
δ_{NCH3} (s)	2.77			
δ_{ArCH3} (s)			2.33	2.33

Table 7.1. ^{1}H NMR chemical shifts (ppm) observed for several ethenoanthracene-based molecules.

[a]2.5×10^{-3} M (aggregated solution). [b]1 is not aggregated at this pH. [c]2×10^{-4} M (not aggregated). [d]This is the diester analog of **29**, a neutral organic soluble molecule.[1a]

tion of CD_3CN (a solvent known to break up aggregation)[1b] brings the proton chemical shifts back to the expected monomeric values at a composition of about 20% CD_3CN by volume (Figure 7.33). For reasons explained above, the presence of CD_3CN is not expected to alter the chemical shifts expected for monomer protons.

The pD 9 experiments are highly encouraging. The low pD observations suggest micelle-like behavior is occurring only at pD ≤ 7. Additionally, chemical shifts and spectral changes observed on dilution or CD_3CN addition suggest that a more organized aggregate is present at pD ≥ 9. The observation of the largest upfield shift for the 3,7-protons is consistent with observations from studies of **1** and the proposed model of Figure 7.4. Given these qualitative results, an appropriate quantitative model was desired. The following section describes the initial attempts at quantifying the observations described here.

7.4.4 Preliminary Results

Although further work is required to establish the stoichiometry of the **58** aggregate, the pD 9 data did fit to a dimer model. Furthermore, data from pD 7 and pD 2 studies (where micelle-like aggregation is presumably occurring) do not fit to this model. The model chosen assumes that a monomeric molecule (M) exists in equilibrium with dimer M_2, and has dimerization constant K_D.[19]

$$2\,M \rightleftharpoons M_2 \tag{7.1}$$

$$K_D = \frac{[M_2]}{[M]^2} \tag{7.2}$$

The mass balance equation for this system is given by

$$[M]_o = [M] + [M_2] \tag{7.3}$$

The changes in chemical shift between the observed chemical shift (δ_{obs}), the monomer chemical shift (δ_{mono}), and the dimer chemical shift (δ_{dimer}) are defined by equations 7.4 and 7.5. Equation 7.6 relates these chemical shifts to K_D and the total and equilibrium concentrations ($[M]_o$ and [M] respectively).[19]

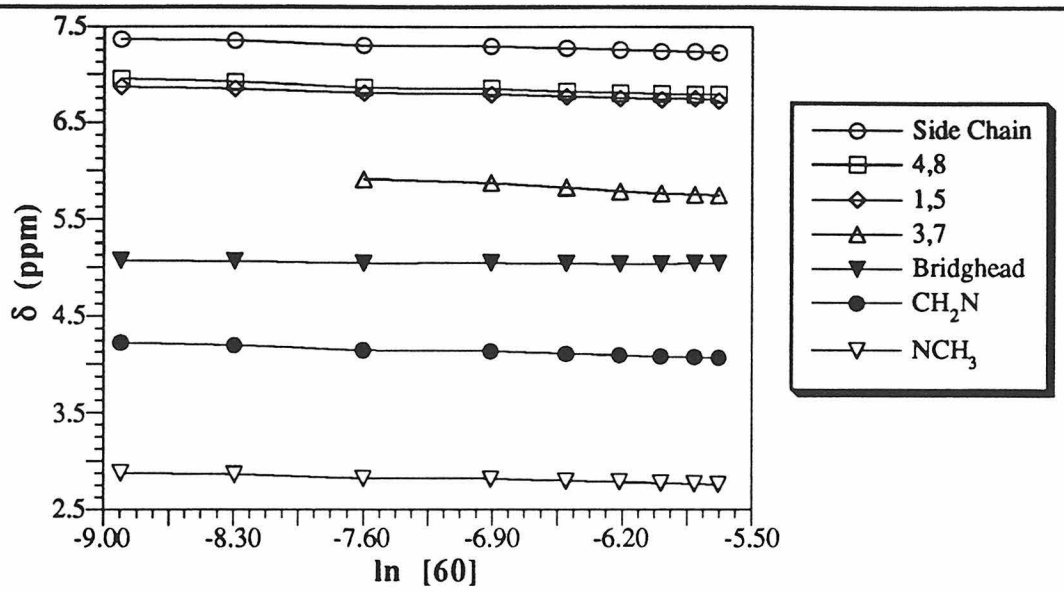

Figure 7.32. Variation of ^{1}H NMR chemical shift with concentration for the protons of 60_R in borate-*d* (pD 9 buffer).

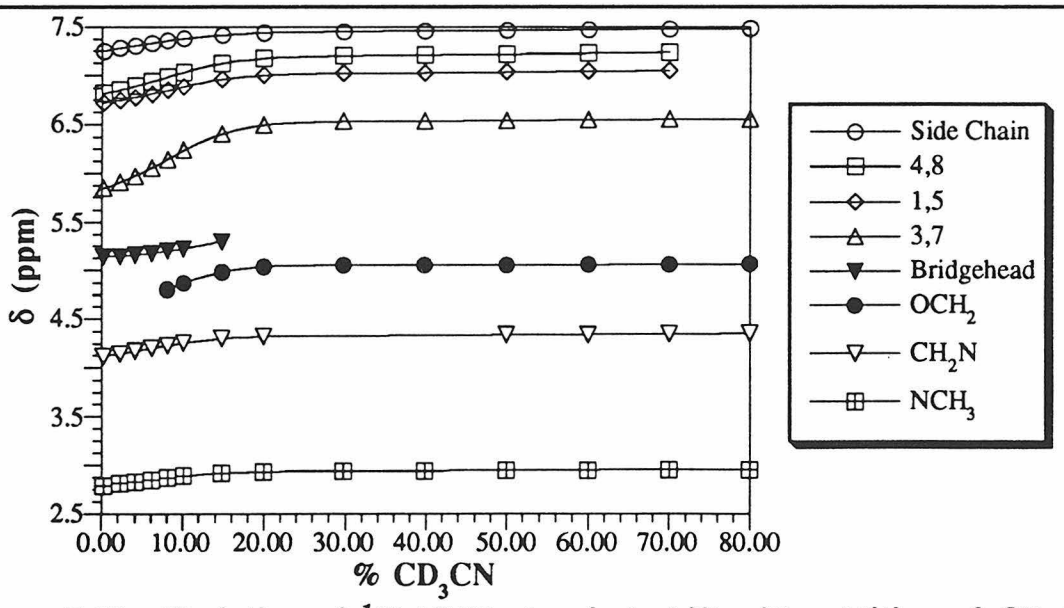

Figure 7.33. Variation of ^{1}H NMR chemical shift with addition of CD_3CN for the protons of 60_R in borate-*d* (pD 9 buffer).

$$\Delta\delta = \delta_{obs} - \delta_{mono} \tag{7.4}$$

$$\Delta\delta_2 = \delta_{dimer} - \delta_{mono} \tag{7.5}$$

$$\Delta\delta = \frac{2K_D[M]^2}{[M]_o}\Delta\delta_2 \tag{7.6}$$

A plot of δ_{obs} vs $2K_D[M]^2/[M]_o$ gives a slope of $\Delta\delta_2$ and an intercept of δ_{mono}.[19] For purposes of applying this model to **60**, δ_{mono} is assumed to be the same as the chemical shifts obtained in 20% CD_3CN/80% borate-*d*. An initial K_D is guessed and then adjusted until a best fit was obtained. In order to fit the results, the concentration of free monomer needed to be known this can be obtained by equation 7.7

$$[M] = \frac{-1 - \sqrt{1 + 8K_D[M]_o}}{4K_D} \tag{7.7}$$

The best-fit straight lines are shown in Figure 7.34 and the results tabulated in Table 7.2. The worst fitting data comes from the shifts for the bridgehead proton. This proton was not present in all the spectra of the experiment being fitted and thus has fewer data points than the other protons being fitted. The dimerization constant ($-\Delta G°_a$ = 7.5 kcal/mol) obtained from this proton is also much larger than value obtained from the other protons, and it can be statistically discarded from a Q-test.[20] The remaining protons give dimerization constants in the 3-5 kcal/mol range (Table 7.2) and with the exception of the 3,7-proton signal, all fitted δ_{mono} values were consistent with experiment (in 20% CD_3CN). δ_{mono} for the 3,7-protons was assumed to be 6.49 ppm, but the fitted value is 6.0 ppm; the dimerization constant obtained from this data set is, however, consistent with the data from the other protons fitting the model. Using an average of the dimerization constants (excluding the bridgehead protons data) gives a value of 4.0 kcal/mol.

The fit to the dimer model is encouraging, but not conclusive. Before the results here can be fully trusted, a broader range of concentrations should be studied (including monomeric concentrations). Additionally, experiments specifically designed to determine

the stoichiometry should be undertaken. The dimerization constant of 4.0 kcal/mol seems low for a system whose critical aggregation concentration (CAC) cannot be measured by NMR; this value most likely represents a lower limit to the actual value.

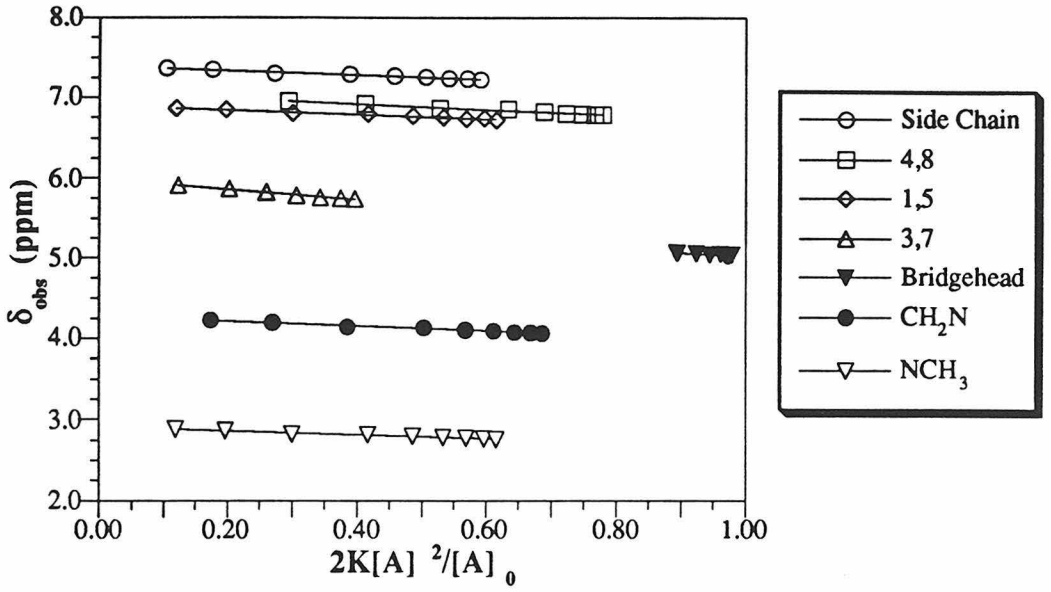

Figure 7.34. Best-fitting lines to the dimer model for all NMR observable proton signals of 60_R in borate-*d* (pD 9 buffer).[19]

Protons	K_D (M^{-1})	$-\Delta G°_a$ (kcal/mol)	δ_{mono} (ppm, fitted)	δ_{mono} (ppm, 20% CD_3CN)
Side chain	5.2×10^2	3.7	7.39	7.44
4,8	2.4×10^3	4.6	7.05	7.17
1,5	6.1×10^2	3.8	6.90	7.00
3,7	1.6×10^2	3.0	5.99	6.49
Bridgehead	3.2×10^5	7.5	5.44	5.23
NCH_2	1.0×10^3	4.1	4.27	4.32
NCH_3	6.1×10^2	3.8	2.90	2.93
Average	4.6×10^4	6.4		
Average (without bridgehead)	8.8×10^2	4.0		

Table 7.2. Fitted and observed data for the protons of 60_R in borate-*d*.

The lack of hydrogen bonding between the polar groups of interacting molecules appears to work well in terms of providing some type of soluble organized assembly. This

chapter concludes with the application of this modification of polar groups to a heteromolecular system.

7.5 Ion-Pairing in Place of Hydrogen Bonding in a Heteromolecular System.

7.5.1 Cationic Heteromonomer Design and Synthesis

Given the preliminary success of eliminating the ability for hydrogen bonding between interacting monomers, it was desired to use this approach on heteromolecular systems. However, given the difficulties encountered in the synthesis of cationic heteromonomers (Section 7.2.2), a molecule which could be quickly prepared was desired for interaction with the polyanionic monomers **9** and **33**.

To meet these goals, it was proposed that ethanoanthracene building block **19** be alkylated with benzyl iodide **68** followed by reduction (**69**), deprotection (**70**), and methylation to give the dicationic heteromonomer **71** (Figure 7.35). Alternately, **69** can be prepared by alkylating ethanoanthracene **75** with **68**; this preparation proved easier for purification of the intermediate than did reduction of **67**. The target molecule **71** would interact with polyanions **9** and **33** to give complexes with a non-zero charge held together through a combination of hydrophobic and electrostatic forces. Hydrophilic hydroxyl groups are used to aid solubility. The synthesis proved successful, but purification of the final product from potassium iodide proved difficult. The studies reported in this section were done with impure samples, although the presence of the potassium salts are thought to have a negligible effect on the results. In future studies of **71**, a synthesis analogous to that of **60** should prove more convenient (Figure 7.36).

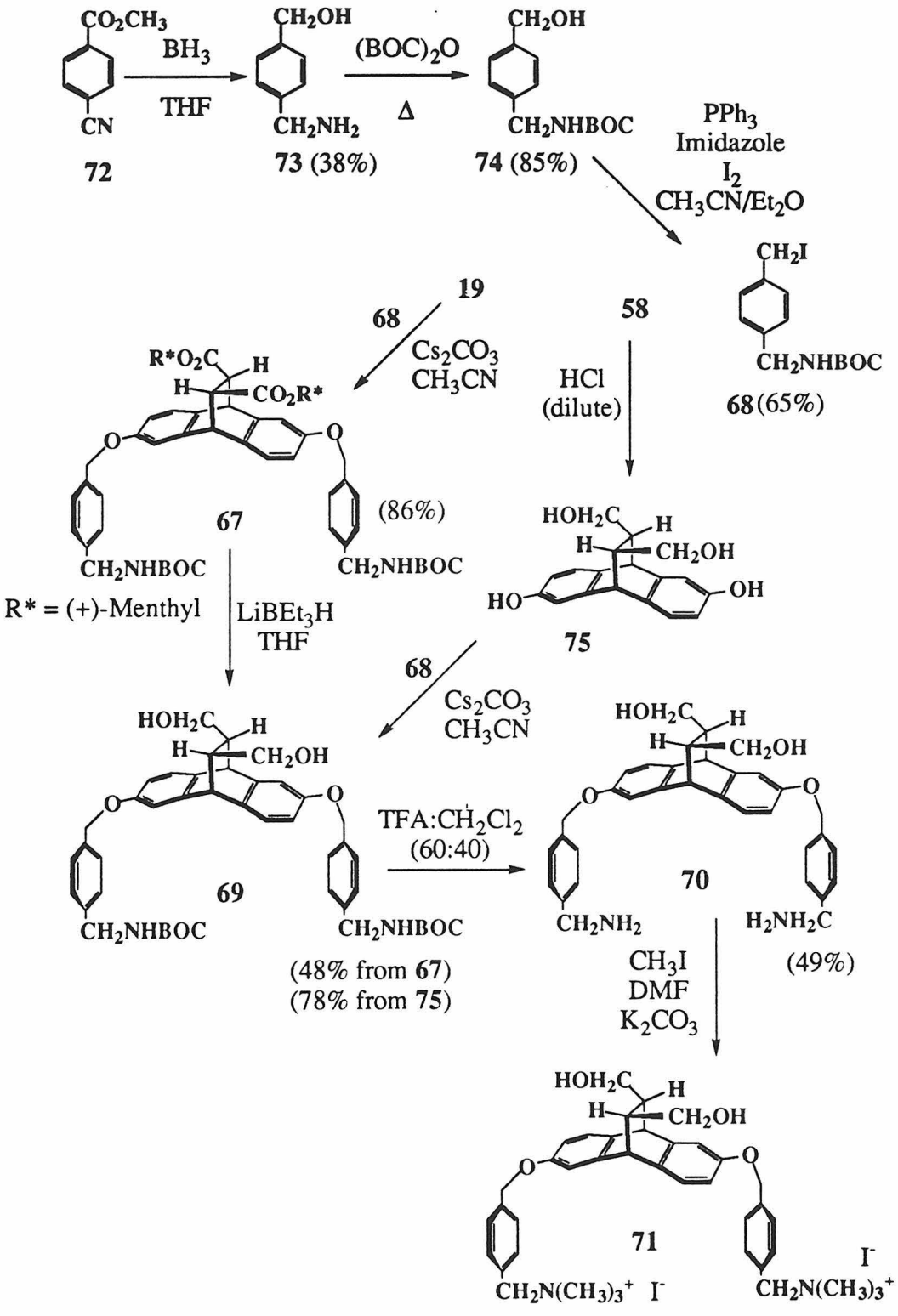

[(*R*, *R*, *R*, *R*)-Stereochemistry of Ethanoanthracene units shown]

Figure 7.35. Synthesis of 71.

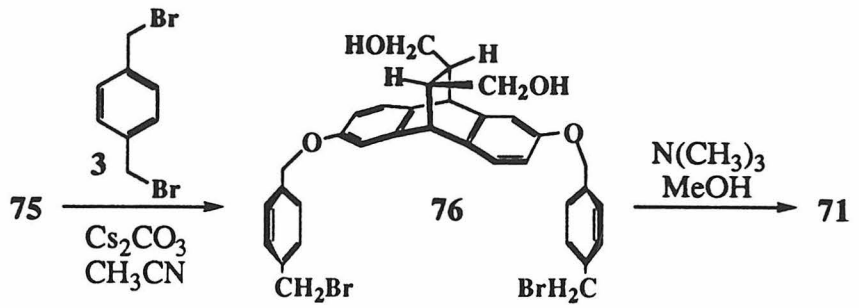

[(*R*, *R*, *R*, *R*)-Stereochemistry of Ethanoanthracene units shown]

Figure 7.36. An alternate synthesis proposed for 71.

7.5.2 Experimental Observations and Results

Three ^{1}H NMR experiments were performed with **71**; interaction with $\mathbf{9_R}$ at pD 7, interaction with $\mathbf{33_R}$ at pD 7, and interaction with $\mathbf{9_S}$ at pD 9. The observed spectral changes were the same in all three experiments, that is upfield shifting of all proton signals for both components on interaction. For both molecules it was the 3,7-proton that showed the greatest upfield shifting (Figures 7.37-7.42).

None of the the plots of Figures 7.37-7.42 were obtained under mol-ratio conditions, and thus the plots may not reflect stiochiometries. However, the pD 7 studies (Figures 7.37-7.40) differ from the pD 9 study (Figures 7.41-7.42) only at the mol ratio of the saturation point. At pD 7 the curves saturate at 2:1 carboxylate:**71** and at pD 9 the curves saturate at 2:1 **71**:carboxylate. Although the stoichiometries may not be 1:1, the spectral changes (upfield shifting of bridgehead and 3,7-proton signals in particular) indicate a non-micelle like aggregate is forming. The likelihood of a non 1:1 stoichiometry may be high due to a low CAC for **71**; the CAC was never measured, but due to limited solubility of **71** in our buffers, it is believed to be low. This may result in non-covalent oligomers of **71** being one of the species present in the solution (however, the spectra of solutions containing only **71** do not show unusual behavior).

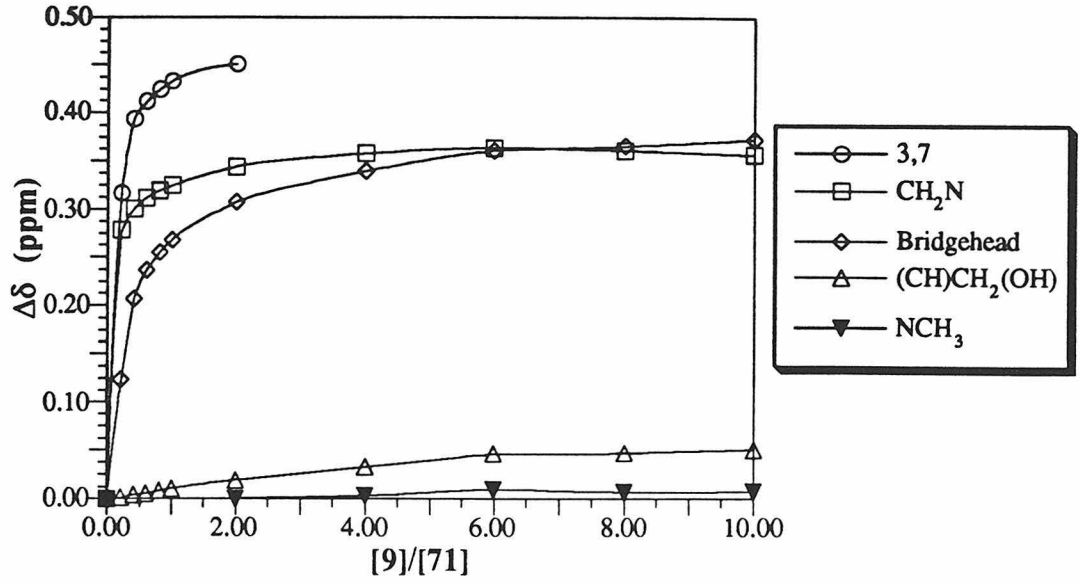

Figure 7.37. Variation of ^{1}H NMR chemical shift with addition of 9_R for the protons of 71_{RR} in phosphate-*d* (pD 7 buffer).

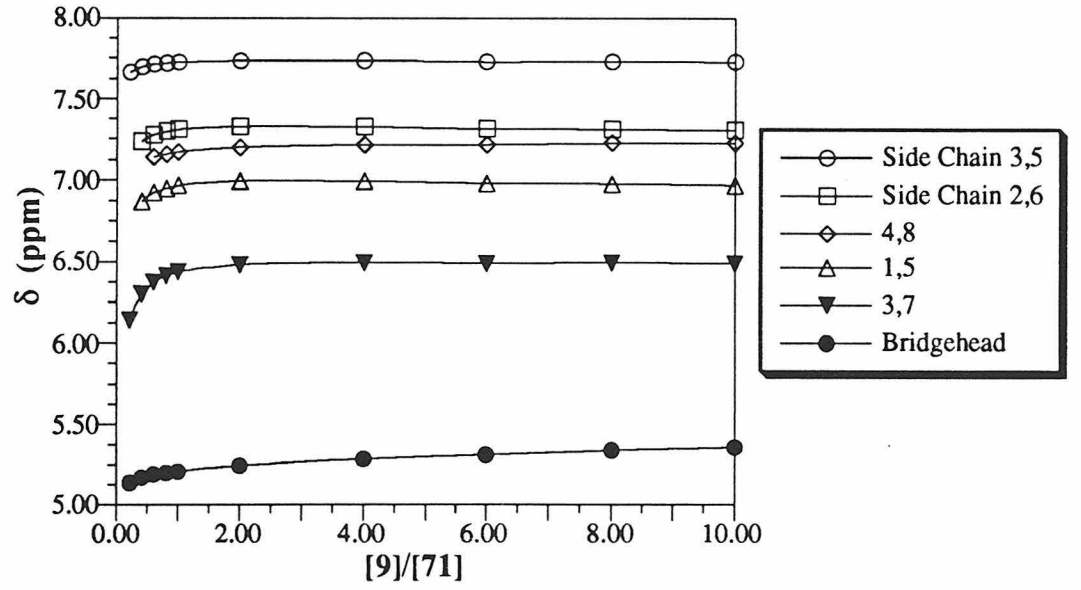

Figure 7.38. Variation of ^{1}H NMR chemical shift on addition to 71_{RR} for the protons of 9_R in phosphate-*d* (pD 7 buffer).

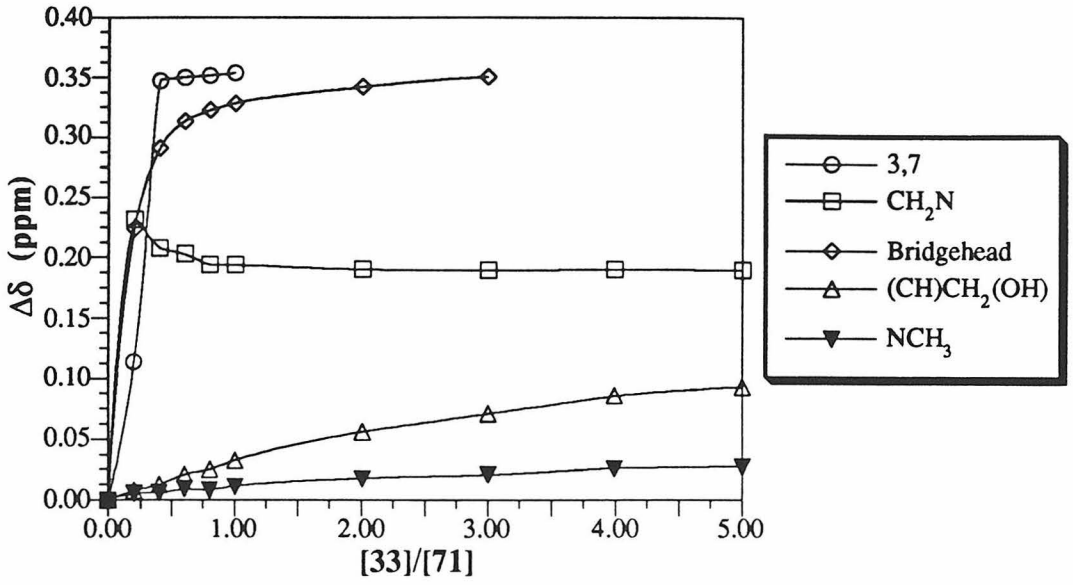

Figure 7.39. Variation of ^{1}H NMR chemical shift with addition of 33_R for the protons of 71_{RR} in phosphate-*d* (pD 7 buffer).

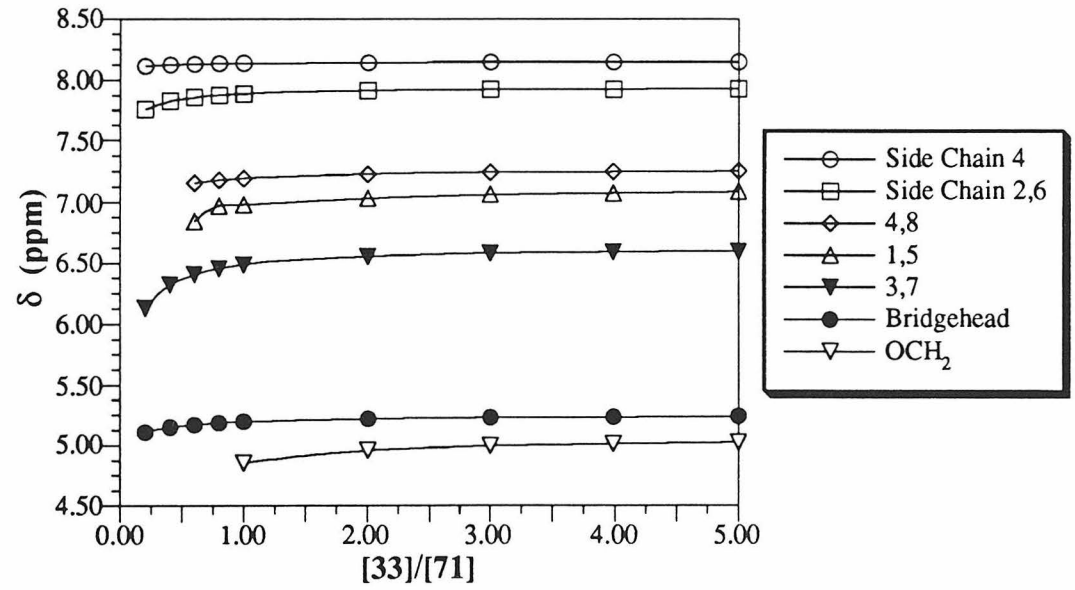

Figure 7.40. Variation of ^{1}H NMR chemical shift on addition to 71_{RR} for the protons of 33_R in phosphate-*d* (pD 7 buffer).

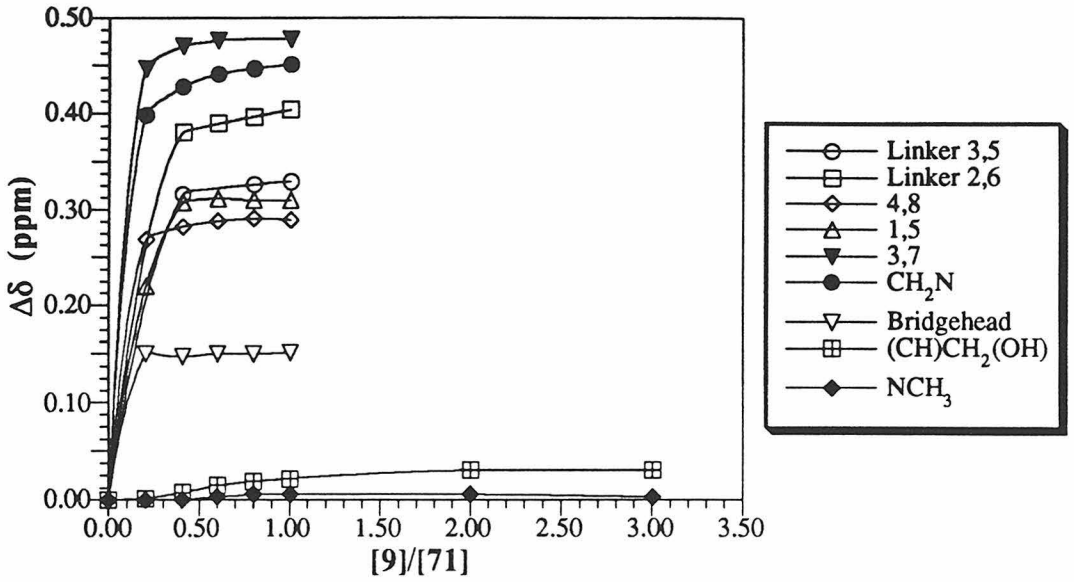

Figure 7.41. Variation of ^{1}H NMR chemical shift with addition of 9_S for the protons of 71_{RR} in borate-*d* (pD 9 buffer).

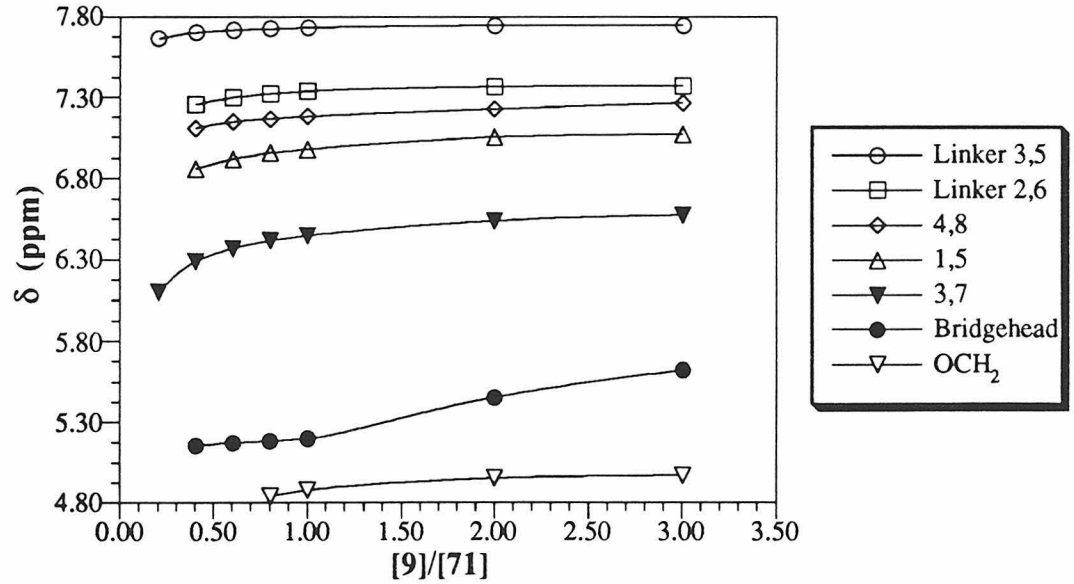

Figure 7.42. Variation of ^{1}H NMR chemical shift on addition to 71_{RR} for the protons of 9_S in borate-*d* (pD 9 buffer).

Given that the spectral changes observed for these experiments were consistent with earlier studies believed to involve dimerization of type U-shape molecules, an attempt was made to model the system as a 1:1 stoichiometry. The data from the **9_R/71** experiment was fitted by the EMUL NMR data-fitting programs.[21] The fitting gave an estimate of a binding constant $-\Delta G^\circ_a \geq 8.0$ kcal/mol, a value higher than can be accurately measured by the NMR methodology being employed (see Chapter 2).[1ab] Alternately, the high binding constant may have resulted from poor fitting due to non 1:1 stoichiometries.

The results are again encouraging. For this system, accurate determination of stoichiometry is critical. Once this has been established, an appropriate model can be used to quantitatively fit the data. Given the observations here, a large association constant is expected.[22]

7.6 Conclusions and Future Directions

7.6.1 General

The studies described in this chapter have established that non-micelle like aggregation will take place between appropriately designed U-shaped molecules in aqueous media. Preliminary results show some agreement with a proposed model of a dimer for homomolecular systems **1** and **60** (Figure 7.4) and for heteromolecular systems such as **9/25** (Figure 7.15). However, the results are not conclusive, and evidence from studies of **9/71** suggest that non 1:1 stoichiometries may also be possible. A number of further studies will be required before these observations can be quantified and reported.

Of particular interest are studies of molecules such as **60** and **9/71**. Systems in which hydrophobic association is inhibited from leading to micelle-like aggregates by the formation of non-hydrogen bonding ion-pairs. Future studies will require the observation of much broader ranges of concentrations than were possible in the initial NMR

experiments. Such studies might employ circular dichroism spectroscopy using cells of various pathlengths, so that both high and low concentrations can be probed. Additionally, experiments with gel-permeation chromatography and/or vapor-phase osmometry could be used to establish stoichiometry. Quantitative determination of stoichiometry is of critical importance, as this information would allow an appropriate quantitative model for describing the system to be chosen.

Another system that showed interesting behavior was the **9/25** system under high pH conditions. Under these conditions, the tetracarboxylate **9** solubilizes the normally insoluble deprotonated **25**. A series of solid-liquid extraction experiments (solid **25** extracted into basic solution by **9**) might provide quantitative estimates of the observed interactions from the initial studies.

Given the success using the **60** and **71** molecular systems, this approach with type B U-shaped molecules should be explored. Work by Jennifer Ma on the interaction of fully methylated analog of **25** (**77**, Figure 7.43) with carboxylates such as **9**, **26**, and **27** is currently underway in the Dougherty labs.[8] The type B systems offer the advantage of greater preorganization for the U-shape and thus should show greater binding affinity than analogous type A molecules.

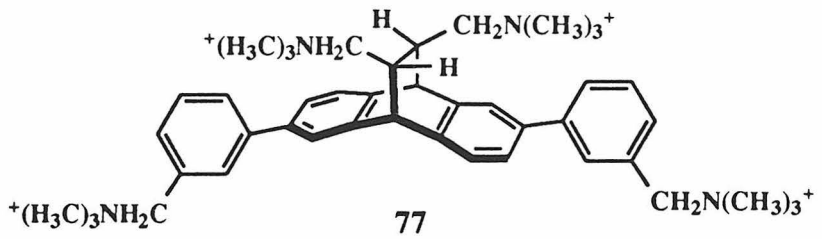

77

[(*R*, *R*, *S*, *S*)-Stereochemistry of Ethanoanthracene Unit Shown]

Figure 7.43. Fully methylated analog of 25.

7.6.2 Future Directions and Alternate Designs

A severe weakness in these self-assembly studies lies in the complexity of the molecules. All the etheno- and ethanoanthracene building blocks require non-trivial syntheses,[1bc] adding the disadvantage of a limited quantity of material to the target molecules. This not only limits the studies that can be done, but also the ability to carry out exploratory syntheses toward new designs (see Sections 7.2.2 and 7.3.3 for example). Given the uncertain molecular features that will work best for the realization of aqueous self-assembling systems, quick syntheses capable of producing enough material to allow crystal growth are desirable.

The type A molecules show potentially interesting self-assembly behavior and provide simpler syntheses than the type B systems. Using a more readily available building block (**78**) and the type A benzyl ether linkages, molecule **79** (Figure 7.44) may be a simple self-assembling system. Figure 7.45 shows a CPK representation of what a dimer of **79** might look like. As with the more complex systems studied in this chapter, the model places the hydrophilic functional groups exterior to the aggregated structure. Once studies on more simple designs like **79** provide insights into the controlling factors of self-assembly behavior, more complex molecules based on type A and type B designs could then be looked at.

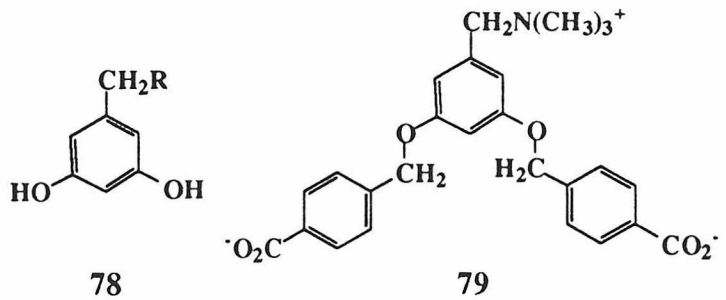

78 79

Figure 7.44. A Less complex self-assembling system.

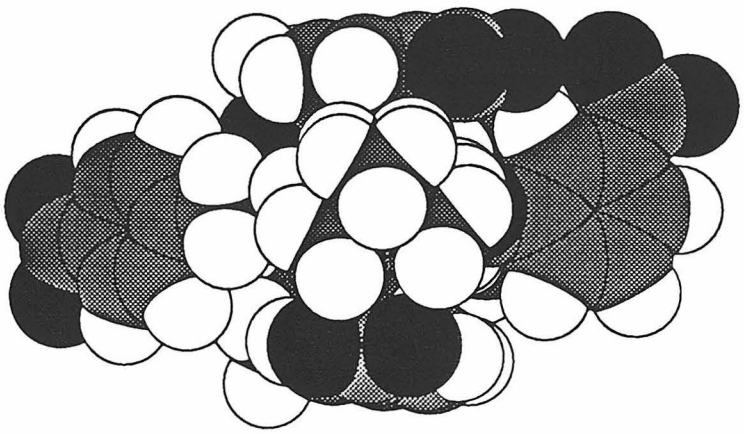

Figure 7.45. CPK representation of a possible structure for a dimer formed by 79.

Alternatively, other recognition elements might be examined. For example, Figure 7.46 shows a diammonium ion formed from a bis(crown-ether) appended ethanoanthracene unit (**80**, Figure 7.46). The concave hydrophobic surfaces from the ethenoanthracenes would aggregate, with crown-complexation of the ammonium holding the stoichiometry as a dimer (as per Figure 7.2). The system has the potential to be controlled by pH; at high pH where the ammonium groups of **80** are deprotonated, the interaction may turn off or micelle-like aggregates may form.

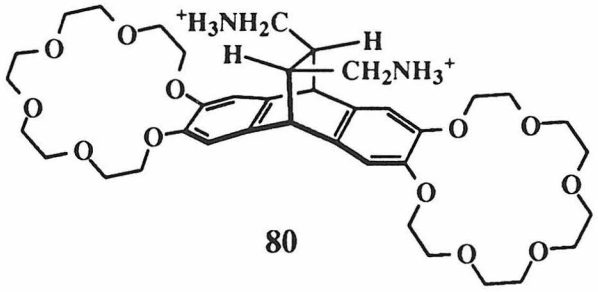

80

Figure 7.46. Using crown ethers as recognition elements for self-assembly.

Another approach could involve the formation of a host-like structure by using an appropriate template to bring together assembling units such as **81** (Figure 7.47).

Depending on the choice of the complimentary groups X and Y, the system could be switched on and off by adjusting the pH. Appropriate neutral solubilizing groups, not complimentary to X or Y, can be chosen from studies on neutral water soluble cyclophane hosts in the Dougherty group.[23]

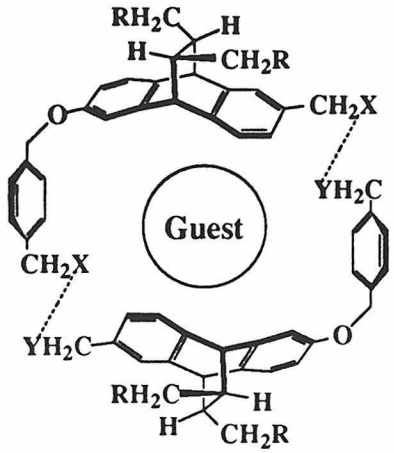

X, Y =Complimentary polar groups
R = Neutral water solubilizing group

[(*R*, *R*, *R*, *R*)-Stereochemistry of Ethanoanthracene units shown]

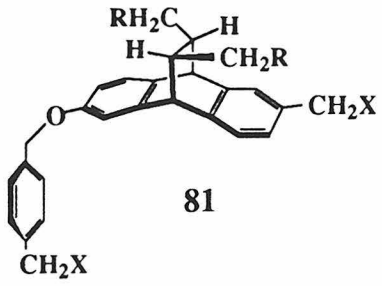

81

Figure 7.47. Template assisted assembly of a host-like structure.

The suggestions outlined here might be modified to suit future experimental results on functional self-assembling molecules (studies of simple systems like **79** are ideally suited to the task of exploring new directions). It is hoped that future studies in this area may provide important insights into the mechanisms by which self-assembling systems operate.

7.7 Experimental Section

7.7.1 General Methods

NMR spectra were recorded on a Bruker AM-500 spectrometer; routine spectra were referenced to the residual proton signals of the solvents and are reported in ppm downfield of 0.0 as δ values. CD spectra were recorded on a JASCO J-600 Spectropolarimeter with either 1.0, 0.5, or 0.1 cm pathlength quartz cells. A standard set of measurement parameters was used in all experiments (see Chapter 2). UV/vis spectra were recorded on a CARY 2200 or Beckman DU-640 spectrophotometer. IR spectra were recorded on a Perkin-Elmer 1600 FT-IR. GC/MS data was obtained on a Hewlett-Packard 5890/5970 GC/MS. Other mass spectral data was obtained from the University of California Riverside, Mass Spectrometry Center. All solvents used in spectroscopy were spectrophotometric or HPLC grade.

All reactions, unless otherwise noted, were stirred magnetically under nitrogen or argon atmosphere. Solvents used in reactions were distilled from drying agents under argon atmosphere; acetonitrile and methylene chloride, CaH_2; THF and ether, sodium benzophenone ketyl. All glassware, septa, and syringes used in reactions were oven-dried and/or stored in a desiccator prior to use, except in cases where aqueous solvents were employed. Ion exchange for NH_4^+ was carried out with Dowex® 50w-x2 cation exchange resin (the resin was treated with concentrated ammonium carbonate then washed with Milli-Q purified water before use). Unless otherwise noted reagents obtained from commercial sources were used without further purification.

Data fitting for the dimer model was set up using an Excel[24] spreadsheet for computing free monomer concentrations.

7.7.2 NMR Studies

Borate-*d* was prepared as previously described.[1bc] Phosphate-*d* was prepared by combining 2.91 ml 0.1 M NaOD (or CsOD) and 5.00 ml KD_2PO_4 followed by dilution to 10.0 ml with D_2O.[25] Variations of the amount of NaOD can be used to alter the pD of the solvent (see reference 23). NMR spectra in D_2O solutions were referenced to the 1.09 ppm peak of 3,3-dimethylglutarate (DMG) as internal standard or the 1.93 ppm peak of acetonitrile added in < 1% by volume as CD_3CN. Experiments were carried out in seven or nine inch long 5 mm diameter quartz NMR tubes. Volumes of aqueous solutions were added using Eppindorf Varipettes; volumes of non-aqueous (and mixed) solvents were added with Hamilton gas-tight syringes. In NMR experiments, volumes were assumed to be additive.

Stock solutions of **60** and **71** were prepared, and aliquots were taken and diluted to known volumes in CD_3OD. The D_2O/CD_3OD solutions were then standardized vs tetramethylammonium hydroxide pentahydrate by NMR integration. Stock solutions of **9**, **26**, **27**, **29** and **30** were prepared by weighing out samples of known purity (as di- and tetraacids) on a Sartorius microbalance followed by dilution to appropriate volumes. The sample purity was determined by fitting circular dichroism data from acetonitrile solutions of the appropriate di- and tetraacids to $\Delta\varepsilon$ values for the 230-350 nm region of the corresponding di- and tetramethyl esters in CH_3CN (as described in Chapter 2). Stock solutions of **33** were prepared by our standard NMR protocols.[1b] Other stock solutions were prepared by weighing out solutes on a Sartorius microbalance followed by dilution to appropriate volumes.

Studies of **1** at varying pD involved taking solutions of **1** in 0.01 M CsOD and lowering the pD by addition of 0.1 M or 1.0 M acetic acid-d_4. In other studies pD was adjusted by adding 0.1 M or 1.0 M solutions of DCl, NaOD, or CsOD.

7.7.3 Circular Dichroism Studies

Stock solutions were prepared by weighing out solutes on a Sartorius microbalance followed by dilution to appropriate volumes. Studies across varying pH's were carried out using the Britton-Robinson buffer system (desired pH is obtained by adding an appropriate volume of 0.2 M NaOH to 100 ml of a solution 0.040 M in acetic acid, 0.040 M in H_3PO_4, and 0.040 M in H_3BO_3).[25] The water used in these preparations was passed through a Milli-Q purification system.

7.7.4 Synthesis

Compounds **3**, **14**, **41**, **45**, **46**, **53**, **56**, **63**, and **72** were obtained from commercial sources. The preparation of **29** and **30** are given in Chapter 2.[1a] **2** and **50** were synthesized as previously reported.[1c] Compounds **19**, **25**, **31-dimethyl ester**, **32-dimethyl ester**, and **37** were prepared in the Dougherty labs.[26] Guanidine free base (**17**) was prepared by ion-exchange of the hydrochloride salt with Amberlite® IRA-400 (OH) ion-exchange resin in methanol and the ion-exchanged material was stored under Argon (the material must be used within two or three days).

(9*R*, 10*R*)-2, 6-Bis(*p*-aminomethylbenzyloxy)-9,10-dihydro-11, 12-dicarboxyethenoanthracene (1_R dicesium salt). In a 25 ml flask 0.030 g (5.0×10^{-5} mol) $\mathbf{5_R}$ was dissolved in 10 ml THF, followed by addition of 0.087 g (5.80×10^{-4} mol) cesium hydroxide and 2.5 ml water. The mixture was allowed to stir in the dark at room temperature overnight and the THF removed by rotary evaporation. The aqueous mixture was brought to pH 7 by addition of 1 M CsOH and the resultant precipitate collected and dried overnight in a vacuum desiccator. ^{1}H NMR (0.01 M CsOD) δ (ppm) 7.43 (d, J = 8.4 Hz), 7.40 (d, J = 8.1 Hz), 7.18 (d, J = 8.2 Hz), 7.02 (d, $J \approx 8$ Hz), 6.53 (dd, $J \approx 2$, 8 Hz), 5.77 (s), 5.06 (s), 3.98 (s).

(9*R*, 10*R*)-2, 6-Bis(*p*-bromomethylbenzyloxy)-9,10-dihydro-11, 12-dicarbomethoxyethenoanthracene (4_R). A 50 ml flask was charged with 0.199 g (5.65×10^{-4} mol) **2**, 1.511 g (5.72×10^{-3} mol) α,α'-dibromo-*p*-xylene (**3**), and 0.930 g (2.85×10^{-3} mol) cesium carbonate. After addition of 30 ml acetonitrile, the mixture was heated to 55 °C and allowed to stir in the dark. After 22 hours TLC (Si gel, 3:1 isooctane:Ethyl Acetate eluant) indicated completion of the reaction, the mixture was filtered, solids washed with acetonitrile, and the filtrate rotovapped to a yellowish solid. This solid was purified by flash chromatography (3:1 isooctane:Ethyl Acetate). Obtained 0.314 g (77%) of product. ^{1}H NMR ($CDCl_3$) δ (ppm) 7.39 (d, J = 8.2 Hz), 7.35 (d, J = 8.3 Hz), 7.25 (d, J = 7.4 Hz), 7.04 (d, J = 2.0 Hz), 6.54 (dd, J = 2.0, 7.4 Hz), 5.33 (s), 4.98 (s), 4.49 (s), 3.77 (s). FAB-MS (*m/e*) 591 (MH^+), 573, 419, 391. FAB-MS (*m/e*) 719, 717 (MH^+), 391. HRMS 717.0487 (MH^+), calculated for $C_{36}H_{31}Br_2O_6$ 717.0497.

(9*R*, 10*R*)-2, 6-Bis(*p*-aminomethylbenzyloxy)-9,10-dihydro-11, 12-dicarbomethoxyethenoanthracene (5_R) [Ammoniolysis]. A suspension of 4_R (0.42 g, 5.84×10^{-5} mol) in 10 ml dry methanol (Aldrich Sure-Seal Bottle) was prepared in a three-neck 25 ml round bottom flask fitted with gas inlet, stopper, and dry-ice condenser. Anhydrous ammonia was condensed into the suspension and allowed to saturate the methanol (as indicated by condensation on the outside of the flask). After saturation, the gas inlet and dry-ice condenser were removed and replaced with stoppers, the mixture was allowed to stir for two hours and then evaporated to a white solid. The solid was dissolved in 1 M HCl and the solution neutralized with 1 M NaOH and placed in a refrigerator for several hours. The white precipitate was collected by vacuum filtration, washed with ice-cold water until the filtrate was neutral, and dried over night in a vacuum desiccator yielding 0.020 g of product (57%). ^{1}H NMR (CD_3CN) δ (ppm) 7.34 (d, J = 8.2 Hz), 7.31 (d, J = 7.8 Hz), 7.25 (d, J = 7.8 Hz), 7.07 (d, J = 2.3 Hz), 6.59 (dd, J = 2.3, 8.5 Hz), 5.38 (s), 5.01 (s), 3.76 (s), 3.71 (s). FAB-MS (*m/e*) 591 (MH^+), 573, 419, 391. HRMS 591.2501 (MH^+), calculated for $C_{36}H_{35}N_2O_6$ 590.2417.

(9*R*, 10*R*)-2, 6-Bis(*p*-aminomethylbenzyloxy)-9,10-dihydro-11, 12-dicarbomethoxyethenoanthracene (5_R) [Nitrile reduction]. A three-neck 25 ml round bottom flask was fitted with two stoppers and a septum. After purging 3 × with dry nitrogen, 0.047 g 6_R (8.06×10^{-5} mol) and 10 ml of THF were added to the flask. Upon complete dissolution of 6_R, 0.15 ml of 1 M BH_3 in THF (2.1×10^{-3} g, 1.5×10^{-4} mol) was added by syringe over a 1 hour period and the mixture allowed to stir at room temperature. After 20 hours TLC (Si gel treated with 10% Et_3N in hexanes, 9:1 CH_2Cl_2:CH_3OH eluant) showed only non-moving spots. The cloudy reaction mixture was quenched with 2 ml conc. HCl and allowed to sit in a refrigerator (4 °C) for several hours, the white precipitate was collected by vacuum filtration washing with ice-cold water until a neutral filtrate was obtained and the solid dried overnight in a vacuum desiccator. The material can be converted to free amine by dissolving in water adding base and collecting the free precipitate. ^{1}H NMR (CD_3CN) δ (ppm) 7.34 (d, J = 8.2 Hz), 7.31 (d, J = 7.8 Hz), 7.25 (d, J = 7.8 Hz), 7.07 (d, J = 2.3 Hz), 6.59 (dd, J = 2.3, 8.5 Hz), 5.38 (s), 5.01 (s), 3.76 (s), 3.71 (s). FAB-MS (*m/e*) 591 (MH^+), 573, 419, 391. HRMS 591.2501 (MH^+), calculated for $C_{36}H_{35}N_2O_6$ 590.2417. Product was never obtained as pure as in the above ammoniolysis preparation, even after recrystallization from methanol.

(9*R*, 10*R*)-2, 6-Bis(*p*-cyanobenzyloxy)-9,10-dihydro-11, 12-dicarbomethoxyethenoanthracene (6_R). A 25 ml flask was charged with 0.115 g (3.26×10^{-5} mol) 2_R, 0.180 g (9.18×10^{-4} mol) *p*-bromomethylbenzonitrile (Aldrich), and 0.545 g (1.67×10^{-3} mol) cesium carbonate. After addition of 15 ml acetonitrile, the mixture was heated to 55 °C and allowed to stir in the dark. After 12 hours TLC (Si gel, 95:5 CH_2Cl_2:Ethyl Acetate eluant) indicated completion of the reaction, the mixture was filtered, solids washed with acetonitrile, and the filtrate rotovapped to a yellowish solid. This solid was purified by flash chromatography (95:5 CH_2Cl_2:Ethyl Acetate). Obtained 0.150 g (80%) of product. ^{1}H NMR ($CDCl_3$) δ (ppm) 7.66 (d, J = 8.1 Hz), 7.49 (d, J = 8.2 Hz), 7.24 (d, $J \approx 8$ Hz), 7.04 (d, $J \approx 2$ Hz), 6.53 (dd, $J \approx 8$ Hz, J = 2.1 Hz), 5.34 (s), 4.06

(s), 3.78 (s). DEI-MS (*m/e*) 582 (M^+), 551, 523, 466, 438, 406, 378, 324, 291, 263, 219, 176, 152, 116, 89, 59. HRMS 582.1790, calculated for $C_{36}H_{26}N_2O_6$ 582.1791.

2, 6-Bis(*p*-carboxybenzyloxy)-9,10-dihydro-11, 12-dicarboxyethenoanthracene (9_R-tetracid). In a 25 ml flask 0.056 g (8.63×10^{-5} mol) $\mathbf{13_R}$ was dissolved in 15 ml THF, followed by addition of 0.220 g (1.47×10^{-3} mol) cesium hydroxide and 5 ml water. The mixture was allowed to stir in the dark at room temperature overnight and the THF removed by rotary evaporation. The aqueous mixture was frozen to -78 °C and lyophilized to give a white powder that was dissolved in water and ion-exchanged for NH_4^+. The ion-exchanged solution was frozen at -78 °C and lyophilized to give 0.028 g of an off-white powder (84.0% pure by circular dichroism, impurities were inorganic salts and water, 46% yield). ^{1}H NMR (CD_3CN) δ (ppm) 7.97 (d, J = 8.3 Hz), 7.50 (d, J = 8.3 Hz), 7.28 (d, J = 8.1 Hz), 7.11 (d, J = 2.4 Hz), 6.62 (dd, J = 2.4, 8.1 Hz), 5.68 (s), 4.10 (s). FAB-MS (*m/e*) 592 (M^+), 557, 523, 439, 420, 391, 363, 343, 286, 259, 186. HRMS 592.1345, calculated for $C_{34}H_{24}O_{10}$ 592.1369.

(9*S*, 10*S*)-2, 6-Bis(*p*-carbomethoxybenzyloxy)-9,10-dihydro-11, 12-dicarbomethoxyethenoanthracene (13_S). A 25 ml flask was charged with 0.150 g (4.26×10^{-4} mol) $\mathbf{2_S}$, 0.303 g (1.32×10^{-3} mol) methyl *p*-bromomethylbenzoate (**14**), and 0.545 g (1.67×10^{-3} mol) cesium carbonate. After addition of 15 ml acetonitrile, the mixture was heated to 55 °C and allowed to stir in the dark. After 11 hours TLC (Si gel, 95:5 CH_2Cl_2:Ethyl Acetate eluant) indicated completion of the reaction, the mixture was filtered, solids washed with acetonitrile, and the filtrate rotovapped to a yellowish oil. This oil was subjected to flash chromatography (95:5 CH_2Cl_2:Ethyl Acetate) and provided 0.278 g (100%) of product as a white solid. ^{1}H NMR ($CDCl_3$) δ (ppm) 8.03 (d, J = 8.4 Hz), 7.45 (d, J = 8.3 Hz), 7.24 (d, J = 8.7 Hz), 7.05 (d, $J \approx 2$ Hz), 6.54 (dd, J = 2.2, 8.5 Hz), 5.33 (s), 5.05 (s), 3.91 (s). FAB-MS (*m/e*) 649 (MH^+), 617, 589, 557, 529, 500, 430, 410, 381, 327. HRMS 649.2049 (MH^+), calculated for $C_{38}H_{33}O_{10}$ 649.2017.

Circular dichroism [(9*S*, 10*S*)-enantiomer, CH_3CN] λ (Δε) [nm ($M^{-1}cm^{-1}$)], 315 (-2.7), 301 (+1.2), 284 (-18.9), 252 (+49.6), 232 (+102.4), 217 (+6.6), 207 (-48.0).

(9*S*, 10*S*)-2, 6-Bis(*p*-carboxamidomethylbenzyloxy)-9,10-dihydro-11, 12-dicarboxamidoethenoanthracene (15_S). A solution of 0.035 g (5.40×10^{-4} mol) 13_S in 5 ml dry methanol (Aldrich Sure-Seal Bottle) was prepared in a three-neck 25 ml round bottom flask fitted with gas inlet, stopper, and dry-ice condenser. Anhydrous ammonia was condensed into the suspension and allowed to saturate the methanol (as indicated by condensation on the outside of the flask). After saturation, the gas inlet and dry-ice condenser were removed and replaced with stoppers. TLC monitoring (Si gel, 9:1 CH_2Cl_2:CH_3OH eluant) indicated the completion of the reaction after 25 days. The reaction mixture was evaporated to a white solid and flash chromatographed (10 → 20% CH_3OH in CH_2Cl_2) yielding 0.022 g of product (69%). ^1H NMR (CD_3CN) δ (ppm) 7.79 (d, J = 7.5 Hz), 7.48 (d, J = 7.7 Hz), 7.28 (d, J = 7.8 Hz), 7.11 (d, J = 2.3 Hz), 6.59 (dd, J = 2.3, 8.5 Hz), 5.45 (s), 4.95 (s).

(9*S*, 10*S*)-2, 6-Bis(*p*-cyanobenzyloxy)-9,10-dihydro-11, 12-dicarboxamidoethenoanthracene (16_S). A solution of 0.049 g (8.41×10^{-5} mol) 6_S in 5 ml dry methanol (Aldrich Sure-Seal Bottle) was prepared in a three-neck 25 ml round bottom flask fitted with gas inlet, stopper, and dry-ice condenser. Anhydrous ammonia was condensed into the suspension and allowed to saturate the methanol (as indicated by condensation on the outside of the flask). After saturation, the gas inlet and dry-ice condenser were removed and replaced with stoppers. TLC monitoring (Si gel, 9:1 CH_2Cl_2:CH_3OH eluant) indicated the completion of the reaction after two days. The reaction mixture was evaporated to a white solid and flash chromatographed (95:5 CH_2Cl_2:CH_3OH) yielding 0.033 g of product (72%). ^1H NMR (CD_3OD) δ (ppm) 7.71 (d, J = 8.1 Hz), 7.58 (d, J = 8.1 Hz), 7.27 (d, J = 8.2 Hz), 7.12 (d, $J \approx 2$ Hz), 6.60 (dd, $J \approx 2$, 8 Hz), 5.40 (s), 5.13 (s). DEI-MS (*m/e*) 552 (M^+), 535, 440, 419, 376, 324, 296,

260, 234, 210, 181, 152, 116, 89, 63. HRMS 552.1785, calculated for $C_{34}H_{24}N_4O_4$ 552.1798.

(9*S*, 10*S*, 11*S*, 12*S*)-2,6-Dihydroxy-9,10-dihydro-11,12-dicarbomethoxyethanoanthracene (20_{SS}). In a 50 ml round bottom flask fitted with a reflux condenser, 1.02 g (1.22×10^{-3} mol) $\mathbf{50_{SS}}$ was dissolved in 25 ml methanol. After addition of methane sulfonic acid (2.0 ml, 2.962 g, 0.031 mol), the solution was brought to reflux. TLC (Si gel, 3:1 Ether:Pet ether eluant) indicated the completion of the reaction after 12 days. The mixture was cooled to room temperature and poured into a two-phase mixture of 100 ml pH 7 phosphate buffer[25] and 100 ml ethyl acetate. The layers were separated, the aqueous layer extracted with ethyl acetate (2×20 ml), and the combined organic layers dried over anhydrous $MgSO_4$. The dry solution was filtered and rotovapped onto Si gel, the Si gel was added as a plug to a flash column and eluted with 3:1 Ether:Pet ether yielding 0.358 g (82%) of product. ^{1}H NMR (CD_3CN) δ (ppm) 7.03 (d, J = 7.9 Hz), 6.81 (d, J = 2.2 Hz), 6.77 (s), 6.49 (dd, J = 2.4, 8.0 Hz), 4.43 (s), 3.58 (s), 3.25 (s). CI-MS (*m/e*) 355 (MH^+), 339, 323, 314, 297, 230, 210, 194, 181, 162, 147, 113, 102, 85, 70, 59. HRMS 355.1199 (MH^+), calculated for $C_{20}H_{19}O_6$ 355.1181.

(9*S*, 10*S*, 11*S*, 12*S*)-2, 6-Bis(*p*-carbomethoxybenzyloxy)-9,10-dihydro-11, 12-dicarbomethoxyethanoanthracene 11,12-Bis[(-)-menthyl ester] (21_{SS}). A 25 ml flask was charged with 0.301 g (4.99×10^{-4} mol) $\mathbf{19_{SS}}$, 0.380 g (1.66×10^{-3} mol) methyl *p*-bromomethylbenzoate (**14**), and 0.899 g (2.76×10^{-3} mol) cesium carbonate. After addition of 20 ml acetonitrile, the mixture was heated to 55 °C and allowed to stir in the dark. After four days TLC (Si gel, 95:5 CH_2Cl_2:Ethyl acetate eluant) indicated completion of the reaction, the mixture was filtered, solids washed with acetonitrile, and the filtrate rotovapped to a yellowish oil. This oil was subjected to flash chromatography (95:5 CH_2Cl_2:Ether) and provided 0.364 g (81%) of product as a white solid. ^{1}H NMR (CD_3CN) δ (ppm) 7.99 (d, J = 8.4 Hz), 7.52 (d, J = 8.4 Hz), 7.08 (d, J = 8.2 Hz), 7.04 (d, J = 2.5 Hz), 6.68 (dd, J = 2.5, 8.2 Hz), 5.11 (s), 5.64 (s), 4.53 (dt, J

= 4.4, 10.9 Hz), 3.86 (s), 3.18 (s), 1.7-1.0 (m), 0.937 (d, J = 7.0), 0.847 (d, J = 6.4), 0.674 (d, J = 7.0). FAB-MS (*m/e*) 899 (MH^+), 623, 573, 506, 209, 181, 149, 121, 35. HRMS 899.4698 (MH^+), calculated for $C_{56}H_{67}O_{10}$ 899.4734.

(9*S*, 10*S*, 11*S*, 12*S*)-2, 6-Bis(*p*-carbomethoxybenzyloxy)-9,10-dihydro-11, 12-dicarbomethoxyethanoanthracene (22_{SS}). A 25 ml flask was charged with 0.093 g (2.64×10^{-4} mol) 20_{SS}, 0.263 g (1.15×10^{-3} mol) methyl *p*-bromomethylbenzoate (**14**), and 0.609 g (1.87×10^{-3} mol) cesium carbonate. After addition of 10 ml acetonitrile, the mixture was heated to 55 °C and allowed to stir in the dark. After two days TLC (Si gel, 95:5 CH_2Cl_2:Ether eluant) indicated completion of the reaction, the mixture was filtered, solids washed with acetonitrile, and the filtrate rotovapped to a yellowish solid. This solid was subjected to flash chromatography (95:5 CH_2Cl_2:Ether) and provided 0.137 g (80%) of product as a white solid. ^1H NMR (CD_3CN) δ (ppm) 7.99 (d, J = 8.3 Hz), 7.52 (d, J = 8.3 Hz), 7.14 (d, J = 8.3 Hz), 7.04 (d, J = 2.5 Hz), 6.70 (dd, J = 2.6, 8.1 Hz), 5.11 (s), 5.05 (s), 4.61 (s), 3.85 (s), 3.58 (s), 3.27 (s). FAB-MS (*m/e*) 650 (M^+), 506, 447, 419, 357. HRMS 650.2139 (M^+), calculated for $C_{38}H_{34}O_{10}$ 650.2151. Circular dichroism [(9*S*, 10*S*, 11*S*, 12*S*)-enantiomer, CH_3CN] λ ($\Delta\varepsilon$) [nm ($M^{-1}cm^{-1}$)], 320 (-1.6), 277 (-6.4), 247 (+42.3), 226 (-66.1), 207 (-81.8).

(9*S*, 10*S*, 11*S*, 12*S*)-2, 6-Bis(*p*-hydroxymethylbenzyloxy)-9,10-dihydro-11, 12-hydroxymethylethanoanthracene (23_{SS}) [Prepared from 21_{SS}]. A solution of 0.359 g (3.99×10^{-4} mol) 23_{SS} in 10 ml THF was prepared in a 100 ml flask fitted with a septum; this was followed by dropwise addition of 4.0 ml 1.0 M $LiBEt_3H$ (4.0×10^{-3} mol) from a syringe. TLC (Ethyl acetate eluant) indicated complete reaction after two days. The mixture was quenched by adding 20 ml ethyl acetate and rotovapped to a colorless oil. The oil was dissolved in 25 ml ethyl acetate and 25 ml water, the layers separated, the aqueous layer extracted with ethyl acetate (3 × 10 ml), and the combined organic layers dried over anhydrous $MgSO_4$. The dried organic solution was

filtered, rotovapped to a white solid, and flash chromatographed (0 → 5% CH_3OH in Ethyl acetate) yielding 0.055 g (26 %) of product. ^1H NMR (CD_3OD) δ (ppm) 7.31 (d, J = 8.3 Hz), 7.26 (d, J = 8.3 Hz), 7.04 (d, $J \approx 8$ Hz), 6.77 (d, $J \approx 2$ Hz), 6.67 (dd, $J \approx 2, 8$ Hz), 4.94 (s), 4.51 (s), 4.12 (s). FAB-MS (*m/e*) 538 (M^+), 521, 450, 443, 391, 363. HRMS 538.2362, calculated for $C_{34}H_{34}O_6$ 538.2355.

(9*S*, 10*S*, 11*S*, 12*S*)-2, 6-Bis(*p*-hydroxymethylbenzyloxy)-9,10-dihydro-11, 12-hydroxymethylethanoanthracene (23_{SS}) [Prepared from 22_{SS}]. A solution of 0.057 g (8.76×10^{-5} mol) 22_{SS} in 2.0 ml THF was prepared in a 25 ml flask fitted with a septum. This was followed by dropwise addition of 0.8 ml 1.0 M $LiBEt_3H$ (8.0×10^{-4} mol) from a syringe. TLC (Si gel, Ethyl acetate eluant) indicated complete reaction after 24 hours. The mixture was quenched by adding 6 ml ethyl acetate and rotovapped to a white solid. The solid was dissolved in 5 ml ethyl acetate and 10 ml water, the layers separated, the aqueous layer extracted with ethyl acetate (3 × 5 ml), and the combined organic layers dried over anhydrous $MgSO_4$. The dried organic solution was filtered, rotovapped to a white solid, and flash chromatographed (Ethyl acetate) yielding 0.031 g (66 %) of product. ^1H NMR (CD_3OD) δ (ppm) 7.31 (d, J = 8.3 Hz), 7.26 (d, J = 8.3 Hz), 7.04 (d, $J \approx 8$ Hz), 6.77 (d, $J \approx 2$ Hz), 6.67 (dd, $J \approx 2, 8$ Hz), 4.94 (s), 4.51 (s), 4.12 (s). FAB-MS (*m/e*) 538 (M^+), 521, 450, 443, 391, 363. HRMS 538.2362, calculated for $C_{34}H_{34}O_6$ 538.2355.

(9*S*, 10*S*, 11*S*, 12*S*)-2, 6-Bis(*p*-carboxybenzyloxy)-9,10-dihydro-11, 12-dicarboxyethanoanthracene (26_{SS}-tetracid). In a 25 ml flask 0.033 g (5.07×10^{-5} mol) 22_{SS} was dissolved in 15 ml THF, followed by addition of 0.118 g (7.87×10^{-4} mol) cesium hydroxide and 5 ml water. The mixture was allowed to stir in the dark at room temperature overnight and the THF removed by rotary evaporation. The aqueous mixture was frozen to -78 °C and lyophilized to give a white powder that was dissolved in water and ion-exchanged for NH_4^+. The ion-exchanged solution was frozen at -78 °C and lyophilized to give 0.038 g of an off-white powder (77.4% pure by circular

dichroism, impurities were inorganic salts and water, 98% yield). ^{1}H NMR (CD_3CN) δ (ppm) 7.96 (d), 7.51 (d), 7.18 (d), 6.96 (d), 6.67 (dd), 5.10 (s), 4.47 (s).

(9*R*, 10*R*, 11*S*, 12*S*)-2, 6-Bis(*p*-carboxybenzyloxy)-9,10-dihydro-11, 12-dicarboxyethanoanthracene (27_{RS}-tetracid). In a 25 ml flask 0.058 g (8.91×10^{-5} mol) **27_{RS}-tetramethyl ester** was dissolved in 15 ml THF, followed by addition of 0.185 g (1.23×10^{-3} mol) cesium hydroxide and 5 ml water. The mixture was allowed to stir in the dark at room temperature overnight and the THF removed by rotary evaporation. The aqueous mixture was frozen to -78 °C and lyophilized to give a white powder that was dissolved in water and ion-exchanged for NH_4^+. The ion-exchanged solution was frozen at -78 °C and lyophilized to give 0.059 g of an off-white powder (53.5% pure by circular dichroism, impurities were inorganic salts and water, 59% yield). ^{1}H NMR (CD_3CN) δ (ppm) 7.96 (d, *J* = 8.3 Hz), 7.51 (d, *J* = 8.3 Hz), 7.15 (d, *J* = 8.3 Hz), 6.98 (d, *J* = 2.2 Hz), 6.66 (dd, *J* = 2.3, 8.3 Hz), 5.10 (s), 4.52 (s), 4.37 (s).

(9*R*, 10*R*, 11*S*, 12*S*)-2, 6-Bis(*p*-carbomethoxybenzyloxy)-9,10-dihydro-11, 12-dicarbomethoxyethanoanthracene (27_{RS}-tetramethyl ester). A 25 ml flask was charged with 0.106 g (2.99×10^{-4} mol) **28_{RS}**, 0.210 g (9.17×10^{-4} mol) methyl *p*-bromomethylbenzoate (**14**), and 0.504 g (1.55×10^{-3} mol) cesium carbonate. After addition of 10 ml acetonitrile, the mixture was heated to 55 °C and allowed to stir in the dark. After 30 hours TLC (Si gel, 95:5 CH_2Cl_2:Ethyl acetate eluant) indicated completion of the reaction, the mixture was filtered, solids washed with acetonitrile, and the filtrate rotovapped to a yellowish solid. This solid was subjected to flash chromatography (95:5 CH_2Cl_2:Ethyl acetate) and provided 0.184 g (95%) of product as a white solid. ^{1}H NMR (CD_3CN) δ (ppm) 7.98 (d, *J* = 8.3 Hz), 7.51 (d, *J* = 8.2 Hz), 7.25 (d, *J* = 8.1 Hz), 6.91 (d, *J* = 2.5 Hz), 6.72 (dd, *J* = 2.5, 8.2 Hz), 5.10 (s), 4.57 (d, *J* = 4.5 Hz), 3.77 (s), 3.54 (s), 3.29 (d, *J* = 4.5 Hz). FAB-MS (*m/e*) 650 (M^+), 619, 506, 357, 242, 209, 178, 166, 121. HRMS 650.2187 (M^+), calculated for $C_{38}H_{34}O_{10}$

650.2151. Circular dichroism [(9*R*, 10*R*, 11*S*, 12*S*)-enantiomer, CH_3CN] λ (Δε) [nm ($M^{-1}cm^{-1}$)], 300 (-2.0), 274 (+5.2), 247 (-35.2), 230 (+60.0), 213 (+38.0), 207 (+47.8).

(9*R*, 10*R*, 11*S*, 12*S*)-2,6-Dihydroxy-9,10-dihydro-11,12-dicarbomethoxyethanoanthracene (28_{RS}). In a 50 ml round bottom flask fitted with a reflux condenser, 0.57 g (9.49×10^{-4} mol) (9*R*, 10*R*, 11*S*, 12*S*)-2,6-Dihydroxy-9,10-dihydro-11,12-dicarbomethoxyethanoanthracene bis[(-)-menthyl ester][27] was dissolved in 15 ml methanol. After addition of methane sulfonic acid (1.6 ml, 2.37 g, 0.025 mol), the solution was brought to reflux. TLC (Si gel, 3:1 Ether:Pet ether eluant) indicated the completion of the reaction after five days. The mixture was cooled to room temperature and poured into a two-phase mixture of 50 ml pH 7 phosphate buffer[25] and 50 ml ethyl acetate. The layers were separated, the aqueous layer extracted with ethyl acetate (3×15 ml), and the combined organic layers dried over anhydrous $MgSO_4$. The dry solution was filtered and rotovapped to a white solid and flash chromatographed (3:1 Ether:Pet ether) yielding 0.297 g (88%) of product. ^1H NMR (CD_3CN) δ (ppm) 7.14 (d, J = 8.0 Hz), 6.73 (s), 6.70 (d, J = 2.4 Hz), 6.52 (dd, J = 2.4, 8.0 Hz), 4.54 (s), 3.58 (s), 3.26 (s). CI-MS (*m/e*) 355 (MH^+), 339, 314, 297, 230, 210, 195, 181, 162, 147, 113. HRMS 355.1178 (MH^+), calculated for $C_{20}H_{19}O_6$ 355.1181.

9,10-dihydro-11, 12-dicarboxyethenoanthracene (31-diacid). In a 25 ml flask 0.035 g (1.08×10^{-4} mol) **31-dimethyl ester** was dissolved in 10 ml THF, followed by addition of 0.095 g (6.3×10^{-4} mol) cesium hydroxide and 2 ml water. The mixture was allowed to stir in the dark at room temperature overnight and the THF removed by rotary evaporation. The aqueous mixture was frozen to -78 °C and lyophilized to give a white powder that was dissolved in water and ion-exchanged for NH_4^+. The ion-exchanged solution was frozen at -78 °C and lyophilized to give 0.036 g of an off-white powder. ^1H NMR (borate-*d*) δ (ppm) 7.45 (d), 7.06 (d), 5.40 (s).

(±)-1,5-bis(*N*-Benzylcarboxamido)-9.10-dihydro-11, 12-dicarboxyethenoanthracene (32-diacid). In a 25 ml flask 0.020 g (3.5×10^{-5} mol) **(±)-32-**

dimethyl ester was dissolved in 10 ml THF, followed by addition of 0.064 g (4.3×10^{-4} mol) cesium hydroxide and 2 ml water. The mixture was allowed to stir in the dark at room temperature overnight and the THF removed by rotary evaporation. The aqueous mixture was frozen to -78 °C and lyophilized to give a white powder that was dissolved in water and ion-exchanged for NH_4^+. The ion-exchanged solution was frozen at -78 °C and lyophilized to give an off-white powder. ^{1}H NMR (DMSO-d_6) δ (ppm) 7.40 (d, J = 7.5 Hz), 7.36 (d, J = 7.5 Hz), 7.26 (d, J = 6.4 Hz), 7.16 (d, J = 7.2 Hz), 7.04 (t, J = 8.4 Hz), 6.96 (s), 6.56 (s), 4.54 (m).

(9*R*, 10*R*)-2, 6-Bis(*p*-carboxybenzyloxy)-9,10-dihydro-11, 12-dicarboxyethanoanthracene (33_R). In a 25 ml flask 0.027 g (3.64×10^{-5} mol) $\mathbf{40_R}$ was dissolved in 10 ml THF, followed by addition of 0.171 g (1.14×10^{-3} mol) cesium hydroxide and 4 ml water. The mixture was allowed to stir in the dark at room temperature overnight and the THF removed by rotary evaporation. The aqueous mixture was frozen to -78 °C and lyophilized to give a white powder that was dissolved in water and ion-exchanged for NH_4^+. The ion-exchanged solution was frozen at -78 °C and lyophilized to give an off-white powder that was immediately dissolved in pD 7 buffer to give a 5.08×10^{-3} M solution (by NMR integration). ^{1}H NMR (phosphate-*d*) δ (ppm) 8.14 (t), 7.92 (d), 7.25 (d), 7.11 (d), 6.61 (dd), 5.21 (s), 4.06 (s).

Diethyl 5-methylisophthalate (38). In a 100 ml flask fitted with a reflux condenser, 0.7 g (3.8×10^{-3}) **37** was dissolved in 50 ml absolute ethanol and the solution brought to reflux. TLC (Si gel, 6:4 Hexane:Ether) indicated completion of the reaction after 17 hours. The solution was cooled to room temperature and poured into a two-phase mixture of 100 ml pH 7 phosphate buffer[25] and 100 ml CH_2Cl_2. The layers were separated, the aqueous layer was extracted with CH_2Cl_2 (3 × 20 ml), the organic layers combined and dried over anhydrous $MgSO_4$. The dry organic solution was rotovapped to an orange oil and flash chromatographed (4 → 40 % Ether in Hexanes) to yield 0.60 g (67

%) of product. ^{1}H NMR (CD_3CN) δ (ppm) 8.45 (t, J = 1.6 Hz), 8.03 (d, J = 1.6 Hz), 4.33 (quartet, J = 7.2 Hz), 2.44 (s), 1.37 (t, J = 7.1 Hz).

Diethyl 5-bromomethylisophthalate (39). In a 50 ml flask fitted with a reflux condenser, 0.60 g (2.5×10^{-3} mol) **38** was dissolved in 20 ml CCl_4, 0.451 g (2.53×10^{-3} mol) NBS and 0.020 g (9.3×10^{-5} mol) benzoyl peroxide were added and the mixture brought to reflux. TLC (Si gel, 6:4 Hexane:Ether) indicated complete reaction after two days. The orange solution was brought to room temperature and rotovapped to an orange solid. Recrystallization from 4% ether in hexanes provided 0.225 (28%) of a white solid. ^{1}H NMR (CD_3CN) δ (ppm) 8.47 (t, J = 1.5 Hz, 1H), 8.25 (d, J = 1.7 Hz, 2H), 4.68 (s, 2H), 4.37 (quartet, J = 7.1 Hz, 4H), 1.37 (t, J = 6.9 Hz, 6H). CI-MS (NH_3) (*m/e*) 348, 332 ($M+NH_4^+$), 315 (MH^+), 254, 237, 191, 182, 168, 150, 135, 110, 95, 86, 73, 58. HRMS 332.0493 ($M+NH_4^+$), calculated for $C_{13}H_{19}BrNO_4$ 332.0498.

(9*R*, 10*R*)-2, 6-Bis(3,5-dicarboethoxybenzyloxy)-9,10-dihydro-11, 12-dicarbomethoxyethenoanthracene (40_R). A 25 ml flask was charged with 0.048 g (1.36×10^{-4} mol) $\mathbf{2_R}$, 0.124 g (5.76×10^{-4} mol) **39**, and 0.227 g (6.97×10^{-4} mol) cesium carbonate. After addition of 10 ml acetonitrile, the mixture was heated to 55 °C and allowed to stir in the dark. After 23 hours TLC (Si gel, 95:5 CH_2Cl_2:Ether eluant) indicated completion of the reaction, the mixture was filtered, solids washed with acetonitrile, and the filtrate rotovapped to a brown oil. This oil was subjected to flash chromatography (95:5 CH_2Cl_2:Ether) and provided 0.103 g (92%) of product as a white solid. ^{1}H NMR (CD_3CN) δ (ppm) 8.48 (d, J = 1.5 Hz), 8.23 (d, J = 1.4 Hz), 7.29 (d, J = 8.1 Hz), 7.11 (d, J = 2.4 Hz), 6.63 (dd, J = 2.5, 8.1 Hz), 5.42 (s), 5.15 (s), 4.36 (quartet, J = 7.1), 3.72 (s), 1.36 (t, J = 7.1). FAB-MS (*m/e*) 821 (MH^+), 820 (M^+), 789, 751, 678, 585, 525, 444, 387, 371, 351, 309, 291, 263, 235, 215, 191, 117. HRMS 820.2769, calculated for $C_{46}H_{44}O_{14}$ 820.2731.

α-Bromo-*p*-tolyl acetate (42). In a 50 ml flask fitted with a reflux condenser, 1.048 g (6.98×10^{-3} mol) **41** was dissolved in 30 ml CCl_4, 1.246 g (7.00×10^{-3} mol)

NBS and 0.020 g (9.3×10^{-5} mol) benzoyl peroxide were added and the mixture brought to reflux. TLC (Si gel, 4% Ether in Hexanes) indicated complete reaction after 21 hours. The solution was brought to room temperature and rotovapped to an orange oil. White crystals formed after sitting in a -20 °C freezer for two hours yielding 0.922 (56%) of product. ^{1}H NMR (CD_3CN) δ (ppm) 8.45 (t, J = 8.3 Hz), 7.07 (d, J = 8.5 Hz), 4.59 (s), 2.23 (s).

Di(2-cyanoethyl)-*N*,*N*-diisopropylaminephosphoramidite (47). A solution of 3.539 g (0.050 mol) 3-hydroxypropionitrile (**46**) and 13.0 ml (9.646 g, 0.075 mol) diisopropylethylamine in 20 ml THF was prepared in a 100 ml three-neck flask fitted with two stoppers and a septum. The solution was cooled to 0 °C and 3.48 ml (5 g, 0.025 mol) dichlorodiisopropylaminophosphine (**45**) was added slowly dropwise from a syringe. The mixture was allowed to stir for two hours and then poured into 75 ml acid-free ethyl acetate. The solution was washed with pH 7 phosphate buffer[25] (3 x 20 ml) and the combined aqueous layers extracted with 30 ml acid-free ethyl acetate. The organic layers were combined and dried over anhydrous $MgSO_4$. The dry organic layer was rotovapped to a cloudy oil and flash chromatographed (5:1 Hexane:Acetone with 0.20% Et_3N) yielding 2.612 g (40%) of a colorless oil. ^{1}H NMR (CD_3CN) δ (ppm) 3.82 (m), 3.64 (m), 2.64 (td), 1.18 (s), 1.16 (s).

(9*S*, 10*S*, 11*S*, 12*S*)-2, 6-Dihydroxy-9,10-dihydro-11, 12-dihydroxymethylethanoanthracene Bis[di(2-cyanoethyl)-phosphate] Ester (48_{SS}). A mixture of 0.051 g (5.67×10^{-5} mol) **52** in 4 ml methanol, 1 ml CH_2Cl_2, and 0.5 ml conc. aqueous HCl was prepared in a 25 ml flask. The mixture was stirred for two hours, then poured into a two-phase mixture of 10 ml ethyl acetate, 15 ml saturated $NaHCO_3$, and 5 ml pH 7 phosphate buffer.[25] The layers were separated and the aqueous layer extracted with ethyl acetate (3×5 ml). The combined organic extracts were dried over anhydrous $MgSO_4$, then rotovapped to a white solid. The solid was flash chromatographed (15% CH_3OH in Ethyl acetate) yielding 0.031 g (82%) of a white solid.

^{1}H NMR (CD_3CN) δ (ppm) 7.12 (d, J = 8.0 Hz), 6.80 (s), 6.79 (d, J = 2.4 Hz), 6.55 (dd, J = 2.4, 8.0 Hz), 4.20 (quartet of doublets), 3.80 (quintet, J = 5.0 Hz), 3.47 (quartet, J = 7.2 Hz), 2.78 (quartet of doublets), 1.22 (t, J = 9.0). FAB-MS (*m/e*) 671 (MH^+). HRMS 671.1707 (MH^+), calculated for $C_{30}H_{33}O_{10}P_2$ 671.1672.

(9*S*, 10*S*, 11*S*, 12*S*)-2, 6-Bis(*tert*-butyldimethylsiloxy)-9,10-dihydro-11, 12-dihydroxymethylethanoanthracene (51_{SS}). A solution of 0.267 g (3.32×10^{-4} mol) 50_{SS} in 5 ml THF was prepared in a 25 ml flask fitted with a septum, this was followed by dropwise addition of 1.7 ml 1.0 M $LiBEt_3H$ (1.7×10^{-3} mol) from a syringe. TLC (Si gel, 6:4 Ethyl acetate:Pet ether eluant) indicated complete reaction after 23 hours. The mixture was quenched by adding 10 ml ethyl acetate and rotovapped to a colorless oil. The oil was dissolved in 20 ml ethyl acetate and 20 ml water, the layers separated, the aqueous layer extracted with ethyl acetate (3 × 5 ml), and the combined organic layers dried over anhydrous $MgSO_4$. The dried organic solution was filtered, rotovapped to a white solid, and flash chromatographed (6:4 Ethyl acetate:Pet ether) yielding 0.112 g (64%) of product. ^{1}H NMR (CD_3CN) δ (ppm) 7.09 (d, J = 7.9 Hz), 6.80 (d, J = 2.1 Hz), 6.57 (dd, J = 2.1, 7.9 Hz), 4.15 (s), 3.06 (m), 2.94 (m), 1.33 (d, J = 5.7 Hz), 0.95 (s), 0.14 (s).

(9*S*, 10*S*, 11*S*, 12*S*)-2, 6-Bis(*tert*-butyldimethylsiloxy)-9,10-dihydro-11, 12-dihydroxymethylethanoanthracene Bis[di(2-cyanoethyl)-phosphate] Ester (52_{SS}). A solution of 0.050 g (9.49×10^{-5} mol) **51** and 0.028 g (4.00×10^{-4}) tetrazole in 2 ml acetonitrile was prepared in a 10 ml round bottom flask. The flask was cooled to 0 °C and 0.076 g (2.8×10^{-4} mol) **47** was added by syringe. The mixture was allowed to warm to room temperature and stir for four hours. At this point 0.082 g (3.23×10^{-4} mol) Iodine in 0.5 ml 2:1:0.8 THF:H_2O:pyridine was added, the iodine color immediately disappeared and addition continued until a slight yellowish color persisted. The reaction was allowed to stir for an additional ten minutes and the mixture rotovapped to a white residue. The residue was dissolved in 5 ml $CHCl_3$ and washed with

5 ml 0.1% aqueous NaHSO3, water (2 × 5 ml), and saturated NaCl (2 × 5 ml). The combined aqueous layers were extracted with 5 ml $CHCl_3$ and the combined organic layers dried over anhydrous $MgSO_4$. The dry solution was rotovapped to a colorless oil and flash chromatographed, eluting first with 6:4 Ethyl acetate:Pet ether then with 95:5 Ethyl acetate:methanol. A yellowish oil was obtained (0.051 g, 60%). ^1H NMR (CD_3CN) δ (ppm) 7.17 (d, J = 8.0 Hz), 6.86 (d, J = 2.4 Hz), 6.63 (dd, J = 2.4, 7.9 Hz), 4.26 (s), 4.20 (quartet of doublets, J = 1.9, 6.0 Hz), 3.80 (quintet, J = 5.2 Hz), 3.44 (quartet, J = 7.3 Hz), 2.78 (quartet of doublets, J = 1.0, 4.0 Hz), 1.67 (t, J = 2.8), 0.96 (s). FAB-MS (*m/e*) 921 (MNa^+), 899 (MH^+), 695, 531, 491, 438, 381, 325, 267, 211, 155. HRMS 899.3446 (MH^+), calculated for $C_{42}H_{61}O_{10}P_2Si_2$ 899.3401.

***p*-Bromomethylbenzyl alcohol (54).** A three-neck 100 ml flask was fitted with a reflux condenser, a 10 ml addition funnel, and a stopper. A solution of 2.555 g (0.0119 mol) *p*-bromomethylbenzoic acid (**53**) in 40 ml THF was prepared in the flask and the apparatus cooled to 0 °C. Once cooled, 10 ml of a 1.0 M solution of BH_3 in THF was added dropwise over a period of 30 minutes; upon complete addition the apparatus was brought back to room temperature and the cooling bath replaced with a heating mantle. The solution was maintained at reflux for five and a half hours, at which point TLC (Si gel, 6:4 Ethyl acetate:Pet ether eluant) indicated a complete reaction. The reaction was quenched by addition of 60 ml water and extracted with ether (3 × 50 ml). The combined organic extracts were washed with saturated $NaHCO_3$ (2 × 50 ml) and 50 ml water, then dried over anhydrous K_2CO_3. The dry solution was rotovapped to a white solid and flash chromatographed (95:5 CH_2Cl_2:Ethyl acetate) yielding 1.993 g (83%) of a white solid. ^1H NMR ($CDCl_3$) δ (ppm) 7.40 (d, J = 6.1 Hz), 7.38 (d, J = 5.1 Hz), 4.70 (d, J = 6.0 Hz), 4.50 (s), 1.65 (t, J = 6.0 Hz). 50 eV EI-MS (*m/e*) 202, 201 (M^+), 121, 103, 91, 77, 72, 61, 51, 43. HRMS 199.9837, calculated for C_8H_9BrO 199.9837.

β-(*p*-Bromomethylphenyl)ethanol (57). A three-neck 100 ml flask was fitted with a reflux condenser, a 10 ml addition funnel, and a stopper. A solution of 2.725

g (0.0119 mol) (*p*-bromophenyl)acetic acid (**56**) in 40 ml THF was prepared in the flask and the apparatus cooled to 0 °C. Once cooled, 10 ml of a 1.0 M solution of BH_3 in THF was added dropwise over a period of 30 minutes. Upon complete addition the apparatus was brought back to room temperature and the cooling bath replaced with a heating mantle. The solution was maintained at reflux for ten hours, at which point TLC (Si gel, 6:4 Ethyl acetate:Pet ether eluant) indicated a complete reaction. The reaction was quenched by addition of 60 ml water and extracted with ether (3 × 50 ml). The combined organic extracts were washed with saturated $NaHCO_3$ (2 × 50 ml) and 50 ml water, then dried over anhydrous K_2CO_3. The dry solution was rotovapped to a white solid and flash chromatographed (95:5 CH_2Cl_2:Ethyl acetate) yielding 1.429 g (56%) of a white solid. ^1H NMR ($CDCl_3$) δ (ppm) 7.35 (d, J = 8.0 Hz), 7.21 (d, J = 7.8 Hz), 4.49 (s), 3.87 (quartet, J = 6.2 Hz), 2.87 (t, J = 6.5 Hz), 1.37 (t, J = 5.7 Hz). 70 eV EI-MS (*m/e*) 216, 214 (M^+), 202, 183, 135, 117, 105, 89, 78, 66, 61, 51, 43. HRMS 214.0011, calculated for $C_9H_{11}BrO$ 213.9993.

(9*R*, 10*R*)-2, 6-Bis(*p*-trimethylaminomethylbenzyloxy)-9,10-dihydro-11, 12-dicarboxy-ethenoanthracene (60_R inner salt). In a 25 ml flask 0.200 g (2.4×10^{-4} mol) $\mathbf{62_R}$ was dissolved in 40 ml THF, followed by addition of 1.949 g (0.013 mol) cesium hydroxide and 10 ml water. The mixture was allowed to stir in the dark at room temperature overnight and the THF removed by rotary evaporation. After addition of 10 ml of water, the cloudy suspension was sonicated and the precipitate allowed to settle. The precipitate was collected, washed with ice cold water, and dried overnight in a vacuum desiccator yielding 0.082 g (53%). ^1H NMR (CD_3OD) δ (ppm) 7.58 (d, J = 8.0 Hz), 7.53 (d, J = 8.1 Hz), 7.23 (d, J = 8.0 Hz), 7.03 (d, J = 2.5 Hz), 6.60 (dd, J = 2.4, 8.0 Hz), 5.80 (s), 5.14 (s), 4.50 (s), 3.11 (s). FAB-MS (*m/e*) 647 ($[M^{2+}\text{-}H^+]^+$), 338, 219, 166. HRMS 647.3143 ($[M^{2+}\text{-}H^+]^+$), calculated for $C_{40}H_{41}N_2O_6$ 647.3121.

(9*R*, 10*R*)-2, 6-Bis(*p*-trimethylaminomethylbenzyloxy)-9,10-dihydro-11, 12-dicarbomethoxyethenoanthracene (62_R). A suspension of $\mathbf{4_R}$

(0.3.14 g, 4.37×10^{-4} mol) in 30 ml dry methanol (Aldrich Sure-Seal Bottle) was prepared in a three-neck 50 ml round bottom flask fitted with gas inlet, stopper, and dry-ice condenser. Anhydrous trimethylamine was condensed into the suspension and allowed to saturate the methanol (as indicated by increasing volume of the suspension). After saturation, the gas inlet and dry-ice condenser were removed and replaced with stoppers, the mixture was allowed to stir for one hour and then evaporated to a white solid. The solid was recrystallized from ethanol, collected by vacuum filtration, and dried overnight in a vacuum desiccator yielding 0.200 g of product (55%). ^{1}H NMR (CD_3CN) δ (ppm) 7.54 (d), 7.48 (d), 7.15 (d), 7.08 (d), 6.60 (dd), 5.13 (s), 4.35 (s), 3.57 (s), 2.97 (s). FAB-MS (*m/e*) 661 ([M-CH_3]$^+$), 648, 602, 447, 419, 363, 335, 312, 251, 233, 194, 180, 163, 121. HRMS 661.3256 ([M-CH_3]$^+$), calculated for $C_{41}H_{45}N_2O_6$ 661.3278.

4-Hydroxymethyl-1-methylpyridinium Iodide (64). To a solution of 0.733 g (6.72×10^{-3} mol) 4-hydroxymethylpyridine (**63**) in 20 ml acetonitrile in a 50 ml flask was added, 2.1 ml (4.78 g, 0.034 mol) CH_3I was added by syringe. After four hours the solution was noticeably yellow, and a white precipitate had formed; the mixture was allowed to continue stirring overnight. The mixture was concentrated under vacuum and slurried with 50 ml ether. The yellowish solid was collected by vacuum filtration and dried overnight under vacuum, yielding 1.409 g (83%) of product. ^{1}H NMR (CD_3OD) δ (ppm) 8.80 (d, J = 6.7 Hz), 8.03 (d, J = 6.0 Hz), 4.91 (s), 4.37 (s).

4-Bromomethyl-1-methylpyridinium Bromide (65). A mixture of 0.506 g (2.02×10^{-3} mol) **64** and 5 ml of 48.5% aqueous HBr were brought to reflux in a 10 ml flask fitted with a condenser. After four and a half hours, the mixture was concentrated to an orange oil and 10 ml absolute ethanol was added. A yellow solid precipitated from the oil, and this was collected by vacuum filtration and dried under vacuum overnight to yield 0.318 g (59%) of product. ^{1}H NMR (CD_3OD) δ (ppm) 8.76 (d, J = 6.6 Hz), 8.05 (d, J = 6.5 Hz), 4.79 (s), 4.34 (s). FAB-MS (*m/e*) 234, 188, 186 (M$^+$), 165, 140, 124, 115. HRMS 185.9910, calculated for C_7H_9NBr 185.9918.

[di*t*-BOC protected] (9*S*, 10*S*, 11*S*, 12*S*)-2, 6-Bis(*p*-aminomethylbenzyloxy)-9,10-dihydro-11, 12-dicarbomethoxyethanoanthracene Bis[di-(-)-menthyl ester] (67_{SS}). A 50 ml flask was charged with 0.057 g (9.49×10^{-5} mol) 19_{SS}, 0.118 g (3.40×10^{-4} mol) **68**, and 0.175 g (5.37×10^{-4} mol) cesium carbonate. After addition of 10 ml acetonitrile, the mixture was allowed to stir in the dark. TLC (Si gel, 95:5 $CHCl_3$:Ether eluant) indicated completion of the reaction after 24 hours, the mixture was filtered, solids washed with acetonitrile, and the filtrate rotovapped to a yellowish solid. This solid was subjected to flash chromatography (6:4 Hexanes:Ether) and provided 0.086 g (86%) of product as a white solid. ^{1}H NMR (CD_3CN) δ (ppm) 7.36 (d, J = 8.0 Hz), 7.25 (d, J = 8.0 Hz), 7.07 (d, J = 8.2 Hz), 7.01 (d, J = 2.4 Hz), 6.66 (dd, J = 2.3, 8.1 Hz), 5.04 (s), 4.58 (s), 4.53 (td), 4.19 (d, J = 6.5 Hz), 3.18 (s), 1.79-1.63 (m), 1.39 (s), 0.94 (d, J = 7.1 Hz), 0.85 (d, J = 6.4 Hz), 0.68 (d, J = 6.7 Hz). FAB-MS (*m/e*) 1050 (MH^+), 886, 648, 373, 210. HRMS 1049.6807 (MH^+), calculated for $C_{64}H_{93}N_2O_{10}$ 1048.6830.

(*t*-BOC protected) *p*-aminomethylbenzyl Iodide (68). In a three-neck 50 ml flask fitted with a septum and two stoppers, 0.251 g (1.06×10^{-3} mol) **74**, 0.469 g (1.79×10^{-3} mol) triphenylphosphine, and 0.141 g (2.07×10^{-3} mol) tetrazole were dissolved in 5 ml ether and 2 ml acetonitrile. The solution was cooled to 0 °C and 0.479 g (1.89×10^{-3} mol) solid iodine was slowly added; a yellow precipitate immediately formed. The mixture was allowed to slowly come to room temperature while stirring in the dark. TLC (Si gel, 6:4 Ethyl acetate:Pet ether eluant) indicated completion of the reaction after four hours. The mixture was rotovapped to a brown oil, 20 ml ether was added and the mixture sonicated and filtered. The filtrate was rotovapped to a red-brown oil and flash chromatographed (6:4 Hexanes:Ether) yielding 0.237 g (65%) of a white solid. ^{1}H NMR (CD_3CN) δ (ppm) 7.36 (d, J = 8.0 Hz), 7.19 (d, J = 8.3 Hz), 4.54 (s), 4.15 (d, J = 6.2 Hz), 1.40 (s). CI-MS (*m/e*) 348 (MH^+), 320, 292, 248, 231, 220, 164, 146, 120, 104, 91, 74, 57. HRMS 348.0465 (MH^+), calculated for $C_{13}H_{19}INO_2$ 348.0460.

[di*t*-BOC protected] (9*S*, 10*S*, 11*S*, 12*S*)-2, 6-Bis(*p*-aminomethylbenzyloxy)-9,10-dihydro-11, 12-dihydroxymethylethanoanthracene (70_{SS}) [Prepared from reduction of 69_{SS}]. A solution of 0.085 g (8.10×10^{-5} mol) 67_{SS} in 2 ml THF was prepared in a 50 ml flask fitted with a septum. This was followed by dropwise addition of 0.5 ml 1.0 M $LiBEt_3H$ (5.0×10^{-4} mol) from a syringe. TLC (6:4 Ethyl acetate:Pet ether eluant) indicated complete reaction after two hours. The mixture was quenched by adding 5 ml ethyl acetate and rotovapped to a colorless oil. The oil was dissolved in 10 ml ethyl acetate and 10 ml water, the layers separated, the aqueous layer extracted with ethyl acetate (3 × 5 ml), and the combined organic layers dried over anhydrous $MgSO_4$. The dried organic solution was filtered, rotovapped to a colorless oil, and flash chromatographed (Ethyl acetate:Pet ether) yielding 0.029 g (48%) of product. ^1H NMR (CD_3CN) δ (ppm) 7.36 (d, *J* = 7.9 Hz), 7.25 (d, *J* = 8.0 Hz), 7.13 (d, *J* = 8.1 Hz), 6.92 (d, *J* = 2.5 Hz), 6.67 (d, *J* = 2.5, 8.0 Hz), 5.01 (s), 4.18 (t, *J* = 6.0 Hz), 3.11 (quartet), 2.95 (quartet), 2.86 (t, *J* = 5.0 Hz), 1.34 (s). FAB-MS (*m/e*) 736 (M^+), 648, 581, 520, 429, 373. HRMS 736.3686, calculated for $C_{44}H_{52}O_8$ 736.3724.

[di*t*-BOC protected] (9*R*, 10*R*, 11*R*, 12*R*)-2, 6-Bis(*p*-aminomethylbenzyloxy)-9,10-dihydro-11, 12-dihydroxymethylethanoanthracene (69_{RR}) [Prepared from alkylation of 75_{RR}]. A 10 ml flask was charged with 0.033 g (1.11×10^{-4} mol) 75_{RR}, 0.132 g (3.80×10^{-4} mol) **68**, and 0.200 g (6.14×10^{-4} mol) cesium carbonate. After addition of 5 ml acetonitrile, the mixture was allowed to stir in the dark. TLC (Si gel, 6:4 Ethyl acetate:Pet ether eluant) indicated completion of the reaction after two days, the mixture was filtered, solids washed with acetonitrile, and the filtrate rotovapped to a yellowish solid. This solid was subjected to flash chromatography (6:4 Ethyl acetate:Pet ether) and provided 0.064 g (78%) of product as a white solid. ^1H NMR (CD_3CN) δ (ppm) 7.36 (d, *J* = 7.9 Hz), 7.25 (d, *J* = 8.0 Hz), 7.13 (d, *J* = 8.1 Hz), 6.92 (d, *J* = 2.5 Hz), 6.67 (d, *J* = 2.5, 8.0 Hz), 5.01 (s), 4.18 (t, *J* = 6.0 Hz), 3.11 (quartet),

2.95 (quartet), 2.86 (t, J = 5.0 Hz), 1.34 (s). FAB-MS (*m/e*) 736 (M^+), 648, 581, 520, 429, 373. HRMS 736.3686, calculated for $C_{44}H_{52}O_8$ 736.3724.

(9*R*, 10*R*, 11*R*, 12*R*)-2, 6-Bis(*p*-aminomethylbenzyloxy)-9,10-dihydro-11, 12-dihydroxymethylethanoanthracene (70_{RR}). To a solution of 0.064 g (8.68×10^{-5} mol) 69_{RR} in 1.5 ml CH_2Cl_2 in a 10 ml flask was added 0.8 ml TFA. The stirring solution was monitored by TLC (Si gel treated with 10% ET_3N in hexanes, 85:15 Ethyl acetate:CH_3OH) which indicated a complete reaction after 30 minutes. The solvent was evaporated in a stream of nitrogen gas and the resultant solid dried overnight under vacuum to yield 0.023 g (49%) product. ^1H NMR (DMSO-d_6) δ (ppm) 7.45 (AB, J = 7.7 Hz, Δν = 22.96 Hz), 7.16 (d, J = 8.1 Hz), 7.07 (d, J = 2.3 Hz), 6.75 (dd, J = 2.4, 8.4 Hz), 5.75 (s), 5.06 (s), 4.22 (s), 4.08 (quartet, J = 5.4 Hz), 4.02 (AB, J = 5.7 Hz), 3.83 (partly covered by water peak), 1.90 (t).

(9*R*, 10*R*, 11*R*, 12*R*)-2, 6-Bis(*p*-trimethylaminomethylbenzyloxy)-9,10-dihydro-11, 12-dihydroxymethylethanoanthracene (71_{RR}). To a 10 ml containing 0.023 g (4.28×10^{-5} mol) 70_{RR}, 0.040 g (2.89×10^{-4} mol), and 1 ml dry DMF (Aldrich Sure-Seal Bottle) was added 0.3 ml (0.68 g, 4.82×10^{-4} mol) CH_3I. The mixture was allowed to stir for one hour, then rotovapped to a yellowish oil, added 5 ml water and froze to -78 °C. The frozen solid was lyophilized to give a yellowish powder; recrystallization from ethanol provided a yellow solid. Mass spectrometry indicated a significant amount of KI was present as impurity. ^1H NMR (CD_3CN) δ (ppm) 7.55 (AB, J = 9.8 Hz, Δν = 29.36 Hz), 7.17 (d, J = 8.1 Hz), 6.96 (d, J = 2.4 Hz), 6.71 (dd, J = 2.6, 8.0 Hz), 5.11 (s), 4.45 (s), 4.21 (s), 3.08 (s), 3.02 (s), 2.59 (t, J = 1.8 Hz).

***p*-aminomethylbenzyl alcohol (73).** A three-neck 100 ml flask was fitted with a reflux condenser, a 10 ml addition funnel, and a stopper. A solution of 2.021 g (0.0137 mol) *p*-cyanobenzoic acid (**72**) in 10 ml THF was prepared in the flask and the apparatus cooled to 0 °C. Once cooled, 72 ml of a 1.0 M solution of BH_3 in THF was added dropwise over a period of one hour; upon complete addition the apparatus was

brought back to room temperature and the cooling bath replaced with a heating mantle and the solution was maintained at reflux for four hours. The reaction was quenched by addition of 10 ml conc. HCl, rotovapped to a white solid and dissolved in 100 ml water. The aqueous solution was washed with 50 ml $CHCl_3$ and made basic with 50/50 w/w NaOH. The basic solution was extracted with $CHCl_3$ (3 × 50 ml) and the combined dried over anhydrous K_2CO_3. The dry solution was rotovapped to give a 0.723 g (38%) of a white solid. ^1H NMR (CD_3CN) δ (ppm) 7.26 (m), 4.54 (s), 3.75 (s). CI-MS (*m/e*) 136 ($[M-H]^+$), 120, 106, 91, 61. HRMS 136.0756 ($[M-H]^+$), calculated for $C_8H_{10}NO$ 136.0763.

(*t*-BOC protected) *p*-aminomethylbenzyl alcohol (74). A 100 ml flask was charged with 0.332 g **73** (2.42×10^{-3} mol) and 0.545 (2.50×10^{-3} mol) BOC anhydride and heated to 100 °C in an oil-bath. After stirring at 100 °C for one and a half hours, the reaction was cooled to room temperature, dissolved in methanol and rotovapped onto a Si gel. The Si gel was added as a plug to a flash column and eluted with 6:4 ethyl acetate:pet ether yielding 0.487 g (85%) of a white solid. ^1H NMR (CD_3CN) δ (ppm) 7.27 (d, J = 8.1 Hz), 7.18 (d, J = 8.0 Hz), 5.74 (br), 4.53 (d, J = 6.0 Hz), 4.18 (d, J = 6.3 Hz), 3.11 (t, J = 5.9 Hz), 1.40 (s). CI-MS (*m/e*) 236 ($[M-H]^+$), 220, 192, 180, 164, 150. HRMS 236.1283 ($[M-H]^+$), calculated for $C_{13}H_{18}NO_3$ 236.1287.

(9*R*, 10*R*, 11*R*, 12*R*)-2, 6-Dihydroxy-9,10-dihydro-11, 12-dihydroxymethylethanoanthracene (75_{RR}). A mixture of 0.224 g (4.25×10^{-4} mol) $\mathbf{51_{RR}}$ in 16 ml methanol, 4 ml CH_2Cl_2, and 2 ml conc. aqueous HCl was prepared in a 25 ml flask. The mixture was stirred for four hours, then poured into a two-phase mixture of 40 ml ethyl acetate, 50 ml saturated $NaHCO_3$, and 10 ml pH 7 phosphate buffer.[25] The layers were separated and the aqueous layer extracted with ethyl acetate (3 × 20 ml). The combined organic extracts were dried over anhydrous $MgSO_4$, then rotovapped to a colorless oil. The oil was flash chromatographed (95:5 Ethyl acetate:CH_3OH) yielding a white solid. ^1H NMR (CD_3CN) δ (ppm) 7.04 (d, J = 7.9 Hz), 6.72 (d, J = 2.4 Hz), 6.66

(s), 6.49 (dd, J = 2.4, 7.9 Hz), 4.07 (s), 3.09 (quintet, J = 5.0 Hz), 3.47 (quintet, J = 5.3 Hz), 2.99 (quintet, J = 4.6 Hz), 2.83 (t, J = 5.1), 1.32 (t, J = 2.9).

7.8 References and Footnotes

1. (a) Forman, J. E.; Barrans, R. E., Jr.; Dougherty, D. A.; *J. Am. Chem. Soc.* **1995**, *117*, 9213-9228. (b) Kearney, P. C.; Mizoue, L. S.; Kumpf, R. A.; Forman, J. E.; McCurdy, A.; Dougherty, D. A. *J. Am. Chem. Soc.* **1993**, *115*, 9907-9919. (c) Petti, M. A.; Shepodd, T. J.; Barrans, R. E., Jr.; Dougherty, D. A. *J. Am. Chem. Soc.* **1988**, *110*, 6825-6840.

2. Hulme, H. C.; *Receptor Biochemistry*, Oxford University Press, New York, 1990.

3. (a) Merz, K. M., Jr.; Le grande, S. M. (eds); *The Protein Folding Problem and Tertiary Structure*, Birkhäuser, Boston, 1994. (b) Lehninger, A. L.; *Biochemistry*, Worth Publishers, Inc.; New York, 1976.

4. Circular dichroism data from solutions of **1** at pH's from 2-12 suggest that the pK_a's are approximately 2, 8, and 10 (isoelectric point approximately 7.5).

5. Day, R. A., Jr.; Underwood, A. C.; *Quantitative Analysis*, Prentice-Hall, 1986.

6. pK_a for model compound **7** from: Dean, J. A. (ed); *Handbook of Organic Chemistry*, McGraw-Hill, 1987.

7. pK_a for model compound **8** from: (a) Perrin, D. D.; *Dissociation Constants of Organic*

Bases in Aqueous Solution, Butterworths, London, 1965. (b) Perrin, D. D.; *Supplement to Dissociation Constants of Organic Bases in Aqueous Solution*, Butterworths, London, 1972.

8. Ma, J. C.; Dougherty, D. A.; *Unpublished Results*.

9. *Aggregation Processes in Solution*, Wyn-Jones, E.; Gormally, J; (eds), Elsevier Scientific Publishing Company, 1983.

10. These molecules are prepared analogously to **9** from the ethanoanthracene building blocks **20** and **28**.

11. Collman, J. P.; Zhang, X.; Wong, K.; *J. Am. Chem. Soc.* **1994**, *116*, 6245-6251.

12. Originally the synthesis was attempted using the dimethyl ester of **37**; however, this compound could not be successfully brominated with NBS. Thus the ethyl ester was finally required to prepare the side chain precursor **39**.

13. Kearney, P. C.; California Institute of Technology, Ph.D. Thesis, 1994.

14. Robertson, S. A.; Noren, J.; Anthony-Cahill, S. J.; Griffith, M. C.; Schultz, P. G.; *Nucleic Acids Res.* **1989**, *17*, 9649-9660.

15. Corbridge, D. E. C.; *Phosphorous–An outline of its Chemistry, Biochemistry, and Technology*, Elsevier, 1990.

16. Bixler, R. L.; Niemann, C.; *J. Am. Chem. Soc.* **1958**, *23*, 575-584.

17. Zincke, T.; Heuser, G.; Möller, W.; *Ann.* **1904**, *333*, 296-345.

18. This is a general observation from studies of ethenoanthracene based cyclophane hosts and other ethenoanthracene based structures in the Dougherty labs.

19. Connors, K. A. *Binding Constants*, Wiley: New York, 1987.

20. Shoemaker, D. P.; Garland, C. W.; Steinfeld, J. I.; Nibler, J. W.; *Experiments in Physical Chemistry*, McGraw-Hill, 1981.

21. (a) Barrans, R. E., Jr.; Dougherty, D. A. *Supramolecular Chem.* **1994**, *4*, 121-130. (b) Barrans, R. E., Jr.; California Institute of Technology, Ph.D. Thesis, 1993.

22. Given the poor fitting results, the other studies of **71** with polycarboxylates $\mathbf{33_R}$ and $\mathbf{9_S}$ were not fitted.

23. Mecozzi, S.; Dougherty, D. A.; *Unpublished Results*.

24. Version 4.0, Microsoft Corp., © 1985-1992.

25. Dean, J. A. (ed); *Lang's Handbook of Chemistry*; McGraw-Hill, 1985.

26. **19**: McCurdy, A.; California Institute of Technology, Ph.D. Thesis, 1995; **25**: See reference 8; **31-dimethyl ester**: See reference 21b; **32-dimethyl ester**: Stauffer, D.A. California Institute of Technology, Ph.D. Thesis, 1989; **37**: This molecule was prepared by Eric Co, a SURF student during the summer of 1994 from a preparation provided by Michael Murray.

27. This is the (9*R*, 10*R*, 11*S*, 12*S*)-diastereomer of **19**.[26].

Chapter 8
Miscellaneous Laboratory Projects.

Chapter 8
Miscellaneous Laboratory Projects.

8.1 Introduction

Chapters 2-7 describe the results of projects which were the major focus of study over the course of the author's residence at Caltech. While these studies comprised the bulk of the work, a number of side projects were also carried out. Several of these other projects are worth mentioning and are reported in this chapter.[1]

8.2 Amides as Neutral Water-Solubilizing Groups

8.2.1 Introduction

A very important question that arises in the studies of cyclophane receptors in the Dougherty group is the role that the charge on the host plays in binding cationic guests.[2] The hosts studied (typified by hosts **P** and **C** in Figure 8.1) all use anionic carboxylate groups to solubilize the organic molecule.[2] The prototypical guests for these hosts are cations such as **1** and electron-deficient neutral guests such as **2** (Figure 8.2). A large amount of data suggests that a strong cation-π effect rather than electrostatic forces is a controlling factor in the observed binding event (as observed in the comparison of binding constants for the guests shown in Figure 8.2, neutral guests are bound with the same affinity by the two hosts, but charged guests are not).[2] While the solubilizing carboxylates should be tightly solvated, resulting in an attenuation of the electrostatic attractions through the aqueous environment, the contribution of the electrostatic attractions between host and

guest may not be negligible. In order to address this issue a neutral water soluble host analog was desired.

Neutral solubilizing groups are not as effective as ionic solubilizing groups for organic molecules.[3] However, with the development of circular dichroism (CD) spectroscopy as a means for studying the cyclophane systems,[2a] micromolar solubility would still allow study. Given the need for only slight solubility, the use of primary amides as neutral solubilizing groups seemed a good place to start. Thus, the tetraamide analog of host P (P_A) was envisioned (Figure 8.3). The preparation and solubility of this molecule are described in the following section.

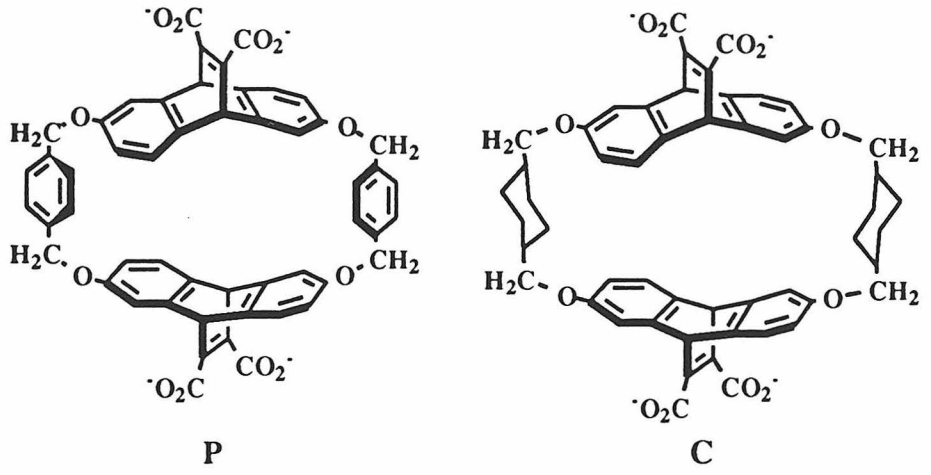

[(*S*, *S*)-Stereochemistry of ethenoanthracene units shown]

Figure 8.1. Anionic cyclophane hosts.[2]

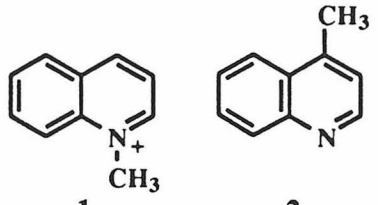

	1	2
$-\Delta G°_a$ (P) =	8.4 kcal/mol	5.9 kcal/mol
$-\Delta G°_a$ (C) =	6.3 kcal/mol	6.0 kcal/mol

Figure 8.2. Prototypical guests and their binding constants with hosts P and C.[2]

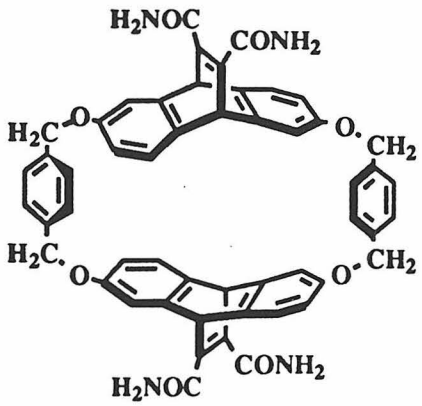

P_A

[(*S*, *S*)-Stereochemistry of ethenoanthracene units shown]

Figure 8.3. Tetraamide analog of host P.

8.2.2 Synthesis and Solubility

Initial attempts to convert the carboxylates of host **P** to amides began with simple ammoniolysis of the host's tetra methyl ester precursor ($\mathbf{P_E}$). Model studies with ethenoanthracene **3** showed the ammoniolysis reaction to give diamide **4** (Figure 8.4) proceeds in high yield. Diamide **4** was found to be sparingly soluble in aqueous media, with a saturated solution having a concentration of around 2 μM (as determined by UV/Visible spectroscopy).[4] These results were very encouraging. It was assumed that the host $\mathbf{P_A}$ would also be more soluble than model compound **4**, as the ratio of polar groups to organic groups is greater in the host.

The ammoniolysis of $\mathbf{P_E}$ (Figure 8.5) was found to proceed much more slowly than that of model compound **3**. After 36 hours, TLC indicated the absence of starting material and the presence of a single product. On isolation, however, this single product turned out to be the triamide monoester **5**. Conversion of **5** to $\mathbf{P_A}$ required an additional six days and gave a product that proved difficult to purify (hence the low yield of isolated material).

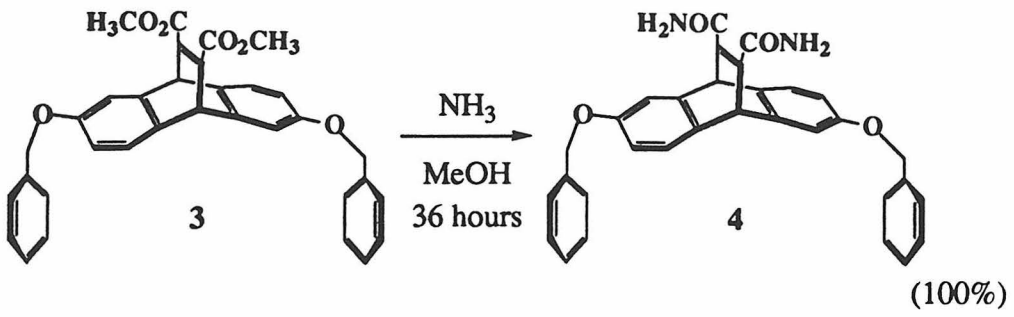

[(*S*, *S*)-Stereochemistry of Ethenoanthracene units shown]

Figure 8.4. Amide preparation by ammoniolysis.

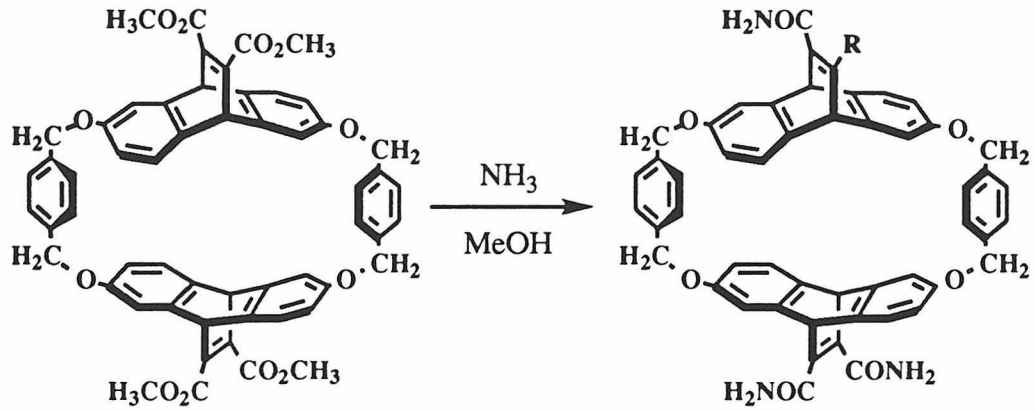

P_E

5, R = $-CO_2CH_3$ (100%)
reaction time = 1 day

[(*S*, *S*)-Stereochemistry of ethenoanthracene units shown]

P_A, R = $-CONH_2$ (8%)
reaction time = 7 days

Figure 8.5. Ammoniolysis of P_E.

Host P_A was found to be readily soluble in chloroform and DMSO, but not soluble in aqueous media. Saturated solutions (prepared by sonication of solid P_A in the solvent and filtering the resultant solution) gave CD signals too weak to be useful in quantitative studies (sub-μM solubility).

The indication of this work was that primary amides cannot impart significant water solubility for the more conformationally rigid cyclophane structure. From this failure it

was deduced that additional hydrophilic groups would be required to provide the desired solubility. One way of introducing this additional hydrophilic character is through hydroxy groups, as described in the next section.

8.2.3 Other Designs

In order to add additional hydrophilic character from hydroxyl groups, amides formed from amines **6-8** were proposed (Figure 8.6). A number of attempts to convert **3** into the appropriate diamide (**9-11**) using conditions analogous to those used in the preparation of **4** failed, even with heating. Heating **3** in neat **6** also failed to provide the diamide **9**.

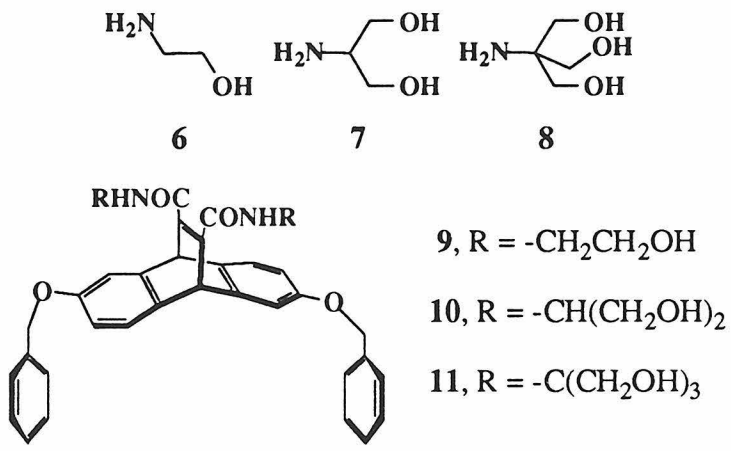

[(*S*, *S*)-Stereochemistry of Ethenoanthracene unit shown]

Figure 8.6. Amines capable of providing more hydrophilic amides.

The project was abandoned at this point. However, later work in the group by Sandro Mecozzi did provide a neutral water soluble host using amides prepared from amine **8** by a base-catalyzed aminolysis with ethano- rather than ethenoanthracene-based cyclophanes.[5]

8.3 Stabilization of Resonance Structures by Binding to a Cyclophane Receptor.

8.3.1 Introduction

Cationic polyene dyes like **12** and **13** have resonance structures that place the formal positive charge on either of the two nitrogen atoms (Figure 8.7). Since host **P** stabilizes cations, it was of interest to see if the host would prefer to bind one of these resonance structures in preference to the other.

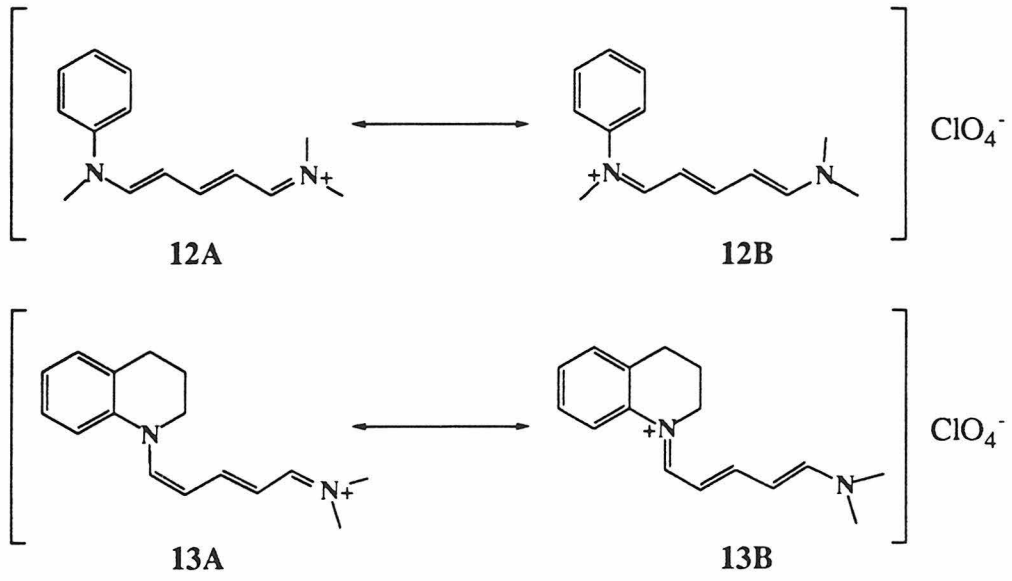

Figure 8.7. Cationic polyene dyes.

8.3.2 Binding Studies

^{1}H NMR binding studies were carried out with dyes **12** and **13**. The experiments showed the expected upfield shifting of guest proton signals, consistent with the guest being bound in the host cavity;[2bc] the relative *D* values for the protons of interest are given in Figure 8.8.[6] However, the dyes were observed to hydrolyze in the pD borate buffer

used in the studies (as indicated by the increasing intensity of the dimethyl amine signal at δ ≈ 2.7 ppm over the course of the experiment, Figure 8.9). This decomposition (Figure 8.9) prevented quantitative binding data from being obtained in the studies.

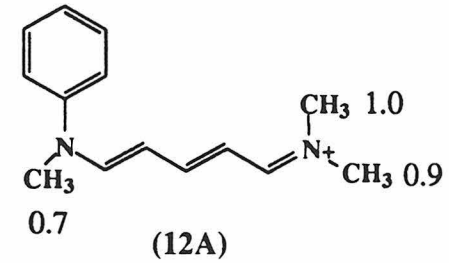

(12A)

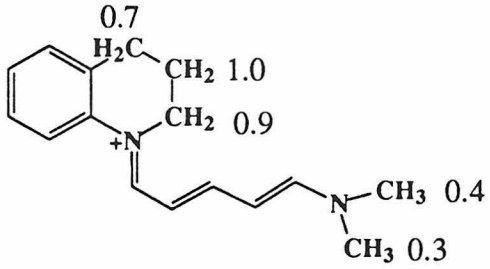

(13B)

Figure 8.8. Relative *D* values observed for dyes 12 and 13 bound by host P in borate-*d*.[6]

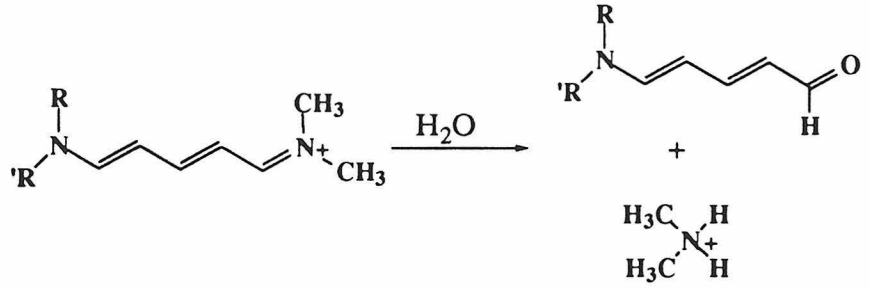

Figure 8.9. Hydrolysis of polyene dyes.[7]

Qualitatively, however, the relative *D* values do give some indication of the binding interaction between the dyes and host **P**. Larger relative *D* values indicate guest protons (or a portion of the guest) that are more preferentially bound within the cavity. Based on the

data in Figure 8.8, it appears that the preferred resonance structures for binding are **12A** and **13B**, a seemingly contradictory result. The data should, however, be viewed with caution, as the exact effect of the decomposing dyes is not clear (note that signals for both hydrolyzed and non-hydrolyzed dyes were observed, and the relative *D* values come from the non-hydrolyzed signals).

In the case of **12**, the binding seems to prefer the more basic nitrogen atom (**12A**), while with **13** the opposite is observed. With **13** the hydrolysis occurs faster than with **12** and the hydrolysis product (a tetrahydronapthalene derivative) is quite hydrophobic. Given the greater hydrophobic character of the aromatic end of the molecule, the result for **13** is not unexpected, whether or not hydrolysis occurs. The slower hydrolysis of **12** may be a result of a preferential binding of the dimethyl amine end of the dye, although the aromatic end of the molecule would be expected to be bound in preference to dimethyl amine. Several CD experiments were attempted in order to use induced CD to shed light on the NMR results. Unfortunately, no induced CD was detected with the dyes. The results are intriguing, yet inconclusive.

8.3.3 Conclusions and Future Directions

The results here suggest significantly different preferences are operating in the binding of **12** vs **13** by host **P**. But these systems were not further explored. Future studies at neutral pH (possibly with neutral hosts)[5] may result in the absence of hydrolysis and may help to answer the questions brought up in these studies.

The observation of preferred binding of a given resonance structure is interesting, particularly given that earlier attempts (see Chapter 4) at determining if the guest azulene (**14**, Figure 8.10) is preferentially bound at the seven-membered ("cationic") ring proved inconclusive.

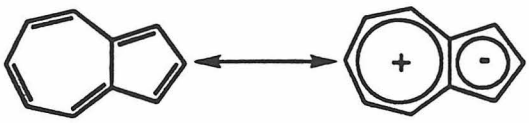

14A 14B

Figure 8.10. Resonance structures of Azulene (14).

8.4 Induction of Circular Dichroism in an Achiral Host

8.4.1 Introduction

Chapter 4 describes the observation of CD induced in achiral guest chromophores by a chiral host. The converse situation in which a chiral guest induces CD in an achiral host is also known, and is generally the result of the guest forcing the host into a chiral comformation.[8] In our laboratories the achiral analog of host **P** ($\mathbf{P_{meso}}$, Figure 8.11) appears well suited for this type of experiment. An appropriate guest should induce the chiral conformation and the strongly interacting chromophores of the host would be expected to show induced CD.

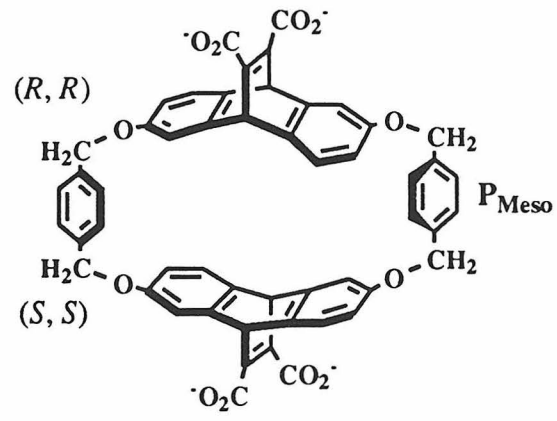

Figure 8.11. Achiral isomer of host P.[2c]

8.4.2 Binding Studies

In Chapter 6, binding constants were measured for chiral guests **15** and **16** with P_{meso}. But in neither case was any induced CD observed. With guest **15**, the metal complex itself has strong CD active absorptions that would hide any weak induced signals in the host. While guest **16** has a weaker CD spectrum, it also has no strong $\pi \rightarrow \pi^*$ transitions whose coupling to the host transitions would result in induced CD by the coupled-oscillator mechanism.[9] Thus CD (if any) induced by guest **16** would be very weak and difficult to detect. The observation of induced CD in the host appeared to require a chiral guest whose CD would not interfere with any signals induced in the host.

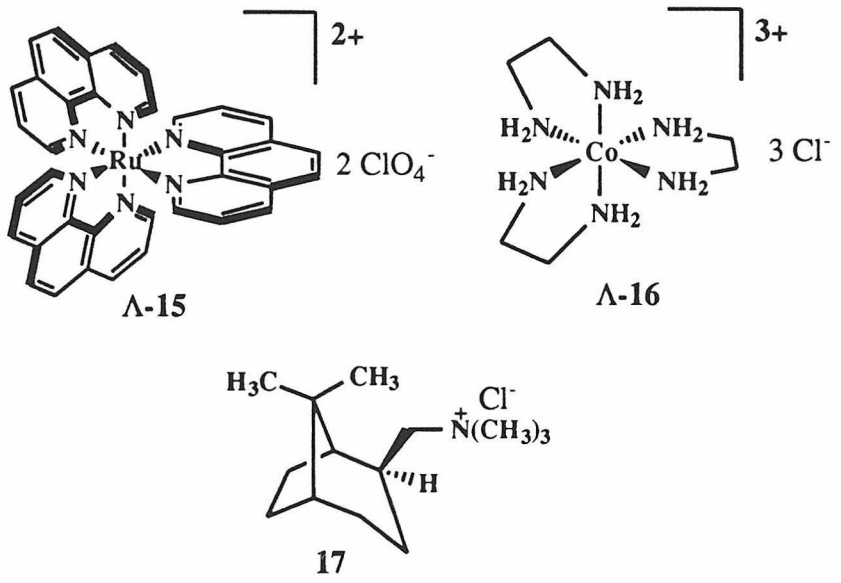

Figure 8.12. Guests studied with P_{meso}.

CD binding experiments with the non-chromophoric guest **17** were attempted in order to try to observe a chiral conformation of P_{meso} without interference from guest CD. However, in these experiments (including under conditions of excess guest), no induced CD could be detected in the host. The result suggests that the conformation of the host cavity is dynamic enough to prevent it from being locked into a stable chiral conformation.

This may be a consequence of the fast-exchange binding conditions observed with cyclophane hosts studied in our laboratories.[2c]

8.4.3 Future Directions

Additional studies with P_{meso} and chiral guests by CD were not undertaken. The results here suggest that in order to bring about induced CD in the host, a strong chromophoric guest is needed. The guests of Figure 8.13 may be useful for future studies. Unfortunately, these guests may also have the disadvantage of obscuring the induced CD in the host with the guest's inherent CD signals.

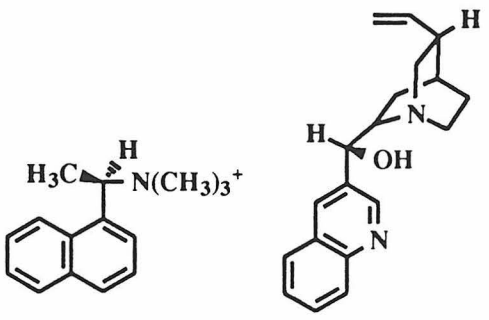

18 19

(cinchonine)

Figure 8.13. Chiral guests expected to induce CD in host P_{meso}.

8.5 Experimental Section

8.5.1 General Methods

CD spectra were recorded on a JASCO J-600 Spectropolarimeter with a 1.0 cm pathlength quartz cell. A standard set of measurement parameters was used in all quantitative experiments: Band Width 1.0 nm, Sensitivity 50 m°/cm, Time Constant 1.0

Sec., Scan Speed 50 nm/min., Step Width 0.2 nm/point, and a minimum of 4 accumulations. UV/Vis spectra were recorded on a Beckman DU-640 spectrophotometer. IR spectra were recorded on a Perkin-Elmer 1600 FT-IR. ^{1}H NMR spectra were recorded on a Bruker AM-500 spectrometer, routine spectra were referenced to the residual proton signals of the solvents and are reported in ppm downfield of 0.0 as δ values. NMR spectra in borate-*d* were referenced to the 1.09 ppm peak of 3,3-dimethylglutarate (DMG) as internal standard. Mass spectral data was obtained from the University of California Riverside, Mass Spectrometry Center.

All reactions, unless otherwise noted, were stirred magnetically under nitrogen or argon atmosphere. Ion exchange for NH_4^+ was carried out with Dowex® 50w-x2 cation exchange resin (the resin was treated with concentrated ammonium carbonate then washed with Milli-Q purified water before use). Unless otherwise noted, reagents obtained from commercial sources were used without further purification.

8.5.2 Binding Studies

Protocols for NMR binding studies in aqueous media have been described previously.[2bc] Host concentrations of borate-*d* solutions were determined using circular dichroism spectroscopy and fitting to known calibration curves (as described in Chapter 2). For guests, samples were weighed out on a Sartorius microbalance followed by dilution to appropriate volumes.

Circular dichroism binding studies are described in Chapter 2 of this manuscript.[2a] Attempts at qualitative detection of induced CD was done using excess concentrations of the appropriate host and/or control molecule with the guest of interest. For these studies the standard measurement parameters were often varied to provide conditions with the highest sensitivity. Fitting UV data from acetonitrile solutions of **P_{meso}-tetraacid** to ε

values for the 230-350 nm region of P_{meso}-tetramethyl ester in CH_3CN provided estimates of purity of samples of the tetraacid (as described for CD data in Chapter 2).

8.5.3 Synthesis

Compounds **P**, P_E, P_{meso}, P_{meso}-tetramethyl ester, **3**, and **17** were prepared by procedures described previously.[2c] Ion-exchange to provide the chloride salt of guest **17** was performed with Dowex® 1X8-400 ion exchange resin. Compounds **6**, **7**, and **8** were obtained from commercial sources. Guests **12** and **13** were gifts from the laboratories of Seth Marder in the Beckman Institute at the California Institute of Technology.[10] Samples of the enantiomers of guest **15** (as chloride salts) were gifts from the laboratories of Professor J. K. Barton at the California Institute of Technology.[11] For purification, **15** was precipitated from aqueous solution as a perchlorate salt and recrystallized from water prior to use (purity was assessed from elemental analysis). Guest **16** was prepared by the literature method and recrystallized and isolated as pure [Λ-$Co(en)_3Cl_3]_2$•NaCl•6 H_2O.[12]

(±)-2, 6-Bis(benzyloxy)-9,10-dihydro-11, 12-dicarboxamidoetheno-anthracene [(±)-4]. A solution of 0.026 g (4.88×10^{-5} mol) (±)-**4** in 5 ml dry methanol (Aldrich Sure-Seal Bottle) was prepared in a three-neck 25 ml round bottom flask fitted with gas inlet, stopper, and dry-ice condenser. Anhydrous ammonia was condensed into the suspension and allowed to saturate the methanol (as indicated by condensation on the outside of the flask). After saturation, the gas inlet and dry-ice condenser were removed and replaced with stoppers. TLC monitoring (Si gel, 95:5 CH_2Cl_2:Ether eluant) indicated the completion of the reaction after 36 hours. The reaction mixture was evaporated to a white solid and flash chromatographed (95:5 CH_2Cl_2:CH_3OH) yielding 0.025 g of product (100%). ^1H NMR ($CDCl_3$) δ (ppm) 7.40 (d, J = 7.6 Hz), 7.36 (t, J = 7.4 Hz), 7.31 (d, J = 7.6 Hz), 7.27 (d, J = 8.5 Hz), 7.10 (d, J = 1.8 Hz), 6.59 (dd, J =

2.3, 7.3 Hz), 5.44 (s), 5.03 (s). FAB-MS (*m/e*) 503 (MH^+), 486, 447, 419, 391. HRMS 503.1969 (MH^+), calculated for $C_{32}H_{27}N_2O_4$ 503.1863. IR (ν, cm^{-1}) 3448, 2370.6, 1654.4 (C=O), 1617.9 (C=O), 1475.3, 1381.8, 1231.8, 1107.0, 1024.6, 737.8, 696.6, 529.5.

(9*S*, 10*S*, 9'*S*, 10'*S*)-5. A solution of 0.014 g (1.54×10^{-5} mol) **(9*S*, 10*S*, 9'*S*, 10'*S*)-P_E** in 10 ml dry methanol (Aldrich Sure-Seal Bottle) was prepared in a three-neck 25 ml round bottom flask fitted with gas inlet, stopper, and dry-ice condenser. Anhydrous ammonia was condensed into the suspension and allowed to saturate the methanol (as indicated by condensation on the outside of the flask). After saturation, the gas inlet and dry-ice condenser were removed and replaced with stoppers. TLC monitoring (Si gel, 95:5 CH_2Cl_2:Ether eluant) indicated the completion of the reaction after 24 hours. The reaction mixture was evaporated to a white solid and flash chromatographed (95:5 CH_2Cl_2:CH_3OH) yielding 0.014 g of product (100%). ^1H NMR ($CDCl_3$) δ (ppm) 7.25 (partly covered by solvent peak), 7.14 (d), 6.93 (d), 6.49 (dd), 5.33 (s), 5.29 (s), 5.00 (AB), 3.71 (s), 3.69 (d), 3.52 (d).

(9*S*, 10*S*, 9'*S*, 10'*S*)-P_A. A solution of 0.014 g (1.548×10^{-5} mol) **(9*S*, 10*S*, 9'*S*, 10'*S*)-5** in 5 ml dry methanol (Aldrich Sure-Seal Bottle) was prepared in a three-neck 25 ml round bottom flask fitted with gas inlet, stopper, and dry-ice condenser. Anhydrous ammonia was condensed into the suspension and allowed to saturate the methanol (as indicated by condensation on the outside of the flask). After saturation, the gas inlet and dry-ice condenser were removed and replaced with stoppers. TLC monitoring (Si gel, 95:5 CH_2Cl_2:CH_3OH eluant) indicated the completion of the reaction after six days. The reaction mixture was evaporated to a white solid and flash chromatographed (9:1 CH_2Cl_2:CH_3OH) yielding 0.001 g of product (8%). ^1H NMR ($CDCl_3$) δ (ppm) 7.22 (partly covered by solvent peak), 7.11 (d, J = 8.1 Hz), 7.05 (s), 6.92 (d, J = 2.1 Hz), 6.42 (dd, J = 2.1, 8.7 Hz), 5.85 (s), 5.36 (s), 5.07 (AB, Δν = 56.5 Hz). FAB-MS (*m/e*) 849 (MH^+), 815, 739, 625, 551, 505, 419, 391, 363, 335, 279. HRMS 849.2924

(MH$^+$), calculated for $C_{52}H_{41}N_4O_8$ 849.2924. Circular dichroism [(9*S*, 10*S*, 9'*S*, 10'*S*)-enantiomer, CH_3CN] λ ($\Delta\varepsilon$) [nm ($M^{-1}cm^{-1}$)], 297 (+16.9), 280 (-4.0), 251 (+149), 226 (-214), 208 (-95.0).

8.6 References and Footnotes

1. Two other projects that do not dispose themselves to discussion are: 1) A number of attempts were made to grow crystals of hosts and host-guest complexes; the only successful result from these experiments is reported in Chapter 3. 2) A large number of samples have been submitted to the UC Riverside Mass Spectrometry center in attempt to observe host-guest complexes and self-assembled structures by electrospray mass spectrometry. As of this writing, no results from these mass spectrometry experiments have been obtained.

2. (a) Forman, J. E.; Barrans, R. E., Jr.; Dougherty, D. A.; *J. Am. Chem. Soc.* **1995**, *117*, 9213-9228. (b) Kearney, P. C.; Mizoue, L. S.; Kumpf, R. A.; Forman, J. E.; McCurdy, A.; Dougherty, D. A. *J. Am. Chem. Soc.* **1993**, *115*, 9907-9919. (c) Petti, M. A.; Shepodd, T. J.; Barrans, R. E., Jr.; Dougherty, D. A. *J. Am. Chem. Soc.* **1988**, *110*, 6825-6840.

3. *Aggregation Processes in Solution*, Wyn-Jones, E.; Gormally, J; (eds), Elsevier Scientific Publishing Company, 1983.

4. The spectra showed absorption intensities for **4** in aqueous solvents equivalent to those of 2 μM solutions of **3** in acetonitrile.

5. Mecozzi, S.; Dougherty, D. A.; *Unpublished Results*.

6. The relative *D* values are upfield shifts observed in ^{1}H NMR signals guest protons in the presence of host, these values have been scaled relative to the highest observed shift (which is assigned a value of 1.0.).

7. Chen, C.-T.; *Personnal Communication.*

8. (a) James, T. D.; Samankumara Sandanayake, K. R. C.; Shinkai, S.; *Supramol. Chem.* **1995**, *6*, 141-157. (b) Morozumi, T.; Shinkai, S.; *Chem. Lett.* **1994**, 1515-1518. (c) Morozumi, T.; Shinkai, S.; *J. Chem. Soc., Chem. Commun.* **1994**, 1219-1220. (d) Kobayashi, K.; Asakawa, Y.; Kikuchi, Y.; Toi, H.; Aoyama, Y.; *J. Am. Chem. Soc.* **1993**, *115*, 2648-2654. (e) Kikuchi, Y.; Kobayashi, K.; Aoyama, Y.; *J. Am. Chem. Soc.* **1992**, *114*, 1351-1358. (f) Arimura, T.; Shinkai, S. *Bull. Chem. Soc. Jpn.* **1991**, *64*, 1896-1900. (g) Arimura, T.; Kawabata, H.; Matsuda, T.; Muramatsu, T.; Satoh, H.; Fujio, K.; Manabe, O.; Shinkai, S. *J. Org. Chem.* **1991**, *56*, 301-306.

9. (a) Volosov, A.; Woody, R. W.; in *Circular Dichroism-Principles and Applications*, Nakanishi, K.; Berova, N.; Woody, R. W. (eds); VCH, 1994, 59-84.(b) Charney, E.; *The Molecular Basis of Optical Activity-Optical Rotatory Dispersion and Circular Dichroism*, Robert E. Krieger Publishing Company: Malabar, FL, 1985. (c) Mason, S. F. *Molecular Optical Activity and the Chiral Discriminations*, Cambridge University Press: Cambridge, 1982. (d) Tinoco, I., Jr. *Adv. Chem. Phys.* **1962**, *4*, 113-160.

10. These dyes were prepared by C.-T. Chen.

11. Methods of preparation and purfication can be found in: (a) Barton, J. K.; Goldberg,

J. M.; Kumar, C. V.; Turro, N. J.; *J. Am. Chem. Soc.* **1986**, *108*, 2081-2088. (b) Barton, J. K.; *Science* **1986**, *233*, 727-734. (c) Kumar, C. V.; Barton, J. K.; Turro, N. J.; *J. Am. Chem. Soc.* **1985**, *107*, 5518-5523. (d) Barton, J. K.; Danishefsky, A. T.; Goldberg, J. M.; *J. Am. Chem. Soc.* **1984**, *106*, 2172-2176.

12. Broomhead, J. A.; Dwyer, F. P.; Hogarth, J. W.; *Inorg. Synth.* **1960**, *6*, 183-186.